THÈSE POUR OBTENIR LE GRADE DE DOCTEUR DE L'UNIVERSITÉ DE MONTPELLIER

En Biologie Santé – Biologie cellulaire

École doctorale Sciences Chimiques et Biologiques pour la Santé

Unité de recherche IRMB, INSERM U1183

Rôles du mésenchyme pulmonaire au cours du développement de l'épithélium bronchique

Présentée par Amel NASRI

Le 20 Juin 2023

Sous la direction du Professeur John de VOS
et du Professeur Arnaud BOURDIN

Devant le jury composé de

Dr. Vasiliki KALATZIS, DR, Institut des Neurosciences, Montpellier – INSERM U1051	Présidente du jury
Pr. Jamila CHAKIR, PR, Institut de cardiologie et pneumologie, Université de Laval	Rapportrice
Pr. Charles PILETTE, PU-PH, Université catholique de Louvain	Rapporteur
Dr. Delphine GRAS, CR, Centre de Recherche CardioVasculaire et Nutrition, Aix-Marseille – U1263	Examinatrice
Dr. Saïd ASSOU, IR, Institut de Médecine Régénératrice et Biothérapie, Montpellier – INSERM U1183	Invité
Pr. John DE VOS, PU-PH, CHU de Montpellier – IRMB INSERM U1183	Directeur de thèse
Pr. Arnaud BOURDIN, PU-PH, CHU de Montpellier – PhyMedExp INSERM U1046	Co-directeur de thèse

UNIVERSITÉ DE MONTPELLIER

Résumé de la thèse

La BPCO est la troisième cause de mortalité dans le monde, causant plus de 3,2 millions de décès en 2017, pour une estimation de 4,4 millions en 2040. Cette augmentation du nombre de cas concerne autant les pays développés que ceux en voie de développement. En France le nombre d'hospitalisations de patients souffrant de BPCO, notamment en unité de soins intensifs, est en constante augmentation. Cela oblige donc les pouvoirs publics à augmenter les enveloppes budgétaires et à repenser les stratégies de prise en charge de cette pathologie.

La BPCO est généralement diagnostiquée tardivement à un stade où les lésions sont peu réversibles. En effet, les signes cliniques sont non spécifiques et apparaissent de façon progressive et insidieuse. Ces symptômes, souvent sous-estimés par les patients et les professionnels de santé, s'aggravent au cours du temps et finissent par nécessiter des hospitalisations. En effet, l'inflammation des voies aériennes et du tissu pulmonaire entrainent des perturbations cellulaires et des anomalies fonctionnelles, souvent irréversibles. La perte des forces de rétraction élastique est la conséquence de la dévastatrice synergie entre obstruction bronchiolaire et rupture des cloisons interalvéolaires. Les parois bronchiques s'épaississent, le muscle lisse s'hypertrophie et le mucus est hyper-sécrété, menant à une obstruction permanente des bronches. L'ensemble de ces changements induisent en aval une destruction progressive des cloisons alvéolaires pulmonaires (emphysème).

Cette dégradation progressive est ponctuée d'exacerbations cliniques comportant le cortège clinique toux, expectorations et dyspnées, souvent provoquées par des infections virales ou bactériennes.

Le tabagisme est la première cause de BPCO, auxquels s'ajoute l'exposition à des particules de pollution, notamment dans les grandes métropoles des pays en voie de développement mais également à la campagne dans les habitations mal ventilées et lieux d'une cuisine au feu de bois, ainsi que l'exposition à des poussières

minérales ou organiques, ou des substances chimiques, une prédisposition multigénique, et des infections respiratoires répétées au cours de l'enfance. L'ensemble de ces facteurs mettent en jeu divers mécanismes moléculaires et cellulaires qui peuvent varier d'un patient à un autre et, font de la BPCO une maladie multifactorielle. Cela aboutit à différents sous-types dont les spécificités et caractéristiques sont encore à identifier. De plus, une forte comorbidité pouvant comporter pathologies cardiaques, gastro-intestinales, cérébrales et musculaires, accentue l'hétérogénéité entre les patients. De récentes études définissent même la BPCO comme un syndrome recouvrant plusieurs pathologies distinctes avec l'ostéoporose et la dépression.

A l'heure actuelle, outre une prévention primaire, seule la prise en charge multidisciplinaire des patients permet d'améliorer leur qualité de vie. Cela comprend notamment un arrêt du tabac, un arrêt d'expositions aux substances toxiques qui favorisent la maladie et la reprise d'une activité physique. De plus, la prise de corticostéroïdes permet de réduire l'inflammation, celle de bronchodilatateurs de longue durée permet de dilater les voies respiratoires et dans les cas plus sévères, l'oxygénothérapie et la ventilation viennent suppléer la fonction respiratoire défaillante.

Cependant, ces traitements n'ont qu'une efficacité limitée dans le temps, et l'hétérogénéité de la BPCO complexifie la prise en charge des patients. De ce fait, le traitement de la BPCO demeure un grand défi car malgré des efforts considérables, aucun traitement curatif n'a pu être mis en place.

Récemment, l'hypothèse physiopathologique dans la genèse de la BPCO est progressivement passée du concept inflammatoire vers celui de l'altération de l'homéostasie épithéliale bronchique. En effet, le rôle central de l'épithélium bronchique dans l'orchestration des réponses aux stimuli extérieurs est mieux compris aujourd'hui. En outre, la sénescence cellulaire, le stress oxydant, une perte de la fonction mitochondriale, une régénération imparfaite ou une prolifération excessive des cellules basales et à mucus (ou hyperplasie), sont des processus reconnus comme étant à l'origine de la BPCO.

Cependant, les modèles d'études utilisés à ce jour présentent de nombreuses limitations et ne permettent pas de comprendre l'ensemble des mécanismes physiopathologiques de la BPCO. C'est notamment le cas, des modèles animaux tels que la souris, le rat ou le cochon d'inde, qui présentent certes des avantages considérables, mais aussi différents inconvénients tels que la variabilité inter-espèce, un arbre bronchique peu représentatif de celui de l'Homme et le manque de reproductibilité de la BPCO au niveau pulmonaire. Les lignées cellulaires immortalisées quant à elles ne permettent pas de générer un épithélium bronchique complet, et sont souvent cultivées de façon immergée.

L'amélioration considérable des techniques de cultures cellulaires *in vitro* permet néanmoins d'isoler et de cultiver des cellules épithéliales bronchiques prélevées sur des patients. Ces cellules primaires offrent une meilleure représentation de la pathologie et de ses différents sous-types. Elles peuvent aussi être cultivées en interface air-liquide (ALI), dont le pôle apical est exposé à l'air et le pôle basal au contact du milieu de culture. Cependant, les cellules sont collectées de façon invasive par bronchoscopie. De plus, ces biopsies ne permettent que de collecter un faible nombre de cellules, qui ne peuvent pas être maintenues longtemps en culture.

L'utilisation de cellules souches humaines pluripotentes induites (iPSCs) permet de pallier ces inconvénients. En effet, les cellules souches ont la capacité de s'auto-renouveler et de se différencier en tout type cellulaire. Les progrès de génération et de maintenance des iPSCs permettent aussi de les différencier en épithélium bronchique fonctionnel *in vitro* et de façon non invasive, en reproduisant les étapes du développement pulmonaire. Ces cellules, dérivées de patients sains ou souffrants de BPCO, gardent bien entendu le fond génétique du patient. De ce fait, leur utilisation est un moyen de pallier le manque de connaissance du développement physiopathologique de la BPCO, en reproduisant *in vitro* certains phénomènes qui se développent *in vivo*.

Ainsi, l'utilisation de ce modèle, par la production en théorie illimitée d'épithélium bronchique de différents fond génétiques et exposés à la pollution ou au tabac, pourrait permettre l'identification de biomarqueurs de la pathologie. Ces

biomarqueurs permettraient d'établir un diagnostic précoce de la BPCO et d'utiliser certains biomarqueurs comme marqueurs prédictifs, garantissant donc une meilleure prise en charge du patient. L'identification *in vitro* puis *in vivo*, et la validation clinique ultérieure de ces biomarqueurs permettront de proposer un traitement adapté au patient et de prédire la réponse aux traitements proposés.

Les travaux de l'équipe ont permis la mise en place d'un protocole robuste pour générer des lignées iPSCs à partir de patients sains ou souffrants de BPCO (groupe avec une forme sévère de BPCO), et leur différenciation avec une bonne reproductibilité en épithélium bronchiques fonctionnels en interface air/liquide, appelés iALI.

Mes travaux de thèse ont permis d'une part, de mettre en place un protocole d'exposition au tabac et à la pollution sur des iALI générés à partir d'iPSCs de donneurs sains et souffrant de BPCO. Ces expositions reproduisent *in vitro* certains phénomènes physiopathologiques qui se développent *in vivo*, tels que l'hypersécrétion de mucus et l'hyperplasie. Les effets de l'exposition à la pollution de type PM2.5 (diamètre aérodynamique de 2.5 µm), particules fines dont l'impact sur l'arbre respiratoire est le plus important, sur l'iALI ont été analysés par scRNA-seq. Cela a permis de mettre en évidence la réponse des cellules épithéliales et mésenchymateuses à cette exposition par l'induction et/ou la répression de gènes exprimés spécifiquement dans des groupes de cellules. De plus, ces travaux qui font l'objet d'un article prêt pour soumission, ont permis de mettre en évidence une population épithéliale transitoire induite à la suite de l'exposition à la pollution.

D'autre part, grâce à ces données de transcriptome et le modèle iALI, j'ai également étudié l'interaction entre le compartiment épithélial et le compartiment mésenchymateux sous-jacent, au cours du développement de l'iALI et à sa phase mature. Ces travaux, récapitulés dans un second papier en cours de rédaction, mettent en évidence 17 interactions impliquées entre autres dans la migration cellulaire, la croissance et la survie cellulaires de l'iALI. De plus, nous avons montré que la transition épithélio-mésenchymateuse est également impliquée dans le développement des iALI, et que les cellules mésenchymateuses peuvent se transdifférencier en cellules épithéliales. Cela souligne donc l'interconnexion entre

l'épithélium et le mésenchyme et met en évidence le rôle, encore peu connu, du contingent mésenchymateux.

Ainsi, les résultats de ma thèse ouvrent de nouvelles perspectives quant à l'utilisation des iPSCs comme modèle d'interaction entre l'épithélium bronchique et son environnement immédiat, y compris dans un contexte d'exposition aux particules de pollution

Abstract

Chronic lung diseases such as chronic obstructive pulmonary disease (COPD) are a major public health problem. Smoking is the main cause of COPD, but air pollution is also a factor, especially fine particulate matter (PM2.5). Several molecular and cellular mechanisms are involved in the development of COPD, leading to different subtypes whose specificities and characteristics remain to be determined.

Despite considerable efforts, there is no effective curative treatment to date. The study models used to date have numerous limitations and do not provide a comprehensive understanding of the pathophysiological mechanisms of COPD.

The use of human induced pluripotent stem cells (iPSCs) allows overcoming these drawbacks, thanks to their stemness, their abilities to self-renew and differentiate into any cell type. These cells, derived from healthy or COPD patients, can be differentiated *in vitro* and non-invasively into functional bronchial epithelium (called iALI) and reproduce *in vitro* certain physiological phenomenon that develop *in vivo*.

In this work, it was possible to establish a protocol for exposures to tobacco and pollution in iALI. In addition, the effects of PM2.5 exposure on iALI were analysed using scRNA-seq and compiled in a first article. Finally, this work is accompanied by the study of the interaction between the epithelial compartment and the adjacent mesenchymal compartment during the development of iALI. Several pathways have been highlighted between these both compartments in iALI and may be further explored. A mesenchymal to epithelial transition was described and this work was resume on a second article. Taken together, this thesis data will help to understand and ameliorate *in vitro* pathophysiological model of COPD.

« La science n'a pas de patrie, parce que le savoir est le patrimoine de l'humanité, le flambeau qui éclaire le monde. »

Louis Pasteur

Remerciements

Je tiens à exprimer ma profonde gratitude aux membres du jury qui ont accepté de juger mes travaux de thèse. Je suis honorée de soutenir ma thèse devant un tel collège de scientifique.

Dr. Vasiliki Kalatzis, je vous suis reconnaissante d'avoir accepté de présider ce jury et d'examiner mon travail. Merci de partager votre expertise dans le domaine des cellules souches pluripotentes induites.

Merci aux rapporteurs, le Pr. Jamila Chakir et le Pr. Charles Pilette, pour votre temps et votre engagement envers l'évaluation de ma thèse. Je suis persuadée que votre expérience dans le domaine pulmonaire, ainsi que vos suggestions, seront particulièrement utiles à l'amélioration de mon travail.

Jamila, merci encore d'avoir accepté d'être rapportrice, ta contribution précieuse a permis de maintenir ma date de soutenance.

Delphine, merci de donner de ton temps pour examiner ces travaux et partager tes connaissances.

Said, merci d'avoir toujours répondu présent. Je te suis reconnaissante pour ton aide et tes idées qui ont permis d'élaborer ce projet.

Je suis également reconnaissante envers mes directeurs de thèse, Pr. John De Vos et Pr. Arnaud Bourdin, qui m'ont permis de réaliser ce travail.

John, je ne vous remercierais jamais assez de m'avoir donné la chance d'être sous votre direction. Vos idées, votre engagement et votre soutien indéfectible ont été essentiels à ma réussite.

Arnaud, merci infiniment pour vos encouragements et vos précieux conseils. Vous avez été une grande source d'inspiration tout au long de ce projet.

Je remercie également mes collègues pour leur amitié et leur contribution, ainsi que toutes les personnes, sans oublier mes amis, qui ont participé à cette aventure.

Enfin, je remercie les membres de ma famille, qui m'ont soutenu à chaque étape de ma vie, notamment les plus difficiles. Je vous dédis ce travail ainsi que ces vers :

Dans ma famille, il y a des histoires,
Des souvenirs de nos ancêtres et de leurs voyages,
Des légendes de héros et de batailles,
Et des rêves d'un avenir plus beau.

Dans ma famille, il y a de la musique,
Des voix qui s'élèvent dans la nuit,
Des chants qui célèbrent l'amour et la vie,
Et des mélodies qui résonnent dans nos cœurs.

Dans ma famille, il y a de l'amour,
Un amour qui nous lie les uns aux autres,
Un amour qui nous aide à traverser les épreuves,
Et un amour qui nous accompagne tout au long de notre vie.

Dans ma famille, il y a de la fierté,
Une fierté de nos racines et de notre culture,
Une fierté de nos traditions et de nos valeurs,
Et une fierté de notre héritage commun.

Dans ma famille, il y a de l'espoir,
Un espoir pour un avenir meilleur,
Un espoir pour la paix et la justice,
Et un espoir pour un monde où règne l'amour et la fraternité.

Dans ma famille, il y a tout ce dont j'ai besoin,
L'amour, la musique, la fierté et l'espoir,
Et je suis reconnaissant chaque jour,
De faire partie de cette famille unique et belle.

Tahar Djaout, Famille

Table of contents

Résumé de la thèse 1

Abstract 6

Remerciements 8

List of Figures 14

List of Tables 15

List of abbreviations 16

GENERAL INTRODUCTION 17

Chapter I | The respiratory tract 18

1) Embryonic lung development 18

a) Gastrulation 18

b) Endoderm lung specialization 21

c) Known embryonic roots of lung diseases 24

2) Histology of the lung 25

a) Proximal airways 26

b) Distal airways 34

c) Mesenchymal compartment 34

3) Single cell RNA sequencing 53

a) Definition 53

b) Workflow 53

c) Challenges and limitations 57

Chapter II | Chronic respiratory diseases 58

1) COPD 58

a) Definition and prevalence 58

b) Physiopathology of COPD 60

c) Models of COPD 64

2) Air pollution 67

a) Definition 67

b) Classification 68

c) Health impact 70

3) Tobacco smoking 72

a) Definition 72

b) Health effects 72

c) Electronic cigarette 73

Chapter III | Induced pluripotent stem cells to study lung development and diseases 75

1) History and description 75

a) Stem cell properties 75

b) Generation of iPSCs 77

c) Challenges and limitations 77

2) Applications 79

a) 2D models 79
b) Organoids 80
c) Other models 81
3) Mimicking lung development 82
a) Initial steps of differentiation 82
b) Lung specialization 83
c) Exposure models 87
AIMS OF THE THESIS 89
RESULTS 91
Article 1 92
Article 2 117
GENERAL DISCUSSION 145
1) Developing an iALI exposure protocol 146
a) Fine particles exposure 146
b) Tobacco exposure 148
c) Limits of iALI model 148
2) Effect of pollution exposure 151
a) Cell lines choice 151
b) Single cell experiment 151
c) Perspectives 153
3) Epithelial and mesenchymal crosstalk 153

a) Functionality of the interactions 153

b) Extracellular matrix 154

c) Mesenchymal to epithelial transition 154

CONCLUSION 156

REFERENCES 157

ANNEXES 188

List of Figures

Figure 1 || **Differentiation of the three embryonic germ layers** 20

Figure 2 || **Timeline of embryonic lung development** 24

Figure 3 || **Structure and cellular composition of the human lungs** 26

Figure 4 || **Overview of the epithelium of the proximal airway** 33

Figure 5 || **General workflow of scRNA-seq** 54

Figure 6 || **Droplet-based microfluidic system** 55

Figure 7 || **Prevalence of COPD worldwide** 59

Figure 8 || **Representation of COPD airways** 62

Figure 9 || **The exposome concept** 68

Figure 10 || **Death attributable to PM2.5 in 2016** 71

Figure 11 || **Effects of smoking and vaping** 74

Figure 12|| **Hierarchy of stem cells** 76

Figure 13 || **Clinical trials with human ESC and human iPSC** 78

Figure 14 || **Representation of in vitro iPSC derived airway** 84

Figure 15 || **Overview of protocols used in lung generation** 85

Figure 16 || **Exposure method in vitro culture** 88

Figure 17 || **Picture of iALI** 147

Figure 18 || **Immunofluorescence of iALI with OCT** 150

Figure 19|| **Epithelial and mesenchymal continuum states** 155

List of Tables

Table 1 || **Summary of animal models of COPD** 65

Table 2 || **Advantages and disadvantages of in vitro lung models** 82

Table 3 || **Specific markers of airway cells** 86

List of abbreviations

ALI *Air-Liquid Interface*

AT1 *Type I Alveolar Cells*

AT2 *Type II Alveolar Cells*

CCSP *Club Cell Secretory Protein*

COPD *Chronic Obstructive Pulmonary Disease*

CRISPR *Clustered Regularly Interspaced Short Palindromic Repeats*

CSE *Cigarette Smoke Extract*

DAPT *(2S)-N-[(3,5-Difluorophenyl) acetyl]-L-alanyl-2-phenyl]glycine1,1-dimethylethyl ester*

EMT *Epithelial to Mesenchymal Transition*

ESC *Embryonic Stem Cells*

FACS *Fluorescence-Activated Cell Sorting*

FGF *Fibroblast Growth Factor*

iALI *ALI from iPSCs*

IL *Interleukin*

iPSCs *Induced Pluripotent Stem Cells*

MET *Mesenchymal to Epithelial Transition*

MMP *Metalloproteinase*

PM *Particulate Matters*

PNEC *Pulmonary Neuroendocrine Cells*

QC *Quality control*

scRNA-seq *Single-cell RNA Sequencing*

tSNE t-Stochastic Neighbourhood Embedding

UMAP *Uniform Manifold Approximation and Projection*

UMI *Unique Molecular Identifier*

VAFE *Ventralized-Anterior Foregut Endoderm*

WHO *World Health Organization*

WNT *Wingless/Integrated*

GENERAL INTRODUCTION

Chapter I | The respiratory tract 18

1) Embryonic lung development 18

2) Histology of lung 25

3) Single cell RNA sequencing 53

Chapter II | Chronic respiratory diseases 58

1) COPD 58

2) Air pollution 67

3) Tobacco smoking 72

Chapter III | Induced pluripotent stem cells 75

1) Definition and historic 75

2) Applications 79

3) Mimic of lung development 82

Chapter I | The respiratory tract

The respiratory system is located at the interface between the body and the environment. This chapter focuses on the development of the lung from embryonic development to adulthood and the utility of single cell RNA sequencing in cell type discovery.

1) Embryonic lung development

To understand the functionality and molecular process of the respiratory tract development, we will focus on embryonic lung development.

a) Gastrulation

Gastrulation was discovered by Alexander Onufrievich Kovalevsky (1840-1901), a Russian Professor of Embryology (Lunn et al., 1999). It begins at the beginning of the third week of development and results in the trilaminar embryo, consisting of three germ layers: ectoderm, mesoderm and endoderm.

Around day 14, epiblast cells proliferate and migrate to a primitive line in the caudal half of the embryo, a region that will give rise to the primitive streak. At the cephalic end, the cells surrounding the primitive streak form the primitive node, which generates the notochord. Gradually, epiblast cells replace the hypoblast by an endoderm layer. Further epiblast cells invaginate and will form the mesoderm between the epiblast and endoderm layers.

The mesoderm can be divided three regions, ranging from the paraxial region to the lateral region: paraxial mesoderm, intermediate mesoderm, lateral plate mesoderm. Furthermore, there are mesenchymal cells that surround the embryo (extraembryonic mesoderm). Finally, the epiblast transitions into the ectoderm.

Each germ layer will contribute mainly to the development of an organ. As shown in Figure 1, the epidermis, and nervous system are formed by the ectoderm (Elshazzly et al., 2022), while the mesoderm gives rise to the dermis, bones, cartilage, most of the cardiovascular system, hematopoietic and lymphatic systems, connective tissue, and reproductive and urinary systems (Gao et al., 2020).

We will now focus on the development of the endoderm and more specifically on our topic, the development of the lung.

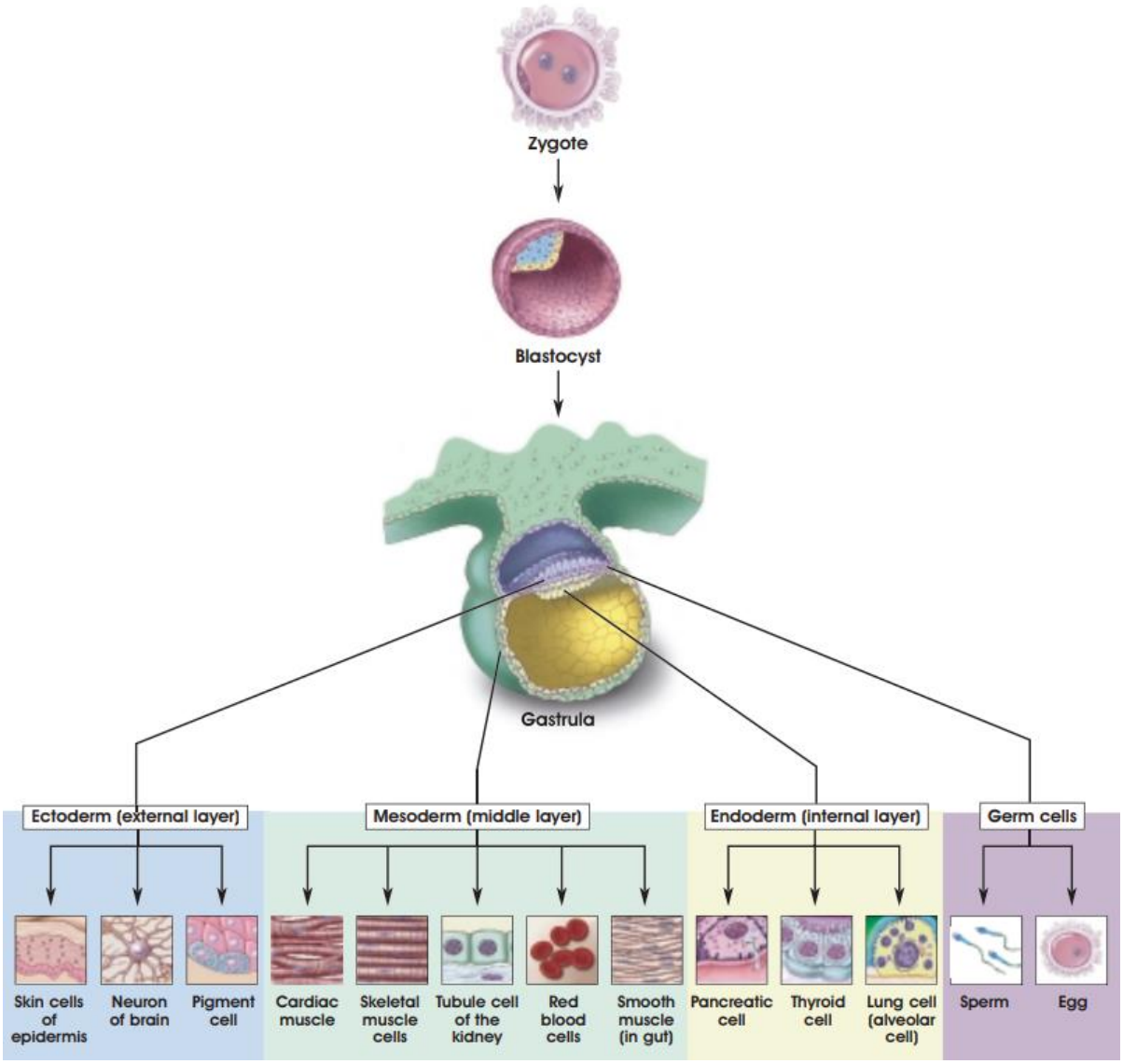

Figure 1 || ***Differentiation of the three embryonic germ layers***

Various tissues and organs arise from the 3 germ layers. These include the epidermis of the skin and its derivatives, and the nervous system for ectoderm. The mesoderm gives rise to the skeletal system, the reproductive system (except the germ cells), the cardiovascular system, the hematopoiesis and the muscular system. And the endoderm forms the epithelial lining of the respiratory tract, digestive tract , liver, pancreas, thymus, and thyroid gland.

From Winslow Terese. « Scientific Progress and Future Research Directions », 2001.

b) Endoderm lung specialization

The endoderm forms the gastrointestinal tract, including the pancreas and liver, and the respiratory system (Grapin-Botton, 2008). The respiratory system is originating from the foregut and includes the pharynx, trachea, and the lungs (Zorn and Wells, 2009). The respiratory tract can be divided into the upper respiratory tract (nose, nasal cavity, pharynx, and larynx) and the lower respiratory tract (trachea, bronchi, bronchioles and alveoli) (Ball et al., 2022).

The development of the lungs extends from the fetal period, when they are involved in the production of amniotic fluid, to birth when the lungs immediately begin their critical function, the exchange of gases between air and blood. The fetal period is divided into 5 stages (Figure 2). At each stage, a precise development is critical to avoid negative consequences for respiratory function after birth, as shown below.

Embryonic stage

The embryonic stage extends between the 3rd and 6th week of organogenesis, and starts with the appearance of a lung bud on the ventral primitive foregut, known as Ventralized-Anterior Foregut Endoderm (VAFE) (Cardoso and Lü, 2006). This bud divides successively in an asymmetric manner to form 3 bronchi on the right and 2 bronchi on the left. Gradually, each bronchial bud extends and branches to form the 5 lobes of the lungs.

Many studies have shown that the adjacent mesenchyme, which is formed from the splanchnopleuric mesoderm a part of the lateral mesoderm, is critical for lung growth and the branching process. (Kimura and Deutsch, 2007; Nasri et al., 2021; Rehman and Bacha, 2022). For example in mice, Fibroblast Growth Factor 10 (FGF) released by lung mesenchymal cells has been shown to regulate budding growth, and double mutant mice are lethal by lack of lung development (Bellusci et al., 1997; Min et al., 1998; Sekine et al., 1999).

Pseudoglandular stage

The pseudoglandular stage begins around week 7 of development. At this stage, the lung shape is more of a glandular-like structure that expands and branches extensively to form preacinar airways (Mullassery and Smith, 2015).

The epithelium is initially composed of progenitor cells that differentiate into ciliated cells, secretory cells, and all the different bronchial cells under various signals, including WNT and Notch signalling (Carsin et al., 2016).

At the end of the 17th week, the lung tree until the terminal bronchioles, is formed. This coincides with a high level of apoptosis and metalloproteinase 9 (MMP) expression in the mesenchymal compartment which develops capillary, cartilage and smooth muscle cells (Kheradmand et al., 2002; Kraljevic et al., 2015; Wongtrakool and Roman, 2008).

Canalicular stage

During the canalicular stage (16th to 26th week), the terminal bronchioles give rise to the acinus. Each acinus contains 3 to 4 bronchioles and are contoured by capillaries from parenchyma, which form the future air-blood barrier. (Schittny, 2017).

In addition, the type II pneumocytes (known as type II alveolar cells (AT2)) appears in the distal epithelium, forming the primitive alveolus. They contain lamellar bodies that store pulmonary surfactant (surface active agent).

The pulmonary surfactant is composed of several proteins such as surfactant protein A-C and various lipids such as glycerophospholipids, neutral lipids and cholesterol (Griese, 1999). Type II pneumocytes then differentiate into squamous type I pneumocytes (also known as type I alveolar cells (AT1)).

Saccular stage

The saccular stage begins around week 25 and continues until birth. Surfactant is secreted over the alveolar surface to reduce surface tension and prevent lung collapse during respiration. (Knudsen and Ochs, 2018). The primitive alveolar sacs expand considerably to form extensive air spaces called saccules (Rehman and Bacha, 2022).

Interstitial fibroblasts secrete extracellular matrix compounds such as collagen and elastin in the intercanal and intersaccular spaces, which may play a role in adjacent epithelial differentiation. (Benjamin et al., 2016; Warburton et al., 2010).

Alveolar stage

The final stage is the alveolar stage, which begins around 36th week and extends into infancy. The mature alveoli develops centripetally and increases in number by a septation process until the formation of the mature lung. The adjacent parenchyma between the alveoli forms a bilayer of capillaries enriched with elastic fibres to ensure efficient gas exchange (Davis and Mychaliska, 2013).

At this stage, surfactant is produced in sufficient quantities which is not the case for preterm infants who may present lung dysfunction resulting in bronchopulmonary dysplasia (Ballard et al., 2019).

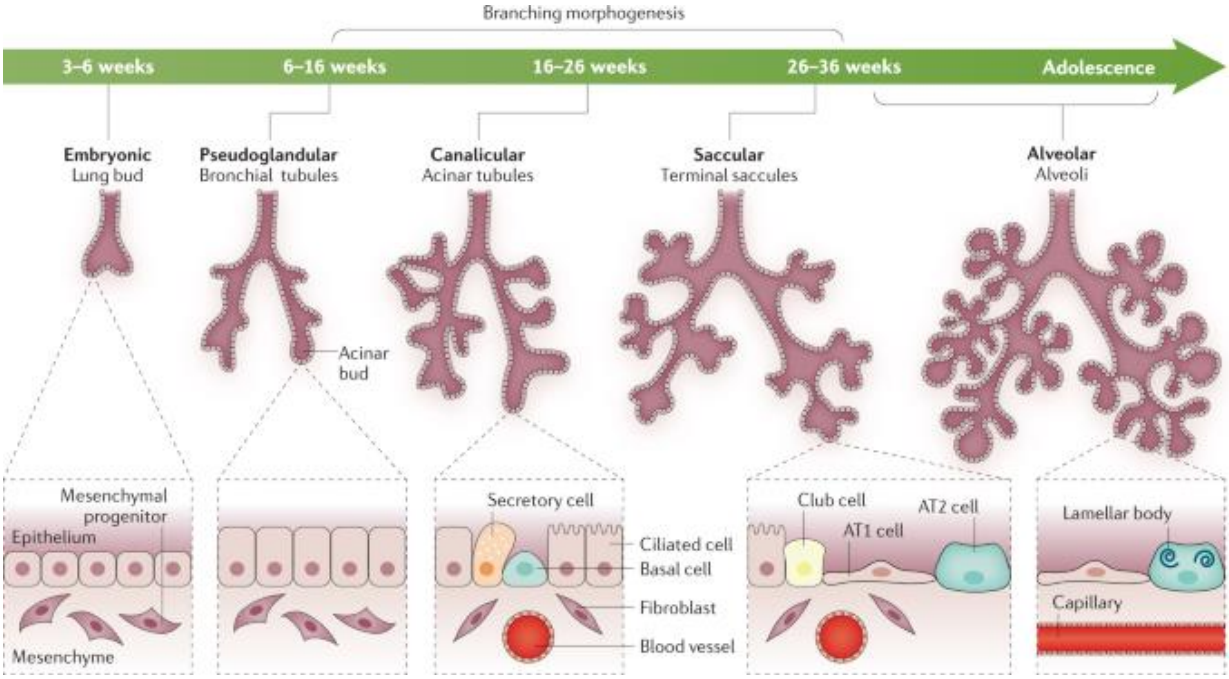

Figure 2 || ***Timeline of embryonic lung development***

Schematic representation of the 5 stages of embryonic lung development in humans, with specific phenotype associated with epithelium and mesenchymal compartment.

From Thébaud Bernard, et al., Nature Reviews Disease Primers, 2019

c) Known embryonic roots of lung diseases

Several abnormalities during lung development can affect final lung function and lead to chronic lung disease (Pechriggl et al., 2022).

As mentioned earlier, bronchopulmonary dysplasia, that manifests as a respiratory distress syndrome after premature birth, is characterized by malformations of the bronchi and alveoli. It affects 40% to 50% of extremely premature infants (Deschamps et al., 2021). Lack of alveolarization may be the cause, as well as pulmonary surfactant deficiency and interstitial disorders (Pierro et al., 2022; Thébaud et al., 2019).

Nevertheless, there are also congenital malformations that occur early in lung development. These include congenital lobar emphysema, bronchogenic cysts,

congenital cystic adenomatoid malformation and bronchopulmonary sequestration (Hall and Stanton, 2017). There is also congenital tracheobronchial branching, which is caused by branching defects but is asymptomatic in most cases (Chassagnon et al., 2016). Congenital tracheobronchial stenosis is also a rare condition that requires surgical correction because the separation between the trachea and esophagus is incomplete (Hewitt et al., 2016). This type of anomaly may be associated with other defects such as cardiac defects (Cardoso and Lü, 2006). Given the widespread use of pre-natal echography, with improved sonographic resolution, lung congenital malformations are now more frequently detected before birth and cared for early during life.

To understand the mechanisms involved in pathological development, it is important to understand what happens at the cellular level.

2) Histology of the lung

The lungs are composed of several distinct cell types, and the cell composition varies depending on the location of the tissues in the lung. The airway epithelium forms a barrier against external influences (pathogens, dusts, chemical compounds) and is supported by the basement membrane, which rests on a mesenchyme (Brune et al., 2015).

We can distinguish the proximal airways (bronchi and bronchioles), the distal airways (alveoli) and the mesenchymal compartment (Figure 3).

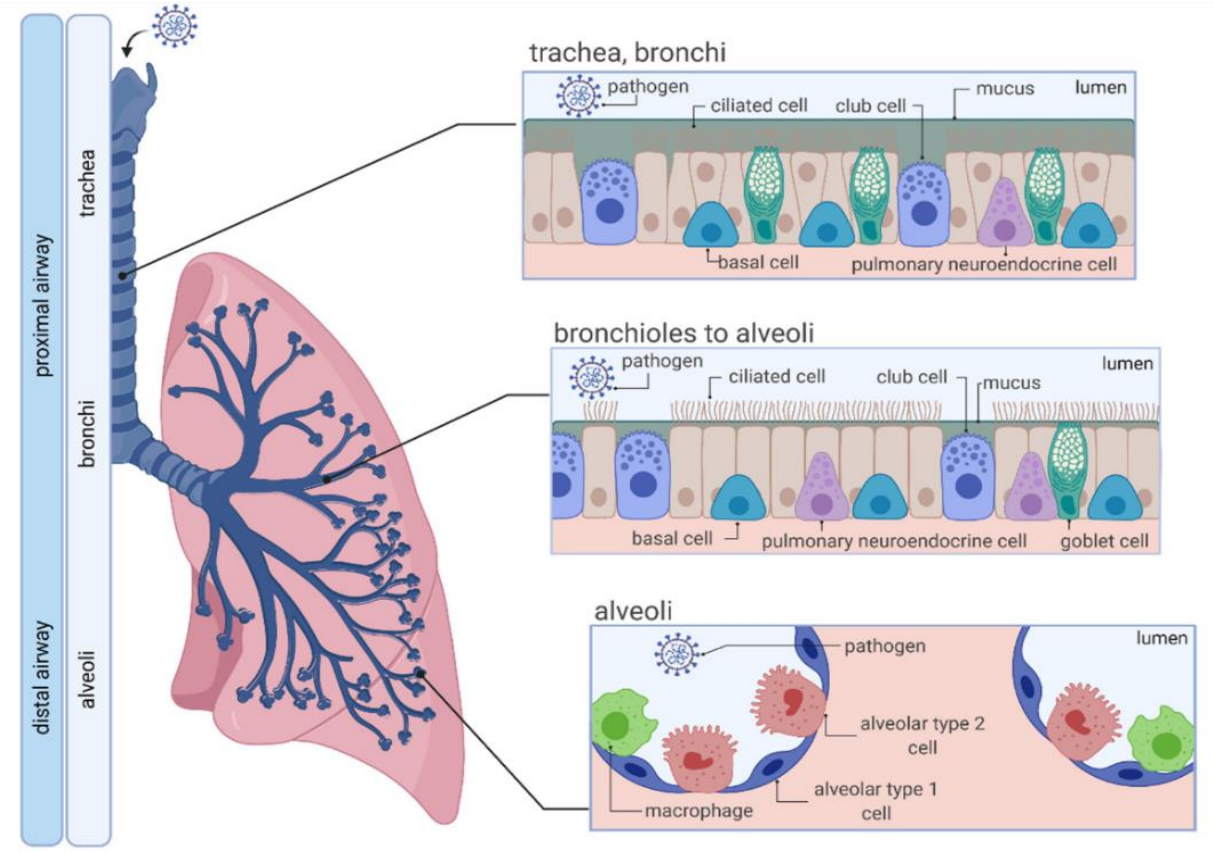

Figure 3 || ***Structure and cellular composition of the human lungs***

From Heinen Natalie, et al., Viruses, 2021

a) Proximal airways

From trachea until bronchioles, the epithelium evolves from a pseudostratified epithelium to a simple cuboidal epithelium (Kia'i and Bajaj, 2022). This accompanies the narrowing of the respiratory tract, from a diameter of around 11 mm for the bronchi to around 1 mm for the bronchioles (Ball et al., 2022; Hampton et al., 2000). This implies a corresponding change in cell composition along the airway as well as the expression of specific markers, as discussed in a later chapter.

Basal cells

Basal cells are small, cuboidal, not in contact with the bronchial lumen, and strongly attached to the basal lamina (Kia'i and Bajaj, 2022). They account for approximately 30% to 10% of the cells in the most proximal and distal airways, respectively (Boers et al., 1998; Crystal, 2014).

Because of their ability to self-renew and differentiate into tracheal bronchial cells, basal cells are referred to as "bronchial multipotent stem cells" (Evans et al., 2001; Hong et al., 2004; Lee et al., 2014; Rock et al., 2009). They play an important role in maintaining homeostasis and may be a potential source of cell therapies to treat diseases such as chronic obstructive pulmonary disease (COPD) (Ghosh et al., 2017; Wijk et al., 2021).

It has been shown that there are several categories of basal cells (Donnelly et al., 1982). For example, "hillocks" are a specific niche for highly proliferating basal cells (Montoro et al., 2018). There are also quiescent basal cells and transitional states such as parabasal or suprabasal cells, depending on their specific protein expression (Ruysseveldt et al., 2021). The Notch signalling pathway may play an important role in this cell fate (Mori et al., 2015; Rock et al., 2011). Nevertheless, their role and function are still controversial and should be elucidated, which is possible by improving cell identification techniques (Barbry et al., 2020; Watson et al., 2015).

Ciliated cells

The ciliated cells are columnar elongated cells that are in direct contact with the basement membrane and the lumen of the bronchus, and are fully differentiated (Mercer et al., 2012; Rawlins and Hogan, 2008). They account for 70% of the epithelium at this level (Yaghi and Dolovich, 2016). As their name implies, they have approximately 300 cilia (4 to 7 µm long) at the apical side that move the mucus and inhaled particles away from the gas exchange area (Tilley et al., 2015). This mucociliary clearance is extremely important for maintaining lung homeostasis,

which can be disrupted in many diseases, including Chronic Obstructive Pulmonary Disease (COPD) (Bustamante-Marin and Ostrowski, 2017).

Inhibition of Notch signaling by a γ-secretase inhibitor called DAPT ((2S)-N-[(3,5-Difluorophenyl)acetyl]-L-alanyl-2-phenyl]glycine1,1-dimethylethyl ester), has been shown to promote differentiation of airway epithelial cells into a ciliated fate *in vitro* (Konishi et al., 2015; Lafkas et al., 2015). In contrast, the activation of Notch signaling pathway favors the differentiation of epithelial cells into secretory cells by suppressing the cilia program (Tsao et al., 2009). Recently, a transient state of secretory cells generating ciliated cells (so-called “deuterosomal cells”) has also been demonstrated (He et al., 2022; Ruiz García et al., 2019; Zaragosi et al., 2020).

Secretory cells

Secretory cells can produce and secrete various proteins on their apical side. We distinguish goblet cells, which are found more in the proximal area, from club cells, which are found more in the distal part of the bronchioles (Boers et al., 1999).

Goblet cells

Goblet cells (also called mucous cells or caliciform cells) represent about 25% of bronchial epithelial cells (Rogers, 2003). They produce and stocks mucous vesicles that can be secreted into the bronchial lumen.

Mucus plays a critical role in mucociliary clearance as it is composed of high molecular weight mucin glycoproteins (Bansil and Turner, 2018, 2006). It leads to the encapsulation of pathogens and dusts, is propelled upward via the ciliary beat and is cleared by deglutition or expectoration. High mucus secretion and goblet cell hyperplasia are found in many patients with chronic lung diseases such as asthma and COPD (Aikawa et al., 1992; Vestbo, 2002; Yang et al., 2017).

Goblet cells are generated in the presence of Notch activity by activation of the transcription factor SPDEF (Sam-pointed domain Ets-like factor) and can

differentiate into ciliated cells, as mentioned previously (Kiyokawa and Morimoto, 2020; Whitsett, 2018).

Club cells

Club cells are another category of secretory cells that are non-ciliated with a dome-shaped apical surface (Rousseaux et al., 2018). They are highly expressed in distal bronchioles (20% of cells), whereas they are barely expressed in proximal bronchioles, in contrast to mice, where they are fully expressed in the conducting airways (Boers et al., 1999; Rawlins et al., 2009).

They secrete Club Cell Secretory Protein (CCSP), a secretoglobulin also called SCGB1A1/CC10, as well as SCGB3A2, and surfactant proteins A, B and D (Barnes, 2015). CSSP has pleiotropic regulatory effects, but is overall an important anti-inflammatory and immunosuppressive with an important role in maintaining lung homeostasis, and the dysregulation of its expression has been found in many diseases, including COPD (Davis and Wypych, 2021; Gamez et al., 2015; Knabe et al., 2019; Laucho-Contreras et al., 2015; Lomas et al., 2008; Martinu et al., 2022).

Club cells express several cytochrome P450 (CYP) enzymes that play an important role in detoxifying inhaled xenobiotics (Barnes, 2015). Of note, the CYP2F isoforms metabolise naphthalene into toxic compounds. This induced cytotoxicity has been exploited to specifically ablate club cells in the mouse respiratory tract, demonstrating their role in epithelial regeneration due to their ability to self-renew, dedifferentiate into basal cells and give rise to ciliated and goblet cells (Montoro et al., 2018; Puchelle et al., 2006; Rawlins et al., 2009; Tata et al., 2013). However, naphthalene toxicity differs greatly between humans and mice. In mice, CYP2F2 expression in lung tissue results in a high cytotoxicity of naphthalene in club cells, whereas the CYP2F1 isozyme expressed in humans has a lower capacity to metabolize polycyclic aromatic hydrocarbons and a lower cytotoxicity for bronchial epithelium (Cruzan et al., 2009).

Overall, club cells are active in xenobiotic metabolism, immune system regulation, and progenitor cell activity.

Neuroendocrine cells

Pulmonary neuroendocrine cells (PNEC) are considered as a rare cell type, accounting for less than 1% of airway cells in adults (Boers et al., 1996). They also derived from the endoderm and are located near ciliated and secretory cells (Rock and Hogan, 2011). They have a pyramidal shape and can occur in isolation or in clusters called neuroendocrine bodies (Kuo and Krasnow, 2015).

PNECs sense airways and respond to stimuli by secreting neuropeptides able to simulate immune responses (Branchfield et al., 2016; Xu et al., 2020). These neuropeptides include neuropeptide Y, bombesin, and serotonin, which act on neighbouring fibroblasts, the nervous system, and the immune system to influence bronchoconstriction, vasodilation, mast cell recruitment, and cytokine secretion (Belvisi et al., 1991; Davis and Wypych, 2021; Subramaniam et al., 2003; J. Xu et al., 2022).

In this context, PNEC hyperplasia has been reported to have various pathological effects in asthma and COPD (Atanasova and Reznikov, 2018; Noguchi et al., 2020). It has also been reported that the use of DAPT increases PNEC (Konishi et al., 2015; Tsao et al., 2009).

Tuft cells and ionocytes

Tuft cells

Tuft cells (or brushed cells) are also a rare cell type, that has been reported in lung, gastrointestinal tract, thymus, auditory tube and others organs (Bornstein et al., 2018; Gerbe et al., 2016; Höfer et al., 1996; Krasteva et al., 2012). They have microvilli at their apical side and can secrete proteins such as acetylcholine and Interleukins-25 (IL-25) (C. Schneider et al., 2019). They act as a chemosensor and have an important immunomodulatory function in the airways, making them a potential target in cancer therapy (Goldfarbmuren et al., 2020; Koh et al., 2023; Li et al., 2022).

Ionocytes

Ionocytes are another rare cell type recently discovered thanks to single-cell RNA sequencing (scRNA-seq) (Montoro et al., 2018; Plasschaert et al., 2018). They are also expressed at less than 1% in the airways and are, like tuft cells, derived from basal cells (Davis and Wypych, 2021; Deprez et al., 2020). Ionocytes highly express the Cystic Fibrosis Transmembrane Conductance Regulator (CFTR), an ABC transporter-class ion channel protein that conducts chloride and that is defective in cystic fibrosis (Paranjapye et al., 2022; Scudieri et al., 2020).

Endothelial cells

The capillary endothelial cells account for a total of 30% of lung cells and are derived from the lateral mesoderm (Crapo et al., 1982; Stone and Stainier, 2019). They play a critical role in supplying nutrients and metabolites and ensure the blood oxygenation through the systemic bronchial circulation and pulmonary circulation system (Huertas et al., 2018). The two pulmonary arteries subdivide into pulmonary arterioles and then into capillaries and microvascular endothelial cells that interact closely with AT1 cells (Niethamer et al., 2020; Stevens et al., 2008). The oxygenated blood is then collected by the pulmonary veins and returned to the left atrium of the heart for distribution to the entire body (Suresh and Shimoda, 2016).

Immune cells

Immune cells play an important role in lung defense and protection, and include circulating, egressed and lung-resident cells (Travaglini et al., 2020). Among lung-resident cells, alveolar macrophages are the most abundant innate immune cells in the lung (Ardain et al., 2020). They coexist with interstitial macrophages and monocyte-derived macrophages in the lung and phagocyte foreign particles, bacteria, and cellular debris (Aegerter et al., 2022). Dendritic cells are also lung resident cells of the innate immune system known as sentinel cells because they present peptide antigens to specific T lymphocytes in the lung lymph nodes, which

act in concert with B lymphocytes as an adaptive immune response (Kopf et al., 2015). Overall, recent efforts to map all lung cell types using scRNAseq identified at least 25 different immune cell types, including, in addition to the monocyte derived cells listed above, different lymphocytes populations (CD4+ and CD8+ memory/effector T lymphocytes, CD4+ and CD8+ naive T lymphocytes, and NK lymphocytes), as well as neutrophils. The interplay between these immune cells and the lung epithelium are critical to the defense against infection, but also in the onset or exacerbation of chronic lung diseases such as asthma or COPD.

A

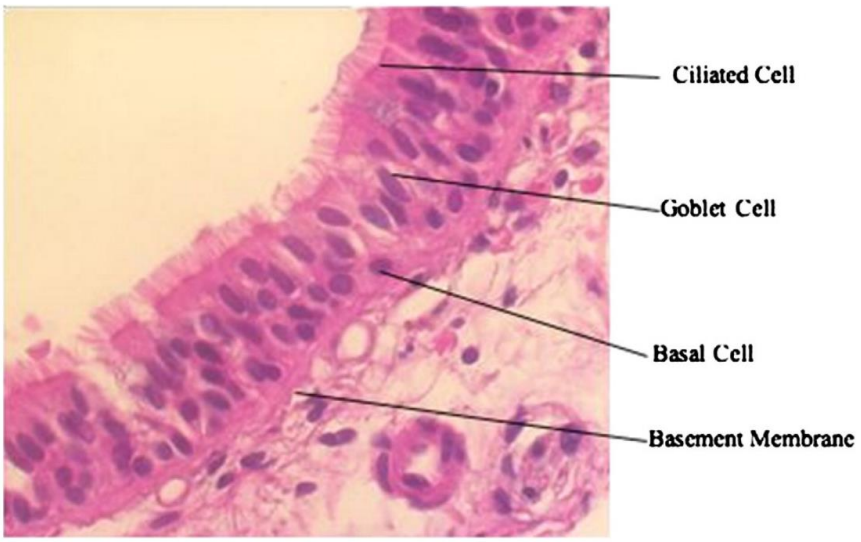

B

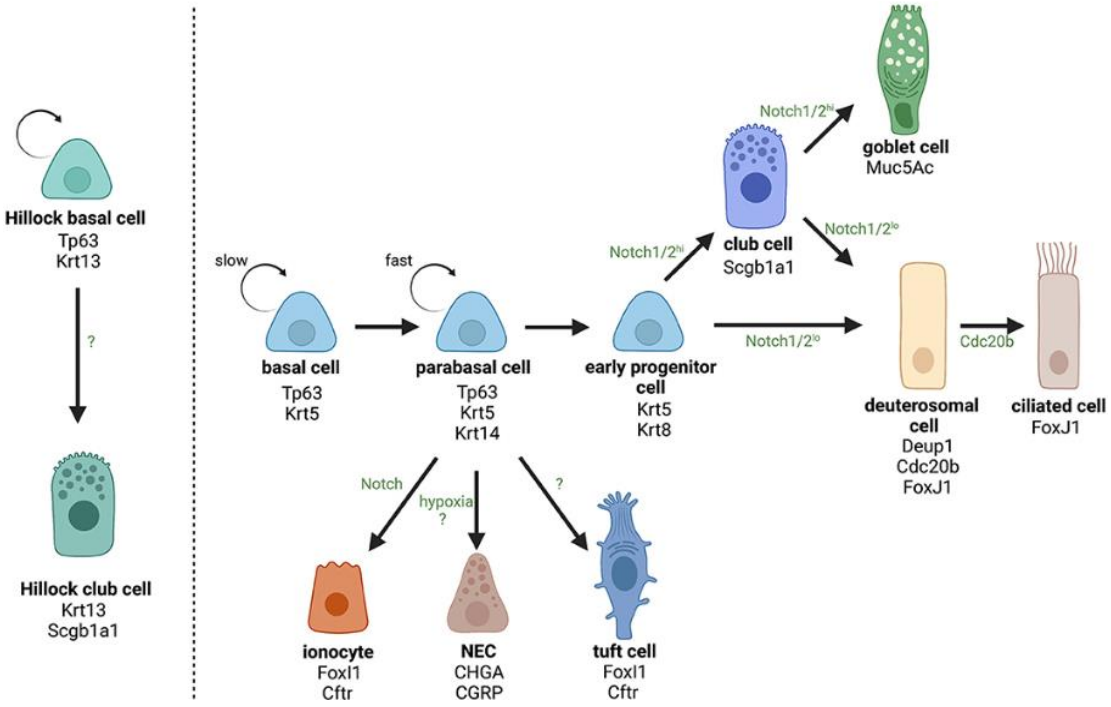

Figure 4 || **Overview of the epithelium of the proximal airway**

*(**A**) Hematoxylin-eosin stain of a bronchial biopsy shows ciliated cells, goblet cells, and basal cells. (**B**) Proposal for the differentiation of precursor basal cells, with their specific markers.*

*Adapted from (**A**) Gras Delphine, et al., Pharmacology & Therapeutics, 2013 and (**B**) Ruysseveldt Emma, et al., Frontiers in Allergy, 2021*

b) Distal airways

As noted above, alveoli are composed mainly by AT1 and AT2 cells.

AT1 cells

AT1 cells are large and flattened prismatic cells, covering more than 95% of the alveolar surface (Dobbs et al., 2010). They are air permeable and adjacent to microcapillary endothelial cells, and play a critical role for the air-blood barrier (Hogan et al., 2014; J. P. Schneider et al., 2019). Some studies have also shown that AT1 may play a role in lung regeneration by maintaining a proliferation and differentiation capacity, but this is still unclear (Jain et al., 2015; Wang et al., 2018).

AT2 cells

AT2 cells are much smaller and more cuboidal than AT1 and account for less than 5% of alveolar cells (Crapo et al., 1982). They produce, stock (through lamellar inclusions), and secrete the surfactant and participate in ion transport (Ruaro et al., 2021). They also have the ability to self-renew and differentiate into AT1 cells in response to lung injury (Aspal and Zemans, 2020; Chan and Liu, 2022). However, AT2 cells can also contribute to lung fibrosis by inducing aberrant wound healing responses with adjacent fibroblasts (Massaro et al., 2023; Parimon et al., 2020; Yao et al., 2021).

c) Mesenchymal compartment

During my thesis, I wrote a review manuscript on the role of the lung mesenchyme during lung development and in the physiopathological context. I also discussed in this article the epithelial to mesenchymal transition (EMT) and its opposite, the mesenchymal to epithelial transition (MET), which highlights cell plasticity, in lung development and disease (Nasri et al., 2021).

cells

MDPI

Review

Roles of Mesenchymal Cells in the Lung: From Lung Development to Chronic Obstructive Pulmonary Disease

Amel Nasri [1], Florent Foisset [1], Engi Ahmed [2,3], Zakaria Lahmar [2,3], Isabelle Vachier [2], Christian Jorgensen [1], Said Assou [1], Arnaud Bourdin [2,3] and John De Vos [1,4,*]

1 Institute for Regenerative Medicine and Biotherapy, Université de Montpellier, INSERM, Centre Hospitalier Universitaire de Montpellier, 34000 Montpellier, France; amel.nasri@inserm.fr (A.N.); florent.foisset@inserm.fr (F.F.); christian.jorgensen@inserm.fr (C.J.); said.assou@inserm.fr (S.A.)
2 Department of Respiratory Diseases, Université de Montpellier, INSERM, Centre Hospitalier Universitaire de Montpellier, 34090 Montpellier, France; noussa31@gmail.com (E.A.); zakaria.lahmar@gmail.com (Z.L.); isabelle.vachier@medbiomed.fr (I.V.); a-bourdin@chu-montpellier.fr (A.B.)
3 PhyMedExp, Université de Montpellier, INSERM, Centre Hospitalier Universitaire de Montpellier, 34295 Montpellier, France
4 Department of Cell and Tissue Engineering, Université de Montpellier, Centre Hospitalier Universitaire de Montpellier, 34000 Montpellier, France
* Correspondence: john.devos@inserm.fr; +33-467337888

Abstract: Mesenchymal cells are an essential cell type because of their role in tissue support, their multilineage differentiation capacities and their potential clinical applications. They play a crucial role during lung development by interacting with airway epithelium, and also during lung regeneration and remodeling after injury. However, much less is known about their function in lung disease. In this review, we discuss the origins of mesenchymal cells during lung development, their crosstalk with the epithelium, and their role in lung diseases, particularly in chronic obstructive pulmonary disease.

Keywords: mesenchyme; lung; development; COPD

check for updates

Citation: Nasri, A.; Foisset, F.; Ahmed, E.; Lahmar, Z.; Vachier, I.; Jorgensen, C.; Assou, S.; Bourdin, A.; De Vos, J. Roles of Mesenchymal Cells in the Lung: From Lung Development to Chronic Obstructive Pulmonary Disease. *Cells* **2021**, *10*, 3467. https://doi.org/10.3390/cells10123467

Academic Editor: Mehdi Najar

Received: 6 November 2021
Accepted: 7 December 2021
Published: 9 December 2021

Publisher's Note: MDPI stays neutral with regard to jurisdictional claims in published maps and institutional affiliations.

Copyright: © 2021 by the authors. Licensee MDPI, Basel, Switzerland. This article is an open access article distributed under the terms and conditions of the Creative Commons Attribution (CC BY) license (https://creativecommons.org/licenses/by/4.0/).

1. Introduction

The lung is a complex organ that carries out the vital task of blood oxygenation. To offer the surface required for this process, the lung gas exchange units (i.e., the alveoli) and the corresponding airways have been multiplied through iterative, fractal branching. This comes at a cost: the direct contact with the external environment of a surface larger than the skin. This contact surface is estimated to be bigger than 100 square meters. The bronchial epithelium is composed of polarized cells attached to a basement membrane and is closely interconnected through junctions, such as adherent junctions, tight junctions, gap junctions, desmosomes and hemi-desmosomes. The bronchial epithelium is composed of different cell types, including ciliated cells, club cells and goblet cells. It functions as a protective barrier and maintains the tissue homeostasis [1–3]. The main protection of the epithelium against external aggression (dusts, airborne particulate matters, noxious compounds, and microbes) is the mucociliary clearance system [4]. Goblet cells secrete mucin glycoproteins to form the mucus that covers bronchioles with a gel layer to trap the inhaled physical matter. Then, cilia on the ciliated cell surface beat to remove these pollutants from the airways.

Like all epithelia, the bronchial epithelium relies on the lung mesenchyme for physical support, nutrient supply [5–8], and key differentiation cues during development. The composition of the lung mesenchyme is still not fully known, but it comprises a large array of cells: endothelial cells, lymphatic cells, pericytes, fibroblasts, mesenchymal stromal cells, smooth muscle cells, and myofibroblasts [9–13]. Mesenchymal stromal cells and fibroblasts are morphologically indistinguishable, and they are differentiated mainly using functional assays [14]. In this review, these different cell types are collectively called "mesenchymal

cells". They have critical supporting roles and display specific features, such as migration and invasion [15]. Gene expression analysis and more recently single-cell mRNA sequencing have been useful to explore the mesenchymal cell diversity. For instance, their transcriptomic signature varies according to their localization in the body [11,14,16–19]. Moreover, a comprehensive catalogue of all mesenchymal cells has been proposed for human [20], and mouse [21] lungs. This list includes already known cell types (airway smooth muscle cells, adventitial fibroblasts, lipofibroblasts, mesothelial cells, myofibroblasts, pericytes, vascular smooth muscle cells), and also novel cell types identified on the basis of their gene expression profile, such as fibromyocytes and alveolar fibroblasts. All these mesenchymal cell types harbor a distinct gene expression signature (Figure 1 shows some of these cell types and their gene expression signature). Discrepancies among studies may reflect differences linked to the exact tissue localization or the species investigated (proximal versus distal pattern species, human versus mouse, etc.), and suggest that the different mesenchymal cell types could represent different steps in a continuous process of differentiation that varies also between different cell types but also between healthy and diseased lung. As the lung mesenchymal compartment contributes to lung homeostasis and repair after injury [22,23], mesenchymal cells are implicated in many lung diseases, particularly asthma, idiopathic pulmonary fibrosis, and chronic obstructive pulmonary disease (COPD). In this review, we highlight the importance of the crosstalk between epithelium and mesenchyme during lung development, adult life, and diseases, with a focus on COPD.

Human

Authors	References	Cell Types	Gene Expression profile
Travaglini et al	[20]	Fibroblasts	BSG, **COL1A2**
		Myofibroblasts	**ACTA2**, ASPN, BSG, **COL1A2**, CREB5, FGF18, TAGLN, WIF1
		Others	
		Alveoli Fibroblasts	**COL1A2**, DKK3, FGFR4 GPC3, MYC, SPINT2, TCF21
		Adventitial Fibroblasts	COL1A1, **COL1A2**, C3, IGFBP4, SERPINF1, SFRP2, PI16, PDGFRL
		Fibromyocytes	ACTA2, ACTG2, MYH11, **COL1A2**, CNN1, CREB5, TAGLN, TBX2
		Lipofibroblasts	APOE, CREM, FST, MAFF, MYC, NFIL3, NR4A3, **PLIN2**, SERPINF1
Habermann et al	[24]	Fibroblasts	**COL14A1**, **COL1A1**, COL3A1, COL6A1, COL6A2, **DCN**, EFEMP1, EFEMP2, FBN1, **FBLN1**, FBLN2, FBLN5, ITBP1, **LAMA2**, MAFP2, MAFP5, MGP, PLIN2
		Myofibroblasts	**ACTA2**, **COL1A1**, COL3A1, COL6A2, **LTBP2**, MGP, **PDGFRA**
		Others	
		Mesothelial Cells	MYC, **WT1**
Reyfman et al	[25]	Fibroblasts	**ACTA2**, CAV1, **COL1A1**, COL3A1, HIF1A, NOTCH2, NOTCH3, PDGFRA, PDGFRB, POSTN, TAGLN, TWIST2, **WNT2**, YAP1, ZEB2
Hein et al	[26]	Smooth Muscle Cell types	**ACTA2**, ACTG2, SM22, MYL9, FOXF1, HHIP, MYH11, WNT5A
		Others	
		Non Smooth Muscle Cell types	EGR1, WNT2

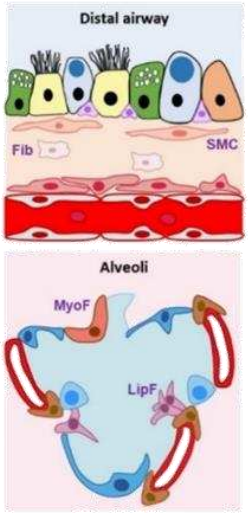

Mouse

Authors	References	Cell Types	Gene Expression profile
Negretti et al	[21]	Fibroblasts	**Acta2**, **Col1a1**, Gyg, Macf1, Mib67, **Wnt 2**
		Myofibroblasts	**Acta2**, Ednrb, Enpp2, Eln, **Pdgfra**, Tgfbi, Wnt5a
		Smooth Muscle Cell types	**Acta2**, Eln, Tgfb2
		Others	
		Adventitial Fibroblasts	Col1a1, Decorin, Lumican, Eln
		Mesothelial Cells	Col1a1, **Dcn**, Eln, Upk3b, **Wt1**
		Pericytes	Acta2, Cox4i2, Col4a1, Pdgfrb
		Lipofibroblasts	Gyg, **Plin2**, Tcf21,
Guo et al	[27]	Fibroblasts	**Col1a1**, **Col1a2**, Fgf10, Fn1, Vcam1, Tcf21,
		Myofibroblasts	**Col1a1**, **Col1a2**, **Pdgfra**, Rgs2, Vim
		Smooth Muscle Cell types	**Acta2**, **Col1a2**, **Col1a1**, Des, Rgs2
		Others	
		Pericytes	**Acta2**, Notch3, Pdgfrb
Strunz et al	[28]	Fibroblasts	Abi3bp, Adamts2, Angpt1, **Col14a1**, Clec3b, C1qtnf7, Cxcl12, **Dcn**, Efemp1, Efemp2, **Fbln1**, Figf, Gas6, Gpc3, Igfbp4, Lama2, Lamc, Ltbp3, Igfbp6, Mdk, Mfap4, Mmp3, Npnt, Serpina3n, Serpinx3m, Serpinf1, Prodoc2, Pkdc2,
		Myofibroblasts	**Acta2**, Amica1, Colfa3, Col12a1, Cxf1, Ctgf, Cthrc1, Grem1, Inhba, Lgals1, Lman1, Low2, Ltbp1, **Ltbp2**, Serpine1, Srpx2, Spp1, S100a6, Tnc, Thbs1, Wisp1
		Smooth Muscle Cell types	Aspn, Crim1, Pgf
Angelidis et al	[29]	Smooth Muscle Cell types	**Acta2**, **Col1a2**
		Others	
		Mesothelial Cells	**Dcn**, Msln
		Interstitial Fibroblasts	**Col1a2**, Dcn, Inmt
		Lipofibroblasts	**Col1a2**, Inmt

Figure 1. Summary of genes expressed in the different lung mesenchymal cell types (distal airways and alveoli), based on different recent studies in human (**left**) [20,24–26] and mouse (**right**) [21,27–29] samples. For fibroblasts cells (Fib), smooth muscle cell types (SMC), myofibroblasts (MyoF) and lipofibroblasts (LipF), genes present in at least two different studies are listed in bold. Distal airway: goblets, ciliated, club and basal cells are green, yellow, blue and lila, respectively. Alveoli: alveolar type 1, alveolar type 2 and pericytes are dark blue, light blue and brown, respectively.

2. Origin of Pulmonary Mesenchymal Cells

At the bilaminar disc stage in the second week of human development, gastrulation starts with the formation of the primitive streak [30]. Cells forming the epiblast undergo epithelial to mesenchymal transition (EMT) and migrate through the primitive streak to form the endoderm and mesoderm cell layers (Figure 2A) [31]. Specifically, the first wave of cells integrates the hypoblast layer and forms the endoderm [30], from which the lung will derive. A second group of cells migrates between the epiblast and endoderm layers

and constitutes the mesoderm layer that will give rise to a large variety of tissues, such as skeletal muscle, bone, cartilage, and many mesenchymal cell types (e.g., fibroblasts, chondroblasts, osteoblasts, blood cells). The mesoderm is a major contributor to trunk and limb stromal cells, but neural crest cells also contribute to mesenchymal cell lineages [32,33], although their specific role in lung mesenchyme is still poorly defined.

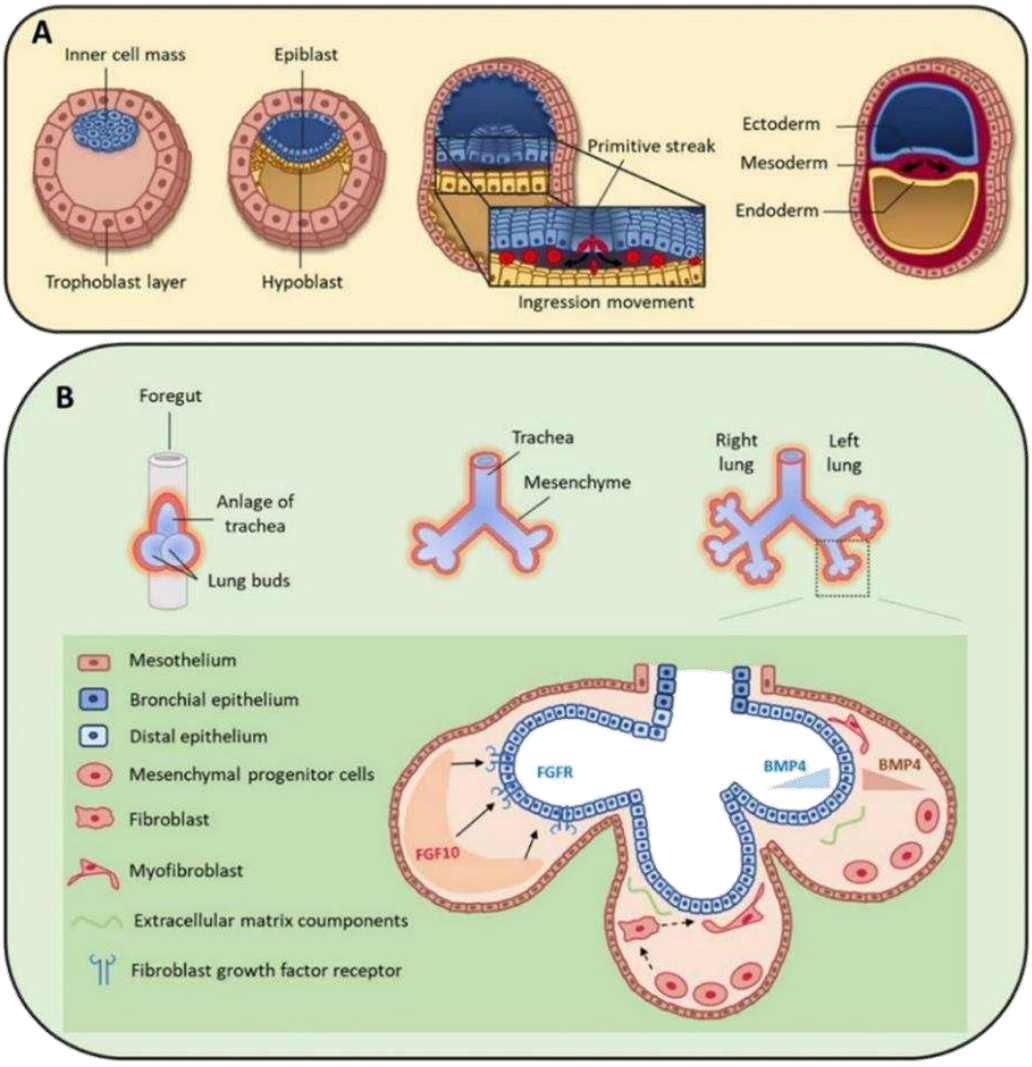

Figure 2. (**A**) During early human embryo development, the inner cell mass differentiates and becomes organized in the epiblast and hypoblast layers. Primitive streak formation leads to an ingression movement of epiblastic cells that elongate and detach from each other via a critical epithelial–mesenchymal transition [31]. This results in the formation of the three germ layers: ectoderm, mesoderm and endoderm. (**B**) On day 22, the foregut forms a ventral outgrowth leading to the formation of larynx and trachea in its proximal part, and lung buds in the distal part. Bifurcation and splitting of the lung buds give rise to the future right and left lungs. These structures grow ventrally to caudally through the surrounding mesenchyme. Mesenchymal progenitor cells secrete many factors, including fibroblast growth factor 10 (FGF10) that interacts with fibroblast growth factor receptor (FGFR) expressed by distal epithelial cells. Moreover, some cytokines, such as bone morphogenic protein 4 (BMP4), are secreted by both epithelial and mesenchymal cells.

3. Mesenchymal Cells during Lung Organogenesis

At the beginning of the fourth week of development, the anterior foregut endoderm develops at the cranial extremity after the cephalocaudal folding of the embryo. The foregut produces a ventral evagination that leads to lung bud development. These buds are surrounded by the splanchnopleuric mesoderm that is part of the lateral mesoderm and will contribute to lung vascularization, cartilage, muscles and conjunctive tissue (Figure 2B). In addition, the embryonic lateral splanchnic mesoderm generates mesothelial cells that form a thin layer of squamous-like cells lining the visceral pleura (mesothelium) [34–36]. Then, at day 26, the lung buds divide into right and left primitive bronchial buds, which are the precursors of the two lungs (Figure 2B).

During the pseudo-glandular stage, a second division at week 5 of development leads to the formation of the future pulmonary lobes by creating three secondary bronchial buds on the right and two on the left side. Each lung bud and the surrounding splanchnopleuric mesoderm grow, elongate and branch until the formation of the terminal bronchioles (17th branching generation) to create the respiratory tree (Figure 2B) [37]. At this stage, the tracheobronchial tree is coated by prismatic epithelial cells, the precursors of ciliated and secretory cells. Bronchioles appears during the canalicular stage (week 16 to 25), forming the basis of the gas exchange units. This is accompanied by geometric modifications of epithelial cells that flatten and by the appearance of capillaries throughout the mesenchyme that surround the bronchioles. Finally, at the saccular stage (week 24 to 40), alveolar ducts start to form. Their formation will continue after birth, and will terminate only in adulthood [7]. Of note, the development of the gas exchange units in utero and during early childhood is critical for achieving full adult lung function [38]. Lung development is the consequence of an interweaved relationship between embryonic lung epithelial and mesenchymal cells, through direct interactions and also indirectly via the secretion of extracellular matrix (ECM) components and growth factors [39–41]. Moreover, the mesothelium plays an important role during lung development [36,42,43], partly by secreting fibroblast growth factor (FGF) 9 [35,44,45].

Fetal airway smooth muscle (ASM) development begins early during gestation (from week 5–6 in human airways) [46]. Fetal ASM surrounds the airways and guides lung development and branching. ASM cells spontaneously contract early in fetal life, with proximal to distal peristaltic-like contractions that displace the amniotic liquid along the lumen [47,48]. At the pseudo-glandular and canalicular stages in pigs [48], the mechanical distention and stretching of the developing lungs, produced by ASM contractions, influence lung growth via mechanotransduction, through the pressure exerted across the airway wall and the surrounding parenchyma. Furthermore, the transmural pressure regulates the rate of airway epithelial bud branching [49].

The next part of this review will focus on some of the most relevant factors implicated in the epithelium–mesenchyme interactions during lung development.

3.1. Peptide Growth Factors

3.1.1. Fibroblast Growth Factors

The large FGF family plays an important role in the regulation of cell differentiation, proliferation and development, including lung branching [50]. Several studies have identified FGFs implicated in the bidirectional signaling between epithelium and mesenchyme during lung development [44,50,51]. For example, FGF10 is expressed in the distal submesothelial mesenchyme and activates FGF receptor 2b (FGFR2b) in the adjacent epithelial cells (Figure 3) to induce lung budding, epithelial cell expansion and migration, and ECM organization [52–54]. Indeed, in *Fgf*$10^{-/-}$ mice, the lung does not develop below the trachea [55,56]. Moreover, Bellusci et al. have identified, in mice, a subtype of Axin2+/FGF10+-resident mesenchymal alveolar niche cells that are close to alveolar type 2 (AT2) stem cells and that control the proliferation and differentiation of AT2 cells [57].

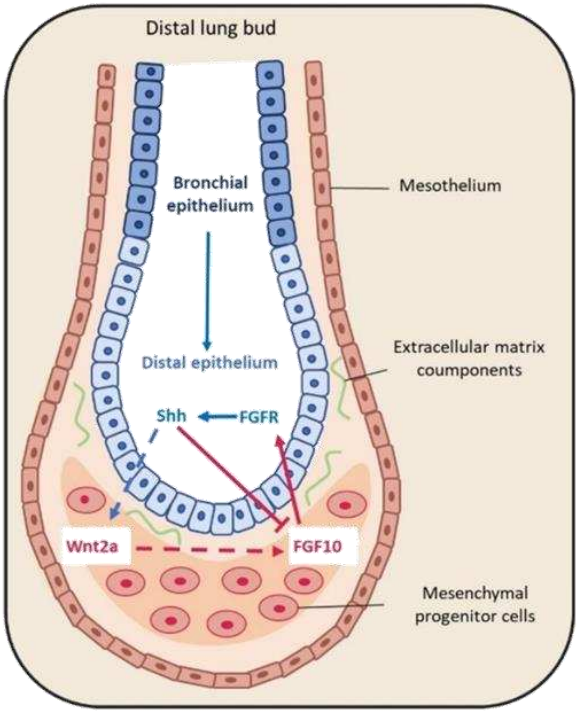

Figure 3. Representative schema of epithelium-mesenchyme interactions during lung budding. Many factors are secreted and exchanged between the lung epithelium (blue arrows) and mesenchyme (red arrows). For instance, fibroblast growth factor 10 (FGF10) is locally expressed by distal submesothelial mesenchymal cells and interacts with its receptor expressed in the distal epithelium. Sonic hedgehog (SHH) is expressed by epithelial cells, and downregulates FGF10 expression through its receptor Patched 1, but also activates FGF10 through the Wnt pathway.

FGF9 is another FGF family member that is expressed in the mesothelium from the pseudo-glandular stage (week 5 to 17) onwards, regulating the local activation of Wnt signaling to promote mesenchymal cell proliferation [35,44] (Figure 3). FGF9 also plays a critical role in lung development, as indicated by the finding that *Fgf9*$^{-/-}$ mice die at the neonatal stage due to lung hypoplasia caused by very reduced mesenchymal cell expansion [58].

3.1.2. Bone Morphogenic Protein 4 (BMP4)

BMP4 belongs to the transforming growth factor superfamily. *Bmp4*$^{-/-}$ mice die early during development, mainly due to an absence of mesoderm differentiation [59]. During lung development, BMP4 expression is detected in the distal epithelium buds and in the adjacent mesenchyme already at the pseudo-glandular stage (week 5 to 17) [60,61]. Conversely, BMP type I receptor (BMPR1) is expressed in both epithelium and mesenchyme (Figure 2B) [62]. In association with sonic hedgehog (SHH), BMP4 antagonizes FGF10 that is expressed in the surrounding mesenchyme [63]. Conditional knock-out of *Bmpr 1a*, the gene encoding the BMP4 receptor in the epithelium, leads to abnormal lung development with reduced cell proliferation, increased apoptosis and abnormal lung morphogenesis. This indicates that BMP4 plays important roles in lung development [64]. Moreover [65], in cultured mouse embryonic lung, reduction of gremlin expression, a BMP4 antagonist, using antisense oligonucleotides promotes epithelial cell proliferation and abnormal lung formation/function. Finally, BMP4 overexpression in the distal bud tips leads to lung hypoplasia, reduction of AT2 cells, and enlargement of the terminal buds [62]. However, the exact role of this signaling pathway during lung development remains debated, because

mathematical models to mimic the FGF10-SHH interaction accurately model bronchial branching independently of BMP4 expression [66,67].

3.1.3. Sonic Hedgehog

SHH also is part of a key developmental signaling pathway. It is implicated in central nervous system patterning, and limb, digit and lung development [68]. In *Shh*$^{-/-}$ mice, a single lobe, lung hypoplasia with absence of left and right asymmetry, enhanced cell death and decreased lung mesenchymal cell proliferation are observed [69]. SHH is expressed with BMP4 in the distal bud epithelium during lung development. It binds to and activates its receptor Patched 1 (PTCH1) that is localized in the adjacent mesenchyme. Patched 1 activation downregulates FGF10 expression [44,52,70]. Indeed, in *Shh*$^{-/-}$ mice, FGF10 expression in the mesenchyme immediately adjacent to the epithelium is increased [71]. In addition, BMP4 is overexpressed and wingless-related integration site family member 2 (WNT2) is downregulated in the mesenchyme. In 2013, Peng et al. [72] identified a cardiopulmonary mesoderm progenitor population that is defined by the expression of WNT2, glioma-associated oncogene 1 (Gli1) and Islet 1, and gives rise to the lung mesenchyme and cardiac lineage in the mouse. This population is regulated by Hedgehog signaling because Gli proteins are the main transcriptional effectors of this pathway, and start to be expressed at the lung organogenesis step [72]. This suggests that SHH is broadly involved in mesenchymal signaling in the developing lung.

3.1.4. Epidermal Growth Factor (EGF)

EGF and its tyrosine kinase receptor EGF-R are expressed in the epithelial and mesenchymal compartments during lung development. EGF stimulates lung branching in fetal mice [40]. In agreement, in *Egfr*$^{-/-}$ mice, neonatal lethality is high and epithelial cell development is impaired in several organs, including the lung [73]. Importantly, lung branching is reduced and alveolarization and septation are deficient in *Egfr*$^{-/-}$ mice [74]. Similarly, mouse lung branching can be inhibited in ex-vivo cultures using antisense oligonucleotides against EGF [40,75]. Furthermore, the interplay between retinoid acid (RA) and EGFR during fetal lung development stimulates lung branching [76].

3.1.5. Retinoic Acid (RA)

RA is essential for normal embryo development, including lung development [77]. In the mouse, retinoic acid receptor (RAR) double knock-out (RARα-/-/RARβ2-/-) leads to agenesis of the left lung and hypoplasia of the right lung [78]. RA is produced by the mesenchyme surrounding the lung primordia, and also by the epithelial compartment of the proximal bronchi [79]. Importantly, a RA-transforming growth factor (TGF)-β-FGF10 interaction has been described during lung bud induction, where RA downregulates TGF-β to allow FGF10 expression [80].

3.1.6. TGF-β

TGF-β, a pleiotropic growth factor and a key EMT inducer, is another modulator of epithelium–mesenchyme interactions in the developing lung [81]. Its three isoforms play a crucial role during lung organogenesis [82]. Their expression is well characterized in the mouse where TGF-β1 is expressed in the mesenchyme, TGF-β2 in the distal epithelium, and TGF-β3 in the proximal mesenchyme and pulmonary mesothelium [83,84]. In *Tgf-β2*$^{-/-}$ mice, the distal airways are collapsed and the proximal airways are dilated [82], whereas in *Tgf-β3*$^{-/-}$ mice lung development is delayed, causing their death [85]. Conversely, *Tgfr-β2* ablation in mesodermal tissue results in abnormal lung branching and lung development, while its ablation in epithelial cells that produce surfactant protein C results in a decrease of alveolar type I (AT1) epithelial cells during post-natal alveolarization [86]. TGF-β also plays a role in FGF10 regulation by RA [80] as illustrated by the finding that ectopic TGF-β1 expression inhibits FGF10-induced lung morphogenesis in cultured embryonic lung endodermal explants [87].

3.1.7. The Hippo Pathway

The Hippo pathway and its downstream targets Yes-associated protein (YAP) and transcriptional coactivator with PDZ-binding motif (TAZ) play major roles in tissue homeostasis, organ development, and organ size [88,89] by regulating various processes, such as cell proliferation/survival, the response to mechanical stress and cell geometry. This pathway involves a kinase cascade and adaptors that ultimately regulate YAP/TAZ activities. The name comes from the Drosophila kinase Hippo, the mammalian orthologs of which are the kinases MST1/2. Upon activation of the Hippo signaling pathway, MST1/2 phosphorylates LATS1/2, thereby activate these kinases that in turn phosphorylate YAP and TAZ. Phosphorylated YAP and TAZ are retained in the cytoplasm or degraded by the ubiquitin system. Conversely, when the Hippo pathway is inactive, YAP and TAZ shuttle to the nucleus where they bind to TEA domain (TEAD) transcription factors and regulates the transcription of many downstream genes [89]. *Taz* knockout mice show abnormal alveolarization, leading to airway enlargement that mimics human emphysema [90,91]. Conditional *Yap* knockout in lung epithelium causes disruption of bronchial morphogenesis [91]. During alveologenesis, YAP/TAZ inactivation by cell crowding orients NKX2.1 activity towards AT2 cells, a mechanism thought to be a negative feedback to limit AT1 cell expansion [92]. In bronchia, YAP is activated in distal airways, and its induction prevents multi-ciliated cell differentiation [93]. These observations suggest a general role of YAP/TAZ in favoring the stem cell compartment at the expenses of terminal differentiation. In line, YAP overexpression in adult tracheal cells results in basal cell hyperplasia and stratification [94]. Interestingly, injury in airway epithelial cells leads to downregulation of hippo signaling that increases the concentration of nuclear YAP [38], and induces FGF10 secretion by the adjacent mesenchymal cells [95]. Moreover, in the absence of *Yap*, epithelial progenitors cannot respond to local TGF-β signaling [93]. Overall, the Hippo pathway plays a critical role in lung development and response to injury directly in epithelial cells or indirectly through epithelium/mesenchyme signaling.

Other factors also are involved in lung development, such as components of the vascular endothelial growth factor (VEGF) and WNT signaling pathways. Their expression is highly regulated in space and time, allowing optimal lung development, at least partly through epithelium-mesenchyme interactions. Single-cell transcriptomic analyses will help to identify all the factors involved in lung development.

3.2. Extracellular Matrix Compounds

The ECM exerts functions of support, structure and stabilization that are essential for organ development and homeostasis. By directly binding to growth factors, it can also modulate the activity of secreted factors [96]. At the end of the human pseudo-glandular stage, proteoglycans, such as decorin and lumican, are located between the epithelium and the mesenchyme compartments, along with collagen type I, III and VI [97]. In ex-vivo cultures of mouse embryonic lungs, decorin binds to and neutralizes exogenous TGF-β with high affinity, thus inhibiting TGF-β signaling [98]. Furthermore, heparan sulfates present in the EMC can stabilize the interaction between growth factors and receptors. For example, Izvolsky et al. [99] showed that endogenous gradients of heparan sulfates, especially highly sulfated heparan sulfates, help lung budding induced by FGF10.

4. Physiological Roles of Mesenchymal Cells in Bronchioles

In the airways, epithelial cells are directly exposed to the outside environment and form a protective barrier against pathogens and toxic particles. Some bronchial epithelial cell populations contribute to epithelium repair, such as basal cells [100], one of the main airway stem cell sources [101], and club cells that can trans-differentiate for epithelium renewal [102–104]. Mesenchymal cells also participate by supporting lung epithelium homeostasis and repair [105,106].

Bronchial epithelium maintains the quiescence of mesenchymal cells through the Hedgehog pathway paracrine signaling [105]. Upon epithelial injury, SHH is downregu-

lated to promote proliferation of peribronchial mesenchymal cells and the repair of the damaged tissue [105]. Peng et al. [72] showed that loss of SHH expression in airway epithelial cells leads to expansion of the surrounding mesenchymal Gli1 population that promotes the increase of the total club cell number and consequently bronchial hyperplasia.

Recently, several new lung mesenchyme cell types that can self-renew and contribute to mesenchyme self-maintenance have been described. Zepp et al. [107] characterized Axin2-Pdgfr+ mesenchymal cells that promote the regeneration and growth of alveolar cells, and Axin2+ myofibrogenic progenitors that contribute to the pathological myofibroblast response after lung injury. The origin of myofibroblasts in the lung is still debated because it requires multiple signals from fibroblasts, pericytes and other cell types [108,109]. Although it is still difficult to distinguish the different mesenchymal cell types, presumably because of an underlying continuum of differentiation, new tools such as single-cell RNA-sequencing will provide new data to expand the taxonomy of mesenchymal cells (Figure 4). In an analysis of mesenchymal cells from multiple tissues, Buechler et al. identified a dermatopontin-positive cell fibroblast population, possibly representing a universal fibroblast cell population that can give rise to other fibroblast subsets in the different tissues [110].

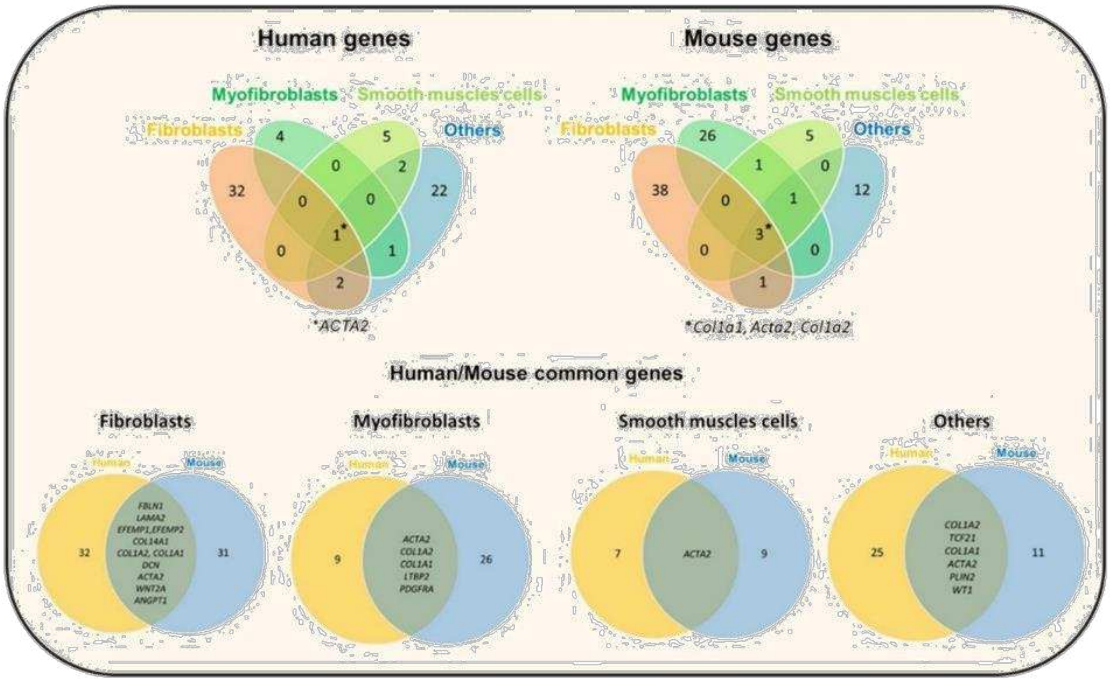

Figure 4. Venn diagrams showing the number of differentially expressed genes in each comparison (between human and mouse) and the overlaps between the four main compared mesenchymal cell types (fibroblasts, myofibroblasts, smooth muscle cells and other cell types). 1* and 3*, number of genes shared by the four cell types. This analysis is based on data from eight single-cell RNA sequencing studies (see Figure 1). The Venn diagrams were generated using the Venny tool.

More recently, Fang et al. [106] tagged with a green fluorescent protein the basic helix-loop-helix transcription factor TWIST2/Dermo1 that is strongly expressed in mouse mesodermal tissues [111]. They found that after lung injury using lipopolysaccharide and naphthalene (a polycyclic aromatic hydrocarbon), the Dermo+ mesenchymal population differentiated into club cells, ciliated cells, goblet cells and neuroendocrine cells. In mice, exposure to naphthalene specifically depletes club cells by binding to CYP2F2 enzymes. These results suggest that besides their pleiotropic (e.g., anti-inflammatory and trophic) effects [112], mesenchymal cells may also directly contribute to epithelium regeneration.

5. Mesenchymal Cells in Chronic Obstructive Pulmonary Disease

Increased environmental susceptibility, as observed in asthma, might be seen as a failure of the innate immune system to prevent the adaptive immunity engagement and the subsequent airway inflammation. Ultimately, this might lead to cell loss and alterations that cause respiratory functional disruption. The lung physiological defense systems and regeneration capacities could be overwhelmed. In some individuals, this can lead to chronic lung diseases, such as COPD, pulmonary fibrosis and lung cancer (see Wolters et al. and Gohy et al. [113,114]). This review will focus on the role of mesenchymal cells in COPD.

5.1. Genetic Contribution

COPD is the third leading cause of death worldwide: more than 3.2 million of deaths in 2017 that should increase to more than 4.4 million by 2040 [115,115]. This chronic airway disease is associated with inflammation and structural changes, leading to permanent bronchial obstruction [116–118]. The insidious progression of the disease might explain its frequent underdiagnosis and late diagnosis [119]. Moreover, COPD is associated with many comorbidities, such as cardiac, gastrointestinal, cerebral and muscular diseases [120–125]. Tobacco smoking is the first cause of COPD in western countries [126–128]. Air pollution, including by biomass combustion [129–131], occupational and non-occupational exposure to dust and chemical agents [132], and repeated airway infections during childhood [133] are now recognized as contributing causes of COPD. Genetic and environmental factors could influence the susceptibility to COPD. Multiple large-cohort genome-wide association studies to understand the link between loci associated with lung function impairment and COPD found many polymorphisms near the Hedgehog Interacting Protein (*HHIP*) gene [134–137] that encodes a physiological inhibitor of SHH [138]. Furthermore, several studies have highlighted a relationship between susceptibility to COPD, *FGF*10 gene variants, and human airway branching variations. For instance, Smith et al., using computed tomography observed greater central airway bifurcation density, bronchial anatomic variations and narrower airway lumens in all lobes of patients with COPD than in controls. They found that these changes were significatively associated with *FGF*10 variants [139]. Gene mutations in components of key signaling pathways involved in lung development may promote COPD development.

The huge heterogeneity in COPD triggers and clinical expression may be explained by the different underlying mechanisms. Indeed, COPD should not be seen as a unique entity, but as a syndrome [140].

5.2. The Epithelial–Mesenchymal Crosstalk

The release of inflammatory mediators, such as TNF-α, interleukin (IL)-6 and IL-8, promotes chronic airway inflammation and ECM deposition [140,141]. In the epithelial cell compartment, goblet and basal cell hyperplasia, squamous metaplasia, mucus hypersecretion and altered cilia beating are the classical structural changes observed in patients with COPD and in smokers [4,142–144]. The contribution of the bronchial mesenchymal compartment to COPD progression is strongly suggested by its role in bronchial injury repair, but this is still debated. Many studies have identified an increase in the expression of mesenchymal markers, such as vimentin and the fibroblast protein S100A4, in COPD lung samples [145]. Myofibroblasts and fibroblasts could remodel the ECM by releasing matrix metalloproteinases, such as MMP9 [146,147]. Interestingly, a recent study identified different fibroblast subtypes that are localized in the lung subepithelial, subpleural and parenchymal regions and that contribute to ECM expansion in pulmonary fibrosis [24]. Similar injury-response mechanisms could be involved in COPD. These data suggest that the epithelial-mesenchymal crosstalk or the "epithelial-mesenchymal trophic unit" plays crucial roles in driving lung pathology [148].

5.3. Peribronchiolar Fibrosis

In COPD, the major site of obstruction is located in the small conducting airways (i.e., bronchioles with a diameter < 2 mm) [149,150]. During COPD, small airways become narrower due to the airway wall thickening and peribronchiolar fibrosis. The mechanisms of peribronchiolar fibrosis are poorly understood, and small airway fibroblasts have not been well characterized. Senescent fibroblasts could have a role in small airway fibrosis [151] due to their increased secretion of collagen 1A1 and 3A1 and increased expression of matrix metalloproteinases (MMP2, MMP9).

Cigarette smoke and oxidative stress may stimulate the release of profibrotic mediators, such as TGF-β and IL-1 beta, by airway epithelial cells [152]. Increased TGF-β1 expression (mRNA and protein) has been observed in epithelial and endothelial cells from small airways of patients with COPD compared with controls [153]. Air–liquid interface culture of airway epithelial cells from patients with COPD showed increased EMT and increased release of TGF-β that were correlated with the degree of peribronchiolar fibrosis and airway obstruction [154]. These profibrotic growth factors may induce a profibrotic phenotype in adjacent airway fibroblasts or promote the differentiation of bronchial smooth muscle cells into myofibroblasts. Indeed, a recent study showed an increase of the αSMA+ myofibroblast population in small airways of patients with COPD compared with controls [155].

5.4. Extracellular Matrix Composition

In COPD, ECM is degraded by enzymes, such as neutrophil elastase, metalloproteinases, hyaluronidases and chondroitinases. It has been shown that in different lung compartments, elastic fibers, elastin, glycosaminoglycans (e.g., hyaluronic acid) and type I collagen decrease drastically, but not fibronectin, tenascin and other collagens. These changes contribute to peri-bronchial fibrosis and progressive emphysema that profoundly impact the respiratory functions (Figure 5) [156–160].

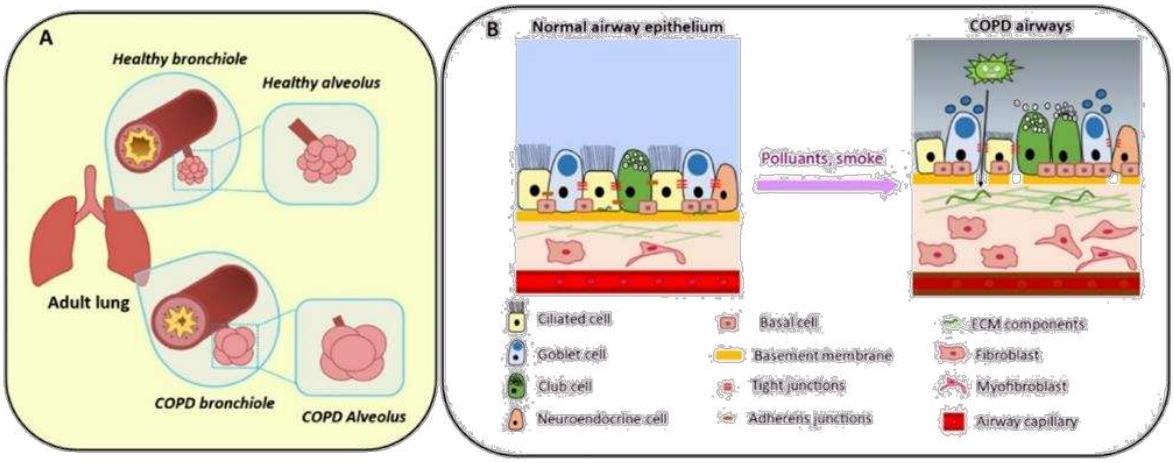

Figure 5. Aspects of COPD development. **(A)** (**Top panel**) Healthy bronchioles present a thin wall and a lumen where mucus is secreted to externalize pathogens. Alveoli contain elastin fibers and regulate gas exchanges between lung and blood. (**Bottom panel**) Over time, chronic exposure to tobacco, air pollution and/or recurrent infections lead to a thickened bronchiole wall associated with airflow obstruction. Emphysema is caused by gas trapping that damages the alveoli, followed by progressive peribronchiolar fibrosis. **(B)** (**Right panel**) In the alveolar-capillary unit, epithelial cells are interconnected and attached to the basement membrane above the mesenchymal compartment. (**Left panel**) Chronic exposure to pollutants damages ciliated cells (leading to impaired mucociliary clearance), alters the epithelial cell barrier and the basement membrane with loss of tight junctions and pathogen penetration in the lower layers. This is associated with mucus plugging and goblet cell hypersecretion. Pro-proliferative fibroblasts and myofibroblasts contribute to extracellular matrix (ECM) deposition that impairs injury repair.

5.5. Epithelial–Mesenchymal Transition

Cigarette smoke also induces EMT in bronchial epithelial cells of smokers and patients with COPD, thus altering epithelial function and contributing to defective lung remodeling [161]. EMT is a morphogenetic cell conversion program of epithelial cells to mesenchymal cells. EMT and mesenchymal–epithelial transition are key processes during embryogenesis and organogenesis [31]. Normally, epithelial cells are polarized and attached to the basement membrane via their basal surface. Depending on the microenvironment conditions and the cell physiological state [162], these cells can lose many epithelial characteristics, such as cell–cell adhesion (Figure 5B) and cell polarity, and acquire features of mesenchymal cells, such as migration and invasion [163–165]. EMT illustrates the epithelial cell phenotype plasticity. Of note, an intermediate "metastable" state where cells co-express markers of both epithelial and mesenchymal cells has been described [166,167]. In chronic airway diseases, EMT is mainly promoted through TGF-β/SMAD signaling [168] that with other signaling pathways promotes myofibroblast proliferation [169,170] and activates several ECM components. By acquiring mesenchymal cell properties, such as migration through the basement membrane, these cells could contribute to peribronchial fibrosis [145,171]. In COPD, EMT could also be promoted by the bronchial epithelium basement membrane fragmentation that facilitates pathogen penetration in the subepithelium and increases local inflammation [172,173]. Hence, mesenchymal cell proliferation and EMT might contribute to COPD pathophysiology and explain some of the observed architectural changes, such as bronchial lumen thickening (Figure 5).

5.6. Airway Smooth Muscle

ASM cells are the main pharmacological target in COPD through inhaled drugs, such as long-acting β-agonists, anticholinergic and corticosteroids. However, little is known about ASM cell changes in COPD. Differently from asthma, no ASM cell alteration (morphology and size) has been observed in the large airways of patients with COPD, and the ASM cell number does not correlate with airflow limitation [174]. Similarly, the proliferation rate of cultured ASM cells from patients with COPD is not increased [175]. Conversely, in small airways, ASM mass is significantly increased in COPD and is inversely correlated with lung function [176].

Some mesenchymal cell populations, such as mesenchymal stromal cells, could have a therapeutic potential in COPD. Indeed, administration of mesenchymal stromal cells in mouse [177] and in rat [178] models of COPD attenuates lung damage. However, it does not improve COPD outcomes [179,180] and therefore, its use is still debated [181–183]. Recently, in patients with COVID-19-associated pneumonia, the systemic delivery of allogeneic mesenchymal stromal cells (MSC) has been proposed. MSC anti-inflammatory properties and their ECM remodeling capacity suggest that MSC- based therapy may prevent fibrosis. Several clinical trials have shown the feasibility of this approach but preliminary data are mixed, possibly due to bronchial inflammation which may dampen their therapeutic efficacy [184]. Therefore, randomized trials are needed before drawing definitive conclusions [185].

6. Conclusions

Lung mesenchyme plays an important role in lung development and homeostasis, and an imbalance or a defect in the mesenchymal cell response to chronic injury could contribute to lung diseases. However, the exact role of the mesenchymal compartment in lung homeostasis and disease is still largely unknown. As a first step to improve this knowledge, it is essential to precisely determine the taxonomy of lung mesenchymal stromal cells during lung development and disease (a task accelerated by single-cell RNA sequencing) and the composition of that niche.

Author Contributions: A.N. wrote the review and made all the figures. F.F., E.A., Z.L., I.V., C.J., S.A., A.B. and J.D.V. have written, reviewed and edited the manuscript. All authors have read and agreed to the published version of the manuscript.

Funding: This work was supported by a grant to F.F. from la Foundation du Souffle.

Institutional Review Board Statement: Not applicable.

Informed Consent Statement: Not applicable.

Data Availability Statement: Not applicable.

Acknowledgments: We thank E. Andermarcher for critical reading of this manuscript.

Conflicts of Interest: The authors declare no conflict of interest.

References

1. Gohy, S.; Hupin, C.; Ladjemi, M.Z.; Hox, V.; Pilette, C. Key role of the epithelium in chronic upper airways diseases. *Clin. Exp. Allergy* **2020**, *50*, 135–146. [CrossRef] [PubMed]
2. Wittekindt, O.H. Tight junctions in pulmonary epithelia during lung inflammation. *Pflug. Arch.* **2017**, *469*, 135–147. [CrossRef]
3. Powell, D.W. Barrier function of epithelia. *Am. J. Physiol.-Gastrointest. Liver Physiol.* **1981**, *241*, G275–G288. [CrossRef] [PubMed]
4. Bustamante-Marin, X.M.; Ostrowski, L.E. Cilia and Mucociliary Clearance. *Cold Spring Harb. Perspect. Biol.* **2017**, *9*, a028241. [CrossRef] [PubMed]
5. Loh, K.M.; Chen, A.; Koh, P.W.; Deng, T.Z.; Sinha, R.; Tsai, J.M.; Barkal, A.A.; Shen, K.Y.; Jain, R.; Morganti, R.M.; et al. Mapping the Pairwise Choices Leading from Pluripotency to Human Bone, Heart, and Other Mesoderm Cell Types. *Cell* **2016**, *166*, 451–467. [CrossRef]
6. Delorme, B.; Chateauvieux, S.; Charbord, P. The concept of mesenchymal stem cells. *Regen. Med.* **2006**, *1*, 497–509. [CrossRef]
7. Bishop, A.E. Pulmonary epithelial stem cells. *Cell Prolif.* **2004**, *37*, 89–96. [CrossRef]
8. Mammoto, A.; Mammoto, T. Vascular Niche in Lung Alveolar Development, Homeostasis, and Regeneration. *Front. Bioeng. Biotechnol.* **2019**, *7*, 318. [CrossRef]
9. Hogan, B.L.M.; Barkauskas, C.E.; Chapman, H.A.; Epstein, J.A.; Jain, R.; Hsia, C.C.W.; Niklason, L.; Calle, E.; Le, A.; Randell, S.H.; et al. Repair and Regeneration of the Respiratory System: Complexity, Plasticity, and Mechanisms of Lung Stem Cell Function. *Cell Stem Cell* **2014**, *15*, 123–138. [CrossRef]
10. McCulley, D.; Wienhold, M.; Sun, X. The Pulmonary Mesenchyme Directs Lung Development. *Curr. Opin. Genet. Dev.* **2015**, *32*, 98–105. [CrossRef] [PubMed]
11. Barron, L.; Gharib, S.A.; Duffield, J.S. Lung Pericytes and Resident Fibroblasts. *Am. J. Pathol.* **2016**, *186*, 2519–2531. [CrossRef]
12. Lee, J.-H.; Tammela, T.; Hofree, M.; Choi, J.; Marjanovic, N.D.; Han, S.; Canner, D.; Wu, K.; Paschini, M.; Bhang, D.H.; et al. Anatomically and Functionally Distinct Lung Mesenchymal Populations Marked by Lgr5 and Lgr6. *Cell* **2017**, *170*, 1149–1163.e12. [CrossRef] [PubMed]
13. Sveiven, S.N.; Nordgren, T.M. Lung-resident mesenchymal stromal cells are tissue-specific regulators of lung homeostasis. *Am. J. Physiol.-Lung Cell. Mol. Physiol.* **2020**, *319*, L197–L210. [CrossRef]
14. Soundararajan, M.; Kannan, S. Fibroblasts and Mesenchymal Stem Cells: Two Sides of the Same Coin? *J. Cell. Physiol.* **2018**, *233*, 9099–9109. [CrossRef]
15. Hay, E.D. The mesenchymal cell, its role in the embryo, and the remarkable signaling mechanisms that create it. *Dev. Dyn.* **2005**, *233*, 706–720. [CrossRef] [PubMed]
16. da Silva Meirelles, L. Mesenchymal stem cells reside in virtually all post-natal organs and tissues. *J. Cell Sci.* **2006**, *119*, 2204–2213. [CrossRef]
17. Rinn, J.L.; Bondre, C.; Gladstone, H.B.; Brown, P.O.; Chang, H.Y. Anatomic Demarcation by Positional Variation in Fibroblast Gene Expression Programs. *PLoS Genet.* **2006**, *2*, e119. [CrossRef]
18. Spadafora, R.; Lu, J.; Khetani, R.S.; Zhang, C.; Iberg, A.; Li, H.; Shi, Y.; Lerou, P.H. Lung-Resident Mesenchymal Stromal Cells Reveal Transcriptional Dynamics of Lung Development in Preterm Infants. *Am. J. Respir. Crit. Care Med.* **2018**, *198*, 961–964. [CrossRef]
19. Abreu, S.C.; Rolandsson Enes, S.; Dearborn, J.; Goodwin, M.; Coffey, A.; Borg, Z.D.; dos Santos, C.C.; Wargo, M.J.; Cruz, F.F.; Loi, R.; et al. Lung inflammatory environments differentially alter mesenchymal stromal cell behavior. *Am. J. Physiol. Lung Cell. Mol. Physiol.* **2019**, *317*, L823–L831. [CrossRef] [PubMed]
20. Travaglini, K.J.; Nabhan, A.N.; Penland, L.; Sinha, R.; Gillich, A.; Sit, R.V.; Chang, S.; Conley, S.D.; Mori, Y.; Seita, J.; et al. A molecular cell atlas of the human lung from single-cell RNA sequencing. *Nature* **2020**, *587*, 619–625. [CrossRef]
21. Negretti, N.M.; Plosa, E.J.; Benjamin, J.T.; Schuler, B.A.; Christian, A.; Jetter, C.; Gulleman, P.; Taylor, C.J.; Nichols, D.; Matlock, K.; et al. A Single Cell Atlas of Lung Development. *bioRxiv* **2021**. [CrossRef]
22. Slavkin, H.C.; Snead, M.L.; Zeichner-David, M.; Jaskoll, T.F.; Smith, B.T. Concepts of epithelial-mesenchymal interactions during development: Tooth and lung organogenesis. *J. Cell. Biochem.* **1984**, *26*, 117–125. [CrossRef]

23. Agha, E.E.; Herold, S.; Alam, D.A.; Quantius, J.; MacKenzie, B.; Carraro, G.; Moiseenko, A.; Chao, C.-M.; Minoo, P.; Seeger, W.; et al. Fgf10-positive cells represent a progenitor cell population during lung development and postnatally. *Development* **2014**, *141*, 296–306. [CrossRef] [PubMed]
24. Habermann, A.C.; Gutierrez, A.J.; Bui, L.T.; Yahn, S.L.; Winters, N.I.; Calvi, C.L.; Peter, L.; Chung, M.-I.; Taylor, C.J.; Jetter, C.; et al. Single-Cell RNA Sequencing Reveals Profibrotic Roles of Distinct Epithelial and Mesenchymal Lineages in Pulmonary Fibrosis. *Sci. Adv.* **2020**, *6*, eaba1972. [CrossRef] [PubMed]
25. Reyfman, P.A.; Walter, J.M.; Joshi, N.; Anekalla, K.R.; McQuattie-Pimentel, A.C.; Chiu, S.; Fernandez, R.; Akbarpour, M.; Chen, C.-I.; Ren, Z.; et al. Single-Cell Transcriptomic Analysis of Human Lung Provides Insights into the Pathobiology of Pulmonary Fibrosis. *Am. J. Respir. Crit. Care Med.* **2019**, *199*, 1517–1536. [CrossRef]
26. Hein, R.F.C.; Wu, J.H.; Tsai, Y.-H.; Wu, A.; Miller, A.J.; Holloway, E.M.; Frum, T.; Conchola, A.S.; Szenker-Ravi, E.; Reversade, B.; et al. R-SPONDIN2^{+} Mesenchymal Cells Form the Bud Tip Progenitor Niche During Human Lung Development. *bioRxiv* **2021**. [CrossRef]
27. Guo, M.; Du, Y.; Gokey, J.J.; Ray, S.; Bell, S.M.; Adam, M.; Sudha, P.; Perl, A.K.; Deshmukh, H.; Potter, S.S.; et al. Single Cell RNA Analysis Identifies Cellular Heterogeneity and Adaptive Responses of the Lung at Birth. *Nat. Commun.* **2019**, *10*, 37. [CrossRef]
28. Strunz, M.; Simon, L.M.; Ansari, M.; Kathiriya, J.J.; Angelidis, I.; Mayr, C.H.; Tsidiridis, G.; Lange, M.; Mattner, L.F.; Yee, M.; et al. Alveolar regeneration through a Krt8+ transitional stem cell state that persists in human lung fibrosis. *Nat. Commun.* **2020**, *11*, 3559. [CrossRef]
29. Angelidis, I. An Atlas of the Aging Lung Mapped by Single Cell Transcriptomics and Deep Tissue Proteomics. *Nat. Commun.* **2019**, *10*, 963. [CrossRef]
30. Solnica-Krezel, L.; Sepich, D.S. Gastrulation: Making and Shaping Germ Layers. *Annu. Rev. Cell Dev. Biol.* **2012**, *28*, 687–717. [CrossRef]
31. Thiery, J.P.; Acloque, H.; Huang, R.Y.J.; Nieto, M.A. Epithelial-Mesenchymal Transitions in Development and Disease. *Cell* **2009**, *139*, 871–890. [CrossRef] [PubMed]
32. Douarin, N.M.L.; Creuzet, S.; Couly, G.; Dupin, E. Neural crest cell plasticity and its limits. *Development* **2004**, *131*, 4637–4650. [CrossRef] [PubMed]
33. Takashima, Y.; Era, T.; Nakao, K.; Kondo, S.; Kasuga, M.; Smith, A.G.; Nishikawa, S.-I. Neuroepithelial Cells Supply an Initial Transient Wave of MSC Differentiation. *Cell* **2007**, *129*, 1377–1388. [CrossRef]
34. Que, J.; Wilm, B.; Hasegawa, H.; Wang, F.; Bader, D.; Hogan, B.L.M. Mesothelium contributes to vascular smooth muscle and mesenchyme during lung development. *Proc. Natl. Acad. Sci. USA* **2008**, *105*, 16626–16630. [CrossRef] [PubMed]
35. Yin, Y.; Wang, F.; Ornitz, D.M. Mesothelial- and epithelial-derived FGF9 have distinct functions in the regulation of lung development. *Development* **2011**, *138*, 3169–3177. [CrossRef]
36. Batra, H.; Antony, V.B. The pleural mesothelium in development and disease. *Front. Physiol.* **2014**, *5*, 284. [CrossRef]
37. Schittny, J.C. Development of the lung. *Cell Tissue Res.* **2017**, *367*, 427–444. [CrossRef]
38. Lange, P.; Celli, B.; Agustí, A.; Boje Jensen, G.; Divo, M.; Faner, R.; Guerra, S.; Marott, J.L.; Martinez, F.D.; Martinez-Camblor, P.; et al. Lung-Function Trajectories Leading to Chronic Obstructive Pulmonary Disease. *N. Engl. J. Med.* **2015**, *373*, 111–122. [CrossRef]
39. Nogawa, H.; Ito, T. Branching Morphogenesis of Embryonic Mouse Lung Epithelium in Mesenchyme-Free Culture. *Development* **1995**, *121*, 1015–1022. [CrossRef]
40. Warburton, D.; Seth, R.; Shum, L.; Horcher, P.G.; Hall, F.L.; Werb, Z.; Slavkin, H.C. Epigenetic role of epidermal growth factor expression and signalling in embryonic mouse lung morphogenesis. *Dev. Biol.* **1992**, *149*, 123–133. [CrossRef]
41. Warburton, D.; El-Hashash, A.; Carraro, G.; Tiozzo, C.; Sala, F.; Rogers, O.; De Langhe, S.; Kemp, P.J.; Riccardi, D.; Torday, J.; et al. Lung Organogenesis. *Curr. Top. Dev. Biol.* **2010**, *90*, 73–158. [CrossRef]
42. Koopmans, T.; Rinkevich, Y. Mesothelial to mesenchyme transition as a major developmental and pathological player in trunk organs and their cavities. *Commun. Biol.* **2018**, *1*, 1–14. [CrossRef]
43. Ariza, L.; Carmona, R.; Cañete, A.; Cano, E.; Muñoz-Chápuli, R. Coelomic epithelium-derived cells in visceral morphogenesis. *Dev. Dyn.* **2016**, *245*, 307–322. [CrossRef] [PubMed]
44. White, A.C.; Xu, J.; Yin, Y.; Smith, C.; Schmid, G.; Ornitz, D.M. FGF9 and SHH signaling coordinate lung growth and development through regulation of distinct mesenchymal domains. *Development* **2006**, *133*, 1507–1517. [CrossRef] [PubMed]
45. Yin, Y.; Ornitz, D.M. FGF9 and FGF10 activate distinct signaling pathways to direct lung epithelial specification and branching. *Sci. Signal.* **2020**, *13*, 621. [CrossRef]
46. Nakamura, K.T.; McCray, P.B. Fetal airway smooth-muscle contractility and lung development. A player in the band or just someone in the audience? *Am. J. Respir. Cell Mol. Biol.* **2000**, *23*, 3–6. [CrossRef]
47. Fayon, M.; Andrieux, A.; Bara, I.; Rebola, M.; Labbé, A.; Marthan, R.; Berger, P. An Age-Wise Comparison of Human Airway Smooth Muscle Proliferative Capacity. *PLoS ONE* **2015**, *10*, e0122446. [CrossRef]
48. Bokka, K.K.; Jesudason, E.C.; Lozoya, O.A.; Guilak, F.; Warburton, D.; Lubkin, S.R. Morphogenetic Implications of Peristalsis-Driven Fluid Flow in the Embryonic Lung. *PLoS ONE* **2015**, *10*, e0132015. [CrossRef]
49. Nelson, C.M.; Gleghorn, J.P.; Pang, M.-F.; Jaslove, J.M.; Goodwin, K.; Varner, V.D.; Miller, E.; Radisky, D.C.; Stone, H.A. Microfluidic chest cavities reveal that transmural pressure controls the rate of lung development. *Development* **2017**, *144*, 4328–4335. [CrossRef] [PubMed]

50. Ornitz, D.M.; Itoh, N. Fibroblast Growth Factors. *Genome Biol.* **2001**, *2*, 3005.1–3005.12. [CrossRef]
51. Shannon, J.M.; Hyatt, B.A. Epithelial-Mesenchymal Interactions in the Developing Lung. *Annu. Rev. Physiol.* **2004**, *66*, 625–645. [CrossRef]
52. Bellusci, S.; Grindley, J.; Emoto, H.; Itoh, N.; Hogan, B.L. Fibroblast Growth Factor 10 (FGF10) and Branching Morphogenesis in the Embryonic Mouse Lung. *Development* **1997**, *124*, 4867–4878. [CrossRef]
53. Park, W.Y.; Miranda, B.; Lebeche, D.; Hashimoto, G.; Cardoso, W.V. FGF-10 Is a Chemotactic Factor for Distal Epithelial Buds during Lung Development. *Dev. Biol.* **1998**, *201*, 125–134. [CrossRef] [PubMed]
54. Lü, J.; Izvolsky, K.I.; Qian, J.; Cardoso, W.V. Identification of FGF10 Targets in the Embryonic Lung Epithelium during Bud Morphogenesis. *J. Biol. Chem.* **2005**, *280*, 4834–4841. [CrossRef]
55. Sekine, K.; Ohuchi, H.; Fujiwara, M.; Yamasaki, M.; Yoshizawa, T.; Sato, T.; Yagishita, N.; Matsui, D.; Koga, Y.; Itoh, N.; et al. Fgf10 is essential for limb and lung formation. *Nat. Genet.* **1999**, *21*, 138–141. [CrossRef]
56. Min, H.; Danilenko, D.M.; Scully, S.A.; Bolon, B.; Ring, B.D.; Tarpley, J.E.; DeRose, M.; Simonet, W.S. Fgf-10 is required for both limb and lung development and exhibits striking functional similarity to Drosophila branchless. *Genes Dev.* **1998**, *12*, 3156–3161. [CrossRef] [PubMed]
57. Taghizadeh, S.; Heiner, M.; Vazquez-Armendariz, A.I.; Wilhelm, J.; Herold, S.; Chen, C.; Zhang, J.S.; Bellusci, S. Characterization in mice of the resident mesenchymal niche maintaining AT2 stem cell proliferation in homeostasis and disease. *Stem Cells* **2021**, *39*, 1382–1394. [CrossRef] [PubMed]
58. Colvin, J.S.; Green, R.P.; Schmahl, J.; Capel, B.; Ornitz, D.M. Male-to-Female Sex Reversal in Mice Lacking Fibroblast Growth Factor 9. *Cell* **2001**, *104*, 875–889. [CrossRef]
59. Winnier, G.; Blessing, M.; Labosky, P.A.; Hogan, B.L. Bone morphogenetic protein-4 is required for mesoderm formation and patterning in the mouse. *Genes Dev.* **1995**, *9*, 2105–2116. [CrossRef]
60. Weaver, M.; Dunn, N.R.; Hogan, B.L. Bmp4 and Fgf10 Play Opposing Roles during Lung Bud Morphogenesis. *Development* **2000**, *127*, 2695–2704. [CrossRef]
61. Weaver, M.; Batts, L.; Hogan, B.L.M. Tissue interactions pattern the mesenchyme of the embryonic mouse lung. *Dev. Biol.* **2003**, *258*, 169–184. [CrossRef]
62. Bellusci, S.; Henderson, R.; Winnier, G.; Oikawa, T.; Hogan, B.L. Evidence from Normal Expression and Targeted Misexpression That Bone Morphogenetic Protein (Bmp-4) Plays a Role in Mouse Embryonic Lung Morphogenesis. *Development* **1996**, *122*, 1693–1702. [CrossRef]
63. Herriges, M.; Morrisey, E.E. Lung development: Orchestrating the generation and regeneration of a complex organ. *Development* **2014**, *141*, 502–513. [CrossRef]
64. Eblaghie, M.C.; Reedy, M.; Oliver, T.; Mishina, Y.; Hogan, B.L.M. Evidence that autocrine signaling through Bmpr1a regulates the proliferation, survival and morphogenetic behavior of distal lung epithelial cells. *Dev. Biol.* **2006**, *291*, 67–82. [CrossRef] [PubMed]
65. Shi, W.; Zhao, J.; Anderson, K.D.; Warburton, D. Gremlin negatively modulates BMP-4 induction of embryonic mouse lung branching morphogenesis. *Am. J. Physiol.-Lung Cell. Mol. Physiol.* **2001**, *280*, L1030–L1039. [CrossRef] [PubMed]
66. Hirashima, T.; Iwasa, Y.; Morishita, Y. Mechanisms for split localization of Fgf10 expression in early lung development. *Dev. Dyn.* **2009**, *238*, 2813–2822. [CrossRef]
67. Menshykau, D.; Kraemer, C.; Iber, D. Branch Mode Selection during Early Lung Development. *PLoS Comput. Biol.* **2012**, *8*, e1002377. [CrossRef]
68. Carballo, G.B.; Honorato, J.R.; de Lopes, G.P.F.; de Sampaio e Spohr, T.C.L. A highlight on Sonic hedgehog pathway. *Cell Commun. Signal.* **2018**, *16*, 11. [CrossRef]
69. Litingtung, Y.; Lei, L.; Westphal, H.; Chiang, C. Sonic hedgehog is essential to foregut development. *Nat. Genet.* **1998**, *20*, 58–61. [CrossRef]
70. Cardoso, W.V.; Lü, J. Regulation of early lung morphogenesis: Questions, facts and controversies. *Development* **2006**, *133*, 1611–1624. [CrossRef]
71. Pepicelli, C.V.; Lewis, P.M.; McMahon, A.P. Sonic hedgehog regulates branching morphogenesis in the mammalian lung. *Curr. Biol.* **1998**, *8*, 1083–1086. [CrossRef]
72. Peng, T.; Tian, Y.; Boogerd, C.J.; Lu, M.M.; Kadzik, R.S.; Stewart, K.M.; Evans, S.M.; Morrisey, E.E. Coordination of heart and lung co-development by a multipotent cardiopulmonary progenitor. *Nature* **2013**, *500*, 589–592. [CrossRef] [PubMed]
73. Miettinen, P.J.; Berger, J.E.; Meneses, J.; Phung, Y.; Pedersen, R.A.; Werb, Z.; Derynck, R. Epithelial immaturity and multiorgan failure in mice lacking epidermal growth factor receptor. *Nature* **1995**, *376*, 337–341. [CrossRef] [PubMed]
74. Miettinen, P.J.; Warburton, D.; Bu, D.; Zhao, J.-S.; Berger, J.E.; Minoo, P.; Koivisto, T.; Allen, L.; Dobbs, L.; Werb, Z.; et al. Impaired Lung Branching Morphogenesis in the Absence of Functional EGF Receptor. *Dev. Biol.* **1997**, *186*, 224–236. [CrossRef] [PubMed]
75. Seth, R.; Shum, L.; Wu, F.; Wuenschell, C.; Hall, F.L.; Slavkin, H.C.; Warburton, D. Role of Epidermal Growth Factor Expression in Early Mouse Embryo Lung Branching Morphogenesis in Culture: Antisense Oligodeoxynucleotide Inhibitory Strategy. *Dev. Biol.* **1993**, *158*, 555–559. [CrossRef] [PubMed]
76. Schuger, L.; Varani, J.; Mitra, R.; Gilbride, K. Retinoic acid stimulates mouse lung development by a mechanism involving epithelial-mesenchymal interaction and regulation of epidermal growth factor receptors. *Dev. Biol.* **1993**, *159*, 462–473. [CrossRef]
77. Mark, M.; Ghyselinck, N.B.; Chambon, P. Function of retinoid nuclear receptors: Lessons from Genetic and Pharmacological Dissections of the Retinoic Acid Signaling Pathway During Mouse Embryogenesis. *Annu. Rev. Pharmacol. Toxicol.* **2006**, *46*, 451–480. [CrossRef]

78. Mendelsohn, C.; Lohnes, D.; Décimo, D.; Lufkin, T.; LeMeur, M.; Chambon, P.; Mark, M. Function of the retinoic acid receptors (RARs) during development (II). Multiple abnormalities at various stages of organogenesis in RAR double mutants. *Development* **1994**, *120*, 2749–2771. [CrossRef]
79. Fernandes-Silva, H.; Araújo-Silva, H.; Correia-Pinto, J.; Moura, R.S. Retinoic Acid: A Key Regulator of Lung Development. *Biomolecules* **2020**, *10*, 152. [CrossRef]
80. Chen, F.; Desai, T.J.; Qian, J.; Niederreither, K.; Lü, J.; Cardoso, W.V. Inhibition of Tgfβ signaling by endogenous retinoic acid is essential for primary lung bud induction. *Development* **2007**, *134*, 2969–2979. [CrossRef]
81. Kahata, K.; Dadras, M.S.; Moustakas, A. TGF-β Family Signaling in Epithelial Differentiation and Epithelial–Mesenchymal Transition. *Cold Spring Harb. Perspect. Biol.* **2018**, *10*, a022194. [CrossRef] [PubMed]
82. Saito, A.; Horie, M.; Nagase, T. TGF-β Signaling in Lung Health and Disease. *Int. J. Mol. Sci.* **2018**, *19*, 2460. [CrossRef] [PubMed]
83. Bragg, A.D.; Moses, H.L.; Serra, R. Signaling to the epithelium is not sufficient to mediate all of the effects of transforming growth factor β and bone morphogenetic protein 4 on murine embryonic lung development. *Mech. Dev.* **2001**, *109*, 13–26. [CrossRef]
84. Warburton, D.; Bellusci, S.; De Langhe, S.; Del Moral, P.-M.; Fleury, V.; Mailleux, A.; Tefft, D.; Unbekandt, M.; Wang, K.; Shi, W. Molecular Mechanisms of Early Lung Specification and Branching Morphogenesis. *Pediatr. Res.* **2005**, *57*, 26–37. [CrossRef] [PubMed]
85. Kaartinen, V.; Voncken, J.W.; Shuler, C.; Warburton, D.; Bu, D.; Heisterkamp, N.; Groffen, J. Abnormal lung development and cleft palate in mice lacking TGF-beta 3 indicates defects of epithelial-mesenchymal interaction. *Nat. Genet.* **1995**, *11*, 415–421. [CrossRef] [PubMed]
86. Chen, H.; Zhuang, F.; Liu, Y.-H.; Xu, B.; del Moral, P.; Deng, W.; Chai, Y.; Kolb, M.; Gauldie, J.; Warburton, D.; et al. TGF-β receptor II in epithelia versus mesenchyme plays distinct roles in the developing lung. *Eur. Respir. J.* **2008**, *32*, 285–295. [CrossRef]
87. Xing, Y.; Li, C.; Hu, L.; Tiozzo, C.; Li, M.; Chai, Y.; Bellusci, S.; Anderson, S.; Minoo, P. Mechanisms of TGFβ Inhibition of Lung Endodermal Morphogenesis: The role of TβRII, Smads, Nkx2.1 and Pten. *Dev. Biol.* **2008**, *320*, 340–350. [CrossRef]
88. Edgar, B.A. From Cell Structure to Transcription: Hippo Forges a New Path. *Cell* **2006**, *124*, 267–273. [CrossRef]
89. Meng, Z.; Moroishi, T.; Guan, K.-L. Mechanisms of Hippo pathway regulation. *Genes Dev.* **2016**, *30*, 1–17. [CrossRef]
90. Makita, R.; Uchijima, Y.; Nishiyama, K.; Amano, T.; Chen, Q.; Takeuchi, T.; Mitani, A.; Nagase, T.; Yatomi, Y.; Aburatani, H.; et al. Multiple renal cysts, urinary concentration defects, and pulmonary emphysematous changes in mice lacking TAZ. *Am. J. Physiol. Ren. Physiol.* **2008**, *294*, F542–F553. [CrossRef] [PubMed]
91. Isago, H.; Mitani, A.; Mikami, Y.; Horie, M.; Urushiyama, H.; Hamamoto, R.; Terasaki, Y.; Nagase, T. Epithelial Expression of YAP and TAZ Is Sequentially Required in Lung Development. *Am. J. Respir. Cell Mol. Biol.* **2020**, *62*, 256–266. [CrossRef] [PubMed]
92. Little, D.R.; Lynch, A.M.; Yan, Y.; Akiyama, H.; Kimura, S.; Chen, J. Differential chromatin binding of the lung lineage transcription factor NKX2-1 resolves opposing murine alveolar cell fates in vivo. *Nat. Commun.* **2021**, *12*, 2509. [CrossRef] [PubMed]
93. Mahoney, J.E.; Mori, M.; Szymaniak, A.D.; Varelas, X.; Cardoso, W.V. The Hippo Pathway Effector Yap Controls Patterning and Differentiation of Airway Epithelial Progenitors. *Dev. Cell* **2014**, *30*, 137–150. [CrossRef]
94. Zhao, R.; Fallon, T.R.; Saladi, S.V.; Pardo-Saganta, A.; Villoria, J.; Mou, H.; Vinarsky, V.; Gonzalez-Celeiro, M.; Nunna, N.; Hariri, L.P.; et al. Yap Tunes Airway Epithelial Size and Architecture by Regulating the Identity, Maintenance, and Self-renewal of Stem Cells. *Dev. Cell* **2014**, *30*, 151–165. [CrossRef]
95. Volckaert, T.; Yuan, T.; Chao, C.-M.; Bell, H.; Sitaula, A.; Szimmtenings, L.; El Agha, E.; Chanda, D.; Majka, S.; Bellusci, S.; et al. Fgf10-Hippo epithelial mesenchymal crosstalk maintains and recruits lung basal stem cells. *Dev. Cell* **2017**, *43*, 48–59.e5. [CrossRef]
96. McGowan, S.E. Extracellular matrix and the regulation of lung development and repair1. *FASEB J.* **1992**, *6*, 2895–2904. [CrossRef] [PubMed]
97. Godoy-Guzmán, C.; San Martin, S.; Pereda, J. Proteoglycan and collagen expression during human air conducting system development. *Eur. J. Histochem.* **2012**, *56*, e29. [CrossRef]
98. Zhao, J.; Sime, P.J.; Bringas, P.; Gauldie, J.; Warburton, D. Adenovirus-mediated decorin gene transfer prevents TGF-β-induced inhibition of lung morphogenesis. *Am. J. Physiol.-Lung Cell. Mol. Physiol.* **1999**, *277*, L412–L422. [CrossRef] [PubMed]
99. Izvolsky, K.I.; Shoykhet, D.; Yang, Y.; Yu, Q.; Nugent, M.A.; Cardoso, W.V. Heparan sulfate–FGF10 interactions during lung morphogenesis. *Dev. Biol.* **2003**, *258*, 185–200. [CrossRef]
100. Kotton, D.N.; Morrisey, E.E. Lung regeneration: Mechanisms, applications and emerging stem cell populations. *Nat. Med.* **2014**, *20*, 822–832. [CrossRef]
101. Rock, J.R.; Onaitis, M.W.; Rawlins, E.L.; Lu, Y.; Clark, C.P.; Xue, Y.; Randell, S.H.; Hogan, B.L.M. Basal cells as stem cells of the mouse trachea and human airway epithelium. *Proc. Natl. Acad. Sci. USA* **2009**, *106*, 12771–12775. [CrossRef] [PubMed]
102. Rawlins, E.L.; Okubo, T.; Xue, Y.; Brass, D.M.; Auten, R.L.; Hasegawa, H.; Wang, F.; Hogan, B.L.M. The role of Scgb1a1+ Clara cells in the long-term maintenance and repair of lung airway, but not alveolar, epithelium. *Cell Stem Cell* **2009**, *4*, 525–534. [CrossRef]
103. Tata, P.R.; Mou, H.; Pardo-Saganta, A.; Zhao, R.; Prabhu, M.; Prabhu, M.; Law, B.M.; Vinarsky, V.; Cho, J.L.; Breton, S.; et al. Dedifferentiation of committed epithelial cells into stem cells in vivo. *Nature* **2013**, *503*, 218–223. [CrossRef]
104. Lafkas, D.; Shelton, A.; Chiu, C.; de Leon Boenig, G.; Chen, Y.; Stawicki, S.S.; Siltanen, C.; Reichelt, M.; Zhou, M.; Wu, X.; et al. Therapeutic antibodies reveal Notch control of transdifferentiation in the adult lung. *Nature* **2015**, *528*, 127–131. [CrossRef] [PubMed]

105. Peng, T.; Frank, D.B.; Kadzik, R.S.; Morley, M.P.; Rathi, K.S.; Wang, T.; Zhou, S.; Cheng, L.; Lu, M.M.; Morrisey, E.E. Hedgehog actively maintains adult lung quiescence and regulates repair and regeneration. *Nature* **2015**, *526*, 578–582. [CrossRef]
106. Fang, S.; Zhang, S.; Dai, H.; Hu, X.; Li, C.; Xing, Y. The role of pulmonary mesenchymal cells in airway epithelium regeneration during injury repair. *Stem Cell Res. Ther.* **2019**, *10*, 366. [CrossRef]
107. Zepp, J.A.; Zacharias, W.J.; Frank, D.B.; Cavanaugh, C.A.; Zhou, S.; Morley, M.P.; Morrisey, E.E. Distinct Mesenchymal Lineages and Niches Promote Epithelial Self-Renewal and Myofibrogenesis in the Lung. *Cell* **2017**, *170*, 1134–1148.e10. [CrossRef]
108. Barnes, J.L.; Gorin, Y. Myofibroblast differentiation during fibrosis: Role of NAD(P)H oxidases. *Kidney Int.* **2011**, *79*, 944–956. [CrossRef] [PubMed]
109. El Agha, E.; Kramann, R.; Schneider, R.K.; Li, X.; Seeger, W.; Humphreys, B.D.; Bellusci, S. Mesenchymal Stem Cells in Fibrotic Disease. *Cell Stem Cell* **2017**, *21*, 166–177. [CrossRef] [PubMed]
110. Buechler, M.B.; Pradhan, R.N.; Krishnamurty, A.T.; Cox, C.; Calviello, A.K.; Wang, A.W.; Yang, Y.A.; Tam, L.; Caothien, R.; Roose-Girma, M.; et al. Cross-tissue organization of the fibroblast lineage. *Nature* **2021**, *593*, 575–579. [CrossRef]
111. Yu, K.; Xu, J.; Liu, Z.; Sosic, D.; Shao, J.; Olson, E.N.; Towler, D.A.; Ornitz, D.M. Conditional inactivation of FGF receptor 2 reveals an essential role for FGF signaling in the regulation of osteoblast function and bone growth. *Development* **2003**, *130*, 3063–3074. [CrossRef]
112. Harrell, C.R.; Jankovic, M.G.; Fellabaum, C.; Volarevic, A.; Djonov, V.; Arsenijevic, A.; Volarevic, V. Molecular mechanisms responsible for anti-inflammatory and immunosuppressive effects of mesenchymal stem cell-derived factors. In *Tissue Engineering and Regenerative Medicine*; Pham, P.V., Ed.; Springer International Publishing: Cham, Switzerland, 2019; pp. 187–206.
113. Wolters, P.J.; Collard, H.R.; Jones, K.D. Pathogenesis of Idiopathic Pulmonary Fibrosis. *Annu. Rev. Pathol.* **2014**, *9*, 157–179. [CrossRef] [PubMed]
114. Gohy, S.T.; Hupin, C.; Pilette, C.; Ladjemi, M.Z. Chronic inflammatory airway diseases: The central role of the epithelium revisited. *Clin. Exp. Allergy* **2016**, *46*, 529–542. [CrossRef] [PubMed]
115. Rabe, K.F.; Watz, H. Chronic obstructive pulmonary disease. *Lancet* **2017**, *389*, 1931–1940. [CrossRef]
116. Barnes, P.J. Chronic Obstructive Pulmonary Disease. *N. Engl. J. Med.* **2000**, *343*, 1969–1971. [CrossRef] [PubMed]
117. Barnes, P.J.; Burney, P.G.J.; Silverman, E.K.; Celli, B.R.; Vestbo, J.; Wedzicha, J.A.; Wouters, E.F.M. Chronic obstructive pulmonary disease. *Nat. Rev. Dis. Primers* **2015**, *1*, 15076. [CrossRef] [PubMed]
118. Celli, B.R.; Wedzicha, J.A. Update on Clinical Aspects of Chronic Obstructive Pulmonary Disease. *N. Engl. J. Med.* **2019**, *381*, 1257–1266. [CrossRef] [PubMed]
119. Perez-Padilla, R.; Thirion-Romero, I.; Guzman, N. Underdiagnosis of chronic obstructive pulmonary disease: Should smokers be offered routine spirometry tests? *Expert Rev. Respir. Med.* **2018**, *12*, 83–85. [CrossRef] [PubMed]
120. Rabe, K.F.; Hurst, J.R.; Suissa, S. Cardiovascular disease and COPD: Dangerous liaisons? *Eur. Respir. Rev.* **2018**, *27*, 180057. [CrossRef]
121. Lee, A.L.; Goldstein, R.S. Gastroesophageal reflux disease in COPD: Links and risks. *Int. J. Chronic Obstr. Pulm. Dis.* **2015**, *10*, 1935–1949. [CrossRef]
122. Lahousse, L.; Tiemeier, H.; Ikram, M.A.; Brusselle, G.G. Chronic obstructive pulmonary disease and cerebrovascular disease: A comprehensive review. *Respir. Med.* **2015**, *109*, 1371–1380. [CrossRef] [PubMed]
123. Gea, J.; Sancho-Muñoz, A.; Chalela, R. Nutritional status and muscle dysfunction in chronic respiratory diseases: Stable phase versus acute exacerbations. *J. Thorac. Dis.* **2018**, *10*, S1332–S1354. [CrossRef]
124. Jaitovich, A.; Barreiro, E. Skeletal Muscle Dysfunction in Chronic Obstructive Pulmonary Disease. What We Know and Can Do for Our Patients. *Am. J. Respir. Crit. Care Med.* **2018**, *198*, 175–186. [CrossRef] [PubMed]
125. Smith, M.C.; Wrobel, J.P. Epidemiology and clinical impact of major comorbidities in patients with COPD. *Int. J. Chronic Obstr. Pulm. Dis.* **2014**, *9*, 871–888. [CrossRef]
126. Anderson, D.O. Smoking And Respiratory Disease. *Am. J. Public Health Nations Health* **1964**, *54*, 1856–1863. [CrossRef]
127. Fletcher, C.; Peto, R. The natural history of chronic airflow obstruction. *Br. Med. J.* **1977**, *1*, 1645–1648. [CrossRef]
128. Laniado-Laborín, R. Smoking and Chronic Obstructive Pulmonary Disease (COPD). Parallel Epidemics of the 21st Century. *Int. J. Environ. Res. Public Health* **2009**, *6*, 209–224. [CrossRef]
129. Fullerton, D.G.; Bruce, N.; Gordon, S.B. Indoor air pollution from biomass fuel smoke is a major health concern in the developing world. *Trans. R. Soc. Trop. Med. Hyg.* **2008**, *102*, 843–851. [CrossRef] [PubMed]
130. Salvi, S.S.; Barnes, P.J. Chronic obstructive pulmonary disease in non-smokers. *Lancet* **2009**, *374*, 733–743. [CrossRef]
131. Jiang, X.-Q.; Mei, X.-D.; Feng, D. Air pollution and chronic airway diseases: What should people know and do? *J. Thorac. Dis.* **2016**, *8*, E31–E40. [CrossRef]
132. Cohen, R.; Patel, A.; Green, F. Lung Disease Caused by Exposure to Coal Mine and Silica Dust. *Semin. Respir. Crit. Care Med.* **2008**, *29*, 651–661. [CrossRef] [PubMed]
133. Martinez, F.D. Early-Life Origins of Chronic Obstructive Pulmonary Disease. *N. Engl. J. Med.* **2016**, *375*, 871–878. [CrossRef]
134. Wilk, J.B.; Chen, T.-H.; Gottlieb, D.J.; Walter, R.E.; Nagle, M.W.; Brandler, B.J.; Myers, R.H.; Borecki, I.B.; Silverman, E.K.; Weiss, S.T.; et al. A genome-wide association study of pulmonary function measures in the Framingham Heart Study. *PLoS Genet.* **2009**, *5*, e1000429. [CrossRef] [PubMed]
135. Pillai, S.G.; Ge, D.; Zhu, G.; Kong, X.; Shianna, K.V.; Need, A.C.; Feng, S.; Hersh, C.P.; Bakke, P.; Gulsvik, A.; et al. A genome-wide association study in chronic obstructive pulmonary disease (COPD): Identification of two major susceptibility loci. *PLoS Genet.* **2009**, *5*, e1000421. [CrossRef] [PubMed]

136. Repapi, E.; Sayers, I.; Wain, L.V.; Burton, P.R.; Johnson, T.; Obeidat, M.; Zhao, J.H.; Ramasamy, A.; Zhai, G.; Vitart, V.; et al. Genome-wide association study identifies five loci associated with lung function. *Nat. Genet.* **2010**, *42*, 36–44. [CrossRef]
137. Soler Artigas, M.; Loth, D.W.; Wain, L.V.; Gharib, S.A.; Obeidat, M.; Tang, W.; Zhai, G.; Zhao, J.H.; Smith, A.V.; Huffman, J.E.; et al. Genome-wide association and large-scale follow up identifies 16 new loci influencing lung function. *Nat. Genet.* **2011**, *43*, 1082–1090. [CrossRef] [PubMed]
138. Chuang, P.-T.; McMahon, A.P. Vertebrate Hedgehog signalling modulated by induction of a Hedgehog-binding protein. *Nature* **1999**, *397*, 617–621. [CrossRef]
139. Smith, B.M.; Traboulsi, H.; Austin, J.H.M.; Manichaikul, A.; Hoffman, E.A.; Bleecker, E.R.; Cardoso, W.V.; Cooper, C.; Couper, D.J.; Dashnaw, S.M.; et al. Human airway branch variation and chronic obstructive pulmonary disease. *Proc. Natl. Acad. Sci. USA.* **2018**, *115*, E974–E981. [CrossRef]
140. Agusti, A.; Faner, R. Lung function trajectories in health and disease. *Lancet Respir. Med.* **2019**, *7*, 358–364. [CrossRef]
141. Barnes, P.J. Inflammatory mechanisms in patients with chronic obstructive pulmonary disease. *J. Allergy Clin. Immunol.* **2016**, *138*, 16–27. [CrossRef]
142. Shaykhiev, R.; Crystal, R.G. Early Events in the Pathogenesis of Chronic Obstructive Pulmonary Disease. Smoking-induced Reprogramming of Airway Epithelial Basal Progenitor Cells. *Ann. Am. Thorac. Soc.* **2014**, *11*, S252–S258. [CrossRef]
143. Baraldo, S.; Turato, G.; Badin, C.; Bazzan, E.; Beghé, B.; Zuin, R.; Calabrese, F.; Casoni, G.; Maestrelli, P.; Papi, A.; et al. Neutrophilic infiltration within the airway smooth muscle in patients with COPD. *Thorax* **2004**, *59*, 308–312. [CrossRef]
144. Leopold, P.L.; O'Mahony, M.J.; Lian, X.J.; Tilley, A.E.; Harvey, B.-G.; Crystal, R.G. Smoking Is Associated with Shortened Airway Cilia. *PLoS ONE* **2009**, *4*, e8157. [CrossRef]
145. Mahmood, M.Q.; Sohal, S.S.; Shukla, S.D.; Ward, C.; Hardikar, A.; Noor, W.D.; Muller, H.K.; Knight, D.A.; Walters, E.H. Epithelial mesenchymal transition in smokers: Large versus small airways and relation to airflow obstruction. *Int. J. Chronic Obs. Pulm. Dis.* **2015**, *10*, 1515–1524. [CrossRef]
146. Higham, A.; Quinn, A.M.; Cançado, J.E.D.; Singh, D. The pathology of small airways disease in COPD: Historical aspects and future directions. *Respir. Res.* **2019**, *20*, 1–11. [CrossRef]
147. Yang, J.; Antin, P.; Berx, G.; Blanpain, C.; Brabletz, T.; Bronner, M.; Campbell, K.; Cano, A.; Casanova, J.; Christofori, G.; et al. Guidelines and definitions for research on epithelial–mesenchymal transition. *Nat. Rev. Mol. Cell Biol.* **2020**, *21*, 341–352. [CrossRef]
148. Osei, E.T.; Hackett, T.-L. Epithelial-mesenchymal crosstalk in COPD: An update from in vitro model studies. *Int. J. Biochem. Cell Biol.* **2020**, *125*, 105775. [CrossRef]
149. Hogg, J.C. Pathophysiology of airflow limitation in chronic obstructive pulmonary disease. *Lancet* **2004**, *364*, 709–721. [CrossRef]
150. McDonough, J.E.; Yuan, R.; Suzuki, M.; Seyednejad, N.; Elliott, W.M.; Sanchez, P.G.; Wright, A.C.; Gefter, W.B.; Litzky, L.; Coxson, H.O.; et al. Small-Airway Obstruction and Emphysema in Chronic Obstructive Pulmonary Disease. *N. Engl. J. Med.* **2011**, *365*, 1567–1575. [CrossRef] [PubMed]
151. Barnes, P.J. Small airway fibrosis in COPD. *Int. J. Biochem. Cell Biol.* **2019**, *116*, 105598. [CrossRef] [PubMed]
152. Araya, J.; Cambier, S.; Markovics, J.A.; Wolters, P.; Jablons, D.; Hill, A.; Finkbeiner, W.; Jones, K.; Broaddus, V.C.; Sheppard, D.; et al. Squamous metaplasia amplifies pathologic epithelial-mesenchymal interactions in COPD patients. *J. Clin. Investig.* **2007**, *117*, 3551–3562. [CrossRef] [PubMed]
153. de Boer, W.I.; van Schadewijk, A.; Sont, J.K.; Sharma, H.S.; Stolk, J.; Hiemstra, P.S.; van Krieken, J.H. Transforming growth factor beta1 and recruitment of macrophages and mast cells in airways in chronic obstructive pulmonary disease. *Am. J. Respir. Crit. Care Med.* **1998**, *158*, 1951–1957. [CrossRef] [PubMed]
154. Gohy, S.T.; Hupin, C.; Fregimilicka, C.; Detry, B.R.; Bouzin, C.; Gaide Chevronay, H.; Lecocq, M.; Weynand, B.; Ladjemi, M.Z.; Pierreux, C.E.; et al. Imprinting of the COPD airway epithelium for dedifferentiation and mesenchymal transition. *Eur. Respir. J.* **2015**, *45*, 1258–1272. [CrossRef]
155. Eapen, M.S.; Lu, W.; Hackett, T.L.; Singhera, G.K.; Mahmood, M.Q.; Hardikar, A.; Ward, C.; Walters, E.H.; Sohal, S.S. Increased myofibroblasts in the small airways, and relationship to remodelling and functional changes in smokers and COPD patients: Potential role of epithelial-mesenchymal transition. *ERJ Open Res.* **2021**, *7*, 00876-2020. [CrossRef]
156. Karakioulaki, M.; Papakonstantinou, E.; Stolz, D. Extracellular matrix remodelling in COPD. *Eur. Respir. Rev.* **2020**, *29*, 190124. [CrossRef]
157. Annoni, R.; Lanças, T.; Tanigawa, R.Y.; Matsushita, M.D.M.; Fernezlian, S.D.M.; Bruno, A.; da Silva, L.F.F.; Roughley, P.J.; Battaglia, S.; Dolhnikoff, M.; et al. Extracellular matrix composition in COPD. *Eur. Respir. J.* **2012**, *40*, 1362–1373. [CrossRef]
158. Eurlings, I.M.; Dentener, M.A.; Cleutjens, J.P.; Peutz, C.J.; Rohde, G.G.; Wouters, E.F.; Reynaert, N.L. Similar matrix alterations in alveolar and small airway walls of COPD patients. *BMC Pulm. Med.* **2014**, *14*, 90. [CrossRef] [PubMed]
159. Bidan, C.M.; Veldsink, A.C.; Meurs, H.; Gosens, R. Airway and Extracellular Matrix Mechanics in COPD. *Front. Physiol.* **2015**, *6*, 346. [CrossRef]
160. Hedström, U.; Hallgren, O.; Öberg, L.; DeMicco, A.; Vaarala, O.; Westergren-Thorsson, G.; Zhou, X. Bronchial extracellular matrix from COPD patients induces altered gene expression in repopulated primary human bronchial epithelial cells. *Sci. Rep.* **2018**, *8*, 3502. [CrossRef]
161. Milara, J.; Peiró, T.; Serrano, A.; Cortijo, J. Epithelial to mesenchymal transition is increased in patients with COPD and induced by cigarette smoke. *Thorax* **2013**, *68*, 410–420. [CrossRef]

162. Nieto, M.A.; Cano, A. The epithelial–mesenchymal transition under control: Global programs to regulate epithelial plasticity. *Semin. Cancer Biol.* **2012**, *22*, 361–368. [CrossRef]
163. Kalluri, R.; Neilson, E.G. Epithelial-mesenchymal transition and its implications for fibrosis. *J. Clin. Investig.* **2003**, *112*, 1776–1784. [CrossRef] [PubMed]
164. Kalluri, R.; Weinberg, R.A. The basics of epithelial-mesenchymal transition. *J. Clin. Investig.* **2009**, *119*, 1420–1428. [CrossRef] [PubMed]
165. Zeisberg, M.; Neilson, E.G. Biomarkers for epithelial-mesenchymal transitions. *J. Clin. Investig.* **2009**, *119*, 1429–1437. [CrossRef] [PubMed]
166. Lee, J.M.; Dedhar, S.; Kalluri, R.; Thompson, E.W. The epithelial–mesenchymal transition: New insights in signaling, development, and disease. *J. Cell Biol.* **2006**, *172*, 973–981. [CrossRef]
167. Nieto, M.A.; Huang, R.Y.-J.; Jackson, R.A.; Thiery, J.P. EMT: 2016. *Cell* **2016**, *166*, 21–45. [CrossRef]
168. Soltani, A.; Sohal, S.S.; Reid, D.; Weston, S.; Wood-Baker, R.; Walters, E.H. Vessel-Associated Transforming Growth Factor-Beta1 (TGF-β1) Is Increased in the Bronchial Reticular Basement Membrane in COPD and Normal Smokers. *PLoS ONE* **2012**, *7*, e39736. [CrossRef]
169. Eapen, M.S.; Sharma, P.; Gaikwad, A.V.; Lu, W.; Myers, S.; Hansbro, P.M.; Sohal, S.S. Epithelial–mesenchymal transition is driven by transcriptional and post transcriptional modulations in COPD: Implications for disease progression and new therapeutics. *Int. J. Chronic Obstr. Pulm. Dis.* **2019**, *14*, 1603–1610. [CrossRef]
170. Baarsma, H.A.; Spanjer, A.I.R.; Haitsma, G.; Engelbertink, L.H.J.M.; Meurs, H.; Jonker, M.R.; Timens, W.; Postma, D.S.; Kerstjens, H.A.M.; Gosens, R. Activation of WNT/β-Catenin Signaling in Pulmonary Fibroblasts by TGF-β1 Is Increased in Chronic Obstructive Pulmonary Disease. *PLoS ONE* **2011**, *6*, e25450. [CrossRef]
171. Sohal, S.S.; Reid, D.; Soltani, A.; Ward, C.; Weston, S.; Muller, H.K.; Wood-Baker, R.; Walters, E.H. Evaluation of epithelial mesenchymal transition in patients with chronic obstructive pulmonary disease. *Respir. Res.* **2011**, *12*, 130. [CrossRef]
172. Heijink, I.H.; Brandenburg, S.M.; Postma, D.S.; van Oosterhout, A.J.M. Cigarette smoke impairs airway epithelial barrier function and cell-cell contact recovery. *Eur. Respir. J.* **2012**, *39*, 419–428. [CrossRef]
173. Sohal, S.S.; Reid, D.; Soltani, A.; Ward, C.; Weston, S.; Muller, H.K.; Wood-Baker, R.; Walters, E.H. Reticular basement membrane fragmentation and potential epithelial mesenchymal transition is exaggerated in the airways of smokers with chronic obstructive pulmonary disease. *Respirology* **2010**, *15*, 930–938. [CrossRef] [PubMed]
174. Johnson, P.R.; Roth, M.; Tamm, M.; Hughes, M.; Ge, Q.; King, G.; Burgess, J.K.; Black, J.L. Airway smooth muscle cell proliferation is increased in asthma. *Am. J. Respir. Crit. Care Med.* **2001**, *164*, 474–477. [CrossRef] [PubMed]
175. Trian, T.; Benard, G.; Begueret, H.; Rossignol, R.; Girodet, P.-O.; Ghosh, D.; Ousova, O.; Vernejoux, J.-M.; Marthan, R.; Tunon-de-Lara, J.-M.; et al. Bronchial smooth muscle remodeling involves calcium-dependent enhanced mitochondrial biogenesis in asthma. *J. Exp. Med.* **2007**, *204*, 3173–3181. [CrossRef] [PubMed]
176. Saetta, M.; Di Stefano, A.; Turato, G.; Facchini, F.M.; Corbino, L.; Mapp, C.E.; Maestrelli, P.; Ciaccia, A.; Fabbri, L.M. CD8+ T-lymphocytes in peripheral airways of smokers with chronic obstructive pulmonary disease. *Am. J. Respir. Crit. Care Med.* **1998**, *157*, 822–826. [CrossRef]
177. Antunes, M.A.; Abreu, S.C.; Cruz, F.F.; Teixeira, A.C.; Lopes-Pacheco, M.; Bandeira, E.; Olsen, P.C.; Diaz, B.L.; Takyia, C.M.; Freitas, I.P.; et al. Effects of different mesenchymal stromal cell sources and delivery routes in experimental emphysema. *Respir. Res.* **2014**, *15*, 1–14. [CrossRef]
178. Gu, W.; Song, L.; Li, X.-M.; Wang, D.; Guo, X.-J.; Xu, W.-G. Mesenchymal stem cells alleviate airway inflammation and emphysema in COPD through down-regulation of cyclooxygenase-2 via p38 and ERK MAPK pathways. *Sci. Rep.* **2015**, *5*, 8733. [CrossRef]
179. Weiss, D.J.; Casaburi, R.; Flannery, R.; LeRoux-Williams, M.; Tashkin, D.P. A Placebo-Controlled, Randomized Trial of Mesenchymal Stem Cells in COPD. *Chest* **2013**, *143*, 1590–1598. [CrossRef]
180. Le Thi Bich, P.; Nguyen Thi, H.; Dang Ngo Chau, H.; Phan Van, T.; Do, Q.; Dong Khac, H.; Le Van, D.; Nguyen Huy, L.; Mai Cong, K.; Ta Ba, T.; et al. Allogeneic umbilical cord-derived mesenchymal stem cell transplantation for treating chronic obstructive pulmonary disease: A pilot clinical study. *Stem Cell Res. Ther.* **2020**, *11*, 60. [CrossRef]
181. Antunes, M.A.; Lapa e Silva, J.R.; Rocco, P.R. Mesenchymal stromal cell therapy in COPD: From bench to bedside. *Int. J. Chronic Obs. Pulm. Dis.* **2017**, *12*, 3017–3027. [CrossRef]
182. Broekman, W.; Khedoe, P.P.S.J.; Schepers, K.; Roelofs, H.; Stolk, J.; Hiemstra, P.S. Mesenchymal stromal cells: A novel therapy for the treatment of chronic obstructive pulmonary disease? *Thorax* **2018**, *73*, 565–574. [CrossRef] [PubMed]
183. Ikonomou, L.; Wagner, D.E.; Turner, L.; Weiss, D.J. Translating Basic Research into Safe and Effective Cell-based Treatments for Respiratory Diseases. *Ann. ATS* **2019**, *16*, 657–668. [CrossRef] [PubMed]
184. Najar, M.; Johanne, M.P.; Jean Pierre, P.; Fahmi, H. Novel Insights for Improving the Therapeutic Safety and Efficiency of Mesenchymal Stromal Cells. *World J. Stem Cells* **2020**, *12*, 1474–1491. [CrossRef] [PubMed]
185. Paris, G.C.; Azevedo, A.A.; Ferreira, A.L.; Azevedo, Y.M.A.; Rainho, M.A.; Oliveira, G.P.; Silva, K.R.; Cortez, E.A.C.; Stumbo, A.C.; Carvalho, S.N.; et al. Therapeutic potential of mesenchymal stem cells in multiple organs affected by COVID-19. *Life Sci.* **2021**, *278*, 119510. [CrossRef]

3) Single cell RNA sequencing

Single-cell RNA sequencing is a powerful technique that has become incontournable for assessing transcriptomes with greater precision compared to bulk RNA sequencing or microarrays. It offers many advantages, but also some limitations, which are discussed in this section.

a) Definition

scRNA-seq was first used in 2009 to sequence the transcriptome of mouse blastomere division (Tang et al., 2009). Since then, the scRNA-seq method has evolved and the price has decreased, but the concept has remained the same.

A distinction is made between bulk RNA-seq, which represents the transcript of a mixture of cells, i.e., the average expression level of the genes of interest, and scRNA-seq, which provides the expression level of genes in each individual cell (R. Ahmed et al., 2022).

This makes it possible to identify a rare cell population, to compare the effect of a drug in exposed and control cells, to understand the heterogeneity of a tumour or cell differentiation during development, etc. (Saliba et al., 2014).

b) Workflow

scRNA-seq involves several steps depending on the protocol used, including single cell isolation, barcoded reverse transcription, cDNA amplification, library sequencing preparation, sequencing, and bioinformatics analysis, as shown in Figure 5 (Lafzi et al., 2018).

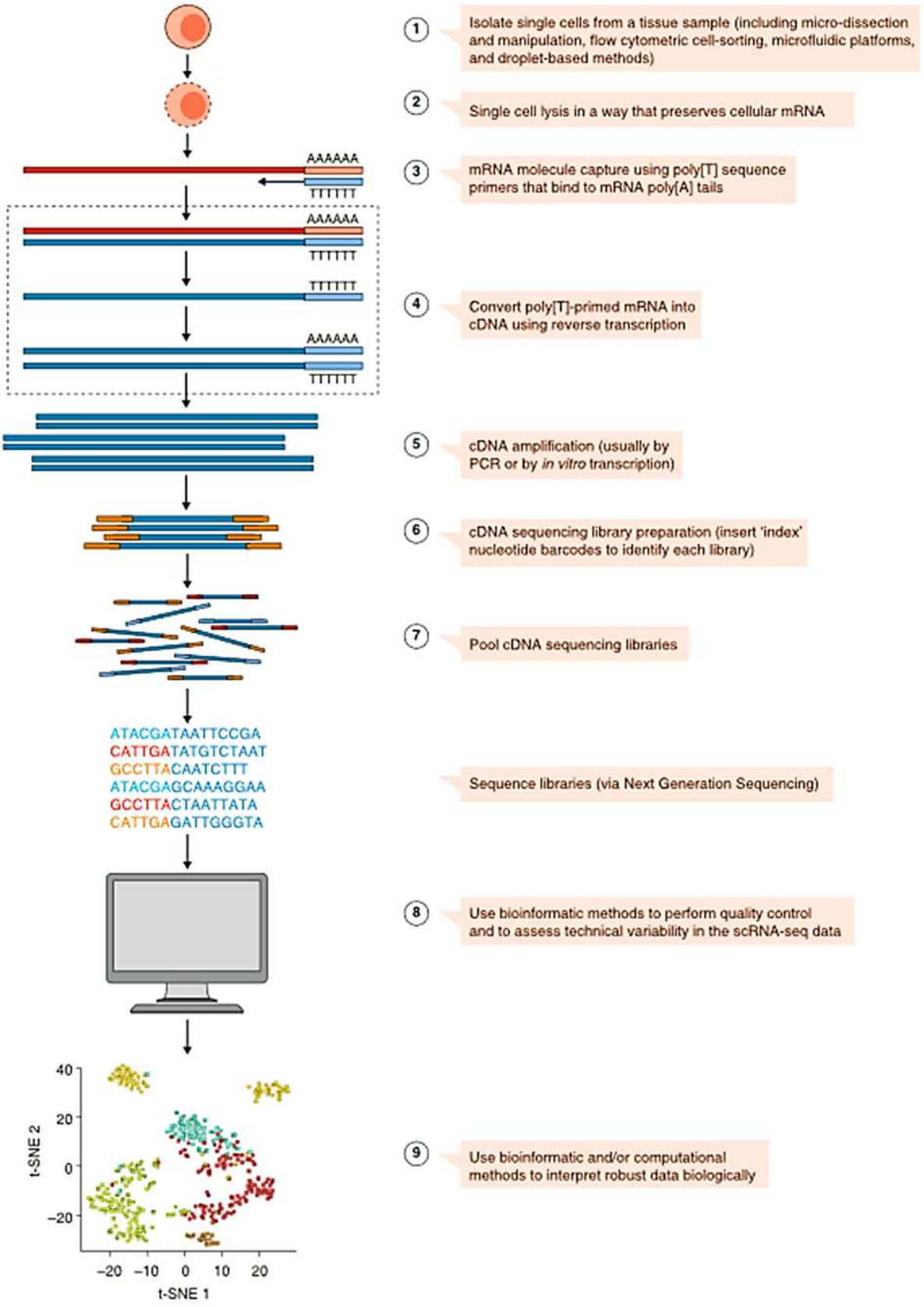

Figure 5 || ***General workflow of scRNA-seq***

From Haque Ashraful, et al., Genome Medicine, 2017

Single cell isolation and library preparation

The first step is to isolate the cells of interest from the tissue or model used for the experiment. This must be a suspension of viable single cells, but may also be a preserved sample or frozen nuclei from a tissue (Guillaumet-Adkins et al., 2017; Habib et al., 2016). It is important to consider that cell dissociation may affect cell viability and transcriptomic profile, such as the use of enzymatic dissociation (van den Brink et al., 2017).

Cells can then be enriched (optional) by fluorescence-activated cell sorting (FACS) or magnetic- activated cell sorting to remove dead cells and debris, as well as pipetting or microfluidics (Lafzi et al., 2018).

Cells are then lyzed and their RNA retro transcribed while preserving the single cells individuality. From example, high-throughput 10X Chromium technology uses droplets to barcode cells. This microfluidics system fuses each cell with an independent gel bead that contains all the material needed to perform reverse transcription. Each bead also contains a unique oligonucleotide barcode composed of adaptors and primers, a specific barcode, a diverse and distinct unique molecular identifier (UMI), and an oligonucleotide for polyadenylation (Figure 6) (Zheng et al., 2017). This enables the recognition of the cell of origin of each sequenced read (i.e., each transcript refers to an UMI that is specific to a given cell). Finally, all cDNAs are pooled, amplified by PCR and prepared for sequencing.

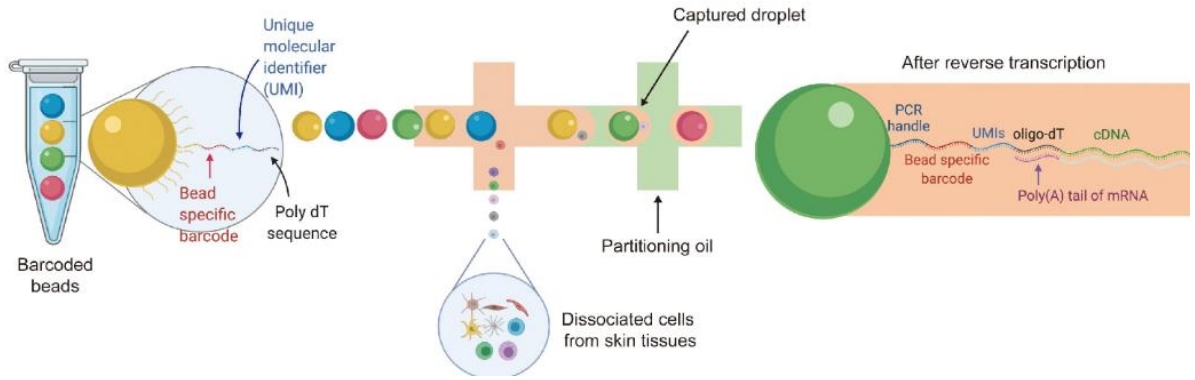

Figure 6 || ***Droplet-based microfluidic system***

From Kim Doyoung, et al., Journal of Dermatological Science, 2020

Bioinformatics analysis

After sequencing is complete, reads must be aligned to the genome using various mapping tools, such as the STAR aligner used by Cell Ranger for 10X Chromium scRNA-seq data to map reads to genes (Chen et al., 2019a). Only reads with high mapping quality should be used to generate the gene expression matrix, which estimates the amount of RNA in each cell for each gene.

scRNA-seq generates a huge amount of data that should be filtered by a quality control (QC) routine to eliminate cells with low capture efficiency, technical noise, multicells, or dead cells (Hwang et al., 2018). This prepossessing data can be analysed using Seurat, an R package that I used during my thesis to analyse our data.

Seurat was developed by the Sajita laboratory and is a highly documented all-in-one tool that can be used for QC, multiple dataset integration, and scRNA-seq analysis (Butler et al., 2018; Hao et al., 2021). It has been reported to be most frequently cited scRNA-seq analysis tool in scientific papers (Jovic et al., 2022).

Briefly, QC involves removing cells with an aberrant high or low number of unique genes and thus with a high percentage of mitochondria, which is typically found in dying cells (Márquez-Jurado et al., 2018). Then, the dataset needs to be normalised to fit the expression measure to the size of the library and to account for the sequencing depth (Evans et al., 2017).

Scaling (or linear transformation) then reduces the oversized counts and allows identification of the most varying genes across cell types. Unsupervised clustering can be performed to group cells, which is a useful method for identifying novel cell populations (Ranjan et al., 2021). Finally, clusters and cells can be visualised by tSNE (t-stochastic Neighbourhood Embedding) or UMAP (Uniform Manifold Approximation and Projection) (Do and Canzar, 2021).

c) Challenges and limitations

scRNA-seq, as mentioned earlier, is an essential tool that offers many opportunities in research. It has been possible to study inaccessible developmental stages in the human embryo, which was unbelievable a few years ago (Tyser et al., 2021; Zhai et al., 2022).

In lung research, it allows characterization of individual cell type populations in healthy and pathological donors, but also during lung development (He et al., 2022; Reyfman et al., 2019; Travaglini et al., 2020). Recently, the Human Cell Atlas Consortium aimed to map all human lung cells in health and disease (Luecken et al., 2022; Schiller et al., 2019). It includes the discovAIR database, where all scRNA-seq research from lung tissue are shared, promising a better understanding of lung diseases. In addition, technological advances provide the ability to visualize transcriptomes in conjunction with scRNA-seq, which improves multi-omics analysis (Chidester et al., 2023; Z. Xu et al., 2022).

However, the scRNA-seq method is subject to some limitations depending on which method is used. 10X Chromium is most efficient in the high-throughput method but has lower sensitivity compared to the low-throughput method (Ding et al., 2020). scRNA-seq also has a low capture efficiency and generates more background noise (Chen et al., 2019b).

In addition, it has been shown that some cells produce new RNA approximately every 3 seconds to maintain a constant state of RNA molecules (Maiuri et al., 2011). However, all the steps required to perform scRNA-seq take time and could interfere with the interpretation of the transcriptome. Nevertheless, new protocols have been developed that allow cryopreservation of cells prior to the scRNA-seq workflow without altering transcriptional profiles (Alles et al., 2017; Guillaumet-Adkins et al., 2017; Pohl et al., 2023).

Chapter II | Chronic respiratory diseases

Chronic lung diseases such as COPD and idiopathic pulmonary fibrosis (IPF), are one of the leading causes of death worldwide and are usually the result of environmental factors. This chapter focuses on COPD, from its physiopathology to its modelling, and addresses its main causes, air pollution and tobacco smoking.

1) COPD

Although certain genetic variants predispose to the development of COPD, the pathophysiological mechanisms of the disease remain poorly understood. Despite considerable efforts, to date there is no any effective therapy, i.e. treatment that could alter the natural history of COPD.

a) Definition and prevalence

Chronic obstructive pulmonary disease is the third leading cause of death worldwide, causing more than 3.2 million deaths in 2017 and an estimated 4.4 million by 2040 ("Global, regional, and national age-sex-specific mortality for 282 causes of death in 195 countries and territories, 1980–2017," 2018; Rabe and Watz, 2017). In some parts of the world, one in ten hospitalizations is due to exacerbations of COPD (Li et al., 2016). In France, the number of hospitalizations for COPD, especially in intensive care units, is steadily increasing, forcing authorities to increase budgetary resources and rethink strategies to treat this disease (Molinari et al., 2016, 2015; Poucineau et al., 2022). With increasing numbers of cases, the management of COPD remains a major challenge for treatment options and public health.

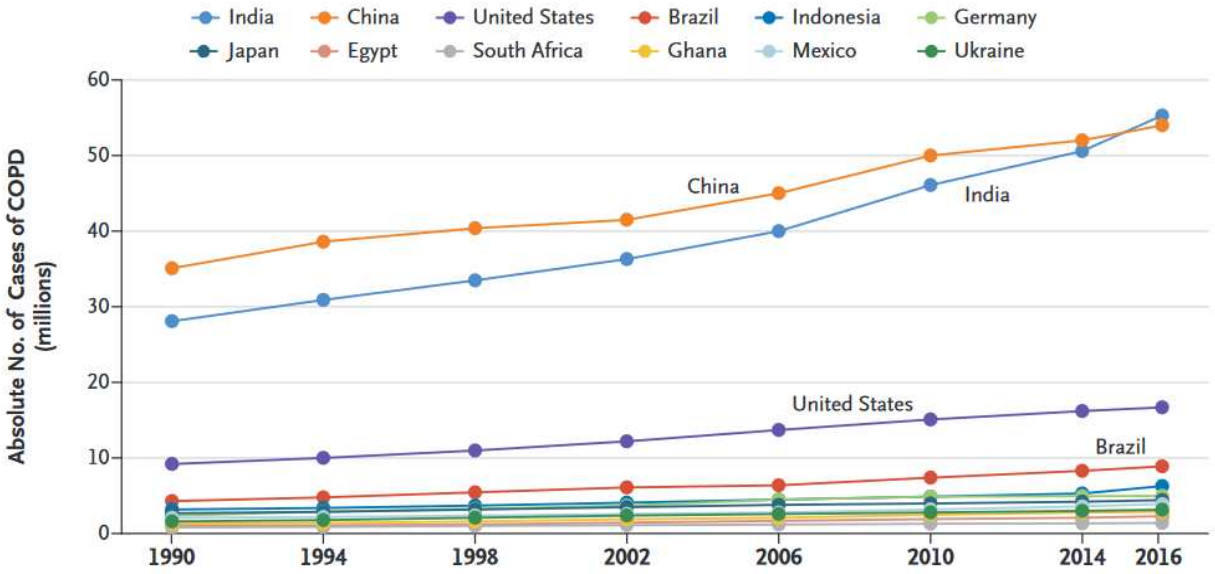

*Figure 7 || **Prevalence of COPD worldwide***

The number of cases of COPD increases in several country including China, India, United States and Brazil.

From Celli Bartolomé R., et al, New England Journal of Medicine, 2019

COPD is a chronic respiratory disease that leads permanent bronchial obstruction, and is usually diagnosed late, when irreversible damage is already substantial, as it begins at the small airway level where it progresses slowly (Barnes, 2000; Barnes et al., 2015; Celli and Wedzicha, 2019; Perez-Padilla et al., 2018). This led to the concept of the 'silent zone' of the lung, as small airway involvement classically does not translate into symptoms or impaired spirometry. In addition, high comorbidity with cardiac, gastrointestinal, cerebral, and muscular involvement increases the heterogeneity between patients (Gea et al., 2018; Hillas et al., 2015; Jaitovich and Barreiro, 2018; Lahousse et al., 2015; Lee and Goldstein, 2015; Rabe et al., 2018; Smith and Wrobel, 2014).

The main cause of COPD is smoking in westernized countries, but air pollution, occupational or non-occupational exposure to organic or mineral dusts or chemicals, woodfire smokes, genetic predisposition and repeated respiratory infections in childhood are also among the causes (Anderson, 1964; Cohen et al.,

2008; Fullerton et al., 2008; Jiang et al., 2016; Laniado-Laborín, 2009; Martinez, 2016; Ragland et al., 2019; Sakornsakolpat et al., 2019; Wadhwa et al., 2019).

Different molecular and cellular mechanisms are involved in all of these factors, which may vary from patient to patient, making COPD a multifactorial disease and leading to different subtypes whose specificities and characteristics remain to be identified (Agustí and Hogg, 2019).

b) Physiopathology of COPD

In the last decade, the pathophysiological hypothesis in the development of COPD has gradually shifted from an inflammatory concept to a disturbed homeostasis of the bronchial epithelium. The central role of the bronchial epithelium in controlling responses to external stimuli is now better understood (Gras et al., 2013; Lambrecht and Hammad, 2012; Whitsett and Alenghat, 2015).

Airflow obstruction

One of the first symptoms of COPD patients is the progressive deterioration of lung function, detected by spirometry as a reduction in expiratory airflow (Tantucci and Modina, 2012). This is the result of airway damage that involves many cellular remodelling processes (Figure 8).

In response to chronic exposure, including tobacco, pollution, toxins, and pathogens, an overproduction of mucus is maintained (Shaykhiev, 2019). This is associated with goblet cell hyperplasia and delayed mucus clearance, with impaired ciliary function and a decrease in the number of ciliated cells (Morgan et al., 2004; Rogers, 2000; Yaghi et al., 2012). This can result in severe mucous cough and disease exacerbations with respiratory distress. In addition, areas of squamous metaplasia with hyperproliferation of basal cells lead to thickening of the epithelium (Figure 8) (Araya et al., 2007; Rigden et al., 2016). Hypersecretion of extracellular matrix compounds and thickening of the mesenchymal compartment also lead to reduction of airflow and progressive emphysema (Barnes et al., 2015;

McDonough et al., 2011). In the end, small airway disease in COPD can be the result of i) luminal mucus plugging due to inversion of the ciliated to goblet cell ratio ii) luminal and parietal inflammatory infiltration, potentially associated with tertiary lymphoid islets iii) squamous metaplasia iv) loss of elastic recoil due to disruption of the alveolar attachments v) smooth muscle hyperplasia vi) enlargement of the submucosal glands vi) peribronchiolar fibrotic changes associated with excess of ECM deposition vii) wall oedema associated with enlarged peribronchiolar vessels and viii) lymphatic compression especially in patients with associated heart failure

Regarding the mesenchymal compartment, EMT has been shown to correlate with peribronchiolar fibrosis observed in COPD patients (Gohy et al., 2015; Milara et al., 2013; Nasri et al., 2021). Blockage of vascular endothelial growth factor receptor has also been associated with alveolar capillary apoptosis leading to emphysema and oxidative stress (Kasahara et al., 2000; Tuder et al., 2003).

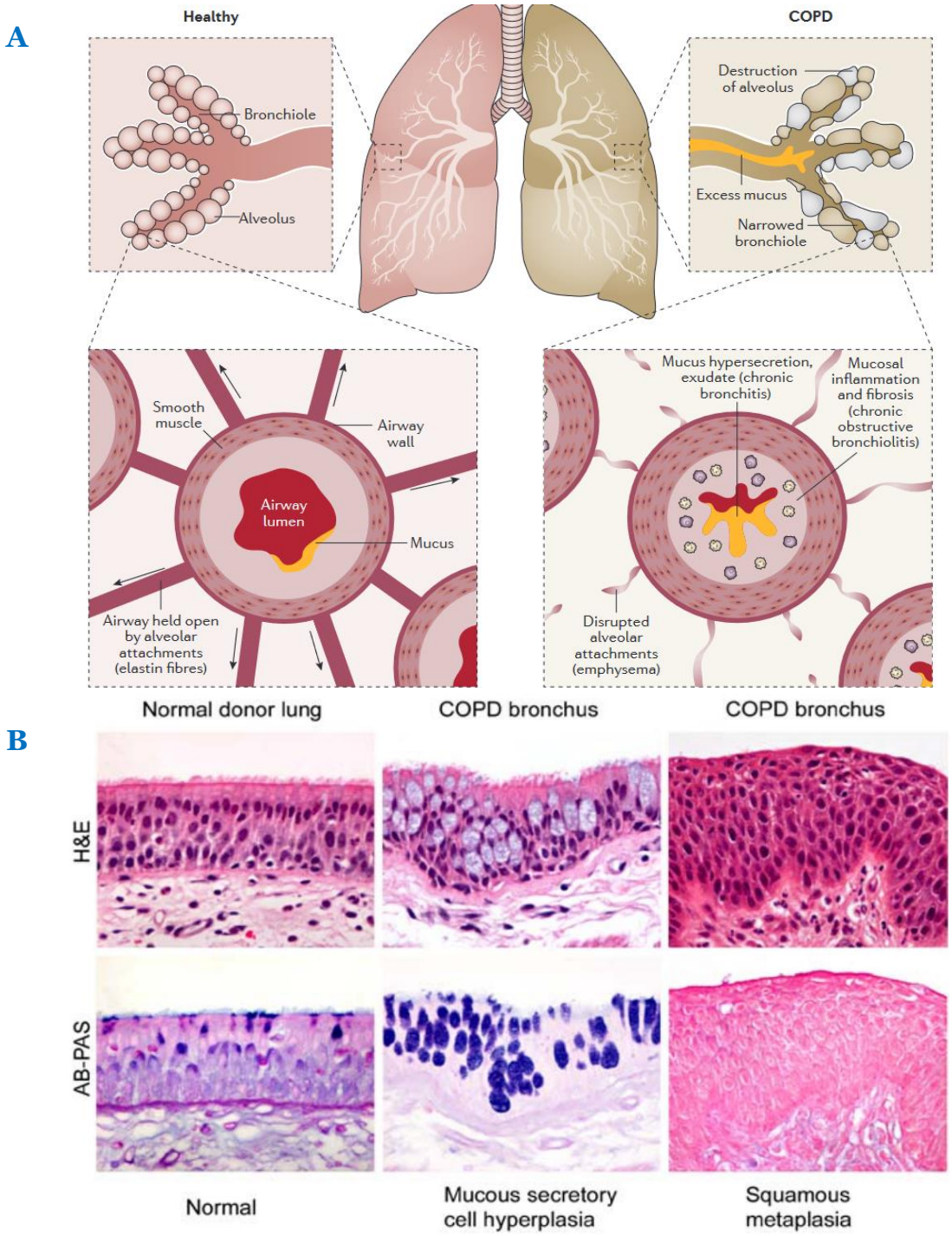

Figure 8 || ***Representation of COPD airways***

*(**A**) Illustration of airway obstruction in COPD associated with emphysema, mucosal inflammation, (**B**) mucus hypersecretion and squamous metaplasia.*

*Adapted from (**A**) Barnes Peter J., et al., Nature Reviews Disease Primers, 2015 and (**B**) Randell S. H. et al., Proceedings of the American Thoracic Society, 2006*

Senescence and oxidative stress

Cellular senescence is now recognised as one of the key processes underlying COPD (Adnot et al., 2015; Barnes, 2017). In mice, exposure to cigarette smoke has been shown to increase the number of senescent cells (Sorrentino et al., 2014; Wu et al., 2022). These cells can influence their neighbouring cells by acting on the microenvironment by secreting the senescence-associated secretory phenotype (SASP), which includes interleukins (IL-6, IL-1, IL1-α, IL1-β and IL-13), chemokines (CXCL8, CXCL1, CCL2) and their receptor (CXCR2), proteases (MMP1, MMP3, MMP10, MMP14), reactive oxygen species, extracellular matrix proteins (fibronectin, collagens, laminin), and other factors (Kumar et al., 2014; Rodier et al., 2009).

This is related to oxidative stress, which is known to promote senescence (Roger et al., 2021). The reactive oxygen species such as superoxide anions and hydroxyl radicals are highly reactive and oxidate proteins, DNA, and lipids, which promotes the inflammatory response in the lung (Kirkham and Rahman, 2006). The antioxidant response is the cellular response to oxidative stress. However, in COPD patients, activation of nuclear factor E2-related factor 2 (NRF2) has been shown to be impaired, resulting in a defect in the antioxidant response (Barnes, 2017). The inflammatory response could also be triggered by repeated infections.

Exacerbation

Viral and bacterial infections promote inflammatory responses in the lungs (Moldoveanu et al., 2008). However, this can lead to acute exacerbation in COPD patients and contribute to rapid decline of lung function (Dransfield et al., 2017) .

This is the case, for example, with the SARS-CoV-2 virus responsible for COVID -19 (Coronavirus Disease 2019), which marked the year 2020 (Samir, 2020). Indeed, COPD patients have been shown to have worse outcomes following SARS-CoV-2 infection (Gerayeli et al., 2021; Singh et al., 2022). They are also more susceptible to this infection because they have high levels of proinflammatory

cytokine proteins and mRNA and produce increased TMPRSS2 and CTSB cofactors that enable SARS-CoV-2 entry (Johansen et al., 2022).

c) Models of COPD

Currently, in addition to early prevention, only multidisciplinary treatment of patients can improve their quality of life. This includes smoking cessation, cessation of exposure to toxic substances, vaccines, resumption of physical activity and lung transplantation. In addition, the use of corticosteroids and long-acting bronchodilators reduce exacerbation rates, improve exercise tolerance, and quality of life; it has been suggested more recently that triple therapy (ICS-LABA-LAMA) reduced overall COPD mortality (Halpin et al., 2020; MacLeod et al., 2021). However, these treatments have limited long-term efficacy, and the heterogeneity of COPD makes patient management more complex (Agustí et al., 2017). In order to understand the pathophysiology and heterogeneity of COPD and devise adapted treatment to each patient, various models have been established.

Animals

Animal models are unavoidable in scientific research and are used in many studies related to understanding the development of COPD, modelling smoking, inflammation models, etc (Ghorani et al., 2017). Different animal species are used depending on the study, as shown in Table 1.

However, animal models have numerous limitations and do not allow to understand all the pathophysiological mechanisms of COPD because they have several drawbacks related to costs, differences between animal species and Human, heterogeneity, and lack of reproducibility for COPD (Tanner and Single, 2019).

Animal model	Advantages	Disadvantages
Mouse	Genetic heterogeneity Diverse responses to lung injury Low comparative costs Abundance of species-specific reagents	Replication of severe COPD not possible Low number of submucosal glands Monopodial airway branching Obligate nose-breather Size makes pulmonary parameter measurement difficult
Rat	Higher lung surface area compared to other rodents Greater size makes procedures easier Fibrotic depositions following smoke exposure	Lower genetic similarity to humans Monopodial airway structure Higher mucociliary clearance No goblet cells Fewer mucosal glands
Guinea pig	Similar inflammatory response to humans Uniform airway epithelial arrangement Docile Anthropomorphic response to smoke inhalation	Axon reflex controls inflammation Low genetic variation Few immunological markers Difficult blood collection (absence of tail/thick skin) Soft palate makes intratracheal procedures challenging
Hamster	Higher nitric oxide production More important ciliated epithelium Moderate goblet cell numbers	Low availability of species-specific reagents Low genetic diversity Aggressive behavior (handling more challenging)
Rabbit	Similar response to histamines and antigens More similar lung structure compared to rodents Larger size (procedures easier) Fairly docile Longer lifespan (longer studies)	Susceptibility to non-experimental disease No cough reflex Monopodial lung structure Different mucus composition
Dog	One lung can be used at a time Larger mouth (easier intratracheal procedure) Greater alveoli number More representative epithelial microstructure than rodents Cough reflex	Few species-specific reagents High housing costs
Pig	Large number of diverse breeds Organ-to-body weight similar to humans Similar lung structure to humans	Narrow mouth (intratracheal procedures challenging) High housing costs
Sheep	Docile Dichotomous lung structure Similar mucus content to humans Similar response to smoke inhalation	Disease progression poorly understood Few species-specific reagents High risk of vomiting during procedure Need for human breathing devices
Non-human primate	Dichotomous airway Genetic similarity Human reagents can be used	Skilled handling required Specialized equipment Higher costs Higher ethical implications

Table 1 || ***Summary of animal models of COPD***

Adapted from Tanner Lloyd, et al., Journal of Innate Immunity, 2020

Immortalised cell lines and primary cells

Immortalised cell lines such as BEAS-2B, have been used to study the effect of pollution, smoke extract and others to modelize COPD (Chen et al., 2020; Fuentes-Mattei et al., 2010; Garcia-Canton et al., 2013). However, it is not possible to generate a complete lung epithelium with immortalised cell lines.

Considerable improvements in cell culture techniques have made it possible to isolate and culture patient-derived cells. Primary cells are obtained from patients and can be grown in layers or cocultured with fibroblasts at air-liquid interface (Adamson et al., 2011; Lee et al., 1984). They allow better visualisation of the disease and its different subtypes in a specific way. They can also be purchased online through the vendor Epithelix™ for example, and used to study the effects of pollution (Despréaux et al., 2023).

However, primary lung cells are obtained by bronchoscopy. ALI cultures are keeping memory and exhibit features of the underlying disease (Vernisse et al., 2023) but this highly depends of the milieu used. In this procedure, only a small number of cells are collected, and rare cell types, neuroendocrine and mesenchymal cells could be lacking (Bukowy-Bieryłło, 2021; Gohy et al., 2015). Moreover, they cannot be kept in culture for a long time, which limits expansion capacities (Rayner et al., 2019). Therefore, new models have been developed with the potential to overcome the limitations currently observed.

Induced pluripotent stem cells

Induced pluripotent stem cells (iPSCs) are unspecialized stem cells that have the ability to self-renew and to differentiate into any cell type (Hui et al., 2011). Advances in iPSC generation and differentiation has opened the way for the non-invasive establishment of airway and lung epithelium *in vitro* by mimicking the lung development (Huang et al., 2014). However, lung derivation protocols are time-consuming, labour-intensive, and expensive (Mertens et al., 2017). This section will be more detailed chapter III.

2) Air pollution

Our anthropocene era is characterised by rapid and abrupt changes in our environment. The explosive growth of the world's population and human activities are significantly altering our environment and the air in the atmosphere. In the face of these changes, the adaptability and plasticity of our respiratory system may be overwhelmed by the rapid deterioration of air quality (Landrigan, 2017; Landrigan et al., 2018). In fact, a proportion of susceptible people chronically exposed to air pollutants develop COPD, which can lead to death.

a) Definition

Air pollution can be the result of natural events such as volcanic eruptions, sandstorms, massive thunderstorms, and massive forest fire smoke, but also human activities (industry, transportation, cooking and heating, chemical pollutants, etc.) (Cascio, 2018; Jia et al., 2023; Tam et al., 2016). These events influence and increase the particle composition that is normally present in indoor and outdoor air (Lonc et al., 2011).

Outdoor air pollution is composed of several components, including ozone (O_3), nitrogen monoxide (NO), carbon monoxide (CO), and particulate matter of various sizes (Leung, 2015). They are mainly emitted in urban areas by industries, carbon combustion, vehicles, airplanes, cigarette smoke, etc (Tu et al., 2022).

Many studies have shown that indoor air quality is also affected by outdoor activities (Asmi et al., 2004; He et al., 2004; Liu et al., 2006). Therefore, the term "exposome" has emerged to describe the totality of environmental influences to which a living being is exposed during its entire life (Figure 9) (Vineis et al., 2020; Wild, 2012). The toxicity of these constituents may depend on the level of exposure and may vary from person to person. However, the fact that they are found indoor increases respiratory issues and the development of diseases such as COPD and asthma, as well as other chronic diseases (Arku et al., 2018; Xu and Jin, 2003).

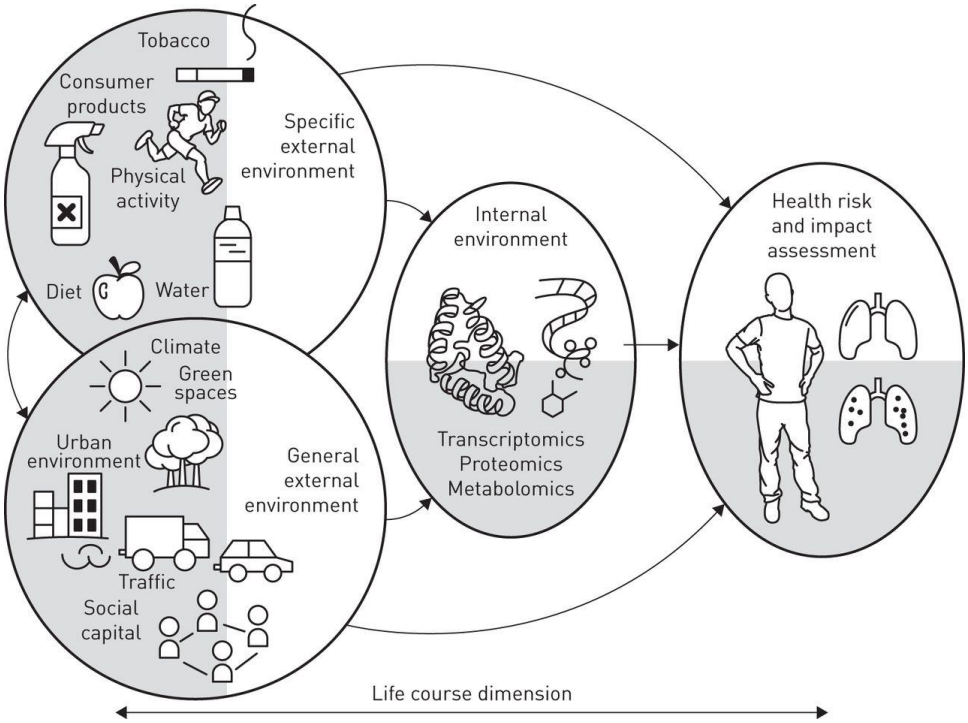

*Figure 9 || **The exposome concept***

External and internal environment influence the health throughout the lifespan

From Siroux Valérie, et al, European Respiratory Review, 2016

b) Classification

Air pollutants are classified into gaseous pollutants and particulate matters (PM).

Gaseous pollutants

Ozone is one of the most monitored gases because it is dangerous. It is concentrated in the stratosphere, the upper atmosphere, where it plays an essential role in shielding much of the sun's ultraviolet rays (Zhang et al., 2019). However, it is also found in the troposphere (lower part of the atmosphere), as oxides of nitrogen (NOx) and volatile organic compounds (VOCs) emitted by motor vehicles or other sources can react in the presence of solar irradiation, leading to ozone formation (Bell et al., 2007; Zhang et al., 2019). In terms of health, ozone pollution is associated with cardiovascular diseases, premature mortality, and respiratory syndromes (Orru et al., 2013).

Nitrogen dioxide has multiple sources such as fossil fuel combustion, vehicle emissions, furnaces, and water heaters (Atkinson et al., 2018; Singh et al., 2016). When inhaled, it penetrates deep into the lungs and is converted into nitric acid, which damages cells and causes dyspnea, bronchospasm, and cough (González-Martín et al., 2021). High levels of nitrogen dioxide are also associated with a reduction in plant growth and crop yield (Manisalidis et al., 2020).

Finally, carbon monoxide is also one of the most dangerous gaseous pollutants. It is emitted mainly from incomplete combustion processes, tobacco smoke, fireplaces, defective heating and densely travelled roads (Singh et al., 2016). Due to its formula, it has a higher affinity for hemoglobin than oxygen and, depending on its concentration, causes tissue hypoxia, irreversible cell damage, and death (González-Martín et al., 2021). It could be shown to independently trigger cardiac failure in patients free of cardiac disease (Andre et al., 2010).

Particulate matters

PM, together with ozone, are the most common air pollutants (Manisalidis et al., 2020). They are defined as airborne substances in the form of tiny solid particles. They often contain high concentrations of toxic metals such as chromium (Cr),

cadmium (Cd), manganese (Mn), nickel (Ni), lead (Pb), arsenic (As), Titanium (Ti), etc. (Martinelli et al., 2013).

They are classified according to their size, i.e., aerodynamic diameter. Thus, there are PM10 (aerodynamic diameter smaller than 10 µm), the fine particles PM2.5 (aerodynamic diameter smaller than 2.5 µm), and the ultrafine particles, also called nanoparticles PM0.1 (aerodynamic diameter smaller than 0.1 µm) (Nazaroff et al., 2004). PM composition and size vary according to their source (Brunekreef, 2005).

Regarding their size, particulate matter can enter indoor spaces through ventilation and reach the human body. PM10 has been shown to be more likely found in the upper respiratory tract, while PM2.5 and nanoparticles can reach the distal alveoli and enter the bloodstream through capillaries (Ma et al., 2022). PM2.5 could be associated with many diseases and is considered the main contributor to the health effects of air pollution (Bowe et al., 2019; Burnett et al., 2018; Martinelli et al., 2013).

c) Health impact

The World Health Organization (WHO) estimates that 7 million deaths per year are attributable to air pollution, including 4.2 million/year from outdoor air pollution and 3.8 million/year from indoor air pollution ("Air pollution," n.d.). According to the Global Burden of Disease Project 2015, a large-scale international study, air pollution, particularly from particulate matter (PM2.5), is the sixth most important risk factor for premature death and is partly responsible for 4.24 million deaths (Figure 10) (GBD 2013 Risk Factors Collaborators et al., 2015). In China, PM2.5 pollution has been shown to be responsible for 15.5% of total mortality, including 40.3% for stroke and 18.7% for chronic obstructive pulmonary disease (COPD) (Song et al., 2017). The benefits in terms of reducing mortality attributable to this pollution would be 85.2% if the air quality objectives for PM2.5 set by WHO were met.

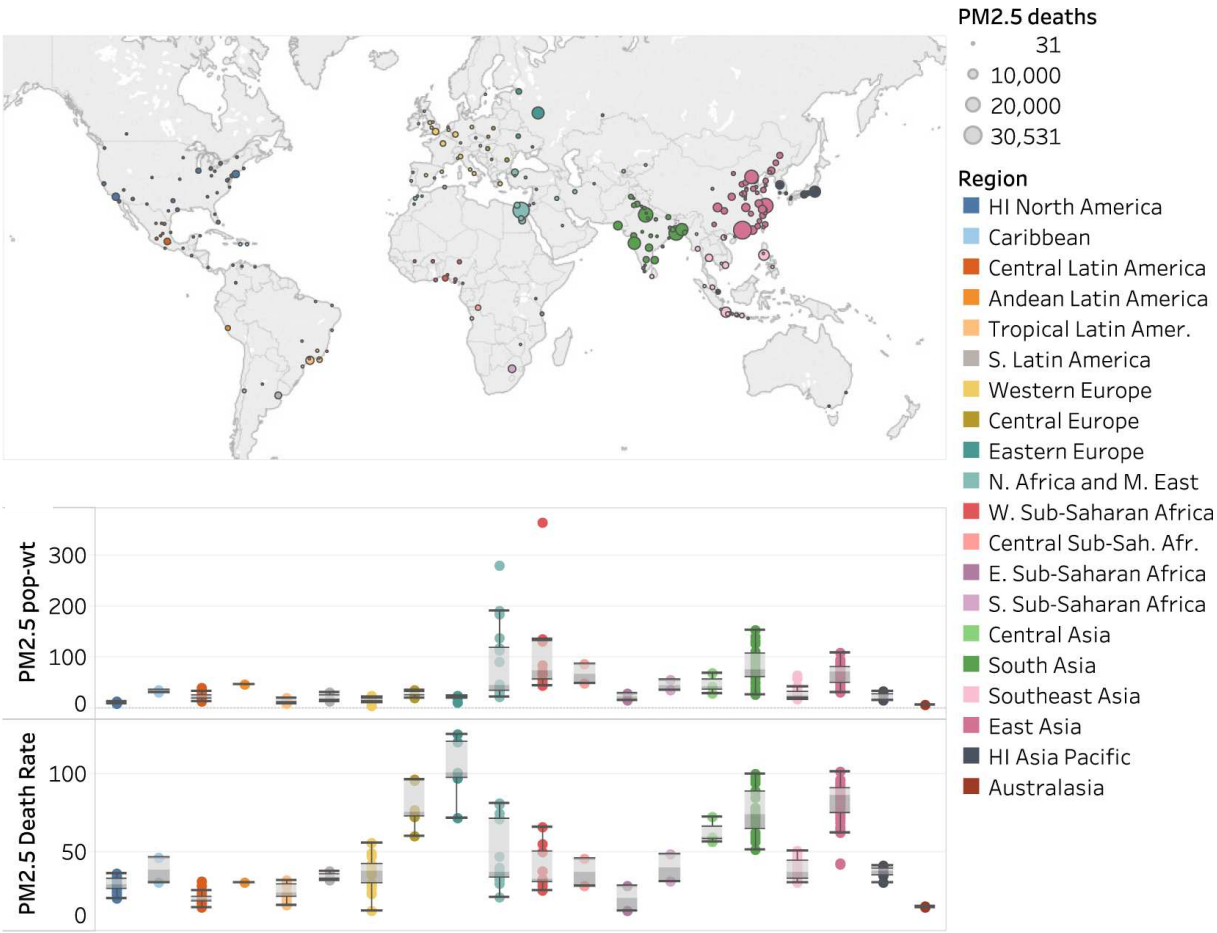

Figure 10 || ***Death attributable to PM2.5 in 2016***

High PM2.5 concentration was associated with cardiopulmonary diseases across 250 cities worldwide

Adapted from Anenberg Susan C. et al., Scientific Reports, 2019

As mentioned above, numerous epidemiological studies have demonstrated the association between air pollution and the decompensation of chronic respiratory diseases such as asthma and COPD (Bouazza et al., 2018; Liu et al., 2017). PM2.5 causes numerous lung cell damages, including oxidative stress and inflammation (Sierra-Vargas et al., 2023). It also increases the risk of influenza and SARS-CoV-2 infection (Scapini et al., 2023; Yu et al., 2022; Zhang et al., 2022). PM2.5 is also associated with an increase in hospitalisation for chronic heart disease, and may lead to depression (Feng et al., 2023; Fu et al., 2022). Consequently, preventive measures to promote environmental protection and limit pollutant emissions can

be taken by policy makers, of course, but also at the level of each individual to maintain healthy air (Bouza et al., 2022).

3) Tobacco smoking

Another important factor in the development of COPD is smoking, and as much as 90% of COPD cases are due to tobacco smoking in westernized countries (Tashkin and Murray, 2009). However, only susceptible smokers develop COPD, and the reason for this susceptibility is not clearly understood (Salvi and Barnes, 2009).

a) Definition

Tobacco smoke is a chemically complex mixture with more than 4000 compounds such as carbon monoxide, nicotine, formaldehyde, and benzene (Engstrom et al., 2003). It depends on the natural tobacco, but also the various ingredients added during the production process, and how the cigarettes are manufactured (Talhout et al., 2006).

Whole cigarette smoke can be divided into 2 phases: the particulate phase, which accounts for 5%, and the vapor phase (95%). Both phases contain various chemical compounds, and toxic combustion products have been shown to be found primarily in the vapor phase (Adamson et al., 2011). This is important because most *in vitro* studies treat cells with cigarette smoke extract (CSE), which involves contacting cigarette smoke with the cell culture medium (Cipollina et al., 2022). However, CSE represents only 5% of the whole cigarette smoke, which may be more relevant for studying the effects of tobacco on cells (Clunes et al., 2008; Phillips et al., 2005).

b) Health effects

Chronic exposure to cigarette smoke triggers inflammation that is correlated with COPD severity (Tran et al., 2021). In fact, inflammation is maintained because the

immune response, including alveolar macrophages, is dysregulated by smoking (Le et al., 2020; Lugg et al., 2022). Passive smoking has the same problem as active smoking in relation to the development of COPD (Dayal et al., 1994; Leuenberger et al., 1994).

Epithelial cells are also severely affected by smoking. Many studies reported cigarette smoke induced mucus hypersecretion, epithelial cell hyperplasia and impaired mucociliary clearance (Laube et al., 2019; Rabe and Watz, 2017).

In addition, oxidative stress has been shown to be associated with cigarette smoke, leading to the formation of oxygenated species and alteration of tissue repair. This is also associated with an increase in senescence, leading to progressive emphysema (Barnes, 2003; Vij et al., 2018).

Finally, tobacco smoking is also related to other morbidities, such as cardiovascular disease (Ambrose and Barua, 2004; Kaplan et al., 2017). Nevertheless, smoking cessation is one of the most cost-effective prevention interventions when combined with physical activity (Rigotti, 2013).

c) Electronic cigarette

The electronic cigarette has recently emerged as a solution to reduce or quit smoking. However, there are more and more studies that show its harmful effects. For example, vaping electronic cigarettes has been shown to cause inflammatory responses and affect the respiratory system (Glynos et al., 2018; Kalininskiy et al., 2021). The same is true for the trend of waterpipe (or shisha) smoking, which is equivalent to smoking more than 100 cigarettes and has been shown to increase oxidative stress (Figure 11) (Badran and Laher, 2020; Patil et al., 2022). All of this

affects various organs, including the lungs, but also cardiovascular functions and promotes cancer development (Münzel et al., 2020).

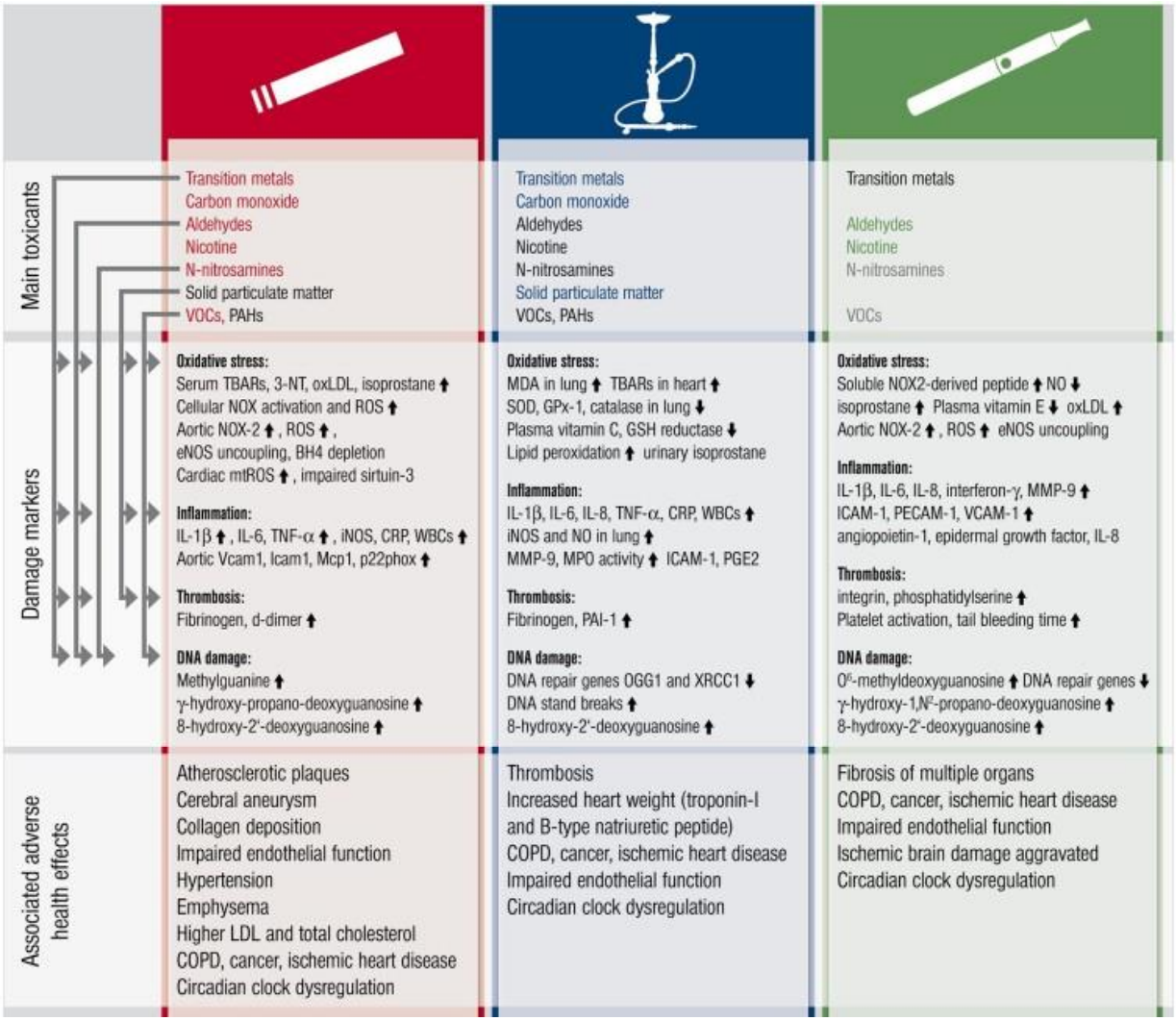

*Figure 11 || **Effects of smoking and vaping***

Cigarettes, shishas and e-cigarettes contain similar toxins that cause various cell damage

Adapted from Münzel Thomas, et al., European Heart Journal, 2020

Chapter III | Induced pluripotent stem cells to study lung development and diseases

Induced pluripotent stem cells offer a variety of research applications, including disease modelling. In this chapter, the properties, limits, and applications of iPSCs, including lung differentiation, will be discussed.

1) History and description

The human body is composed of more than 200 cell types. Each cell type has a specific function in maintaining homeostasis and the integrity of our body. Nevertheless, they all originate from a unicellular zygote.

a) Stem cell properties

Stem cells are characterised by their ability to self-renew, proliferate infinitely and differentiate into all cell types (the potency ability) (Chagastelles and Nardi, 2011; Kolios and Moodley, 2013).

"Potency" is the ability to give rise to a specialised cell type (Balistreri et al., 2020). Depending on the cell type, we can distinguish several potencies. The fertilised egg or zygote is a **totipotent** stem cell that gives rise to a whole body and extraembryonic tissues (e.g., placenta).

Inner cell mass, found in the blastocyte, are **pluripotent** stem cells that have the ability to form all human tissues (expect extraembryonic). In 1981, Evans and Kaufman isolated the ICM from mouse blastocysts and cultured them *in vitro* for the first time, giving rise to embryonic stem cells (ESCs) (Evans and Kaufman, 1981).

In 1998, the first human ESCs were cultured on feeder cells (mouse embryonic fibroblasts) (Thomson et al., 1998). These cell lines are able to proliferate without losing their pluripotency, maintaining their genetic stability after multiple passages, and differentiate into the three germ layers by forming teratomas in immunodeficient mice.

Potency is gradually lost during stem cell specialisation (Figure 12). This is the case with **multipotent** and **unipotent** cells, which are maintained during development and adulthood and can generate many (multi-) or one (uni-) specific cell types to maintain tissue integrity (Kolios and Moodley, 2013). This is the case, for example, with mesenchymal stem cells.

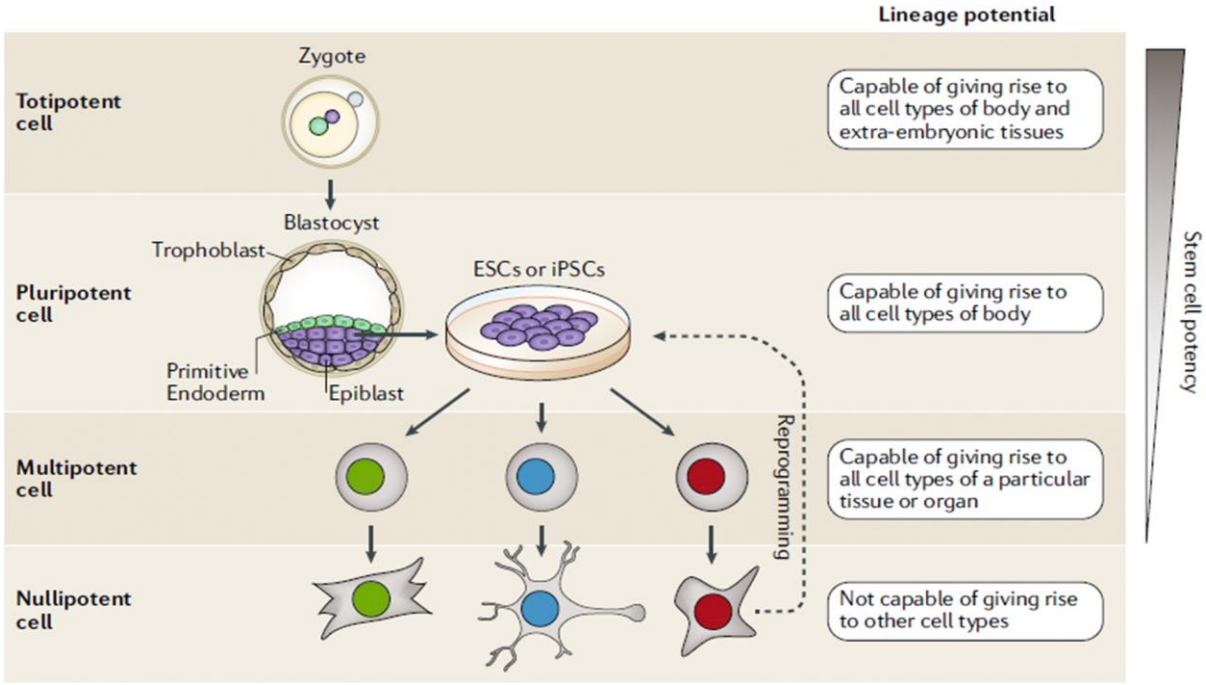

*Figure 12|| **Hierarchy of stem cells***

From Balistreri Carmela Rita, et al., Molecular Biology Reports, 2020

b) Generation of iPSCs

The ethical use of human ESCs is still debated worldwide because it involves the destruction of a human embryo (Volarevic et al., 2018). To circumvent this problem, Kazutoshi Takahashi and Shinya Yamanaka proposed in 2006 to reprogram somatic differentiated cells into iPSCs (Takahashi and Yamanaka, 2006).

To this end, they transiently overexpressed 24 factors, involved in murine pluripotency, in mouse fibroblasts and observed induction of pluripotency. They were then able to shorten the list to 4 transcription factors KLF4, SOX2, OCT3/4, and c-MYC, known as the "Yamanaka cocktail", that were as efficient as the 24 in inducing pluripotency (Takahashi and Yamanaka, 2006). These pluripotent cells were termed 'induced pluripotent stem cells (iPSCs)'. A year later, the same feat was achieved in human fibroblasts with the same cocktail (Takahashi et al., 2007), or with the variant list OCT4, SOX2, NANOG and LIN28 (Yu et al., 2007).

This scientific revolution earned the Nobel Prize in Medicine in 2012 to Shinya Yamanaka, a prize shared with John Gurdon for his earlier work on nuclear transfer of intestinal epithelial cells into denucleated Xenopus oocytes (Gurdon, 1962).

c) Challenges and limitations

Since the advent of iPSCs, many protocols have been developed to improve reprogramming, such as the use of nonintegrative vectors (Shi et al., 2017) or the reprogramming of mononucleated blood cells into iPSCs (Ahmed et al., 2021). Culture conditions also evolved from the use of feeder cells such as irradiated murine fibroblasts to the use of extracellular matrix (e.g., Matrigel® and Geltrex® made from animal and synthetic laminin or gelatin) and xeno-free media (Villa-Diaz et al., 2013).

iPSCs have been used intensively in developmental biology to understand the different steps of differentiation that lead to organ formation, as well as the

principle of auto-organisation, in particular in the blooming field of organoids (Lancaster and Knoblich, 2014). They also enable advances in medicine. In regenerative medicine, iPSCs are produced according to good manufacturing practices (GMP) and used as cell therapies (Yamanaka, 2012). In 2021, 90 trials were reported worldwide using iPSCs, but also human ESCs, with a major focus on degenerative eye diseases and immunotherapies against cancer (Figure 13) (Ilic and Ogilvie, 2022). iPSCs are also increasingly useful for disease modelling to recapitulate the phenotype of the disease with the genetic background of the patients to screen drug candidates (Doss and Sachinidis, 2019).

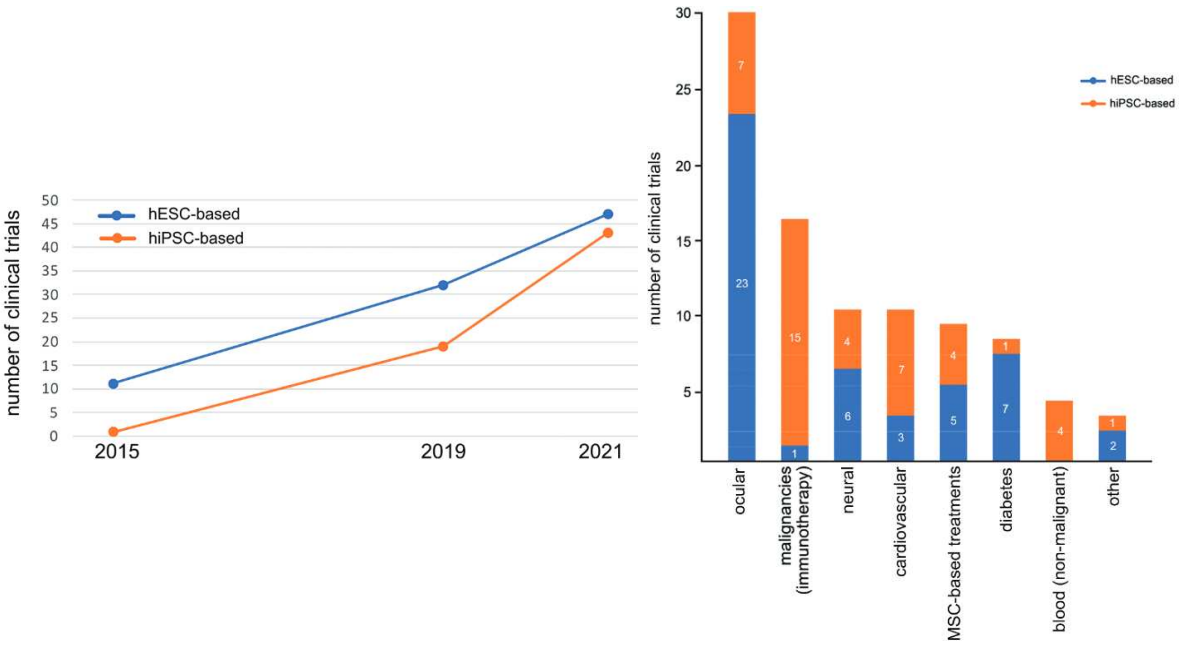

*Figure 13 || **Clinical trials with human ESC and human iPSC***

The number of clinical trials is increasing rapidly (left), with most trials performed in ocular diseases.

From Ilic Dusko, et al., Stem Cells, 2022

However, iPSCs have several limitations as sources of cell for clinical application. First, they have a potential for tumorigenicity, and may form teratomas if injected pluripotent (Ben-David and Benvenisty, 2011). In addition, when maintained in culture, iPSCs can also develop random genomic abnormalities, and some of those can be selected during passaging (Assou et al., 2020, 2018). To ensure genetic

integrity, iPSCs can be screened using karyotype, sequencing, and also digital droplet PCR to detect copy number variations (De Vos et al., 2020).

Furthermore, variability has been shown to exist between human iPSCs, mainly due to the genetic background of the patient (Rouhani et al., 2014). This could greatly limit personalised therapy, as differentiation is highly variable depending on the iPSCs lines used *in vitro* due to their DNA methylation, gene expression, and chromatin status (Nishizawa et al., 2016; Ortmann and Vallier, 2017). But this variability between iPSCs also confirms that they are relevant for human genetic studies.

Finally, *in vitro* conditions could also contribute to iPSCs variability by varying technical and culture conditions and affecting the reproducibility of differentiation protocols (Y. Liu et al., 2019). Several solutions have been proposed to circumvent this problem, such as using iPSCs banks or common cell lines and purifying key stages of the differentiated subpopulation, but the cost remains high (Huang et al., 2019; Inoue et al., 2014).

2) Applications

As mentioned earlier, iPSCs have the patient's genetic background and best representation of the patient's subtype (Mertens et al., 2017). Given the endless potentially unlimited use of iPSC, many studies have been conducted to mimic early steps of embryonic development and to model organs such as the lung and pathological developments.

a) 2D models

iPSCs are widely used in 2-dimentional (2D) cultures, to model and understand disease (Liu et al., 2018). In the past, human lung cell cultures were grown on plastic and immersed in media, but this has been replaced by air-liquid interface (ALI) culture, thanks to the use of Transwell® (Adamson et al., 2011). In this way,

the physiological function of the airway could be mimicked with an apico-basal polarity.

As discussed in the next section, advances in the development of protocols for targeted lung differentiation have enabled the use of iPSC. These include ALI cultures in which differentiated cells are plated on Transwell® coated with a matrix (Berical et al., 2022; Hawkins et al., 2021). But also a coculture model combining multiple cell types, including fibroblasts, endothelial cells and nerves (Burkhanova et al., 2022; Foisset et al., 2023).

However, 2D models have some limitations, especially in disease modeling. These include the lack of niche environment, loss of organ structure, and immaturity of the system (Liu et al., 2018).

b) Organoids

Organoid 3D cultures have revolutionized *in vitro* models and have a strong ethical potential (Koo et al., 2021). They can recapitulate the 3D structure of organs by self-assembling and growing with or without cell supports or on a scaffold that mimics the extracellular matrix (Liu et al., 2018). This is to be distinguished from "spheroid", which are mostly derived from primary cell lines and are less durable in 3D culture (Moreira et al., 2022).

The first human lung organoid generated from iPSCs was first developed in 2015 (Dye et al., 2015). This model consisted of all cell types of the lung, including epithelial cells of the proximal airway and cells of the mesenchymal lineage. Many other protocols have been developed to generate different lung organoids (Hawkins et al., 2021; Hein et al., 2022; Miller et al., 2019; Werder et al., 2022a). They are very promising for the study of respiratory diseases (Hughes et al., 2023).

To improve the relevance of organoids in practice, certain challenges must be overcome. Accumulation of dead cells and accessibility to nutrients by all cells are among the limitations of their use due to the lack of vascularization (Zhao et al.,

2022). In addition, organoids are heterogeneous and exhibit variabilities in size or in cell type composition, due to the lack of a standardized protocol (Hughes et al., 2023). Another limitation is the lack of mimicking of the physiological niche, which can be improved by co-culture or variant strategies such as organ-on-a-chip (Agraval and Chu, 2022).

c) Other models

In order to solve problems caused by the different 2D and 3D models, numerous solutions have been developed.

This is the case of organ-on-chip, which consists of microfluidic cell cultures to biomimetically recapitulate one or more tissues (Leung et al., 2022). This resulted in compartmentalised coculture of different cell types, including those derived from the same donor (Nawroth et al., 2019). For example, small airway-on-chip has been developed by assembling COPD patient-derived cells in the upper ALI microfluidic channel with small airway epithelial cells and in the lower microfluidic channel with endothelial cells perfused with the medium (Benam et al., 2016). Another, more complex organ-on-chip system was developed with cells from liver, heart and lung to study interaction between the tissue (Skardal et al., 2017).

In addition, recent studies have attempted to assemble multiple organoids to create assembloid models (Sharma et al., 2020). This may lead to advanced co-culture to mimic complex organs and study the function of each cell type. This has been used with iPSC-derived neurons of the dorsal and ventral forebrains, which were combined into an assembloid to mimic brain regions (Marton and Paşca, 2020). An assembloid-like culture using primary cells has also been reported in the lung but needs to be improved (Ramamoorthy et al., 2019; Varankar et al., 2022).

All these models have advantages and limitations depending on their use Table 2. Given the technological advances *in vitro*, perhaps the gastruloid models will improve our understanding of morphogenesis and organogenesis to overcome the problems encountered (Gupta et al., 2021).

In vitro model	Advantages	Disadvantages
2D ALI culture	• Simple and easy handling • Mimic lung ALI • Relatively low cost • Unlimited cell supply • Scalability (high-throughput) • Suitable for drug/particle permeability and transport studies	• Limited physiological relevance: immortalized/tumoral phenotypes, inability to recapitulate the native 3D pulmonary microenvironment
Spheroids/organoids	• Representation of multiple cell types • Strong cell-cell and cell-ECM communication (3D environment) • Emulation of native physiological processes in lung organoids (e.g., surfactant secretion, particle clearance) • Suitable for biobanking	• High cost • Complex protocols for spheroid/organoid development and maintenance • Usually associated with poorly characterized, animal-derived products (e.g., Matrigel) • Lack of vascularization and interorgan communication • Difficulty in achieving fully differentiated phenotypes • Lack of mechanical stimulation
Lung-on-chip devices	• Representation of multiple lung tissue compartments (epithelium, mesenchymal tissue, blood vessels) • Efficient emulation of the lung microenvironment (ALI, shear flow, biochemical gradients, mechanical breathing motions) • Possibility for interconnected multiorgan devices (interorgan communication) • Possibility for automation • Incorporation of sensors for monitoring of biological parameters	• Early stage of development • High complexity • Frequent lack of an immune compartment • Challenges in the co-culture of multiple cell types (particularly from different tissue compartments or organs) • Relatively low throughput

Table 2 || ***Advantages and disadvantages of in vitro lung models***

Adapted from Moreira, Anabela, et al., Advanced Biology, 2022

3) Mimicking lung development

Several teams worked to mimic the lung development *in vitro*. This includes the reproduction of the first stages of lung development, the study of the different factors affecting these stages, and at last, the specialisation in bronchial or alveolar epithelium.

a) Initial steps of differentiation

As shown in the first chapter, the development of the lung has been well described in the literature thanks to the mouse model, allowing the possibility to mimic the early steps of lung embryogenesis (Varma et al., 2020).

Dual activation of the Nodal/TGFβ and Wnt signaling pathways with a high concentration of activin A and the use of molecules such as CHIR99021 at low

concentration (GSK3b inhibitor) and LDN193189 (BMP receptor inhibitor) lead to differentiation into the definitive endoderm stage (Matsuno et al., 2016; McIntyre et al., 2014). This stage is characterized by the expression of various factors including SOX17 (SRY-Box Transcription Factor 17), FOXA2 (Forkhead box protein A2) and CXCR4 (C-X-C Motif Chemokine Receptor 4) (Green et al., 2011; Yiangou et al., 2018).

Further differentiation into the anterior foregut stage can be induced by dual inhibition of BMP and TGFβ signaling pathways (Green et al., 2011; Hawkins et al., 2016; Wong and Rossant, 2013). However, this dual inhibition at this stage may not be required in the absence of activin A (E. Ahmed et al., 2022; Matsuno et al., 2016).

Lung progenitors expressing NK2 homeobox 1 (NKX2.1), also known as thyroid transcription factor 1 (TTF1), are formed during the VAFE. This stage is generally induced only by dual inhibition of the TGFβ and BMP pathways depending on the protocol, respectively by SB-431542 and LDN193189 molecules, but sometimes also by additional activation of FGF signaling (Varma et al., 2020). This stage is also characterized by expression of the markers FOXA2 and SOX2 (SRY-box transcription factor 2) (Gomperts, 2014).

b) Lung specialization

Following the VAFE stage, proximal or distal airway epithelium can be generated by polarization using 2D ALI cultures or by 3D cultures (Figure 14). In contrast to the early stages of differentiation, which are more standardized and common between different laboratories, a variety of protocols can be used.

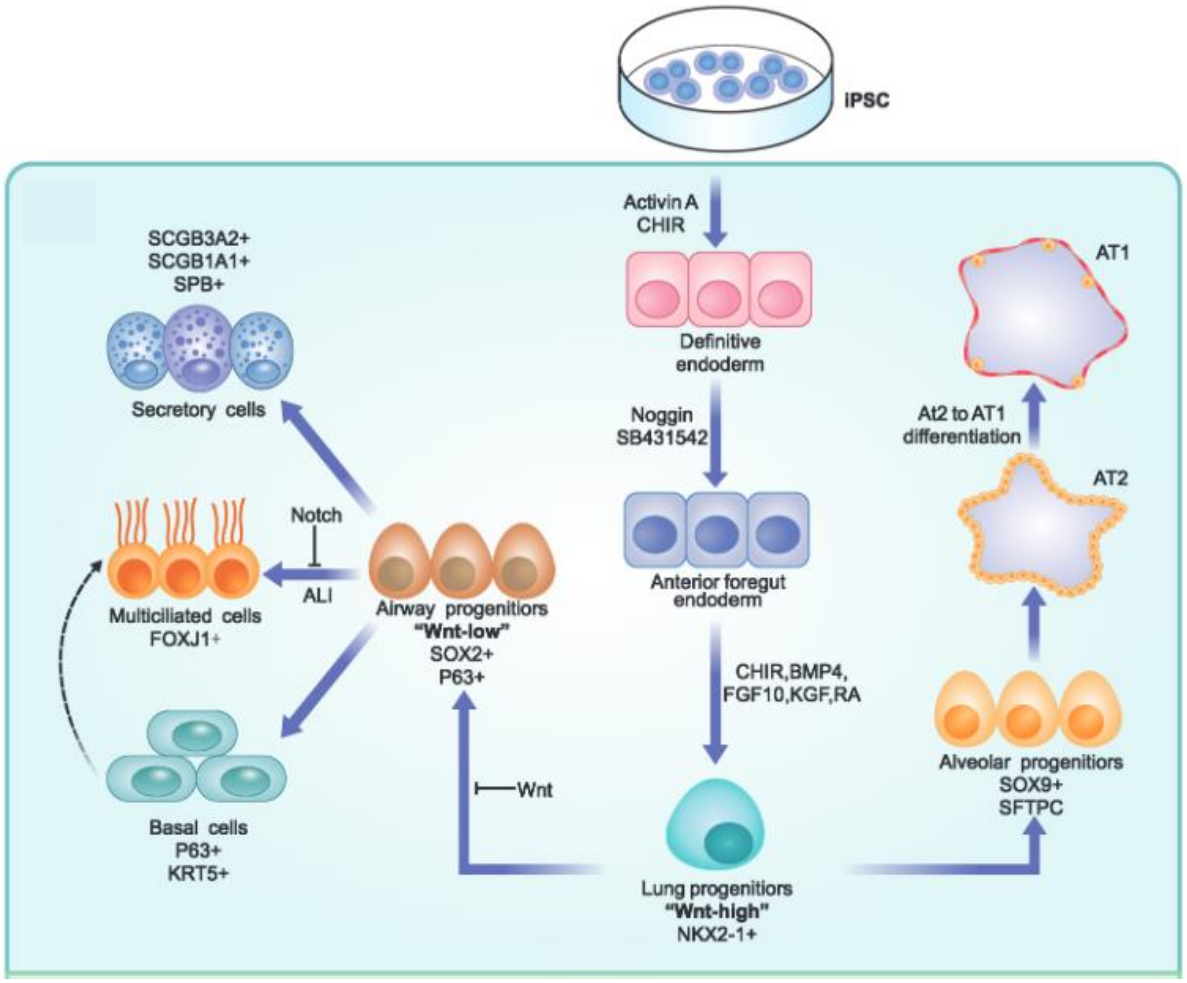

Figure 14 || ***Representation of in vitro iPSC derived airway***

Adapted from Yu Fenggang, et al., Stem Cells, 2023

Cell culture condition

NKX2.1 lung progenitor cells can be sorted to purify, expand, save time, and limit contamination using the NKX2.1-GFP (green fluorescent protein) reported cell line and membrane markers such as $CD47^{high}$ $C26^{low}$ (Drick et al., 2020; Hawkins et al., 2017; Hein et al., 2022).

The next steps of differentiation depend on the media, which can be commercial (example PneumaCult™) or self-produced. It contains several factors that promote

lung cell differentiation, including FGF7, FGF10 and BMP4 (Jacob et al., 2019; Rodrigues Toste de Carvalho et al., 2021).

Inhibition of Wnt signaling has been shown to promote bronchial differentiation, while its activation promotes alveolar differentiation (Figure 15) (Aros et al., 2021; Huang et al., 2014; Mou et al., 2012). As mentioned above, inhibition of Notch signaling favors the differentiation of functional ciliated cells. This can be done by adding DAPT or LY441575 to the media (Firth et al., 2014). All these steps take between 30 and 50 days to finally obtain a fully differentiated epithelium (Varma et al., 2020).

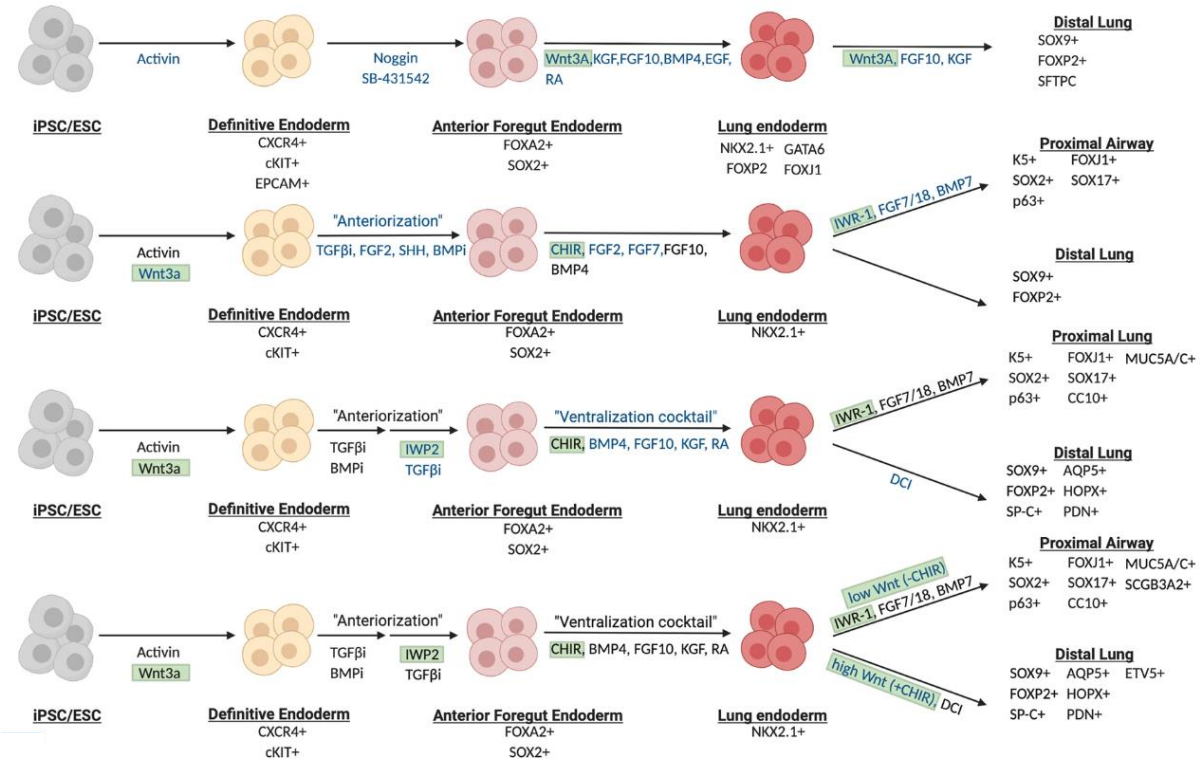

*Figure 15 || **Overview of protocols used in lung generation***

From 2011 (top) to 2017 (bottom) several protocols were developed to differentiate iPSC or ESC into distal and proximal airway cells.

Adapted from Aros Cody J., et al., Communications Biology, 2021

Cell specificity

Several markers are specifically expressed in each epithelial cell type, facilitating their identification during the differentiation process, for example by immunofluorescence or qPCR. This is the case for FOXJ1 for ciliated cells, KRT5 for basal cells, MUC5AC for goblet cells, CCSP for club cells, or CHGA for neuroendocrine cells (Table 3).

Region	Cell Type	Associated Markers for Cell Characterization
Proximal Airway	Ciliated Cell	FOXJ1, AcTUB
	Goblet Cell	MUC5AC, MUC5B
	Club Cell	CCSP, SCGB1A1, SCGB3A2
	Basal Cell	P63, KRT5, NGFR, ITGA6, ITGB4
Distal Lung	Alveolar epithelial cell type I (AEC I)	HOPX, PDPN, AQP5
	Alveolar epithelial cell type II (AEC II)	SPB, SPC, HT2-280

Table 3 || ***Specific markers of airway cells***

Adapted from Varma Ratna, et al., Advanced Drug Delivery Reviews, 2020

Advances in scRNA-seq technologies have led to better characterization of each cell type. With respect to the different protocols used to generate bronchial and alveolar epithelium, cellular heterogeneity and smaller subsets can be identified with the advent of these technologies (Yu et al., 2023). For example, an airway secretory cell population called “RAS” expressing SCGB3A2 has been found to regenerate alveoli in organoid cultures (Basil et al., 2022).

This is also true for transitory populations such as basaloid-like cells found after EMT induction in ALI primary cell culture (Uthaya Kumar et al., 2022). In *ex vivo* organoid cultures, a pre-alveolar type-1 transitional cell state has also been detected during differentiation of alveolar type-2 epithelial cells to AT1 (Kobayashi et al., 2020; Verheyden and Sun, 2020). All these advances make it possible to increase the value of in vitro models, especially in modelling lung diseases.

c) Exposure models

iPSCs provide the possibility to design and study the effect of various chemical compounds such as tobacco and pollution on human tissues (Figure 16). Culture methods are evolving, allowing for example, miniaturization of the ALI culture, leading to better screening capability (Bluhmki et al., 2021).

As mentioned earlier, tobacco smoking can be modelled by using CSE or exposure chambers. All of these techniques have demonstrated efficacy *in vitro*. For example, in primary cells cultured in ALI, CSE exposure was reported to promote goblet cell differentiation through activation of NOTCH3 (Bodas et al., 2021). In AT2 derived from iPSCs and also cultured in ALI, the transcriptomic response was assessed after CSE exposure and electronic cigarette vapor (Abo et al., 2022). This work allowed the authors to select genes of interest and knock them out using the CRISPR system to investigate their biological function and the relevance of their dysfunction in AT2 (Werder et al., 2022b).

It is also possible to study the effects of pollution using iPSC. In iPSC-derived alveolar organoid cultures, PM2.5 diesel pollution at concentrations of 50 and 100 µg/ml was shown to promote EMT and disrupt alveolar development (Kim et al., 2020). In addition, exposure to pollutants collected in France has been shown to induce a CYP1B1 inflammatory response in ALI cultures (Despréaux et al., 2023). Exposure to pollutants can be performed at the basal side directly in the media, but also in apical with an aerosol solution (Lu et al., 2022; Panas et al., 2014).

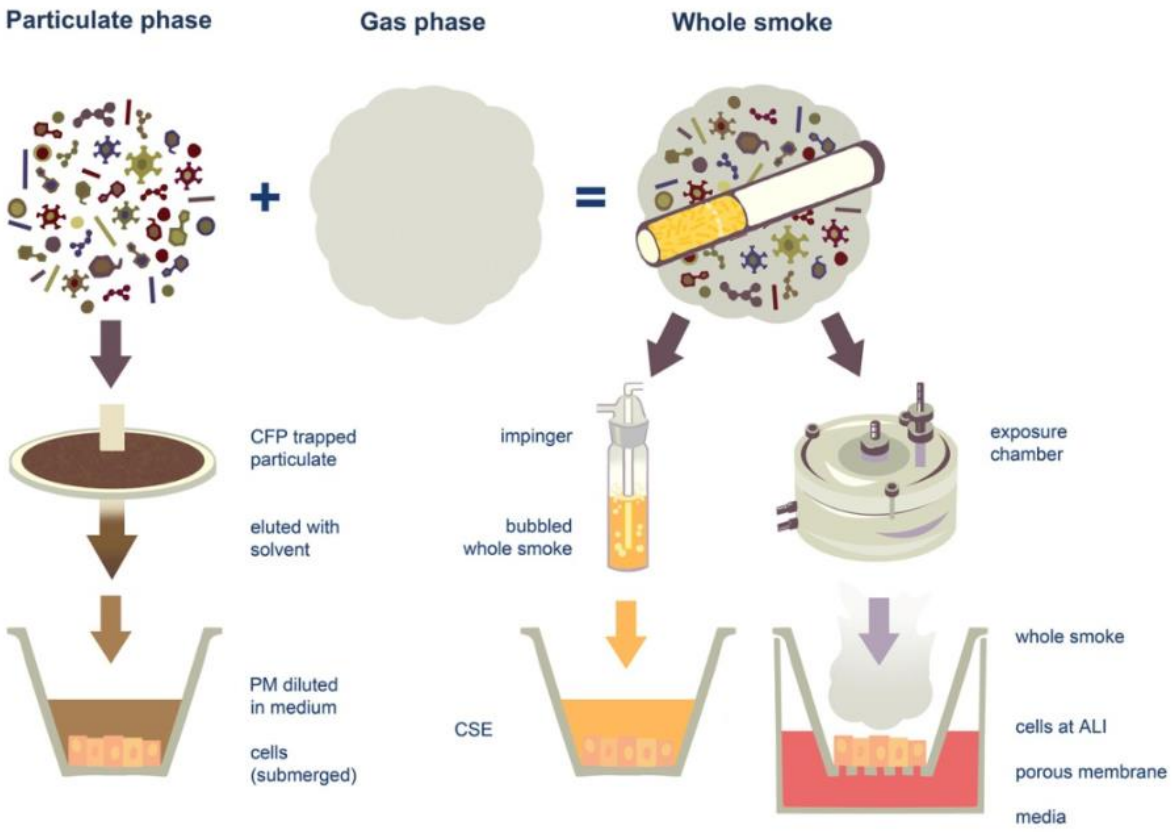

*Figure 16 || **Exposure method in vitro culture***

Particulate matters can be diluted in the medium and exposed to the cells (left). Tobacco smoking can be mimicked by CSE (middle) or by using an exposure chamber (right).

Adapted from Adamson Jason, et al., Bronchitis, 2011

AIMS OF THE THESIS

As described above, COPD is a multifactorial disease that develops insidiously over time. It is associated with airway remodelling, particularly of the bronchial epithelium, and alteration of the regenerative mechanism due to an acute inflammatory response.

Chronic pollution and tobacco smoking are major causes of COPD. However, only the more susceptible patients develop COPD. The specific physiopathological development and mechanism that occurs in the most susceptible patients is not clear but is essential to identify early biomarkers and therapeutic targets.

In fact, biomarkers have recently gained acceptance in the diagnosis and selection of patients most likely to benefit from specific treatments. The *in vitro* or *in vivo* identification and subsequent clinical validation of these biomarkers will allow to propose a treatment adapted to the patient and to predict the response to the proposed treatments.

As shown earlier, animal models have a variable phenotype compared with humans, and in vivo results are not truly applicable to human pathology. Also, the use of primary cells cultured in ALI is very robust, but bronchoscopy is an invasive method, and the number of cells collected as well as their in vitro expansion are limited, hence necessitating multiple donors.

By contrast, iPSCs are an unlimited source of cells. They can be differentiated into airways by mimicking the lung development of healthy and COPD donors. Due to their self-renewal property and a specific telomere maintenance system and metabolism, they can be kept in culture for an infinite time, with a doubling time of two days, implying a major in vitro amplification capacity. Combined with high-throughput sequencing techniques, substantial iPSC-derived epithelium quantities can provide the mean to screen for new COPD biomarkers.

iPSCs have been used in this context in many studies to differentiate them into bronchial or alveolar epithelium in ALI culture. At the start of this project, the laboratories of Professors John De Vos and Arnaud Bourdin have developed a protocol to differentiate iPSCs into functional bronchial epithelium cultured in ALI, called iALI.

The general objective of my thesis is to study the roles of pulmonary mesenchyme during bronchial epithelial development and response to pollution, in the context of the iALI model. We hypothesized that it may play an important role during the generation of iALI, but also in a pathological context.

Based on the iALI technology, the focus of my thesis was the following:

1) Developing a protocol of exposure to tobacco and pollution on iALI, derived from healthy and COPD donors, reproducing in vitro certain pathophysiological phenomena that develop in vivo

2) Precisely identify the effects of pollution exposure on iALI using scRNA-seq on a susceptible iPSCs cell line

3) Study the interaction between epithelium and mesenchymal compartment during the development of iALI

RESULTS

Article 1

The aim of this study was to provide evidence that iALI can be used to model biological responses induced by exposure to air pollution particles.

During my thesis, I set up a robust protocol for PM2.5 exposure in iALI. To determine the effects of this exposure on the different cell types composing iALI, we performed scRNA-seq and analysed the generated data using the Seurat package that I learned as part of my thesis.

Additional results confirming the presence of a transitory population described in the manuscript, which were not available at the time of writing this manuscript, will be added later.

A human pluripotent stem cells bronchial epithelium model with submucosae to study pollution exposure

Amel Nasri[1], Chloé Bourguignon[1], Florent Foisset[1], Carine Bourdais[1], Engi Ahmed[2,3], Aurélie Fort[2], Markus Tammia[4], Tina Baker[4], Kristofer Thorn[4], Daniel Noel[1], Isabelle Vachier[2], Said Assou[1], Arnaud Bourdin[2,3,*], John De Vos[1,5*]

[1] IRMB, Univ Montpellier, INSERM, CHU Montpellier, Montpellier, France

[2] Department of Respiratory Diseases, Univ Montpellier, CHU Montpellier, INSERM, Montpellier, France

[3] PhyMedExp, Univ Montpellier, INSERM, CHU Montpellier, Montpellier, France

[4] AstraZeneca, Göteborg, Sweden

[5] Department of Cell and Tissue Engineering, Univ Montpellier, CHU Montpellier, Montpellier, France

[*] To whom correspondence should be addressed:
John De Vos. IRMB, Hôpital St Eloi, 80 avenue Augustin Fliche. 34295 Montpellier. France. +33 467337888 john.devos@inserm.fr
Arnaud Bourdin, Department of Respiratory Diseases, Hôpital Arnaud de Villeneuve, Montpellier, France. Email: a-bourdin@chu-montpellier.fr

Key words: plasticity, pollution, air-liquid interface, single-cell RNA-sequencing

ABSTRACT

Induced pluripotent stem cells (iPSCs) offer a new approach for modelling lung diseases such as chronic obstructive pulmonary disease (COPD). We have generated a functional air-liquid interface bronchial epithelium from human iPSC (iALI) that recapitulates the main cell types of the tissue, including a marked sub epithelial stroma. Using this model, we measured the effects of pollution exposure, using single-cell RNA sequencing, and identified gene signatures induced by pollutant exposure. One of

these signatures is common to all cell types, while several others are restricted to specific cell types. These data show that iALI is a promising tool for modelling the respiratory airway response to environmental pollution.

INTRODUCTION

Chronic lung diseases such as Chronic Obstructive Pulmonary Disease (COPD) are one of the first leading causes of death in the world and are generally the consequence of bronchus exposure (Barnes et al., 2015; Rabe and Watz, 2017). Air pollution was responsible of 9 million deaths worldwide in 2015 (Landrigan et al., 2018) and related to several disease, including COPD (Ko and Kyung, 2022; Soriano et al., 2020). Incomplete combustion of fuels and biomass results in combustion-derived particulate matter (PM). Fine particulate matter with a diameter of less than 2.5 µm (Kim et al., 2015) ($PM_{2.5}$) is a well-documented atmospheric pollution which can penetrate deep into the respiratory tree and produce more adverse effects than coarse particles with a 2.5 – 10µ diameter (Landrigan et al., 2018; C. Liu et al., 2019). PM can produce acute toxic health effects such as respiratory irritation symptoms, exacerbation of chronic lung diseases and excess mortality (Logan, 1953). Chronic long-term exposure to PM2.5 contribute also to the development of COPD (Blayac et al., 2022; Lu et al., 2022).

Induced pluripotent stem (iPSC) cells offer an unprecedented opportunity to study the effect of air pollutants on human bronchial epithelial cells in unlimited quantities and model pathologies (Chandy et al., 2022). We have recently developed *in vitro* iPSC-derived bronchial epithelium modeling technology called iALI, which include ciliated cells, secretory cells, basal cells and neuroendocrine cells (E. Ahmed et al., 2022). This culture system contains both epithelial and mesenchymal cell populations and supports epithelial cell differentiation that mimics key aspects of the lung development. Our knowledge of pollution pathogenesis is still incomplete. To address this gap, we used the iALI model to study the impact of exposure of PM2.5 pollution on in vitro bronchial epithelium, on the cellular architecture and transcriptomic level. By using single cell RNA-sequencing we profile the transcriptome of individual epithelial and mesenchymal cells from iALI cultures and uncovered that iALI model includes a large mesenchymal compartment on which the bronchial epithelium is resting.

In this study, we provide a detailed effects of Prague $PM_{2.5}$ particles on iALI model which (i) reveals variation in transcriptomic response according to the cell types, (ii) identify the emergence of a previously uncharacterized transitory epithelial cell population with an intermediate cell state and (iii) characterizes cell states related to pollution exposure. The resulting data provide large information about the effects of $PM_{2.5}$ particles on iALI model and also open the way for further investigation of how $PM_{2.5}$ affects human airway epithelium.

RESULTS

iPSC-derived bronchial epithelium displays key morphological and expression patterns of bronchi

iALI were generated as previously described (E. Ahmed et al., 2022) (Fig 1A). An EPCAM/CD326+ epithelium relies on an EPCAM- VIM+ mesenchymal compartment (Fig 1B-C). Basal cells (TP63+, KRT5+) built a single cell layer in contact with the basal membrane at the bottom of the epithelium. Goblet cells (MUC5AC+), neuroendocrine cells (CHGA+) secretory cells, were regularly observed either as individual cells or clusters of cells (Fig 1D). Tubulin beta 4 (TUBIV)+ ciliated cells covered large swathes of the iALI surface (Fig 1E) and were functional (Supplemental video S1). We did not observe ionocytes, nor club cells. For this latter cell category, the use of DAPT during the second week of ALI culture may explain the lack of this cell type (Kiyokawa and Morimoto, 2020; Konishi et al., 2015; Tsao et al., 2009). In summary, iALI included most bronchial epithelium cell types, resting on a mesenchymal sub-mucosae.

iALI response to moderate and chronic particulate matter exposure

To examine the effect fine particle pollution on the iPSC-derived bronchial epithelium, we exposed the cells to SRM2786, a well characterized fine particulate matter (Schantz et al., 2016) that is also known to induce cell damage and apoptosis on epithelial cells (Ru et al., 2017), with a median diameter of 2.06 µm as measured by electron microscopy (IQR: 1.41) (Fig 2A-C). Exposure was carried out every day for two weeks on the basal side at concentrations of 10µg/mL, 50µg/mL or 100µg/mL (Upadhyay et al., 2022). The exposure was started on day 33, after cilia began to be functional (Fig 2A). The median diameter measured by electron microscopy of SRM2786 was 2.06

µm, (IQR: 1.41) (Fig 2B, 2C). To study the early response to injury, we focused on the expression of the mucins (Crosby and Waters, 2010). We observed that after pollution exposure, the number of goblet cells increased significantly, mucins MUC5B and MUC5AC mRNA expression increased, and MUC5AC protein induction was evidenced by immunofluorescence and dot blot (Fig 2D, 2E, 2F and 2G). Of note, ciliated cells functionality was not affected at this level of pollution exposure, as evidenced by live imaging (Supplemental Fig S2).

Transcriptional taxonomy of iALI

Human cells respond to tissue aggression by several response waves, including the induction of innate immunity and a tissue repair program. Our iALI model offers the opportunity to study the airway response to pollution independently from professional immune cells. In order to decipher the cell-type response to pollution, we carried-out single cell RNA sequencing (scRNA-seq) analysis. As our data showed that the iCOPD2 iPSC line responded more to pollution exposure (data not shown), we compared exposed and non-exposed iCOPD2 iALI by single cell analysis. Histological analysis and preliminary scRNAseq data indicated that epithelial cells are outnumbered by mesenchymal cells in iALI. Therefore, in order to analyze a similar number of cells of both populations, we purified the EPCAM+ epithelial cell population and the EPCAM- mesenchymal cells of exposed and non-exposed iALI by flow cytometry before scRNAseq. (Fig 3A and 3B). We obtained 10 817 high-quality cells for further analyses. Of these, 3 706 cells were EPAM+ and 7 111 cells EPCAM- corresponding to the epithelial and mesenchymal population respectively (Fig 3C and D). Clustering identified 9 transcriptionally cell clusters, evidenced by uniform manifold approximation and projection (UMAP) visualization (Fig 3E). Importantly, the EPCAM+ and EPCAM- populations were clearly separated. The clusters could be annotated based on known marker genes and literature evidence (Table 1). The EPCAM+ epithelial cells comprised KRT5+, TP63+ basal cells, FOXJ1+ multi-ciliated cells, NEUROD1+ neuroendocrine cells and a transitory epithelial cell population (Fig 3F). A secretory cells cluster was enriched in MUC5B+, TFF3+ and LYZ+ cells, and these genes were shared by other epithelial clusters, in line with a developmental proximity between secretory cells, ciliated cells and neuroendocrine cells (He et al., 2022; Ruiz García et al., 2019; Sountoulidis et al., 2023) (Fig. 3G). The mesenchymal EPCAM-

126 population comprised 3 close mesenchymal populations (Mesenchymal 1, 2 et 3) and
127 one cluster enriched in cycling cells MIK67 (Proliferating mesenchyme) (Fig 3E). These
128 four mesenchymal populations were PDGFRA+ and COL1A1High. Overall, many
129 genes previously described were identified in iALI and assigned to their cognate cell
130 type (Table 1) (Fig 3F). Finally, gene set enrichment analysis (GSEA) revealed that
131 most of the top upregulated KEGG terms were associated with cilium assembly,
132 microtubule, epithelial cell differentiation and epithelial development (Fig 3H). Overall,
133 iPSC differentiated into a complex bronchial epithelium resting on a mesenchymal
134 submucosae mimicking normal airways.
135
136 **iALI cell subtypes respond specifically to pollution exposure**
137 Next, we explored the effects of pollution on the iALI model, by comparing 6 038 control
138 cells versus 4 779 cells that were exposed to pollution (Fig 4A). A global analysis
139 showed that 6 genes were induced by pollution with a fold change > 2 and a p-value >
140 10^6, including cytochrome cytochrome P450 family 1 subfamily B member 1 (CYP1B1),
141 a procarcinogens-metabolizing enzyme known to be induced by polycyclic aromatic
142 hydrocarbons (PAHs) (Fig 4B-C)(Chang et al., 2006). The single cell data was an
143 opportunity to assess the differential response to pollution across the diverse cell types
144 of human bronchial epithelium. Indeed, while some genes such as CYP1B1 was
145 induced similarly in all 9 cell populations, other genes such as LYZ or LCN2 had an
146 induction profile very different across clusters (Fig 4D). Indeed, some cell populations
147 respond more vigorously than others to pollution, as we found that basal cells or
148 secretory cells had respectively 926 and 598 genes differentially expressed. In
149 contrast, ciliated cells and mesenchymal cells 2 exhibited minimal differential gene
150 expression (Fig 4D/E). Of note, the induction of CXCL14 in basal cells, which may be
151 an early response to aggression by signaling through chemokines to attract white blood
152 cells.
153
154 **An epithelial transition population is induced by pollution exposure**
155 We observed that transitory epithelial cells were predominantly present following
156 pollution exposure rather than in the control condition (Fig 5A). This observation
157 suggests that this specific cell population was induced by pollution aggression. This
158 cell population was entitled “transitory” because it shares part of its gene expression

profile with all other epithelial cells while also displaying a strong specific signature (Fig. 5B). The top gene expression signature included the serine peptidase inhibitor SPINK1, the peptide GHRL, a known endogenous ligand for the growth hormone secretagogue receptor (GHSR), lysozyme (LYZ), an enzyme able to hydrolysate certain bacterial mucopolysaccharides that has anti-bacterial activity against a number of bacterial species and lipocalin 2 (LCN2), a neutrophil gelatinase-associated lipocalin that plays a role in innate immunity by limiting bacterial growth as a result of sequestering iron-containing siderophores. The signature also included serum amyloid A1 (SAA1) a major acute phase protein that is highly expressed in response to inflammation and tissue injury, and chromogranin A (CHGA), a gene typically expressed in neuroendocrine cells (Fig 5C. We performed immunofluorescence on iALI and confirmed a cell population with a high expression of CHGA in pollution condition, exhibiting a different expression distribution than neuroendocrine cells (Fig 5D). Thus, these results collectively provide evidence that fine particulate matter alters the gene expression of a distinct cell group characterized by a specific signature, including CHGA (Fig. 5E).

DISCUSSION

In this study, we investigated the effects of air pollution on iALI, a bronchial epithelium obtained from patient-derived iPSCs. The iALI model, that was previously described by Ahmed et al., is generated through a simplified differentiation protocol that encompasses crucial developmental stages, including the primitive streak and the ventral anterior foregut endoderm (vAFE). Remarkably, this model does not require a cell sorting step. Histologically, the iALI structure faithfully recapitulates normal airways by incorporating both bronchial epithelium and underlying stroma. Because the surface of iALI is not perfectly flat, it represents a self-organized cellular structure intermediate between strictly two-dimensional (2D) systems and three-dimensional (3D) structures like floating organoids. It can be conceptualized as a 2.5D organoid, where the epithelium is forced to adopt a partially flattened organization. This arrangement promotes improved visualization and facilitates direct experimental manipulations. Single cell analysis confirmed the proximity of iALI with airway epithelium as shown by a similar cell composition, including a sub-mucosae.

This allowed us to assess the direct effect of fine particle matter on the different respiratory airway cell populations. Interestingly, we found that epithelial cell respond much more to air pollution than mesenchymal cells, even though a gene such as CYP1B1 was induced in most cell types. CYP1B1 is normally expressed in human lung and lung-derived cell lines (Spivack et al., 2001) and is also important for detoxifying different xenobiotics (Esteves et al., 2021). Strikingly, we found a transitory epithelial cell population induced by pollution exposure, expressing gene from secretory and neuroendocrine cells such as LYZ1 and CHGA respectively. This cell population, that has a basal and intermediate distribution in the bronchial epithelium, could either reflect a transient state of differentiation between basal cells and more differentiated cells such as secretory and neuroendocrine cells, or reflect the reprogramming of a cell population induced by the pollution aggression. The expression of genes such as LCN2 and LYZ1, which are involved in bacterial response, as well as SAA1, associated with inflammation, suggests that the observed cell population may be involved in a targeted reprogramming process aimed at mounting a global response to aggression (López-Campos et al., 2013; Mohammed et al., 2020; Treekitkarnmongkol et al., 2021).

Although iALI model used in this study contain multiple epithelial and mesenchymal cell types, it's remained incomplete as they lack immune cells and vasculature, which create a critical environment relevant for pathological processes. Thus, future investigations of airway epithelium $PM_{2.5}$ exposure effects will also benefit from the introduction of additional cell types that are present *in vivo* (for instance, endothelial cells and macrophages) to provide a more sophisticated *in vitro* model for evaluating biological effects associated with $PM_{2.5}$ exposure.

In conclusion, we have developed a robust protocol using iALI the reproduce in vitro the effects of pollution exposure and this allowed us to uncover a new intermediate cell population that is induced upon fine particle exposure, termed 'transitory epithelial cells'. Hence, this novel model holds great potential for broader applications in investigating the impact of the inhaled exposome. It could be employed to assess the cellular response to various airborne aggressors, including gases such as ozone, nitrogen dioxide, and sulfur dioxide, as well as industrial chemicals, pesticides, fine and ultrafine particles originating from sources like smoking, dust, plastics, fuel

exhaust, agricultural fires, and open-fire cooking. Additionally, the model offers opportunities to explore its response to infectious diseases, particularly viral infections.

FIGURES & LEGENDS

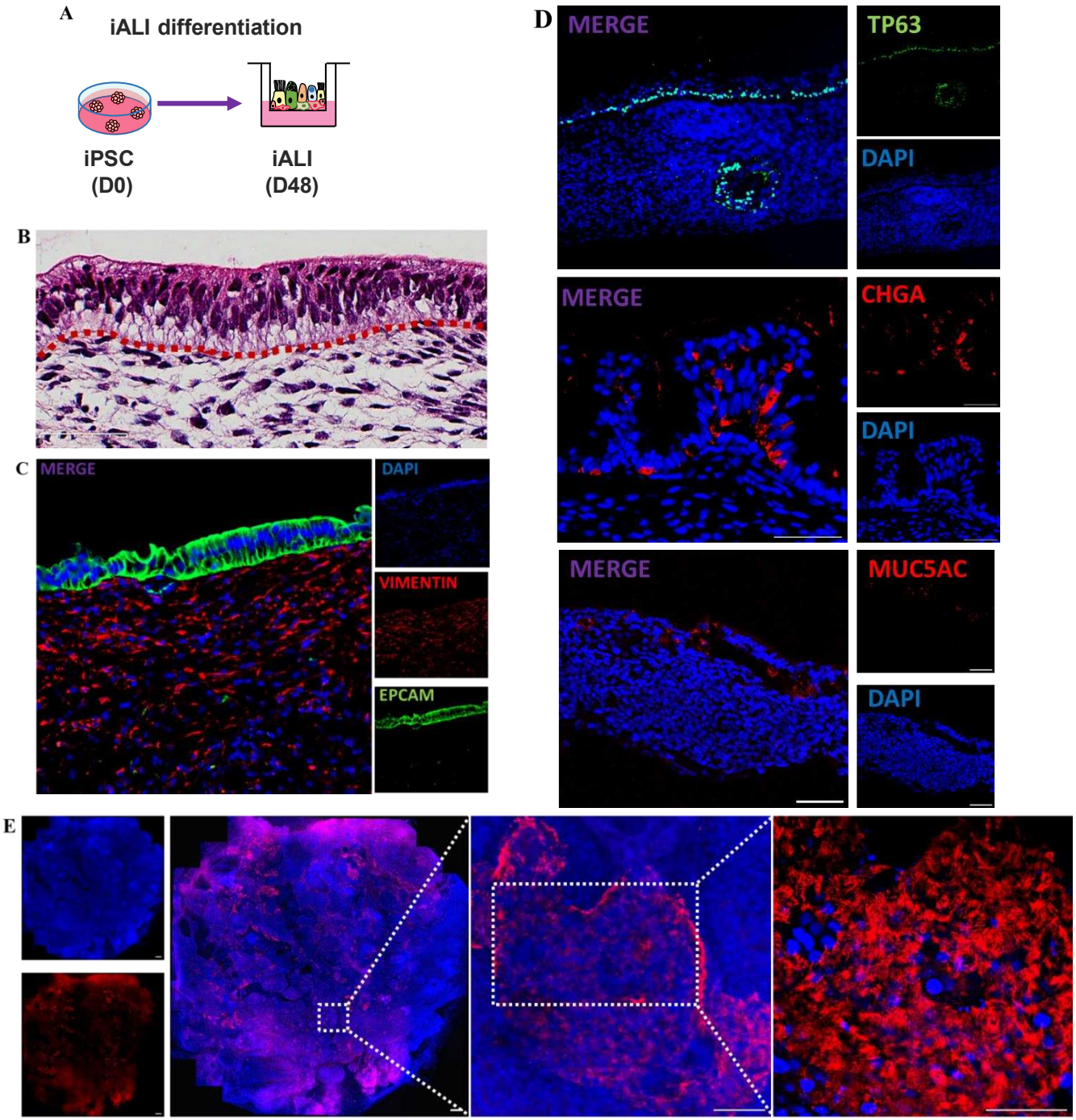

Figure 1. Characterization of iALI

(A) iALI are generated after 48 days of cultured as previously described. (B) HES staining of iALI transversal slide, with delimitation of epithelium and mesenchymal compartment visible

by (C) immunofluorescence of EPCAM and vimentin staining respectively. (D) Immunofluorescence of basal cells (expressing TP63), neuroendocrine cells (expressing CHGA) and goblet cells (expressing MUC5AC) on transversal paraffin sections; scale bar: 50 µm. (E) Ciliated cells at 10,40 and 63 magnification, distributed over the entire surface of iALI ; scale bar: 500µm and 50 µm.

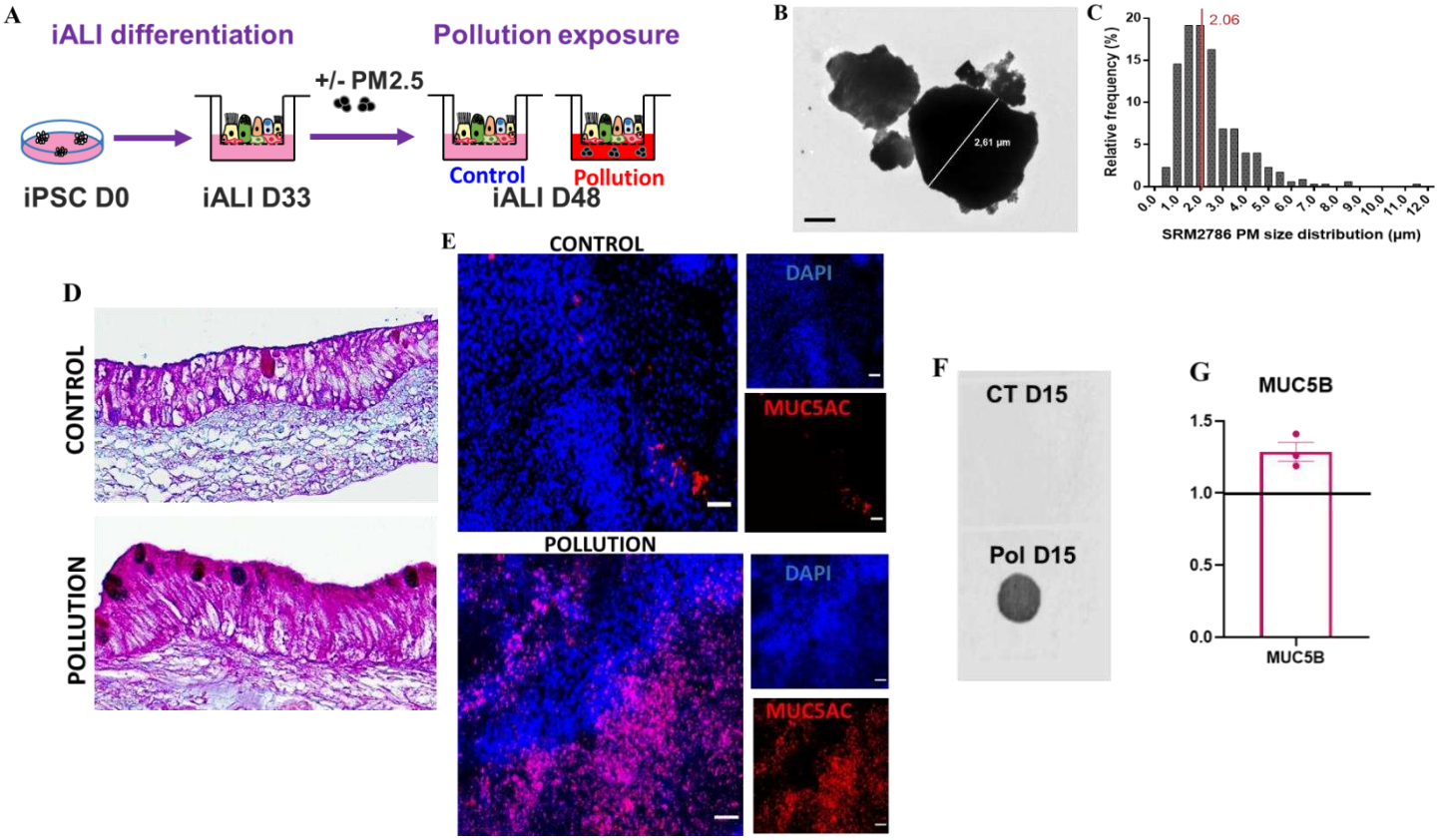

Figure 2. Establishment of pollution exposure protocol

(A) Schematic summary of experimental exposure to pollution. (B) Suspension of SRM2786 particulate matter size was dried out on a Formvar® coated copper grid and assessed by transmission electronic microscopy Tecnai F20 200KV; scale bar: 1 µm. (C) The longest axis of particulate matter median was 2.06 µm as mentioned by the red line. (D) PAS-BA staining on iALI paraffin section on control and exposure condition. (E) Immunofluorescence of protein MUC5AC in whole iALI in both condition; scale bar: 50 µm. (F) Mucus secretion validated by dot blot on control and exposure condition, and (G) relative expression of MUC5B mRNA in exposure condition compared to control (GraphPad 9.4.1).

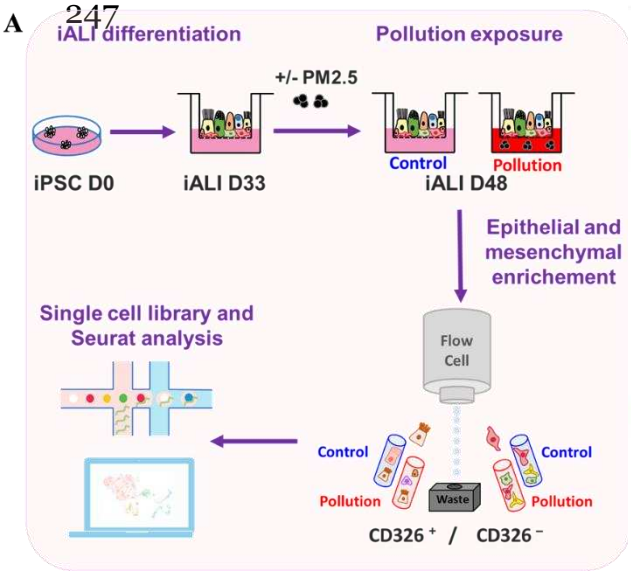
A
iALI differentiation
Pollution exposure
+/- PM2.5
iPSC D0
iALI D33
Control
Pollution
iALI D48
Epithelial and mesenchymal enrichement
Single cell library and Seurat analysis
Flow Cell
Control
Pollution
Waste
Control
Pollution
CD326 + / CD326 −

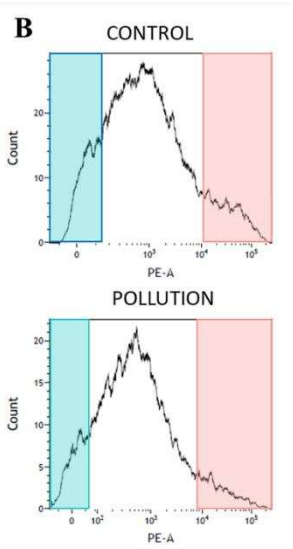
B
CONTROL
Count
PE-A
POLLUTION
Count
PE-A

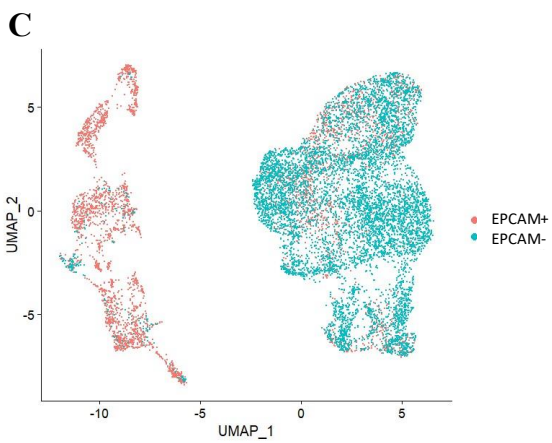
C
UMAP_2
UMAP_1
EPCAM+
EPCAM-

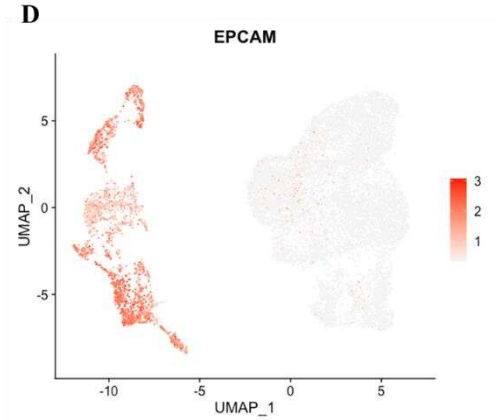
D
EPCAM
UMAP_2
UMAP_1

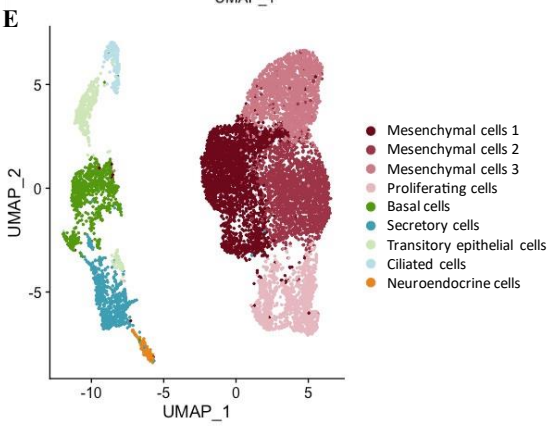
E
UMAP_2
UMAP_1
Mesenchymal cells 1
Mesenchymal cells 2
Mesenchymal cells 3
Proliferating cells
Basal cells
Secretory cells
Transitory epithelial cells
Ciliated cells
Neuroendocrine cells

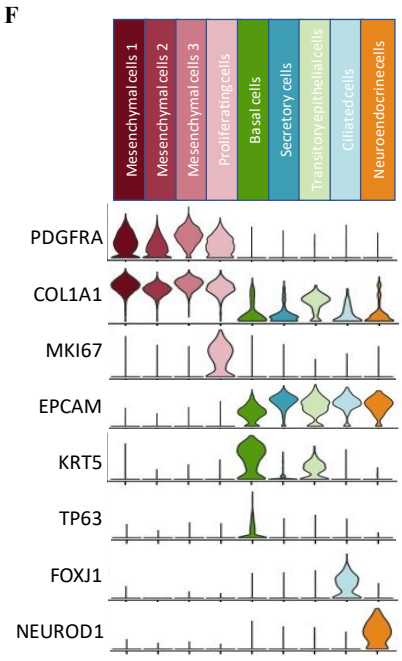
F
Mesenchymal cells 1
Mesenchymal cells 2
Mesenchymal cells 3
Proliferating cells
Basal cells
Secretory cells
Transitory epithelial cells
Ciliated cells
Neuroendocrine cells
PDGFRA
COL1A1
MKI67
EPCAM
KRT5
TP63
FOXJ1
NEUROD1

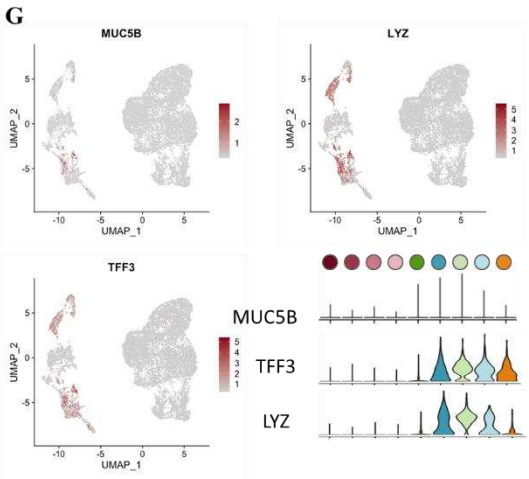
G
MUC5B
LYZ
TFF3
UMAP_2
UMAP_1
MUC5B
TFF3
LYZ

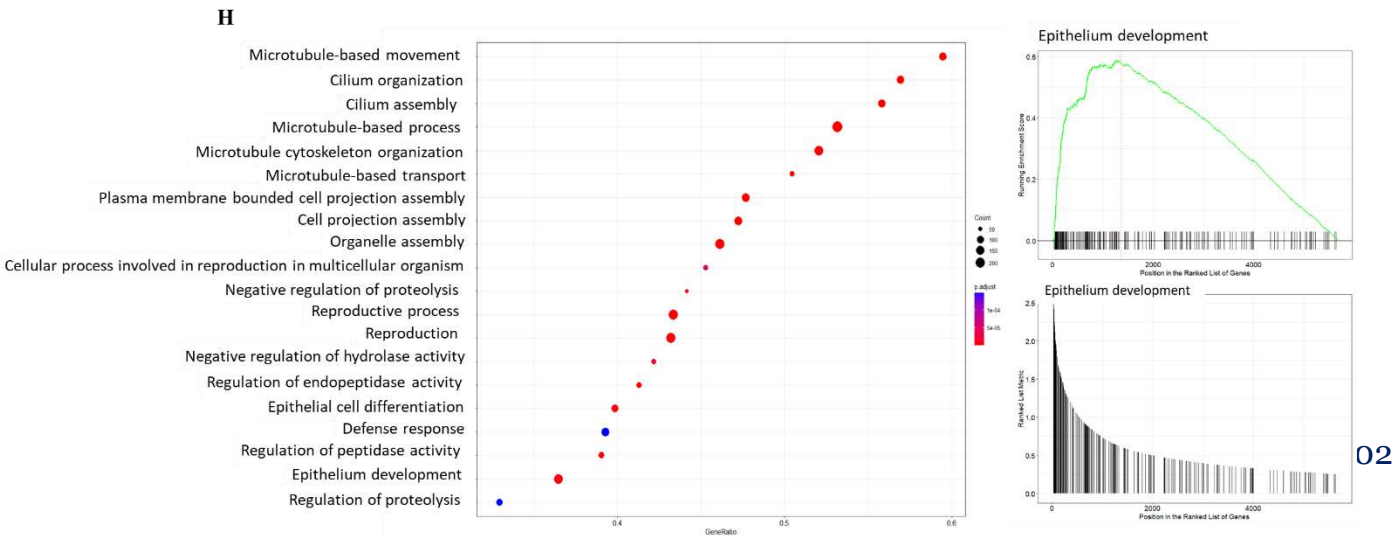
H
Microtubule-based movement
Cilium organization
Cilium assembly
Microtubule-based process
Microtubule cytoskeleton organization
Microtubule-based transport
Plasma membrane bounded cell projection assembly
Cell projection assembly
Organelle assembly
Cellular process involved in reproduction in multicellular organism
Negative regulation of proteolysis
Reproductive process
Reproduction
Negative regulation of hydrolase activity
Regulation of endopeptidase activity
Epithelial cell differentiation
Defense response
Regulation of peptidase activity
Epithelium development
Regulation of proteolysis
GeneRatio
Epithelium development
Epithelium development

Figure 3. scRNA-sequencing characterization of iALI in control and under pollution exposure

(A) Schematic summary of the single cell experiment and exposure protocol. (B) Sorting of cells based on their expression of CD326- (blue) and CD326+ (red) in the control and exposure conditions, top and bottom, respectively. (C) UMAP projection of scRNA-seq datasets from iALI stained by CD326- condition (epithelial or mesenchymal). (D) UMAP plot of EPCAM expression on (E) identified clusters. (F) Violin plot of expression levels of specific genes for each cluster. (G) Feature plot and violin plot of specific genes of secretory cell population. (H) Correlation of epithelial development by gene set enrichment analysis.

Figure 4. Effects of pollution exposure

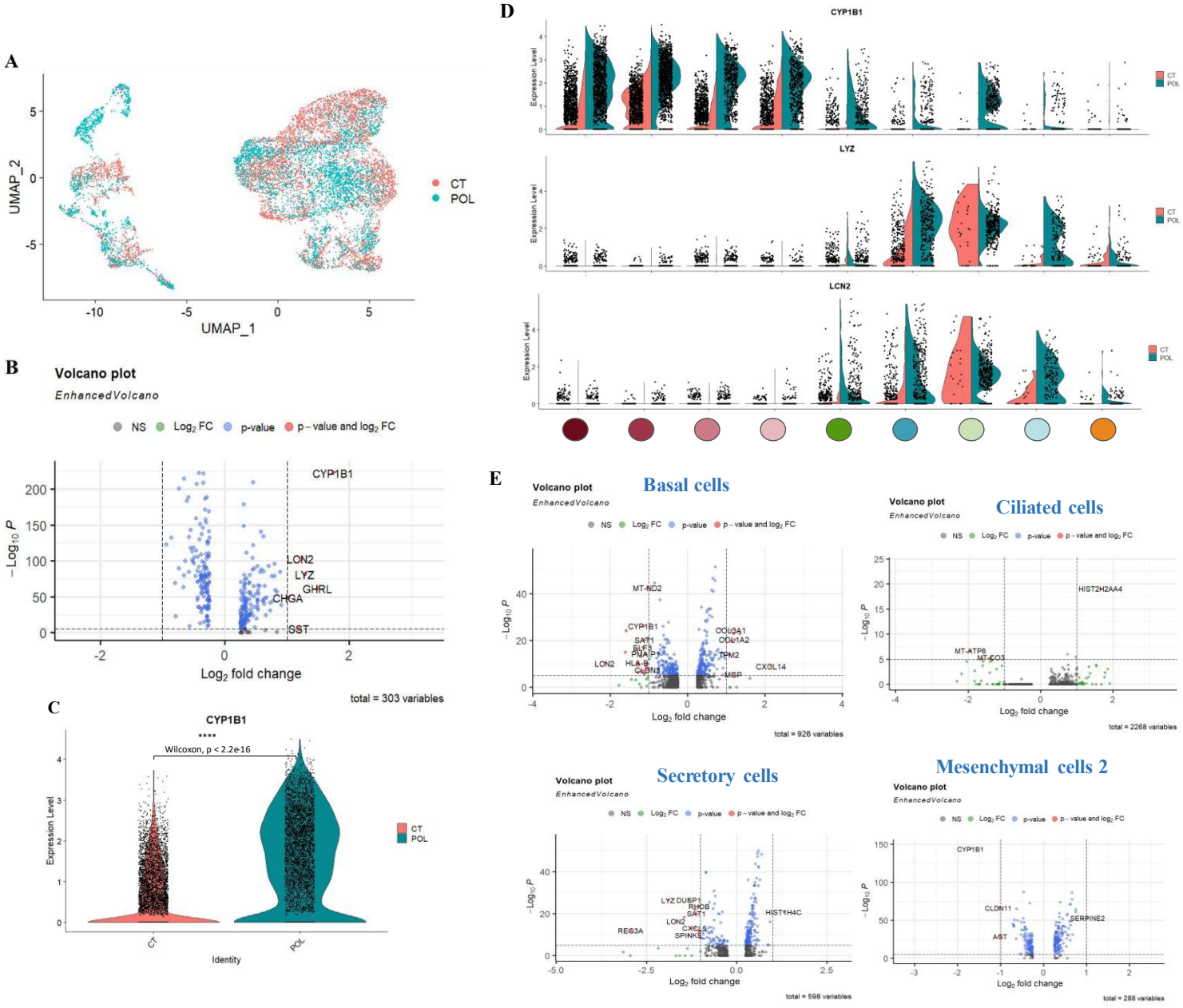

(A) UMAP plot of control and exposure condition. (B) Volcano plot of genes enhanced in exposure condition. (C) Vinplot of CYP1B1 in control and exposure condition. (D) Volcano plot of genes enhanced in exposure condition in basal, ciliated, secretory and mesenchymal cell clusters. (E) Vinplot of specific genes on all cell cluster, depending of condition.

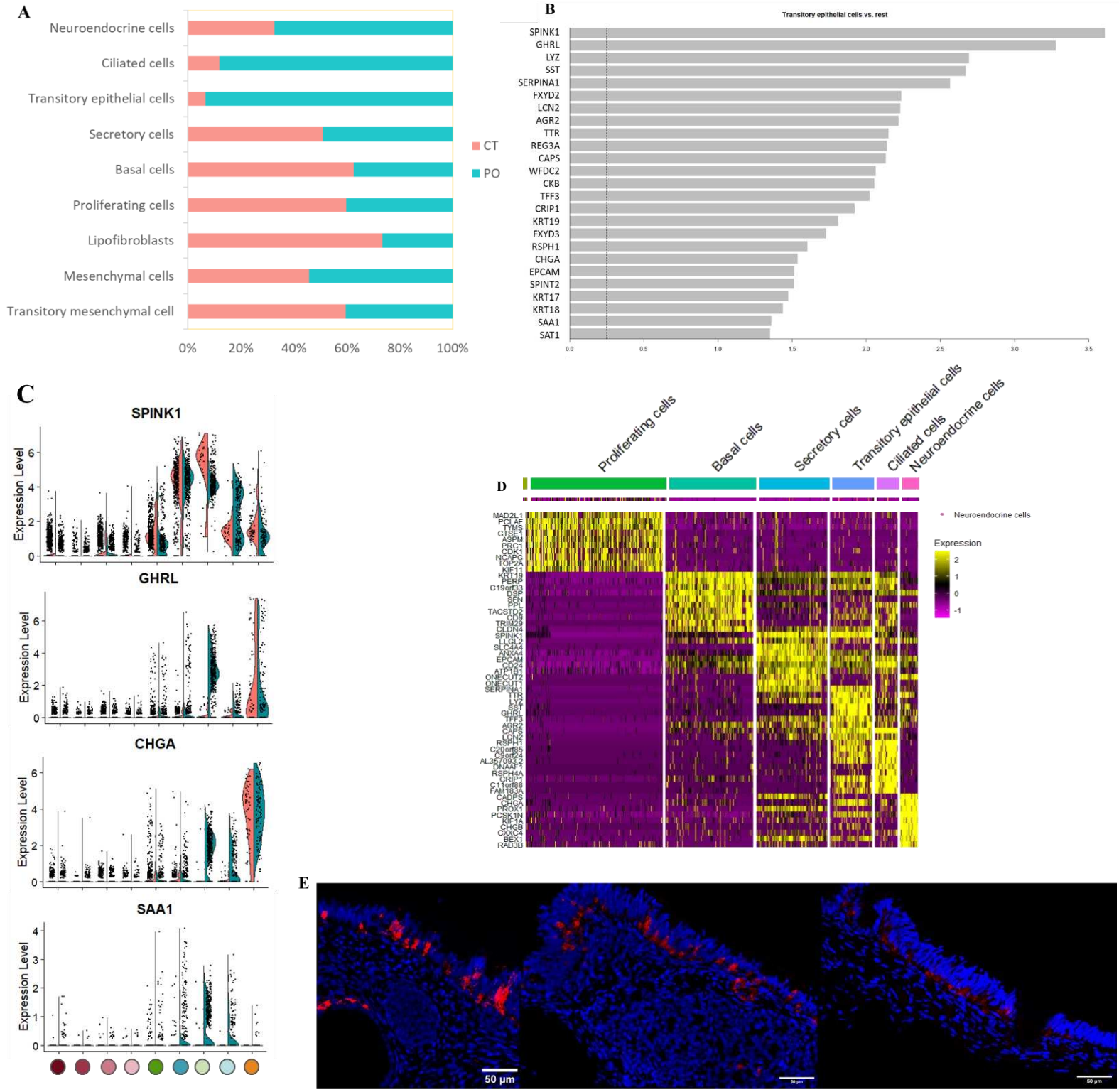

Figure 5. Transitory cell population revealed

(A) Proportions of cell types in iALI depending on control and exposure condition. (B) Vinplot of specific genes expressed on control and exposure condition on specific cell clusters. (C) Specific genes expressed in the transitory epithelial cell population with (D) enhanced genes in exposure compared to control condition. (E) Immunofluorescence of CHGA (in red) and DAPI (in blue) on paraffin sections of iALI under pollution exposure (magnification 63 and 40).

TABLES

Table 1: Selection of specific markers genes based on litterature

	Ciliated cells	Ciliated/secretory	Goblet cells	RAS cells	Goblet/ secretory cells	Club cells	Basal cells	Neuroendocrine
Uthaya Kumar, et al. "Bronchial Epithelium Epithelial-Mesenchymal Plasticity Forms Aberrant Basaloid-like Cells in Vitro." American Journal of Physiology-Lung Cellular and Molecular Physiology, 2022	SNTN, FOXJ1, PIFO, TPPP3, TMEM190		SCGB1A1, SCGB3A1, MUC5B, BPIFA1, TSPAN8			SCGB1A1, SCGB3A1, S100A9	BCAM, TP63, LGALS, KRT15	
Sountoulidis, et al. "Developmental Origins of Cell Heterogeneity in the Human Lung." Preprint. Developmental Biology, 2022.	DNAH12, RSPH1, DNAH11, C20orf85, SNTN, FOXJ1					SCGB3A2, TLL1, NEGR1,THSD4, ANOS1		CHGA, NRXN1, HEPACAM2, PTPRN2, KCNB2, GHRL, GRP, TFF3, SYT1, AC109466.1
Basil, et al. "Human Distal Airways Contain a Multipotent Secretory Cell That Can Regenerate Alveoli." Nature, 2022	FOXJ1, C20orf85, C9orf24, C1orf194, SNTN, TSPAN19, C013264.2,ROPN1L, DNAAF1	HES6, CDC20, CCDC74A, FOXJ1	MUC5B,DMBT1	MGP, SOX14,KLK11, SCGB3A2, SCGB1A1	SCGB1A1, TSPAN8, CYP2F1, C16orf89, MUC5AC, MUC5B, NTS	SCGB1A1, BPIFB1, LCN2, TSPAN8	KRT5, KRT17, S100A2,CHI3L1, S100A2, IGFBP2, KRT15, BCAM, CLCA2, CSTA	GRP, CPE, CHGA
Vieira Braga, et al. "A Cellular Census of Human Lungs Identifies Novel Cell States in Health and in Asthma." Nature Medicine, 2019	TMEM190,SNTN, RP11–356K23.1, ERICH3, C9orf135, APOD, RRAD, C2orf40, DNAH12, C20orf85, C1orf194, DYNLRB2, LRRIQ1, FAM183A, TSPAN19, OMG, PIFO, KCTD12		TFCP2L1 , CEACA, M5, PSCA, S100A4, ASRGL1,IDO1, LYNX1, LYPD2, CXCL10, IL-19, S100A8,SLC26A4,NOS2, PI3, CSF3			CXCL6, TFF3, MUC5B,MSMB, SCGB1A1, BPIFB1,SCGB3A1, TSPAN8,MUC5AC	KRT5, HBEGF, SERPINB13, SERPINB4 , NPPC, CYR61, S100A2, DST, KRT17, BCAM, NPCC, TP63	
Travaglini, et al. "A Molecular Cell Atlas of the Human Lung from Single-Cell RNA Sequencing." Nature , 2020	FOXJ1, C20orf85, CAPS, C1orf194, FAM183A, RFX3, ZNF473 , TP73, ZNF440 , SIX1, EHF, TETV6		ETV6			EHF, SIX1, AHR, ADIPOR1, INSR	KRT17, KRT5, MIR205HG, SCGB3A2, SERPINB3, CLCA2, HMGB, PITX1, BCL11A, EHF	ST18, HOXB2, OTP, MYT1L, ASCL1, MEIS2, PITX1, BCL11A, PROX1
Garc, et al. "Novel Dynamics of Human Mucociliary Differentiation Revealed by Single-Cell RNA Sequencing of Nasal Epithelial Cultures," 2019	C11orf192, C11orf16, C4orf47, C5orf49, C7orf57, C9orf9, CCDC176, CCDC19, CCDC74A, DNAH12, ENKUR, FOXJ1, KIF9, LRRIQ1, MNS1, MUC12, ROPNL1, RSPH4A, SPEF1, TTC40						CENPF	
Hawkins, et al. "Derivation of Airway Basal Stem Cells from Human Pluripotent Stem Cells." Cell Stem Cell, 2021	FOXJ1 , TUBB4B, CCNO, SNTN, TUBA1A, LDLRAD1, MORN2 , ODF3B, CAPS, CFAP53 , TMEM190, C9orf24, DYNLRB2, FAM93B, AL357093.2, C1orf194, PIFO, CCDC1446, RSPH1, C20orf85, CAPSL, TPPP3				SCGB1A1, SCGB3A2, MUC5B, KIAA1324, SFTPA2, GSTA1, CXCL1, C3		TP63, KRT5, KRT17, CCND2, DST, FN1, PMEPA1, TAGLN, COL3A1, TNFRSF12A, SH3BGRL3, SPARC, S100A2, MYL9, FST, IGFBP7,COMP, MMP10, TPM2, VIM	
Carraro, Gianni, Apoorva Mulay, Changfu Yao, Takako Mizuno, Bindu Konda, Martin Petrov, Daniel Lafkas, et al. "Single Cell Reconstruction of Human Basal Cell Diversity in Normal and IPF Lung," n.d., 35.	C5orf49, DNAAF1, CETN2, SNTN, AL357093.2, PIFO, ODF3B, MORN2, TUBA1A, C9orf116, C1orf194, FAM183A , OMG, RSPH1, C20orf85, C9orf24, TPPP3, TMEM190, CAPS				AC020656.1, AZGP1, ZG16B, LTF, PRR4, PRB4, PRB3, LYZ, SCGB3A1 , PI3, BPIFA1 , BPIFB1	MUC5B, TFF3, MSMB, SCGB1A1, MUC5AC, BPIFA1, VMO1	ATP1B3,MYC,FHL2, BCAM, ADIRF, DST, SFN, PHLDA1, AREG, KRT6A, KRT14, MMP10, KRT5, S100A2, KRT17	
Habermann, et al. "Single-Cell RNA Sequencing Reveals Profibrotic Roles of Distinct Epithelial and Mesenchymal Lineages in Pulmonary Fibrosis." Science Advances, 2020					MUC5B, SCGB1A1, SCGB3A2		KRT5, KRT17, SCGB1A1, SFTPC	
He, et al. "A Human Fetal Lung Cell Atlas Uncovers Proximal-Distal Gradients of Differentiation and Key Regulators of Epithelial Fates." Developmental Biology, 2022	FOXJ1, AREG, ALOX15		SCGB3A2, NXPH4, SPDEF, SCGB3A1, LTF, KRT4, CYTL1			SCGB3A2	IL33, IGFBP4, IGFBP6, KISS1, SOX9	UCHL1, GHRL, ASCL1
Madissoon, et al. "A Spatial Multi-Omics Atlas of the Human Lung Reveals a Novel Immune Cell Survival Niche." Cell Biology, 2021	FOXJ1		SCGB1A1				KRT14	
Duclos, et al. "Characterizing Smoking-Induced Transcriptional Heterogeneity in the Human Bronchial Epithelium at Single-Cell Resolution." Science Advances, 2019	FOXJ1		MUC5AC			SCGB1A1	KRT5	

MATERIAL AND METHODS

Cell lines and culture condition

hiPSC lines culture

The hiPSC lines UHOMi002-A (named HY03) and UHOMi003-A (called ICOPD2) were reprogrammed in our laboratory as previously described (Ahmed et al., 2021; Fieldes et al., 2020). Briefly, the two pluripotent cell lines were incubated daily in Essential 8™

277 medium (Thermo Fisher Scientific) at 37 °C, 5% CO2, and growth in feeder-free
278 Geltrex matrix (Thermo Fisher Scientific). Every 4 days, cells were passaged with a
279 Versene solution (Thermo Fisher Scientific) and plated in a ratio of 1:10 to 1:15 with
280 10µM of Rho-associated kinase inhibitor Y-27632 (Tocris).

281 ### iALI differentiation

282 To generate iALI, each cell lines were plated at 80 000 cells/cm^2 and differentiated in
283 ventralized-anterior foregut endoderm on 35mm dishes before plated mechanically in
284 transwells (Corning™) coated with Geltrex as described in (E. Ahmed et al., 2022).
285 Cells were polarized at day 12 and maintained in PneumaCult™-ALI Medium
286 (Stemcell) until day 40-48. Media was changed daily on basolateral side.

287

288 ## Pollution exposure

289 ### Particulate matter type collection and extraction

290 SRM2786 were purchased from National Institute of Standards and Technology (NIST)
291 and collected in a major exhibition center of Prague in 2005, according to its certificate
292 (Schantz et al., 2016). SRM2786 were suspended in PneumaCult™-ALI Medium
293 (Stemcell) at 50 mg/µL and sonicated during 30 min before being aliquoted in aliquots
294 protected from light and stored at -20 according to the manufacture's
295 recommendations.

296 ### Exposure protocol

297 Differentiating iALI cells were exposed continuously during 15 days to SRM2786
298 between day 33 (when cilia appears) and day 48 in basolateral side. The
299 PneumaCult™-ALI medium containing the SRM2786 was prepared according to the
300 desired final concentration (10µg/mL, 50µg/mL or 100µg/mL) and changed every day
301 with a vortex before each use. To avoid sedimentation of particles in the transwell
302 membrane, a wash with PBS$^{-/-}$ was performed when needed at the basolateral side
303 before adding media.

304 ## Single cell RNA sequencing

305 ### Cells dissociation and isolation by FACS

306 At day 48, 12 iALI control and 12 iALI exposed were dissociated with Trypsin (15min,
307 37°C) and gently detached from Transwells by pipetting, filtered through a 40 µm
308 porosity (Corning) with a solution of PneumaCult™-ALI Medium complemented with
309 SVF 5% and then centrifuged (1200 rpm for 5 min). Cells were resuspended in 1,5 mL
310 of PneumaCult™-ALI Medium complemented with 0,4% of BSA and labeled with
311 isotype-PE (2 iALI for each condition) or CD326 antibody (10 iALI for each condition)
312 during 30 min at 4°C. Cells were washed and then sorted on BD FACSAria™.

313 **Single cell library preparation and sequencing**

314 The concentration of freshly sorted cells was adjusted to 1000 cells/µl in PBS-/-
315 complemented with 0.01% of BSA and 10 000 cells were targeted for cDNA
316 preparation and put through the 10X Genomics Chromium Next GEM Single Cell 3'
317 v3.1. After cDNA preparation and clean-up, the quality of cDNA was checked on an
318 Agilent Bioanalyzer DNA High Sensitivity chip. Library preparation was performed
319 according to the manufacturer's instructions using the Chromium Chip B Single Cell
320 kit, and Chromium Multiplex Kit (10X Genomics). Sequencing was performed in paired-
321 end mode and a NovaSeq sequencer (Illumina) at the AstraZenca core facility
322 (Göteborg, Sweden). First, the cell ranger mkfastq and cellranger count pipelines were
323 used for the initial quality control, sample demultiplexing, mapping, and raw data
324 quantification. Briefly, fastq files were run with the Count application using default
325 parameters and were aligned to the human genome reference sequence GRCh38.

326 **Single cell data analysis**

327 Cell Ranger files were loaded into Seurat v.4.2.0 and treated firstly individually
328 according to the standard analysis pipeline (Hao et al., 2021) Briefly, for each dataset,
329 the minimal number of cells was 100 with a minimal UMI across all cells of 1000 and
330 cells with a percentage of mitochondrial counts >10% were removed. Then, extreme
331 outliers thresholds of unique features counts were removed visually depending of each
332 violin plots (maximum 8000 and minimum 1500). Next, the 4 datasets were merged by
333 using the merge function of Seurat, and then log normalized and scaled by default.
334 PCA (Principal component analysis) was performed and based on elbowplot the top
335 15 PCs were used for clustering analysis, with the Seurat function "FindClusters" by
336 increasing the resolution parameter (0.2 was chosen here), and Uniform Manifold
337 Approximation and Projection (UMAP) visualization. Differentially expressed genes

(DEGs) were identified with Seurat's "FindAllMarkers" and "FindMarkers" function based on non-parametric Wilcoxon rank-sum test as default. Each cluster was then identified within the specific gene expression for a cell type known in literature (Nasri et al., 2021) (T1).

Pathway enrichment analyses

The KEGG pathway enrichment analysis and Gene Set Enrichment analysis (GSEA) was performed using the ClusterProfiler package (Wu et al., 2021). Only genes with a q-value <0.05 were retained.

Reverse transcription-quantitative polymerase chain reaction

RNA extraction was performed using RNeasy Mini Kit (Qiagen) and RNA was quantify by Nanodrop (Thermo Fisher Scientific). Reverse transcription was performed with SuperScript™ First-Strand Synthesis System (Invitrogen) as recommended by the manufacturer with 500 ng RNA. Quantitative PCR (qPCR) was then performed using 8µL of LightCycler® 480 SYBR Green I Master (Roche) with 2 µL of cDNA (1:20 dilution) and 0.5 µL of each primer diluted at 10 µM (Integrated DNA Technologies IDT). Plates were then centrifuged at 1000 rpm for 1 minute and cycled on a LightCycler 480 apparatus with the following program: 1 cycle of 95°C for 10s; 45 cycles of 95°C for 10s, 60°C for 15s; 72°C for 15s, 1 cycle 95°C for 5s, 65°C for 1min, 97°C. Each sample was amplified in triplicate and gene expression levels were normalized to the expression of the housekeeping gene GAPDH. Results were expressed as fold change compared to the non-exposed control using the following formula: $2^{-\Delta\Delta Ct}$, where ΔΔCt = ΔCt exposed - ΔCt control.

Dot blot

On day 33 and day 48, 500 µL of $PBS^{+/+}$ was added to the apical side of the iALI. After incubation at 37°C for 5 min, the supernatant was collected and stored at -80°C before analysis. Then, 10 µl of the diluted sample was applied to the nitrocellulose membrane and allowed to dry thoroughly for 30 minutes. The membrane was blocked for 1 hour at RT in Odyssey® blocking buffer and incubated for 2 hours at RT with the primary antibody in 50% blocking buffer/ 50% $PBS^{-/-}$ 0.1% Tween. After washing three times with PBST, the membrane was incubated with the secondary antibody (1/30 000) in

50% blocking buffer/ 50% PBS 0.1% Tween for 1 hour at RT. Finally, after 3 washes in PBST and another in PBS, the membrane was read with Odyssey®.

Paraffin sections

iALI were fixed in 4% paraformaldehyde (PFA) for 24 hours at 4°C. Then, samples were cut from transwells, the membrane removed, and embedded in low-melting agarose 0.5% (Thermo Fisher Scientific). Samples were then cut in half, placed in a cassette (one cassette for one iALI) on the newly cut slices, stored in 70% ethanol at 4°C, and sent to RHEM for parrafin embedding, sectioning, and histological staining. Paraffin sections were cut at a thickness of 3 to 5 µm. Deparaffinization was performed by placing the sections in Neoclear for 3 minutes and progressively decreasing ethanol concentration for 6 minutes, 3 minutes, and 3 minutes in 100%, 70%, and 50%, respectively. Finally, the sections were placed in boiling Neoclear for 20 minutes, and immunofluorescence staining was performed after the slides cooled.

Immunofluorescence staining

Samples were fixed in 4% PFA at room temperature (RT) for 15 min, and then permeabilized with PBS containing 0.5% Triton X-100 for 15 min. Cells were blocked with 10% of donkey serum in PBS complemented with 1% BSA and 0.1% Triton X-100 (solution A) at RT for 60 min. Samples were incubated with primary antibodies (diluted in solution A) at 4°C overnight and after several washes with PBS containing 0.025% Triton X-100, were incubated with secondary antibodies (dilution 1/1000) at RT for 60 min protected from light. Nuclei were stained with DAPI (1:5000) for 2 min. Samples were mounted in glycerol 100% and stored in the dark at 4°C. Image acquisition was performed with Leica TCS SP5 and Leica SP8 confocal microscope (CARTIGEN platform). Images were analyzed with ImageJ (Fiji).

ACKNOWLEDGEMENT

We acknowledge the “Réseau d’Histologie Expérimentale de Montpellier” - RHEM facility supported by SIRIC Montpellier Cancer Grant INCa_Inserm_DGOS_12553, the european regional development foundation and the Occitanie region (FEDER-FSE 2014-2020 Languedoc Roussillon), REACT-EU (Recovery Assistance for Cohesion

401 and the Territories of Europe), IBiSA and Ligue contre le cancer for processing our
402 animal tissues, with histology technics and expertise.
403
404 **DISCLOSURE OF POTENTIAL CONFLICTS OF INTEREST**
405
406 **Supplemental Figures**
407 **Figures S1: Videomicroscopy of cilia beating**

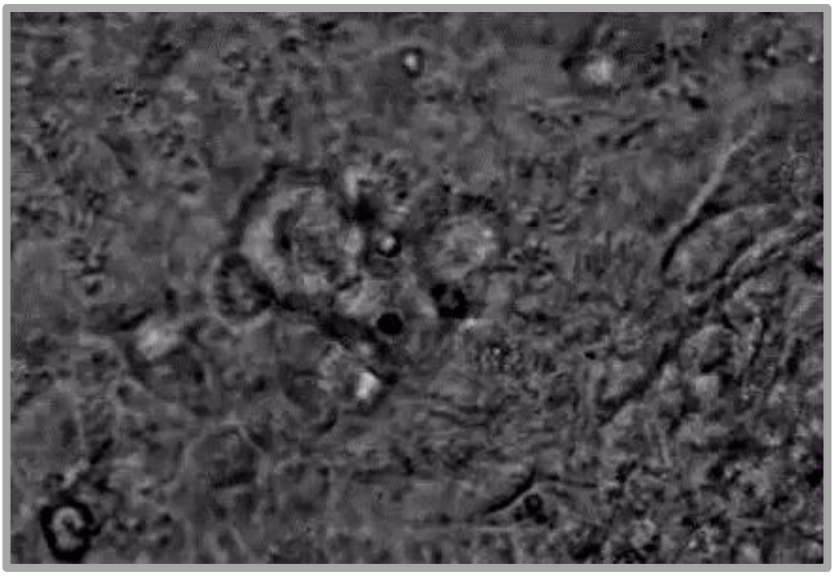

408
409 **Figures S2: Videomicroscopy of cilia beating under pollution**
410 **exposure**

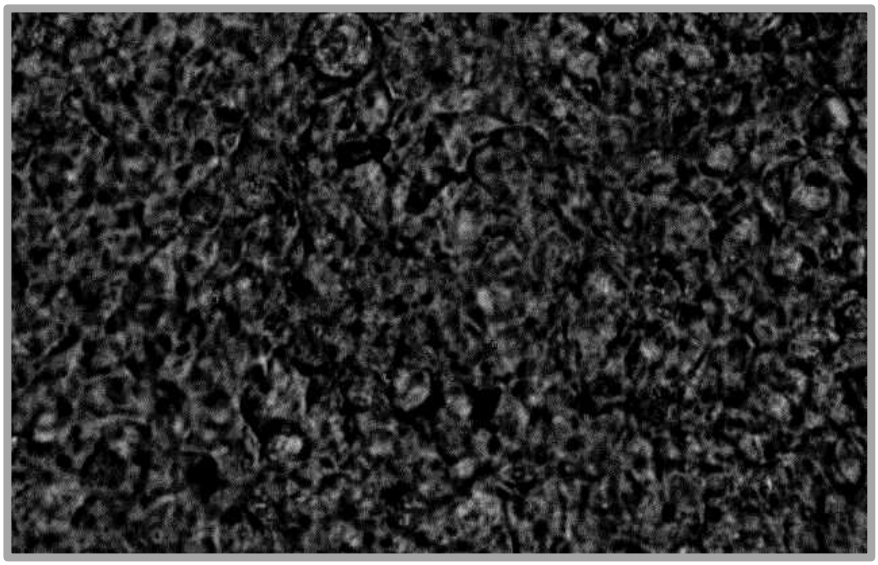

411

412 # REFERENCES

413 Ahmed, E., Fieldes, M., Bourguignon, C., Mianné, J., Petit, A., Jory, M., Cazevieille, C., Boukhaddaoui,
414 H., Garnett, J.P., Hirtz, C., Massiera, G., Vachier, I., Assou, S., Bourdin, A., De Vos, J., 2022.
415 Differentiation of Human Induced Pluripotent Stem Cells from Patients with Severe COPD into
416 Functional Airway Epithelium. Cells 11, 2422.

417 Ahmed, E., Fieldes, M., Mianné, J., Bourguignon, C., Nasri, A., Vachier, I., Assou, S., Bourdin, A., De Vos,
418 J., 2021. Generation of four severe early-onset chronic obstructive pulmonary disease (COPD) patient-
419 derived induced pluripotent stem cell lines from peripheral blood mononuclear cells. Stem Cell
420 Research 56, 102550.

421 Barnes, P.J., Burney, P.G.J., Silverman, E.K., Celli, B.R., Vestbo, J., Wedzicha, J.A., Wouters, E.F.M., 2015.
422 Chronic obstructive pulmonary disease. Nat Rev Dis Primers 1, 15076.

423 Blayac, M., Coll, P., Urbach, V., Fanen, P., Epaud, R., Lanone, S., 2022. The Impact of Air Pollution on
424 the Course of Cystic Fibrosis: A Review. Frontiers in Physiology 13.

425 Chandy, M., Obal, D., Wu, J.C., 2022. Elucidating effects of environmental exposure using human-
426 induced pluripotent stem cell disease modeling. EMBO Mol Med 14, e13260.

427 Chang, H., Chang, L.W., Cheng, Y.-H., Tsai, W.-T., Tsai, M.-X., Lin, P., 2006. Preferential induction of
428 CYP1A1 and CYP1B1 in CCSP-positive cells. Toxicol Sci 89, 205–213.

429 Crosby, L.M., Waters, C.M., 2010. Epithelial repair mechanisms in the lung. Am J Physiol Lung Cell Mol
430 Physiol 298, L715–L731.

431 Esteves, F., Rueff, J., Kranendonk, M., 2021. The Central Role of Cytochrome P450 in Xenobiotic
432 Metabolism-A Brief Review on a Fascinating Enzyme Family. J Xenobiot 11, 94–114.

433 Fieldes, M., Ahmed, E., Bourguignon, C., Mianné, J., Martin, M., Arnould, C., Vachier, I., Assou, S., De
434 Vos, J., Bourdin, A., 2020. Generation of the induced pluripotent stem cell line UHOMi002-A from
435 peripheral blood mononuclear cells of a healthy male donor. Stem Cell Research 49, 102037.

436 Hao, Y., Hao, S., Andersen-Nissen, E., Mauck, W.M., Zheng, S., Butler, A., Lee, M.J., Wilk, A.J., Darby, C.,
437 Zager, M., Hoffman, P., Stoeckius, M., Papalexi, E., Mimitou, E.P., Jain, J., Srivastava, A., Stuart, T.,
438 Fleming, L.M., Yeung, B., Rogers, A.J., McElrath, J.M., Blish, C.A., Gottardo, R., Smibert, P., Satija, R.,
439 2021. Integrated analysis of multimodal single-cell data. Cell 184, 3573-3587.e29.

440 He, P., Lim, K., Sun, D., Pett, J.P., Jeng, Q., Polanski, K., Dong, Z., Bolt, L., Richardson, L., Mamanova, L.,
441 Dabrowska, M., Wilbrey-Clark, A., Madissoon, E., Tuong, Z.K., Dann, E., Suo, C., Goh, I., Yoshida, M.,
442 Nikolić, M.Z., Janes, S.M., He, X., Barker, R.A., Teichmann, S.A., Marioni, J.C., Meyer, K.B., Rawlins, E.L.,
443 2022. A human fetal lung cell atlas uncovers proximal-distal gradients of differentiation and key
444 regulators of epithelial fates. Cell 185, 4841-4860.e25.

445 Kim, K.-H., Kabir, E., Kabir, S., 2015. A review on the human health impact of airborne particulate
446 matter. Environment International 74, 136–143.

447 Kiyokawa, H., Morimoto, M., 2020. Notch signaling in the mammalian respiratory system, specifically
448 the trachea and lungs, in development, homeostasis, regeneration, and disease. Dev Growth Differ 62,
449 67–79.

Ko, U.W., Kyung, S.Y., 2022. Adverse Effects of Air Pollution on Pulmonary Diseases. Tuberc Respir Dis (Seoul) 85, 313–319.

Konishi, S., Gotoh, S., Tateishi, K., Yamamoto, Y., Korogi, Y., Nagasaki, T., Matsumoto, H., Muro, S., Hirai, T., Ito, I., Tsukita, S., Mishima, M., 2015. Directed Induction of Functional Multi-ciliated Cells in Proximal Airway Epithelial Spheroids from Human Pluripotent Stem Cells. Stem Cell Reports 6, 18–25.

Landrigan, P.J., Fuller, R., Acosta, N.J.R., Adeyi, O., Arnold, R., Basu, N. (Nil), Baldé, A.B., Bertollini, R., Bose-O'Reilly, S., Boufford, J.I., Breysse, P.N., Chiles, T., Mahidol, C., Coll-Seck, A.M., Cropper, M.L., Fobil, J., Fuster, V., Greenstone, M., Haines, A., Hanrahan, D., Hunter, D., Khare, M., Krupnick, A., Lanphear, B., Lohani, B., Martin, K., Mathiasen, K.V., McTeer, M.A., Murray, C.J.L., Ndahimananjara, J.D., Perera, F., Potočnik, J., Preker, A.S., Ramesh, J., Rockström, J., Salinas, C., Samson, L.D., Sandilya, K., Sly, P.D., Smith, K.R., Steiner, A., Stewart, R.B., Suk, W.A., van Schayck, O.C.P., Yadama, G.N., Yumkella, K., Zhong, M., 2018. The Lancet Commission on pollution and health. The Lancet 391, 462–512.

Liu, C., Chen, R., Sera, F., Vicedo-Cabrera, A.M., Guo, Y., Tong, S., Coelho, M.S.Z.S., Saldiva, P.H.N., Lavigne, E., Matus, P., Valdes Ortega, N., Osorio Garcia, S., Pascal, M., Stafoggia, M., Scortichini, M., Hashizume, M., Honda, Y., Hurtado-Díaz, M., Cruz, J., Nunes, B., Teixeira, J.P., Kim, H., Tobias, A., Íñiguez, C., Forsberg, B., Åström, C., Ragettli, M.S., Guo, Y.-L., Chen, B.-Y., Bell, M.L., Wright, C.Y., Scovronick, N., Garland, R.M., Milojevic, A., Kyselý, J., Urban, A., Orru, H., Indermitte, E., Jaakkola, J.J.K., Ryti, N.R.I., Katsouyanni, K., Analitis, A., Zanobetti, A., Schwartz, J., Chen, J., Wu, T., Cohen, A., Gasparrini, A., Kan, H., 2019. Ambient Particulate Air Pollution and Daily Mortality in 652 Cities. New England Journal of Medicine 381, 705–715.

Logan, W.P.D., 1953. Mortality in the London fog incident, 1952. Lancet 1, 336–338.

López-Campos, J.L., Calero, C., Rojano, B., López-Porras, M., Sáenz-Coronilla, J., Blanco, A.I., Sánchez-López, V., Tobar, D., Montes-Worboys, A., Arellano, E., 2013. C-Reactive Protein and Serum Amyloid A Overexpression in Lung Tissues of Chronic Obstructive Pulmonary Disease Patients: A Case-Control Study. Int J Med Sci 10, 938–947.

Lu, Z., Coll, P., Maitre, B., Epaud, R., Lanone, S., 2022. Air pollution as an early determinant of COPD. Eur Respir Rev 31, 220059.

Mohammed, A., Alghetaa, H.K., Zhou, J., Chatterjee, S., Nagarkatti, P., Nagarkatti, M., 2020. Protective effects of Δ9-tetrahydrocannabinol against enterotoxin-induced acute respiratory distress syndrome are mediated by modulation of microbiota. British Journal of Pharmacology 177, 5078–5095.

Nasri, A., Foisset, F., Ahmed, E., Lahmar, Z., Vachier, I., Jorgensen, C., Assou, S., Bourdin, A., De Vos, J., 2021. Roles of Mesenchymal Cells in the Lung: From Lung Development to Chronic Obstructive Pulmonary Disease. Cells 10, 3467.

Rabe, K.F., Watz, H., 2017. Chronic Obstructive Pulmonary Disease. The Lancet 389, 1931-1940,.

Ru, Q., Xiong, Q., Chen, L., Tian, X., Yue, K., Ma, B., Liu, L., Wu, R., Xu, C., Pi, M., Li, C., 2017. Lipopolysaccharide accelerates fine particulate matter-induced cell apoptosis in human lung bronchial epithelial cells. Int J Occup Med Environ Health.

Ruiz García, S., Deprez, M., Lebrigand, K., Cavard, A., Paquet, A., Arguel, M.-J., Magnone, V., Truchi, M., Caballero, I., Leroy, S., Marquette, C.-H., Marcet, B., Barbry, P., Zaragosi, L.-E., 2019. Novel dynamics

490 of human mucociliary differentiation revealed by single-cell RNA sequencing of nasal epithelial
491 cultures. Development 146, dev177428.

492 Schantz, M.M., Cleveland, D., Heckert, N.A., Kucklick, J.R., Leigh, S.D., Long, S.E., Lynch, J.M., Murphy,
493 K.E., Olfaz, R., Pintar, A.L., Porter, B.J., Rabb, S.A., Vander Pol, S.S., Wise, S.A., Zeisler, R., 2016.
494 Development of two fine particulate matter standard reference materials (<4 μm and <10 μm) for the
495 determination of organic and inorganic constituents. Anal Bioanal Chem 408, 4257–4266.

496 Soriano, J.B., Kendrick, P.J., Paulson, K.R., Gupta, V., Abrams, E.M., Adedoyin, R.A., Adhikari, T.B.,
497 Advani, S.M., Agrawal, A., Ahmadian, E., Alahdab, F., Aljunid, S.M., Altirkawi, K.A., Alvis-Guzman, N.,
498 Anber, N.H., Andrei, C.L., Anjomshoa, M., Ansari, F., Antó, J.M., Arabloo, J., Athari, S.M., Athari, S.S.,
499 Awoke, N., Badawi, A., Banoub, J.A.M., Bennett, D.A., Bensenor, I.M., Berfield, K.S.S., Bernstein, R.S.,
500 Bhattacharyya, K., Bijani, A., Brauer, M., Bukhman, G., Butt, Z.A., Cámera, L.A., Car, J., Carrero, J.J.,
501 Carvalho, F., Castañeda-Orjuela, C.A., Choi, J.-Y.J., Christopher, D.J., Cohen, A.J., Dandona, L., Dandona,
502 R., Dang, A.K., Daryani, A., de Courten, B., Demeke, F.M., Demoz, G.T., De Neve, J.-W., Desai, R.,
503 Dharmaratne, S.D., Diaz, D., Douiri, A., Driscoll, T.R., Duken, E.E., Eftekhari, A., Elkout, H., Endries, A.Y.,
504 Fadhil, I., Faro, A., Farzadfar, F., Fernandes, E., Filip, I., Fischer, F., Foroutan, M., Garcia-Gordillo, M.A.,
505 Gebre, A.K., Gebremedhin, K.B., Gebremeskel, G.G., Gezae, K.E., Ghoshal, A.G., Gill, P.S., Gillum, R.F.,
506 Goudarzi, H., Guo, Y., Gupta, R., Hailu, G.B., Hasanzadeh, A., Hassen, H.Y., Hay, S.I., Hoang, C.L., Hole,
507 M.K., Horita, N., Hosgood, H.D., Hostiuc, M., Househ, M., Ilesanmi, O.S., Ilic, M.D., Irvani, S.S.N., Islam,
508 S.M.S., Jakovljevic, M., Jamal, A.A., Jha, R.P., Jonas, J.B., Kabir, Z., Kasaeian, A., Kasahun, G.G., Kassa,
509 G.M., Kefale, A.T., Kengne, A.P., Khader, Y.S., Khafaie, M.A., Khan, E.A., Khan, J., Khubchandani, J., Kim,
510 Y.-E., Kim, Y.J., Kisa, S., Kisa, A., Knibbs, L.D., Komaki, H., Koul, P.A., Koyanagi, A., Kumar, G.A., Lan, Q.,
511 Lasrado, S., Lauriola, P., La Vecchia, C., Le, T.T., Leigh, J., Levi, M., Li, S., Lopez, A.D., Lotufo, P.A.,
512 Madotto, F., Mahotra, N.B., Majdan, M., Majeed, A., Malekzadeh, R., Mamun, A.A., Manafi, N., Manafi,
513 F., Mantovani, L.G., Meharie, B.G., Meles, H.G., Meles, G.G., Menezes, R.G., Mestrovic, T., Miller, T.R.,
514 Mini, G., Mirrakhimov, E.M., Moazen, B., Mohammad, K.A., Mohammed, S., Mohebi, F., Mokdad, A.H.,
515 Molokhia, M., Monasta, L., Moradi, M., Moradi, G., Morawska, L., Mousavi, S.M., Musa, K.I., Mustafa,
516 G., Naderi, M., Naghavi, M., Naik, G., Nair, S., Nangia, V., Nansseu, J.R., Nazari, J., Ndwandwe, D.E.,
517 Negoi, R.I., Nguyen, T.H., Nguyen, C.T., Nguyen, H.L.T., Nixon, M.R., Ofori-Asenso, R., Ogbo, F.A.,
518 Olagunju, A.T., Olagunju, T.O., Oren, E., Ortiz, J.R., Owolabi, M.O., P a, M., Pakhale, S., Pana, A., Panda-
519 Jonas, S., Park, E.-K., Pham, H.Q., Postma, M.J., Pourjafar, H., Poustchi, H., Radfar, A., Rafiei, A., Rahim,
520 F., Rahman, M.H.U., Rahman, M.A., Rawaf, S., Rawaf, D.L., Rawal, L., Reiner Jr., R.C., Reitsma, M.B.,
521 Roever, L., Ronfani, L., Roro, E.M., Roshandel, G., Rudd, K.E., Sabde, Y.D., Sabour, S., Saddik, B., Safari,
522 S., Saleem, K., Samy, A.M., Santric-Milicevic, M.M., Sao Jose, B.P., Sartorius, B., Satpathy, M., Savic, M.,
523 Sawhney, M., Sepanlou, S.G., Shaikh, M.A., Sheikh, A., Shigematsu, M., Shirkoohi, R., Si, S., Siabani, S.,
524 Singh, V., Singh, J.A., Soljak, M., Somayaji, R., Soofi, M., Soyiri, I.N., Tefera, Y.M., Temsah, M.-H., Tesfay,
525 B.E., Thakur, J.S., Toma, A.T., Tortajada-Girbés, M., Tran, K.B., Tran, B.X., Tudor Car, L., Ullah, I.,
526 Vacante, M., Valdez, P.R., van Boven, J.F.M., Vasankari, T.J., Veisani, Y., Violante, F.S., Wagner, G.R.,
527 Westerman, R., Wolfe, C.D.A., Wondafrash, D.Z., Wondmieneh, A.B., Yonemoto, N., Yoon, S.-J., Zaidi,
528 Z., Zamani, M., Zar, H.J., Zhang, Y., Vos, T., 2020. Prevalence and attributable health burden of chronic
529 respiratory diseases, 1990–2017: a systematic analysis for the Global Burden of Disease Study 2017.
530 The Lancet Respiratory Medicine 8, 585–596.

531 Sountoulidis, A., Marco Salas, S., Braun, E., Avenel, C., Bergenstråhle, J., Theelke, J., Vicari, M.,
532 Czarnewski, P., Liontos, A., Abalo, X., Andrusivová, Ž., Mirzazadeh, R., Asp, M., Li, X., Hu, L., Sariyar, S.,
533 Martinez Casals, A., Ayoglu, B., Firsova, A., Michaëlsson, J., Lundberg, E., Wählby, C., Sundström, E.,
534 Linnarsson, S., Lundeberg, J., Nilsson, M., Samakovlis, C., 2023. A topographic atlas defines
535 developmental origins of cell heterogeneity in the human embryonic lung. Nat Cell Biol 25, 351–365.

536 Spivack, S.D., Hurteau, G.J., Reilly, A.A., Aldous, K.M., Ding, X., Kaminsky, L.S., 2001. CYP1B1 expression
537 in human lung. Drug Metab Dispos 29, 916–922.

538 Treekitkarnmongkol, W., Hassane, M., Sinjab, A., Chang, K., Hara, K., Rahal, Z., Zhang, J., Lu, W.,
539 Sivakumar, S., McDowell, T.L., Kantrowitz, J., Zhou, J., Lang, W., Xu, L., Ochieng, J.K., Nunomura-
540 Nakamura, S., Deng, S., Behrens, C., Raso, M.G., Fukuoka, J., Reuben, A., Ostrin, E.J., Parra, E., Solis,
541 L.M., Spira, A.E., McAllister, F., Cascone, T., Wistuba, I.I., Moghaddam, S.J., Scheet, P.A., Fujimoto, J.,
542 Kadara, H., 2021. Augmented Lipocalin-2 Is Associated with Chronic Obstructive Pulmonary Disease
543 and Counteracts Lung Adenocarcinoma Development. Am J Respir Crit Care Med 203, 90–101.

544 Tsao, P.-N., Vasconcelos, M., Izvolsky, K.I., Qian, J., Lu, J., Cardoso, W.V., 2009. Notch signaling controls
545 the balance of ciliated and secretory cell fates in developing airways. Development 136, 2297–2307.

546 Upadhyay, S., Chakraborty, A., Thimraj, T.A., Baldi, M., Steneholm, A., Ganguly, K., Gerde, P., Ernstgård,
547 L., Palmberg, L., 2022. Establishment of Repeated In Vitro Exposure System for Evaluating Pulmonary
548 Toxicity of Representative Criteria Air Pollutants Using Advanced Bronchial Mucosa Models. Toxics 10,
549 277.

550 Wu, T., Hu, E., Xu, S., Chen, M., Guo, P., Dai, Z., Feng, T., Zhou, L., Tang, W., Zhan, L., Fu, X., Liu, S., Bo,
551 X., Yu, G., 2021. clusterProfiler 4.0: A universal enrichment tool for interpreting omics data. Innovation
552 2.
553
554

Article 1 - Discussion

To reproduce pollution exposure shown in literature, I chose to begin the exposure at day 33 of iALI, when ciliated cells begin to beat (E. Ahmed et al., 2022). Initially, exposures were performed by adding media supplemented with SRM2786 on the apical side to mimic what occurs in the adult lung. However, we observed that the epithelial cells began to die within three days.

To overcome these difficulties, the exposure was performed each day at the basal side of iALI, for two weeks (the duration will be discussed later). The unique conformation of iALI, with some epithelial cells in immediate contact with the mesenchyme, supports the establishment of this procedure. As the exposure is performed at the basal side, several results discussed in this Article show an inflammatory response to pollution.

Furthermore, some differences between the HY03 and the ICOP2 cell lines were noticeable, such as an epithelial hyperplasia for ICOPD2, but these results are inconclusive because of the use of only two iPSC lines. It should be interesting to further explore this point by including other cell lines. The lab has derived four iPSC lines derived from COPD and two control lines. Now that precise experimental conditions to expose iALI to pollution have been set up, such a project is feasible.

Article 2

This study aimed to investigate the crosstalk between the epithelial and mesenchymal compartments during iALI differentiation.

To achieve this objective, scRNA-seq data generated was used to identify all receptors and ligands specific to both the epithelium and to the mesenchyme sides (part of the scRNA-seq dataset of Article 1). The identified ligand-receptor pairs were then analyzed to determine their associated pathways based on existing literature. To highlight the role of the mesenchymal compartment in the model, EpCAM-negative stromal cells were sorted and cultured separately from epithelial cells. It was observed that these stromal cells have the ability to transdifferentiate into epithelial cells, which, to the best of my knowledge, had only been previously shown in one paper on a mouse model.

These initial results require further confirmation, and future experiments will be implemented to build upon this study.

Analysis of the stromal compartment in vitro iPSC-derived bronchial epithelium suggests a contribution of mesenchymal cells to epithelium transition during bronchial development

Amel Nasri[1], Florent Foisset[1], Carine Bourdais[1], Engi Ahmed[2,3], Markus Tammia[4], Tina Baker[4], Kristofer Thorn[4], Isabelle Vachier[2], Daniele Noel[1], Christian Jorgensen[1], Said Assou[1], Arnaud Bourdin[2,3*], John De Vos[1,5*]

[1] IRMB, Univ Montpellier, INSERM, CHU Montpellier, Montpellier, France

[2] Department of Respiratory Diseases, Univ Montpellier, CHU Montpellier, INSERM, Montpellier, France

[3] PhyMedExp, Univ Montpellier, INSERM, CHU Montpellier, Montpellier, France

[4] AstraZeneca, Göteborg, Sweden

[5] Department of Cell and Tissue Engineering, Univ Montpellier, CHU Montpellier, Montpellier, France

[*] To whom correspondence should be addressed:
John De Vos. IRMB, Hôpital St Eloi, 80 avenue Augustin Fliche. 34295 Montpellier. France. +33 467337888 john.devos@inserm.fr
Arnaud Bourdin, Department of Respiratory Diseases, Hôpital Arnaud de Villeneuve, Montpellier, France. Email: a-bourdin@chu-montpellier.fr

Key words: MET, EMT, crosstalk, interaction

ABSTRACT

During the respiratory tract development, the mesenchyme codevelop with the lung epithelium, and the stromal component interacts with the adjacent epithelium. We recently developed an iPSC-derived bronchial epithelium at air/liquid interface (iALI) model and observed a large stromal compartment below the epithelium. We performed single-cell RNA sequencing to identify interactions between these two compartments and identify several signalling cascades (ligand/receptor) that reflect a crosstalk between epithelium and mesenchymal cells during bronchial differentiation. Finally, we show that the mesenchymal compartment of iALI has the ability to transdifferentiate into epithelial cells in ALI culture, undergoing a mesenchymal to epithelium transition. These data provide a unique in vitro model to study the developmental role of mesenchymal cells during lung formation.

INTRODUCTION

The interaction of epithelium and mesenchymal cells is crucial during lung development. Many studies have shown that this interaction leads to branching, elongation, and maturation of the lung (Nasri et al., 2021; Park et al., 1998; Seth et al., 1993; Weaver et al., 2003). Indeed, several factors required for epithelial development are secreted by mesenchymal cells, including fibroblast growth factors (FGF) (Lü et al., 2005). Epithelial cells also secrete factors that act on supporting stromal cells and influence branching, angiogenesis, and other signalling pathways (Zhao et al., 2005). Several of these bilateral interactions have been described in vivo using mouse models but also in embryonic human lung.

We previously developed an in vitro model of bronchial differentiation using induced pluripotent stem cells (iPSCs) (E. Ahmed et al., 2022). Surprisingly, we observed that an important mesenchymal compartment develops during iALI differentiation. In the present study, we investigated whether the iALI model reflects the interaction between epithelium and mesenchymal cells reported in the literature. To this end, we analysed

each ligand and receptor expressed in epithelial and mesenchymal populations using single-cell RNA sequencing. Given the high proportion of stromal cells in our model, and a strong expression of genes involved in epithelium to mesenchyme (EMT)/mesenchyme to epithelium (MET) processes, we also investigated whether mesenchymal cells could differentiate into epithelial cells. Strikingly, we observed a profound plasticity of the stromal compartment, raising the possibility that MET may contribute to lung development or to lung diseases.

RESULTS

iALI contains epithelial and mesenchymal compartments

A preliminary single-cell RNA sequencing experiment analysing iALI revealed a large mesenchymal cell population, that was three time more abundant than the epithelial compartment (1929 mesenchymal cells vs 529 epithelial cells) (data not shown). This could be explained either by a loss of epithelial cells during the microfluidic single cell encapsulation step because of more rigid cell membrane of the epithelial cells, or indeed by a large mesenchymal compartment. Histology analysis confirms a late mesenchymal cell population right under the epithelium, in line with the composition of embryonic and fetal airways (He et al., 2022; Sountoulidis et al., 2023) (Fig.3D). Therefore, to enrich the epithelial cell population in our single cell analysis, we labelled iALI cells with the CD326/EPCAM antibody after 48 days of culture and sorted them based on this expression to perform single-cell RNA sequencing on an epithelial (CD326+) sample and a mesenchymal (CD326-) sample (Fig. 1A). We obtained 6038 high-quality cells for further analyses. Of these, 2039 cells were EPCAM+ and 3999 cells EPCAM- corresponding to the epithelial and mesenchymal/fibrobast population respectively. Seven clusters were identified in epithelial cells, including multi ciliated cells, basal cells, secretory cells, neuroendocrine cells, and, more surprisingly, two EMT cell populations (Fig. 1B). The epithelial compartment also contained a highly proliferative cell population (Fig. 1C). Interestingly, many of the proliferating epithelial cells also co-expressed genes involved in EMT/MET. Each cluster was annotated by

the specific expression of several marker based on literature evidence, including FOXJ1, TP63, MUC5B, NEUROD1, ZEB1, TWIST1, and MKI67 (Fig. 1D). Clustering of the mesenchymal cell population identified 5 groups of cells: 3 very close mesenchymal populations (1, 2 and 3), a proliferative population and a small epithelial population (Fig. 1E). With the exception of the epithelial cluster, general fibroblast markers like PDGFRA, COL1A1 or DCN were found to be widely expressed among all clusters.The proliferative cluster highly expressed genes associated with cell proliferation such as MKI67 (Fig. 1F-G). The epithelial cells expressed a high level of EPCAM RNA (Fig. 1G). This small population was possibly a contamination by epithelial cells that lost the surface expression of EPCAM through the action of trypsin, that was used for cell dissociation before single cell analysis, thus being sorted in the EPCAM- compartment. Except for the epithelial cells, all EPCAM- cells expressed genes involved in EMT/MET such as ZEB1, ZEB2 and TWIST1. Taken together, these data confirm that iALI is composed of both epithelium and mesenchymal cells, and that these two cell population harbour cells expressing EMT/MET genes.

Intercellular signaling matrix between epithelium and mesenchymal cells in iPS-derived bronchial epithelium

Fibroblasts are structural cells that underline the architecture of organs, support the homeostasis of epithelial cells. They have key roles in wound healing and diseases. To uncover potential signaling pathways between bronchial epithelium and the underlying stroma, we used CellChatDB to predict signalling interactions by identifying ligand-receptor pairs across both compartments (Fig 2A, 2B) (Garcia-Alonso et al., 2022). The analysis revealed that there were 10 signaling cascades starting from the epithelium in the direction of mesenchymal cells, and 7 in the reverse direction (Fig 2C). As previously reported, FGFR2 and FGFR4 were expressed in the epithelium, while FGF2, FGF10, FGF1, and FGF7 were expressed in the stroma (Fig 2D) (Bellusci et al., 1997; Lü et al., 2005; Nasri et al., 2021). Strikingly, mesenchymal cells also expressed receptors such as NOTCH2 and EGFR, with specific ligands expressed by the epithelium (Fig 2E and SF1). Furthermore, we identified several other pathways

involved in the crosstalk between the epithelium and stroma, in domains such as angiogenesis, immunomodulation, epithelial-mesenchymal transition (EMT), and cell growth regulation (Fig 2F-G, and Supplemental FigS2). These findings strongly suggest that iALI development is driven by an active crosstalk between epithelial cells and mesenchymal cells.

Inhibiting the mesenchymal compartment during iALI differentiation

We then investigated the impact that impeding the mesenchymal component during the differentiation of iALI could have on the epithelium. We initiated the inhibition of the TGFβ pathway on day 19 of iALI differentiation and continued it for either 7 or 21 days (Fig 3A) (Huang et al., 2014; Wei et al., 2017). We used LDN (250 nM) and SB431542 (10 µM) to inhibit the TGFβ pathways and confirmed the inhibition of SMAD2 phosphorylation by western blot (Fig 3B) (Albers et al., 2018). TGFβ signaling blockade had a considerable impact on the iALI. Vimentine staining, a critical intermediate filament of fibroblasts, almost disappeared at day 21, while the thickness of the mesenchymal compartment decreased in correlation with the duration of TGFβ inhibition (Fig 3C). We observed a decrease in the number of mesenchymal cells, that correlated with a reduction in the height of the iALI section (Fig 3D). Importantly, the alteration of the thickness and biology of the mesenchymal compartment at 21 days of TGFβ inhibition had a drastic impact on the epithelium with a near complete epithelial cells disappearance (Fig 3E). These results suggest that the stroma is a necessary compartment for the normal differentiation of bronchial epithelium in the iALI model, which reflects what is observed during development (Nasri et al., 2021).

iALI mesenchymal cells undergo a MET during in vitro culture

To evaluate the supportive effect of mesenchymal cells on epithelial cells, we sorted iALI cells based on CD326 expression, and re-cultured them on Geltrex, either each cell population alone or in combination (Fig 4A-B). However, CD326+ epithelial cells never recovered, suggesting that single cell dissociation of differentiated bronchial epithelial cells induced irreversible apoptosis. Interestingly, long term culture of

CD326- mesenchymal cells resulted in the appearance of numerous bud-like epithelial structures (Fig 4C). The epithelial cell component was detected as soon as the first week of culture but increased sharply at about two months of culture (Fig 4D). Interestingly, the epithelial structures contained basal cells, ciliated-like cells and neuroendocrine cells, and (Fig 4E, F, SF3). With the fact that both mesenchymal and epithelial iALI cell populations contain cells that express EMT/MET transcription factors such as ZEB1, ZEB2 and TWIST1, these data strongly suggest that iALI-derived mesenchymal cells can undergo MET and may contribute to the bronchial epithelium.

DISCUSSION

We observed that the in vitro development of bronchial epithelium from iPS cells came with the development of a large stromal cell compartment beneath the epithelial layer. In this study, we aimed to analyze the role of these mesenchymal cells and their interactions with the overlaying bronchial epithelium in iPSC-derived airways. Based on histology data, immunofluorescence and single cell data, we established that these mesenchymal cells were mostly fibroblasts. Fibroblasts play a crucial role in sustaining epithelia by participate in tissue homeostasis by producing extracellular matrix, providing mechanical support, creating signaling niches and regulating tissue homeostasis (Plikus et al., 2021).

We first investigated the role of this mesenchymal contingent by scRNAseq analysis. Noteworthy, a sub population was actively proliferating with cells either in M or G2 phases of the cell cycle, expressing markers of cell proliferation and cell division such as MKI67, CDK1 or MAD2L1. The remarkable proliferation observed is analogous to the dynamic growth observed in embryonic and fetal mesenchyme (Rawlins, 2011). Similarly, the importance of the stromal compartment, larger than the epithelial compartment, is also reminiscent of the fetal stage of lung development (Sountoulidis et al., 2023). These observations suggest that, despite its conventional histological arrangement with a pseudo stratified multi-ciliated organization, the iALI is still a developing bronchial epithelium that did not reached full adulthood at this stage. The single cell resolution of the transcriptomic data allowed us to identify at least 17

interactions between the epithelial and the fibroblastic compartment, involved in cell growth and survival, cell migration, angiogenesis, immunomodulation, and others, suggesting an active role for these fibroblasts during the bronchial epithelium development. To further investigate the contribution of the stromal compartment, we antagonized the mesenchymal compartment development. As expected, inhibiting fibroblasts development resulted in inhibition of the overlaying epithelium, further underlining the crucial role for the stroma during iALI formation.

An important questioning that these observations raised was the origin of these fibroblasts. Indeed, the iALI production involves several steps mimicking bronchial epithelium development, including definitive endoderm (DE) and vAFE steps. The fibroblasts observed in iALI may origin from these intermediate cell populations. Indeed, though the differentiation protocol involves highly enriched cell populations, with a purity usually > 80%, there are still non endodermal cells present, that may contain mesenchymal cells that later differentiate into fibroblasts. This hypothesis is also backed by the common origin of DE and mesoderm derivatives, the transient mesendoderm precursor cell population(Weidgang et al., 2013). As our findings demonstrated the essential role of the stromal compartment in the formation of the bronchial epithelium in iALI, it is plausible to suggest that these contaminants might play a beneficial role in the iALI model. Hence, the necessity of cell sorting during vAFE differentiation, when vAFE differentiation is not optimal, as reported in some protocols, may result in the unintended consequence of lacking mesenchymal cells and therefore incomplete bronchial epithelium development. Another explanation for this stroma layer is EMT. Indeed, we show that a large sup-population of epithelial cells express markers of EMT/MET. EMT occurs normally and is largely instrumental during embryonic development (Yang et al., 2020). It is possible that part of this TWIST1+ cell population transdifferentiate into proliferating mesenchymal cell that in fine contribute to the fibroblasts found in the iALI stromal population.

Finally, consistent with a marked expression of EMT/MET markers in the mesenchymal population, re-culture of EPCAM- cells resulted in expansion of EPCAM+ epithelial structures, including cell types typical of bronchial epithelium, suggesting that some of the mesenchymal cells may give differentiate into epithelial cells. Taken together,

these observations suggest that cell fate during iALI may be less fixed than expected, with exchange between the two compartments, epithelial and mesenchymal. It will be important in further studies to quantify these phenomena and explore to what extent these observations in the iALI model can be translated into basal airway homeostasis, regeneration of the epithelium after insults such as viral infection or exposure to pollution, and to the initiation and maintenance of chronic diseases such as IPF or COPD.

209 **FIGURES LEGENDS**

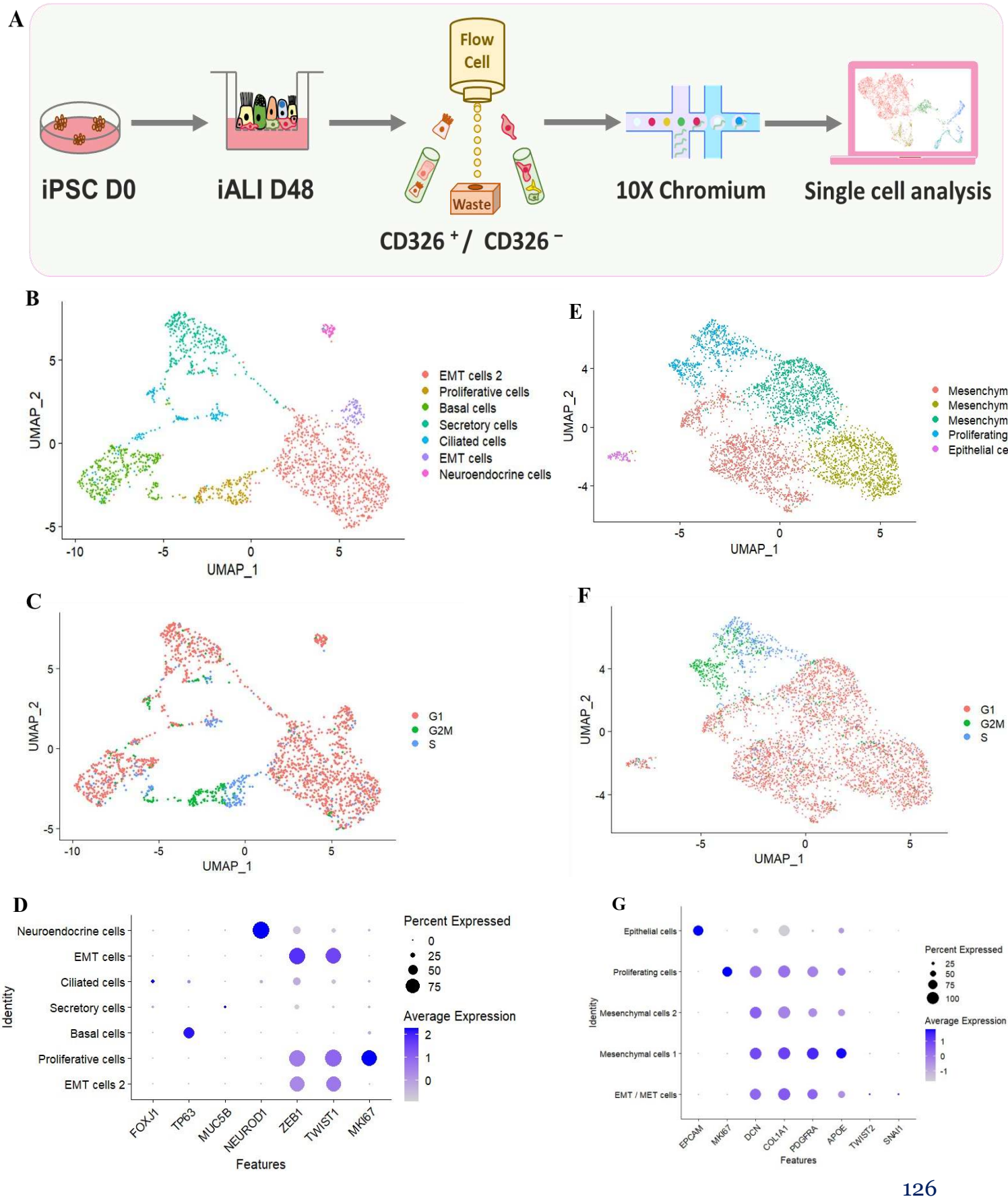

Figure 1. Characterization of epithelial and mesenchymal compartment

(A) Schematization of the experimentation. (B) UMAP of the epithelial cell clusters. (C) UMAP of cycle phase of the epithelial cell clusters. (D) Dot plot of specific genes of epithelial compartment. (E) UMAP of the mesenchymal cell clusters. (F) UMAP of cycle phase of the mesenchymal cell clusters. (G) Dot plot of specific genes of mesenchymal compartment.

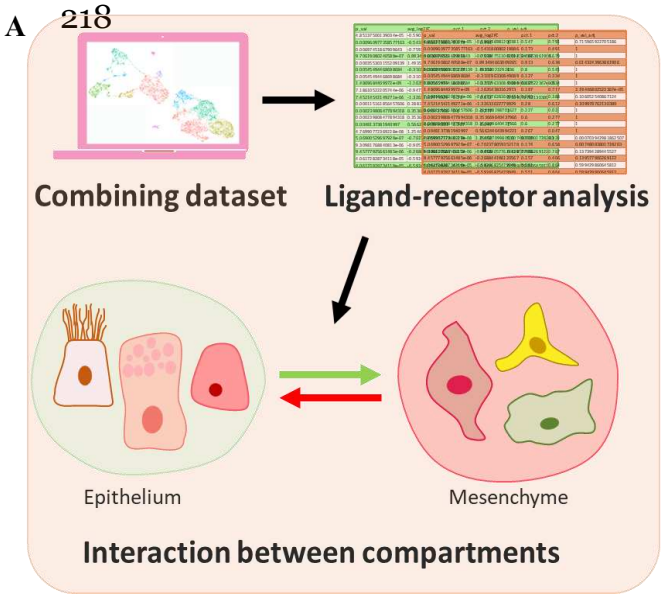
A
Combining dataset
Ligand-receptor analysis
Epithelium
Mesenchyme
Interaction between compartments

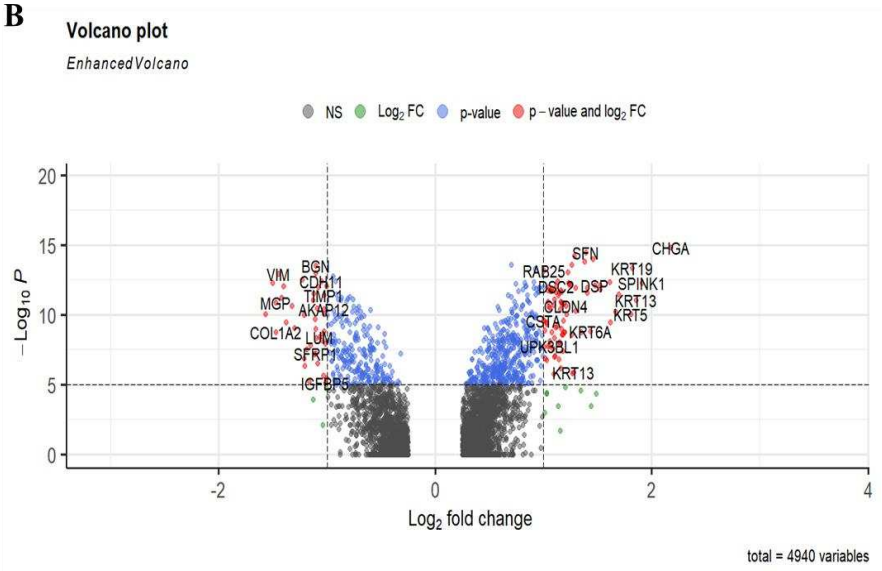
B
Volcano plot
EnhancedVolcano
NS
Log2 FC
p-value
p – value and log2 FC
−Log10 P
Log2 fold change
total = 4940 variables

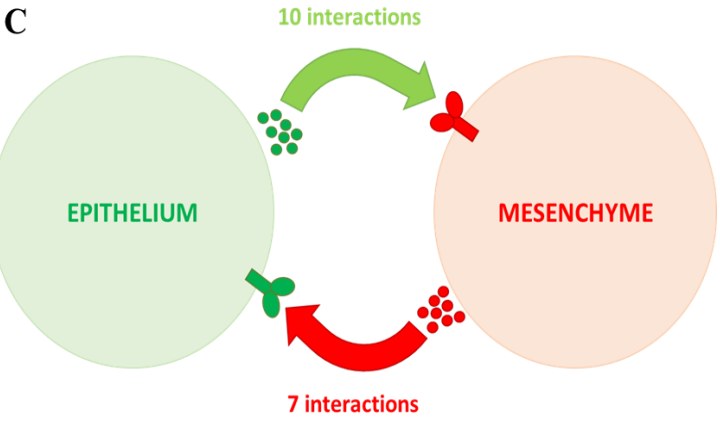
C
10 interactions
EPITHELIUM
MESENCHYME
7 interactions

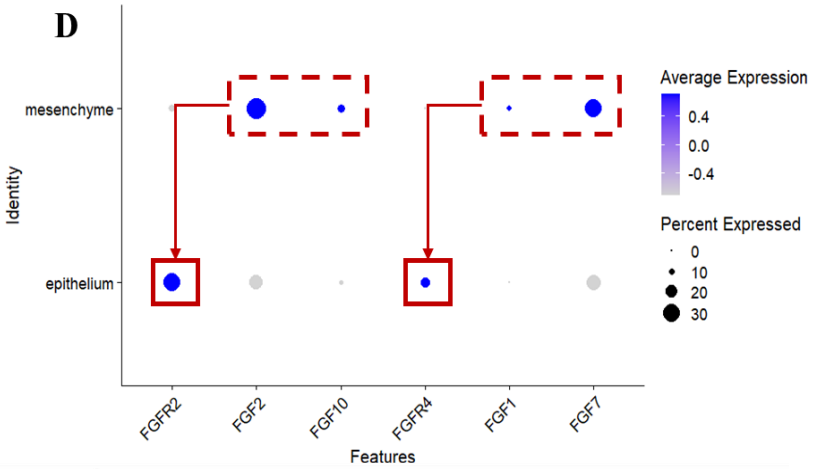
D
mesenchyme
epithelium
Identity
Features
Average Expression
Percent Expressed

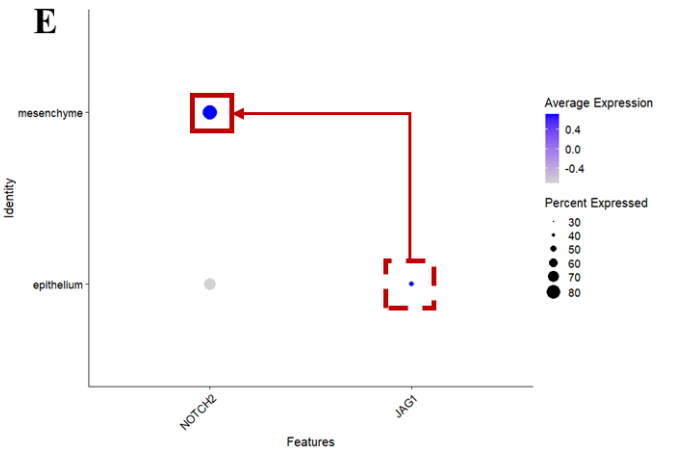
E
mesenchyme
epithelium
Identity
Features
Average Expression
Percent Expressed

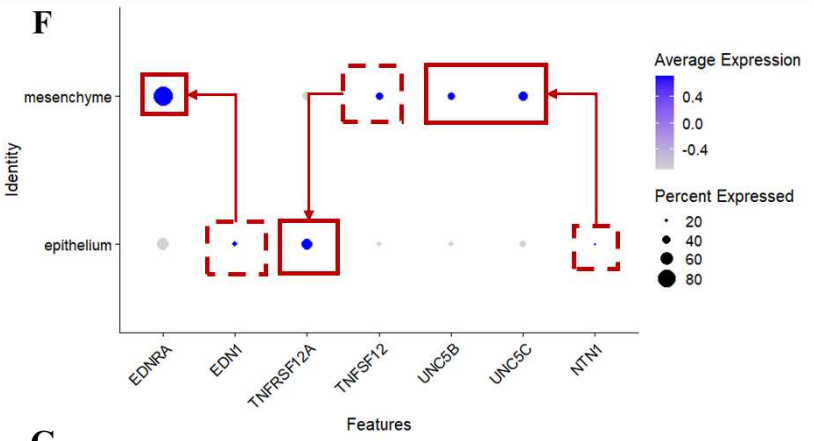
F
mesenchyme
epithelium
Identity
Features
Average Expression
Percent Expressed

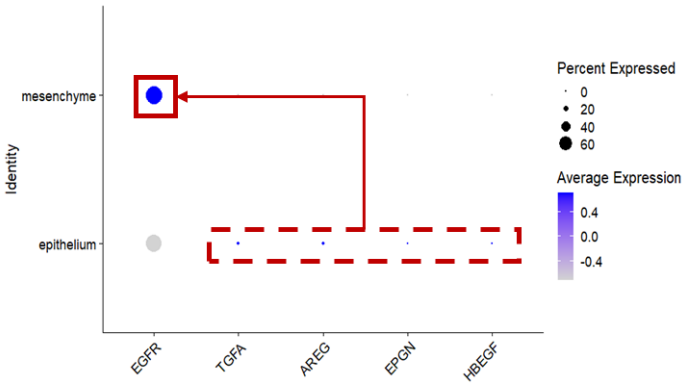
mesenchyme
epithelium
Identity
Percent Expressed
Average Expression

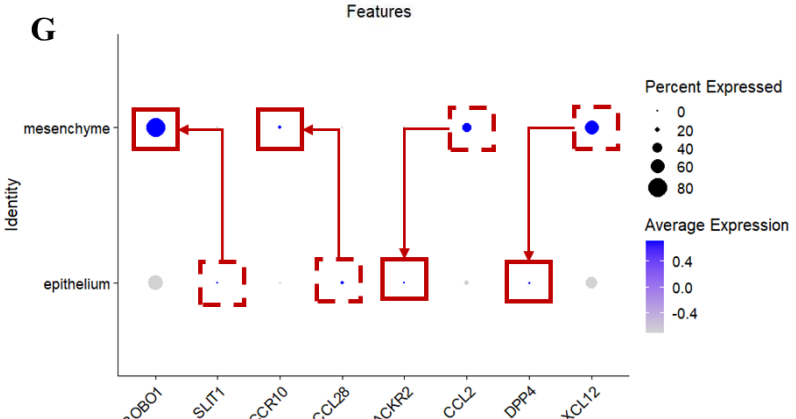
G
mesenchyme
epithelium
Identity
Percent Expressed
Average Expression

Figure 2. Interactions between epithelium and mesenchymal cells in iALI

(A) Steps to identify interactions between epithelium and mesenchymal cells. (B) Volcano plot of genes amplified in stroma (left) and epithelium (right). (C) Summary of the number of interactions between receptors and ligands of the epithelial and mesenchymal compartments. (D-G) Curated ligand-receptor interaction predictions from CellChatDB between epithelium and mesenchymal cells in iALI. Dot plots visualize gene expression by cell type; arrows indicate the predicted direction of signalling from ligands to receptors. Receptors are depicted as solid-lined squares, while ligands are represented as dotted-lined squares. (D) FGF pathway. (E) Notch (upper plot) and EGFR (bottom plot) pathways. (F) Angiogenesis pathways. (G) Immunomodulation.

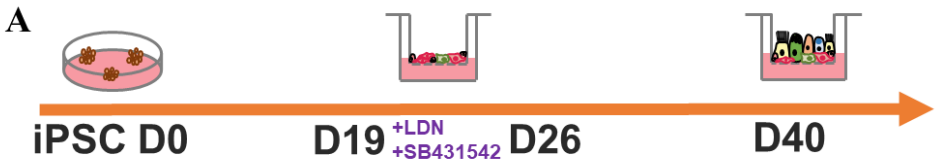
A
iPSC D0
D19
+LDN
+SB431542
D26
D40

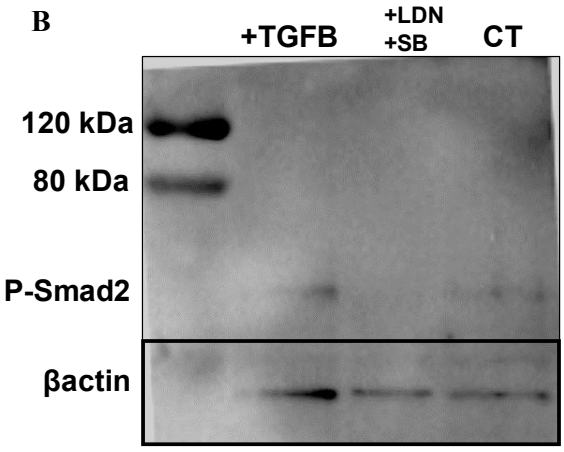
B
+TGFB
+LDN
+SB
CT
120 kDa
80 kDa
P-Smad2
βactin

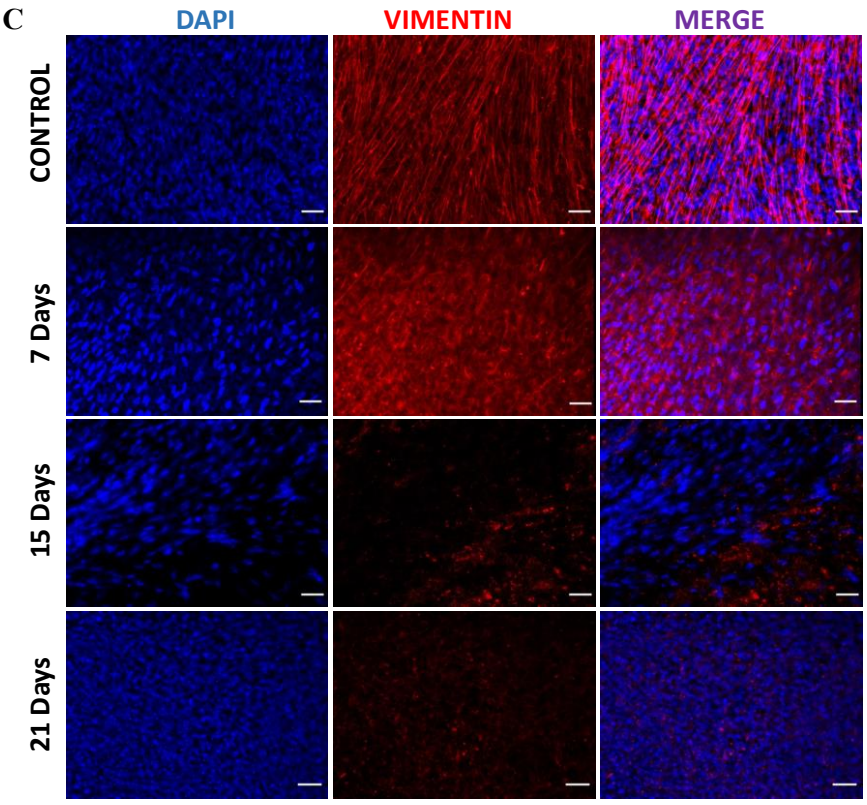
C
DAPI
VIMENTIN
MERGE
CONTROL
7 Days
15 Days
21 Days

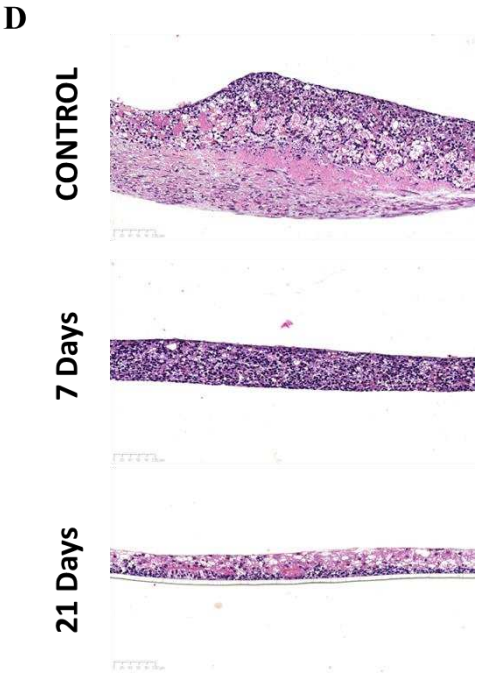
D
CONTROL
7 Days
21 Days

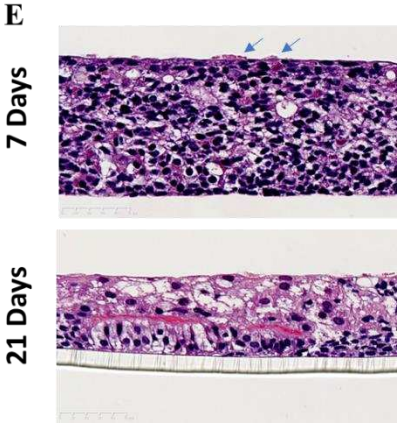
E
7 Days
21 Days

Figure 3. Effects of TGFβ pathway inhibition

(A) Protocol procedure of inhibition of the TGFβ pathway. (B) Immunofluorescence of the mesenchymal compartment with vimentin on iALI, on days 7, 15, and 21 of TGFβ pathway inhibition (scale bar 50 µm). (C) Western blot of phospho-Smad2 protein under control, inhibitory and overexpressing TGFβ conditions. (D) HES staining of paraffin section of iALI at days 7 and 21 of inhibition of TGFβ pathway. (E) Epithelium with and without ciliated cells (arrows) on days 7 and 21 of TGFβ pathway inhibition.

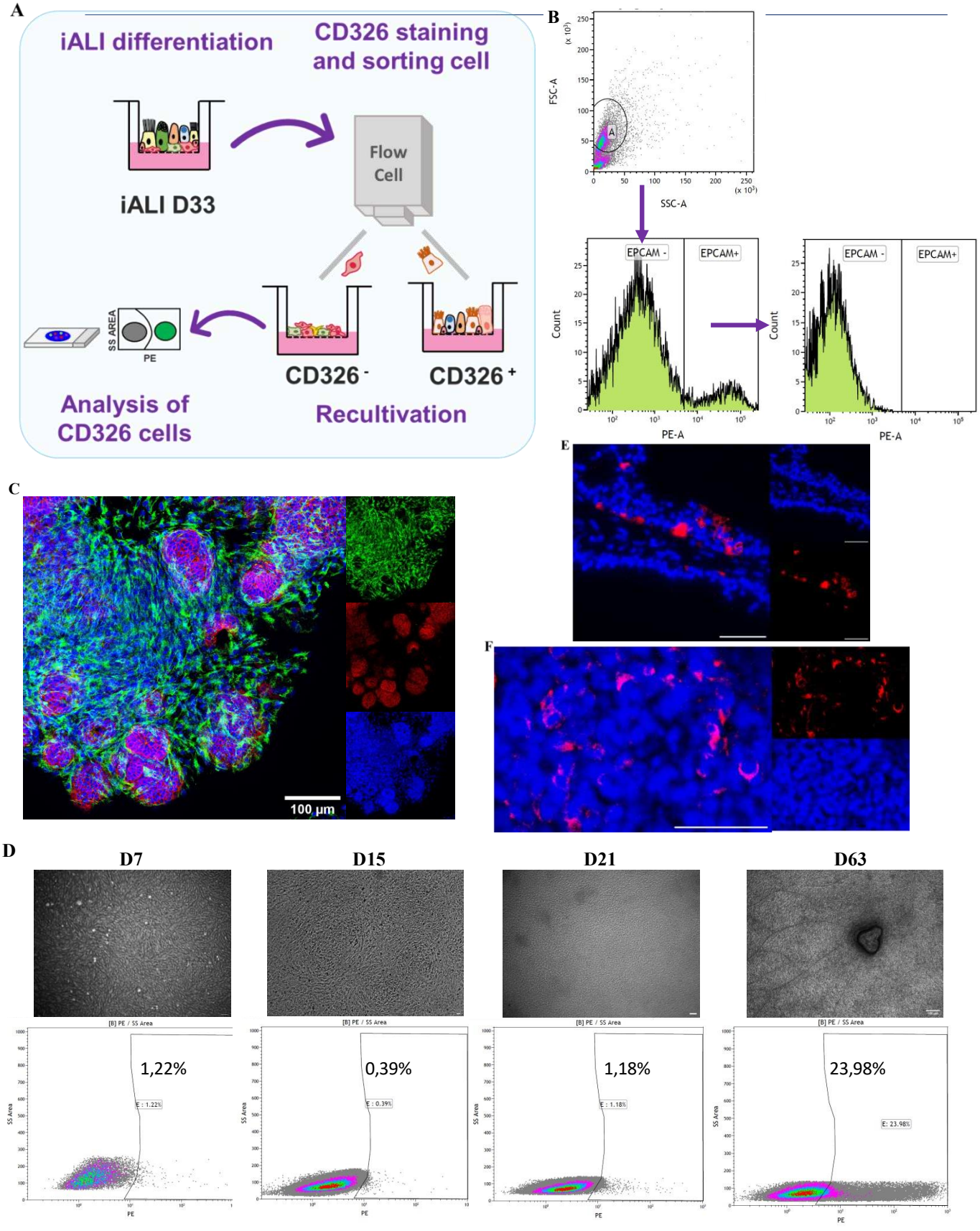
A
iALI differentiation
CD326 staining and sorting cell
Flow Cell
iALI D33
SS AREA
PE
CD326 -
CD326 +
Analysis of CD326 cells
Recultivation
B
FSC-A
SSC-A
EPCAM -
EPCAM+
Count
PE-A
C
100 µm
D
D7
D15
D21
D63
1,22%
0,39%
1,18%
23,98%
SS Area
PE
E
F

240

Figure 4. Reculturing of iALI mesenchymal cells

(A) Schematic of the experimental procedure. (B) FACS workflow analysis of EPCAM- (CD326-) cells based on isotype parameters (top) and review of mesenchymal cells (bottom left). (C) Time course of EPCAM protein expression by FACS analysis of the recultured mesenchymal cells. (D) Immunofluorescence of epithelial (EPCAM in red) and mesenchymal (VIMENTIN in green) compartments after 63 days of reculture. Immunofluorescence of (E) neuroendocrine (CHGA in red) and (F) ciliated (TUBB4) cells, in paraffin section after 63 days of recultivation; scale bar 50 µm.

SUPLEMMENTAL FIGURE

252

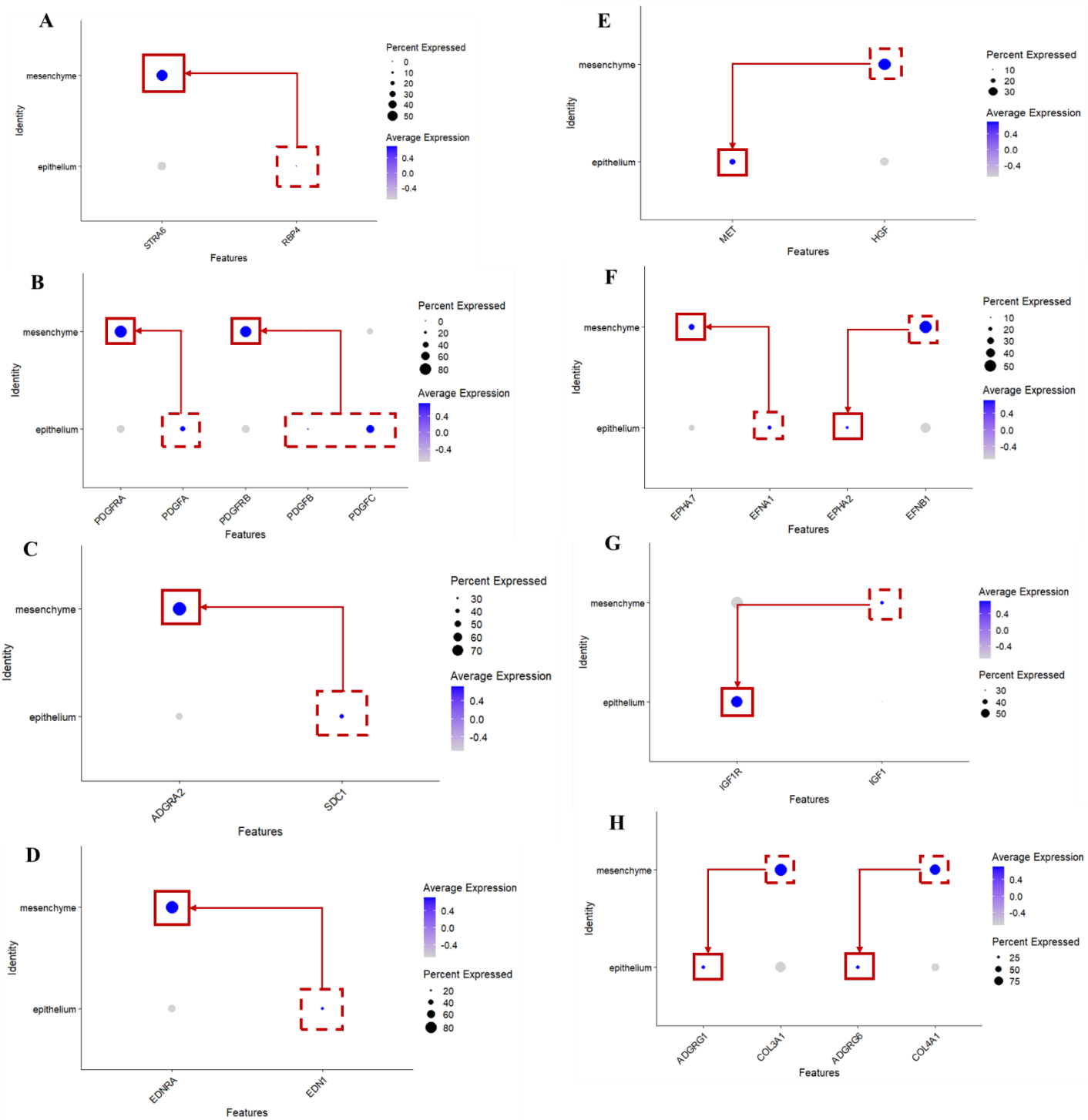

253 **SF1. Analysis of ligand-receptors pairs**

254 (A), (B), (C), (D) dot plot of several pathways expressing the receptor in
255 mesenchymal compartment and ligand in epithelium. (E), (F), (G) dot plot of

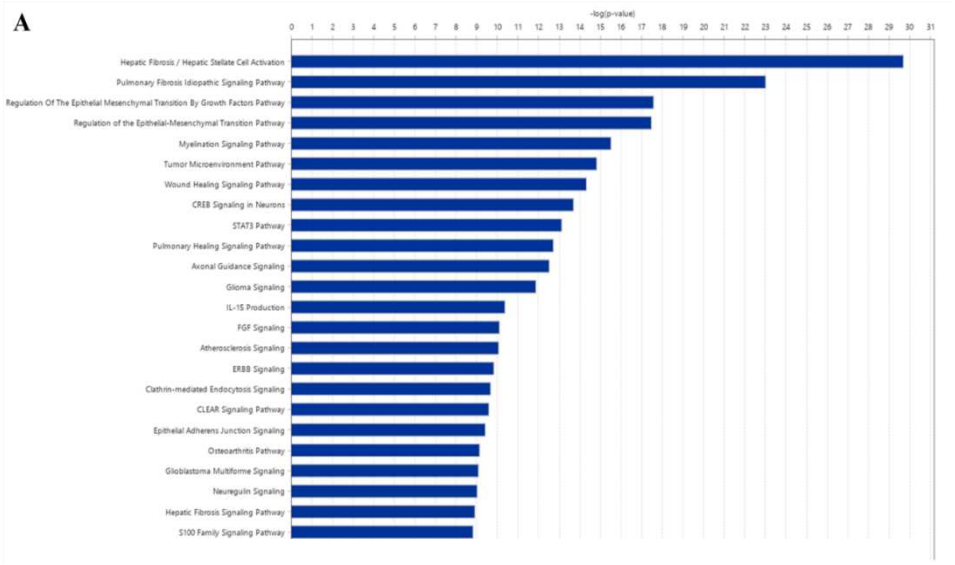

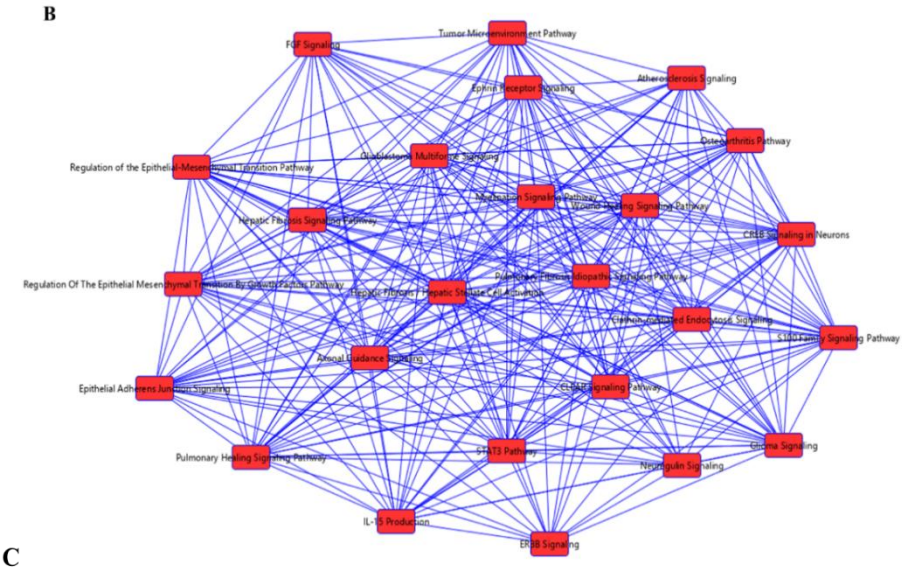

C

Canonical Pathways	-log(p-value)	Ratio	Genes
Hepatic Fibrosis / Hepatic Stellate Cell Activation	2,97E+01	1,13E-01	CCL2,COL3A1,COL4A1,EDN1,EDNRA,EGFR,FGF1,FGF2,FGFR2,HGF,IGF1,IGF1R,IGF2,IL1RAP,IL1RAPL1,MET,PDGFA,PDGFB,PDGFC,PDGFRA,PDGFRB,TGFA
Pulmonary Fibrosis Idiopathic Signaling Pathway	2,30E+01	6,44E-02	AREG,COL3A1,COL4A1,CXCL12,EDN1,EDNRA,EGFR,FGF2,FGFR2,FGFR4,JAG1,NOTCH1,NOTCH2,NOTCH3,NOTCH4,PDGFA,PDGFB,PDGFC,PDGFRA,PDGFRB,TGFA
Regulation Of The Epithelial Mesenchymal Transitic	1,76E+01	7,81E-02	EGFR,FGF1,FGF10,FGF2,FGF7,FGFR2,FGFR4,HGF,MET,PDGFA,PDGFB,PDGFC,PDGFRA,PDGFRB,TNFSF12
Regulation of the Epithelial-Mesenchymal Transitior	1,75E+01	7,69E-02	EGFR,FGF1,FGF10,FGF2,FGF7,FGFR2,FGFR4,HGF,JAG1,MET,NOTCH1,NOTCH2,NOTCH3,NOTCH4,PDGFRB
Myelination Signaling Pathway	1,55E+01	4,89E-02	ADGRG6,EGFR,ERBB3,FGF2,FGFR2,FGFR4,IGF1,IGF1R,NOTCH1,NOTCH2,NRG1,PDGFA,PDGFB,PDGFC,PDGFRA,PDGFRB
Tumor Microenvironment Pathway	1,48E+01	7,26E-02	CCL2,COL3A1,CXCL12,FGF1,FGF10,FGF2,FGF7,HGF,IGF1,IGF2,PDGFA,PDGFB,PDGFC
Wound Healing Signaling Pathway	1,43E+01	5,56E-02	COL3A1,COL4A1,EGFR,FGF2,FGF7,FGFR2,HBEGF,IL1RAP,IL1RAPL1,PDGFA,PDGFB,PDGFC,TGFA,TNFSF12
CREB Signaling in Neurons	1,37E+01	2,97E-02	ADGRA2,ADGRG1,ADGRG6,CCR10,CMKLR1,EDNRA,EGFR,FGF2,FGFR2,FGFR4,HGF,IGF1,IGF1R,PDGFB,PDGFRA,PDGFRB,PTH1R,TGFA
STAT3 Pathway	1,31E+01	8,15E-02	EGFR,FGF2,FGFR2,FGFR4,HGF,IGF1,IGF1R,PDGFB,PDGFRA,PDGFRB,TGFA
Pulmonary Healing Signaling Pathway	1,27E+01	6,03E-02	CXCL12,EGFR,FGF10,FGF7,FGFR2,HBEGF,JAG1,NOTCH1,NOTCH2,NOTCH3,NOTCH4,PDGFC
Axonal Guidance Signaling	1,25E+01	3,14E-02	CXCL12,EFNA1,EFNB1,EPHA2,EPHA7,IGF1,MET,NTN1,PDGFA,PDGFB,PDGFC,ROBO1,SLIT1,SLIT2,UNC5B,UNC5C
Glioma Signaling	1,19E+01	0,08	EGFR,IGF1,IGF1R,IGF2,PDGFA,PDGFB,PDGFC,PDGFRA,PDGFRB,TGFA
IL-15 Production	1,04E+01	7,32E-02	EGFR,EPHA2,ERBB3,FGFR2,FGFR4,IGF1R,MET,PDGFRA,PDGFRB
FGF Signaling	1,01E+01	9,30E-02	FGF1,FGF10,FGF2,FGF7,FGFR2,FGFR4,HGF,MET
Atherosclerosis Signaling	1,01E+01	6,77E-02	CCL2,COL3A1,CXCL12,PDGFA,PDGFB,PDGFC,RBP4,TNFRSF12A,TNFSF12
ERBB Signaling	9,82E+00	8,60E-02	AREG,BTC,EGFR,ERBB3,HBEGF,NRG1,NRG2,TGFA
Clathrin-mediated Endocytosis Signaling	9,67E+00	4,81E-02	FGF1,FGF10,FGF2,FGF7,IGF1,MET,PDGFA,PDGFB,PDGFC,RBP4
CLEAR Signaling Pathway	9,58E+00	3,86E-02	EGFR,FGF2,FGFR2,FGFR4,HGF,IGF1,IGF1R,PDGFB,PDGFRA,PDGFRB,TGFA
Epithelial Adherens Junction Signaling	9,41E+00	5,73E-02	EGFR,FGF1,HGF,IGF1R,MET,NOTCH1,NOTCH2,NOTCH3,NOTCH4
Osteoarthritis Pathway	9,13E+00	4,24E-02	FGF2,IL1RAP,IL1RAPL1,JAG1,NOTCH1,PDGFC,PTH1R,PTHLH,RARRES2,RBP4
Glioblastoma Multiforme Signaling	9,08E+00	5,26E-02	EGFR,IGF1,IGF1R,IGF2,PDGFA,PDGFB,PDGFC,PDGFRA,PDGFRB
Neuregulin Signaling	9,02E+00	6,84E-02	AREG,BTC,EGFR,ERBB3,HBEGF,NRG1,NRG2,TGFA
Hepatic Fibrosis Signaling Pathway	8,90E+00	2,84E-02	CCL2,COL3A1,EDN1,EDNRA,FGF2,IL1RAP,IL1RAPL1,PDGFA,PDGFB,PDGFC,PDGFRA,PDGFRB
S100 Family Signaling Pathway	8,82E+00	1,94E-02	ADGRA2,ADGRG1,ADGRG6,AREG,BTC,CCR10,CMKLR1,EDNRA,EGFR,FGFR2,FGFR4,HBEGF,PDGFC,PTH1R,TGFA
Ephrin Receptor Signaling	8,44E+00	4,46E-02	CXCL12,EFNA1,EFNB1,EPHA2,EPHA7,FGF1,PDGFA,PDGFB,PDGFC
HIF1α Signaling	8,33E+00	4,33E-02	EDN1,FGF2,HGF,IGF1,IGF2,MET,PDGFB,PDGFC,TGFA
Breast Cancer Regulation by Stathmin1	8,27E+00	2,19E-02	ADGRA2,ADGRG1,ADGRG6,CCR10,CMKLR1,EDNRA,FGF2,HGF,IGF1,PDGFB,PDGFC,PTH1R,TGFA
PPAR Signaling	7,81E+00	6,54E-02	IL1RAP,IL1RAPL1,PDGFA,PDGFB,PDGFC,PDGFRA,PDGFRB
Sperm Motility	7,54E+00	3,50E-02	EGFR,EPHA2,ERBB3,FGFR2,FGFR4,IGF1R,MET,PDGFRA,PDGFRB
Airway Pathology in Chronic Obstructive Pulmonar	7,51E+00	5,93E-02	CCL2,FGF1,FGF10,FGF2,FGF7,RBP4,TNFSF12
Notch Signaling	7,25E+00	1,32E-01	JAG1,NOTCH1,NOTCH2,NOTCH3,NOTCH4
Human Embryonic Stem Cell Pluripotency	7,17E+00	3,98E-02	FGF2,FGFR2,FGFR4,PDGFA,PDGFB,PDGFC,PDGFRA,PDGFRB
FAK Signaling	7,09E+00	1,44E-02	ADGRA2,ADGRG1,ADGRG6,CCR10,CMKLR1,COL3A1,EDNRA,EFNA1,EFNB1,EGFR,IGF1R,MET,PDGFRA,PDGFRB,PTH1R

pathways expressing the receptor in epithelial compartment and specific ligand in mesenchymal cells.

258 **SF2. Pathway implicated on ligand receptors analysis**(A) Top pathway
259 highlighted on all interactions between epithelium and stroma crosstalk. (B)

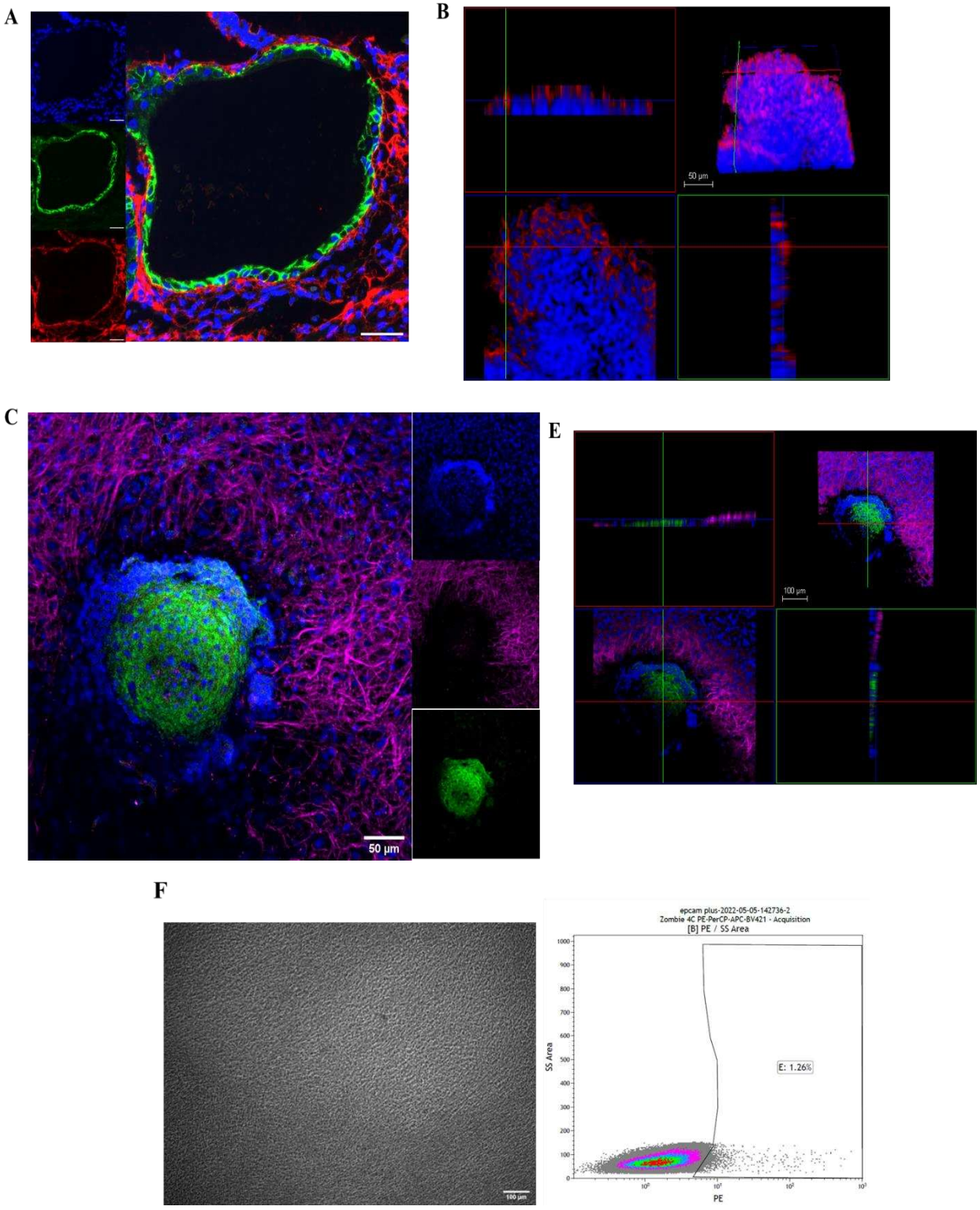

Summary of identified pathways and their interconnection. (C) Table of genes implicated in identified pathways.

SF3. Mesenchymal recultures cells undergoes a MET

(A) Immunofluorescence of Vimentin (red) and Epcam (green) on paraffin section of recultured mesenchymal cells at day 60. (B) Immunofluorescence on whole iALI of TUBB4 (red) on recultured mesenchymal cells at day 67, with x and y axes. (C) Immunofluorescence on whole iALI of TP63 (green) and DECORIN (violet) on recultured mesenchymal cells at day 67, (E) with x and y axes. (F) FACS and aspect of $CD326^{+}$ recultured epithelial cells at day 63.

MATERIAL AND METHODS

hiPSC lines culture and iALI differentiation

The hiPSC lines UHOMi002-A and UHOMi003-A (Ahmed et al., 2021; Fieldes et al., 2020), were incubated daily in Essential 8™ medium (Thermo Fisher Scientific) at 37 °C, 5% CO2, and growth in feeder-free Geltrex matrix (Thermo Fisher Scientific). Each cell lines were plated at 80 000 cells/cm^2 and differentiated in iALI as previously shown (E. Ahmed et al., 2022). Media was changed daily on basolateral side.

Inhibition of TGFβ

To inhibit TGFβ pathway, LDN (250 nM, Biotechne) and SB431542 (10 µM, Biotechne) were added to PneumaCult™-ALI Medium in basolateral side. The media was changed daily and these cytokines were used during 7, 15 or 21 days. After that, only PneumaCult™-ALI Medium is used until the end of the differentiation.

Flow cytometric analysis and cell sorting

iALI were dissociated with Trypsin (15min, 37°C) and gently detached from Transwells. Then, dissociated cells were filtered through a 40 µm porosity (Corning) with a solution

of PneumaCult™-ALI Medium and then centrifuged (1200 rpm for 5 min). Cells were resuspended in 1,5 mL of PneumaCult™-ALI Medium and labeled with isotype-PE (2 iALI) or CD326 antibody (10 iALI) during 30 min at 4°C. Cells were washed and then sorted on BD FACSAria™, with MRI platform.

Reculturing of mesenchymal cells

At day 33 of iALI, sorted CD326- cells, were replated at 300 000 cells per Transwells coated with Geltrex and immerged on PneumaCult™-ALI Medium. PneumaCult™-ALI Medium were removed from the apical the next day of the experimentation, when the cells have adhered, and changed every day in basal.

scRNA-seq experiments

The concentration of freshly sorted cells was adjusted to 1000 cells/µl in PBS-/- complemented with 0.01% of BSA and 10 000 cells were targeted for cDNA preparation and put through the 10X Genomics Chromium Next GEM Single Cell 3' v3.1. After cDNA preparation and clean-up, the quality of cDNA was checked on an Agilent Bioanalyzer DNA High Sensitivity chip. scRNA-seq library preparation and sequencing were carried out by the Princeton Genomics Core Facility using the Chromium Single Cell 3' Library and Gel Bead Kit v3 on the Chromium Controller (10X Genomics) following manufacturer protocols. The quality of libraries was determined using an Agilent 2100 Bioanalyzer and a High Sensitivity DNA kit (Agilent, Santa Clara, CA, USA). Libraries were sequenced on AstraZenca platform (Göteborg, Sweden), followed by computational alignment using CellRanger. Illumina sequencing libraries were prepared from the PCR-amplified cDNA CD326+ and CD326- samples using the DNA library prep kit (Illumina). The CellRanger software was used to run the count pipeline with default settings on all Fastq files from each sample to generate gene-barcode matrices using the human reference genome.

scRNA-seq analysis

scRNA-seq data were imported into R and processed using the Seurat package. Clusters and expression levels of genes of interest were visualized using the uniform

manifold approximation and projection (UMAP) dimensional reduction. We identified low-quality cells based on three metrics: (1) High number of UMIs (≥1000); (2) Cells with less than 1 500 or more than 8 000 genes detected; (3) High percent of mitochondrial gene counts (≥10%). After low-quality cells were filtered out, we employed a global-scaling normalization method “LogNormalize” that normalizes the gene expression. Datasets from CD326+ and CD326- samples were processed first separately and then together, using the Seurat integration tools. To compare clusters between datasets, we carried out Pearson correlation analysis on gene expression profiles for pairs of clusters, then performed unsupervised hierarchical clustering. Differentially expressed genes (DEGs) were investigated in each epithelial or mesenchymal sub-cluster using Seurat’s FindMarkers function. DEGs were filtered based on a >2-fold change and a maximum p value of 0.05.

Ligand receptor analysis

Single cell dataset used previously was used to perform this study (Nasri et al., Unpublished data). The genes specifically expressed in epithelial and mesenchymal cells were obtained by using the Seurat function “FindAllMarkers”. Then, genes were annotated using AnnotationHub package (Maintainer et al., 2023). Identified ligands and receptors were then run on CellPhoneBD online platform, to identify couples.

Paraffin sections

iALI were fixed in 4% paraformaldehyde (PFA) for 24 hours at 4°C and after PBS-/- washes, were cut from Transwells and embedded in low-melting agarose 0.5% (Thermo Fisher Scientific). Samples were then cut in half, placed in a cassette on the newly cut slices, stored in 70% ethanol at 4°C, and sent to RHEM for parrafin embedding, sectioning, and histological staining. Paraffin sections were cut at a thickness of 3 µm. Deparaffinization was performed by placing the sections in Neoclear for 3 minutes and progressively decreasing ethanol concentration for 6 minutes, 3 minutes, and 3 minutes in 100%, 70%, and 50%, respectively. Finally, the sections were placed in boiling Neoclear for 20 minutes, and immunofluorescence staining was performed after the slides cooled.

Immunofluorescence staining

Samples were fixed in 4% PFA at RT for 15 min, and permeabilized with PBS 0.5% Triton X-100 for 15 min. Cells were blocked with 10% of donkey serum in PBS complemented with 1% BSA, 0.1% Triton X-100 (solution A) at RT for 60 min. Samples were incubated with primary antibodies (diluted in solution A) at 4°C overnight and after several washes with PBS containing 0.025% Triton X-100, were incubated with secondary antibodies (dilution 1/1000) at RT for 60 min protected from light. Nuclei were stained with DAPI (1:5000) for 2 min. Samples were mounted in glycerol 100% and stored in the dark at 4°C. Image acquisition was performed with Leica SP8 confocal microscope (CARTIGEN platform) and analyzed with ImageJ (Fiji).

Analysis

Graph analyses were performed using GraphPad 9.4.1 (Prism).

ACKNOWLEDGEMENT

We acknowledge the “Réseau d’Histologie Expérimentale de Montpellier” - RHEM facility supported by SIRIC Montpellier Cancer Grant INCa_Inserm_DGOS_12553, the european regional development foundation and the Occitanie region (FEDER-FSE 2014-2020 Languedoc Roussillon), REACT-EU (Recovery Assistance for Cohesion and the Territories of Europe), IBiSA and Ligue contre le cancer for processing our animal tissues, with histology technics and expertise.

DISCLOSURE OF POTENTIAL CONFLICTS OF INTEREST

REFERENCES

Ahmed, E., Fieldes, M., Bourguignon, C., Mianné, J., Petit, A., Jory, M., Cazevieille, C., Boukhaddaoui, H., Garnett, J.P., Hirtz, C., Massiera, G., Vachier, I., Assou, S., Bourdin, A., De Vos, J., 2022. Differentiation of Human Induced Pluripotent Stem Cells from Patients with Severe COPD into Functional Airway Epithelium. Cells 11, 2422.

Ahmed, E., Fieldes, M., Mianné, J., Bourguignon, C., Nasri, A., Vachier, I., Assou, S., Bourdin, A., De Vos, J., 2021. Generation of four severe early-onset chronic obstructive pulmonary disease (COPD) patient-derived induced pluripotent stem cell lines from peripheral blood mononuclear cells. Stem Cell Research 56, 102550.

Albers, R.E., Selesniemi, K., Natale, D.R.C., Brown, T.L., 2018. TGF-β induces Smad2 Phosphorylation, ARE Induction, and Trophoblast Differentiation. Int J Stem Cells 11, 111–120.

Bellusci, S., Grindley, J., Emoto, H., Itoh, N., Hogan, B.L., 1997. Fibroblast growth factor 10 (FGF10) and branching morphogenesis in the embryonic mouse lung. Development 124, 4867–4878.

Fieldes, M., Ahmed, E., Bourguignon, C., Mianné, J., Martin, M., Arnould, C., Vachier, I., Assou, S., De Vos, J., Bourdin, A., 2020. Generation of the induced pluripotent stem cell line UHOMi002-A from peripheral blood mononuclear cells of a healthy male donor. Stem Cell Research 49, 102037.

Garcia-Alonso, L., Lorenzi, V., Mazzeo, C.I., Alves-Lopes, J.P., Roberts, K., Sancho-Serra, C., Engelbert, J., Marečková, M., Gruhn, W.H., Botting, R.A., Li, T., Crespo, B., van Dongen, S., Kiselev, V.Y., Prigmore, E., Herbert, M., Moffett, A., Chédotal, A., Bayraktar, O.A., Surani, A., Haniffa, M., Vento-Tormo, R., 2022. Single-cell roadmap of human gonadal development. Nature 607, 540–547.

He, P., Lim, K., Sun, D., Pett, J.P., Jeng, Q., Polanski, K., Dong, Z., Bolt, L., Richardson, L., Mamanova, L., Dabrowska, M., Wilbrey-Clark, A., Madissoon, E., Tuong, Z.K., Dann, E., Suo, C., Goh, I., Yoshida, M., Nikolić, M.Z., Janes, S.M., He, X., Barker, R.A., Teichmann, S.A., Marioni, J.C., Meyer, K.B., Rawlins, E.L., 2022. A human fetal lung cell atlas uncovers proximal-distal gradients of differentiation and key regulators of epithelial fates. Cell 185, 4841-4860.e25.

Huang, S.X.L., Islam, M.N., O'Neill, J., Hu, Z., Yang, Y.-G., Chen, Y.-W., Mumau, M., Green, M.D., Vunjak-Novakovic, G., Bhattacharya, J., Snoeck, H.-W., 2014. Efficient generation of lung and airway epithelial cells from human pluripotent stem cells. Nat Biotechnol 32, 84–91.

Lü, J., Izvolsky, K.I., Qian, J., Cardoso, W.V., 2005. Identification of FGF10 Targets in the Embryonic Lung Epithelium during Bud Morphogenesis. J. Biol. Chem 280, 4834-4841,.

Maintainer, B.P., Morgan, M., Carlson, M., Tenenbaum, D., Arora, S., Oberchain, V., Morrell, K., Shepherd, L., 2023. AnnotationHub: Client to access AnnotationHub resources.

Nasri, A., Foisset, F., Ahmed, E., Lahmar, Z., Vachier, I., Jorgensen, C., Assou, S., Bourdin, A., De Vos, J., 2021. Roles of Mesenchymal Cells in the Lung: From Lung Development to Chronic Obstructive Pulmonary Disease. Cells 10, 3467.

Park, W.Y., Miranda, B., Lebeche, D., Hashimoto, G., Cardoso, W.V., 1998. FGF-10 Is a Chemotactic Factor for Distal Epithelial Buds during Lung Development. Developmental Biology 201, 125-134,.

404 Plikus, M.V., Wang, X., Sinha, S., Forte, E., Thompson, S.M., Herzog, E.L., Driskell, R.R., Rosenthal, N.,
405 Biernaskie, J., Horsley, V., 2021. Fibroblasts: Origins, definitions, and functions in health and disease.
406 Cell 184, 3852–3872.

407 Rawlins, E.L., 2011. The building blocks of mammalian lung development. Developmental Dynamics
408 240, 463–476.

409 Seth, R., Shum, L., Wu, F., Wuenschell, C., Hall, F.L., Slavkin, H.C., Warburton, D., 1993. Role of
410 Epidermal Growth Factor Expression in Early Mouse Embryo Lung Branching Morphogenesis in
411 Culture: Antisense Oligodeoxynucleotide Inhibitory Strategy. Developmental Biology 158, 555–559.

412 Sountoulidis, A., Marco Salas, S., Braun, E., Avenel, C., Bergenstråhle, J., Theelke, J., Vicari, M.,
413 Czarnewski, P., Liontos, A., Abalo, X., Andrusivová, Ž., Mirzazadeh, R., Asp, M., Li, X., Hu, L., Sariyar,
414 S., Martinez Casals, A., Ayoglu, B., Firsova, A., Michaëlsson, J., Lundberg, E., Wählby, C., Sundström,
415 E., Linnarsson, S., Lundeberg, J., Nilsson, M., Samakovlis, C., 2023. A topographic atlas defines
416 developmental origins of cell heterogeneity in the human embryonic lung. Nat Cell Biol 25, 351–365.

417 Weaver, M., Batts, L., Hogan, B.L.M., 2003. Tissue Interactions Pattern the Mesenchyme of the
418 Embryonic Mouse Lung. Developmental Biology 258, 169-184,.

419 Wei, Y., Kim, T.J., Peng, D.H., Duan, D., Gibbons, D.L., Yamauchi, M., Jackson, J.R., Le Saux, C.J., Calhoun,
420 C., Peters, J., Derynck, R., Backes, B.J., Chapman, H.A., 2017. Fibroblast-specific inhibition of TGF-β1
421 signaling attenuates lung and tumor fibrosis. J Clin Invest 127, 3675–3688.

422 Weidgang, C.E., Russell, R., Tata, P.R., Kühl, S.J., Illing, A., Müller, M., Lin, Q., Brunner, C., Boeckers,
423 T.M., Bauer, K., Kartikasari, A.E.R., Guo, Y., Radenz, M., Bernemann, C., Weiß, M., Seufferlein, T.,
424 Zenke, M., Iacovino, M., Kyba, M., Schöler, H.R., Kühl, M., Liebau, S., Kleger, A., 2013. TBX3 Directs
425 Cell-Fate Decision toward Mesendoderm. Stem Cell Reports 1, 248–265.

426 Yang, J., Antin, P., Berx, G., Blanpain, C., Brabletz, T., Bronner, M., Campbell, K., Cano, A., Casanova, J.,
427 Christofori, G., 2020. Guidelines and Definitions for Research on Epithelial–Mesenchymal Transition.
428 Nature Reviews Molecular Cell Biology 21, 341-352,.

429 Zhao, L., Wang, K., Ferrara, N., Vu, T.H., 2005. Vascular endothelial growth factor co-ordinates proper
430 development of lung epithelium and vasculature. Mechanisms of Development 122, 877–886.

431

432

Article 2 - Discussion

The analysis of the single-cell dataset during my thesis allowed to identify all the ligands and receptors expressed in both the epithelial and mesenchymal compartments of iALI. Based on the literature, the analysis enabled the identification of various signalling pathways sumarized in this article. Due to time constraints, this work remained descriptive and requires further development. It will be interesting to study the impact of inhibiting or enhancing the expression of identified pathways on iALI differentiation.

Regarding the mesenchymal to epithelial transition (MET), as the same transcriptional factors, such as TWIST1/2, SNAIL, and ZEB1/2, are involved in both EMT and MET, it can be challenging to differentiate between the two solely by scRNA-seq. However, the results obtained after reculturing mesenchymal cells in this article strongly suggest that a MET process is active during iALI development. Nevertheless, the epithelial cells derived from mesenchymal cells in my reculture experiment should be further characterised, in particular by scRNA-seq.

GENERAL DISCUSSION

The aim of this thesis was to propose a new *in vitro* model for studying the effects of external exposure, such as fine particle pollution and tobacco, which can lead to chronic respiratory diseases such as asthma and COPD. Another aim was to investigate, using this model, the epithelial and mesenchymal crosstalk driving iALI bronchial differentiation, which likely reflects fetal lung development. The role played by early events that occurred during lung differentiation and growth is now recognized as a major determinant of impaired lung function characteristic of COPD; obvious ethical issues impose working on animal models. iALI is by consequence offering this unique opportunity of assessing early events in a human model. In the following sections, I discuss my results and highlights the perspectives that my work offers.

1) Developing an iALI exposure protocol

My lab developed an original protocol for differentiating iPSCs into a bronchial epithelium, iALI, that mimics the various stages of bronchial development. iALI includes most if not all epithelial cells found in the airways such as ciliated cells, secretory cells, neuroendocrine cells, basal cells and a high level of a less described mesenchymal cell population (E. Ahmed et al., 2022). The functionality of iALI cells has been largely reported, such as the presence of beating cilia on multiciliated cells or mucus secretion upon smoke extract exposition. Thus, iALI was appears as an ideal model to develop exposure protocols involving airborne particles such as fine particles pollutants and/or tobacco.

a) Fine particles exposure

The first step in developing the exposure protocol was to select the optimal range of particles to be used. As previously mentioned, the involvement of fine particles in the pathogenesis of COPD has been strongly established.

To avoid batch bias, we chose to use a reference material, the fine particulate matter SRM2786 (NIST™). These fine particles were collected at a major exhibition

center in Prague in 2005, according to its certificate (Schantz et al., 2016), and are delivered in a vial containing aggregates of particulate matter ranging from 500 µm to 1 mm in diameter. It was crucial to homogeneously resuspend these particles in a medium (in this case, PneumaCult™-ALI Medium from Stemcell) and obtain an average diameter near 2.5 µm. To achieve this, we sonicated the particles for more than 30 minutes several times and determined the appropriate concentration for use as shown in Article 1.

As previously demonstrated, epithelial lung cells such as BEAS 2B or HBEC are usually directly exposed to pollutants on their apical side. This was abandoned due to several reasons. Firstly, when epithelial cells are in ALI conditions, adding media on the apical side can induce stress on the cells. This point is important because it creates a notable difference with embryonic lung development, which does not occur at the air-liquid interface. Secondly, SRM2786 particles are denser than the medium, and after 24 hours of culture, they accumulate on top of the cells (Figure 17), potentially affecting their viability. These PM2.5 cannot be washed out as they are strongly adhering to the epithelium, precluding iterative exposure.



*Figure 17 || **Picture of iALI***

Accumulation of pollution exposure on the top of iALI (right) compared to control condition (left).

Additionally, to assess whether fine particles can penetrate inside the cells, we collaborated with Dr. Laurence Berry from the University of Montpellier to perform

electron microscopy on control and exposed iALI. The goal was to analyse if fine particles can be found inside the cells and if they affect their morphology, especially mitochondria which have previously shown to be impacted (Ke et al., 2021). At the time of writing my manuscript, the collection of electron microscopy is still ongoing.

b) Tobacco exposure

During my thesis, I also worked on the effect of tobacco on iALI. The aim of this project was to study the regeneration of iALI after exposure to cigarette smoke extract (CSE) on the basal side, based on a recent paper (Bodas et al., 2021). To achieve this, iALI were exposed during one week to CSE from day 33 to day 40 of differentiation, after which the CSE was removed until day 48. The aim was to model passive exposure that commonly occurs in children (less in westernized countries but still very present worldwide).

To investigate the impact of tobacco and the regeneration process after tobacco removal, several experiments were performed on both cell lines (this topic will be discussed later). These experiments included qPCR analysis of oxidative stress genes, immunofluorescence, paraffin sections, HES stainings, and measurement of transepithelial electrical resistance (TEER).

The results obtained from these experiments need to be analyzed further and integrated into a research paper. However, as my initial experiments, they have allowed an exposure protocol to be established and have been helpful in demonstrating somes limitations of our model.

c) Limits of iALI model

iALI models have numerous advantages, such as the simplicity and robustness of the protocol. However, some limitations can be discussed.

While the use of commercialized media such as PneumaCult™-ALI Medium from Stemcell Technologies is very efficient, it could also affect iALI development. The composition of the media is not disclosed by the manufacturer, so the other compounds used are not known. As shown in Article 2, the activation of some signalling pathways such as the TGF β could affect the percentage of the mesenchymal compartment, potentially impacting the quality of iALI. Hence, an efficient commercial differentiation medium is an excellent tool to set up a specific differentiation, but it latter becomes an obstacle to precisely understand and master the processes that are involved. For instance in our model, we wonder whether the successful differentiation is epithelium-dependant or whether it also involves the underlying mesenchyme via the TGFbeta pathway?

Another limitation of iALI models is that their thickness increases with the duration of culture due to the mesenchymal layer. As the iALI gets thicker, it becomes more autofluorescent, necessitating the systematic use of confocal microscopy. To perform immunofluorescence, paraffin sections were very critical to understand and vizualise the architecture of iALI, as if sections could often break. During my thesis, I also tried the OCT technique, and the immunofluorescence signal was improved (Figure 18). Nevertheless, it was more challenging than paraffin due to the fragility of iALI.

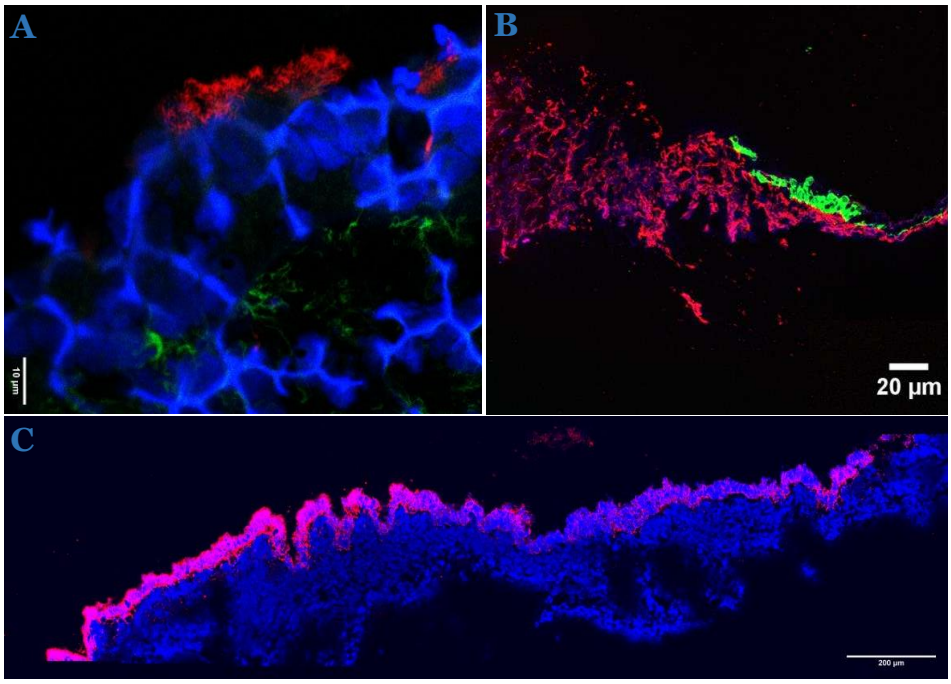

*Figure 18 || **Immunofluorescence of iALI with OCT***

*(**A**) Immunofluorescence of tubulin β4 (red) and vimentin (green), (B) KRT5 (green) and vimentin (red) and (**C**) Epcam (red).*

Finally, during the first step of iALI differentiation, the percentage of NKX2.1 cell progenitors approaches 80-90%, sometimes less. To limit contamination from non-NKX2.1+ cells, such as cells from the digestive tract and mesoderm, and to eventually reduce excessive mesenchymal proliferation, it may be helpful to purify these progenitors. One method consists in purifying then amplifying basal cells based on the surface marker NGFR, as described by Pr. Kotton's laboratory (Hawkins et al., 2021). Another one, is the use of the NKX2.1-p63 modified cell line (coupled with GFP for NKX2.1 and Tomato for TP63), which we obtained from Dr. Ruth Olmer's laboratory (Drick et al., 2020). We acquired this cell line to amplify the basal cell, improve iALI homogeneity and freeze these progenitor cells. However, during iALI differentiation of this cell line, autofluorescence increases and make it difficult to sort enough basal cells.

2) Effect of pollution exposure

Once the exposure protocol was developed, we performed scRNA-seq on both control and pollution exposed samples to study the impact of pollution on iALI. This work resulted in Article 1, and certain aspects of this work can be discussed.

a) Cell lines choice

For each experiment, two iPSCs cell lines were used: UHOMi002-A (named HY03) and UHOMi003-A (named ICOPD2) (Ahmed et al., 2021; Fieldes et al., 2020). HY03 was derived from a healthy patient, while ICOPD2 was derived from a patient with very early and severe COPD. scRNA-seq was performed on both cell lines, but the data from HY03 were insufficient due to a low number of cells. Only the ICOPD2 library was suitable for analysis, and this data is used in the two manuscripts. The fixation protocol is now available in the laboratory thanks to the work of Dr. Said Assou.

Notable differences were observed in the daily culture of the cell lines, such as easier handling, decreased mortality, and better differentiation for the ICOPD2 line paradoxically. However, it is not clear whether these differences are related to random cell line variability or to the genotype specifically linked to COPD susceptibility. This can only be addressed by studying the effect of exposure on other iPSCs lines, derived from patients with severe COPD such as ICOPD8 and ICOPD9 cell lines that have been derived in the lab but not yet studied, and control lines from healthy individuals or heavy smokers without COPD such as the SMOK1 cell line. Theses analysis will be highly interesting to compare control to COPD iPSCs, to find specific hallmarks not erased by reprogramming.

b) Single cell experiment

The effect of pollution exposure on iALI that we observed was quite low, as shown in Article 1, so we wanted to increase the exposure. The concentration of

particulate mater of 50 µg/mL was found to be effective in inducing mucus hypersecretion in iALI, while 100 µg/mL was quite toxic (Montgomery et al., 2020). Recently, we decided to increase the duration of PM 50 µg/mL exposure from 15 days to 30 days, to enhance the observed effects.

All experiments were conducted multiple times to ensure the reliability of the observed results. However, it is important to note that there is high intra-heterogeneity between different Transwells from the same differentiation and a high inter-heterogeneity between different iALI differentiations. To decrease this variability, we are testing different approaches, including forcing differentiation on a fibroblast-loaded chitosan/collagen matrix, improving the differentiation culture media to better control the noise in differentiation that we observed, and reducing the size of the insert to increase the number of assays and thereby select the inserts by visual inspection.

In addition, as previously mentioned, biases can be introduced during single cell experimentation. There is a time lag of 3 hours between the cell collection and the start of scRNA-seq, which may impact both cell viability and transcriptome (Massoni-Badosa et al., 2020). Furthermore, the Notch inhibitor DAPT was used for one week on iALI samples that were subject to scRNA-seq. As mentioned earlier, DAPT can have a positive effect on the number of neuroendocrine cells, while negatively affecting secretory cells. However, it is no longer used in my recent cell differentiation experiments. Additionally, the proportion of cells captured using 10X Chromium technology may be slightly impacted as well. Finally, to delve deeper, it would be interesting to investigate the impact of pollution exposure on the epigenome of iALI. Currently, this study is being conducted to examine the effect of tobacco exposure on ALI and iALI DNA methylation by RRBS-Seq (E. Ahmed, Manuscript in preparation).

c) Perspectives

In order to identify potential biomarkers induced by the exposome, biomarkers that could identify patients at risk of developing COPD, it appears essential to increase the number of iALI samples. To achieve this, as discussed above, miniaturization is an attractive option (Bluhmki et al., 2021). During my thesis, I experimented cultures in 24-well Transwell, which produced excellent results, similar to the commonly used 12-well plates. Building on this work, we are collaborating with the team of Professor Delphine Muriaux from CEMIPAI in Montpellier to further miniaturize iALI (S. Assou et al, Submitted). Currently, we are using 48 Transwell plates and have achieved promising results.

Finally, in regard to the functionality of iALI, we have also collaborated with Dr. Naranjo-Gomez's team to investigate whether iALI can activate human neutrophils, particularly under pollution exposure. These experiments have been performed only twice and should be repeated to confirm and improve the results obtained. However, the discovery of an immunomodulation pathway during the analysis of epithelial and mesenchymal crosstalk as reported in Article 2 is quite promising.

3) Epithelial and mesenchymal crosstalk

The study of the interaction between epithelium and mesenchyme in iALI differentiation was described in Article 2.

a) Functionality of the interactions

As previously said, it should be interesting to investigate the functionality of identified interactions. For instance, chemokine pathways CCR10/CCL28 and ACKR2/CCL2, which are known to coordinate lung inflammation, they could be quantified under exposome conditions and chemotaxis of human polynuclear or neutrophil cells could be tested (Chen et al., 2015; Russo et al., 2018). Additionally, the expression of EDNRA/END1 (endothelin pathway) and the expertise of the

pathologists from CHU of Montpellier on iALI paraffin sections suggest the likely presence of endothelial cells, although further validation is needed. Lastly, several interactions with the ECM, such as ADGRA2/SDC1 (syndecan pathway), highlight the significance of the coating.

b) Extracellular matrix

During iALI differentiation, all cells are grown on Geltrex™ matrix. To incorporate specific ECM proteins, a collaboration has been established with the team of Professor Gilles Subra to test the formulation of a synthetic hydrogel matrix ('Legogel') (Montheil et al., 2018). We have tested this experimental matrix for iPSCs cell lines maintenance but with little success. The efficacy of the chitosan/collagen I matrix (see below) will help us to design a revised Legogel version, that will be tested both for pluripotent stem cell maintenance and differentiation.

Additionally, a collaboration with Dr. Nelly Frossard has resulted in the establishment by my co-PhD student Florent Foisset of a collagen I-chitosan matrix embedded with human pulmonary fibroblasts. This matrix leads to a remarkable iALI epithelium differentiation and offers the possibility to be innervated by the addition of neuronal cells (Foisset et al., 2023).

c) Mesenchymal to epithelial transition

As substantiated by our single-cell analysis (Article 1 and Article 2), an EMT process likely occurs during iALI differentiation. Additionally, it has been observed in response to pollution exposure, and its role should be elucidated further through experimentation. In fact, it will be worth to investigate whether EMT is enhanced in ICOPD2 cell lines, as observed in COPD patients following exposure to tobacco or pollution (Milara et al., 2013; Nasri et al., 2021; Soltani et al., 2012).

Interestingly, mesenchymal cells extracted from iALI undergo MET when recultured. As shown in Figure 19, cells can switch between epithelial, mesenchymal, and metastable intermediate states depending on regulators such as transcription factors and epigenetic markers, and in response to EMT/MET signals (e.g., hypoxia, growth factors) (Nieto et al., 2016).

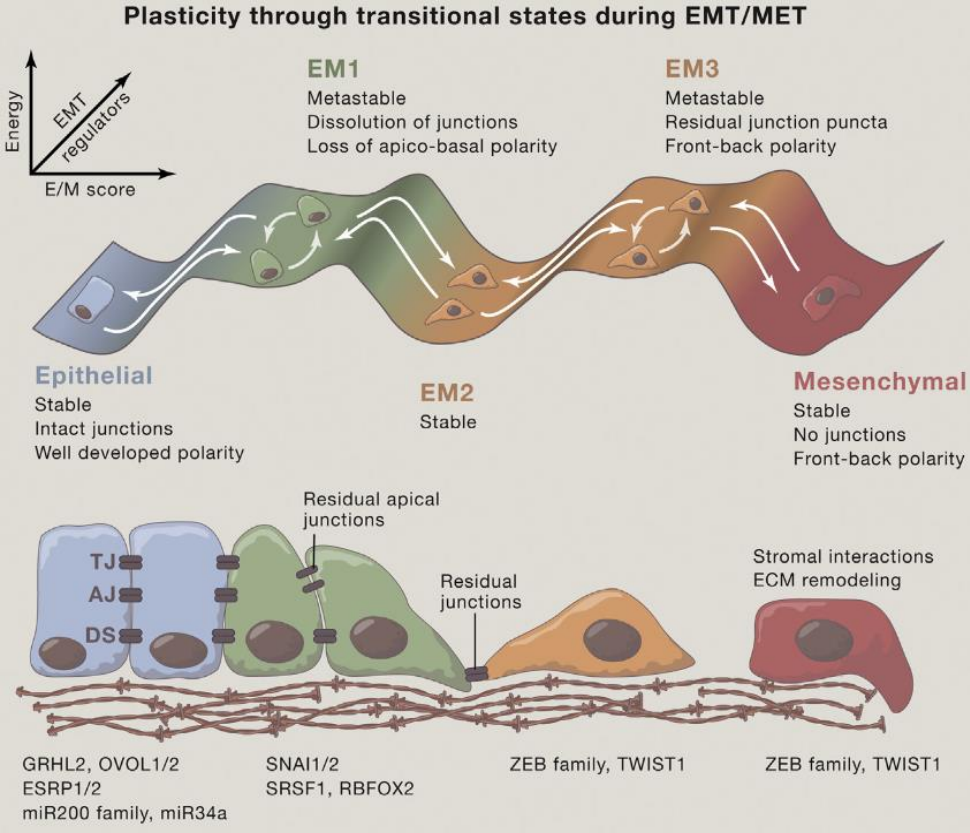

*Figure 19 || **Epithelial and mesenchymal continuum states***

Adapted from Nieto M. Angela, et al., Cell, 2016

Further possibilities need to be explored. MET might be a physiological process that can help in epithelial regeneration after viral or pollution-induced lesions and as such should be forced to improve regeneration? iALI-derived mesenchymal cells maybe an interesting cell population candidate for bronchial epithelial cell therapy? What is the level of MET in adults and could it occur in a physiopathological context such as COPD and fibrosis?

CONCLUSION

In conclusion, the aim of this thesis was to study the role of the mesenchymal compartment during bronchial differentiation and propose a novel in vitro model to study the impact of the exposome on the development of chronic respiratory diseases such as COPD.

An exposure protocol for fine particles was successfully developed using the iALI model, and scRNA-seq results demonstrated an inflammatory response to pollution. Moreover, investigation of the epithelial and mesenchymal crosstalk led to the identification of several signalling pathways that may contribute to bronchial differentiation.

Overall, this work offers promising perspectives for future research on respiratory pathologies and provides a better understanding of the potential of in vitro models to investigate the effects of external exposure and elucidate the role of the pulmonary mesenchyme.

REFERENCES

Abo, K.M., Sainz de Aja, J., Lindstrom-Vautrin, J., Alysandratos, K.-D., Richards, A., Garcia-de-Alba, C., Huang, J., Hix, O.T., Werder, R.B., Bullitt, E., Hinds, A., Falconer, I., Villacorta-Martin, C., Jaenisch, R., Kim, C.F., Kotton, D.N., Wilson, A.A., 2022. Air-liquid interface culture promotes maturation and allows environmental exposure of pluripotent stem cell–derived alveolar epithelium. JCI Insight 7, e155589.

Adamson, J., Haswell, L.E., Phillips, G., Gaça, M.D., Adamson, J., Haswell, L.E., Phillips, G., Gaça, M.D., 2011. In Vitro Models of Chronic Obstructive Pulmonary Disease (COPD), Bronchitis. IntechOpen.

Adnot, S., Amsellem, V., Boyer, L., Marcos, E., Saker, M., Houssaini, A., Kebe, K., Dagouassat, M., Lipskaia, L., Boczkowski, J., 2015. Telomere Dysfunction and Cell Senescence in Chronic Lung Diseases: Therapeutic Potential. Pharmacol Ther 153, 125–134.

Aegerter, H., Lambrecht, B.N., Jakubzick, C.V., 2022. Biology of lung macrophages in health and disease. Immunity 55, 1564–1580.

Agraval, H., Chu, H.W., 2022. Lung Organoids in Smoking Research: Current Advances and Future Promises. Biomolecules 12, 1463.

Agustí, A., Celli, B., Faner, R., 2017. What does endotyping mean for treatment in chronic obstructive pulmonary disease? The Lancet 390, 980–987.

Agustí, A., Hogg, J.C., 2019. Update on the Pathogenesis of Chronic Obstructive Pulmonary Disease. N Engl J Med 381, 1248–1256.

Ahmed, E., Fieldes, M., Bourguignon, C., Mianné, J., Petit, A., Jory, M., Cazevieille, C., Boukhaddaoui, H., Garnett, J.P., Hirtz, C., Massiera, G., Vachier, I., Assou, S., Bourdin, A., De Vos, J., 2022. Differentiation of Human Induced Pluripotent Stem Cells from Patients with Severe COPD into Functional Airway Epithelium. Cells 11, 2422.

Ahmed, E., Fieldes, M., Mianné, J., Bourguignon, C., Nasri, A., Vachier, I., Assou, S., Bourdin, A., De Vos, J., 2021. Generation of four severe early-onset chronic obstructive pulmonary disease (COPD) patient-derived induced pluripotent stem cell lines from peripheral blood mononuclear cells. Stem Cell Research 56, 102550.

Ahmed, R., Zaman, T., Chowdhury, F., Mraiche, F., Tariq, M., Ahmad, I.S., Hasan, A., 2022. Single-Cell RNA Sequencing with Spatial Transcriptomics of Cancer Tissues. International Journal of Molecular Sciences 23, 3042.

Aikawa, T., Shimura, S., Sasaki, H., Ebina, M., Takishima, T., 1992. Marked goblet cell hyperplasia with mucus accumulation in the airways of patients who died of severe acute asthma attack. Chest 101, 916–921.

Air pollution [WWW Document], n.d.

Albers, R.E., Selesniemi, K., Natale, D.R.C., Brown, T.L., 2018. TGF-β induces Smad2 Phosphorylation, ARE Induction, and Trophoblast Differentiation. Int J Stem Cells 11, 111–120.

Alles, J., Karaiskos, N., Praktiknjo, S.D., Grosswendt, S., Wahle, P., Ruffault, P.-L., Ayoub, S., Schreyer, L., Boltengagen, A., Birchmeier, C., Zinzen, R., Kocks, C., Rajewsky, N., 2017. Cell fixation and preservation for droplet-based single-cell transcriptomics. BMC Biol 15, 44.

Ambrose, J.A., Barua, R.S., 2004. The pathophysiology of cigarette smoking and cardiovascular disease: An update. Journal of the American College of Cardiology 43, 1731–1737.

Anderson, D.O., 1964. Smoking And Respiratory Disease. Am J Public Health Nations Health 54, 1856–1863.

Andre, L., Boissière, J., Reboul, C., Perrier, R., Zalvidea, S., Meyer, G., Thireau, J., Tanguy, S., Bideaux, P., Hayot, M., Boucher, F., Obert, P., Cazorla, O., Richard, S., 2010. Carbon Monoxide Pollution Promotes Cardiac Remodeling and Ventricular Arrhythmia in Healthy Rats. Am J Respir Crit Care Med 181, 587–595.

Araya, J., Cambier, S., Markovics, J.A., Wolters, P., Jablons, D., Hill, A., Finkbeiner, W., Jones, K., Broaddus, V.C., Sheppard, D., Barzcak, A., Xiao, Y., Erle, D.J., Nishimura, S.L., 2007. Squamous metaplasia amplifies pathologic epithelial-mesenchymal interactions in COPD patients. J Clin Invest 117, 3551–3562.

Ardain, A., Marakalala, M.J., Leslie, A., 2020. Tissue-resident innate immunity in the lung. Immunology 159, 245–256.

Arku, R.E., Birch, A., Shupler, M., Yusuf, S., Hystad, P., Brauer, M., Team, the P., 2018. Characterizing exposure to household air pollution within the Prospective Urban Rural Epidemiology (PURE) Study. Environment international 114, 307.

Aros, C.J., Pantoja, C.J., Gomperts, B.N., 2021. Wnt signaling in lung development, regeneration, and disease progression. Commun Biol 4, 1–13.

Asmi, A.J., Pirjola, L.H., Kulmala, M., 2004. A sectional aerosol model for submicron particles in indoor air. Scandinavian Journal of Work, Environment & Health 30, 63–72.

Aspal, M., Zemans, R.L., 2020. Mechanisms of ATII-to-ATI Cell Differentiation during Lung Regeneration. Int J Mol Sci 21, 3188.

Assou, S., Bouckenheimer, J., De Vos, J., 2018. Concise Review: Assessing the Genome Integrity of Human Induced Pluripotent Stem Cells: What Quality Control Metrics? Stem Cells 36, 814–821.

Assou, S., Girault, N., Plinet, M., Bouckenheimer, J., Sansac, C., Combe, M., Mianné, J., Bourguignon, C., Fieldes, M., Ahmed, E., Commes, T., Boureux, A., Lemaître, J.-M., De Vos, J., 2020. Recurrent Genetic Abnormalities in Human Pluripotent Stem Cells: Definition and Routine Detection in Culture Supernatant by Targeted Droplet Digital PCR. Stem Cell Reports 14, 1–8.

Atanasova, K.R., Reznikov, L.R., 2018. Neuropeptides in asthma, chronic obstructive pulmonary disease and cystic fibrosis. Respir Res 19, 149.

Atkinson, Richard.W., Butland, Barbara.K., Anderson, H.Ross., Maynard, Robert.L., 2018. Long-term Concentrations of Nitrogen Dioxide and Mortality. Epidemiology 29, 460–472.

Badran, M., Laher, I., 2020. Waterpipe (shisha, hookah) smoking, oxidative stress and hidden disease potential. Redox Biol 34, 101455.

Balistreri, C.R., De Falco, E., Bordin, A., Maslova, O., Koliada, A., Vaiserman, A., 2020. Stem cell therapy: old challenges and new solutions. Mol Biol Rep 47, 3117–3131.

References

Ball, M., Hossain, M., Padalia, D., 2022. Anatomy, Airway, in: StatPearls. StatPearls Publishing, Treasure Island (FL).

Ballard, P.L., Keller, R.L., Truog, W.E., Chapin, C., Horneman, H., Segal, M.R., Ballard, R.A., 2019. Surfactant Status and Respiratory Outcome in Premature Infants Receiving Late Surfactant Treatment. Pediatr Res 85, 305–311.

Bansil, R., Turner, B.S., 2018. The biology of mucus: Composition, synthesis and organization. Adv Drug Deliv Rev 124, 3–15.

Bansil, R., Turner, B.S., 2006. Mucin structure, aggregation, physiological functions and biomedical applications. Current Opinion in Colloid & Interface Science 11, 164–170.

Barbry, P., Cavard, A., Chanson, M., Jaffe, A.B., Plasschaert, L.W., 2020. Regeneration of airway epithelial cells to study rare cell states in cystic fibrosis. Journal of Cystic Fibrosis, ECFS Cystic Fibrosis Research 19, S42–S46.

Barnes, P.J., 2017. Senescence in COPD and Its Comorbidities. Annu Rev Physiol 79, 517–539.

Barnes, P.J., 2015. Club Cells, Their Secretory Protein, and COPD. CHEST 147, 1447–1448.

Barnes, P.J., 2003. New Concepts in Chronic Obstructive Pulmonary Disease. Annual Review of Medicine 54, 113–129.

Barnes, P.J., 2000. Chronic obstructive pulmonary disease. N Engl J Med 343, 269–280.

Barnes, P.J., Burney, P.G.J., Silverman, E.K., Celli, B.R., Vestbo, J., Wedzicha, J.A., Wouters, E.F.M., 2015. Chronic obstructive pulmonary disease. Nat Rev Dis Primers 1, 15076.

Basil, M.C., Cardenas-Diaz, F.L., Kathiriya, J.J., Morley, M.P., Carl, J., Brumwell, A.N., Katzen, J., Slovik, K.J., Babu, A., Zhou, S., Kremp, M.M., McCauley, K.B., Li, S., Planer, J.D., Hussain, S.S., Liu, X., Windmueller, R., Ying, Y., Stewart, K.M., Oyster, M., Christie, J.D., Diamond, J.M., Engelhardt, J.F., Cantu, E., Rowe, S.M., Kotton, D.N., Chapman, H.A., Morrisey, E.E., 2022. Human distal airways contain a multipotent secretory cell that can regenerate alveoli. Nature 604, 120–126.

Bell, M.L., Goldberg, R., Hogrefe, C., Kinney, P.L., Knowlton, K., Lynn, B., Rosenthal, J., Rosenzweig, C., Patz, J.A., 2007. Climate change, ambient ozone, and health in 50 US cities. Climatic Change 82, 61–76.

Bellusci, S., Grindley, J., Emoto, H., Itoh, N., Hogan, B.L., 1997. Fibroblast growth factor 10 (FGF10) and branching morphogenesis in the embryonic mouse lung. Development 124, 4867–4878.

Belvisi, M.G., Stretton, C.D., Barnes, P.J., 1991. Bombesin-induced bronchoconstriction in the guinea pig: mode of action. J Pharmacol Exp Ther 258, 36–41.

Benam, K.H., Villenave, R., Lucchesi, C., Varone, A., Hubeau, C., Lee, H.-H., Alves, S.E., Salmon, M., Ferrante, T.C., Weaver, J.C., Bahinski, A., Hamilton, G.A., Ingber, D.E., 2016. Small airway-on-a-chip enables analysis of human lung inflammation and drug responses in vitro. Nat Methods 13, 151–157.

Ben-David, U., Benvenisty, N., 2011. The tumorigenicity of human embryonic and induced pluripotent stem cells. Nat Rev Cancer 11, 268–277.

Benjamin, J.T., van der Meer, R., Im, A.M., Plosa, E.J., Zaynagetdinov, R., Burman, A., Havrilla, M.E., Gleaves, L.A., Polosukhin, V.V., Deutsch, G.H., Yanagisawa, H., Davidson, J.M., Prince, L.S., Young, L.R., Blackwell, T.S., 2016. Epithelial-Derived Inflammation Disrupts Elastin Assembly and Alters Saccular Stage Lung Development. The American Journal of Pathology 186, 1786–1800.

Berical, A., Beermann, M.L., Suzuki, S., LeSuer, J., Matte, T., Davis, B., Kotton, D., Hawkins, F., 2022. Generation of Airway Epithelial Cell Air-Liquid Interface Cultures from Human Pluripotent Stem Cells. JoVE 63882.

Blayac, M., Coll, P., Urbach, V., Fanen, P., Epaud, R., Lanone, S., 2022. The Impact of Air Pollution on the Course of Cystic Fibrosis: A Review. Frontiers in Physiology 13.

Bluhmki, T., Traub, S., Müller, A.-K., Bitzer, S., Schruf, E., Bammert, M.-T., Leist, M., Gantner, F., Garnett, J.P., Heilker, R., 2021. Functional human iPSC-derived alveolar-like cells cultured in a miniaturized 96-Transwell air–liquid interface model. Sci Rep 11, 17028.

Bodas, M., Moore, A.R., Subramaniyan, B., Georgescu, C., Wren, J.D., Freeman, W.M., Brown, B.R., Metcalf, J.P., Walters, M.S., 2021. Cigarette Smoke Activates NOTCH3 to Promote Goblet Cell Differentiation in Human Airway Epithelial Cells. Am J Respir Cell Mol Biol 64, 426–440.

Boers, J.E., Ambergen, A.W., Thunnissen, F.B.J.M., 1999. Number and Proliferation of Clara Cells in Normal Human Airway Epithelium. Am J Respir Crit Care Med 159, 1585–1591.

Boers, J.E., Ambergen, A.W., Thunnissen, F.B.J.M., 1998. Number and Proliferation of Basal and Parabasal Cells in Normal Human Airway Epithelium. Am J Respir Crit Care Med 157, 2000–2006.

Boers, J.E., den Brok, J.L., Koudstaal, J., Arends, J.W., Thunnissen, F.B., 1996. Number and proliferation of neuroendocrine cells in normal human airway epithelium. Am J Respir Crit Care Med 154, 758–763.

Bornstein, C., Nevo, S., Giladi, A., Kadouri, N., Pouzolles, M., Gerbe, F., David, E., Machado, A., Chuprin, A., Tóth, B., Goldberg, O., Itzkovitz, S., Taylor, N., Jay, P., Zimmermann, V.S., Abramson, J., Amit, I., 2018. Single-cell mapping of the thymic stroma identifies IL-25-producing tuft epithelial cells. Nature 559, 622–626.

Bouazza, N., Foissac, F., Urien, S., Guedj, R., Carbajal, R., Tréluyer, J.-M., Chappuy, H., 2018. Fine particulate pollution and asthma exacerbations. Arch Dis Child 103, 828–831.

Bouza, E., Vargas, F., Alcázar, B., Álvarez, T., Asensio, Á., Cruceta, G., Gracia, D., Guinea, J., Gil, M.A., Linares, C., Muñoz, P., Olier, E., Pastor, P., Pedro-Botet, M.L., Querol, X., Tovar, J., Urrutia, I., Villar, F., Palomo, E., 2022. Air pollution and health prevention: A document of reflection. Rev Esp Quimioter 35, 307–332.

Bowe, B., Xie, Y., Yan, Y., Al-Aly, Z., 2019. Burden of Cause-Specific Mortality Associated With PM2.5 Air Pollution in the United States. JAMA Network Open 2, e1915834.

Branchfield, K., Nantie, L., Verheyden, J.M., Sui, P., Wienhold, M.D., Sun, X., 2016. Pulmonary neuroendocrine cells function as airway sensors to control lung immune response. Science 351, 707–710.

Brune, K., Frank, J., Schwingshackl, A., Finigan, J., Sidhaye, V.K., 2015. Pulmonary epithelial barrier function: some new players and mechanisms. Am J Physiol Lung Cell Mol Physiol 308, L731–L745.

Brunekreef, B., 2005. Epidemiological evidence of effects of coarse airborne particles on health. European Respiratory Journal 26, 309–318.

References

Bukowy-Bieryłło, Z., 2021. Long-term differentiating primary human airway epithelial cell cultures: how far are we? Cell Commun Signal 19, 63.

Burkhanova, U., Harris, A., Leir, S.-H., 2022. Enhancement of airway epithelial cell differentiation by pulmonary endothelial cell co-culture. Stem Cell Res 65, 102967.

Burnett, R., Chen, H., Szyszkowicz, M., Fann, N., Hubbell, B., Pope, C.A., Apte, J.S., Brauer, M., Cohen, A., Weichenthal, S., Coggins, J., Di, Q., Brunekreef, B., Frostad, J., Lim, S.S., Kan, H., Walker, K.D., Thurston, G.D., Hayes, R.B., Lim, C.C., Turner, M.C., Jerrett, M., Krewski, D., Gapstur, S.M., Diver, W.R., Ostro, B., Goldberg, D., Crouse, D.L., Martin, R.V., Peters, P., Pinault, L., Tjepkema, M., van Donkelaar, A., Villeneuve, P.J., Miller, A.B., Yin, P., Zhou, M., Wang, L., Janssen, N.A.H., Marra, M., Atkinson, R.W., Tsang, H., Quoc Thach, T., Cannon, J.B., Allen, R.T., Hart, J.E., Laden, F., Cesaroni, G., Forastiere, F., Weinmayr, G., Jaensch, A., Nagel, G., Concin, H., Spadaro, J.V., 2018. Global estimates of mortality associated with long-term exposure to outdoor fine particulate matter. Proceedings of the National Academy of Sciences 115, 9592–9597.

Bustamante-Marin, X.M., Ostrowski, L.E., 2017. Cilia and Mucociliary Clearance. Cold Spring Harb Perspect Biol 9, a028241.

Butler, A., Hoffman, P., Smibert, P., Papalexi, E., Satija, R., 2018. Integrating single-cell transcriptomic data across different conditions, technologies, and species. Nat Biotechnol 36, 411–420.

Cardoso, W.V., Lü, J., 2006. Regulation of Early Lung Morphogenesis: Questions, Facts and Controversies. Development 133, 1611-1624,.

Carsin, A., Mazenq, J., Ilstad, A., Dubus, J.-C., Chanez, P., Gras, D., 2016. Bronchial epithelium in children: a key player in asthma. European Respiratory Review 25, 158–169.

Cascio, W.E., 2018. Wildland fire smoke and human health. Science of The Total Environment 624, 586–595.

Celli, B.R., Wedzicha, J.A., 2019. Update on Clinical Aspects of Chronic Obstructive Pulmonary Disease. N Engl J Med 381, 1257–1266.

Chagastelles, P.C., Nardi, N.B., 2011. Biology of stem cells: an overview. Kidney International Supplements, Stem Cells and Kidney Disease 1, 63–67.

Chan, M., Liu, Y., 2022. Function of epithelial stem cell in the repair of alveolar injury. Stem Cell Res Ther 13, 170.

Chandy, M., Obal, D., Wu, J.C., 2022. Elucidating effects of environmental exposure using human-induced pluripotent stem cell disease modeling. EMBO Mol Med 14, e13260.

Chang, H., Chang, L.W., Cheng, Y.-H., Tsai, W.-T., Tsai, M.-X., Lin, P., 2006. Preferential induction of CYP1A1 and CYP1B1 in CCSP-positive cells. Toxicol Sci 89, 205–213.

Chassagnon, G., Morel, B., Carpentier, E., Ducou Le Pointe, H., Sirinelli, D., 2016. Tracheobronchial Branching Abnormalities: Lobe-based Classification Scheme. RadioGraphics 36, 358–373.

Chen, C., Li, Y.-R., Lin, S.-H., Chang, H.-H., Chai, W.-H., Chan, P.-C., Lin, C.-H., 2020. Tiotropium/Olodaterol treatment reduces cigarette smoke extract-induced cell death in BEAS-2B bronchial epithelial cells. BMC Pharmacology and Toxicology 21, 74.

Chen, G., Ning, B., Shi, T., 2019a. Single-Cell RNA-Seq Technologies and Related Computational Data Analysis. Frontiers in Genetics 10.

Chen, G., Ning, B., Shi, T., 2019b. Single-Cell RNA-Seq Technologies and Related Computational Data Analysis. Frontiers in Genetics 10.

Chen, Z., Kim, S., Essani, A.B., Volin, M.V., Vila, O.M., Swedler, W., Arami, S., Volkov, S., Sardin, L.V., Sweiss, N., Shahrara, S., 2015. Characterizing the expression and function of CCL28 and its corresponding receptor CCR10 in RA pathogenesis. Ann Rheum Dis 74, 1898–1906.

Chidester, B., Zhou, T., Alam, S., Ma, J., 2023. SPICEMIX enables integrative single-cell spatial modeling of cell identity. Nat Genet 55, 78–88.

Cipollina, C., Bruno, A., Fasola, S., Cristaldi, M., Patella, B., Inguanta, R., Vilasi, A., Aiello, G., La Grutta, S., Torino, C., Pace, E., 2022. Cellular and Molecular Signatures of Oxidative Stress in Bronchial Epithelial Cell Models Injured by Cigarette Smoke Extract. Int J Mol Sci 23, 1770.

Clunes, L.A., Bridges, A., Alexis, N., Tarran, R., 2008. In Vivo Versus In Vitro Airway Surface Liquid Nicotine Levels Following Cigarette Smoke Exposure. J Anal Toxicol 32, 201–207.

Cohen, R., Patel, A., Green, F., 2008. Lung Disease Caused by Exposure to Coal Mine and Silica Dust. Semin Respir Crit Care Med 29, 651–661.

Crapo, J.D., Barry, B.E., Gehr, P., Bachofen, M., Weibel, E.R., 1982. Cell number and cell characteristics of the normal human lung. Am Rev Respir Dis 126, 332–337.

Crosby, L.M., Waters, C.M., 2010. Epithelial repair mechanisms in the lung. Am J Physiol Lung Cell Mol Physiol 298, L715–L731.

Cruzan, G., Bus, J., Banton, M., Gingell, R., Carlson, G., 2009. Mouse specific lung tumors from CYP2F2-mediated cytotoxic metabolism: an endpoint/toxic response where data from multiple chemicals converge to support a mode of action. Regul Toxicol Pharmacol 55, 205–218.

Crystal, R.G., 2014. Airway Basal Cells. The “Smoking Gun” of Chronic Obstructive Pulmonary Disease. Am J Respir Crit Care Med 190, 1355–1362.

Davis, J.D., Wypych, T.P., 2021. Cellular and functional heterogeneity of the airway epithelium. Mucosal Immunol 14, 978–990.

Davis, R.P., Mychaliska, G.B., 2013. Neonatal pulmonary physiology. Seminars in Pediatric Surgery, Neonatal Physiology 22, 179–184.

Dayal, H.H., Khuder, S., Sharrar, R., Trieff, N., 1994. Passive Smoking in Obstructive Respiratory Diseases in an Industrialized Urban Population. Environmental Research 65, 161–171.

De Vos, J., Girault, N., Mianné, J., Bourguignon, C., Fieldes, M., Nasri, A., Ahmed, E., Boureux, A., Assou, S., 2020. Non-invasive and rapid test for routine detection of recurrent genetic abnormalities in human pluripotent stem cells. Cytotherapy 22, S27.

Deprez, M., Zaragosi, L.-E., Truchi, M., Becavin, C., Ruiz García, S., Arguel, M.-J., Plaisant, M., Magnone, V., Lebrigand, K., Abelanet, S., Brau, F., Paquet, A., Pe’er, D., Marquette, C.-H., Leroy, S., Barbry, P., 2020. A Single-Cell Atlas of the Human Healthy Airways. Am J Respir Crit Care Med 202, 1636–1645.

References

Deschamps, J., Boucekine, M., Fayol, L., Dubus, J.C., Nauleau, S., Garcia, P., Boubred, F., 2021. Neighborhood Disadvantage and Early Respiratory Outcomes in Very Preterm Infants with Bronchopulmonary Dysplasia. The Journal of Pediatrics 237, 177-182.e1.

Despréaux, P., Jeanton, C., Desaulle, D., Al Zallouha, M., Verdin, A., Momas, I., Achard, S., 2023. Innovative graph analysis method to assess gene expression modulation after fine particles exposures of 3D human airway epithelia. Environmental Research 221, 115296.

Ding, J., Adiconis, X., Simmons, S.K., Kowalczyk, M.S., Hession, C.C., Marjanovic, N.D., Hughes, T.K., Wadsworth, M.H., Burks, T., Nguyen, L.T., Kwon, J.Y.H., Barak, B., Ge, W., Kedaigle, A.J., Carroll, S., Li, S., Hacohen, N., Rozenblatt-Rosen, O., Shalek, A.K., Villani, A.-C., Regev, A., Levin, J.Z., 2020. Systematic comparison of single-cell and single-nucleus RNA-sequencing methods. Nat Biotechnol 38, 737–746.

Do, V.H., Canzar, S., 2021. A generalization of t-SNE and UMAP to single-cell multimodal omics. Genome Biology 22, 130.

Dobbs, L., Johnson, M., Vanderbilt, J., Allen, L., Gonzalez, R., 2010. The Great Big Alveolar TI Cell: Evolving Concepts and Paradigms. Cell Physiol Biochem 25, 055–062.

Donnelly, G.M., Haack, D.G., Heird, C.S., 1982. Tracheal epithelium: cell kinetics and differentiation in normal rat tissue. Cell Tissue Kinet 15, 119–130.

Doss, M.X., Sachinidis, A., 2019. Current Challenges of iPSC-Based Disease Modeling and Therapeutic Implications. Cells 8, 403.

Dransfield, M.T., Kunisaki, K.M., Strand, M.J., Anzueto, A., Bhatt, S.P., Bowler, R.P., Criner, G.J., Curtis, J.L., Hanania, N.A., Nath, H., Putcha, N., Roark, S.E., Wan, E.S., Washko, G.R., Wells, J.M., Wendt, C.H., Make, B.J., COPDGene Investigators, 2017. Acute Exacerbations and Lung Function Loss in Smokers with and without Chronic Obstructive Pulmonary Disease. Am J Respir Crit Care Med 195, 324–330.

Drick, N., Sahabian, A., Pongpamorn, P., Merkert, S., Göhring, G., Welte, T., Martin, U., Olmer, R., 2020. Generation of a NKX2.1 – p63 double transgenic knock-in reporter cell line from human induced pluripotent stem cells (MHHi006-A-4). Stem Cell Research 42, 101659.

Dye, B.R., Hill, D.R., Ferguson, M.A., Tsai, Y.-H., Nagy, M.S., Dyal, R., Wells, J.M., Mayhew, C.N., Nattiv, R., Klein, O.D., White, E.S., Deutsch, G.H., Spence, J.R., 2015. In vitro generation of human pluripotent stem cell derived lung organoids. eLife 4, e05098.

Elshazzly, M., Lopez, M.J., Reddy, V., Caban, O., 2022. Embryology, Central Nervous System, in: StatPearls. StatPearls Publishing, Treasure Island (FL).

Engstrom, P.F., Clapper, M.L., Schnoll, R.A., 2003. Physiochemical Composition of Tobacco Smoke. Holland-Frei Cancer Medicine. 6th edition.

Esteves, F., Rueff, J., Kranendonk, M., 2021. The Central Role of Cytochrome P450 in Xenobiotic Metabolism-A Brief Review on a Fascinating Enzyme Family. J Xenobiot 11, 94–114.

Evans, C., Hardin, J., Stoebel, D.M., 2017. Selecting between-sample RNA-Seq normalization methods from the perspective of their assumptions. Brief Bioinform 19, 776–792.

Evans, M.J., Kaufman, M.H., 1981. Establishment in culture of pluripotential cells from mouse embryos. Nature 292, 154–156.

Evans, M.J., Van Winkle, L.S., Fanucchi, M.V., Plopper, C.G., 2001. Cellular and molecular characteristics of basal cells in airway epithelium. Exp Lung Res 27, 401–415.

Feng, Y.-T., Lang, C.-F., Chen, C., Harry Asena, M., Fang, Y., Zhang, R.-D., Jiang, L.-Q., Fang, X., Chen, Y., He, Y.-S., Wang, P., Pan, H.-F., 2023. Association between air pollution exposure and coronary heart disease hospitalization in a humid sub-tropical region of China: A time-series study. Front Public Health 10, 1090443.

Fieldes, M., Ahmed, E., Bourguignon, C., Mianné, J., Martin, M., Arnould, C., Vachier, I., Assou, S., De Vos, J., Bourdin, A., 2020. Generation of the induced pluripotent stem cell line UHOMi002-A from peripheral blood mononuclear cells of a healthy male donor. Stem Cell Research 49, 102037.

Firth, A.L., Dargitz, C.T., Qualls, S.J., Menon, T., Wright, R., Singer, O., Gage, F.H., Khanna, A., Verma, I.M., 2014. Generation of multiciliated cells in functional airway epithelia from human induced pluripotent stem cells. Proc Natl Acad Sci U S A 111, E1723–E1730.

Foisset, F., Lehalle, C., Nasri, A., Bourdais, C., Morichon, L., Petit, A., Vachier, I., Assou, S., Bourdin, A., Frossard, N., De Vos, J., 2023. Fabrication d'un épithélium bronchique innervé à partir d'une prise de sang. Revue des Maladies Respiratoires.

Fu, Z., Liu, Q., Liang, J., Weng, Z., Li, W., Xu, J., Zhang, X., Xu, C., Huang, T., Gu, A., 2022. Air pollution, genetic factors and the risk of depression. Science of The Total Environment 850, 158001.

Fuentes-Mattei, E., Rivera, E., Gioda, A., Sanchez-Rivera, D., Roman-Velazquez, F.R., Jimenez-Velez, B.D., 2010. Use of Human Bronchial Epithelial Cells (BEAS-2B) to Study Immunological Markers Resulting From Exposure to PM2.5 Organic Extract from Puerto Rico. Toxicol Appl Pharmacol 243, 381–389.

Fullerton, D.G., Bruce, N., Gordon, S.B., 2008. Indoor air pollution from biomass fuel smoke is a major health concern in the developing world. Transactions of the Royal Society of Tropical Medicine and Hygiene 102, 843–851.

Gamez, A.S., Gras, D., Petit, A., Knabe, L., Molinari, N., Vachier, I., Chanez, P., Bourdin, A., 2015. Supplementing defect in club cell secretory protein attenuates airway inflammation in COPD. Chest 147, 1467–1476.

Gao, X., Cui, X., Zhang, X., Zhao, C., Zhang, N., Zhao, Y., Ren, Y., Su, C., Ge, L., Wu, S., Yang, J., 2020. Differential genetic mutations of ectoderm, mesoderm, and endoderm-derived tumors in TCGA database. Cancer Cell International 20, 595.

Garcia-Alonso, L., Lorenzi, V., Mazzeo, C.I., Alves-Lopes, J.P., Roberts, K., Sancho-Serra, C., Engelbert, J., Marečková, M., Gruhn, W.H., Botting, R.A., Li, T., Crespo, B., van Dongen, S., Kiselev, V.Y., Prigmore, E., Herbert, M., Moffett, A., Chédotal, A., Bayraktar, O.A., Surani, A., Haniffa, M., Vento-Tormo, R., 2022. Single-cell roadmap of human gonadal development. Nature 607, 540–547.

Garcia-Canton, C., Minet, E., Anadon, A., Meredith, C., 2013. Metabolic characterization of cell systems used in in vitro toxicology testing: Lung cell system BEAS-2B as a working example. Toxicology in Vitro 27, 1719–1727.

GBD 2013 Risk Factors Collaborators, Forouzanfar, M.H., Alexander, L., Anderson, H.R., Bachman, V.F., Biryukov, S., Brauer, M., Burnett, R., Casey, D., Coates, M.M., Cohen, A., Delwiche, K., Estep, K., Frostad, J.J., Astha, K.C., Kyu, H.H., Moradi-Lakeh, M., Ng, M., Slepak, E.L., Thomas, B.A., Wagner, J., Aasvang, G.M., Abbafati, C., Abbasoglu Ozgoren, A., Abd-Allah, F., Abera, S.F., Aboyans, V., Abraham, B., Abraham, J.P.,

References

Abubakar, I., Abu-Rmeileh, N.M.E., Aburto, T.C., Achoki, T., Adelekan, A., Adofo, K., Adou, A.K., Adsuar, J.C., Afshin, A., Agardh, E.E., Al Khabouri, M.J., Al Lami, F.H., Alam, S.S., Alasfoor, D., Albittar, M.I., Alegretti, M.A., Aleman, A.V., Alemu, Z.A., Alfonso-Cristancho, R., Alhabib, S., Ali, R., Ali, M.K., Alla, F., Allebeck, P., Allen, P.J., Alsharif, U., Alvarez, E., Alvis-Guzman, N., Amankwaa, A.A., Amare, A.T., Ameh, E.A., Ameli, O., Amini, H., Ammar, W., Anderson, B.O., Antonio, C.A.T., Anwari, P., Argeseanu Cunningham, S., Arnlöv, J., Arsenijevic, V.S.A., Artaman, A., Asghar, R.J., Assadi, R., Atkins, L.S., Atkinson, C., Avila, M.A., Awuah, B., Badawi, A., Bahit, M.C., Bakfalouni, T., Balakrishnan, K., Balalla, S., Balu, R.K., Banerjee, A., Barber, R.M., Barker-Collo, S.L., Barquera, S., Barregard, L., Barrero, L.H., Barrientos-Gutierrez, T., Basto-Abreu, A.C., Basu, A., Basu, S., Basulaiman, M.O., Batis Ruvalcaba, C., Beardsley, J., Bedi, N., Bekele, T., Bell, M.L., Benjet, C., Bennett, D.A., Benzian, H., Bernabé, E., Beyene, T.J., Bhala, N., Bhalla, A., Bhutta, Z.A., Bikbov, B., Bin Abdulhak, A.A., Blore, J.D., Blyth, F.M., Bohensky, M.A., Bora Başara, B., Borges, G., Bornstein, N.M., Bose, D., Boufous, S., Bourne, R.R., Brainin, M., Brazinova, A., Breitborde, N.J., Brenner, H., Briggs, A.D.M., Broday, D.M., Brooks, P.M., Bruce, N.G., Brugha, T.S., Brunekreef, B., Buchbinder, R., Bui, L.N., Bukhman, G., Bulloch, A.G., Burch, M., Burney, P.G.J., Campos-Nonato, I.R., Campuzano, J.C., Cantoral, A.J., Caravanos, J., Cárdenas, R., Cardis, E., Carpenter, D.O., Caso, V., Castañeda-Orjuela, C.A., Castro, R.E., Catalá-López, F., Cavalleri, F., Çavlin, A., Chadha, V.K., Chang, J.-C., Charlson, F.J., Chen, H., Chen, W., Chen, Z., Chiang, P.P., Chimed-Ochir, O., Chowdhury, R., Christophi, C.A., Chuang, T.-W., Chugh, S.S., Cirillo, M., Claßen, T.K.D., Colistro, V., Colomar, M., Colquhoun, S.M., Contreras, A.G., Cooper, C., Cooperrider, K., Cooper, L.T., Coresh, J., Courville, K.J., Criqui, M.H., Cuevas-Nasu, L., Damsere-Derry, J., Danawi, H., Dandona, L., Dandona, R., Dargan, P.I., Davis, A., Davitoiu, D.V., Dayama, A., de Castro, E.F., De la Cruz-Góngora, V., De Leo, D., de Lima, G., Degenhardt, L., del Pozo-Cruz, B., Dellavalle, R.P., Deribe, K., Derrett, S., Des Jarlais, D.C., Dessalegn, M., deVeber, G.A., Devries, K.M., Dharmaratne, S.D., Dherani, M.K., Dicker, D., Ding, E.L., Dokova, K., Dorsey, E.R., Driscoll, T.R., Duan, L., Durrani, A.M., Ebel, B.E., Ellenbogen, R.G., Elshrek, Y.M., Endres, M., Ermakov, S.P., Erskine, H.E., Eshrati, B., Esteghamati, A., Fahimi, S., Faraon, E.J.A., Farzadfar, F., Fay, D.F.J., Feigin, V.L., Feigl, A.B., Fereshtehnejad, S.-M., Ferrari, A.J., Ferri, C.P., Flaxman, A.D., Fleming, T.D., Foigt, N., Foreman, K.J., Paleo, U.F., Franklin, R.C., Gabbe, B., Gaffikin, L., Gakidou, E., Gamkrelidze, A., Gankpé, F.G., Gansevoort, R.T., García-Guerra, F.A., Gasana, E., Geleijnse, J.M., Gessner, B.D., Gething, P., Gibney, K.B., Gillum, R.F., Ginawi, I.A.M., Giroud, M., Giussani, G., Goenka, S., Goginashvili, K., Gomez Dantes, H., Gona, P., Gonzalez de Cosio, T., González-Castell, D., Gotay, C.C., Goto, A., Gouda, H.N., Guerrant, R.L., Gugnani, H.C., Guillemin, F., Gunnell, D., Gupta, Rahul, Gupta, Rajeev, Gutiérrez, R.A., Hafezi-Nejad, N., Hagan, H., Hagstromer, M., Halasa, Y.A., Hamadeh, R.R., Hammami, M., Hankey, G.J., Hao, Y., Harb, H.L., Haregu, T.N., Haro, J.M., Havmoeller, R., Hay, S.I., Hedayati, M.T., Heredia-Pi, I.B., Hernandez, L., Heuton, K.R., Heydarpour, P., Hijar, M., Hoek, H.W., Hoffman, H.J., Hornberger, J.C., Hosgood, H.D., Hoy, D.G., Hsairi, M., Hu, G., Hu, H., Huang, C., Huang, J.J., Hubbell, B.J., Huiart, L., Husseini, A., Iannarone, M.L., Iburg, K.M., Idrisov, B.T., Ikeda, N., Innos, K., Inoue, M., Islami, F., Ismayilova, S., Jacobsen, K.H., Jansen, H.A., Jarvis, D.L., Jassal, S.K., Jauregui, A., Jayaraman, S., Jeemon, P., Jensen, P.N., Jha, V., Jiang, F., Jiang, G., Jiang, Y., Jonas, J.B., Juel, K., Kan, H., Kany Roseline, S.S., Karam, N.E., Karch, A., Karema, C.K., Karthikeyan, G., Kaul, A., Kawakami, N., Kazi, D.S., Kemp, A.H., Kengne, A.P., Keren, A., Khader, Y.S., Khalifa, S.E.A.H., Khan, E.A., Khang, Y.-H., Khatibzadeh, S., Khonelidze, I., Kieling, C., Kim, D., Kim, S., Kim, Y., Kimokoti, R.W., Kinfu, Y., Kinge, J.M., Kissela, B.M., Kivipelto, M., Knibbs, L.D., Knudsen, A.K., Kokubo, Y., Kose, M.R., Kosen, S., Kraemer, A., Kravchenko, M., Krishnaswami, S., Kromhout, H., Ku, T., Kuate Defo, B., Kucuk Bicer, B., Kuipers, E.J., Kulkarni, C., Kulkarni, V.S., Kumar, G.A., Kwan, G.F., Lai, T., Lakshmana Balaji, A., Lalloo, R., Lallukka, T., Lam, H., Lan, Q., Lansingh, V.C., Larson, H.J., Larsson, A., Laryea, D.O., Lavados, P.M., Lawrynowicz, A.E., Leasher, J.L., Lee, J.-T., Leigh, J., Leung, R., Levi, M., Li, Yichong, Li, Yongmei, Liang, J., Liang, X., Lim, S.S., Lindsay, M.P., Lipshultz, S.E., Liu, S., Liu, Y., Lloyd, B.K., Logroscino, G., London, S.J., Lopez, N., Lortet-Tieulent, J., Lotufo, P.A., Lozano, R., Lunevicius, R., Ma, J., Ma, S., Machado, V.M.P., MacIntyre, M.F., Magis-Rodriguez, C., Mahdi, A.A., Majdan, M., Malekzadeh, R., Mangalam, S., Mapoma, C.C., Marape, M., Marcenes, W., Margolis, D.J., Margono, C., Marks, G.B., Martin, R.V., Marzan, M.B., Mashal, M.T., Masiye, F., Mason-Jones, A.J., Matsushita, K., Matzopoulos, R., Mayosi, B.M., Mazorodze, T.T., McKay, A.C., McKee, M., McLain, A., Meaney, P.A., Medina, C., Mehndiratta, M.M., Mejia-Rodriguez, F., Mekonnen, W.,

Melaku, Y.A., Meltzer, M., Memish, Z.A., Mendoza, W., Mensah, G.A., Meretoja, A., Mhimbira, F.A., Micha, R., Miller, T.R., Mills, E.J., Misganaw, A., Mishra, S., Mohamed Ibrahim, N., Mohammad, K.A., Mokdad, A.H., Mola, G.L., Monasta, L., Montañez Hernandez, J.C., Montico, M., Moore, A.R., Morawska, L., Mori, R., Moschandreas, J., Moturi, W.N., Mozaffarian, D., Mueller, U.O., Mukaigawara, M., Mullany, E.C., Murthy, K.S., Naghavi, M., Nahas, Z., Naheed, A., Naidoo, K.S., Naldi, L., Nand, D., Nangia, V., Narayan, K.M.V., Nash, D., Neal, B., Nejjari, C., Neupane, S.P., Newton, C.R., Ngalesoni, F.N., Ngirabega, J. de D., Nguyen, G., Nguyen, N.T., Nieuwenhuijsen, M.J., Nisar, M.I., Nogueira, J.R., Nolla, J.M., Nolte, S., Norheim, O.F., Norman, R.E., Norrving, B., Nyakarahuka, L., Oh, I.-H., Ohkubo, T., Olusanya, B.O., Omer, S.B., Opio, J.N., Orozco, R., Pagcatipunan, R.S., Pain, A.W., Pandian, J.D., Panelo, C.I.A., Papachristou, C., Park, E.-K., Parry, C.D., Paternina Caicedo, A.J., Patten, S.B., Paul, V.K., Pavlin, B.I., Pearce, N., Pedraza, L.S., Pedroza, A., Pejin Stokic, L., Pekericli, A., Pereira, D.M., Perez-Padilla, R., Perez-Ruiz, F., Perico, N., Perry, S.A.L., Pervaiz, A., Pesudovs, K., Peterson, C.B., Petzold, M., Phillips, M.R., Phua, H.P., Plass, D., Poenaru, D., Polanczyk, G.V., Polinder, S., Pond, C.D., Pope, C.A., Pope, D., Popova, S., Pourmalek, F., Powles, J., Prabhakaran, D., Prasad, N.M., Qato, D.M., Quezada, A.D., Quistberg, D.A.A., Racapé, L., Rafay, A., Rahimi, K., Rahimi-Movaghar, V., Rahman, S.U., Raju, M., Rakovac, I., Rana, S.M., Rao, M., Razavi, H., Reddy, K.S., Refaat, A.H., Rehm, J., Remuzzi, G., Ribeiro, A.L., Riccio, P.M., Richardson, L., Riederer, A., Robinson, M., Roca, A., Rodriguez, A., Rojas-Rueda, D., Romieu, I., Ronfani, L., Room, R., Roy, N., Ruhago, G.M., Rushton, L., Sabin, N., Sacco, R.L., Saha, S., Sahathevan, R., Sahraian, M.A., Salomon, J.A., Salvo, D., Sampson, U.K., Sanabria, J.R., Sanchez, L.M., Sánchez-Pimienta, T.G., Sanchez-Riera, L., Sandar, L., Santos, I.S., Sapkota, A., Satpathy, M., Saunders, J.E., Sawhney, M., Saylan, M.I., Scarborough, P., Schmidt, J.C., Schneider, I.J.C., Schöttker, B., Schwebel, D.C., Scott, J.G., Seedat, S., Sepanlou, S.G., Serdar, B., Servan-Mori, E.E., Shaddick, G., Shahraz, S., Levy, T.S., Shangguan, S., She, J., Sheikhbahaei, S., Shibuya, K., Shin, H.H., Shinohara, Y., Shiri, R., Shishani, K., Shiue, I., Sigfusdottir, I.D., Silberberg, D.H., Simard, E.P., Sindi, S., Singh, A., Singh, G.M., Singh, J.A., Skirbekk, V., Sliwa, K., Soljak, M., Soneji, S., Søreide, K., Soshnikov, S., Sposato, L.A., Sreeramareddy, C.T., Stapelberg, N.J.C., Stathopoulou, V., Steckling, N., Stein, D.J., Stein, M.B., Stephens, N., Stöckl, H., Straif, K., Stroumpoulis, K., Sturua, L., Sunguya, B.F., Swaminathan, S., Swaroop, M., Sykes, B.L., Tabb, K.M., Takahashi, K., Talongwa, R.T., Tandon, N., Tanne, D., Tanner, M., Tavakkoli, M., Te Ao, B.J., Teixeira, C.M., Téllez Rojo, M.M., Terkawi, A.S., Texcalac-Sangrador, J.L., Thackway, S.V., Thomson, B., Thorne-Lyman, A.L., Thrift, A.G., Thurston, G.D., Tillmann, T., Tobollik, M., Tonelli, M., Topouzis, F., Towbin, J.A., Toyoshima, H., Traebert, J., Tran, B.X., Trasande, L., Trillini, M., Trujillo, U., Dimbuene, Z.T., Tsilimbaris, M., Tuzcu, E.M., Uchendu, U.S., Ukwaja, K.N., Uzun, S.B., van de Vijver, S., Van Dingenen, R., van Gool, C.H., van Os, J., Varakin, Y.Y., Vasankari, T.J., Vasconcelos, A.M.N., Vavilala, M.S., Veerman, L.J., Velasquez-Melendez, G., Venketasubramanian, N., Vijayakumar, L., Villalpando, S., Violante, F.S., Vlassov, V.V., Vollset, S.E., Wagner, G.R., Waller, S.G., Wallin, M.T., Wan, X., Wang, H., Wang, J., Wang, L., Wang, W., Wang, Y., Warouw, T.S., Watts, C.H., Weichenthal, S., Weiderpass, E., Weintraub, R.G., Werdecker, A., Wessells, K.R., Westerman, R., Whiteford, H.A., Wilkinson, J.D., Williams, H.C., Williams, T.N., Woldeyohannes, S.M., Wolfe, C.D.A., Wong, J.Q., Woolf, A.D., Wright, J.L., Wurtz, B., Xu, G., Yan, L.L., Yang, G., Yano, Y., Ye, P., Yenesew, M., Yentür, G.K., Yip, P., Yonemoto, N., Yoon, S.-J., Younis, M.Z., Younoussi, Z., Yu, C., Zaki, M.E., Zhao, Y., Zheng, Y., Zhou, M., Zhu, J., Zhu, S., Zou, X., Zunt, J.R., Lopez, A.D., Vos, T., Murray, C.J., 2015. Global, regional, and national comparative risk assessment of 79 behavioural, environmental and occupational, and metabolic risks or clusters of risks in 188 countries, 1990-2013: a systematic analysis for the Global Burden of Disease Study 2013. Lancet 386, 2287–2323.

Gea, J., Sancho-Muñoz, A., Chalela, R., 2018. Nutritional status and muscle dysfunction in chronic respiratory diseases: stable phase versus acute exacerbations. J Thorac Dis 10, S1332–S1354.

Gerayeli, F.V., Milne, S., Cheung, C., Li, X., Yang, C.W.T., Tam, A., Choi, L.H., Bae, A., Sin, D.D., 2021. COPD and the risk of poor outcomes in COVID-19: A systematic review and meta-analysis. eClinicalMedicine 33.

References

Gerbe, F., Sidot, E., Smyth, D.J., Ohmoto, M., Matsumoto, I., Dardalhon, V., Cesses, P., Garnier, L., Pouzolles, M., Brulin, B., Bruschi, M., Harcus, Y., Zimmermann, V.S., Taylor, N., Maizels, R.M., Jay, P., 2016. Intestinal epithelial tuft cells initiate type 2 mucosal immunity to helminth parasites. Nature 529, 226–230.

Ghorani, V., Boskabady, M.H., Khazdair, M.R., Kianmeher, M., 2017. Experimental animal models for COPD: a methodological review. Tob Induc Dis 15, 25.

Ghosh, M., Ahmad, S., White, C.W., Reynolds, S.D., 2017. Transplantation of Airway Epithelial Stem/Progenitor Cells: A Future for Cell-Based Therapy. Am J Respir Cell Mol Biol 56, 1–10.

Global, regional, and national age-sex-specific mortality for 282 causes of death in 195 countries and territories, 1980–2017: a systematic analysis for the Global Burden of Disease Study 2017, 2018. . Lancet 392, 1736–1788.

Glynos, C., Bibli, S.-I., Katsaounou, P., Pavlidou, A., Magkou, C., Karavana, V., Topouzis, S., Kalomenidis, I., Zakynthinos, S., Papapetropoulos, A., 2018. Comparison of the effects of e-cigarette vapor with cigarette smoke on lung function and inflammation in mice. American Journal of Physiology-Lung Cellular and Molecular Physiology 315, L662–L672.

Gohy, S.T., Hupin, C., Fregimilicka, C., Detry, B.R., Bouzin, C., Chevronay, H.G., Lecocq, M., Weynand, B., Ladjemi, M.Z., Pierreux, C.E., Birembaut, P., Polette, M., Pilette, C., 2015. Imprinting of the COPD airway epithelium for dedifferentiation and mesenchymal transition. European Respiratory Journal 45, 1258–1272.

Goldfarbmuren, K.C., Jackson, N.D., Sajuthi, S.P., Dyjack, N., Li, K.S., Rios, C.L., Plender, E.G., Montgomery, M.T., Everman, J.L., Bratcher, P.E., Vladar, E.K., Seibold, M.A., 2020. Dissecting the cellular specificity of smoking effects and reconstructing lineages in the human airway epithelium. Nat Commun 11, 2485.

Gomperts, B.N., 2014. Induction of multiciliated cells from induced pluripotent stem cells. Proceedings of the National Academy of Sciences 111, 6120–6121.

González-Martín, J., Kraakman, N.J.R., Pérez, C., Lebrero, R., Muñoz, R., 2021. A state–of–the-art review on indoor air pollution and strategies for indoor air pollution control. Chemosphere 262, 128376.

Grapin-Botton, A., 2008. Endoderm specification, in: StemBook. Harvard Stem Cell Institute, Cambridge (MA).

Gras, D., Chanez, P., Vachier, I., Petit, A., Bourdin, A., 2013. Bronchial epithelium as a target for innovative treatments in asthma. Pharmacology & Therapeutics 140, 290–305.

Green, M.D., Chen, A., Nostro, M.-C., d'Souza, S.L., Schaniel, C., Lemischka, I.R., Gouon-Evans, V., Keller, G., Snoeck, H.-W., 2011. Generation of anterior foregut endoderm from human embryonic and induced pluripotent stem cells. Nat Biotechnol 29, 267–272.

Griese, M., 1999. Pulmonary surfactant in health and human lung diseases: state of the art. Eur Respir J 13, 1455–1476.

Guillaumet-Adkins, A., Rodríguez-Esteban, G., Mereu, E., Mendez-Lago, M., Jaitin, D.A., Villanueva, A., Vidal, A., Martinez-Marti, A., Felip, E., Vivancos, A., Keren-Shaul, H., Heath, S., Gut, M., Amit, I., Gut, I., Heyn, H., 2017. Single-cell transcriptome conservation in cryopreserved cells and tissues. Genome Biol 18, 45.

Gupta, A., Lutolf, M.P., Hughes, A.J., Sonnen, K.F., 2021. Bioengineering in vitro models of embryonic development. Stem Cell Reports 16, 1104–1116.

Gurdon, J.B., 1962. The Developmental Capacity of Nuclei taken from Intestinal Epithelium Cells of Feeding Tadpoles. Development 10, 622–640.

Habib, N., Li, Y., Heidenreich, M., Swiech, L., Avraham-Davidi, I., Trombetta, J.J., Hession, C., Zhang, F., Regev, A., 2016. Div-Seq: Single-nucleus RNA-Seq reveals dynamics of rare adult newborn neurons. Science 353, 925–928.

Hall, N.J., Stanton, M.P., 2017. Long-term outcomes of congenital lung malformations. Seminars in Pediatric Surgery, Long-term outcomes in Pediatric Surgery 26, 311–316.

Halpin, D.M.G., Criner, G.J., Dransfield, M.T., Han, M.K., Hartley, B., Harvey, C., Jones, C.E., Kato, M., Lange, P., Lettis, S., Lomas, D.A., Martinez, F.J., Martin, N., Singh, D., Wise, R., Zheng, J., Lipson, D.A., 2020. Triple Versus Dual Combination Therapy in Chronic Obstructive Pulmonary Disease in Asian Countries: Analysis of the IMPACT Trial. Pulm Ther 7, 101–118.

Hampton, T., Armstrong, S., Russell, W.J., 2000. Estimating the diameter of the left main bronchus. Anaesth Intensive Care 28, 540–542.

Hao, Y., Hao, S., Andersen-Nissen, E., Mauck, W.M., Zheng, S., Butler, A., Lee, M.J., Wilk, A.J., Darby, C., Zager, M., Hoffman, P., Stoeckius, M., Papalexi, E., Mimitou, E.P., Jain, J., Srivastava, A., Stuart, T., Fleming, L.M., Yeung, B., Rogers, A.J., McElrath, J.M., Blish, C.A., Gottardo, R., Smibert, P., Satija, R., 2021. Integrated analysis of multimodal single-cell data. Cell 184, 3573-3587.e29.

Hawkins, F., Kramer, P., Jacob, A., Driver, I., Thomas, D.C., McCauley, K.B., Skvir, N., Crane, A.M., Kurmann, A.A., Hollenberg, A.N., Nguyen, S., Wong, B.G., Khalil, A.S., Huang, S.X.L., Guttentag, S., Rock, J.R., Shannon, J.M., Davis, B.R., Kotton, D.N., 2017. Prospective isolation of NKX2-1–expressing human lung progenitors derived from pluripotent stem cells. J Clin Invest 127, 2277–2294.

Hawkins, F., Rankin, S.A., Kotton, D.N., Zorn, A.M., 2016. The Genetic Programs Regulating Embryonic Lung Development and Induced Pluripotent Stem Cell Differentiation, in: Jobe, A., Whitsett, J., Abman, S. (Eds.), Fetal and Neonatal Lung Development. Cambridge University Press, Cambridge, pp. 1–21.

Hawkins, F.J., Suzuki, S., Beermann, M.L., Barillà, C., Wang, R., Villacorta-Martin, C., Berical, A., Jean, J.C., Suer, J.L., Matte, T., Simone-Roach, C., Tang, Y., Schlaeger, T.M., Crane, A.M., Matthias, N., Huang, S.X.L., Randell, S.H., Wu, J., Spence, J.R., Carraro, G., Stripp, B.R., Rab, A., Sorsher, E.J., Horani, A., Brody, S.L., Davis, B.R., Kotton, D.N., 2021. Derivation of Airway Basal Stem Cells from Human Pluripotent Stem Cells. Cell Stem Cell 28, 79-95.e8.

He, C., Morawska, L., Hitchins, J., Gilbert, D., 2004. Contribution from indoor sources to particle number and mass concentrations in residential houses. Atmospheric Environment 38, 3405–3415.

He, P., Lim, K., Sun, D., Pett, J.P., Jeng, Q., Polanski, K., Dong, Z., Bolt, L., Richardson, L., Mamanova, L., Dabrowska, M., Wilbrey-Clark, A., Madissoon, E., Tuong, Z.K., Dann, E., Suo, C., Goh, I., Yoshida, M., Nikolić, M.Z., Janes, S.M., He, X., Barker, R.A., Teichmann, S.A., Marioni, J.C., Meyer, K.B., Rawlins, E.L., 2022. A human fetal lung cell atlas uncovers proximal-distal gradients of differentiation and key regulators of epithelial fates. Cell 185, 4841-4860.e25.

Hein, R.F.C., Conchola, A.S., Fine, A.S., Xiao, Z., Frum, T., Brastrom, L.K., Akinwale, M.A., Childs, C.J., Tsai, Y.-H., Holloway, E.M., Huang, S., Mahoney, J., Heemskerk, I., Spence, J.R., 2022. Stable iPSC-derived NKX2-1+ lung bud tip progenitor organoids give rise to airway and alveolar cell types. Development 149, dev200693.

References

Hewitt, R.J., Butler, C.R., Maughan, E.F., Elliott, M.J., 2016. Congenital tracheobronchial stenosis. Seminars in Pediatric Surgery, SI: Pediatric Airway Disease 25, 144–149.

Hillas, G., Perlikos, F., Tsiligianni, I., Tzanakis, N., 2015. Managing comorbidities in COPD. Int J Chron Obstruct Pulmon Dis 10, 95–109.

Höfer, D., Püschel, B., Drenckhahn, D., 1996. Taste receptor-like cells in the rat gut identified by expression of alpha-gustducin. Proc Natl Acad Sci U S A 93, 6631–6634.

Hogan, B.L.M., Barkauskas, C.E., Chapman, H.A., Epstein, J.A., Jain, R., Hsia, C.C.W., Niklason, L., Calle, E., Le, A., Randell, S.H., Rock, J., Snitow, M., Krummel, M., Stripp, B.R., Vu, T., White, E.S., Whitsett, J.A., Morrisey, E.E., 2014. Repair and Regeneration of the Respiratory System: Complexity, Plasticity, and Mechanisms of Lung Stem Cell Function. Cell Stem Cell 15, 123–138.

Hong, K.U., Reynolds, S.D., Watkins, S., Fuchs, E., Stripp, B.R., 2004. Basal Cells Are a Multipotent Progenitor Capable of Renewing the Bronchial Epithelium. Am J Pathol 164, 577–588.

Huang, C.-Y., Liu, C.-L., Ting, C.-Y., Chiu, Y.-T., Cheng, Y.-C., Nicholson, M.W., Hsieh, P.C.H., 2019. Human iPSC banking: barriers and opportunities. Journal of Biomedical Science 26, 87.

Huang, S.X.L., Islam, M.N., O'Neill, J., Hu, Z., Yang, Y.-G., Chen, Y.-W., Mumau, M., Green, M.D., Vunjak-Novakovic, G., Bhattacharya, J., Snoeck, H.-W., 2014. Efficient generation of lung and airway epithelial cells from human pluripotent stem cells. Nat Biotechnol 32, 84–91.

Huertas, A., Guignabert, C., Barberà, J.A., Bärtsch, P., Bhattacharya, J., Bhattacharya, S., Bonsignore, M.R., Dewachter, L., Dinh-Xuan, A.T., Dorfmüller, P., Gladwin, M.T., Humbert, M., Kotsimbos, T., Vassilakopoulos, T., Sanchez, O., Savale, L., Testa, U., Wilkins, M.R., 2018. Pulmonary vascular endothelium: the orchestra conductor in respiratory diseases: Highlights from basic research to therapy. Eur Respir J 51, 1700745.

Hughes, T., Dijkstra, K.K., Rawlins, E.L., Hynds, R.E., 2023. Open questions in human lung organoid research. Front Pharmacol 13, 1083017.

Hui, H., Tang, Y., Hu, M., Zhao, X., Hui, H., Tang, Y., Hu, M., Zhao, X., 2011. Stem Cells: General Features and Characteristics, Stem Cells in Clinic and Research. IntechOpen.

Hwang, B., Lee, J.H., Bang, D., 2018. Single-cell RNA sequencing technologies and bioinformatics pipelines. Exp Mol Med 50, 1–14.

Ilic, D., Ogilvie, C., 2022. Pluripotent Stem Cells in Clinical Setting—New Developments and Overview of Current Status. Stem Cells 40, 791–801.

Inoue, H., Nagata, N., Kurokawa, H., Yamanaka, S., 2014. iPS cells: a game changer for future medicine. EMBO J 33, 409–417.

Jacob, A., Vedaie, M., Roberts, D.A., Thomas, D.C., Villacorta-Martin, C., Alysandratos, K.-D., Hawkins, F., Kotton, D.N., 2019. Derivation of self-renewing lung alveolar epithelial type II cells from human pluripotent stem cells. Nat Protoc 14, 3303–3332.

Jain, R., Barkauskas, C.E., Takeda, N., Bowie, E.J., Aghajanian, H., Wang, Q., Padmanabhan, A., Manderfield, L.J., Gupta, M., Li, D., Li, L., Trivedi, C.M., Hogan, B.L.M., Epstein, J.A., 2015. Plasticity of Hopx+ Type I alveolar cells to regenerate Type II cells in the lung. Nat Commun 6, 6727.

Jaitovich, A., Barreiro, E., 2018. Skeletal Muscle Dysfunction in Chronic Obstructive Pulmonary Disease. What We Know and Can Do for Our Patients. Am J Respir Crit Care Med 198, 175–186.

Jia, Z., Chen, Q., Na, H., Yang, Y., Zhao, J., 2023. Impacts of industrial agglomeration on industrial pollutant emissions: Evidence found in the Lanzhou–Xining urban agglomeration in western China. Front Public Health 10, 1109139.

Jiang, X.-Q., Mei, X.-D., Feng, D., 2016. Air pollution and chronic airway diseases: what should people know and do? J Thorac Dis 8, E31–E40.

Johansen, M.D., Mahbub, R.M., Idrees, S., Nguyen, D.H., Miemczyk, S., Pathinayake, P., Nichol, K., Hansbro, N.G., Gearing, L.J., Hertzog, P.J., Gallego-Ortega, D., Britton, W.J., Saunders, B.M., Wark, P.A., Faiz, A., Hansbro, P.M., 2022. Increased SARS-CoV-2 Infection, Protease, and Inflammatory Responses in Chronic Obstructive Pulmonary Disease Primary Bronchial Epithelial Cells Defined with Single-Cell RNA Sequencing. Am J Respir Crit Care Med 206, 712–729.

Jovic, D., Liang, X., Zeng, H., Lin, L., Xu, F., Luo, Y., 2022. Single-cell RNA sequencing technologies and applications: A brief overview. Clin Transl Med 12, e694.

Kalininskiy, A., Kittel, J., Nacca, N.E., Misra, R.S., Croft, D.P., McGraw, M.D., 2021. E-cigarette exposures, respiratory tract infections, and impaired innate immunity: a narrative review. Pediatr Med 4, 5.

Kaplan, A., Abidi, E., Ghali, R., Booz, G.W., Kobeissy, F., Zouein, F.A., 2017. Functional, Cellular, and Molecular Remodeling of the Heart under Influence of Oxidative Cigarette Tobacco Smoke. Oxid Med Cell Longev 2017, 3759186.

Kasahara, Y., Tuder, R.M., Taraseviciene-Stewart, L., Le Cras, T.D., Abman, S., Hirth, P.K., Waltenberger, J., Voelkel, N.F., 2000. Inhibition of VEGF receptors causes lung cell apoptosis and emphysema. J Clin Invest 106, 1311–1319.

Ke, S., Liu, Q., Zhang, X., Yao, Y., Yang, X., Sui, G., 2021. Cytotoxicity analysis of biomass combustion particles in human pulmonary alveolar epithelial cells on an air–liquid interface/dynamic culture platform. Particle and Fibre Toxicology 18, 31.

Kheradmand, F., Rishi, K., Werb, Z., 2002. Signaling through the EGF receptor controls lung morphogenesis in part by regulating MT1-MMP-mediated activation of gelatinase A/MMP2. Journal of Cell Science 115, 839–848.

Kia'i, N., Bajaj, T., 2022. Histology, Respiratory Epithelium, StatPearls [Internet]. StatPearls Publishing.

Kim, J.-H., Kim, J., Kim, W.J., Choi, Y.H., Yang, S.-R., Hong, S.-H., 2020. Diesel Particulate Matter 2.5 Induces Epithelial-to-Mesenchymal Transition and Upregulation of SARS-CoV-2 Receptor during Human Pluripotent Stem Cell-Derived Alveolar Organoid Development. Int J Environ Res Public Health 17, 8410.

Kim, K.-H., Kabir, E., Kabir, S., 2015. A review on the human health impact of airborne particulate matter. Environment International 74, 136–143.

Kimura, J., Deutsch, G.H., 2007. Key Mechanisms of Early Lung Development. Pediatr Dev Pathol 10, 335–347.

Kirkham, P., Rahman, I., 2006. Oxidative stress in asthma and COPD: Antioxidants as a therapeutic strategy. Pharmacology & Therapeutics 111, 476–494.

References

Kiyokawa, H., Morimoto, M., 2020. Notch signaling in the mammalian respiratory system, specifically the trachea and lungs, in development, homeostasis, regeneration, and disease. Dev Growth Differ 62, 67–79.

Knabe, L., Petit, A., Vernisse, C., Charriot, J., Pugnière, M., Henriquet, C., Sasorith, S., Molinari, N., Chanez, P., Berthet, J.-P., Suehs, C., Vachier, I., Ahmed, E., Bourdin, A., 2019. CCSP counterbalances airway epithelial-driven neutrophilic chemotaxis. Eur Respir J 54, 1802408.

Knudsen, L., Ochs, M., 2018. The micromechanics of lung alveoli: structure and function of surfactant and tissue components. Histochem Cell Biol 150, 661–676.

Ko, U.W., Kyung, S.Y., 2022. Adverse Effects of Air Pollution on Pulmonary Diseases. Tuberc Respir Dis (Seoul) 85, 313–319.

Kobayashi, Y., Tata, A., Konkimalla, A., Katsura, H., Lee, R.F., Ou, J., Banovich, N.E., Kropski, J.A., Tata, P.R., 2020. Persistence of a regeneration-associated, transitional alveolar epithelial cell state in pulmonary fibrosis. Nat Cell Biol 22, 934–946.

Koh, J., Kim, H., Moon, K.C., Lee, C., Lee, K., Ryu, H.S., Jung, K.C., Jeon, Y.K., 2023. Molecular Classification of Extrapulmonary Neuroendocrine Carcinomas With Emphasis on POU2F3-positive Tuft Cell Carcinoma. Am J Surg Pathol 47, 183–193.

Kolios, G., Moodley, Y., 2013. Introduction to Stem Cells and Regenerative Medicine. RES 85, 3–10.

Konishi, S., Gotoh, S., Tateishi, K., Yamamoto, Y., Korogi, Y., Nagasaki, T., Matsumoto, H., Muro, S., Hirai, T., Ito, I., Tsukita, S., Mishima, M., 2015. Directed Induction of Functional Multi-ciliated Cells in Proximal Airway Epithelial Spheroids from Human Pluripotent Stem Cells. Stem Cell Reports 6, 18–25.

Koo, B.-K., Bartfeld, S., Alev, C., 2021. Organoids: ready for the revolution? J Mol Med 99, 441–442.

Kopf, M., Schneider, C., Nobs, S.P., 2015. The development and function of lung-resident macrophages and dendritic cells. Nat Immunol 16, 36–44.

Kraljevic, D., Vukojevic, K., Karan, D., Rajic, B., Todorovic, J., Miskovic, J., Tomic, V., Kordic, M., Soljic, V., 2015. Proliferation, apoptosis and expression of matrix metalloproteinase-9 in human fetal lung. Acta Histochemica, Immunomarkers in human developing and pediatric neoplastic tissues 117, 444–450.

Krasteva, G., Hartmann, P., Papadakis, T., Bodenbenner, M., Wessels, L., Weihe, E., Schütz, B., Langheinrich, A.C., Chubanov, V., Gudermann, T., Ibanez-Tallon, I., Kummer, W., 2012. Cholinergic chemosensory cells in the auditory tube. Histochem Cell Biol 137, 483–497.

Kumar, M., Seeger, W., Voswinckel, R., 2014. Senescence-Associated Secretory Phenotype and Its Possible Role in Chronic Obstructive Pulmonary Disease. Am J Respir Cell Mol Biol 51, 323–333.

Kuo, C.S., Krasnow, M.A., 2015. Formation of a Neurosensory Organ by Epithelial Cell Slithering. Cell 163, 394–405.

Lafkas, D., Shelton, A., Chiu, C., Leon Boenig, G., Chen, Y., Stawicki, S.S., Siltanen, C., Reichelt, M., Zhou, M., Wu, X., 2015. Therapeutic Antibodies Reveal Notch Control of Transdifferentiation in the Adult Lung. Nature 528, 127-131,.

Lafzi, A., Moutinho, C., Picelli, S., Heyn, H., 2018. Tutorial: guidelines for the experimental design of single-cell RNA sequencing studies. Nat Protoc 13, 2742–2757.

Lahousse, L., Tiemeier, H., Ikram, M.A., Brusselle, G.G., 2015. Chronic obstructive pulmonary disease and cerebrovascular disease: A comprehensive review. Respiratory Medicine 109, 1371–1380.

Lambrecht, B.N., Hammad, H., 2012. The airway epithelium in asthma. Nat Med 18, 684–692.

Lancaster, M.A., Knoblich, J.A., 2014. Organogenesis in a dish: modeling development and disease using organoid technologies. Science 345, 1247125.

Landrigan, P.J., 2017. Air pollution and health. The Lancet Public Health 2, e4–e5.

Landrigan, P.J., Fuller, R., Acosta, N.J.R., Adeyi, O., Arnold, R., Basu, N. (Nil), Baldé, A.B., Bertollini, R., Bose-O'Reilly, S., Boufford, J.I., Breysse, P.N., Chiles, T., Mahidol, C., Coll-Seck, A.M., Cropper, M.L., Fobil, J., Fuster, V., Greenstone, M., Haines, A., Hanrahan, D., Hunter, D., Khare, M., Krupnick, A., Lanphear, B., Lohani, B., Martin, K., Mathiasen, K.V., McTeer, M.A., Murray, C.J.L., Ndahimananjara, J.D., Perera, F., Potočnik, J., Preker, A.S., Ramesh, J., Rockström, J., Salinas, C., Samson, L.D., Sandilya, K., Sly, P.D., Smith, K.R., Steiner, A., Stewart, R.B., Suk, W.A., van Schayck, O.C.P., Yadama, G.N., Yumkella, K., Zhong, M., 2018. The Lancet Commission on pollution and health. The Lancet 391, 462–512.

Laniado-Laborín, R., 2009. Smoking and Chronic Obstructive Pulmonary Disease (COPD). Parallel Epidemics of the 21st Century. Int J Environ Res Public Health 6, 209-224,.

Laube, B.L., Carson, K.A., Sharpless, G., Paulin, L.M., Hansel, N.N., 2019. Mucociliary Clearance in Former Tobacco Smokers with Both Chronic Obstructive Pulmonary Disease and Chronic Bronchitis and the Effect of Roflumilast. J Aerosol Med Pulm Drug Deliv 32, 189–199.

Laucho-Contreras, M.E., Polverino, F., Gupta, K., Taylor, K.L., Kelly, E., Pinto-Plata, V., Divo, M., Ashfaq, N., Petersen, H., Stripp, B., Pilon, A.L., Tesfaigzi, Y., Celli, B.R., Owen, C.A., 2015. Protective role for club cell secretory protein-16 (CC16) in the development of COPD. European Respiratory Journal 45, 1544–1556.

Le, Y., Wang, Y., Zhou, L., Xiong, J., Tian, J., Yang, X., Gai, X., Sun, Y., 2020. Cigarette smoke-induced HMGB1 translocation and release contribute to migration and NF-κB activation through inducing autophagy in lung macrophages. J Cell Mol Med 24, 1319–1331.

Lee, A.L., Goldstein, R.S., 2015. Gastroesophageal reflux disease in COPD: links and risks. Int J Chron Obstruct Pulmon Dis 10, 1935–1949.

Lee, J.-H., Bhang, D.H., Beede, A., Huang, T.L., Stripp, B.R., Bloch, K.D., Wagers, A.J., Tseng, Y.-H., Ryeom, S., Kim, C.F., 2014. Lung Stem Cell Differentiation in Mice Directed by Endothelial Cells via a BMP4-NFATc1-Thrombospondin-1 Axis. Cell 156, 440–455.

Lee, T.C., Wu, R., Brody, A.R., Barrett, J.C., Nettesheim, P., 1984. Growth and differentiation of hamster tracheal epithelial cells in culture. Exp Lung Res 6, 27–45.

Leuenberger, P., Schwartz, J., Ackermann-Liebrich, U., Blaser, K., Bolognini, G., Bongard, J.P., Brandli, O., Braun, P., Bron, C., Brutsche, M., 1994. Passive smoking exposure in adults and chronic respiratory symptoms (SAPALDIA Study). Swiss Study on Air Pollution and Lung Diseases in Adults, SAPALDIA Team. Am J Respir Crit Care Med 150, 1222–1228.

Leung, C.M., de Haan, P., Ronaldson-Bouchard, K., Kim, G.-A., Ko, J., Rho, H.S., Chen, Z., Habibovic, P., Jeon, N.L., Takayama, S., Shuler, M.L., Vunjak-Novakovic, G., Frey, O., Verpoorte, E., Toh, Y.-C., 2022. A guide to the organ-on-a-chip. Nat Rev Methods Primers 2, 1–29.

References

Leung, D.Y.C., 2015. Outdoor-indoor air pollution in urban environment: challenges and opportunity. Frontiers in Environmental Science 2.

Li, J., Sun, S., Tang, R., Qiu, H., Huang, Q., Mason, T.G., Tian, L., 2016. Major air pollutants and risk of COPD exacerbations: a systematic review and meta-analysis. Int J Chron Obstruct Pulmon Dis 11, 3079–3091.

Li, L., Ma, M., Duan, T., Sui, X., 2022. The critical roles and therapeutic implications of tuft cells in cancer. Front Pharmacol 13, 1047188.

Liu, C., Chen, R., Sera, F., Vicedo-Cabrera, A.M., Guo, Y., Tong, S., Coelho, M.S.Z.S., Saldiva, P.H.N., Lavigne, E., Matus, P., Valdes Ortega, N., Osorio Garcia, S., Pascal, M., Stafoggia, M., Scortichini, M., Hashizume, M., Honda, Y., Hurtado-Díaz, M., Cruz, J., Nunes, B., Teixeira, J.P., Kim, H., Tobias, A., Íñiguez, C., Forsberg, B., Åström, C., Ragettli, M.S., Guo, Y.-L., Chen, B.-Y., Bell, M.L., Wright, C.Y., Scovronick, N., Garland, R.M., Milojevic, A., Kyselý, J., Urban, A., Orru, H., Indermitte, E., Jaakkola, J.J.K., Ryti, N.R.I., Katsouyanni, K., Analitis, A., Zanobetti, A., Schwartz, J., Chen, J., Wu, T., Cohen, A., Gasparrini, A., Kan, H., 2019. Ambient Particulate Air Pollution and Daily Mortality in 652 Cities. New England Journal of Medicine 381, 705–715.

Liu, C., Oikonomopoulos, A., Sayed, N., Wu, J.C., 2018. Modeling human diseases with induced pluripotent stem cells: from 2D to 3D and beyond. Development 145, dev156166.

Liu, Sha, Zhou, Y., Liu, Suixin, Chen, X., Zou, W., Zhao, D., Li, X., Pu, J., Huang, L., Chen, J., Li, B., Liu, Shiliang, Ran, P., 2017. Association between exposure to ambient particulate matter and chronic obstructive pulmonary disease: results from a cross-sectional study in China. Thorax 72, 788–795.

Liu, W., Zhang, J., Zhang, L., Turpin, B.J., Weisel, C.P., Morandi, M.T., Stock, T.H., Colome, S., Korn, L.R., 2006. Estimating contributions of indoor and outdoor sources to indoor carbonyl concentrations in three urban areas of the United States. Atmospheric Environment 40, 2202–2214.

Liu, Y., Mi, Y., Mueller, T., Kreibich, S., Williams, E.G., Van Drogen, A., Borel, C., Frank, M., Germain, P.-L., Bludau, I., Mehnert, M., Seifert, M., Emmenlauer, M., Sorg, I., Bezrukov, F., Bena, F.S., Zhou, H., Dehio, C., Testa, G., Saez-Rodriguez, J., Antonarakis, S.E., Hardt, W.-D., Aebersold, R., 2019. Multi-omic measurements of heterogeneity in HeLa cells across laboratories. Nat Biotechnol 37, 314–322.

Logan, W.P.D., 1953. Mortality in the London fog incident, 1952. Lancet 1, 336–338.

Lomas, D.A., Silverman, E.K., Edwards, L.D., Miller, B.E., Coxson, H.O., Tal-Singer, R., Evaluation of COPD Longitudinally to Identify Predictive Surrogate Endpoints (ECLIPSE) investigators, 2008. Evaluation of serum CC-16 as a biomarker for COPD in the ECLIPSE cohort. Thorax 63, 1058–1063.

Lonc, E., Plewa, K., Lonc, E., Plewa, K., 2011. Comparison of Indoor and Outdoor Bioaerosols in Poultry Farming, Advanced Topics in Environmental Health and Air Pollution Case Studies. IntechOpen.

López-Campos, J.L., Calero, C., Rojano, B., López-Porras, M., Sáenz-Coronilla, J., Blanco, A.I., Sánchez-López, V., Tobar, D., Montes-Worboys, A., Arellano, E., 2013. C-Reactive Protein and Serum Amyloid A Overexpression in Lung Tissues of Chronic Obstructive Pulmonary Disease Patients: A Case-Control Study. Int J Med Sci 10, 938–947.

Lü, J., Izvolsky, K.I., Qian, J., Cardoso, W.V., 2005. Identification of FGF10 Targets in the Embryonic Lung Epithelium during Bud Morphogenesis. J. Biol. Chem 280, 4834-4841,.

Lu, Z., Coll, P., Maitre, B., Epaud, R., Lanone, S., 2022. Air pollution as an early determinant of COPD. Eur Respir Rev 31, 220059.

Luecken, M.D., Zaragosi, L.-E., Madissoon, E., Sikkema, L., Firsova, A.B., Domenico, E.D., Kümmerle, L., Saglam, A., Berg, M., Gay, A.C.A., Schniering, J., Mayr, C.H., Abalo, X.M., Larsson, L., Sountoulidis, A., Teichmann, S.A., Eunen, K. van, Koppelman, G.H., Saeb-Parsy, K., Leroy, S., Powell, P., Sarkans, U., Timens, W., Lundeberg, J., Berge, M. van den, Nilsson, M., Horváth, P., Denning, J., Papatheodorou, I., Schultze, J.L., Schiller, H.B., Barbry, P., Petoukhov, I., Misharin, A.V., Adcock, I.M., Papen, M. von, Theis, F.J., Samakovlis, C., Meyer, K.B., Nawijn, M.C., 2022. The discovAIR project: a roadmap towards the Human Lung Cell Atlas. European Respiratory Journal 60.

Lugg, S.T., Scott, A., Parekh, D., Naidu, B., Thickett, D.R., 2022. Cigarette smoke exposure and alveolar macrophages: mechanisms for lung disease. Thorax 77, 94–101.

Lunn, M.P.T., Manji, H., Choudhary, P.P., Hughes, R.A.C., Thomas, P.K., 1999. Chronic inflammatory demyelinating polyradiculoneuropathy: a prevalence study in south east England. Journal of Neurology, Neurosurgery & Psychiatry 66, 677–680.

Ma, Z., Meng, X., Chen, C., Chao, B., Zhang, C., Li, W., 2022. Short-term effects of different PM2.5 ranges on daily all-cause mortality in Jinan, China. Sci Rep 12, 5665.

MacLeod, M., Papi, A., Contoli, M., Beghé, B., Celli, B.R., Wedzicha, J.A., Fabbri, L.M., 2021. Chronic obstructive pulmonary disease exacerbation fundamentals: Diagnosis, treatment, prevention and disease impact. Respirology 26, 532–551.

Maintainer, B.P., Morgan, M., Carlson, M., Tenenbaum, D., Arora, S., Oberchain, V., Morrell, K., Shepherd, L., 2023. AnnotationHub: Client to access AnnotationHub resources.

Maiuri, P., Knezevich, A., De Marco, A., Mazza, D., Kula, A., McNally, J.G., Marcello, A., 2011. Fast transcription rates of RNA polymerase II in human cells. EMBO Rep 12, 1280–1285.

Manisalidis, I., Stavropoulou, E., Stavropoulos, A., Bezirtzoglou, E., 2020. Environmental and Health Impacts of Air Pollution: A Review. Front Public Health 8, 14.

Márquez-Jurado, S., Díaz-Colunga, J., das Neves, R.P., Martinez-Lorente, A., Almazán, F., Guantes, R., Iborra, F.J., 2018. Mitochondrial levels determine variability in cell death by modulating apoptotic gene expression. Nat Commun 9, 389.

Martinelli, N., Olivieri, O., Girelli, D., 2013. Air particulate matter and cardiovascular disease: A narrative review. European Journal of Internal Medicine 24, 295–302.

Martinez, F.D., 2016. Early-Life Origins of Chronic Obstructive Pulmonary Disease. New England Journal of Medicine 375, 871-878,.

Martinu, T., Todd, J.L., Gelman, A.E., Guerra, S., Palmer, S.M., 2022. Club Cell Secretory Protein in Lung Disease: Emerging Concepts and Potential Therapeutics. Annu Rev Med.

Marton, R.M., Pașca, S.P., 2020. Organoid and Assembloid Technologies for Investigating Cellular Crosstalk in Human Brain Development and Disease. Trends in Cell Biology 30, 133–143.

Massaro, M., Wu, S., Baudo, G., Liu, H., Collum, S., Lee, H., Stigliano, C., Segura-Ibarra, V., Karmouty-Quintana, H., Blanco, E., 2023. Lipid nanoparticle-mediated mRNA delivery in lung fibrosis. Eur J Pharm Sci 106370.

References

Massoni-Badosa, R., Iacono, G., Moutinho, C., Kulis, M., Palau, N., Marchese, D., Rodríguez-Ubreva, J., Ballestar, E., Rodriguez-Esteban, G., Marsal, S., Aymerich, M., Colomer, D., Campo, E., Julià, A., Martín-Subero, J.I., Heyn, H., 2020. Sampling time-dependent artifacts in single-cell genomics studies. Genome Biology 21, 112.

Matsuno, K., Mae, S.-I., Okada, C., Nakamura, M., Watanabe, A., Toyoda, T., Uchida, E., Osafune, K., 2016. Redefining definitive endoderm subtypes by robust induction of human induced pluripotent stem cells. Differentiation 92, 281–290.

McDonough, J.E., Yuan, R., Suzuki, M., Seyednejad, N., Elliott, W.M., Sanchez, P.G., Wright, A.C., Gefter, W.B., Litzky, L., Coxson, H.O., Paré, P.D., Sin, D.D., Pierce, R.A., Woods, J.C., McWilliams, A.M., Mayo, J.R., Lam, S.C., Cooper, J.D., Hogg, J.C., 2011. Small-Airway Obstruction and Emphysema in Chronic Obstructive Pulmonary Disease. N Engl J Med 365, 1567–1575.

McIntyre, B.A.S., Alev, C., Mechael, R., Salci, K.R., Lee, J.B., Fiebig-Comyn, A., Guezguez, B., Wu, Y., Sheng, G., Bhatia, M., 2014. Expansive Generation of Functional Airway Epithelium From Human Embryonic Stem Cells. Stem Cells Translational Medicine 3, 7–17.

Mercer, R.R., Russell, M.L., Roggli, V.L., Crapo, J.D., 2012. Cell number and distribution in human and rat airways. American journal of respiratory cell and molecular biology.

Mertens, T.C.J., Karmouty-Quintana, H., Taube, C., Hiemstra, P.S., 2017. Use of airway epithelial cell culture to unravel the pathogenesis and study treatment in obstructive airway diseases. Pulmonary Pharmacology & Therapeutics 45, 101–113.

Milara, J., Peiró, T., Serrano, A., Cortijo, J., 2013. Epithelial to Mesenchymal Transition Is Increased in Patients with COPD and Induced by Cigarette Smoke. Thorax 68, 410-420,.

Miller, A.J., Dye, B.R., Ferrer-Torres, D., Hill, D.R., Overeem, A.W., Shea, L.D., Spence, J.R., 2019. Generation of lung organoids from human pluripotent stem cells in vitro. Nat Protoc 14, 518–540.

Min, H., Danilenko, D.M., Scully, S.A., Bolon, B., Ring, B.D., Tarpley, J.E., DeRose, M., Simonet, W.S., 1998. Fgf-10 Is Required for Both Limb and Lung Development and Exhibits Striking Functional Similarity to Drosophila Branchless. Genes Dev 12, 3156-3161,.

Mohammed, A., Alghetaa, H.K., Zhou, J., Chatterjee, S., Nagarkatti, P., Nagarkatti, M., 2020. Protective effects of Δ9-tetrahydrocannabinol against enterotoxin-induced acute respiratory distress syndrome are mediated by modulation of microbiota. British Journal of Pharmacology 177, 5078–5095.

Moldoveanu, B., Otmishi, P., Jani, P., Walker, J., Sarmiento, X., Guardiola, J., Saad, M., Yu, J., 2008. Inflammatory mechanisms in the lung. J Inflamm Res 2, 1–11.

Molinari, N., Briand, C., Vachier, I., Malafaye, N., Aubas, P., Georgescu, V., Roche, N., Chanez, P., Bourdin, A., 2015. Hospitalizations for COPD Exacerbations: Trends and Determinants of Death. COPD 12, 621–627.

Molinari, N., Chanez, P., Roche, N., Ahmed, E., Vachier, I., Bourdin, A., 2016. Rising total costs and mortality rates associated with admissions due to COPD exacerbations. Respir Res 17, 149.

Montgomery, M.T., Sajuthi, S.P., Cho, S.-H., Everman, J.L., Rios, C.L., Goldfarbmuren, K.C., Jackson, N.D., Saef, B., Cromie, M., Eng, C., Medina, V., Elhawary, J.R., Oh, S.S., Rodriguez-Santana, J., Vladar, E.K., Burchard,

E.G., Seibold, M.A., 2020. Genome-Wide Analysis Reveals Mucociliary Remodeling of the Nasal Airway Epithelium Induced by Urban PM2.5. Am J Respir Cell Mol Biol 63, 172–184.

Montheil, T., Echalier, C., Martinez, J., Subra, G., Mehdi, A., 2018. Inorganic polymerization: an attractive route to biocompatible hybrid hydrogels. J. Mater. Chem. B 6, 3434–3448.

Montoro, D.T., Haber, A.L., Biton, M., Vinarsky, V., Lin, B., Birket, S., Yuan, F., Chen, S., Leung, H.M., Villoria, J., Rogel, N., Burgin, G., Tsankov, A., Waghray, A., Slyper, M., Waldmann, J., Nguyen, L., Dionne, D., Rozenblatt-Rosen, O., Tata, P.R., Mou, H., Shivaraju, M., Bihler, H., Mense, M., Tearney, G.J., Rowe, S.M., Engelhardt, J.F., Regev, A., Rajagopal, J., 2018. A revised airway epithelial hierarchy includes CFTR-expressing ionocytes. Nature 560, 319–324.

Moreira, A., Müller, M., Costa, P.F., Kohl, Y., 2022. Advanced In Vitro Lung Models for Drug and Toxicity Screening: The Promising Role of Induced Pluripotent Stem Cells. Advanced Biology 6, 2101139.

Morgan, L., Pearson, M., de Iongh, R., Mackey, D., van der Wall, H., Peters, M., Rutland, J., 2004. Scintigraphic measurement of tracheal mucus velocity in vivo. Eur Respir J 23, 518–522.

Mori, M., Mahoney, J.E., Stupnikov, M.R., Paez-Cortez, J.R., Szymaniak, A.D., Varelas, X., Herrick, D.B., Schwob, J., Zhang, H., Cardoso, W.V., 2015. Notch3-Jagged signaling controls the pool of undifferentiated airway progenitors. Development 142, 258–267.

Mou, H., Zhao, R., Sherwood, R., Ahfeldt, T., Lapey, A., Wain, J., Sicilian, L., Izvolsky, K., Lau, F.H., Musunuru, K., Cowan, C., Rajagopal, J., 2012. Generation of Multipotent Lung and Airway Progenitors from Mouse ESCs and Patient-Specific Cystic Fibrosis iPSCs. Cell Stem Cell 10, 385–397.

Mullassery, D., Smith, N.P., 2015. Lung development. Seminars in Pediatric Surgery, Congenital Lung Lesions 24, 152–155.

Münzel, T., Hahad, O., Kuntic, M., Keaney, J.F., Deanfield, J.E., Daiber, A., 2020. Effects of tobacco cigarettes, e-cigarettes, and waterpipe smoking on endothelial function and clinical outcomes. Eur Heart J 41, 4057–4070.

Nasri, A., Foisset, F., Ahmed, E., Lahmar, Z., Vachier, I., Jorgensen, C., Assou, S., Bourdin, A., De Vos, J., 2021. Roles of Mesenchymal Cells in the Lung: From Lung Development to Chronic Obstructive Pulmonary Disease. Cells 10, 3467.

Nawroth, J.C., Barrile, R., Conegliano, D., van Riet, S., Hiemstra, P.S., Villenave, R., 2019. Stem cell-based Lung-on-Chips: The best of both worlds? Adv Drug Deliv Rev 140, 12–32.

Nazaroff et al., 2004. Indoor particle dynamics. Indoor Air 14, 175–183.

Niethamer, T.K., Stabler, C.T., Leach, J.P., Zepp, J.A., Morley, M.P., Babu, A., Zhou, S., Morrisey, E.E., 2020. Defining the role of pulmonary endothelial cell heterogeneity in the response to acute lung injury. eLife 9, e53072.

Nieto, M.A., Huang, R.Y.-J., Jackson, R.A., Thiery, J.P., 2016. EMT: 2016. Cell 166, 21–45.

Nishizawa, M., Chonabayashi, K., Nomura, M., Tanaka, A., Nakamura, M., Inagaki, A., Nishikawa, M., Takei, I., Oishi, A., Tanabe, K., Ohnuki, M., Yokota, H., Koyanagi-Aoi, M., Okita, K., Watanabe, A., Takaori-Kondo, A., Yamanaka, S., Yoshida, Y., 2016. Epigenetic Variation between Human Induced Pluripotent Stem Cell Lines Is an Indicator of Differentiation Capacity. Cell Stem Cell 19, 341–354.

References

Noguchi, M., Furukawa, K.T., Morimoto, M., 2020. Pulmonary neuroendocrine cells: physiology, tissue homeostasis and disease. Dis Model Mech 13, dmm046920.

Orru, H., Andersson, C., Ebi, K.L., Langner, J., Åström, C., Forsberg, B., 2013. Impact of climate change on ozone-related mortality and morbidity in Europe. European Respiratory Journal 41, 285–294.

Ortmann, D., Vallier, L., 2017. Variability of human pluripotent stem cell lines. Current Opinion in Genetics & Development, Cell reprogramming 46, 179–185.

Panas, A., Comouth, A., Saathoff, H., Leisner, T., Al-Rawi, M., Simon, M., Seemann, G., Dössel, O., Mülhopt, S., Paur, H.-R., Fritsch-Decker, S., Weiss, C., Diabaté, S., 2014. Silica nanoparticles are less toxic to human lung cells when deposited at the air–liquid interface compared to conventional submerged exposure. Beilstein J. Nanotechnol. 5, 1590–1602.

Paranjapye, A., Leir, S.-H., Huang, F., Kerschner, J.L., Harris, A., 2022. Cell function and identity revealed by comparative scRNA-seq analysis in human nasal, bronchial and epididymis epithelia. Eur J Cell Biol 101, 151231.

Parimon, T., Yao, C., Stripp, B.R., Noble, P.W., Chen, P., 2020. Alveolar Epithelial Type II Cells as Drivers of Lung Fibrosis in Idiopathic Pulmonary Fibrosis. Int J Mol Sci 21, 2269.

Park, W.Y., Miranda, B., Lebeche, D., Hashimoto, G., Cardoso, W.V., 1998. FGF-10 Is a Chemotactic Factor for Distal Epithelial Buds during Lung Development. Developmental Biology 201, 125-134,.

Patil, S., Mahuli, A.V., Warnakulasuriya, S., 2022. Effects of smoking shisha, cancer risk, and strategies for prevention of shisha habit. J Oral Biol Craniofac Res 12, 439–443.

Pechriggl, E., Blumer, M., Tubbs, R.S., Olewnik, Ł., Konschake, M., Fortélny, R., Stofferin, H., Honis, H.R., Quinones, S., Maranillo, E., Sanudo, J., 2022. Embryology of the Abdominal Wall and Associated Malformations—A Review. Front Surg 9, 891896.

Perez-Padilla, R., Thirion-Romero, I., Guzman, N., 2018. Underdiagnosis of chronic obstructive pulmonary disease: should smokers be offered routine spirometry tests? Expert Review of Respiratory Medicine 12, 83–85.

Phillips, J., Kluss, B., Richter, A., Massey, E., 2005. Exposure of bronchial epithelial cells to whole cigarette smoke: assessment of cellular responses. Altern Lab Anim 33, 239–248.

Pierro, M., Van Mechelen, K., van Westering-Kroon, E., Villamor-Martínez, E., Villamor, E., 2022. Endotypes of Prematurity and Phenotypes of Bronchopulmonary Dysplasia: Toward Personalized Neonatology. Journal of Personalized Medicine 12, 687.

Plasschaert, L.W., Žilionis, R., Choo-Wing, R., Savova, V., Knehr, J., Roma, G., Klein, A.M., Jaffe, A.B., 2018. A single cell atlas of the tracheal epithelium reveals the CFTR-rich pulmonary ionocyte. Nature 560, 377–381.

Plikus, M.V., Wang, X., Sinha, S., Forte, E., Thompson, S.M., Herzog, E.L., Driskell, R.R., Rosenthal, N., Biernaskie, J., Horsley, V., 2021. Fibroblasts: Origins, definitions, and functions in health and disease. Cell 184, 3852–3872.

Pohl, S.T., Prada, M.L., Espinet, E., Jurkowska, R., 2023. Practical Considerations for Complex Tissue Dissociation for Single-Cell Transcriptomics. Methods Mol Biol 2584, 371–387.

Poucineau, J., Delory, T., Lapidus, N., Hejblum, G., Chouaïd, C., Le Cœur, S., Khlat, M., 2022. Hospital admissions and mortality for acute exacerbations of COPD during the COVID-19 pandemic: A nationwide study in France. Front Med (Lausanne) 9, 995016.

Puchelle, E., Zahm, J.-M., Tournier, J.-M., Coraux, C., 2006. Airway Epithelial Repair, Regeneration, and Remodeling after Injury in Chronic Obstructive Pulmonary Disease. Proceedings of the American Thoracic Society 3, 726–733.

Rabe, K.F., Hurst, J.R., Suissa, S., 2018. Cardiovascular disease and COPD: dangerous liaisons? Eur Respir Rev 27, 180057.

Rabe, K.F., Watz, H., 2017. Chronic Obstructive Pulmonary Disease. The Lancet 389, 1931-1940,.

Ragland, M.F., Benway, C.J., Lutz, S.M., Bowler, R.P., Hecker, J., Hokanson, J.E., Crapo, J.D., Castaldi, P.J., DeMeo, D.L., Hersh, C.P., Hobbs, B.D., Lange, C., Beaty, T.H., Cho, M.H., Silverman, E.K., 2019. Genetic Advances in Chronic Obstructive Pulmonary Disease. Insights from COPDGene. Am J Respir Crit Care Med 200, 677–690.

Ramamoorthy, P., Thomas, S.M., Kaushik, G., Subramaniam, D., Chastain, K.M., Dhar, A., Tawfik, O., Kasi, A., Sun, W., Ramalingam, S., Gunewardena, S., Umar, S., Mammen, J.M., Padhye, S.B., Weir, S.J., Jensen, R.A., Sittampalam, G.S., Anant, S., 2019. Metastatic Tumor-in-a-Dish, a Novel Multicellular Organoid to Study Lung Colonization and Predict Therapeutic Response. Cancer Research 79, 1681–1695.

Ranjan, B., Schmidt, F., Sun, W., Park, J., Honardoost, M.A., Tan, J., Arul Rayan, N., Prabhakar, S., 2021. scConsensus: combining supervised and unsupervised clustering for cell type identification in single-cell RNA sequencing data. BMC Bioinformatics 22, 186.

Rawlins, E.L., 2011. The building blocks of mammalian lung development. Developmental Dynamics 240, 463–476.

Rawlins, E.L., Hogan, B.L.M., 2008. Ciliated epithelial cell lifespan in the mouse trachea and lung. Am J Physiol Lung Cell Mol Physiol 295, L231–L234.

Rawlins, E.L., Okubo, T., Xue, Y., Brass, D.M., Auten, R.L., Hasegawa, H., Wang, F., Hogan, B.L.M., 2009. The Role of Scgb1a1+ Clara Cells in the Long-Term Maintenance and Repair of Lung Airway, but Not Alveolar, Epithelium. Cell Stem Cell 4, 525-534,.

Rayner, R.E., Makena, P., Prasad, G.L., Cormet-Boyaka, E., 2019. Optimization of Normal Human Bronchial Epithelial (NHBE) Cell 3D Cultures for in vitro Lung Model Studies. Sci Rep 9, 500.

Rehman, S., Bacha, D., 2022. Embryology, Pulmonary, StatPearls [Internet]. StatPearls Publishing.

Reyfman, P.A., Walter, J.M., Joshi, N., Anekalla, K.R., McQuattie-Pimentel, A.C., Chiu, S., Fernandez, R., Akbarpour, M., Chen, C.-I., Ren, Z., Verma, R., Abdala-Valencia, H., Nam, K., Chi, M., Han, S., Gonzalez-Gonzalez, F.J., Soberanes, S., Watanabe, S., Williams, K.J.N., Flozak, A.S., Nicholson, T.T., Morgan, V.K., Winter, D.R., Hinchcliff, M., Hrusch, C.L., Guzy, R.D., Bonham, C.A., Sperling, A.I., Bag, R., Hamanaka, R.B., Mutlu, G.M., Yeldandi, A.V., Marshall, S.A., Shilatifard, A., Amaral, L.A.N., Perlman, H., Sznajder, J.I., Argento, A.C., Gillespie, C.T., Dematte, J., Jain, M., Singer, B.D., Ridge, K.M., Lam, A.P., Bharat, A., Bhorade, S.M., Gottardi, C.J., Budinger, G.R.S., Misharin, A.V., 2019. Single-Cell Transcriptomic Analysis of Human Lung Provides Insights into the Pathobiology of Pulmonary Fibrosis. Am J Respir Crit Care Med 199, 1517–1536.

References

Rigden, H.M., Alias, A., Havelock, T., O'Donnell, R., Djukanovic, R., Davies, D.E., Wilson, S.J., 2016. Squamous Metaplasia Is Increased in the Bronchial Epithelium of Smokers with Chronic Obstructive Pulmonary Disease. PLoS One 11, e0156009.

Rigotti, N.A., 2013. Smoking cessation in patients with respiratory disease: existing treatments and future directions. Lancet Respir Med 1, 241–250.

Rock, J.R., Gao, X., Xue, Y., Randell, S.H., Kong, Y.-Y., Hogan, B.L.M., 2011. Notch-Dependent Differentiation of Adult Airway Basal Stem Cells. Cell Stem Cell 8, 639–648.

Rock, J.R., Hogan, B.L.M., 2011. Epithelial Progenitor Cells in Lung Development, Maintenance, Repair, and Disease. Annual Review of Cell and Developmental Biology 27, 493–512.

Rock, J.R., Onaitis, M.W., Rawlins, E.L., Lu, Y., Clark, C.P., Xue, Y., Randell, S.H., Hogan, B.L.M., 2009. Basal Cells as Stem Cells of the Mouse Trachea and Human Airway Epithelium. Proc Natl Acad Sci U S A 106, 12771-12775,.

Rodier, F., Coppé, J.-P., Patil, C.K., Hoeijmakers, W.A.M., Muñoz, D.P., Raza, S.R., Freund, A., Campeau, E., Davalos, A.R., Campisi, J., 2009. Persistent DNA damage signalling triggers senescence-associated inflammatory cytokine secretion. Nat Cell Biol 11, 973–979.

Rodrigues Toste de Carvalho, A.L., Liu, H.-Y., Chen, Y.-W., Porotto, M., Moscona, A., Snoeck, H.-W., 2021. The in vitro multilineage differentiation and maturation of lung and airway cells from human pluripotent stem cell–derived lung progenitors in 3D. Nat Protoc.

Roger, I., Milara, J., Belhadj, N., Cortijo, J., 2021. Senescence Alterations in Pulmonary Hypertension. Cells 10, 3456.

Rogers, D.F., 2003. The airway goblet cell. Int J Biochem Cell Biol 35, 1–6.

Rogers, D.F., 2000. Mucus Hypersecretion in Chronic Obstructive Pulmonary Disease, in: Chronic Obstructive Pulmonary Disease: Pathogenesis to Treatment. John Wiley & Sons, Ltd, pp. 65–83.

Rouhani, F., Kumasaka, N., Brito, M.C. de, Bradley, A., Vallier, L., Gaffney, D., 2014. Genetic Background Drives Transcriptional Variation in Human Induced Pluripotent Stem Cells. PLOS Genetics 10, e1004432.

Rousseaux, C.G., Wallig, M.A., Haschek, W.M., Bolon, B., 2018. Chapter 1 - An Overview of Toxicologic Pathology, in: Wallig, M.A., Haschek, W.M., Rousseaux, C.G., Bolon, B. (Eds.), Fundamentals of Toxicologic Pathology (Third Edition). Academic Press, pp. 1–12.

Ru, Q., Xiong, Q., Chen, L., Tian, X., Yue, K., Ma, B., Liu, L., Wu, R., Xu, C., Pi, M., Li, C., 2017. Lipopolysaccharide accelerates fine particulate matter-induced cell apoptosis in human lung bronchial epithelial cells. Int J Occup Med Environ Health.

Ruaro, B., Salton, F., Braga, L., Wade, B., Confalonieri, P., Volpe, M.C., Baratella, E., Maiocchi, S., Confalonieri, M., 2021. The History and Mystery of Alveolar Epithelial Type II Cells: Focus on Their Physiologic and Pathologic Role in Lung. Int J Mol Sci 22, 2566.

Ruiz García, S., Deprez, M., Lebrigand, K., Cavard, A., Paquet, A., Arguel, M.-J., Magnone, V., Truchi, M., Caballero, I., Leroy, S., Marquette, C.-H., Marcet, B., Barbry, P., Zaragosi, L.-E., 2019. Novel dynamics of human mucociliary differentiation revealed by single-cell RNA sequencing of nasal epithelial cultures. Development 146, dev177428.

Russo, R.C., Savino, B., Mirolo, M., Buracchi, C., Germano, G., Anselmo, A., Zammataro, L., Pasqualini, F., Mantovani, A., Locati, M., Teixeira, M.M., 2018. The atypical chemokine receptor ACKR2 drives pulmonary fibrosis by tuning influx of CCR2+ and CCR5+ IFNγ-producing γδT cells in mice. American Journal of Physiology-Lung Cellular and Molecular Physiology 314, L1010–L1025.

Ruysseveldt, E., Martens, K., Steelant, B., 2021. Airway Basal Cells, Protectors of Epithelial Walls in Health and Respiratory Diseases. Frontiers in Allergy 2.

Sakornsakolpat, P., Prokopenko, D., Lamontagne, M., Reeve, N.F., Guyatt, A.L., Jackson, V.E., Shrine, N., Qiao, D., Bartz, T.M., Kim, D.K., Lee, M.K., Latourelle, J.C., Li, X., Morrow, J.D., Obeidat, M., Wyss, A.B., Bakke, P., Barr, R.G., Beaty, T.H., Belinsky, S.A., Brusselle, G.G., Crapo, J.D., de Jong, K., DeMeo, D.L., Fingerlin, T.E., Gharib, S.A., Gulsvik, A., Hall, I.P., Hokanson, J.E., Kim, W.J., Lomas, D.A., London, S.J., Meyers, D.A., O'Connor, G.T., Rennard, S.I., Schwartz, D.A., Sliwinski, P., Sparrow, D., Strachan, D.P., Tal-Singer, R., Tesfaigzi, Y., Vestbo, J., Vonk, J.M., Yim, J.-J., Zhou, X., Bossé, Y., Manichaikul, A., Lahousse, L., Silverman, E.K., Boezen, H.M., Wain, L.V., Tobin, M.D., Hobbs, B.D., Cho, M.H., SpiroMeta Consortium, International COPD Genetics Consortium, 2019. Genetic landscape of chronic obstructive pulmonary disease identifies heterogeneous cell-type and phenotype associations. Nat Genet 51, 494–505.

Saliba, A.-E., Westermann, A.J., Gorski, S.A., Vogel, J., 2014. Single-cell RNA-seq: advances and future challenges. Nucleic Acids Research 42, 8845–8860.

Salvi, S.S., Barnes, P.J., 2009. Chronic obstructive pulmonary disease in non-smokers. Lancet 374, 733–743.

Samir, D., 2020. Oxidative Stress Associated with SARS-Cov-2 (COVID-19) Increases the Severity of the Lung Disease - A Systematic Review. J Infect Dis Epidemiol 6.

Scapini, V., Torres, S., Rubilar-Torrealba, R., 2023. Meteorological, PM2.5 and PM10 factors on SARS-COV-2 transmission: The case of Southern Regions in Chile. Environ Pollut 120961.

Schantz, M.M., Cleveland, D., Heckert, N.A., Kucklick, J.R., Leigh, S.D., Long, S.E., Lynch, J.M., Murphy, K.E., Olfaz, R., Pintar, A.L., Porter, B.J., Rabb, S.A., Vander Pol, S.S., Wise, S.A., Zeisler, R., 2016. Development of two fine particulate matter standard reference materials (<4 µm and <10 µm) for the determination of organic and inorganic constituents. Anal Bioanal Chem 408, 4257–4266.

Schiller, H.B., Montoro, D.T., Simon, L.M., Rawlins, E.L., Meyer, K.B., Strunz, M., Vieira Braga, F.A., Timens, W., Koppelman, G.H., Budinger, G.R.S., Burgess, J.K., Waghray, A., van den Berge, M., Theis, F.J., Regev, A., Kaminski, N., Rajagopal, J., Teichmann, S.A., Misharin, A.V., Nawijn, M.C., 2019. The Human Lung Cell Atlas: A High-Resolution Reference Map of the Human Lung in Health and Disease. Am J Respir Cell Mol Biol 61, 31–41.

Schittny, J.C., 2017. Development of the Lung. Cell Tissue Res 367, 427-444,.

Schneider, C., O'Leary, C.E., Locksley, R.M., 2019. Regulation of immune responses by tuft cells. Nat Rev Immunol 19, 584–593.

Schneider, J.P., Wrede, C., Hegermann, J., Weibel, E.R., Mühlfeld, C., Ochs, M., 2019. On the Topological Complexity of Human Alveolar Epithelial Type 1 Cells. Am J Respir Crit Care Med 199, 1153–1156.

Scudieri, P., Musante, I., Venturini, A., Guidone, D., Genovese, M., Cresta, F., Caci, E., Palleschi, A., Poeta, M., Santamaria, F., Ciciriello, F., Lucidi, V., Galietta, L.J.V., 2020. Ionocytes and CFTR Chloride Channel Expression in Normal and Cystic Fibrosis Nasal and Bronchial Epithelial Cells. Cells 9, 2090.

References

Sekine, K., Ohuchi, H., Fujiwara, M., Yamasaki, M., Yoshizawa, T., Sato, T., Yagishita, N., Matsui, D., Koga, Y., Itoh, N., 1999. Fgf10 Is Essential for Limb and Lung Formation. Nature Genetics 21, 138-141,.

Seth, R., Shum, L., Wu, F., Wuenschell, C., Hall, F.L., Slavkin, H.C., Warburton, D., 1993. Role of Epidermal Growth Factor Expression in Early Mouse Embryo Lung Branching Morphogenesis in Culture: Antisense Oligodeoxynucleotide Inhibitory Strategy. Developmental Biology 158, 555–559.

Sharma, A., Sances, S., Workman, M.J., Svendsen, C.N., 2020. Multi-Lineage Human iPSC-Derived Platforms for Disease Modeling and Drug Discovery. Cell Stem Cell 26, 309–329.

Shaykhiev, R., 2019. Emerging biology of persistent mucous cell hyperplasia in COPD. Thorax 74, 4–6.

Shi, Y., Inoue, H., Wu, J.C., Yamanaka, S., 2017. Induced pluripotent stem cell technology: a decade of progress. Nat Rev Drug Discov 16, 115–130.

Sierra-Vargas, M.P., Montero-Vargas, J.M., Debray-García, Y., Vizuet-de-Rueda, J.C., Loaeza-Román, A., Terán, L.M., 2023. Oxidative Stress and Air Pollution: Its Impact on Chronic Respiratory Diseases. Int J Mol Sci 24, 853.

Singh, D., Kumar, A., Kumar, K., Singh, B., Mina, U., Singh, B.B., Jain, V.K., 2016. Statistical modeling of O3, NOx, CO, PM2.5, VOCs and noise levels in commercial complex and associated health risk assessment in an academic institution. Science of The Total Environment 572, 586–594.

Singh, D., Mathioudakis, A.G., Higham, A., 2022. Chronic obstructive pulmonary disease and COVID-19: interrelationships. Curr Opin Pulm Med 28, 76–83.

Skardal, A., Murphy, S.V., Devarasetty, M., Mead, I., Kang, H.-W., Seol, Y.-J., Shrike Zhang, Y., Shin, S.-R., Zhao, L., Aleman, J., Hall, A.R., Shupe, T.D., Kleensang, A., Dokmeci, M.R., Jin Lee, S., Jackson, J.D., Yoo, J.J., Hartung, T., Khademhosseini, A., Soker, S., Bishop, C.E., Atala, A., 2017. Multi-tissue interactions in an integrated three-tissue organ-on-a-chip platform. Sci Rep 7, 8837.

Smith, M.C., Wrobel, J.P., 2014. Epidemiology and clinical impact of major comorbidities in patients with COPD. Int J Chron Obstruct Pulmon Dis 9, 871–888.

Soltani, A., Sohal, S.S., Reid, D., Weston, S., Wood-Baker, R., Walters, E.H., 2012. Vessel-Associated Transforming Growth Factor-Beta1 (TGF-B1) Is Increased in the Bronchial Reticular Basement Membrane in COPD and Normal Smokers. PLOS ONE 7, 39736,.

Song, C., He, J., Wu, L., Jin, T., Chen, X., Li, R., Ren, P., Zhang, L., Mao, H., 2017. Health burden attributable to ambient PM2.5 in China. Environ Pollut 223, 575–586.

Soriano, J.B., Kendrick, P.J., Paulson, K.R., Gupta, V., Abrams, E.M., Adedoyin, R.A., Adhikari, T.B., Advani, S.M., Agrawal, A., Ahmadian, E., Alahdab, F., Aljunid, S.M., Altirkawi, K.A., Alvis-Guzman, N., Anber, N.H., Andrei, C.L., Anjomshoa, M., Ansari, F., Antó, J.M., Arabloo, J., Athari, S.M., Athari, S.S., Awoke, N., Badawi, A., Banoub, J.A.M., Bennett, D.A., Bensenor, I.M., Berfield, K.S.S., Bernstein, R.S., Bhattacharyya, K., Bijani, A., Brauer, M., Bukhman, G., Butt, Z.A., Cámera, L.A., Car, J., Carrero, J.J., Carvalho, F., Castañeda-Orjuela, C.A., Choi, J.-Y.J., Christopher, D.J., Cohen, A.J., Dandona, L., Dandona, R., Dang, A.K., Daryani, A., de Courten, B., Demeke, F.M., Demoz, G.T., De Neve, J.-W., Desai, R., Dharmaratne, S.D., Diaz, D., Douiri, A., Driscoll, T.R., Duken, E.E., Eftekhari, A., Elkout, H., Endries, A.Y., Fadhil, I., Faro, A., Farzadfar, F., Fernandes, E., Filip, I., Fischer, F., Foroutan, M., Garcia-Gordillo, M.A., Gebre, A.K., Gebremedhin, K.B., Gebremeskel, G.G., Gezae, K.E., Ghoshal, A.G., Gill, P.S., Gillum, R.F., Goudarzi, H., Guo, Y., Gupta, R., Hailu, G.B.,

Hasanzadeh, A., Hassen, H.Y., Hay, S.I., Hoang, C.L., Hole, M.K., Horita, N., Hosgood, H.D., Hostiuc, M., Househ, M., Ilesanmi, O.S., Ilic, M.D., Irvani, S.S.N., Islam, S.M.S., Jakovljevic, M., Jamal, A.A., Jha, R.P., Jonas, J.B., Kabir, Z., Kasaeian, A., Kasahun, G.G., Kassa, G.M., Kefale, A.T., Kengne, A.P., Khader, Y.S., Khafaie, M.A., Khan, E.A., Khan, J., Khubchandani, J., Kim, Y.-E., Kim, Y.J., Kisa, S., Kisa, A., Knibbs, L.D., Komaki, H., Koul, P.A., Koyanagi, A., Kumar, G.A., Lan, Q., Lasrado, S., Lauriola, P., La Vecchia, C., Le, T.T., Leigh, J., Levi, M., Li, S., Lopez, A.D., Lotufo, P.A., Madotto, F., Mahotra, N.B., Majdan, M., Majeed, A., Malekzadeh, R., Mamun, A.A., Manafi, N., Manafi, F., Mantovani, L.G., Meharie, B.G., Meles, H.G., Meles, G.G., Menezes, R.G., Mestrovic, T., Miller, T.R., Mini, G., Mirrakhimov, E.M., Moazen, B., Mohammad, K.A., Mohammed, S., Mohebi, F., Mokdad, A.H., Molokhia, M., Monasta, L., Moradi, M., Moradi, G., Morawska, L., Mousavi, S.M., Musa, K.I., Mustafa, G., Naderi, M., Naghavi, M., Naik, G., Nair, S., Nangia, V., Nansseu, J.R., Nazari, J., Ndwandwe, D.E., Negoi, R.I., Nguyen, T.H., Nguyen, C.T., Nguyen, H.L.T., Nixon, M.R., Ofori-Asenso, R., Ogbo, F.A., Olagunju, A.T., Olagunju, T.O., Oren, E., Ortiz, J.R., Owolabi, M.O., P a, M., Pakhale, S., Pana, A., Panda-Jonas, S., Park, E.-K., Pham, H.Q., Postma, M.J., Pourjafar, H., Poustchi, H., Radfar, A., Rafiei, A., Rahim, F., Rahman, M.H.U., Rahman, M.A., Rawaf, S., Rawaf, D.L., Rawal, L., Reiner Jr., R.C., Reitsma, M.B., Roever, L., Ronfani, L., Roro, E.M., Roshandel, G., Rudd, K.E., Sabde, Y.D., Sabour, S., Saddik, B., Safari, S., Saleem, K., Samy, A.M., Santric-Milicevic, M.M., Sao Jose, B.P., Sartorius, B., Satpathy, M., Savic, M., Sawhney, M., Sepanlou, S.G., Shaikh, M.A., Sheikh, A., Shigematsu, M., Shirkoohi, R., Si, S., Siabani, S., Singh, V., Singh, J.A., Soljak, M., Somayaji, R., Soofi, M., Soyiri, I.N., Tefera, Y.M., Temsah, M.-H., Tesfay, B.E., Thakur, J.S., Toma, A.T., Tortajada-Girbés, M., Tran, K.B., Tran, B.X., Tudor Car, L., Ullah, I., Vacante, M., Valdez, P.R., van Boven, J.F.M., Vasankari, T.J., Veisani, Y., Violante, F.S., Wagner, G.R., Westerman, R., Wolfe, C.D.A., Wondafrash, D.Z., Wondmieneh, A.B., Yonemoto, N., Yoon, S.-J., Zaidi, Z., Zamani, M., Zar, H.J., Zhang, Y., Vos, T., 2020. Prevalence and attributable health burden of chronic respiratory diseases, 1990–2017: a systematic analysis for the Global Burden of Disease Study 2017. The Lancet Respiratory Medicine 8, 585–596.

Sorrentino, J.A., Krishnamurthy, J., Tilley, S., Alb, J.G., Burd, C.E., Sharpless, N.E., 2014. *p16^{INK4a}* reporter mice reveal age-promoting effects of environmental toxicants. J Clin Invest 124, 169–173.

Sountoulidis, A., Marco Salas, S., Braun, E., Avenel, C., Bergenstråhle, J., Theelke, J., Vicari, M., Czarnewski, P., Liontos, A., Abalo, X., Andrusivová, Ž., Mirzazadeh, R., Asp, M., Li, X., Hu, L., Sariyar, S., Martinez Casals, A., Ayoglu, B., Firsova, A., Michaëlsson, J., Lundberg, E., Wählby, C., Sundström, E., Linnarsson, S., Lundeberg, J., Nilsson, M., Samakovlis, C., 2023. A topographic atlas defines developmental origins of cell heterogeneity in the human embryonic lung. Nat Cell Biol 25, 351–365.

Spivack, S.D., Hurteau, G.J., Reilly, A.A., Aldous, K.M., Ding, X., Kaminsky, L.S., 2001. CYP1B1 expression in human lung. Drug Metab Dispos 29, 916–922.

Stevens, T., Phan, S., Frid, M.G., Alvarez, D., Herzog, E., Stenmark, K.R., 2008. Lung Vascular Cell Heterogeneity. Proc Am Thorac Soc 5, 783–791.

Stone, O.A., Stainier, D.Y.R., 2019. Paraxial Mesoderm Is the Major Source of Lymphatic Endothelium. Dev Cell 50, 247-255.e3.

Subramaniam, M., Sugiyama, K., Coy, D.H., Kong, Y., Miller, Y.E., Weller, P.F., Wada, K., Wada, E., Sunday, M.E., 2003. Bombesin-like peptides and mast cell responses: relevance to bronchopulmonary dysplasia? Am J Respir Crit Care Med 168, 601–611.

Suresh, K., Shimoda, L.A., 2016. Lung Circulation. Compr Physiol 6, 897–943.

Takahashi, K., Tanabe, K., Ohnuki, M., Narita, M., Ichisaka, T., Tomoda, K., Yamanaka, S., 2007. Induction of Pluripotent Stem Cells from Adult Human Fibroblasts by Defined Factors. Cell 131, 861–872.

References

Takahashi, K., Yamanaka, S., 2006. Induction of Pluripotent Stem Cells from Mouse Embryonic and Adult Fibroblast Cultures by Defined Factors. Cell 126, 663–676.

Talhout, R., Opperhuizen, A., van Amsterdam, J.G.C., 2006. Sugars as tobacco ingredient: Effects on mainstream smoke composition. Food and Chemical Toxicology 44, 1789–1798.

Tam, E., Miike, R., Labrenz, S., Sutton, A.J., Elias, T., Davis, J., Chen, Y.-L., Tantisira, K., Dockery, D., Avol, E., 2016. Volcanic air pollution over the Island of Hawai'i: Emissions, dispersal, and composition. Association with respiratory symptoms and lung function in Hawai'i Island school children. Environment International 92–93, 543–552.

Tang, F., Barbacioru, C., Wang, Y., Nordman, E., Lee, C., Xu, N., Wang, X., Bodeau, J., Tuch, B.B., Siddiqui, A., Lao, K., Surani, M.A., 2009. mRNA-Seq whole-transcriptome analysis of a single cell. Nat Methods 6, 377–382.

Tanner, L., Single, A.B., 2019. Animal Models Reflecting Chronic Obstructive Pulmonary Disease and Related Respiratory Disorders: Translating Pre-Clinical Data into Clinical Relevance. J Innate Immun 1–23.

Tantucci, C., Modina, D., 2012. Lung function decline in COPD. Int J Chron Obstruct Pulmon Dis 7, 95–99.

Tashkin, D.P., Murray, R.P., 2009. Smoking cessation in chronic obstructive pulmonary disease. Respir Med 103, 963–974.

Tata, P.R., Mou, H., Pardo-Saganta, A., Zhao, R., Prabhu, M., Prabhu, M., Law, B.M., Vinarsky, V., Cho, J.L., Breton, S., Sahay, A., Medoff, B.D., Rajagopal, J., 2013. Dedifferentiation of committed epithelial cells into stem cells in vivo. Nature 503, 218–223.

Thébaud, B., Goss, K.N., Laughon, M., Whitsett, J.A., Abman, S.H., Steinhorn, R.H., Aschner, J.L., Davis, P.G., McGrath-Morrow, S.A., Soll, R.F., Jobe, A.H., 2019. Bronchopulmonary dysplasia. Nat Rev Dis Primers 5, 1–23.

Thomson, J.A., Itskovitz-Eldor, J., Shapiro, S.S., Waknitz, M.A., Swiergiel, J.J., Marshall, V.S., Jones, J.M., 1998. Embryonic Stem Cell Lines Derived from Human Blastocysts. Science 282, 1145–1147.

Tilley, A.E., Walters, M.S., Shaykhiev, R., Crystal, R.G., 2015. Cilia Dysfunction in Lung Disease. Annu Rev Physiol 77, 379–406.

Tran, H.B., Hamon, R., Jersmann, H., Ween, M.P., Asare, P., Haberberger, R., Pant, H., Hodge, S.J., 2021. AIM2 nuclear exit and inflammasome activation in chronic obstructive pulmonary disease and response to cigarette smoke. J Inflamm (Lond) 18, 19.

Travaglini, K.J., Nabhan, A.N., Penland, L., Sinha, R., Gillich, A., Sit, R.V., Chang, S., Conley, S.D., Mori, Y., Seita, J., Berry, G.J., Shrager, J.B., Metzger, R.J., Kuo, C.S., Neff, N., Weissman, I.L., Quake, S.R., Krasnow, M.A., 2020. A molecular cell atlas of the human lung from single-cell RNA sequencing. Nature 587, 619–625.

Treekitkarnmongkol, W., Hassane, M., Sinjab, A., Chang, K., Hara, K., Rahal, Z., Zhang, J., Lu, W., Sivakumar, S., McDowell, T.L., Kantrowitz, J., Zhou, J., Lang, W., Xu, L., Ochieng, J.K., Nunomura-Nakamura, S., Deng, S., Behrens, C., Raso, M.G., Fukuoka, J., Reuben, A., Ostrin, E.J., Parra, E., Solis, L.M., Spira, A.E., McAllister, F., Cascone, T., Wistuba, I.I., Moghaddam, S.J., Scheet, P.A., Fujimoto, J., Kadara, H., 2021. Augmented Lipocalin-2 Is Associated with Chronic Obstructive Pulmonary Disease and Counteracts Lung Adenocarcinoma Development. Am J Respir Crit Care Med 203, 90–101.

Tsao, P.-N., Vasconcelos, M., Izvolsky, K.I., Qian, J., Lu, J., Cardoso, W.V., 2009. Notch signaling controls the balance of ciliated and secretory cell fates in developing airways. Development 136, 2297–2307.

Tu, W.-J., Chao, B., Wang, L., 2022. Prevalence of stroke in China: overestimated? The Lancet Public Health 7, e404.

Tuder, R.M., Zhen, L., Cho, C.Y., Taraseviciene-Stewart, L., Kasahara, Y., Salvemini, D., Voelkel, N.F., Flores, S.C., 2003. Oxidative Stress and Apoptosis Interact and Cause Emphysema Due to Vascular Endothelial Growth Factor Receptor Blockade. Am J Respir Cell Mol Biol 29, 88–97.

Tyser, R.C.V., Mahammadov, E., Nakanoh, S., Vallier, L., Scialdone, A., Srinivas, S., 2021. Single-cell transcriptomic characterization of a gastrulating human embryo. Nature 600, 285–289.

Upadhyay, S., Chakraborty, A., Thimraj, T.A., Baldi, M., Steneholm, A., Ganguly, K., Gerde, P., Ernstgård, L., Palmberg, L., 2022. Establishment of Repeated In Vitro Exposure System for Evaluating Pulmonary Toxicity of Representative Criteria Air Pollutants Using Advanced Bronchial Mucosa Models. Toxics 10, 277.

Uthaya Kumar, D.B., Motakis, E., Yurieva, M., Kohar, V., Martinek, J., Wu, T.-C., Khoury, J., Grassmann, J., Lu, M., Palucka, K., Kaminski, N., Koff, J.L., Williams, A., 2022. Bronchial epithelium epithelial-mesenchymal plasticity forms aberrant basaloid-like cells in vitro. American Journal of Physiology-Lung Cellular and Molecular Physiology ajplung.00254.2021.

van den Brink, S.C., Sage, F., Vértesy, Á., Spanjaard, B., Peterson-Maduro, J., Baron, C.S., Robin, C., van Oudenaarden, A., 2017. Single-cell sequencing reveals dissociation-induced gene expression in tissue subpopulations. Nat Methods 14, 935–936.

Varankar, S.S., Cardoso, E.C., Lee, J.-H., 2022. Ex situ-armus: experimental models for combating respiratory dysfunction. Current Opinion in Genetics & Development 75, 101946.

Varma, R., Soleas, J.P., Waddell, T.K., Karoubi, G., McGuigan, A.P., 2020. Current strategies and opportunities to manufacture cells for modeling human lungs. Adv Drug Deliv Rev 161, 90–109.

Verheyden, J.M., Sun, X., 2020. A transitional stem cell state in the lung. Nat Cell Biol 22, 1025–1026.

Vernisse, C., Tuaillon, E., Suehs, C., Gras, D., Bedin, A.S., Charriot, J., Knabe, L., Vachier, I., Chanez, P., Petit, A., Bourdin, A., 2023. Airway epithelial type-2 alarmin profiles: Blood eosinophil counts remain in memory. Eur J Immunol 53, e2250101.

Vestbo, J., 2002. Epidemiological studies in mucus hypersecretion. Novartis Found Symp 248, 3–12; discussion 12-19, 277–282.

Vij, N., Chandramani-Shivalingappa, P., Van Westphal, C., Hole, R., Bodas, M., 2018. Cigarette smoke-induced autophagy impairment accelerates lung aging, COPD-emphysema exacerbations and pathogenesis. Am J Physiol Cell Physiol 314, C73–C87.

Villa-Diaz, L.G., Ross, A.M., Lahann, J., Krebsbach, P.H., 2013. The evolution of human pluripotent stem cell culture: from feeder cells to synthetic coatings. Stem Cells 31, 1–7.

Vineis, P., Robinson, O., Chadeau-Hyam, M., Dehghan, A., Mudway, I., Dagnino, S., 2020. What is new in the exposome? Environ Int 143, 105887.

References

Volarevic, V., Markovic, B.S., Gazdic, M., Volarevic, A., Jovicic, N., Arsenijevic, N., Armstrong, L., Djonov, V., Lako, M., Stojkovic, M., 2018. Ethical and Safety Issues of Stem Cell-Based Therapy. Int J Med Sci 15, 36–45.

Wadhwa, R., Aggarwal, T., Malyla, V., Kumar, N., Gupta, G., Chellappan, D.K., Dureja, H., Mehta, M., Satija, S., Gulati, M., Maurya, P.K., Collet, T., Hansbro, P.M., Dua, K., 2019. Identification of biomarkers and genetic approaches toward chronic obstructive pulmonary disease. J Cell Physiol jcp.28482.

Wang, Y., Tang, Z., Huang, H., Li, Jiao, Wang, Z., Yu, Y., Zhang, C., Li, Juan, Dai, H., Wang, F., Cai, T., Tang, N., 2018. Pulmonary alveolar type I cell population consists of two distinct subtypes that differ in cell fate. Proceedings of the National Academy of Sciences 115, 2407–2412.

Warburton, D., El-Hashash, A., Carraro, G., Tiozzo, C., Sala, F., Rogers, O., De Langhe, S., Kemp, P.J., Riccardi, D., Torday, J., 2010. Lung Organogenesis. Curr Top Dev Biol 90, 73-158,.

Watson, J.K., Rulands, S., Wilkinson, A.C., Wuidart, A., Ousset, M., Van Keymeulen, A., Göttgens, B., Blanpain, C., Simons, B.D., Rawlins, E.L., 2015. Clonal Dynamics Reveal Two Distinct Populations of Basal Cells in Slow-Turnover Airway Epithelium. Cell Reports 12, 90–101.

Weaver, M., Batts, L., Hogan, B.L.M., 2003. Tissue Interactions Pattern the Mesenchyme of the Embryonic Mouse Lung. Developmental Biology 258, 169-184,.

Wei, Y., Kim, T.J., Peng, D.H., Duan, D., Gibbons, D.L., Yamauchi, M., Jackson, J.R., Le Saux, C.J., Calhoun, C., Peters, J., Derynck, R., Backes, B.J., Chapman, H.A., 2017. Fibroblast-specific inhibition of TGF-β1 signaling attenuates lung and tumor fibrosis. J Clin Invest 127, 3675–3688.

Weidgang, C.E., Russell, R., Tata, P.R., Kühl, S.J., Illing, A., Müller, M., Lin, Q., Brunner, C., Boeckers, T.M., Bauer, K., Kartikasari, A.E.R., Guo, Y., Radenz, M., Bernemann, C., Weiß, M., Seufferlein, T., Zenke, M., Iacovino, M., Kyba, M., Schöler, H.R., Kühl, M., Liebau, S., Kleger, A., 2013. TBX3 Directs Cell-Fate Decision toward Mesendoderm. Stem Cell Reports 1, 248–265.

Werder, R.B., Huang, J., Abo, K.M., Hix, O.T., Minakin, K., Alysandratos, K.-D., Merritt, C., Berthiaume, K., Alber, A.B., Burgess, C.L., Kotton, D.N., Wilson, A.A., 2022a. Generating 3D Spheres and 2D Air-Liquid Interface Cultures of Human Induced Pluripotent Stem Cell-Derived Type 2 Alveolar Epithelial Cells. J Vis Exp.

Werder, R.B., Liu, T., Abo, K.M., Lindstrom-Vautrin, J., Villacorta-Martin, C., Huang, J., Hinds, A., Boyer, N., Bullitt, E., Liesa, M., Silverman, E.K., Kotton, D.N., Cho, M.H., Zhou, X., Wilson, A.A., 2022b. CRISPR interference interrogation of COPD GWAS genes reveals the functional significance of desmoplakin in iPSC-derived alveolar epithelial cells. Sci Adv 8, eabo6566.

Whitsett, J.A., 2018. Airway Epithelial Differentiation and Mucociliary Clearance. Ann Am Thorac Soc 15, S143–S148.

Whitsett, J.A., Alenghat, T., 2015. Respiratory epithelial cells orchestrate pulmonary innate immunity. Nat Immunol 16, 27–35.

Wijk, S.C., Prabhala, P., Michaliková, B., Sommarin, M., Doyle, A., Lang, S., Kanzenbach, K., Tufvesson, E., Lindstedt, S., Leigh, N.D., Karlsson, G., Bjermer, L., Westergren-Thorsson, G., Magnusson, M., 2021. Human Primary Airway Basal Cells Display a Continuum of Molecular Phases from Health to Disease in Chronic Obstructive Pulmonary Disease. Am J Respir Cell Mol Biol 65, 103–113.

Wild, C.P., 2012. The exposome: from concept to utility. International Journal of Epidemiology 41, 24–32.

Wong, A.P., Rossant, J., 2013. Generation of Lung Epithelium from Pluripotent Stem Cells. Curr Pathobiol Rep 1, 137–145.

Wongtrakool, C., Roman, J., 2008. Apoptosis of mesenchymal cells during the pseudoglandular stage of lung development affects branching morphogenesis. Exp Lung Res 34, 481–499.

Wu, H., Ma, H., Wang, L., Zhang, H., Lu, L., Xiao, T., Cheng, C., Wang, P., Yang, Y., Wu, M., Wang, S., Zhang, J., Liu, Q., 2022. Regulation of lung epithelial cell senescence in smoking-induced COPD/emphysema by microR-125a-5p via Sp1 mediation of SIRT1/HIF-1a. Int J Biol Sci 18, 661–674.

Wu, T., Hu, E., Xu, S., Chen, M., Guo, P., Dai, Z., Feng, T., Zhou, L., Tang, W., Zhan, L., Fu, X., Liu, S., Bo, X., Yu, G., 2021. clusterProfiler 4.0: A universal enrichment tool for interpreting omics data. Innovation 2.

Xu, J., Xu, L., Sui, P., Chen, J., Moya, E.A., Hume, P., Janssen, W.J., Duran, J.M., Thistlethwaite, P., Carlin, A., Gulleman, P., Banaschewski, B., Goldy, M.K., Yuan, J.X.-J., Malhotra, A., Pryhuber, G., Crotty-Alexander, L., Deutsch, G., Young, L.R., Sun, X., 2022. Excess neuropeptides in lung signal through endothelial cells to impair gas exchange. Developmental Cell 57, 839-853.e6.

Xu, J., Yu, H., Sun, X., 2020. Less Is More: Rare Pulmonary Neuroendocrine Cells Function as Critical Sensors in Lung. Developmental Cell 55, 123–132.

Xu, Z., Jin, Y., 2003. [Main indoor air pollutants and their health impacts]. Wei Sheng Yan Jiu 32, 279–283.

Xu, Z., Wang, X., Fan, L., Wang, F., Lin, B., Wang, J., Trevejo-Nuñez, G., Chen, W., Chen, K., 2022. Integrative analysis of spatial transcriptome with single-cell transcriptome and single-cell epigenome in mouse lungs after immunization. iScience 25, 104900.

Yaghi, A., Dolovich, M.B., 2016. Airway Epithelial Cell Cilia and Obstructive Lung Disease. Cells 5, 40.

Yaghi, A., Zaman, A., Cox, G., Dolovich, M.B., 2012. Ciliary beating is depressed in nasal cilia from chronic obstructive pulmonary disease subjects. Respiratory Medicine 106, 1139–1147.

Yamanaka, S., 2012. Induced Pluripotent Stem Cells: Past, Present, and Future. Cell Stem Cell 10, 678–684.

Yang, J., Antin, P., Berx, G., Blanpain, C., Brabletz, T., Bronner, M., Campbell, K., Cano, A., Casanova, J., Christofori, G., 2020. Guidelines and Definitions for Research on Epithelial–Mesenchymal Transition. Nature Reviews Molecular Cell Biology 21, 341-352,.

Yang, J., Zuo, W.-L., Fukui, T., Chao, I., Gomi, K., Lee, B., Staudt, M.R., Kaner, R.J., Strulovici-Barel, Y., Salit, J., Crystal, R.G., Shaykhiev, R., 2017. Smoking-Dependent Distal-to-Proximal Repatterning of the Adult Human Small Airway Epithelium. Am J Respir Crit Care Med 196, 340–352.

Yao, C., Guan, X., Carraro, G., Parimon, T., Liu, X., Huang, G., Mulay, A., Soukiasian, H.J., David, G., Weigt, S.S., Belperio, J.A., Chen, P., Jiang, D., Noble, P.W., Stripp, B.R., 2021. Senescence of Alveolar Type 2 Cells Drives Progressive Pulmonary Fibrosis. Am J Respir Crit Care Med 203, 707–717.

Yiangou, L., Ross, A.D.B., Goh, K.J., Vallier, L., 2018. Human Pluripotent Stem Cell-Derived Endoderm for Modeling Development and Clinical Applications. Cell Stem Cell 22, 485–499.

References

Yu, F., Liu, F., Liang, X., Duan, L., Li, Q., Pan, G., Ma, C., Liu, M., Li, M., Wang, P., Zhao, X., 2023. iPSC-Derived Airway Epithelial Cells: Progress, Promise, and Challenges. Stem Cells 41, 1–10.

Yu, J., Vodyanik, M.A., Smuga-Otto, K., Antosiewicz-Bourget, J., Frane, J.L., Tian, S., Nie, J., Jonsdottir, G.A., Ruotti, V., Stewart, R., Slukvin, I.I., Thomson, J.A., 2007. Induced Pluripotent Stem Cell Lines Derived from Human Somatic Cells. Science 318, 1917–1920.

Yu, Z., Bellander, T., Bergström, A., Dillner, J., Eneroth, K., Engardt, M., Georgelis, A., Kull, I., Ljungman, P., Pershagen, G., Stafoggia, M., Melén, E., Gruzieva, O., 2022. Association of Short-term Air Pollution Exposure With SARS-CoV-2 Infection Among Young Adults in Sweden. JAMA Netw Open 5, e228109.

Zaragosi, L.E., Deprez, M., Barbry, P., 2020. Using single-cell RNA sequencing to unravel cell lineage relationships in the respiratory tract. Biochem Soc Trans 48, 327–336.

Zhai, J., Guo, J., Wan, H., Qi, L., Liu, L., Xiao, Z., Yan, L., Schmitz, D.A., Xu, Y., Yu, D., Wu, X., Zhao, W., Yu, K., Jiang, X., Guo, F., Wu, J., Wang, H., 2022. Primate gastrulation and early organogenesis at single-cell resolution. Nature 612, 732–738.

Zhang, J. (Jim), Wei, Y., Fang, Z., 2019. Ozone Pollution: A Major Health Hazard Worldwide. Front Immunol 10, 2518.

Zhang, Y., Wang, S., Feng, Z., Song, Y., 2022. Influenza incidence and air pollution: Findings from a four-year surveillance study of prefecture-level cities in China. Front Public Health 10, 1071229.

Zhao, L., Wang, K., Ferrara, N., Vu, T.H., 2005. Vascular endothelial growth factor co-ordinates proper development of lung epithelium and vasculature. Mechanisms of Development 122, 877–886.

Zhao, Z., Chen, X., Dowbaj, A.M., Sljukic, A., Bratlie, K., Lin, L., Fong, E.L.S., Balachander, G.M., Chen, Z., Soragni, A., Huch, M., Zeng, Y.A., Wang, Q., Yu, H., 2022. Organoids. Nat Rev Methods Primers 2, 1–21.

Zheng, G.X.Y., Terry, J.M., Belgrader, P., Ryvkin, P., Bent, Z.W., Wilson, R., Ziraldo, S.B., Wheeler, T.D., McDermott, G.P., Zhu, J., Gregory, M.T., Shuga, J., Montesclaros, L., Underwood, J.G., Masquelier, D.A., Nishimura, S.Y., Schnall-Levin, M., Wyatt, P.W., Hindson, C.M., Bharadwaj, R., Wong, A., Ness, K.D., Beppu, L.W., Deeg, H.J., McFarland, C., Loeb, K.R., Valente, W.J., Ericson, N.G., Stevens, E.A., Radich, J.P., Mikkelsen, T.S., Hindson, B.J., Bielas, J.H., 2017. Massively parallel digital transcriptional profiling of single cells. Nat Commun 8, 14049.

Zorn, A.M., Wells, J.M., 2009. Vertebrate Endoderm Development and Organ Formation. Annu Rev Cell Dev Biol 25, 221–251.

ANNEXES

bioRxiv preprint doi: https://doi.org/10.1101/2023.04.15.536998; this version posted April 17, 2023. The copyright holder for this preprint (which was not certified by peer review) is the author/funder, who has granted bioRxiv a license to display the preprint in perpetuity. It is made available under aCC-BY-NC-ND 4.0 International license.

Human airway ex vivo models: new tools to study the airway epithelial cell response to SARS-CoV-2 infection

Said Assou [1,#,*], Engi Ahmed [1,2], Lisa Morichon [1,3], Amel Nasri [1], Florent Foisset [1], Carine Bourdais [1], Nathalie Gros [3], Sonia Wong [4], Aurelie Petit [2], Isabelle Vachier [2], Delphine Muriaux [3,5], Arnaud Bourdin [2, #,*], John De Vos [1,6, #]

[1] IRMB, Univ Montpellier, INSERM, CHU Montpellier, Montpellier, F34295, France

[2] Department of Respiratory Diseases, CHU Montpellier, Arnaud de Villeneuve Hospital, INSERM, Montpellier 34000, France; PhyMedExp, University of Montpellier, INSERM U1046, CNRS UMR 9214.

[3] CEMIPAI, Univ Montpellier, CNRS UAR3725, Montpellier, France.

[4] CEFE, Univ Montpellier, CNRS, EPHE, IRD, Montpellier, France

[5] IRIM, Univ Montpellier, CNRS UMR9004, Montpellier, France.

[6] Department of Cell and Tissue Engineering, Saint-Eloi Hospital, Montpellier, F34295 France.

[#] Co-senior authors.

Short title: SARS-CoV-2 signatures in *ex vivo* airway models

[*] **Corresponding authors**:

Said Assou, Institute for Research in Regenerative Medicine and Biotherapy, Hôpital Saint-Eloi, 80 Avenue Augustin Fliche, 34295 Montpellier Cedex 5, France. Fax: 33-(0) 4-67-33-57-23. Email: said.assou@inserm.fr.

Arnaud Bourdin, Department of Respiratory Diseases, CHU Montpellier, Arnaud de Villeneuve Hospital, 34000, Montpellier. France. Email: a-bourdin@chu-montpellier.fr

bioRxiv preprint doi: https://doi.org/10.1101/2023.04.15.536998; this version posted April 17, 2023. The copyright holder for this preprint (which was not certified by peer review) is the author/funder, who has granted bioRxiv a license to display the preprint in perpetuity. It is made available under aCC-BY-NC-ND 4.0 International license.

Abstract

Airway-liquid interface cultures of primary epithelial cells and of induced pluripotent stem cell-derived airway epithelial cells (ALI and iALI, respectively) are physiologically relevant models for respiratory virus infection studies because they can mimic the *in vivo* human bronchial epithelium. Here, we investigated gene expression profiles in human airway cultures (ALI and iALI models) infected or not with severe acute respiratory syndrome coronavirus 2 (SARS-CoV-2) using publicly available and our own bulk and single-cell transcriptome datasets. SARS-CoV-2 infection significantly increased the expression of interferon-stimulated genes (*IFI44*, *IFIT1*, *IFIT3*, *IFI35*, *IRF9*, *MX1*, *OAS1*, *OAS3* and *ISG15*) and inflammatory genes (*NFKBIA*, *CSF1*, *FOSL1*, *IL32* and *CXCL10*) at day 4 post-infection, indicating activation of the interferon and immune responses to the virus. Extracellular matrix genes (*ITGB6*, *ITGB1* and *GJA1*) also were altered in infected cells. Single-cell RNA sequencing data revealed that SARS-CoV-2 infection damaged the respiratory epithelium, particularly mature ciliated cells. The expression of genes encoding intercellular communication and adhesion proteins also was deregulated, suggesting a mechanism to promote shedding of infected epithelial cells. These data demonstrate that ALI/iALI models help to understand the airway epithelium response to SARS-CoV-2 infection and are a key tool for developing COVID-19 treatments.

bioRxiv preprint doi: https://doi.org/10.1101/2023.04.15.536998; this version posted April 17, 2023. The copyright holder for this preprint (which was not certified by peer review) is the author/funder, who has granted bioRxiv a license to display the preprint in perpetuity. It is made available under aCC-BY-NC-ND 4.0 International license.

Introduction

The rapid spread of Severe Acute Respiratory Syndrome Coronavirus 2 (SARS-CoV-2) in humans has posed a serious global health threat. Coronaviruses are part of a large family of viruses that cause illnesses ranging from common colds to severe respiratory diseases, including COVID-19 caused by SARS-CoV-2. SARS-CoV-2 is a single positive-stranded RNA enveloped virus that replicates in epithelial cells [1]. Upon infection, SARS-CoV-2 binds the host ACE2 receptor through its spike protein, and enters the cells by fusion of the viral membrane with the epithelial cell membrane or by endocytosis [2]. After binding, the spike protein can be cleaved by TMPRSS2, a host membrane serine protease, facilitating viral entry [1]. Then, the virus replicates inside epithelial cells and produces newly synthetized viral particles that are secreted by the host cells [3].

Due to the COVID-19 long- and short-term effects on human health and the need to limit the emergence of novel virus variants, significant efforts have been dedicated to understand the viral infection mechanisms and to develop antiviral drugs using physiologically relevant *in vitro* culture models that mimic *in vivo* phenotypes. Human airway epithelial cells in culture are traditionally used for modeling respiratory diseases [4]. These cells can be obtained from lung tissue biopsies and are cultured as primary airway epithelial cells in air-liquid interface (ALI) systems that support epithelial cell differentiation and mimic key aspects of the mucosal epithelium [5]. They can also be derived by differentiation of induced pluripotent stem cells (iPSCs) in ALI systems (i.e. iALI) [6–9]. In both ALI and iALI systems, epithelial cells are cultured on a permeable membrane with the medium in the basal chamber and the epithelium exposed to air at the apical side of the membrane. In this system, cells are in contact with air and can be induced to differentiate into a functional pseudo-stratified epithelium. Several studies confirmed that ALI culture transcriptomic profiles are very similar to those of *in vivo* airway epithelium obtained by bronchial brushing or biopsy [10,11]. ALI

bioRxiv preprint doi: https://doi.org/10.1101/2023.04.15.536998; this version posted April 17, 2023. The copyright holder for this preprint (which was not certified by peer review) is the author/funder, who has granted bioRxiv a license to display the preprint in perpetuity. It is made available under aCC-BY-NC-ND 4.0 International license.

and iALI models can be infected by viruses and have been used to model various mechanisms of viral pathogenesis [12,13]. SARS-CoV-2 can replicate in both models [1,14] and infection can be limited by interferon. This demonstrated interferon therapeutic potential for COVID-19 treatments and the usefulness of these models as a high-throughput screening tool [15,16]. Additionally, ALI and iALI cultures from patients with respiratory diseases (e.g. chronic obstructive pulmonary disease) recapitulate some of the *in vivo* disease characteristics, and are used to assess the impact of smoke exposure on viral infection [12,17,18]. Therefore, ALI and iALI cultures could help to understand SARS-CoV-2 effects in bronchial epithelium, by analyzing the transcriptomic changes upon infection. ALI models are very helpful to identify the key initiating steps of viral injury and innate epithelial cell defense that may or may not lead to cell infection and replication. Increasing the number of models and of donors will improve the robustness of the identified pathways by reducing the inter-individual heterogeneity in viral susceptibility.

Various omic-based studies, including *in vivo* (human samples) and *in vitro* (model systems) transcriptome profiling studies (bulk RNA sequencing), have highlighted the molecular changes induced by SARS-CoV-2 infection [19–21]. The recent advent of single-cell RNA-sequencing (scRNA-seq) provides a precious approach to carefully analyze gene expression and cell composition. For instance, scRNA-seq has been used to identify the cells in the human respiratory system with the highest expression of transmembrane receptors for SARS-CoV-2 [22], and to show that in ALI cultures of nasal epithelial cells, ciliated and goblet/secretory cells express progressively SARS-CoV-2 entry factors. Moreover, in infected human bronchial epithelial–derived ALI cultures, scRNA-seq [23] revealed that ciliated cells are a major SARS-CoV-2 target.

In the present study, we analyzed bulk and single-cell RNA-seq datasets to provide a detailed picture of the gene expression changes in ALI and iALI models following SARS-CoV-2

bioRxiv preprint doi: https://doi.org/10.1101/2023.04.15.536998; this version posted April 17, 2023. The copyright holder for this preprint (which was not certified by peer review) is the author/funder, who has granted bioRxiv a license to display the preprint in perpetuity. It is made available under aCC-BY-NC-ND 4.0 International license.

infection. This analysis highlighted the molecular mechanisms involved in the induction of the hyper-inflammatory state and innate immune response, including interferon signaling, chemokines and extracellular matrix (ECM), and identified potential regulatory microRNAs (miRNAs) for therapeutic interventions.

Methods

ALI culture of primary airway epithelial cells and iPSC-derived airway epithelium for scRNA-seq analysis

Primary Human Bronchial Epithelial Cells (HBEC) were expanded and differentiated in ALI culture following the protocol given by StemCell Technologies. Briefly, cells were dissociated mechanically from bronchial biopsy specimens obtained by fiberoptic bronchoscopy (approval number: 2013 11 05; NCT02354677) and cultured in PneumaCult-Ex Plus expansion medium (cat #05041, StemCell Technologies, France) for 15 days. After the expansion phase, differentiation was initiated by seeding 1.1×10^5 cells/insert on Transwell^R polyester membranes (ref 3460, Corning, Kennebunk, United States). Once epithelial cells reached confluence, the apical growth medium was removed, and the basal medium was replaced by PneumaCult™-ALI maintenance medium (cat #05002, StemCell Technologies, France) (i.e. day 0 of ALI culture). Epithelial cells were allowed to differentiate at 37°C, 5% CO_2 for 28 days.

iPSC-derived airway epithelium on ALI (iALI model) was generated as previously described [6]. Briefly, the major stages of embryonic lung development were recapitulated as follows: stage 1, definitive endoderm (day 0–3) using activin A; stage 2, anterior foregut endoderm (day 4–8); stage 3, lung progenitor specification (day 9); and stage 4, epithelial layer (day 14). After 40 days, the airway epithelium on iALI displayed morphologic and functional

bioRxiv preprint doi: https://doi.org/10.1101/2023.04.15.536998; this version posted April 17, 2023. The copyright holder for this preprint (which was not certified by peer review) is the author/funder, who has granted bioRxiv a license to display the preprint in perpetuity. It is made available under aCC-BY-NC-ND 4.0 International license.

similarities with primary human airway epithelial cells and included different airway cell types (basal, secretory, and multi-ciliated cells).

ScRNA-seq and data analysis

Non-infected ALI and iALI cultures were dissociated with trypsin into single-cell suspensions. Cell viability and aggregation were tested before starting the single-cell library preparation. The concentration of freshly dissociated cells was adjusted to 1000 cells/µl in HBSS/0.05% BSA and then the 10x Chromium Controller and the Chromium Single Cell 3' Reagent kit V3.1 were used for performing the scRNAseq experiments. Library preparation was performed according to the manufacturer's instructions using the Chromium Chip B Single Cell kit, and Chromium Multiplex Kit (10X Genomics). Sequencing was performed in paired-end mode with an S1 flow cell (28/8/87 cycles) and a NovaSeq 6000 sequencer (Illumina) at the MGX core facility of Montpellier, France. First, the cell ranger mkfastq and cellranger count pipelines were used for the initial quality control, sample demultiplexing, mapping, and raw data quantification. Briefly, fastq files were run with the Count application using default parameters and were aligned to the human genome reference sequence GRCh38, filtered and counted. The C-loop software (version 6.2.0) was used to visualize clusters and sub-clusters of transcriptionally related cells and to identify candidate genes the expression of which was enriched in specific clusters. Clustering results were visualized with the t-distributed Stochastic Neighbor Embedding (tSNE) technique. Bronchial cell (biopsy/brushing samples) datasets included in [24] were analyzed through a COVID-19 Cell Atlas website portal and were visualized using Uniform Manifold Approximation and Projection (UMAP).

Functional enrichment analysis of bulk RNA-seq datasets

bioRxiv preprint doi: https://doi.org/10.1101/2023.04.15.536998; this version posted April 17, 2023. The copyright holder for this preprint (which was not certified by peer review) is the author/funder, who has granted bioRxiv a license to display the preprint in perpetuity. It is made available under aCC-BY-NC-ND 4.0 International license.

The unique bulk RNA-seq signature was obtained from a publicly available list of differential expressed genes between primary human lung epithelium infected with SARS-CoV-2 (multiplicity of infection, MOI, = 2 for 24 h) and mock-treated controls [20]. The GO functional enrichment and pathway enrichment analyses were performed with ShinyGO [26] and Gene Set Enrichment Analysis (GSEA) (http://www.broadinstitute.org/gsea/). GO annotations were divided in three categories: biological process, molecular function, and cellular component. In the enrichment analysis, the Fisher' exact test was used to test whether genes were enriched in a term, and an adjusted p value <0.05 was set as the screening condition. The GenGo Metacore software was used to identify miRNA targets. Heatmaps and gene networks were generated with Ingenuity Pathway Analysis (IPA, QIAGEN, Redwood City, CA, USA).

Analysis of publicly available single-cell RNA-seq datasets

A public scRNA-seq dataset (GEO accession number: GSE166766) of HBEC ALI culture samples infected with SARS-CoV-2 (MOI ~0.01) was also analyzed [25]. The Velocyto® package was used to investigate the gene expression dynamics in the scRNA-seq data before virus infection and at day 3 post-infection (dpi). RNA velocity quantifies the change in the state of a cell over time by distinguishing unspliced and spliced mRNAs reads. To obtain de counts of spliced and unspliced mRNAs reads, Velocyto used the outputs of CellRanger (version 3.0.2) alignments with the command line 'run10x' and the transcriptome GRCh38.p12 (accession NCBI:GCA_000001405.27). At this step, loom files were created for the input data of the scVelo tool [26]. This python package allowed normalizing with the scv.pp.normalize_per_cell() function and transform scv.pp.log1p(). Genes were filtered by keeping only the 2000 top highly variable genes (n_top_genes = 2000 parameters for scv.pp.filter_and_normalize function). Then, moments were calculated for each cell across its nearest neighbors with n_neighbors set to 30 and the first 10 PCs using the scv.pp.moments()

bioRxiv preprint doi: https://doi.org/10.1101/2023.04.15.536998; this version posted April 17, 2023. The copyright holder for this preprint (which was not certified by peer review) is the author/funder, who has granted bioRxiv a license to display the preprint in perpetuity. It is made available under aCC-BY-NC-ND 4.0 International license.

function. Then, cell velocities were estimated using scvelo.tl.velocity() based on a stochastic model of transcriptional dynamics. To visualize the velocity graph, data were projected on the UMAP space and clusters defined by the CellRanger pipeline were colored. After cluster identification on Seurat V4 [27], the function cluster_analysis from the SingleCellSignalR package [28] was used to compute paracrine interactions between cell clusters and to predict ligand–target links between interacting cells by combining their expression level with prior knowledge on gene regulatory networks and signaling pathways. To compare ALI and iALI samples, genes identified in our samples were combined with other publicly available datasets that used infected iPSC-derived AT2 cells (iAT2) [16], specifically for the genes related to inflammatory and interferon responses and extracellular ECM.

SARS-CoV-2 virus stock and titration

The hCoV-19/France/HDF-IPP11602i/2021 (21A - Delta – B.1.617.2) strain was supplied by the National Reference Centre for Respiratory Viruses hosted by Institut Pasteur (Paris, France). The human sample from which this strain was isolated was provided by Dr Guiheneuf Raphaël, CH Simone Veil, Beauvais France. The strain was propagated in VeroE6 cells with DMEM containing 25mM HEPES at 37°C and 5% CO_2 and viruses were harvested 72 hours post-inoculation. Virus stocks were stored at -80°C. Viruses from infected cell culture supernatants were titrated with the plaque assays on a monolayer of VeroE6 cells and 100µL of virus serial dilutions. The plaque forming unit (PFU) values were determined by crystal violet staining and then by scoring the wells displaying cytopathic effects. The virus titer was determined as the number of PFU/mL, and MOI was the PFU/cell ratio.

Reverse transcription-quantitative polymerase chain reaction (RT-qPCR)

bioRxiv preprint doi: https://doi.org/10.1101/2023.04.15.536998; this version posted April 17, 2023. The copyright holder for this preprint (which was not certified by peer review) is the author/funder, who has granted bioRxiv a license to display the preprint in perpetuity. It is made available under aCC-BY-NC-ND 4.0 International license.

RNA was extracted from cells using the QIAshredder kit (QIAGEN, Redwood city, CA, USA) and the RNeasy mini kit (Qiagen, Redwood city, CA, USA) according to the manufacturer's instructions. Viral RNA was quantified by RT-qPCR in triplicate as described [29], using the Luna Universal One-Step RT-qPCR Kit (New England Biolabs, Ipswich, MA, USA) and a BIORAD CFX Opus 384 system. Relative gene expression was calculated for each triplicate by normalizing to *GAPDH* level (control) and using the formula $2^{-\Delta Ct}$. Primers are listed in Supplementary Table S1.

Immunofluorescence analysis

iALI cultures were fixed in 4% paraformaldehyde for 4 hours. After three PBS washes, iALI samples were stored in PBS at 4°C. Samples were permeabilized in 0.5% Triton X-100/PBS at room temperature for 20 min and then blocked with PBS/0.1% Triton X-100/1% bovine serum albumin (BSA)/10% donkey serum at room temperature for at least 1h. Primary antibodies against p63 (AF1916, Biotechne, Minneapolis, MN, USA), TubIV (T7941, Sigma, Saint Louis, MO, USA) and SARS-CoV-2 M protein membrane (100-401-A55, Rockland Immunochemicals, Pottstown, PA, USA) were diluted (1/100, 1/200 and 1/200, respectively) in PBS/1%BSA/0.1%, Triton X-100 and added to the samples for overnight incubation. Then, samples were washed three times with PBS/0.025% Triton X-100 before incubation (room temperature for 2h) with the following secondary antibodies: anti-mouse coupled to Alexafluor 555 (A31570, Invitrogen, Waltham, MA, USA), anti-rabbit coupled to Alexafluor 488 (A21206, Invitrogen, Waltham, MA, USA) and anti-goat coupled to Alexafluor 647 (A21447, Invitrogen, Waltham, MA, USA) (all diluted to 1/1000 in PBS/1% BSA/0.1%, Triton X-100. After three washes in PBS/0.025% Triton X-100, samples were incubated with DAPI (D9542, Sigma, Saint Louis, MO, USA), diluted 1/2500 in PBS, for 5 min and rinsed in PBS. Then, iALI samples were separated for their support and mounted between glass slides.

bioRxiv preprint doi: https://doi.org/10.1101/2023.04.15.536998; this version posted April 17, 2023. The copyright holder for this preprint (which was not certified by peer review) is the author/funder, who has granted bioRxiv a license to display the preprint in perpetuity. It is made available under aCC-BY-NC-ND 4.0 International license.

Confocal images were acquired using a Cell-Discoverer 7 LSM900 confocal laser-scanning microscope (Zeiss, Germany) at 40x magnification, and processed with Zen Blue.

Statistical analysis

Data are presented as the mean ± SEM, unless otherwise specified. Statistical analyses were performed with the GraphPad Prism 5 software (Student's *t*-test; GraphPad). The shown data were from representative experiments, with similar results in at least three independent biological replicates, unless otherwise specified. Differences were evaluated using the Student's *t*-test. A p value ≤ 0.05 was considered significant.

Results

Cellular landscapes of non-infected human lung epithelium models

One of the challenges in COVID-19 research is the need of physiologically relevant *in vitro* cell culture models to mimic the native environment. To this aim, non-infected HBEC in ALI culture and iPSC-derived epithelial-like cells in iALI culture were analyzed by scRNA-seq to generate a comprehensive repertoire of the cell populations present in these models. Single-cell transcriptome data were obtained also from lung epithelium collected by bronchial biopsy or brushing (Figure 1A). Analysis of these scRNA-seq data from these three models (biopsy/brushing bronchial cells, ALI, and iALI cultures) (Figure 1B) showed that most epithelial cell markers, such as *SCGB1A1/CC10* (secretoglobin family 1A member 1; secretory cells), *TP63* (tumor protein p63; basal cells), and *FOXJ1* (forkhead box J1; multi-ciliated cells) were present in the three sample types. This suggested that non-infected ALI and iALI models contain the essential cell types necessary for bronchial epithelium function and can be used as experimental *ex vivo* models to study SARS-CoV-2 infectivity. Comparison of the single-cell landscapes indicated that unlike the biopsy/brushing and ALI

bioRxiv preprint doi: https://doi.org/10.1101/2023.04.15.536998; this version posted April 17, 2023. The copyright holder for this preprint (which was not certified by peer review) is the author/funder, who has granted bioRxiv a license to display the preprint in perpetuity. It is made available under aCC-BY-NC-ND 4.0 International license.

models, the iALI model expressed *ASCL1*, a marker of neuroendocrine cells, but not *FOXI1* (ionocyte marker) and all models express *POU2F3* (tuft cell marker). In addition, immune cells were an important cell fraction in biopsy/brushing samples (Figure 1C), but were absent in the ALI and iALI models. This major difference may help to (i) understand the epithelial-intrinsic innate inflammatory response to SARS-CoV-2 infection; (ii) identify the key epithelial target cells; and (iii) compare the molecular mechanisms triggered in the absence (iALI and ALI) and the presence (biopsy–brushing samples) of immune cells.

Cell-specific expression of single-stranded RNA virus receptors in non-infected human lung epithelium models

The expression of receptors to which single-stranded RNA (ssRNA) viruses can bind is a key factor for virus infection and transmission. Analysis of scRNA-seq data from the three non-infected lung epithelium models showed that *CDHR3* (encoding cadherin related family member 3, the entry receptor for rhino-virus C) [30] was specifically expressed in ciliated cells, and *CD55* (Coxsackie-virus B1 receptor) [30] in secretory cells (Figure 1D). *ACE2* (SARS-CoV-2 receptor) was expressed by ciliated, secretory and basal cells. Moreover, in biopsy/brushing samples, $ACE2^{+}$ cells were overrepresented among all epithelial cell types compared with immune cells, including macrophage, endothelial and dendritic cells (Figure 1D). This is in line with a recent study reporting the absence of viral transcripts in bronchoalveolar fluid and peripheral blood mononuclear cell samples collected from patients with COVID-19 [31]. Collectively, scRNA-seq data analysis of the three cell culture models showed expression of ssRNA virus receptors in secretory, ciliated and basal cells, suggesting the possibility of modeling ssRNA virus infection, including SARS-CoV-2, in airway epithelium *in vitro*.

bioRxiv preprint doi: https://doi.org/10.1101/2023.04.15.536998; this version posted April 17, 2023. The copyright holder for this preprint (which was not certified by peer review) is the author/funder, who has granted bioRxiv a license to display the preprint in perpetuity. It is made available under aCC-BY-NC-ND 4.0 International license.

Changes induced by SARS-CoV-2 infection in the ALI model

A recent bulk RNA-seq dataset [20] was used to compare the gene expression profiles of infected and non-infected human bronchial epithelium in order to identify the "SARS-CoV-2 bulk RNA-seq signature" induced by SARS-CoV-2 infection in the ALI model (Supplementary Table S2). GO biological process and molecular function analyses of this "SARS-CoV-2 bulk RNA-seq signature" showed significant overexpression of genes implicated in immune response, cytokines and chemokine activity (Figure 2A). The GO cellular component enrichment analysis showed that many differentially expressed genes were related to ECM and ECM regulators (Figure 2A). GSEA confirmed the significant upregulation of the interferon and inflammatory pathways (Figure 2B). Heatmaps revealed that the core transcriptional response included genes implicated in "immune cell trafficking", "inflammatory response", "cellular movement", "inflammatory response" and "cell-to-cell signaling and interaction" (Figure 2C), which is consistent with the biological processes and molecular functions highlighted above. The top categories, ranked in accordance with their −log(P-value), are shown in Supplementary Table S3. In total, 146 enriched canonical pathways were identified (Supplementary Table S4). The interferon signaling pathway was ranked first with a −log (P-value) of 14.1. Many genes belonging to the interferon machinery implicated in the antiviral response and viral replication were identified (Figure 2D), such as interferon-induced genes (*IFI27*, *IFI35*, *IFI44*, *IFI44L*, *IFIH1*, *IFIT1*, *IFIT3*, *IFITM1*, *IFITM3*), interferon regulatory factors (*IRF7* and *IRF9*), interferon-stimulated genes (*ISG15* and *ISG20*), MX dynamin-like GTPases (*MX1* and *MX2*), oligoadenylate synthetases (*OAS1*, *OAS2* and *OAS3*) and the master suppressor of cytokine signaling (*SOCS3*). With a Z-score >2 as a threshold of significant activation, the following signaling pathways were identified as activated: '*IL17* signaling' (Z-score=5.099), '*HMGB1* signaling' (Z-score=4), '*TREM1* signaling' (Z-score=3.742), 'Toll-like Receptor signaling' (Z-score=2.53), '*IL-8* signaling' (Z-

bioRxiv preprint doi: https://doi.org/10.1101/2023.04.15.536998; this version posted April 17, 2023. The copyright holder for this preprint (which was not certified by peer review) is the author/funder, who has granted bioRxiv a license to display the preprint in perpetuity. It is made available under aCC-BY-NC-ND 4.0 International license.

score=4.123), 'iNOS signaling' (Z-score=3.162), '*IL-6* signaling' (Z-score=3.37), '*TNFR1* signaling' (Z-score=2.121), '*IL-1* signaling' (Z-score=3) and '*PI3K/AKT* signaling' (Z-score=2.333). Conversely, some of the enriched signaling pathways had Z-scores lower than -2, such as 'inhibition of matrix metalloproteases' (Z-score=-2), '*PPAR* signaling' (Z-score=-3.606) and 'erythropoietin signaling pathway' (Z-score=-2.524). Concerning upstream regulators (Supplementary Figure S1, Supplementary Table S5), the highest ranked regulatory effects with consistency scores up to 4.8 strongly suggested that the upstream regulators *TNF*, *IL1A* and *F2* may be responsible for the gene expression changes in the SARS-CoV-2 bulk RNA-seq signature. IPA analysis predicted that these upstream regulators are involved in chemotaxis, invasion and cell movement, mainly through induction of their targets, including many genes associated with the innate immune response (*IL1B*, *NFKBIA*, *CXCL1*, *NOD2*, *PLAUR*, *C3*, *ITGB2*, *S100A8*, *PLAU*, *S100A9*, *IL1A*, *TNF*), cytokine and chemokine activities (*CCL20*, *CXCL2*, *CXCL3*, *CXCL5*, *CXCL6*, *CXCL8*, *CXCL10*, *IL6*, *IL8*, *IL32*, *IL33*, *CSF3*, *CSF2*, *CSF1*), and genes implicated in ECM degradation, such as matrix metalloproteases (*MMP13*, *MMP9*, *MMP1*). These metalloproteases are connected to pro-inflammatory chemokines and play an operative role in ECM degradation during inflammation that can be triggered by virus infection. Our data highlighted and confirmed that matrix metalloproteinases play key roles in viral infection and its progression [32] through airway remodeling (i.e. loss of the epithelium barrier integrity [33] and elastin degradation in the ECM [34]).

Conserved expression of the epithelial cell response to SARS-CoV-2 infection in the iALI model

Then, bulk RNA sequencing datasets of iPSC-derived alveolar epithelial type 2-like cells (iAT2) infected by SARS-CoV-2 and mock-infected [16] at 1 and 4 dpi were analyzed to

bioRxiv preprint doi: https://doi.org/10.1101/2023.04.15.536998; this version posted April 17, 2023. The copyright holder for this preprint (which was not certified by peer review) is the author/funder, who has granted bioRxiv a license to display the preprint in perpetuity. It is made available under aCC-BY-NC-ND 4.0 International license.

312 determine whether the SARS-CoV-2 bulk RNA-seq signature observed in the ALI model was
313 present also in the iALI model. Analysis of the temporal distribution of RNA-seq reads
314 allowed identifying four major gene groups (Figure 3A): (a) genes that were upregulated early
315 (at 1 dpi) and the expression of which gradually increased from 1 to 4 dpi (*NFKBIA*, *CSF1*,
316 *IL32* and *FOSL1)*; (b) genes that were upregulated early and the expression of which was not
317 changed at 4 dpi (*IL23A*, *CXCL10*, *CXCL20* and *PLAUR)*; (c) genes that were upregulated at
318 1 dpi and were then downregulated at 4 dpi (*CXCL3*, *CXCL5*, *CXCL1* and *LOX)*; and (d)
319 genes that were upregulated only at 4 dpi (*MMP9* and *MMP13*). In addition, and like in the
320 ALI model, in the COVID-19 iALI model, the interferon response was activated, as indicated
321 by the upregulation of genes encoding interferon induced proteins and interferon regulatory
322 factors (Figure 3B). This suggests that the ALI and iALI models share common interferon
323 response regulation features. Conversely, the expression kinetics of ECM-related genes
324 showed that some genes (*ITGB6*, *ITGB1*, *GJA1*, *VIM* and the ECM regulator *PLOD2*, which
325 encode proteins of the host cell cytoskeleton structure) were progressively downregulated
326 during SARS-CoV-2 infection in the iALI model (Figure 3C). This indicated that the ECM
327 and adhesion pathways are affected during cell-to-cell SARS-CoV-2 transmission. Moreover,
328 the expression of *EpCAM* (epithelial cell adhesion molecule), an epithelial cell surface
329 marker, progressively decreased, and that of the stromal cell marker *COL1A1* progressively
330 increased (Figure 3D), suggesting epithelial mesenchymal transition.
331
332 **Experimental validation of the epithelial cell response to SARS-CoV-2 infection in the**
333 **iALI model**
334 To gain insight into the molecular basis of SARS-CoV-2 infection in the iALI model, iALI
335 bronchial epithelium was exposed to SARS-CoV-2 Delta at low MOI (0.05) to let the
336 infection take hold for 4 days and then the expression of interferon-induced genes and

bioRxiv preprint doi: https://doi.org/10.1101/2023.04.15.536998; this version posted April 17, 2023. The copyright holder for this preprint (which was not certified by peer review) is the author/funder, who has granted bioRxiv a license to display the preprint in perpetuity. It is made available under aCC-BY-NC-ND 4.0 International license.

regulatory factors, viral entry genes and ECM genes was investigated. Viral DNA quantification confirmed infection of iALI cultures. The virus was detected at the apical side at 1 dpi and also at 4 dpi (Figure 4A). Moreover, SARS-CoV-2 membrane protein colocalized with tubulin α 4a (TubIV), suggesting preferential infection of ciliated cells (Figure 4B). RT-qPCR analysis of infected cells showed activation of the interferon signaling pathways at 1 dpi and 4 dpi. Interferon-induced proteins (*IFI44*, *IFIT1*, *IFIT3*, *IFI35*), interferon regulatory factors (*IRF9*, *MX1*, *ISG15*), oligoadenylate synthetases (*OAS1*, *OAS3*) and chemokine ligand (*CXCL10*) were upregulated at 4 dpi (Figure 4C). Conversely, viral infection did not alter the expression of genes encoding adhesion molecules, such as *GJA1* and *ITGB1*, unlike what observed upon infection at higher MOI (0.5) (Figure 3C). In agreement with this observation, trans-barrier electrical resistance (TEER) of iPSC-derived epithelial cells was comparable in non-infected and infected (at low MOI = 0.05) iALI cultures from 1 to 4 dpi, indicating that at this infection level, epithelium integrity was not disrupted (Figure 4D). Altogether, these data show that the iALI model is a faithful and sensitive model for SARS-CoV-2 infection.

Epithelial cell communication networks in response to SARS-CoV2 infection

ALI cultures include different cell types connected by tight and adherens junctions. Communication between epithelial cells occurs through the release of a variety of small molecules, including cytokines and chemokines. To investigate the impact of SARS-CoV2 infection on ligand/receptor interaction between the different airway cell types, scRNA-seq data from HBEC ALI cultures infected or not with SARS-CoV-2 (MOI 0.01) were analyzed using the SingleCellSignalR method. Comparison of the summary chord diagram indicated a decrease in the number of paracrine interactions between the main epithelial cell types after 2dpi (Figure 5A), which strongly suggests an impact of SARS-CoV2 infection on intercellular communications. For instance, expression of receptor tyrosine kinase (*RET*) and its ligand

bioRxiv preprint doi: https://doi.org/10.1101/2023.04.15.536998; this version posted April 17, 2023. The copyright holder for this preprint (which was not certified by peer review) is the author/funder, who has granted bioRxiv a license to display the preprint in perpetuity. It is made available under aCC-BY-NC-ND 4.0 International license.

artemin (*ARTN*), one of the most preeminent interacting pair between neuroendocrine cells and other epithelial cells, was strongly decreased at 3 dpi (Figure 5B). This suggests that neuroendocrine cells are particularly sensitive to environmental stimuli (e.g., viral infection), and act as a rheostat to orchestrate ALI-culture responses.

RNA velocity reveals discrepancies between non-infected and infected epithelium in the ALI model

To further characterize the ALI model transcriptional dynamics in response to virus infection, the single-cell RNA velocity was measured in SARS-CoV-2 infected and non-infected epithelial ALI cultures using a dynamic model of transcriptional state based on unspliced and spliced transcript counts [26]. Cell trajectory analysis revealed that non-infected ALI epithelial cells displayed two distinct bifurcation points through two different epithelial transition states. The first bifurcation point included basal cells (*TP63*-/*KRT5*+) that directly differentiate into ciliated cells, and the second bifurcation point mainly included basal cells (*TP63*+/*KRT5*+) that preferentially differentiate into secretory cells and then into ciliated cells. This placed secretory cells in an intermediate position between basal cells and mature ciliated cells (*DNAH9*+) (Figure 5C). Velocity ordering analysis in infected cells revealed a change in the ciliated cell differentiation trajectory. Indeed, basal cells were all oriented to differentiate into ciliated cells through a secretory cell state. Moreover, *DNAH9*+ infected cell mapping within ALI epithelial cells revealed that ciliated cells were more susceptible to infection compared with other cell types, like *DNAH9*+ mature ciliated cells that are preferentially eliminated during SARS-CoV-2 infection (Figure 5D). Collectively, the dynamic ALI airway model provides a useful tool for *in vitro* studies on SARS-CoV-2/other virus infection and antiviral testing.

bioRxiv preprint doi: https://doi.org/10.1101/2023.04.15.536998; this version posted April 17, 2023. The copyright holder for this preprint (which was not certified by peer review) is the author/funder, who has granted bioRxiv a license to display the preprint in perpetuity. It is made available under aCC-BY-NC-ND 4.0 International license.

Potential miRNA regulators of the epithelial cell intrinsic response to SARS-CoV-2 infection

The GenGo Metacore software was then used to identify miRNAs that regulate the epithelial cell response genes after SARS-CoV-2 infection in the ALI and iALI models (i.e. potential antiviral targets). This analysis identified 167 miRNAs that regulate the key epithelial cell intrinsic genes deregulated upon viral infection (Figures 3A-B). Among these miRNAs, 44 were regulators of interferon response genes and 123 regulated inflammatory response genes (complete list of miRNAs in Supplementary Table S6). More than 54% of the interferon gene targets were regulated by more than one miRNA. For instance, *SOCS3* and *MX2* were targeted by 24 and 5 miRNAs, respectively (Figure 6A). The inflammatory genes regulated by the highest number of miRNAs were *MMP9* (n = 29 miRNAs), *NFKBIA* (n = 19), *MMP13* (n = 19), *CSF1* (n = 12), *FOSL1* (n = 11) and *LOX* (n = 11) (Figure 6B). *MIR34a* was identified as a potential regulator of *MMP9*, *NFKBIA*, *FOSL1*, *CXCL10*, whereas *MIR203* and *MIR19* were common regulators of *NFKBIA, MMP13, SOCS3*. *MIR138-5p* and *MIR-326-3p* are validated regulators of *ISG15* and *ISG20*. *MIR650, MIR541-3p* and *MIR302d-3p* regulated several interferon□stimulated genes, including *MX1*, *MX2, IRF7* and *IRF9*. *CSF1* and *LOX* were targets of *MIR130a* and *MIR29*, respectively. These miRNAs can attenuate the inflammatory response and inhibit key coagulation cascade factors, thus preventing inflammatory epithelium damage. Therefore, they are potential miRNA-based therapeutics against COVID-19.

Discussion

The human airways are lined by an epithelium with three abundant specialized cell types (basal, secretory, and multi-ciliated cells) and some rare cell types (neuroendocrine cells, tuft cells and ionocytes) [35–37], on a stroma composed of mesenchymal cells, smooth muscle

bioRxiv preprint doi: https://doi.org/10.1101/2023.04.15.536998; this version posted April 17, 2023. The copyright holder for this preprint (which was not certified by peer review) is the author/funder, who has granted bioRxiv a license to display the preprint in perpetuity. It is made available under aCC-BY-NC-ND 4.0 International license.

411 cells and immune cells [38]. Primary HBECs cultured in ALI conditions can be used to study
412 airways *in vitro*. More recently, our group and others have generated functional airway
413 epithelium from human iPSCs (iALI models) with a marked similarity to the airway
414 epithelium *in vivo* [6,8,39–41]. As expected, scRNA-seq analysis of ALI and iALI models
415 showed that immune cells, which are found in biopsy/brushing-derived primary cultures, were
416 absent in these models. Conversely, the stromal component was exclusively found in ALI and
417 iALI models, suggesting a role in the epithelium maintenance. Of note, neuroendocrine cells
418 were mostly identified in the iALI model, compared with the ALI model. Our analysis
419 characterized rare cell types, such as ionocytes, that strongly express *FOXI1* and *ASCL3*
420 [36,42].
421 SARS-CoV-2 infection in ALI and iALI models induces virus-linked epithelial disruption,
422 loss of mature ciliated cells, and triggers intrinsic immune responses. Despite the differences
423 in terms of cell composition, the ALI and iALI models exhibit relevant proportions of airway
424 cell types, express virus receptors (ACE2, CDHR3, CD55), and have been used to model
425 various mechanisms of SARS-CoV-2 pathogenesis [43]. These models provide a suitable and
426 reliable platform for researchers to study SARS-CoV-2 pathogenesis during infection.
427 In this study we analyzed the bulk and single-cell transcriptomes of ALI and iALI cultures
428 infected with SARS-CoV-2. This highlighted the emergence of pro-inflammatory and
429 interferon signatures in which epithelial cells activated the expression of several cytokines,
430 chemokines, interferon, and downregulated ECM-related genes in response to SARS-CoV-2
431 at different times after infection. Most of these genes play essential roles in virus control and
432 also in disease development. For instance, many chemokines (*CCL2*, *CCL3*, *CCL20*, *CXCL1*,
433 *CXCL3*, *CXCL10*, *IL-8*) associated with inflammatory responses were expressed in the ALI
434 and iALI models. *CCL2*, *CXCL10* (called *IP-10*) and *IL-8* are associated with airway
435 inflammation, and high serum levels of these chemokines were found in patients with severe

bioRxiv preprint doi: https://doi.org/10.1101/2023.04.15.536998; this version posted April 17, 2023. The copyright holder for this preprint (which was not certified by peer review) is the author/funder, who has granted bioRxiv a license to display the preprint in perpetuity. It is made available under aCC-BY-NC-ND 4.0 International license.

436 SARS [44]. *CCL3* also is involved in viral infections [45]. Our detailed analysis of the
437 transcriptional response to SARS-CoV-2 infection showed that ALI and iALI cultures
438 produced an unbalanced cytokine response, with preferential upregulation of genes encoding
439 cytokines (for instance *IL-6*, *IL-1β* and *IL-33*) that are mainly implicated in the defense
440 against extracellular aggression. Several studies showed that IL-6 serum levels are increased
441 in patients with COVID-19 [46]. IL-6 is involved in acute inflammation due to its implication
442 in controlling the acute phase response [47]. IL-6 production is increased by TNF- α and IL-
443 1β [48]. In animal models of SARS-CoV-infection, TNF activity neutralization provides
444 protection against SARS-CoV morbidity and mortality [49]. A large number of data showed
445 the role of interferons in SARS-CoV2 infection. Interferons exercise their biological functions
446 by regulating the expression of interferon-stimulated genes (ISGs). ISG upregulation has been
447 described in various cells from patients with severe COVID-19 [50,51]. Here, we found that
448 infection with SARS-CoV-2 induced a strong interferon response in ALI and iALI cultures,
449 marked by high expression of *ISG15* (key factor in the innate immune response to SARS-
450 CoV-2 infection), *ISG20* (with antiviral activity against RNA viruses), *IRF-7* (the master
451 regulator of interferon responses) [52], and of several ISGs (*IFITM1, IFITM3*, *IRF9*, *IFI27*,
452 *OAS2*, *MX1*, *MX2*, *SOCS3*) involved in the regulation of the host defense responses to the
453 virus [53]. This suggests that *in vitro*, ALI/iALI epithelium can develop an intrinsic response
454 to SARS-CoV-2 infection focused on the activation of the interferon pathways. This is in line
455 with a study showing strong expression of many ISGs in the respiratory tract of patients with
456 COVID-19, supporting the idea that interferon-mediated immune response plays a key role in
457 SARS-CoV-2 infection control [51].
458 Although SARS-CoV-2 pathogenesis has not been fully understood, it seems that excessive
459 immune responses play a key role. Evidence suggests that immune response deregulation
460 causes lung damage [54]. Here we found that in infected ALI and iALI cultures, chemokines

bioRxiv preprint doi: https://doi.org/10.1101/2023.04.15.536998; this version posted April 17, 2023. The copyright holder for this preprint (which was not certified by peer review) is the author/funder, who has granted bioRxiv a license to display the preprint in perpetuity. It is made available under aCC-BY-NC-ND 4.0 International license.

and cytokines, including IL-6, IL-1β, interferon and TNF, were upregulated to coordinate all aspects of the immunogenic response to SARS-CoV-2 infection. Additionally, SARS CoV2-related pneumonia with severe respiratory failure is characterized by enhanced ECM [55]. Similarly, in infected ALI cultures, cells expressing *MMP9*, an enzyme that participate in ECM remodeling, were markedly increased. The molecular pathways involved in *MMP-9* regulation during SARS-CoV2 infection are not known. Ueland et al. suggested that *MMP-9* may be an early indicator of respiratory failure in patients with COVID-19 [56], and Hsu et al. reported an important increase of MMP-9 concentration in the plasma of patients who developed acute respiratory distress syndrome [57]. Conversely, in infected ALI cultures, cells expressing ECM-related genes (e.g. *VIM*, *ITGB1*, *ITGB6*, *GJA1* and *PLOD2*) were decreased compared with control cultures. Vimentin and integrin are critical targets for SARS-CoV-2 host cell invasion [58,59]. Identifying the molecular mechanisms that lead to their regulation will be pivotal to understand their role in epithelium damage and reparation during SARS CoV2 infection.

Another important question we addressed concerned the miRNA role in the regulation of genes deregulated in infected ALI/iALI cultures. Recent investigations revealed that miRNAs are implicated in viral pathogenesis by altering the miRNA-modulated host gene regulation or the host immune system [60]. The variation of miRNA levels during virus infection and their role in modulating SARS-CoV-2 infection in human cells have been well described [17]. Thus, miRNA-antagonists or -mimics could be used to develop new therapeutic strategies for the treatment of patients with COVID-19 [61]. The anti-viral response by miRNAs may implicate the regulation of their mRNA targets that participate in the cellular response to viral infection. Interferon signaling was one of the primary effectors against SARS-CoV2 infections in both ALI and iALI models. Moreover, genes encoding members of this pathway are direct targets of many miRNAs. For instance, *MIR138* regulates *ISG15* expression by

bioRxiv preprint doi: https://doi.org/10.1101/2023.04.15.536998; this version posted April 17, 2023. The copyright holder for this preprint (which was not certified by peer review) is the author/funder, who has granted bioRxiv a license to display the preprint in perpetuity. It is made available under aCC-BY-NC-ND 4.0 International license.

direct binding to its 3′ untranslated region (UTR) [62]. Similarly, *MIR326-3p* reduces the activity of an *ISG20* 3′ UTR luciferase reporter [63]. *MIR650*, *MIR29a-3p* and *MIR130a-3p* regulate other ISGs, such as *MX1*, *MX2*, *IFITM3* and *IFITM1* [64–66]. Moreover, many miRNAs target the 3'UTR site of matrix metalloprotease-encoding genes. For instance, *MIR34a* and *MIR19* target *NFKBIA* [67] (critical for SARS-CoV-2 entry in the cells) and *MMP9* [68] (macrophage-derived biomarker associated with inflammation), whereas *MIR130a* targets the 3'UTR of pro-inflammatory metabolite genes (e.g. *LOX* [69] that interacts with SARS-CoV-2) [70]. Altogether, different culture models are necessary to validate the biological effect of these candidate miRNAs to SARS-CoV-2 infection and to understand the interactions between host ISGs, cytokines and miRNAs. More investigations are needed to determine the expression profiles of key miRNAs during viral infection, to better predict disease severity, and to develop new therapeutic options based on these miRNAs for COVID-19 treatment and/or prevention.

Conclusions

Here, we characterized of two ALI and iALI airway models to understand SARS-CoV-2 infection pathogenesis. We identified the inflammatory and interferon profiles induced in these models in response to SARS-CoV-2 infection. Understanding the long COVID19 effects remains a challenge and will require also these models.

Funding

Supported by grants from the University Hospital of Montpellier (Appel d'offre interne, projet CILIPS 9174, projet INVECCO), the association Vaincre la Mucoviscidose (Grant #RIF20170502048), the Fondation pour la Recherche Médicale (Grant #FDM20170638083),

bioRxiv preprint doi: https://doi.org/10.1101/2023.04.15.536998; this version posted April 17, 2023. The copyright holder for this preprint (which was not certified by peer review) is the author/funder, who has granted bioRxiv a license to display the preprint in perpetuity. It is made available under aCC-BY-NC-ND 4.0 International license.

the Labex Numev (ANR-10-LAB-20), and Astrazenca. The acquisition of the Cell-Discoverer 7 LSM900 microscope was funded by FEDER-FSE Région Occitanie throughout the MIP-FISH project. Part of this research project was supported by the CNRS INSB funding through the VIROCRIB program.

Author contributions

Conceptualization and supervision: S.A., A.B and J.D.V.; Resources, A.B., J.D.V.; Data analysis and interpretation: S.A., A.B, A.N., S.W., N.G., D.M., A.B., J.D.V; Collection and/or assembly of data: S.A., E.A, F.F., C.B., A.P., I.V., D.M., A.B., J.D.V; Validation, L.M., N.G., D.M.; Writing – Original Draft, S.A, A.B, J.D.V.; Writing – Review & Editing, S.A., E.A, L.M., D.M., A.B., J.D.V.. Scientific and technical support: all authors listed have made a substantial, direct, intellectual contribution to the work, reviewed the final manuscript, and approved it for publication

Ethics declarations

Ethics approval and consent to participate

Subjects were recruited at Arnaud de Villeneuve hospital, Montpellier, France, under study protocols approved by the ethics committee - RRR study, NCT02354677, 2013-A01405-40 and INVECCO study, NCT03181204, 2017-A00252-51. All patients have been informed and agreed to participate by signing written consent forms.

Conflict of interest

A.B. reports grants, personal fees, non-financial support and other from AstraZeneca; J.D.V. reports personal fees and other from Stem Genomics, personal fees and other from MedXCell Science, personal fees from Gilead, personal fees from Celgene, outside the submitted work. In addition, J.D.V. and S.A. have a pending patent EP20150306389. S.A. reports personal

bioRxiv preprint doi: https://doi.org/10.1101/2023.04.15.536998; this version posted April 17, 2023. The copyright holder for this preprint (which was not certified by peer review) is the author/funder, who has granted bioRxiv a license to display the preprint in perpetuity. It is made available under aCC-BY-NC-ND 4.0 International license.

fees and other from Stem Genomics, outside the submitted work. E.A, L.M., A.N., F.F., C.B., S.W., A.P., I.V., D.M., declare no conflict of interest.

Data set availability

Publicly available data were obtained from GEO datasets: GSE147507 and GSE166766**.** Interactive exploration tools: https://www.covid19cellatlas.org/index.healthy.html and https://cellxgene.cziscience.com/d/cellular_census_of_human_lungs_bronchi-17.cxg/. The gene expression profile from publicly RNA-seq data can be browsed with an interactive web-tool at: https://crem.shinyapps.io/iAEC2infection/ (GSE153277).

Figures

Figure 1: **Distribution of the different airway epithelial cell types the three lung tissue models**. (A) Schematic representation of the scRNA-seq experimental workflow: airway epithelium sources (biopsy/brushing-derived cells, ALI culture of primary bronchial epithelial cells and iALI culture of iPSC-derived epithelial-like cells), generation of scRNA-seq libraries and sequencing, computational analysis to identify cell types. The brushing/biopsy epithelium scRNA-seq data were from [24]. The ALI and iALI scRNA-seq data were generated in our laboratory (see Methods). (B) Contribution of each cell type in the three models. UMAP and tSNE were used to show the contribution of *SCGB1A1*+, *TP63*+, *FOXJ1*+, *FOXI1*, *POU2F3*+, and *ASCL1*+ cells (dark gray). (C) UMAP projection of the different cell types. The feature plots display the subset of airway epithelial cells obtained from biopsy/brushing of healthy donors [24]. (D) Maps of the expression of ssRNA virus receptors in single cells from the three models. UMAP and tSNE were used to show the cell types that express the ACE2, CDHR3 and CD55 receptors.

bioRxiv preprint doi: https://doi.org/10.1101/2023.04.15.536998; this version posted April 17, 2023. The copyright holder for this preprint (which was not certified by peer review) is the author/funder, who has granted bioRxiv a license to display the preprint in perpetuity. It is made available under aCC-BY-NC-ND 4.0 International license.

555

556 **Figure 2: Analysis of GO terms enriched in the unique bulk RNA-seq signature of the**
557 **ALI model upon SARS-CoV-2 infection**. (A) Pathway enrichment analyses were performed
558 with human gene names. The size of the blue dots corresponds to the enrichment (FDR) and
559 bigger dots indicate more significant *p*-values. The biological process, molecular function,
560 and cellular component categories revealed the high enrichment of immune response and
561 cytokine/chemokine activities upon SARS-CoV-2 infection. (B) GSEA performed using the
562 unique bulk RNA-seq signature upon SARS-CoV-2 infection. The heat map shows the
563 (clustered) genes in the leading-edge subsets and the dynamic expression of genes involved in
564 immune response, interferon response, defense response, TNF-signaling and response to
565 cytokines. (C) Enrichment heat map (IPA) showing the dynamic activity of canonical
566 pathways after SARS-CoV-2 infection. Each colored rectangle is a biological function and the
567 color range indicates its activation state (orange for an activated pathway with Z-score > 2,
568 and blue for an inhibited pathway with Z-score <–2). The pathways were classified into
569 different types according to the IPA database. (D) The network shows the interactions of
570 interferon (IFN)-stimulated genes. Nodes shaded in pink represent protein-coding genes that
571 are upregulated in the ALI model upon SARS-CoV-2 infection. Labels in nodes and edges
572 (lines) illustrate the nature of the relationship between genes and their functions. A dotted line
573 represents an indirect interaction and a solid line a direct interaction. IPA, Ingenuity Pathway
574 Analysis. GO, Gene Ontology.

575

576 **Figure 3**: **Dynamic gene expression changes in the iALI model upon SARS-CoV-2**
577 **infection**. Expression levels of (A) inflammatory cytokines/chemokines, including (a) genes
578 that were upregulated early and the expression of which gradually increased upon SARS-
579 CoV-2 infection, from 1 to 4 dpi; (b) genes that were upregulated early and the expression of

bioRxiv preprint doi: https://doi.org/10.1101/2023.04.15.536998; this version posted April 17, 2023. The copyright holder for this preprint (which was not certified by peer review) is the author/funder, who has granted bioRxiv a license to display the preprint in perpetuity. It is made available under aCC-BY-NC-ND 4.0 International license.

580 which remained constant between 1 and 4 dpi; (c) genes that were upregulated specifically at
581 1 dpi and were then downregulated at 4 dpi; and (d) genes that became upregulated at 4 dpi.
582 Expression of genes implicated in the (B) interferon response, (C) extracellular matrix, and
583 (D) epithelial/stromal gene upon. Normalized expression levels (counts per million reads)
584 were quantified by RNA-seq using data from [16] (human iPSC-derived AT2 cells infected or
585 not with SARS-CoV-2).
586
587 **Figure 4**: **Validation of SARS-CoV-2 infection in the iALI model.** (A) iALI cultures were
588 infected with SARS-CoV-2 Delta (MOI=0.05) and viral RNA was quantified by RT-qPCR
589 (gene E/mL). iALI cultures were washed by adding culture medium at the apical side at 37°C
590 for 15 min, then viral RNA was extracted and quantified in triplicate by RT-qPCR
591 (amplification of the viral envelope gene). Data are from three independent experiment (a, b,
592 c) using three different iALI cultures. The standard deviation shows the result variability. (B)
593 iALI cultures were stained with anti-SARS-CoV-2 M protein (viral membrane, green), anti-α-
594 tubulin (ciliated cell marker, orange) and anti-P63 (basal cell marker, red) antibodies. Nuclei
595 were counterstained with DAPI (blue). SARS-CoV-2 was identified on the motile cilia. Scale
596 bar: 20 µm. (C) RT-qPCR analysis of the expression of genes encoding inflammatory and
597 interferon-related factors in iALI cultures infected with SARS-CoV-2 (MOI 0.05) at 1 dpi and
598 4 dpi. Data are the mean ± SEM of three independent experiments with three technical
599 replicates/each (9 samples); $^{*}p < 0.05$, $^{**}p < 0.01$, $^{***}p < 0.001$, $^{****}p < 0.0001$, ns: not significant
600 (Student's *t* test). (D) Transepithelial resistance was measured daily with an EVOM2 (WPI,
601 Friedberg, Germany), while the apical side was submerged with culture medium.
602 Measurement were done after 10 min of incubation at 37°C. MOI: multiplicity of cellular
603 infection.
604

bioRxiv preprint doi: https://doi.org/10.1101/2023.04.15.536998; this version posted April 17, 2023. The copyright holder for this preprint (which was not certified by peer review) is the author/funder, who has granted bioRxiv a license to display the preprint in perpetuity. It is made available under aCC-BY-NC-ND 4.0 International license.

Figure 5: Paracrine interactions and single-cell trajectories in SARS-CoV-2-infected ALI cultures. (A) Circos plot showing potential interactions (ligands-receptors) made by various epithelial cell types in non-infected (Mock) and SARS-CoV-2-infected ALI cultures at 1, 2, and 3 dpi. The smallest number of paracrine interactions was observed in infected cultures at 2 and 3 dpi. Arrows point to the receptors. (B) Violin plots showing the expression of the ligand *ARTN* and its receptor *RET* in the various airway cell types identified by scRNA-seq before (CTR) and after SARS-CoV-2 infection (1 and 3 dpi). (C) The velocity field revealed two distinct tracks used by basal cells to form ciliated cells in non-infected ALI cultures (mock), but not in SARS-CoV-2-infected cultures (2 dpi). (D) Left, gene expression of known markers of premature (*FOXJ1*+) and mature ciliated cells (*DNAH9*+) is visualized on the t-SNE plot in the mock sample. Right, the t-SNE plot shows the absence of mature ciliated cells (*DNAH9*+) at 2 dpi.

Figure 6: **Identification of miRNA targets as potential COVID-19 therapeutics.** Schematic representation of potential miRNAs that target some genes implicated in the interferon and inflammatory responses upon SARS-CoV-2 infection of ALI cultures. Only the miRNAs experimentally validated are represented. In the figure change into: Number of miRNAs targeting a gene.

Supplementary Tables

Table S1: Primer pairs used for validation by RT-qPCR

Table S2: List of the 515 genes specific to the SARS-CoV-2 bulk RNA-seq signature (transcriptome analysis by Blanco-Melo, D et al. [20]).

Table S3: List of the top GO categories identified by Ingenuity Pathway Analysis using the 515 genes listed in Table S2.

bioRxiv preprint doi: https://doi.org/10.1101/2023.04.15.536998; this version posted April 17, 2023. The copyright holder for this preprint (which was not certified by peer review) is the author/funder, who has granted bioRxiv a license to display the preprint in perpetuity. It is made available under aCC-BY-NC-ND 4.0 International license.

Table S4: List of the 146 enriched canonical pathways identified in the SARS-CoV-2 bulk RNA-seq signature.

Table S5: Lists of genes targeted by the upstream regulator's *TNF*, *IL1A* and *F2* identified using IPA Upstream Regulator Analysis.

Table S6: Exhaustive lists of miRNAs that are putative regulators of genes implicated in interferon and inflammatory responses upon SARS-CoV-2 infection of ALI cultures retrieved by GenGo Metacore.

Supplementary Figure

Figure S1: Mechanistic networks showing the interactions between upstream regulators (*TNF*, *IL1A*, *F2*) and their target genes identified in the SARS-CoV-2 bulk RNA-seq signature. The IPA upstream regulator analysis is based on the expected causal effects between upstream regulators and targets.

References

1. Hoffmann M, Kleine-Weber H, Schroeder S, Krüger N, Herrler T, Erichsen S, et al. SARS-CoV-2 Cell Entry Depends on ACE2 and TMPRSS2 and Is Blocked by a Clinically Proven Protease Inhibitor. Cell. 2020;181:271-280.e8.

2. Jelev V, Mermerski K, Djakov L, Vassilev V. [Cases of mycoplasma abortion in swine]. Zentralblatt Vet Reihe B J Vet Med Ser B. 1972;19:588–97.

3. Bracquemond D, Muriaux D. Betacoronavirus Assembly: Clues and Perspectives for Elucidating SARS-CoV-2 Particle Formation and Egress. mBio. 2021;12:e0237121.

4. Hiemstra PS, Tetley TD, Janes SM. Airway and alveolar epithelial cells in culture. Eur Respir J. 2019;54:1900742.

5. Knabe L, Petit A, Vernisse C, Charriot J, Pugnière M, Henriquet C, et al. CCSP counterbalances airway epithelial-driven neutrophilic chemotaxis. Eur Respir J. 2019;54:1802408.

6. Ahmed E, Fieldes M, Bourguignon C, Mianné J, Petit A, Jory M, et al. Differentiation of Human Induced Pluripotent Stem Cells from Patients with Severe COPD into Functional Airway Epithelium. Cells. 2022;11:2422.

bioRxiv preprint doi: https://doi.org/10.1101/2023.04.15.536998; this version posted April 17, 2023. The copyright holder for this preprint (which was not certified by peer review) is the author/funder, who has granted bioRxiv a license to display the preprint in perpetuity. It is made available under aCC-BY-NC-ND 4.0 International license.

7. Huang SXL, Islam MN, O'Neill J, Hu Z, Yang Y-G, Chen Y-W, et al. Efficient generation of lung and airway epithelial cells from human pluripotent stem cells. Nat Biotechnol. 2014;32:84–91.

8. McCauley KB, Hawkins F, Serra M, Thomas DC, Jacob A, Kotton DN. Efficient Derivation of Functional Human Airway Epithelium from Pluripotent Stem Cells via Temporal Regulation of Wnt Signaling. Cell Stem Cell. 2017;20:844-857.e6.

9. McCauley KB, Alysandratos K-D, Jacob A, Hawkins F, Caballero IS, Vedaie M, et al. Single-Cell Transcriptomic Profiling of Pluripotent Stem Cell-Derived SCGB3A2+ Airway Epithelium. Stem Cell Rep. 2018;10:1579–95.

10. Pezzulo AA, Starner TD, Scheetz TE, Traver GL, Tilley AE, Harvey B-G, et al. The air-liquid interface and use of primary cell cultures are important to recapitulate the transcriptional profile of in vivo airway epithelia. Am J Physiol Lung Cell Mol Physiol. 2011;300:L25-31.

11. Dvorak A, Tilley AE, Shaykhiev R, Wang R, Crystal RG. Do airway epithelium air-liquid cultures represent the in vivo airway epithelium transcriptome? Am J Respir Cell Mol Biol. 2011;44:465–73.

12. Shirato K, Kawase M, Matsuyama S. Wild-type human coronaviruses prefer cell-surface TMPRSS2 to endosomal cathepsins for cell entry. Virology. 2018;517:9–15.

13. Djidrovski I, Georgiou M, Hughes GL, Patterson EI, Casas-Sanchez A, Pennington SH, et al. SARS-CoV-2 infects an upper airway model derived from induced pluripotent stem cells. Stem Cells Dayt Ohio. 2021;39:1310–21.

14. Abo KM, Ma L, Matte T, Huang J, Alysandratos KD, Werder RB, et al. Human iPSC-derived alveolar and airway epithelial cells can be cultured at air-liquid interface and express SARS-CoV-2 host factors. BioRxiv Prepr Serv Biol. 2020;2020.06.03.132639.

15. Vanderheiden A, Ralfs P, Chirkova T, Upadhyay AA, Zimmerman MG, Bedoya S, et al. Type I and Type III Interferons Restrict SARS-CoV-2 Infection of Human Airway Epithelial Cultures. J Virol. 2020;94:e00985-20.

16. Huang J, Hume AJ, Abo KM, Werder RB, Villacorta-Martin C, Alysandratos K-D, et al. SARS-CoV-2 Infection of Pluripotent Stem Cell-Derived Human Lung Alveolar Type 2 Cells Elicits a Rapid Epithelial-Intrinsic Inflammatory Response. Cell Stem Cell. 2020;27:962-973.e7.

17. Osan JK, DeMontigny BA, Mehedi M. Immunohistochemistry for protein detection in PFA-fixed paraffin-embedded SARS-CoV-2-infected COPD airway epithelium. STAR Protoc. 2021;2:100663.

18. Ahmed E, Sansac C, Assou S, Gras D, Petit A, Vachier I, et al. Lung development, regeneration and plasticity: From disease physiopathology to drug design using induced pluripotent stem cells. Pharmacol Ther. 2018;183:58–77.

19. Gordon DE, Jang GM, Bouhaddou M, Xu J, Obernier K, White KM, et al. A SARS-CoV-2 protein interaction map reveals targets for drug repurposing. Nature. 2020;583:459–68.

bioRxiv preprint doi: https://doi.org/10.1101/2023.04.15.536998; this version posted April 17, 2023. The copyright holder for this preprint (which was not certified by peer review) is the author/funder, who has granted bioRxiv a license to display the preprint in perpetuity. It is made available under aCC-BY-NC-ND 4.0 International license.

20. Blanco-Melo D, Nilsson-Payant BE, Liu W-C, Uhl S, Hoagland D, Møller R, et al. Imbalanced Host Response to SARS-CoV-2 Drives Development of COVID-19. Cell. 2020;181:1036-1045.e9.

21. Messina F, Giombini E, Agrati C, Vairo F, Ascoli Bartoli T, Al Moghazi S, et al. COVID-19: viral-host interactome analyzed by network based-approach model to study pathogenesis of SARS-CoV-2 infection. J Transl Med. 2020;18:233.

22. Lukassen S, Chua RL, Trefzer T, Kahn NC, Schneider MA, Muley T, et al. SARS-CoV-2 receptor ACE2 and TMPRSS2 are primarily expressed in bronchial transient secretory cells. EMBO J. 2020;39:e105114.

23. Fiege JK, Thiede JM, Nanda HA, Matchett WE, Moore PJ, Montanari NR, et al. Single cell resolution of SARS-CoV-2 tropism, antiviral responses, and susceptibility to therapies in primary human airway epithelium. PLoS Pathog. 2021;17:e1009292.

24. Vieira Braga FA, Kar G, Berg M, Carpaij OA, Polanski K, Simon LM, et al. A cellular census of human lungs identifies novel cell states in health and in asthma. Nat Med. 2019;25:1153–63.

25. Ravindra NG, Alfajaro MM, Gasque V, Huston NC, Wan H, Szigeti-Buck K, et al. Single-cell longitudinal analysis of SARS-CoV-2 infection in human airway epithelium identifies target cells, alterations in gene expression, and cell state changes. PLoS Biol. 2021;19:e3001143.

26. Bergen V, Lange M, Peidli S, Wolf FA, Theis FJ. Generalizing RNA velocity to transient cell states through dynamical modeling. Nat Biotechnol. 2020;38:1408–14.

27. Hao Y, Hao S, Andersen-Nissen E, Mauck WM, Zheng S, Butler A, et al. Integrated analysis of multimodal single-cell data. Cell. 2021;184:3573-3587.e29.

28. Cabello-Aguilar S, Alame M, Kon-Sun-Tack F, Fau C, Lacroix M, Colinge J. SingleCellSignalR: inference of intercellular networks from single-cell transcriptomics. Nucleic Acids Res. 2020;48:e55.

29. Corman VM, Landt O, Kaiser M, Molenkamp R, Meijer A, Chu DK, et al. Detection of 2019 novel coronavirus (2019-nCoV) by real-time RT-PCR. Euro Surveill Bull Eur Sur Mal Transm Eur Commun Dis Bull. 2020;25:2000045.

30. Zhang Z, Zhu Z, Chen W, Cai Z, Xu B, Tan Z, et al. Cell membrane proteins with high N-glycosylation, high expression and multiple interaction partners are preferred by mammalian viruses as receptors. Bioinforma Oxf Engl. 2019;35:723–8.

31. Mason PR, Gwanzura L. Reduced lymphocyte responses to mitogens in natural and experimental trichomoniasis. Infect Immun. 1990;58:3553–7.

32. Yeo SJ, Yun YJ, Lyu MA, Woo SY, Woo ER, Kim SJ, et al. Respiratory syncytial virus infection induces matrix metalloproteinase-9 expression in epithelial cells. Arch Virol. 2002;147:229–42.

bioRxiv preprint doi: https://doi.org/10.1101/2023.04.15.536998; this version posted April 17, 2023. The copyright holder for this preprint (which was not certified by peer review) is the author/funder, who has granted bioRxiv a license to display the preprint in perpetuity. It is made available under aCC-BY-NC-ND 4.0 International license.

734 33. Vermeer PD, Denker J, Estin M, Moninger TO, Keshavjee S, Karp P, et al. MMP9
735 modulates tight junction integrity and cell viability in human airway epithelia. Am J Physiol
736 Lung Cell Mol Physiol. 2009;296:L751-762.

737 34. Mecham RP, Broekelmann TJ, Fliszar CJ, Shapiro SD, Welgus HG, Senior RM. Elastin
738 degradation by matrix metalloproteinases. Cleavage site specificity and mechanisms of
739 elastolysis. J Biol Chem. 1997;272:18071–6.

740 35. Montoro DT, Haber AL, Biton M, Vinarsky V, Lin B, Birket SE, et al. A revised airway
741 epithelial hierarchy includes CFTR-expressing ionocytes. Nature. 2018;560:319–24.

742 36. Plasschaert LW, Žilionis R, Choo-Wing R, Savova V, Knehr J, Roma G, et al. A single-
743 cell atlas of the airway epithelium reveals the CFTR-rich pulmonary ionocyte. Nature.
744 2018;560:377–81.

745 37. Goldfarbmuren KC, Jackson ND, Sajuthi SP, Dyjack N, Li KS, Rios CL, et al. Dissecting
746 the cellular specificity of smoking effects and reconstructing lineages in the human airway
747 epithelium. Nat Commun. 2020;11:2485.

748 38. Barkauskas CE, Chung M-I, Fioret B, Gao X, Katsura H, Hogan BLM. Lung organoids:
749 current uses and future promise. Dev Camb Engl. 2017;144:986–97.

750 39. Miller AJ, Hill DR, Nagy MS, Aoki Y, Dye BR, Chin AM, et al. In Vitro Induction and
751 In Vivo Engraftment of Lung Bud Tip Progenitor Cells Derived from Human Pluripotent
752 Stem Cells. Stem Cell Rep. 2018;10:101–19.

753 40. Chen Y-W, Huang SX, de Carvalho ALRT, Ho S-H, Islam MN, Volpi S, et al. A three-
754 dimensional model of human lung development and disease from pluripotent stem cells. Nat
755 Cell Biol. 2017;19:542–9.

756 41. Huang SXL, Green MD, de Carvalho AT, Mumau M, Chen Y-W, D'Souza SL, et al. The
757 in vitro generation of lung and airway progenitor cells from human pluripotent stem cells. Nat
758 Protoc. 2015;10:413–25.

759 42. Wohnhaas CT, Gindele JA, Kiechle T, Shen Y, Leparc GG, Stierstorfer B, et al. Cigarette
760 Smoke Specifically Affects Small Airway Epithelial Cell Populations and Triggers the
761 Expansion of Inflammatory and Squamous Differentiation Associated Basal Cells. Int J Mol
762 Sci. 2021;22:7646.

763 43. Zhu N, Wang W, Liu Z, Liang C, Wang W, Ye F, et al. Morphogenesis and cytopathic
764 effect of SARS-CoV-2 infection in human airway epithelial cells. Nat Commun.
765 2020;11:3910.

766 44. Chien J-Y, Hsueh P-R, Cheng W-C, Yu C-J, Yang P-C. Temporal changes in
767 cytokine/chemokine profiles and pulmonary involvement in severe acute respiratory
768 syndrome. Respirol Carlton Vic. 2006;11:715–22.

769 45. Melchjorsen J, Sørensen LN, Paludan SR. Expression and function of chemokines during
770 viral infections: from molecular mechanisms to in vivo function. J Leukoc Biol. 2003;74:331–
771 43.

bioRxiv preprint doi: https://doi.org/10.1101/2023.04.15.536998; this version posted April 17, 2023. The copyright holder for this preprint (which was not certified by peer review) is the author/funder, who has granted bioRxiv a license to display the preprint in perpetuity. It is made available under aCC-BY-NC-ND 4.0 International license.

772 46. McGonagle D, Sharif K, O'Regan A, Bridgewood C. The Role of Cytokines including
773 Interleukin-6 in COVID-19 induced Pneumonia and Macrophage Activation Syndrome-Like
774 Disease. Autoimmun Rev. 2020;19:102537.

775 47. Brocker C, Thompson D, Matsumoto A, Nebert DW, Vasiliou V. Evolutionary divergence
776 and functions of the human interleukin (IL) gene family. Hum Genomics. 2010;5:30–55.

777 48. Hunter CA, Jones SA. IL-6 as a keystone cytokine in health and disease. Nat Immunol.
778 2015;16:448–57.

779 49. McDermott JE, Mitchell HD, Gralinski LE, Eisfeld AJ, Josset L, Bankhead A, et al. The
780 effect of inhibition of PP1 and TNFα signaling on pathogenesis of SARS coronavirus. BMC
781 Syst Biol. 2016;10:93.

782 50. Lee JS, Park S, Jeong HW, Ahn JY, Choi SJ, Lee H, et al. Immunophenotyping of
783 COVID-19 and influenza highlights the role of type I interferons in development of severe
784 COVID-19. Sci Immunol. 2020;5:eabd1554.

785 51. Zhou Z, Ren L, Zhang L, Zhong J, Xiao Y, Jia Z, et al. Heightened Innate Immune
786 Responses in the Respiratory Tract of COVID-19 Patients. Cell Host Microbe. 2020;27:883-
787 890.e2.

788 52. Honda K, Yanai H, Negishi H, Asagiri M, Sato M, Mizutani T, et al. IRF-7 is the master
789 regulator of type-I interferon-dependent immune responses. Nature. 2005;434:772–7.

790 53. Schneider WM, Chevillotte MD, Rice CM. Interferon-stimulated genes: a complex web of
791 host defenses. Annu Rev Immunol. 2014;32:513–45.

792 54. Li G, Fan Y, Lai Y, Han T, Li Z, Zhou P, et al. Coronavirus infections and immune
793 responses. J Med Virol. 2020;92:424–32.

794 55. George PM, Wells AU, Jenkins RG. Pulmonary fibrosis and COVID-19: the potential role
795 for antifibrotic therapy. Lancet Respir Med. 2020;8:807–15.

796 56. Ueland T, Holter JC, Holten AR, Müller KE, Lind A, Bekken GK, et al. Distinct and early
797 increase in circulating MMP-9 in COVID-19 patients with respiratory failure. J Infect.
798 2020;81:e41–3.

799 57. Hsu AT, Barrett CD, DeBusk GM, Ellson CD, Gautam S, Talmor DS, et al. Kinetics and
800 Role of Plasma Matrix Metalloproteinase-9 Expression in Acute Lung Injury and the Acute
801 Respiratory Distress Syndrome. Shock Augusta Ga. 2015;44:128–36.

802 58. Suprewicz Ł, Swoger M, Gupta S, Piktel E, Byfield FJ, Iwamoto DV, et al. Extracellular
803 vimentin as a target against SARS-CoV-2 host cell invasion. BioRxiv Prepr Serv Biol.
804 2021;2021.01.08.425793.

805 59. Sigrist CJ, Bridge A, Le Mercier P. A potential role for integrins in host cell entry by
806 SARS-CoV-2. Antiviral Res. 2020;177:104759.

807 60. Trobaugh DW, Klimstra WB. MicroRNA Regulation of RNA Virus Replication and
808 Pathogenesis. Trends Mol Med. 2017;23:80–93.

bioRxiv preprint doi: https://doi.org/10.1101/2023.04.15.536998; this version posted April 17, 2023. The copyright holder for this preprint (which was not certified by peer review) is the author/funder, who has granted bioRxiv a license to display the preprint in perpetuity. It is made available under aCC-BY-NC-ND 4.0 International license.

809 61. Hanna J, Hossain GS, Kocerha J. The Potential for microRNA Therapeutics and Clinical
810 Research. Front Genet. 2019;10:478.

811 62. Zuo C, Sheng X, Liu Z, Ma M, Xiong S, Deng H, et al. MicroRNA-138 enhances TRAIL-
812 induced apoptosis through interferon-stimulated gene 15 downregulation in hepatocellular
813 carcinoma cells. Tumour Biol J Int Soc Oncodevelopmental Biol Med.
814 2017;39:1010428317710410.

815 63. Chai W, Li J, Shangguan Q, Liu Q, Li X, Qi D, et al. Lnc-ISG20 Inhibits Influenza A
816 Virus Replication by Enhancing ISG20 Expression. J Virol. 2018;92:e00539-18.

817 64. Pichulik T, Khatamzas E, Liu X, Brain O, Delmiro Garcia M, Leslie A, et al. Pattern
818 recognition receptor mediated downregulation of microRNA-650 fine-tunes MxA expression
819 in dendritic cells infected with influenza A virus. Eur J Immunol. 2016;46:167–77.

820 65. Liang Y, Li E, Min J, Gong C, Gao J, Ai J, et al. miR□29a suppresses the growth and
821 metastasis of hepatocellular carcinoma through IFITM3. Oncol Rep. 2018;40:3261–72.

822 66. Bhanja Chowdhury J, Shrivastava S, Steele R, Di Bisceglie AM, Ray R, Ray RB.
823 Hepatitis C virus infection modulates expression of interferon stimulatory gene IFITM1 by
824 upregulating miR-130A. J Virol. 2012;86:10221–5.

825 67. Hart M, Walch-Rückheim B, Friedmann KS, Rheinheimer S, Tänzer T, Glombitza B, et
826 al. miR-34a: a new player in the regulation of T cell function by modulation of NF-κB
827 signaling. Cell Death Dis. 2019;10:46.

828 68. Jia L-F, Wei S-B, Mitchelson K, Gao Y, Zheng Y-F, Meng Z, et al. miR-34a inhibits
829 migration and invasion of tongue squamous cell carcinoma via targeting MMP9 and MMP14.
830 PloS One. 2014;9:e108435.

831 69. Boufraqech M, Nilubol N, Zhang L, Gara SK, Sadowski SM, Mehta A, et al. miR30a
832 inhibits LOX expression and anaplastic thyroid cancer progression. Cancer Res.
833 2015;75:367–77.

834 70. Seethy AA, Singh S, Mukherjee I, Pethusamy K, Purkayastha K, Sharma JB, et al.
835 Potential SARS-CoV-2 interactions with proteins involved in trophoblast functions - An in-
836 silico study. Placenta. 2021;103:141–51.

837

Figure 1

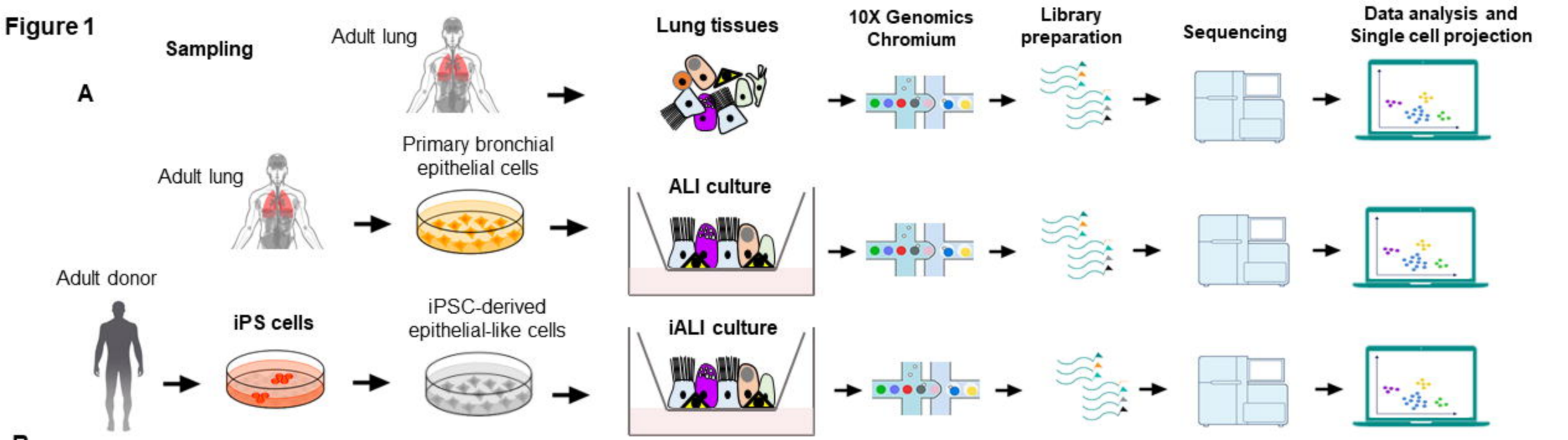

B

Epithelial Cell type	Marker	Model		
		Biopsy -brushing	ALI	iALI
Secretory cells	SCGB1A1	●	●	●
Basal cells	TP63	●	●	●
Ciliated cells	FOXJ1	●	●	●
Ionocyte cells	FOXI1	●	●	●
Tuft cells	POU2F3	●	●	●
Neuroendocrine cells	ASCL1	●	●	●

● Under-represented
● Overrepresented

C

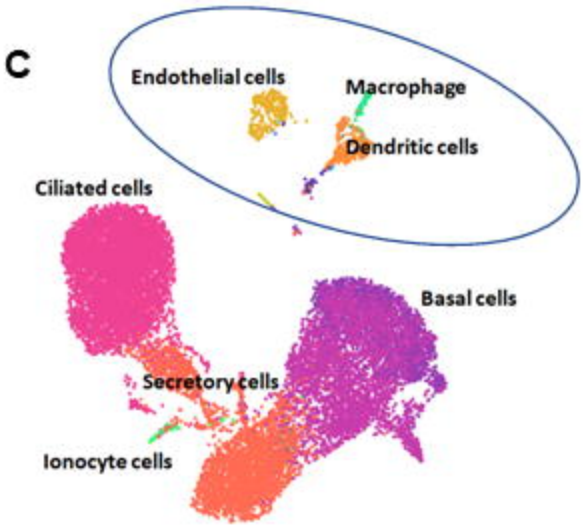

D

ssRNA virus	Receptor	Model		
		Biopsy - brushing	ALI	iALI
SARS Coronavirus	ACE2			
Rhino- Virus C	CDHR3			
Coxsackie-Virus B1	CD55			

Ciliated cells
Secretory cells
Basal cells
Ionocyte cells

Figure 2

A

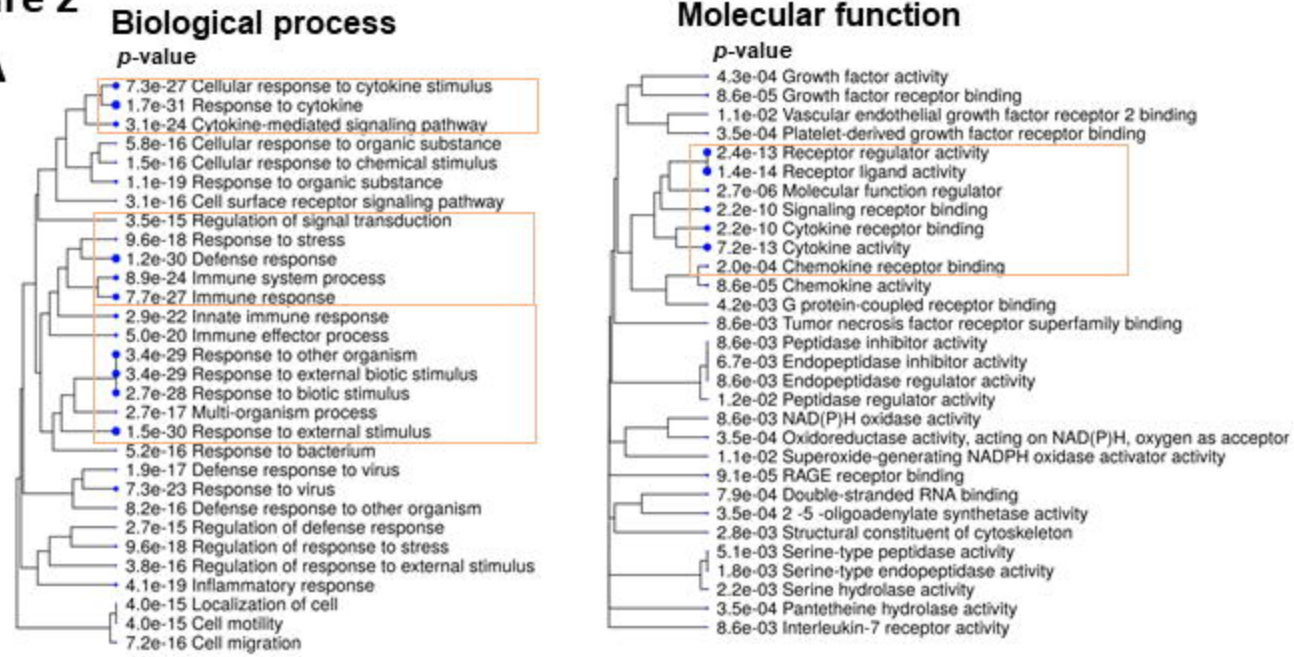

B

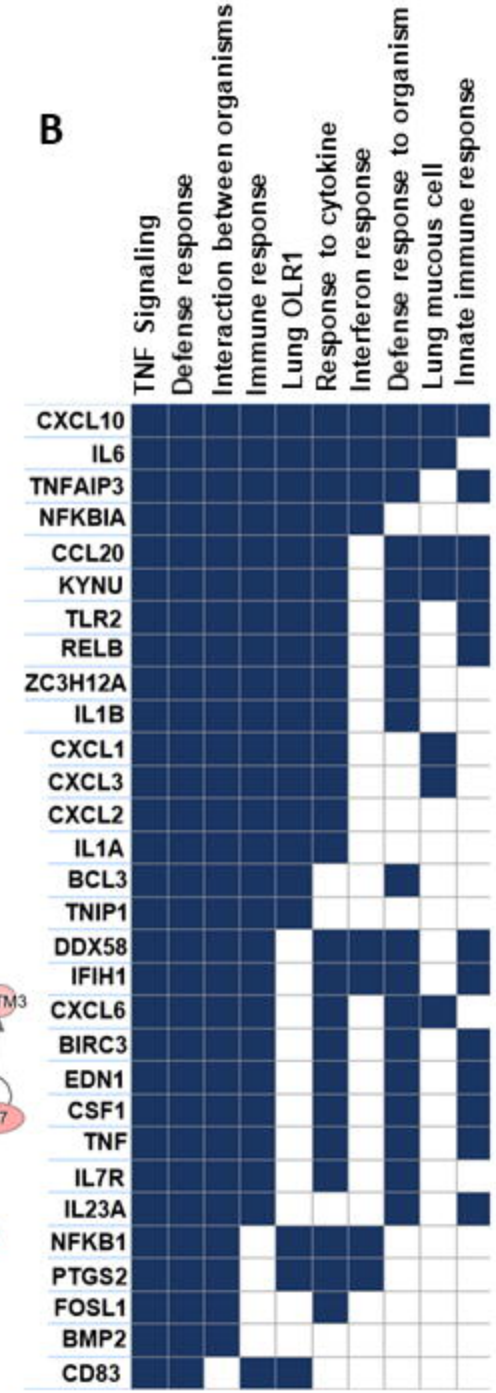

C

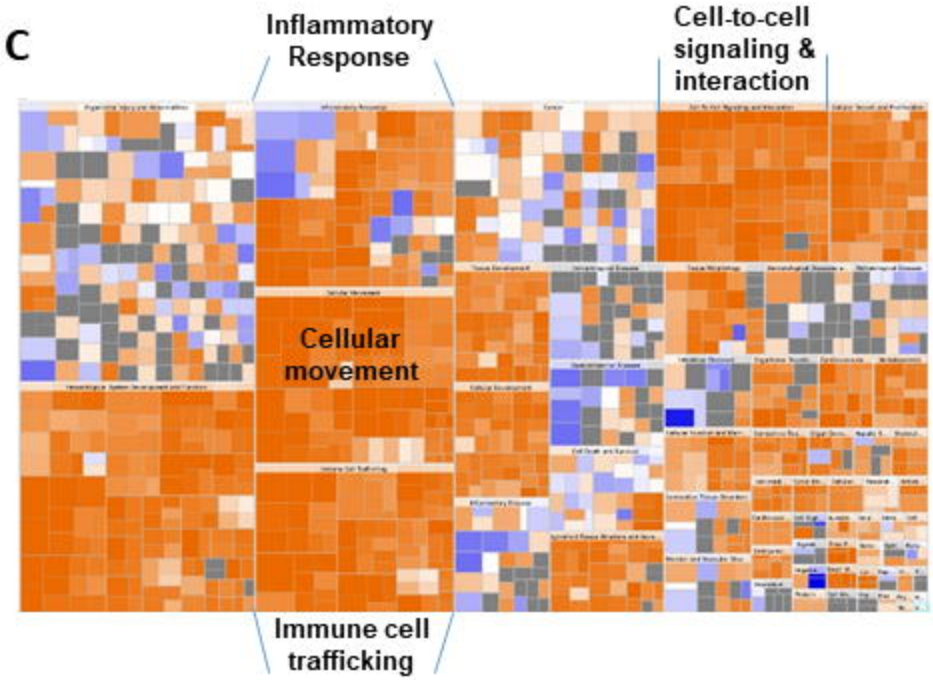

D

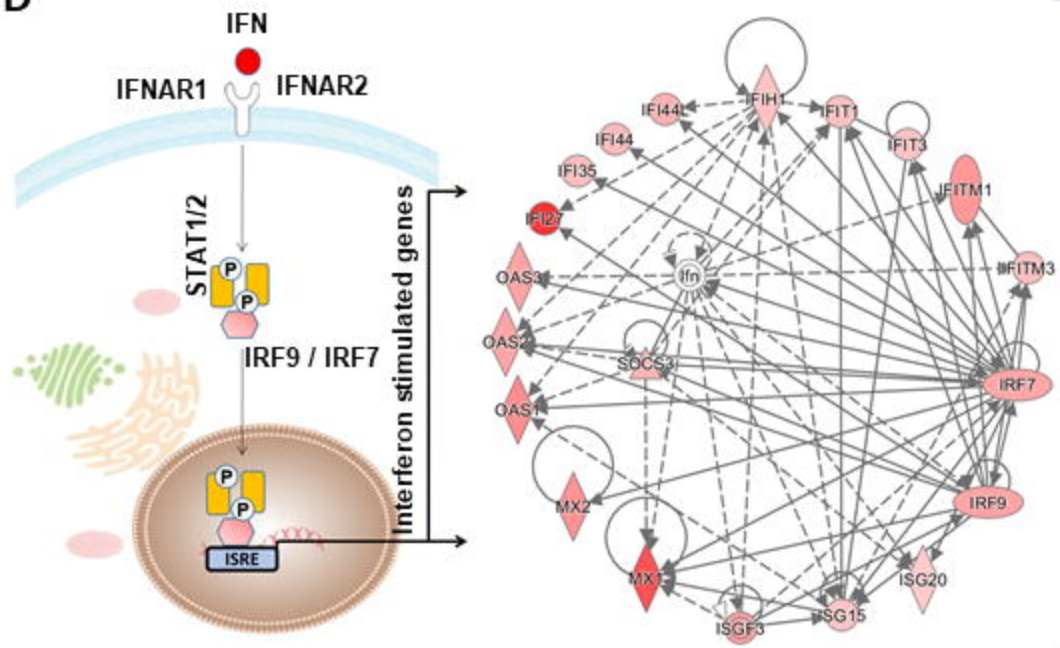

Figure 3

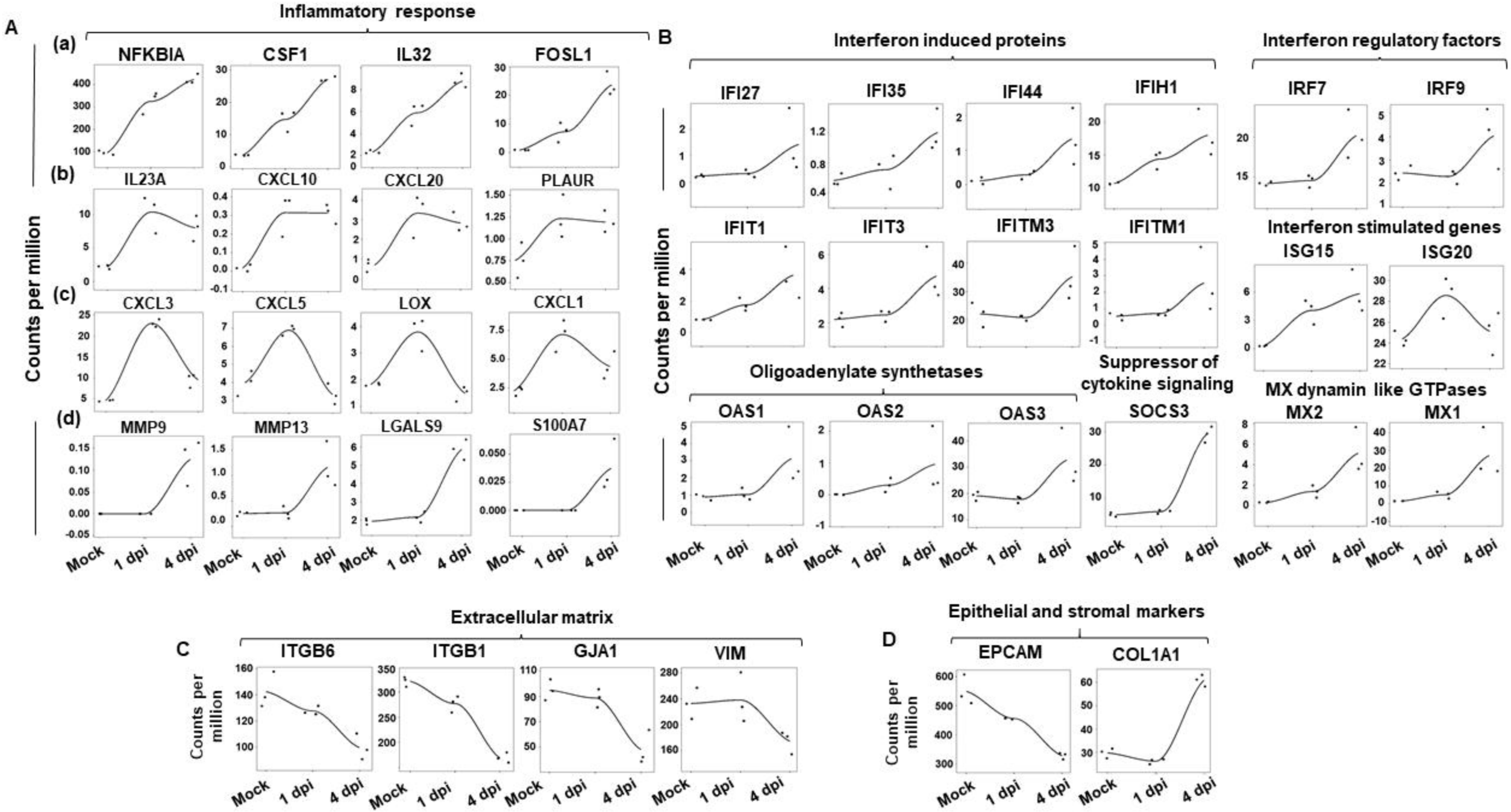
A
Inflammatory response
(a)
NFKBIA
CSF1
IL32
FOSL1
(b)
IL23A
CXCL10
CXCL20
PLAUR
(c)
CXCL3
CXCL5
LOX
CXCL1
(d)
MMP9
MMP13
LGALS9
S100A7
Counts per million
Mock
1 dpi
4 dpi
B
Interferon induced proteins
IFI27
IFI35
IFI44
IFIH1
IFIT1
IFIT3
IFITM3
IFITM1
Interferon regulatory factors
IRF7
IRF9
Interferon stimulated genes
ISG15
ISG20
Oligoadenylate synthetases
OAS1
OAS2
OAS3
Suppressor of cytokine signaling
SOCS3
MX dynamin like GTPases
MX2
MX1
C
Extracellular matrix
ITGB6
ITGB1
GJA1
VIM
Counts per million
D
Epithelial and stromal markers
EPCAM
COL1A1
Counts per million

Figure 4

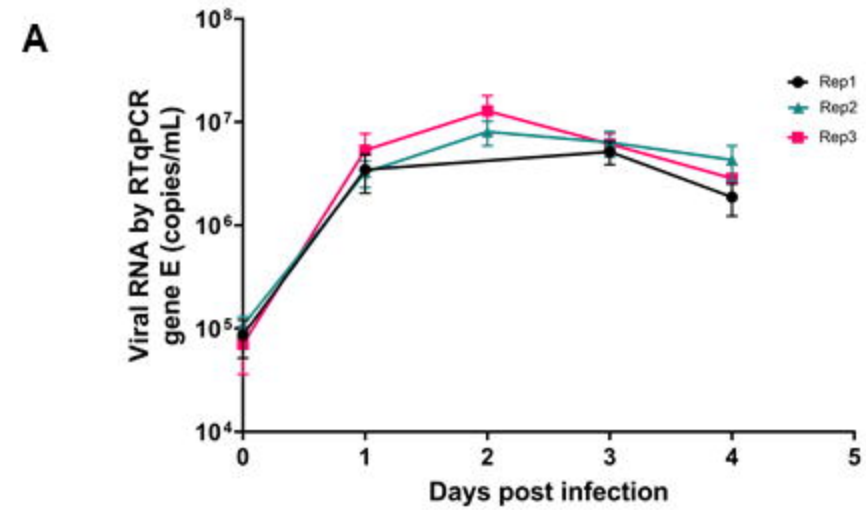
A
Viral RNA by RTqPCR gene E (copies/mL)
Days post infection
Rep1
Rep2
Rep3

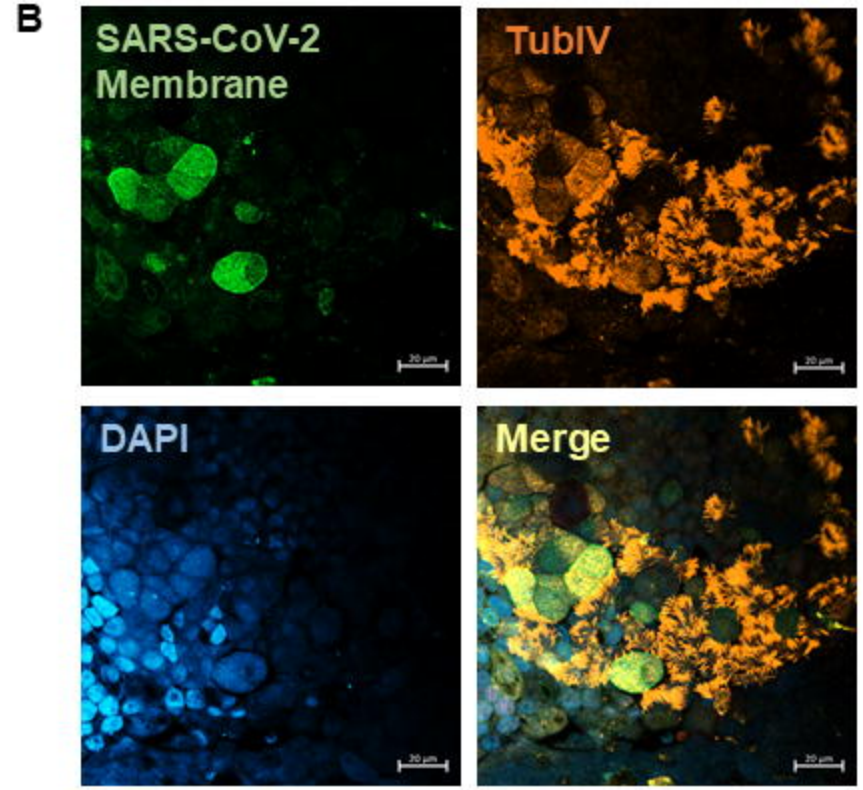
B
SARS-CoV-2 Membrane
TubIV
DAPI
Merge

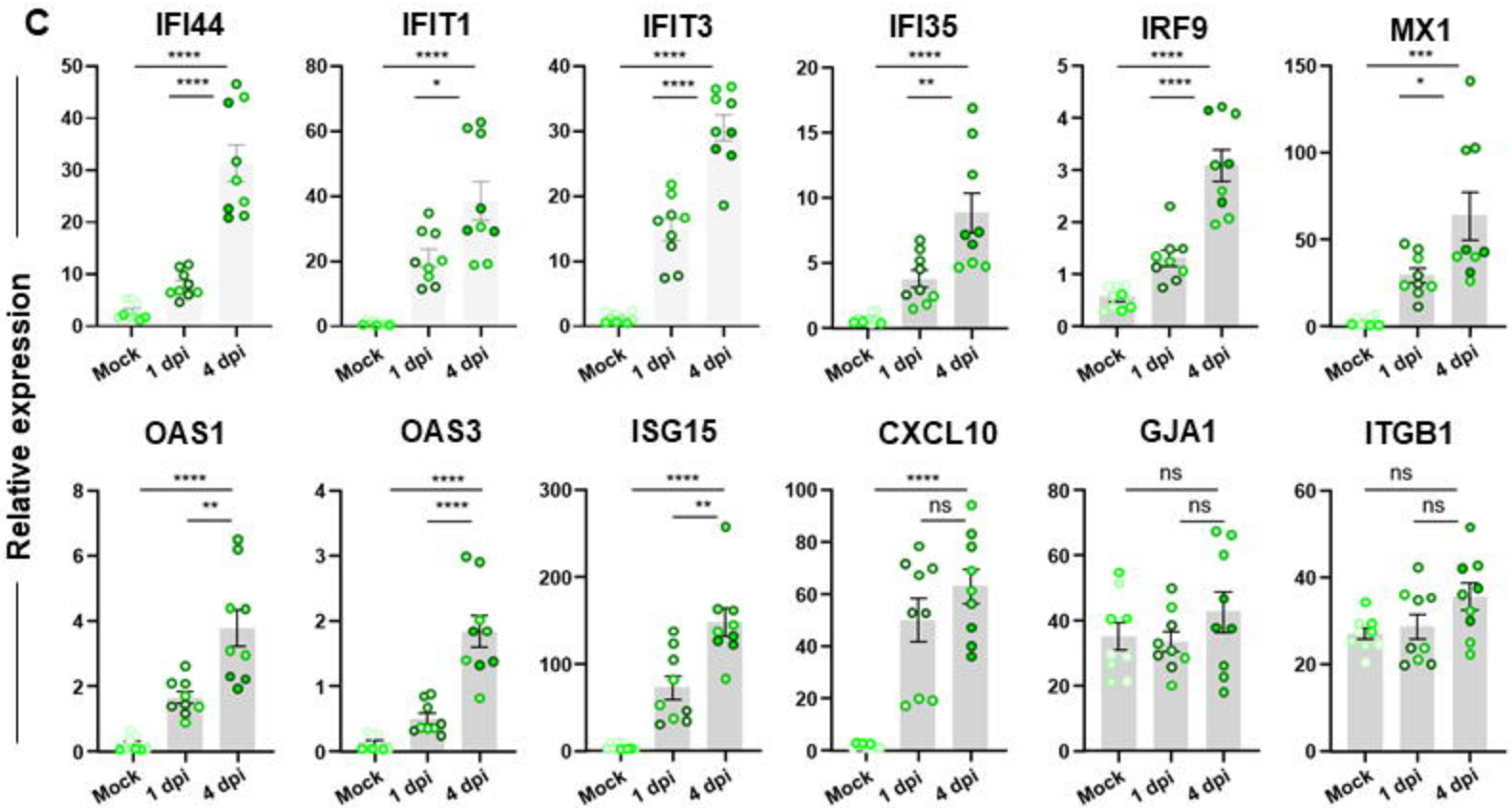
C
IFI44
IFIT1
IFIT3
IFI35
IRF9
MX1
OAS1
OAS3
ISG15
CXCL10
GJA1
ITGB1
Relative expression
Mock
1 dpi
4 dpi
ns

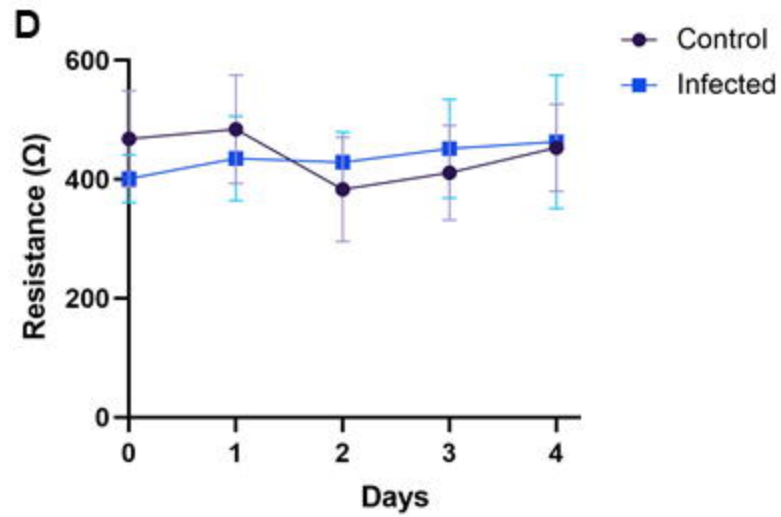
D
Resistance (Ω)
Days
Control
Infected

Figure 5

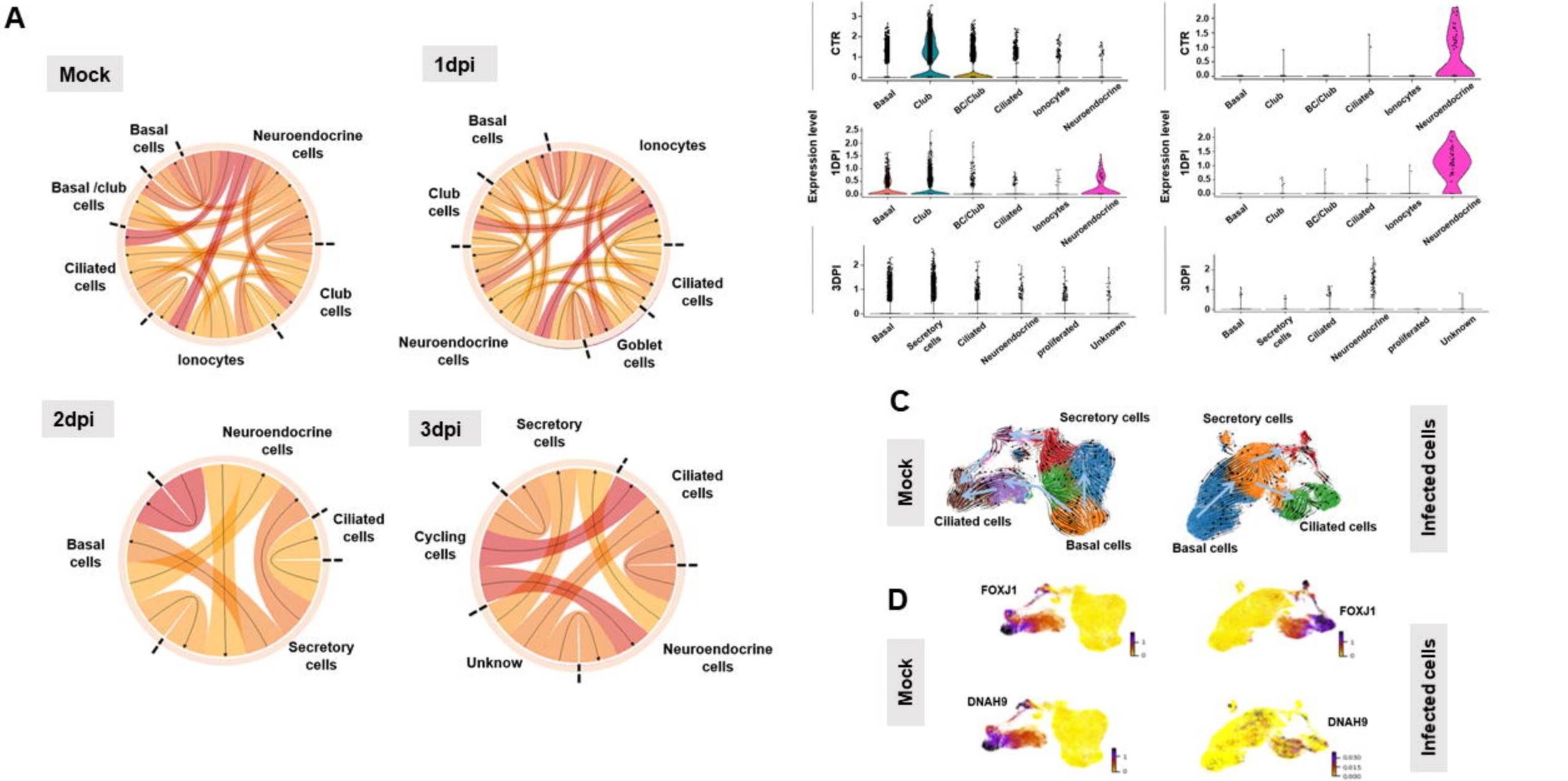
A
Mock
Basal cells
Neuroendocrine cells
Basal /club cells
Ciliated cells
Club cells
Ionocytes
1dpi
Basal cells
Ionocytes
Club cells
Ciliated cells
Neuroendocrine cells
Goblet cells
2dpi
Neuroendocrine cells
Ciliated cells
Basal cells
Secretory cells
3dpi
Secretory cells
Ciliated cells
Cycling cells
Unknow
Neuroendocrine cells
B
Ligand: ARTN
Receptor: RET
Expression level
CTR
1DPI
3DPI
Basal
Club
BC/Club
Ciliated
Ionocytes
Neuroendocrine
Secretory cells
proliferated
Unknown
C
Mock
Secretory cells
Ciliated cells
Basal cells
Infected cells
D
FOXJ1
DNAH9

Figure 6

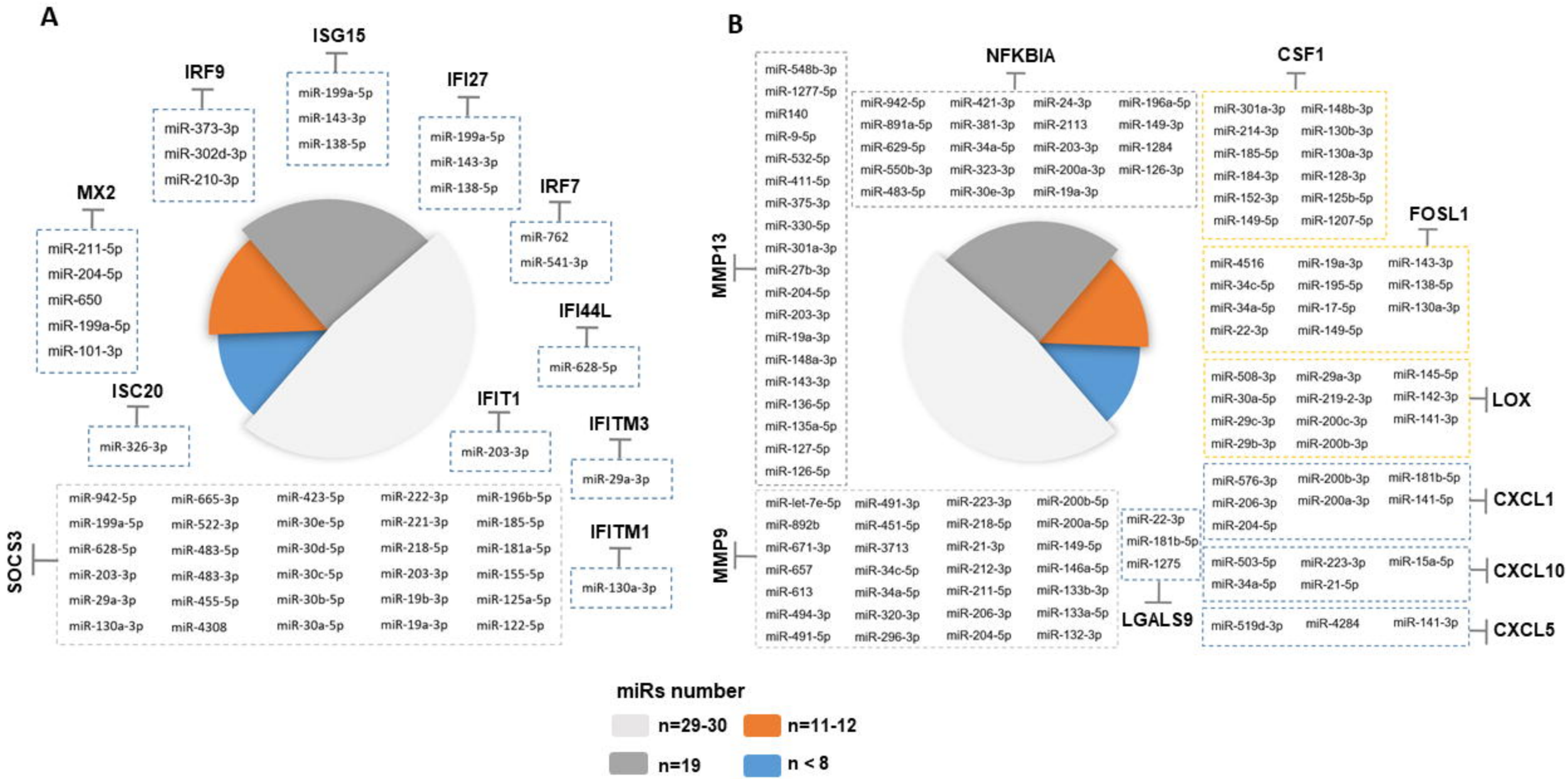
A
ISG15
miR-199a-5p
miR-143-3p
miR-138-5p
IRF9
miR-373-3p
miR-302d-3p
miR-210-3p
IFI27
miR-199a-5p
miR-143-3p
miR-138-5p
MX2
miR-211-5p
miR-204-5p
miR-650
miR-199a-5p
miR-101-3p
IRF7
miR-762
miR-541-3p
IFI44L
miR-628-5p
ISC20
miR-326-3p
IFIT1
miR-203-3p
IFITM3
miR-29a-3p
IFITM1
miR-130a-3p
SOCS3
miR-942-5p miR-665-3p miR-423-5p miR-222-3p miR-196b-5p
miR-199a-5p miR-522-3p miR-30e-5p miR-221-3p miR-185-5p
miR-628-5p miR-483-5p miR-30d-5p miR-218-5p miR-181a-5p
miR-203-3p miR-483-3p miR-30c-5p miR-203-3p miR-155-5p
miR-29a-3p miR-455-5p miR-30b-5p miR-19b-3p miR-125a-5p
miR-130a-3p miR-4308 miR-30a-5p miR-19a-3p miR-122-5p
B
MMP13
miR-548b-3p
miR-1277-5p
miR140
miR-9-5p
miR-532-5p
miR-411-5p
miR-375-3p
miR-330-5p
miR-301a-3p
miR-27b-3p
miR-204-5p
miR-203-3p
miR-19a-3p
miR-148a-3p
miR-143-3p
miR-136-5p
miR-135a-5p
miR-127-5p
miR-126-5p
NFKBIA
miR-942-5p miR-421-3p miR-24-3p miR-196a-5p
miR-891a-5p miR-381-3p miR-2113 miR-149-3p
miR-629-5p miR-34a-5p miR-203-3p miR-1284
miR-550b-3p miR-323-3p miR-200a-3p miR-126-3p
miR-483-5p miR-30e-3p miR-19a-3p
CSF1
miR-301a-3p miR-148b-3p
miR-214-3p miR-130b-3p
miR-185-5p miR-130a-3p
miR-184-3p miR-128-3p
miR-152-3p miR-125b-5p
miR-149-5p miR-1207-5p
FOSL1
miR-4516 miR-19a-3p miR-143-3p
miR-34c-5p miR-195-5p miR-138-5p
miR-34a-5p miR-17-5p miR-130a-3p
miR-22-3p miR-149-5p
LOX
miR-508-3p miR-29a-3p miR-145-5p
miR-30a-5p miR-219-2-3p miR-142-3p
miR-29c-3p miR-200c-3p miR-141-3p
miR-29b-3p miR-200b-3p
CXCL1
miR-576-3p miR-200b-3p miR-181b-5p
miR-206-3p miR-200a-3p miR-141-5p
miR-204-5p
CXCL10
miR-503-5p miR-223-3p miR-15a-5p
miR-34a-5p miR-21-5p
CXCL5
miR-519d-3p miR-4284 miR-141-3p
MMP9
miR-let-7e-5p miR-491-3p miR-223-3p miR-200b-5p
miR-892b miR-451-5p miR-218-5p miR-200a-5p
miR-671-3p miR-3713 miR-21-3p miR-149-5p
miR-657 miR-34c-5p miR-212-3p miR-146a-5p
miR-613 miR-34a-5p miR-211-5p miR-133b-3p
miR-494-3p miR-320-3p miR-206-3p miR-133a-5p
miR-491-5p miR-296-3p miR-204-5p miR-132-3p
LGALS9
miR-22-3p
miR-181b-5p
miR-1275
miRs number
n=29-30
n=11-12
n=19
n < 8



Production of innervated bronchial epithelium from a blood sample

Florent Foisset, Christine Lehalle, Amel Nasri, Carine Bourdais, Lisa Morichon, Aurélie Petit, Isabelle Vachier, Said Assou, Arnaud Bourdin, Nelly Frossard, et al.

▶ **To cite this version:**

Florent Foisset, Christine Lehalle, Amel Nasri, Carine Bourdais, Lisa Morichon, et al.. Production of innervated bronchial epithelium from a blood sample. Revue des Maladies Respiratoires, 2023, 23, pp.S0761-8425. 10.1016/j.rmr.2023.01.021 . hal-03989840

HAL Id: hal-03989840
https://hal.science/hal-03989840

Submitted on 15 Feb 2023

HAL is a multi-disciplinary open access archive for the deposit and dissemination of scientific research documents, whether they are published or not. The documents may come from teaching and research institutions in France or abroad, or from public or private research centers.

L'archive ouverte pluridisciplinaire **HAL**, est destinée au dépôt et à la diffusion de documents scientifiques de niveau recherche, publiés ou non, émanant des établissements d'enseignement et de recherche français ou étrangers, des laboratoires publics ou privés.



Distributed under a Creative Commons Attribution - NonCommercial - NoDerivatives| 4.0 International License

Fabrication d'un épithélium bronchiqueinnervé à partir d'une prise de sang

Production of innervated bronchial epithelium from a blood sample

F. Foisseta,b, C. Lehalleb, A. Nasria, C. Bourdaisa,L. Morichona, A. Petitc, I. Vachierc, S. Assoua,A. Bourdinc,d, N. Frossardb, J. De Vosa,e,∗

a *IRMB (institut de médecine régénératrice et de biothérapies), Inserm UMR 1183, université Montpellier, CHU de Montpellier, Montpellier, France*

b *LIT (laboratoire d'innovation thérapeutique), UMR7200 CNRS-université de Strasbourg, faculté de pharmacie, Illkirch, France*

c *Département de pneumologie, CHU de Montpellier, Montpellier, France*

d *PhyMedExp, université de Montpellier, Inserm U1046, CNRS UMR 9214, Montpellier, France*

e *Département d'ingénierie cellulaire et tissulaire, université de Montpellier, CHU de Montpellier, 80, avenue Augustin-Fliche, 34295 Montpellier cedex 5, France*

MOTS CLÉS

Asthme ;Inflammation neurogène ;Cellules souches pluripotente sinduites ;Épithélium bronchique ;Innervation sensitive

∗**Auteur correspondant.**

Adresse e-mail *:*

john.devos@inserm.fr (J. De Vos).

Résumé

L'asthme est une maladie respiratoire fréquente, sévère dans 3 à 5 % des cas. L'inflammation chronique de l'épithélium bronchique joue un rôle clé dans sa physiopathologie. Le système nerveux sensitif périphérique contribue à cette inflammation des voies aériennes via une activation par l'environnement bronchique. Cependant les mécanismes d'action mis enjeu ne sont à ce jour pas bien connus, notamment par manque de modèles fiables. Nous avons mis en place, à partir de cellules souches pluripotentes induites reprogrammées à partir de cellules sanguines, un modèle d'épithélium bronchique innervé par des neurones sensitifs. Ce dernier permettra notamment de mieux comprendre les mécanismes d'action sous-jacents à l'inflammation neurogène.

Introduction

L'épithélium bronchique constitue une barrière physique essentielle dans la protection du poumon contre les agressions extérieures [1]. Cependant, il joue également un rôle central dans la physiopathologie de nombreuses maladies telle que l'asthme, une maladie inflammatoire chronique fréquente des voies aériennes, de sévérité plus ou moins importante, pouvant affecter la qualité de vie des patients et pour lesquels les traitements actuels restent essentiellement symptomatiques [2,3]. Le système nerveux sensitif périphérique participe à l'inflammation en communiquant avec l'environnement bronchique [4]. L'innervation des voies respiratoires comprend des fibres afférentes (sensorielles) et des fibres efférentes parasympathiques et sympathiques. Les fibres afférentes et efférentes sont connectées via le tronc cérébral et sont à l'origine du réflexe de toux, de la régulation du diamètre bronchique, de l'ampliation respiratoire ou encore de la sécrétion de mucus. Les fibres afférentes peuvent également amplifier l'inflammation des voies respiratoires par la libération de neurotransmetteurs directement au niveau bronchique via un réflexe d'axone, processus par lequel les fibres afférentes non myélinisées de type C entraînent la libération locale de neuropeptides, indépendamment de toute implication du système nerveux central (SNC), initiant ainsi une réaction inflammatoire, de la sécrétion de mucus et une bronchoconstriction [4]. Le réflexe d'axone est médié parle relargage de neuropeptides tels que la neurokinine A ,la substance P, le CGRP ou la neuromédine U [5,6]. Cette inflammation neurogène a été décrite dans de nombreux organes et a été documentée dans les voies respiratoires de plusieurs espèces, notamment le rat et le cochon d'inde. Cependant, l'importance du réflexe d'axone en physiologie humaine et dans l'asthme en particulier reste débattue en raison de la fréquence dans les tissus humains des fibres nerveuses exprimant les neuropeptides impliqués dans ce réflexe [5] et par manque d'un modèle humain fiable. Un modèle *in vitro* de bronche innervée en 3 dimensions (3D)pourrait permettre l'étude de l'inflammation neurogène et d'établir les réponses inflammatoires aux allergènes, aux infections ou irritants qui pourraient être potentialisées par ces interactions neuro-immunes. Nous avons développé à l'aide de cellules souches pluripotentes induites (iPSCs) un modèle 3D d'épithélium bronchique innervé (Fig. 1).

Modèle 3D d'épithélium innervé à partir de cellules souches pluripotentes induites

Les cellules souches pluripotentes induites (iPSC) sont obtenues à partir de cellules somatiques par reprogrammation renforçant l'expression transitoire des quatre facteurs de pluripotence (OCT4, SOX2, KLF4 et cMYC) également appelé le cocktail de Yamanaka [7]. Les iPSCs sont caractérisées par une capacité d'auto-renouvellement avec une prolifération intense, ce qui en fait une source illimitée de cellules d'un même donneur. Elles sont également capables de se différencier en tout type cellulaire de l'organisme (pluripotence).

Elles offrent donc la possibilité de produire des types cellulaires tissus-spécifiques, utiles à la modélisation *in vitro* des tissus sains ou pathologiques, y compris pulmonaires et bronchiques. La modélisation de l'épithélium bronchique à partir d'iPSCs offre un nouveau modèle d'étude des pathologies respiratoires en complément des modèles animaux et des modèles cellulaires primaires, et présente des avantages notables, comme la reproductibilité des lots de tissus bronchiques car tous issus de mêmes donneurs, et la possibilité de modifications génétiques des cellules iPSC par la technologie CRISPR/Cas9 [8].

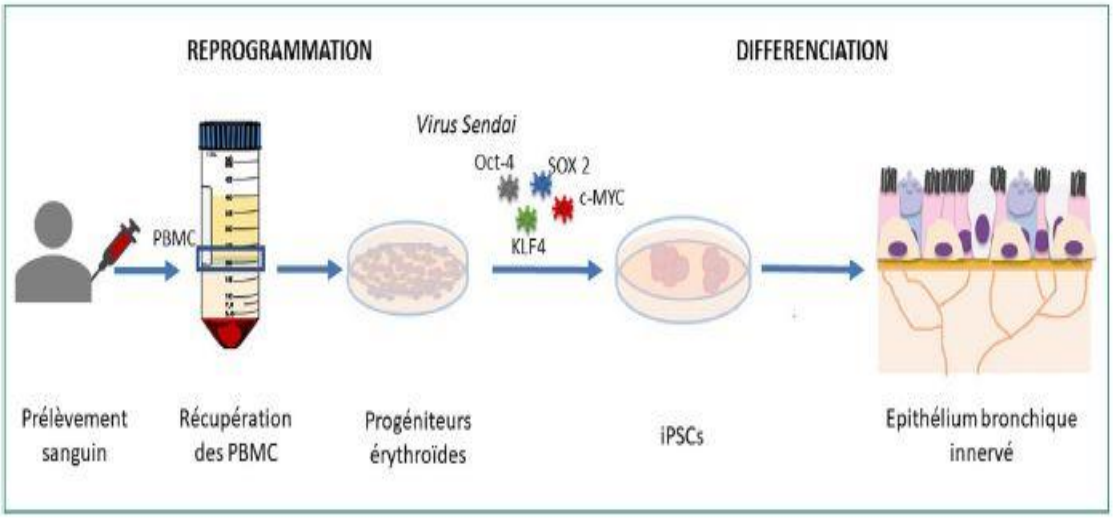

Figure 1. Construction d'un épithélium bronchique présentant une innervation sensitive à partir de cellules sanguines.

Étape 1 : isolation des cellules mononucléées du sang ; Étape 2 : différenciation en progéniteurs érythroïdes ; Étape 3 : transduction des 4 facteurs de pluripotence à l'aide du virus Sendai ; Étape 4 : différenciation des iPSCs en épithélium bronchique et en neurones et construction du modèle.

Nous avons produit des iPSCs à partir de cellules mononucléées obtenues de cinq millilitres de sang de donneurs sains ou de patients atteints de dyskinésie ciliaire primitive, de bronchopneumonie chronique obstructive (BPCO)ou d'asthme. Ces iPSCs ont ensuite été différenciées en épithélium bronchique sur une matrice collagène-chitosan d'après un protocole de différenciation par bio-mimétisme mis en place au laboratoire et qui mime successivement toutes les étapes du développement pulmonaire [9]. Cet épithélium présente des cellules multi-ciliées, des cellules basales, des cellules à mucus, des cellules clubs et des cellules neuroendocrines (Fig. 2). Il est fonctionnel avec un battement ciliaire physiologique (15 Hz) et une sécrétion de mucus. Cet épithélium repose sur une lame basale sous laquelle se trouve une muqueuse sous-épithéliale composée de cellules de type mésenchymateux exprimant la décorine. et dont certaines sont positives pour l'actine ACTA2, suggérant la présence de myofibroblastes. En parallèle à cette différenciation bronchique, nous avons entrepris de différencier ces mêmes iPSCs en neurones sensitifs, en se basant sur un protocole

de différenciation issu de la littérature [10]. Ces neurones sensitifs ont été ensemencés après dépôt sous la matrice collagène-chitosan support de l'épithélium bronchique. L'étude de la fonctionnalité des circuits neuronaux réalisés par les neurones de l'épithélium est en cours d'évaluation.

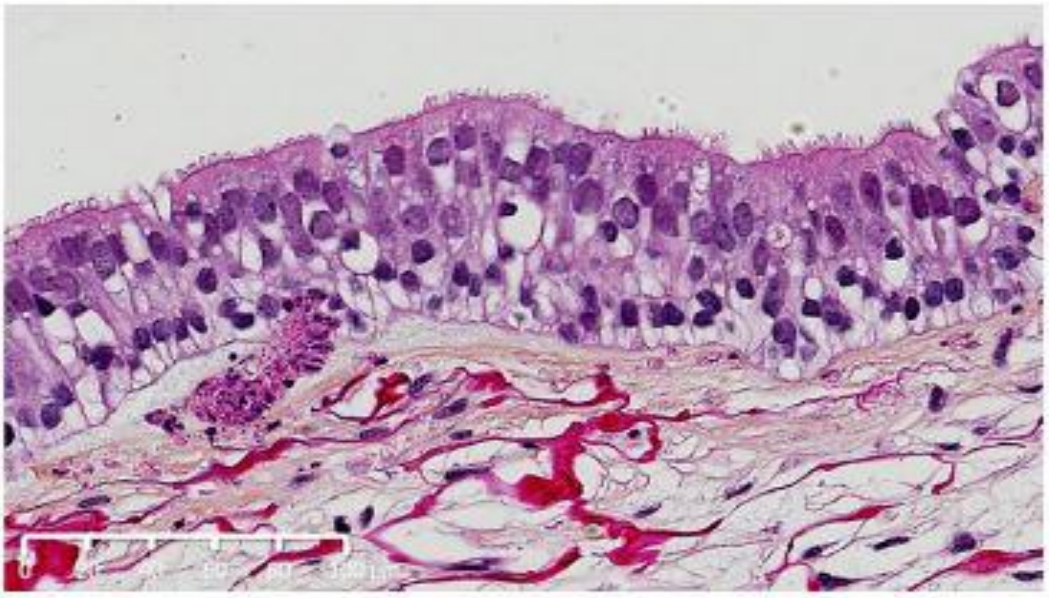

Figure 2. Coloration HES d'une coupe en paraffine présentant un épithélium bronchique obtenu après différenciation à partir de cellules iPS.

Les différents types cellulaires sont présents, notamment les cellules ciliées, reposant sur une lame basale et une muqueuse sous-épithéliale.

Conclusion et perspectives

En partant d'une simple prise de sang, il nous est possible, grâce à la reprogrammation et la différenciation dirigée, dégénérer de façon quasiment illimitée un épithélium bronchique fonctionnel présentant la plupart des types cellulaires attendus et reposant sur une sous-muqueuse innervée. Une fois que l'innervation sera optimisée, en densifiant l'innervation de la matrice par l'ajout de facteurs neuro-trophiques ou par l'ajout de cellules de Schwann dérivées d'iPSCs, il sera possible de stimuler les neurones sensitifs et de voir l'effet de cette stimulation sur l'épithélium, ce qui représenterait un modèle pour l'étude de l'inflammation neurogène. Un tel modèle pourra par la suite servir à des tests pharmacologiques dans un but final de médecine personnalisée des maladies respiratoires telles que l'asthme.

Déclaration des liens d'intérêts

Les auteurs déclarent ne pas avoir de liens d'intérêts.

Références

[1] Vareille M, Kieninger E, Edwards MR, et al. The airway epithelium: soldier in the fight against respiratory viruses. ClinMicrobiol Rev 2011;24:210—29

.[2] Wu TD, Brigham EP, McCormack MC. Asthma in the primary care setting. Med Clin North Am 2019;103:435—52.

[3] Raherison-Semjen C, Guilleminault L, Billiart I, et al. Mise à jour des recommandations pour la prise en charge et le suivi des patients asthmatiques adultes sous l'égide de la Société de pneumologie de langue française (SPLF) et de la Société pédiatrique de pneumologie et allergologie (SP2A). Version courte. Rev Mal Respir 2021;38:e1—13.

[4] Barnes J. Asthma as an axon reflex. Lancet 1986;327:242—5

.[5] Barnes PJ. Neurogenic inflammation in the airways. Respir Phy-siol 2001;125:145—54.

[6] Cardoso V, Chesné J, Ribeiro H, et al. Neuronal regulation of type 2 innate lymphoid cells via neuromedin U. Nature2017;549:277—81.

[7] De Vos J, Bouckenheimer J, Sansac C, et al. Human induced pluripotent stem cells: a disruptive innovation. Curr Res TranslMed 2016;64:91—6.

[8] Mianné J, Nasri A, Van CN, et al. CRISPR/Cas9-mediated gene knockout and interallelic gene conversion in human induced pluripotent stem cells using non-integrative bacteriophage-chimeric retrovirus-like particles. BMC Biol 2022;20:8.

[9] Ahmed E, Fieldes M, Bourguignon C, et al. Differentia-tion of human induced pluripotent stem cells from patients with severe COPD into functional airway epithelium. Cells2022;11:2422

.[10] Muller Q, Beaudet M-J, De Serres-Bérard T, et al. Development of an innervated tissue-engineered skin with human sensoryneurons and Schwann cells differentiated from iPS cells. Acta Biomater 2018;82:93—101.3

Mianné et al. BMC Biology (2022) 20:8
https://doi.org/10.1186/s12915-021-01214-x

BMC Biology

RESEARCH ARTICLE Open Access

CRISPR/Cas9-mediated gene knockout and interallelic gene conversion in human induced pluripotent stem cells using non-integrative bacteriophage-chimeric retrovirus-like particles

Joffrey Mianné[1], Amel Nasri[1], Chloé Nguyen Van[1], Chloé Bourguignon[1], Mathieu Fieldès[1], Engi Ahmed[1], Christine Duthoit[2], Nicolas Martin[2], Hugues Parrinello[3,4], Anaïs Louis[3,4], Alexandra Iché[2], Régis Gayon[2], Florine Samain[2], Lucille Lamouroux[2], Pascale Bouillé[2], Arnaud Bourdin[5], Said Assou[1] and John De Vos[1,6*]

Abstract

Background: The application of CRISPR/Cas9 technology in human induced pluripotent stem cells (hiPSC) holds tremendous potential for basic research and cell-based gene therapy. However, the fulfillment of these promises relies on the capacity to efficiently deliver exogenous nucleic acids and harness the repair mechanisms induced by the nuclease activity in order to knock-out or repair targeted genes. Moreover, transient delivery should be preferred to avoid persistent nuclease activity and to decrease the risk of off-target events. We recently developed bacteriophage-chimeric retrovirus-like particles that exploit the properties of bacteriophage coat proteins to package exogenous RNA, and the benefits of lentiviral transduction to achieve highly efficient, non-integrative RNA delivery in human cells. Here, we investigated the potential of bacteriophage-chimeric retrovirus-like particles for the non-integrative delivery of RNA molecules in hiPSC for CRISPR/Cas9 applications.

Results: We found that these particles efficiently convey RNA molecules for transient expression in hiPSC, with minimal toxicity and without affecting the cell pluripotency and subsequent differentiation. We then used this system to transiently deliver in a single step the CRISPR-Cas9 components (Cas9 mRNA and sgRNA) to generate gene knockout with high indel rate (up to 85%) at multiple loci. Strikingly, when using an allele-specific sgRNA at a locus harboring compound heterozygous mutations, the targeted allele was not altered by NHEJ/MMEJ, but was repaired at high frequency using the homologous wild type allele, i.e., by interallelic gene conversion.

* Correspondence: john.devos@inserm.fr
[1]IRMB, Univ Montpellier, INSERM, CHU Montpellier, Hôpital St Eloi, 80 avenue Augustin Fliche, 34295 Montpellier, France
[6]Department of Cell and Tissue Engineering, Univ Montpellier, CHU Montpellier, Montpellier, France
Full list of author information is available at the end of the article

© The Author(s). 2021 **Open Access** This article is licensed under a Creative Commons Attribution 4.0 International License, which permits use, sharing, adaptation, distribution and reproduction in any medium or format, as long as you give appropriate credit to the original author(s) and the source, provide a link to the Creative Commons licence, and indicate if changes were made. The images or other third party material in this article are included in the article's Creative Commons licence, unless indicated otherwise in a credit line to the material. If material is not included in the article's Creative Commons licence and your intended use is not permitted by statutory regulation or exceeds the permitted use, you will need to obtain permission directly from the copyright holder. To view a copy of this licence, visit http://creativecommons.org/licenses/by/4.0/. The Creative Commons Public Domain Dedication waiver (http://creativecommons.org/publicdomain/zero/1.0/) applies to the data made available in this article, unless otherwise stated in a credit line to the data.

Conclusions: Our results highlight the potential of bacteriophage-chimeric retrovirus-like particles to efficiently and safely deliver RNA molecules in hiPSC, and describe for the first time genome engineering by gene conversion in hiPSC. Harnessing this DNA repair mechanism could facilitate the therapeutic correction of human genetic disorders in hiPSC.

Keywords: hiPSC, Transduction, CRISPR, Retrovirus-like particles, Gene conversion, Knock-out

Background

Human pluripotent and induced stem cells (hPSC and hiPSC, respectively) can self-renew, display unlimited proliferative potential, and can differentiate into any cell type of the three germ layers (ectoderm, mesoderm, endoderm). Therefore, they hold tremendous potential not only for basic research and disease modeling, but also for cell production for clinical applications [1, 2]. This potential has been magnified by the development of gene editing tools, particularly those based on clustered regularly interspaced short palindromic repeats (CRISPR) technologies, to genetically manipulate the hPSC genome [3, 4]. This has allowed the generation of numerous lines with isogenic controls that have become invaluable tools for gene function analysis, genetic disorder modeling, and autologous or allogenic tissue generation for cell-based therapies [1, 2].

However, delivering nucleic acids in hPSC for overexpression or genetic engineering is still a challenging task. This can be explained by several factors, including inefficient delivery systems for hPSC, high cell death rates following transfection using standard transfection tools, difficulties to sub-clone these cells, and low tolerance to DNA double-strand breaks (DSB) [4–6]. Despite recent improvements based on new strategies, such as the transfection of ribonucleoprotein complexes, and the development of new gene transfer tools to enhance delivery in hPSC [7–14], new systems are still required to efficiently deliver nucleic acids in hPSC with minimal toxicity.

Particularly, it would be important to develop a system to efficiently deliver RNA molecules for transient overexpression without transgene insertion in the genome. Currently, mRNA molecules can be delivered in hPSC by electroporation and lipofection or via non-viral particles. However, these systems are usually highly toxic and result in low transfection efficacy. Recently, several groups have described non-integrative RNA delivery systems that are based on modified viral particles and that combine the viral vector high transduction efficacy and low toxicity, without genome integration of the viral payload [15–20]. Several of these systems rely on bacteriophage-chimeric retrovirus-like particles to encapsulate concomitantly (but with variable efficiency) different types of RNA molecules, for instance CRISPR-associated protein 9 (Cas9) mRNA and the CRISPR-associated protein 9 (Cas9) necessary for CRISPR/Cas9 gene editing [21, 22]. Therefore, we asked whether one of these systems could be used to deliver RNA molecules for transient overexpression and genome engineering in hiPSC. To this aim, we targeted three genes [multiciliate differentiation and DNA synthesis associated cell cycle protein (*MCIDAS*), and coiled-coil domain containing 40 (*CCDC40*)] implicated in the pathogenesis of primary ciliary dyskinesia (PCD), a rare pulmonary genetic disorder, and two genes with therapeutic interest for T-cell engineering [T cell receptor alpha constant (*TRAC*) and C-X-C chemokine receptor type 4 (*CXCR4*)].

First, we found that bacteriophage-chimeric retrovirus-like particles can very efficiently transduce hiPSC lines with minimal toxicity and no impact on pluripotency. Then, we used this system to simultaneously and efficiently transfer sgRNA and Cas9 mRNA for non-homologous end-joining (NHEJ)/micro-homology end-joining (MMEJ)-based gene editing at multiple loci. Finally, we demonstrated for the first time that interallelic gene conversion is a DNA repair mechanism that can be activated in hiPSC following introduction of a DNA DSB. This mechanism was harnessed to correct a heterozygous mutation in a patient hiPSC line and for converting heterozygous mutations into homozygous mutations.

Results

Bacteriophage-chimeric retrovirus-like (LentiFlash®) particles for highly efficient and transient RNA delivery in hiPSC

To investigate whether LentiFlash® particles can transduce hiPSC, we generated particles containing the fluorescent reporter ZsGreen mRNA (LF-ZsGreen) and used them at three doses (0.5, 2, and 5 pg p24/cell) to transduce a hiPSC line (HY03) derived from a healthy individual [23]. Analysis of ZsGreen expression by fluorescence microscopy and flow cytometry at 48 h post-transduction revealed that more than 97% of cells were transduced (all three tested doses) and that fluorescence signal intensity was dose-dependent (n = 3) (Fig. 1a–c). Moreover, cell counting and lactate dehydrogenase (LDH; a marker of cytotoxicity) quantification in supernatant confirmed the low toxicity observed by optical microscopy, without significant increase in LDH concentration or cell loss after transduction with particles at the concentration of 0.5 and 2 pg p24/cell. We observed only a slight increase in LDH concentration at the highest dose tested (5 pg p24/cell), without any effect on cell proliferation (Fig. 1d, e). ZsGreen

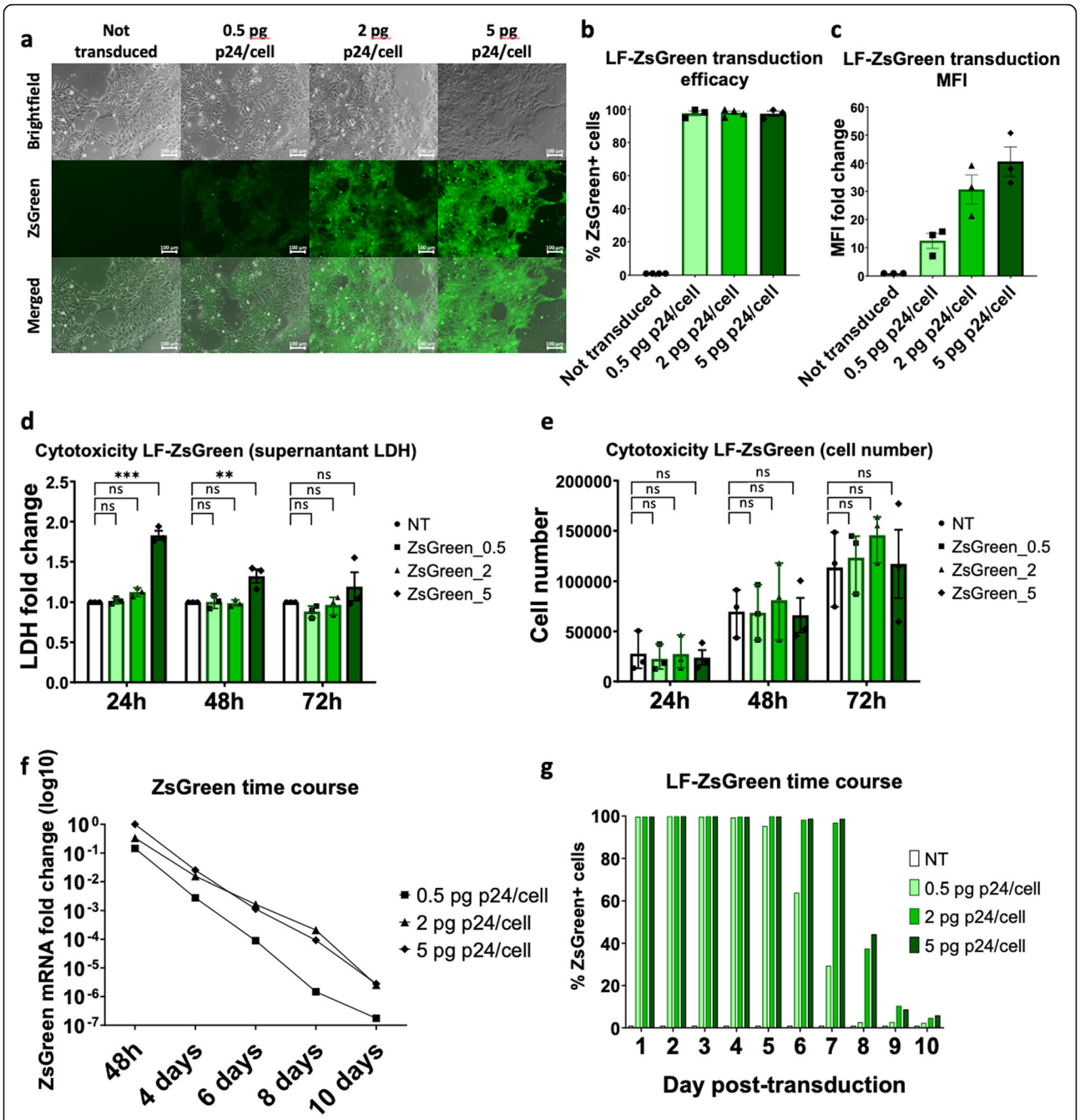

Fig. 1 LentiFlash® particles allow the highly efficient delivery of RNA molecules in hiPSC. **a** Fluorescent microscopy analysis of HY03 hiPSC 48 h post-transduction with LF-ZsGreen particles at 0.5, 2, or 5 pg p24/cell. **b** Transduction efficacy by flow cytometry analysis of ZsGreen-positive HY03 cells at 48 h post-transduction, and **c** mean fluorescent intensity (MFI) fold change assessed by cytometry analysis at 48 h post-transduction (same conditions as in **a**). **d** Fold change of lactate dehydrogenase (LDH) concentration in HY03 cell supernatant samples collected at 24, 48, and 72 h post-transduction (same conditions as in **a**); NT, not transduced cells ($n = 1$); ns, not significant; $^{**}P < 0.005$; $^{***}P < 0.0005$. **e** Cell number at 24, 48, and 72 h post-transduction (same conditions as in **a**); NT, not transduced cells ($n = 1$); ns, not significant. **f** Fold change of ZsGreen mRNA level in HY03 cells in function of time. The sample corresponding to cells transduced with 5 pg p24/cell and analyzed at 48 h was arbitrarily defined as the reference (=1) (same conditions as in **a**, $n = 1$). **g** Flow cytometry analysis of ZsGreen-positive cells for 10 days after transduction (NT, not transduced cells)

expression monitoring by real-time quantitative PCR (qPCR) and flow cytometry analysis for 10 days revealed the transient nature of the system with a sharp decline in ZsGreen mRNA level over time, followed by a progressive decrease in ZsGreen protein expression (Fig. 1f, g). This decrease was dose-dependent and reached control levels

at day 10. The percentage of ZsGreen-positive cells peaked at 24 h post-transduction (all three doses), whereas the fluorescence signal intensity reached its maximum at 48 h (Fig. 1 g, and Fig. S1a-b). These findings confirmed previous data obtained in HeLa cells (data not shown) and clearly show that we can specifically quantify ZsGreen RNA (by qPCR) and ZsGreen protein expression (by cytometry) in cells transduced with LentiFlash® particles. The detection of ZsGreen RNA demonstrates that the RNA contained in the LentiFlash® particles was efficiently transferred in the transduced cells. These experiments also showed that while ZsGreen RNA expression decreased already at 48 h after transduction, ZsGreen protein levels remained high for 5–10 days (in function of the used dose) because the protein half-life is quite long. These results suggest that after transduction of LentiFlash® particles, protein expression in target cells is correlated with the RNA delivery. Transduced hiPSC retained a pluripotent morphology and expressed pluripotency markers, as indicated by the expression of NANOG, OCT3/4, SOX2, and SSEA4 (Fig. S1c). Pluripotency was confirmed by differentiating transduced cells into definitive endoderm that expressed CXCR4, FOXA2, and SOX17 (Fig. S1d). We replicated these results in two additional hiPSC lines, one derived from a patient with PCD (PCD_02:30 line) [24] and the other from a patient with chronic obstructive pulmonary disease (COPD) (iCOPD9_B27 line) (Fig. S2).

Efficient CRISPR/Cas9-mediated NHEJ/MMEJ genome editing in hiPSC

Then, we asked whether LentiFlash® particles could be used to transiently deliver CRISPR/Cas9 reagents in hiPSC for genome engineering. To this aim, we first generated a non-clonal GFP-reporter stable cell line (HY03-GFP) by transducing HY03 cells with integrative recombinant lentiviral particles (ILV-EF1-GFP) (Fig. S3). Then, we transduced HY03-GFP cells with LentiFlash® particles that carry a sgRNA targeting the *GFP* sequence and the Cas9 mRNA (LF-CRISPR/Cas9-GFP) at three doses (0.5, 2, and 5 pg p24/cell) to assess NHEJ/MMEJ-mediated *GFP* knock-out. Six days post-transduction, fluorescent microscopy and flow cytometry analysis showed that GFP expression was absent in more than 90% of cells at the highest dose tested (Fig. 2a, b). Sanger sequencing and Interference of CRISPR Edits (ICE) analysis confirmed the high frequency of NHEJ/MMEJ mutations at the targeted *GFP* sequence (Fig. 2c).

Then, we generated four additional LentiFlash® vectors (LF-CRISPR/Cas9-MCIDAS, LF-CRISPR/Cas9-DNAH5, LF-CRISPR/Cas9-TRAC, and LF-CRISPR/Cas9-CXCR4) to target two endogenous genes involved in motile ciliary biology (*MCIDAS* and *DNAH5*) and two endogenous genes implicated in T-cell biology (*TRAC* and *CXCR4*). Transduction of HY03 hiPSC with increasing doses resulted in dose-dependent NHEJ/MMEJ-mediated mutagenesis at all four loci, as indicated by Sanger sequencing and ICE analysis. The indel rates obtained were gene-dependent, with mutagenesis rates of 86, 36, 40, and 28% for *MCIDAS*, *DNAH5*, *TRAC*, and *CXCR4*, respectively (Fig. 2c). For DNAH5, in line with the ICE analysis, NGS-based amplicon sequencing showed that 49.5% of reads displayed deletions, confirming a high efficiency of CRISPR/Cas9 editing (Fig. S4). As seen for ZsGreen expression, Cas9 mRNA level monitoring by real-time qPCR for 7 days confirmed the rapid mRNA decline after LF-CRISPR/Cas9-MCIDAS (0.5 pg p24/cell) or LF-CRISPR/Cas9-CXCR4 (7.5 pg p24/cell) transduction (Fig. 2d). This is particularly interesting for limiting Cas9 activity over time and reducing potential off-target mutations. To demonstrate that Cas9 mRNA and sgRNA are co-packaged in LentiFlash® particles, we assessed CRISPR/Cas9 targeting efficiency using various batches of LentiFlash® particles to edit the GFP gene in a clonal HCT116 cell line that contains one copy of GFP per cell. Specifically, we analyzed GFP expression at day 7 after transduction of LentiFlash® particles that express (i) Cas9-MS2 alone, (ii) sgRNAGFP-PP7 and Cas9 without the MS2 aptamers (two different plasmids), (iii) sgRNAGFP-PP7 and Cas9-MS2 (two different plasmids), and (iv) sgRNAGFP-PP7 and Cas9-MS2 (both in the same expression plasmid, which corresponds to the LentiFlash® generation process used for the iPSC experiments described in this article). We observed 75% of GFP editing when cells were transduced with sgRNAGFP-PP7 or Cas9 without the MS2 aptamers. This indicated that some Cas9 proteins are passively packaged or embedded with the guide packaging. When Cas9 RNA is actively packaged, the editing efficiency increased to more than 90% (supplementary Fig. S5). As expected, we obtained the best editing efficiency (97.7%) using LentiFlash® particles produced with a single expression plasmid that allows the active packaging of sgRNA-PP7 and Cas9-MS2. These data show that although the Cas9 protein is passively packaged during the production process, the CRISPR/Cas9 system is more efficient when Cas9 is actively packaged thanks to the presence of MS2 aptamers.

Sub-cloning of cells transduced with 0.5 pg p24/cell LF-CRISPR/Cas9-DNAH5 or LF-CRISPR/Cas9-MCIDAS particles and screening by high-resolution melting analysis (HRMA) confirmed gene editing, with 78% and 82% of clones mutated at the *DNAH5* and *MCIDAS* locus, respectively (Fig. 2e). Sanger sequencing of *DNAH5* and *MCIDAS* in 11 and 20 randomly selected mutant clones (according to the HRMA results) confirmed the targeted mutagenesis (Fig. 2f). Furthermore, the characterization of two knock-out cell lines (one for *DNAH5* and one for *MCIDAS*) confirmed the expression

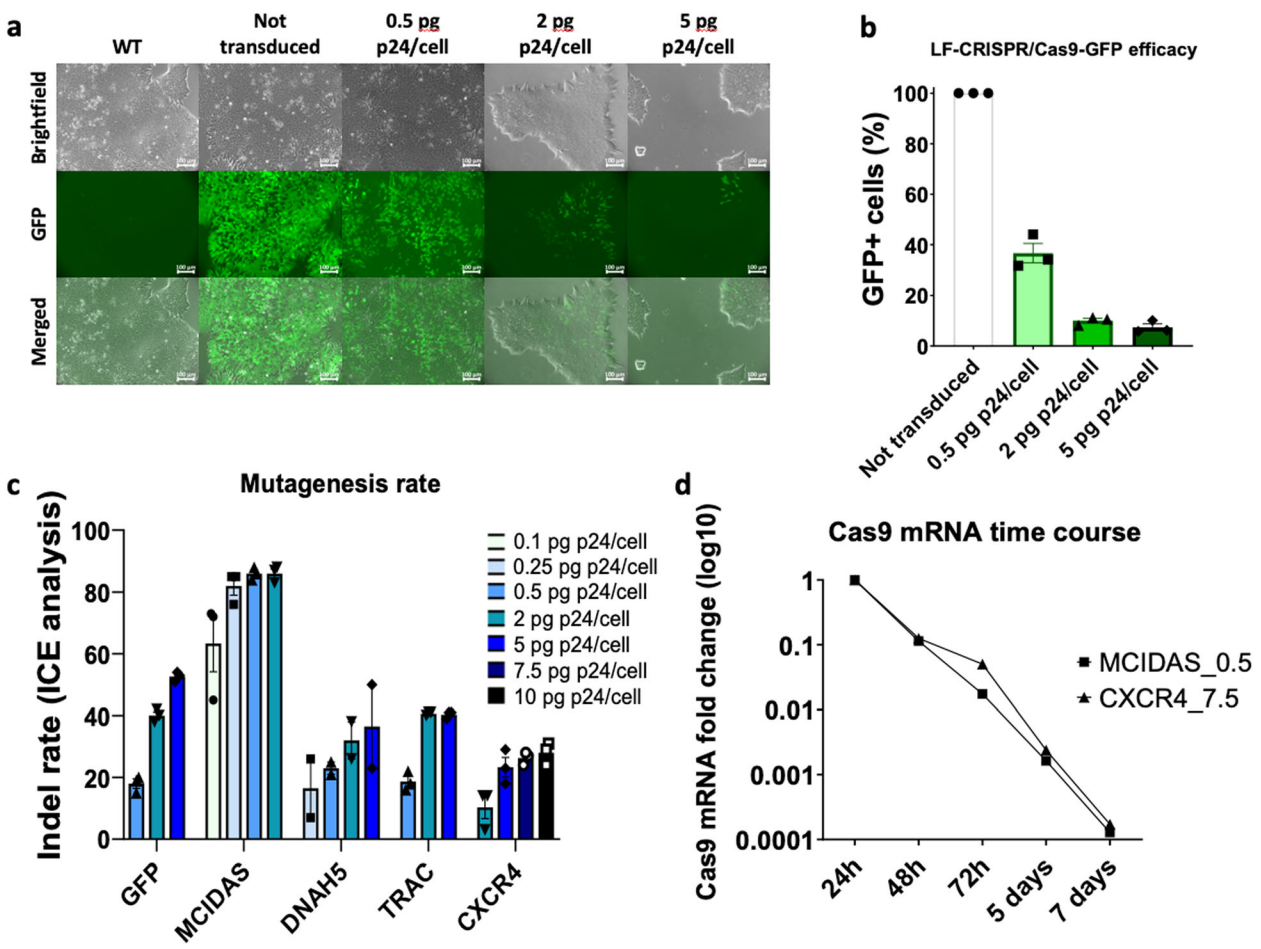

e

	# clones analysed by HRMA	# WT	# Mutants	% mutants
DNAH5_0.5	55	12	43	78.2
MCIDAS_0.5	29	5	24	82.8

f

	# clones analysed by Sanger seq.	# Het (%)	# Comp-Het (%)	# Hom (%)	# mosaic (%)
DNAH5	11	5 (45)	3 (27)	0 (0)	3 (27)
MCIDAS	20	0 (0)	5 (25)	6 (30)	9 (45)

Fig. 2 The LentiFlash® system can be used for the efficient CRISPR/Cas9-mediated modification of hiPSC. **a** Fluorescent microscopy analysis of HY03-GFP cells at day 6 post-transduction with LF-CRISPR/Cas9-GFP particles at 0.5, 2, or 5 pg p24/cell. Wild-type cells (WT) are parental HY03 cells. **b** Transduction efficacy measured by flow cytometry quantification of GFP-positive HY03-GFP cells at day 6 post-transduction with LF-CRISPR/Cas9-GFP particles at 0.5, 2, or 5 pg p24/cell (NT, not transduced = 100%). **c** Indel rate at five loci (*GFP*, *MCIDAS*, *DNAH5*, *TRAC*, and *CXCR4*) using increasing doses of LentiFlash® particles harboring CRISPR/Cas9 to target the indicated genes (from 0.1 to 10 pg p24/cell) in HY03 hiPSC cells at day 3 post-transduction. Data were obtained by ICE decomposition analysis after Sanger sequencing of the targeted loci. **d** Fold change of Cas9 mRNA level in HY03 cells transduced with LF-CRISPR/Cas9-MCIDAS or LF-CRISPR/Cas9-CXCR4 (0.5 and 7.5 pg p24/cell, respectively). The samples corresponding to cells analyzed at 24 h were arbitrarily defined as the reference (=1) (n = 1) **e** HRMA results of clones obtained following HY03 cells transduction with LF-CRISPR/Cas9-DNAH5 and LF-CRISPR/Cas9-MCIDAS particles at 0.5 pg p24/cell. WT, wild type. **f** Sanger sequencing analysis of clones identified as mutated by HRMA. Het, heterozygote; Comp-Het, compound heterozygote; Hom, homozygote

of pluripotency markers (NANOG, OCT3/4, SOX2, and SSEA4), the absence of the most recurrent genomic abnormalities found in hiPSC, and the absence of Cas9 genomic integration (Fig. S6).

Finally, to confirm the data reproducibility, we performed CRISPR/Cas9 editing in the other two hiPSC lines (PCD_02:30 and iCODP9_B27) using optimized particle concentrations. This resulted in comparable mutagenesis rates in all cell lines for the four targeted genes (Fig. S7).

Allele-specific gene editing induces interallelic gene conversion in hiPSC

The PCD_02:30 hiPSC line was derived from a patient with PCD harboring *CCDC40* compound heterozygous mutations [24]. The two heterozygous pathogenic variants correspond to a 2-nucleotide frameshift deletion in exon 7 (Δ-2nt, allele 1) and a single nucleotide polymorphism in the splice site acceptor of exon 19 (G > A, allele 2). To investigate whether a CRISPR/Cas9 reframing approach could restore the reading frame in allele 1, we designed an allele-specific sgRNA that encompasses in its seed region the Δ-2nt variant (Fig. 3a). We then used this sgRNA to generate the corresponding LentiFlash® particles (LF-CRISPR/Cas9-CCDC40-YGT). Transduction of the PCD_02:30 hiPSC line did not lead to the generation of indels at the targeted locus, but decreased the percentage of Δ-2nt alleles and increased the percentage of wild type allele (WT) at this position, as indicated by Sanger sequencing and ICE analysis (Fig. 3b). These results were reproducible (n = 3) and dose-dependent, with an increase of the WT allele percentage from 50% (heterozygous state) to 90% after transduction with LF-CRISPR/Cas9-CCDC40-YGT particles at 5 pg p24/cell. To determine whether these results were due to larger deletions of the targeted Δ-2nt allele with a resulting over-representation of the WT sequence, we counted the copies of the WT allele by droplet digital PCR (ddPCR). In agreement with the Sanger sequencing data, the WT allele copy number was increased in a dose-dependent manner (n = 3), with a mean copy number of 1.43 (equivalent to 71% of WT alleles compared with 90% by ICE analysis) for the 5 pg p24/cell condition (Fig. 3b). This confirmed that the targeted Δ-2nt allele was corrected to a WT allele. To confirm that our sgRNA design was allele-specific, we transduced the HY03 hiPSC line (WT at the *CCDC40* locus) with LF-CRISPR/Cas9-CCDC40-YGT particles at 5 pg p24/cell. We did not detect any indel by Sanger sequencing, confirming the sgRNA specificity (data not shown). This finding was not specific to the use of the LentiFlash® system because we obtained interallelic gene conversion also by electroporating the PCD_02:30 iPSC line with CRISPR/Cas9 RNPs targeting the Δ-2nt allele, albeit at a lower efficiency (interallelic gene conversion occurring, on average, in 42% of cells) (Fig. S8a). Of note, the electroporation conditions must be optimized for each cell line. Indeed, the conditions used to electroporate PCD_02:30 iPSC resulted in complete loss of HY03 hiPSC viability (data not shown). Therefore, we concluded that allele-specific targeting of the Δ-2nt pathogenic variant resulted in DNA repair mediated by interallelic gene conversion.

To determine whether this phenomenon was conserved upon loss of pluripotency, we differentiated PCD_02:30 hiPSC into neural progenitors (Fig. S8b). Transduction of these progenitors with LF-CRISPR/Cas9-CCDC40-YGT at 0.5, 2, and 5 pg p24/cell gave similar results as those obtained with the parental hiPSC line: increase of the WT allele percentage from 50 (heterozygous state) to 90% after transduction at the highest dose. This suggests that interallelic gene conversion occurs also after hPSC differentiation and loss of pluripotency (Fig. S8c).

Finally, to determine whether interallelic gene conversion could occur at another locus and more generally whether this genome engineering approaches could be harnessed to convert heterozygous mutations to homozygous mutations, we derived three heterozygous clonal lines with a frameshift mutation in *DNAH5* (DNAH5_A6, DNAH5_C3, and DNAH5_B5; Fig. S9). These clones were obtained by transducing the HY03 hiPSC line with LF-CRISPR/Cas9-DNAH5 (see above), and harbored one allele with an indel (7nt deletion [Δ-7nt], 1nt insertion [Δ+1nt], or a combination of 1nt deletion with 2nt insertion [Δ-1/+2nt] for DNAH5_A6, DNAH5_C3, and DNAH5_B5, respectively) that disrupted the sgRNA binding site, and a WT allele that could be targeted to introduce a DSB. Transduction with LF-CRISPR/Cas9-DNAH5 at the optimized dose of 0.5 pg p24/cell showed the absence of off-target mutations at sites containing up to three mismatches and the absence of the most recurrent genomic abnormalities found in hiPSC (Fig. S9). It also resulted in gene conversion with an increase of the mutant allele copy number specific to each clone (the Δ-7nt for DNAH5_A6, Δ+1nt for DNAH5_C3 and Δ-1/+2nt for DNAH5_B5), as indicated by Sanger sequencing and ICE analysis (Fig. S10). These results confirmed that allele-specific targeting in hiPSC results in DNA repair mediated by interallelic gene conversion.

Discussion

Our data show that LentiFlash® particles very efficiently deliver non-integrative RNA molecules in hiPSC. We demonstrated that this system can be used to transiently express RNA molecules in up to 97% of transduced cells. Moreover, this highly efficient transduction system does not cause marked cytotoxicity

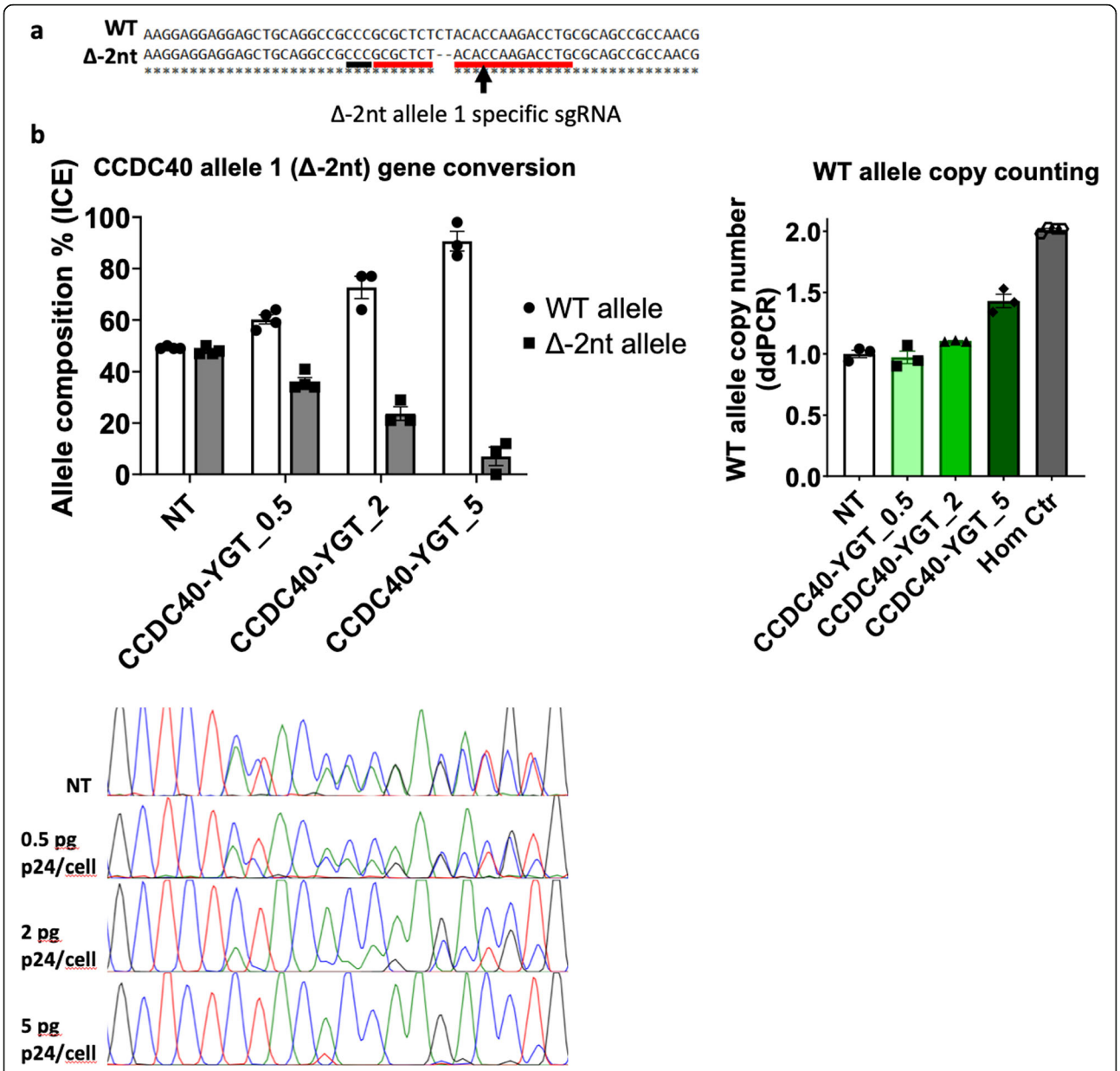

Fig. 3 Allele-specific targeting of a pathogenic allele results in gene conversion. **a** Allele-specific sgRNA design strategy to target the *CCDC40* allele 1 (Δ-2nt) in the PCD_02:30 hiPSC line. The protospacer sequence is underlined in red, and the protospacer adjacent motif in black. **b** Targeting of Δ-2nt allele by transducing PCD_02:30 cells with LF-CRISPR/Cas9-CCDC40-YGT particles at 0.5, 2, and 5 pg p24/cell results in dose-dependent interallelic gene conversion. Top left: Allelic composition at the targeted locus. Top right: Wild type (WT) allele copy number was measured by droplet digital PCR (ddPCR). Bottom: Representative Sanger sequencing chromatograms. ICE, Inference of CRISPR Edits; Hom, homozygote; NT, not transduced

and thus allows reducing the number of cells to be used and performing experiments directly after transduction, without the need of an extended recovery period. This could be particularly interesting for many applications, including the expression of selected transcription factors to direct hPSC differentiation.

Furthermore, thanks to its versatility, this system can be used to deliver simultaneously various RNA types, including the Cas9 mRNA and sgRNA for CRISPR/Cas9-based gene editing. Our result shows that the LentiFlash® technology allows packaging both the Cas9 RNA and the Cas9 protein, especially because the corresponding encoding DNA is efficiently transfected in the producer cells. The editing rates we obtained in HCT116 cells that contain one copy of the target gene per cell cannot be extrapolated to the level of expression of

endogenous genes where many factors can interfere with the editing efficiency (gene copy number, availability of the gene within chromatin, sgRNA design). In fact, a small amount of Cas9 protein might efficiently edit a gene present as a single copy per cell, but be ineffective in other gene configurations [25]. We demonstrated that LentiFlash® particles can be exploited to efficiently manipulate the hiPSC genome via the NHEJ/MMEJ repair pathways. By targeting five genes in three different hiPSC lines, we could generate indels in up to 85% of the targeted alleles. Moreover, we did not observe off-target events at any of the loci analyzed in the five stable cell lines generated in this study.

Thanks to the use of the active cellular entrance pathway of classical lentiviral vectors, LentiFlash® delivery does not disrupt cell integrity, differently from other transfection systems, such as electroporation and lipofection. This results in very low cell toxicity and minimal cell death after transduction (Fig. 1d, e). This easy-to-use technology is also very efficient (> 97% of cells expressed the transgene of interest) (Fig. 1), thus saving time and work linked to cell selection or sorting. Recent studies showed that lentivirus-like particles (LVLP) can be generated with an approach similar to the one described in the present work to obtain a CRISPR/Cas9 system using saCas9, SpCas9, or adenine-based editing systems [15, 26, 27]. The design of these LVLP (number and location of the MS2 coat protein, number of MS2 aptamer repeats, and 3′UTR modification) was different from ours. Like these authors, we observed that LentiFlash® particles were morphologically similar to conventional lentiviral vectors [20]. Differently from us, these authors reported that the viral titers were decreased when MCP was cloned into the matrix gene. Indeed, the titers we obtained with these vector batches remained high, and they are in the best design configuration for efficient gene editing. Other groups used similar bacteriophage systems to create particles that can transfer RNA into target cells using a slightly different design compared with ours [15, 18, 19]. Briefly, Knopp et al. replaced the nucleocapsid by a genetically fused MS2 heterodimer to generate non-integrating gammaretroviral murine leukemia virus-based CRISPR/Cas9 all-in-one particles. Lindel et al. used a transient prototype foamy virus (PFV) vector system to deliver Cas9 mRNA combined with an integration-deficient retroviral vector (IDRV) to carry the sgRNA, allowing efficient gene editing. They also showed that sgRNA delivery using the transient PFV vector was less efficient than with the IDRV vector, but resulted in significant editing rates when transduced 24 h after the Cas9 mRNA-carrying transient PFV. Although LentiFlash® particles contain RNPs, sgRNA and RNA for Cas9 are actively encapsidated via the MS2 coat protein-aptamer interaction. We think that some editing activity can be attributed to passively packaged or embedded Cas9 protein and that this activity might be maintained by the expression of Cas9 RNA. This might explain the increased editing efficiency when using the active packaging system. LentiFlash® particles allow the delivery of RNA molecules in the cell cytoplasm, without any viral sequence, thus completely avoiding reverse transcription and integration in the cell genome (Fig. S6e). Therefore, LentiFlash® particles could be an interesting tool for transient expression for gene overexpression, gene editing, or transcription factor-based differentiation.

Considering the high capacity of LentiFlash® particles to efficiently deliver CRISPR/Cas9 reagents at multiple loci, we investigated whether this system could be used in a reframing strategy at a pathogenic locus. Therefore, we designed a sgRNA specific for a pathogenic variant in a patient-derived hiPSC line, to introduce indels in the close vicinity of this frameshift mutation. To our surprise, this did not result in the generation of indels, but in interallelic gene conversion that allowed correcting the variant to a WT sequence in more than 40% of transduced cells. Interestingly, this phenomenon was conserved following hiPSC differentiation to neural progenitors, suggesting that it is not restricted to pluripotent cells. Furthermore, we confirmed gene conversion after allele-specific targeting of a frameshift mutation at an additional locus (*DNAH5*) in three clones derived from a second hiPSC line (HY03). To the best of our knowledge, interallelic gene conversion has never been described in hPSC.

Gene conversion is a form of homologous recombination that is initiated by DNA DSB and results in the unidirectional transfer of genetic material from the intact homologous sequence to the region that contains the DSB. This phenomenon is well documented during meiosis and is a recognized driver not only of human genome evolution, but also of inherited diseases. However, it is also involved in the occasional phenotype reversion of genetic diseases, such as epidermolysis bullosa [28]. More recently, this DNA repair mechanism was described in other cell types after CRISPR/Cas9-mediated DNA DSB. One report demonstrated interallelic gene conversion in cultured human cells, including human embryonic kidney cells (HEK293T) and human primary lung stromal cells [29], but only in 2.3% and 0.15% of the alleles, respectively. Two other reports described interallelic gene conversion in mouse embryonic stem cells, with different yields: 4×10^{-5} in the study by Susani et al. [30] and 40% in the study by Wu et al. [31]. As we did in our study, Wu et al. used an allele-specific sgRNA that included the variant sequence in the protospacer adjacent motif. Finally, several articles described this phenomenon after CRISPR/Cas9 injection in early

embryos. Although interallelic gene conversion in embryos has been controversial [32–35], this DNA repair mechanism has been shown to be activated in mouse [31], rat [36], and human embryos [37–39]. Although the embryo number and targeted loci remain low, interallelic gene conversion following CRISPR/Cas9 mutagenesis seems to occur more frequently in embryos: 28% in the rat (2/7 embryos) [36], 18% in the mouse (4/22 embryos) [31], and up to 40% in human embryos [37, 38]. Moreover, this DNA repair pathway can be modulated through the use of exogenous molecules. For instance, the 53BP1 inhibitor i53 increases gene conversion in different human and mouse cell lines [40]. Moreover, RAD51 was recently used to increase interallelic gene conversion in mouse embryos from 26 to 74% by Wilde et al. [41]. These studies indicate that interallelic gene conversion might be a conserved DNA repair mechanism activated at high frequency during early mammalian embryogenesis and consequently also in pluripotent stem cells. As DNA damage response can be cell-type specific [42], and the DNA repair response is more efficient in pluripotent stem cells than in somatic cells [43, 44], we investigated whether interallelic gene conversion is also active beyond the pluripotency stage. We obtained similar results in neural progenitors derived from the same hPSC line, suggesting that this phenomenon is at least conserved in some cell types.

Conclusions

Our data show, for the first time, the occurrence of interallelic gene conversion in hiPSC after CRISPR/Cas9 induced DSB. This repair process is observed at a high rate only when one allele is specifically targeted. Interallelic gene conversion in hiPSC could be used to efficiently engineer their genome without donor DNA template. Moreover, unraveling the molecular machinery responsible for gene conversion in hiPSC could lead to the development of strategies to modulate and increase this DNA repair pathway in differentiated cells. This could provide a simple way to convert heterozygote alleles to a homozygous state at targeted loci, opening the way to correct human recessive genetic disorders caused by compound heterozygous mutations and human autosomal dominant genetic disorders.

Methods

hiPSC lines, culture, and passaging

Three hiPSC lines reprogrammed in the laboratory were used: (i) HY03 (alternative name listed in the hPSCReg registry: UHOMi002-A), derived from an healthy individual [23]; (ii) PCD_02:30 (alternative name listed in the hPSCReg registry: UHOMi001-A), derived from a patient with primary ciliary dyskinesia harboring compound heterozygous mutations in the *CCDC40* gene [24]; and (iii) iCOPD9_B27, derived from a patient with chronic obstructive pulmonary disease (COPD) [45]. The three hiPSC lines were maintained in undifferentiated state in feeder-free conditions on growth factor-reduced Geltrex matrix (Thermo Fisher Scientific) in Essential 8™ (E8) medium (Thermo Fisher Scientific) at 37 °C in a humidified atmosphere of 5% CO_2 in air. Cells were dissociated using Versene (Thermo Fisher Scientific) for single-cell passaging every 4–5 days (when cells reached 70–80% confluence) followed by plating (1:10 to 1:20 ratio) with 10 μM of the ROCK inhibitor Y-27632 (Tocris). The E8 medium was changed daily.

sgRNA design and selection

DNAH5 and *MCIDAS* sgRNAs were selected to target a sequence in an exon shared by all the gene transcripts and to be as specific as possible using the freely available CRISPOR online tool (http://crispor.tefor.net/) [46]. For the *CCDC40* reframing/gene conversion experiment, the sgRNA was selected using CRISPOR online tool in order to include the "Δ-2nt, allele 1" mutation [c.1116_1117delCT, p.Y378Hfs] and to produce a DNA DSB as close as possible to the mutation. The sgRNAs targeting *TRAC*, *CXCR4*, and *GFP* were previously described [47–49]. The sgRNA sequences are listed in Supplementary Table S1.

Integrative lentiviral vector particle production, purification, and quantification by quantitative PCR

Three plasmids were used to produce the recombinant lentiviral particles ILV-EF1-GFP. A first plasmid pLV-GagPol (wt) provided a nucleic acid encoding viral gag and pol genes lacking vif, vpr, vpu, and nef genes. A second plasmid pVSVG provided a nucleic acid encoding the vesicular stomatitis virus envelope glycoprotein (VSV-G). A third self-inactivating expression plasmid encoded the GFP fluorescent reporter under the control of the human elongation factor 1 alpha promoter (EF1a) (Fig. S11). Viral particles were produced in a 10-layer CellSTACK chamber (6360cm^2, Corning) after transfection of the three plasmids in HEK293T cells using the standard calcium phosphate procedure. Twenty-four hours post-transfection, the supernatant was discarded and replaced by fresh medium and cells were incubated at 37 °C in a humidified atmosphere of 5% CO_2 in air. After medium change, supernatant was collected, clarified by centrifugation at 3000 *g* for 5 min, and microfiltered through 0.45-μm pore size sterile filter units (Stericup, Millipore). Supernatant was harvested several times, and finally, all samples were pooled (crude harvest). The crude harvest was concentrated and purified by ultrafiltration and diafiltration.

Transduction unit (TU) titration assays of the pooled supernatants were performed as follows. HCT116 cells

were seeded in 96-well plates. Twenty-four hours later, transduction was performed using pooled supernatants and the rLV-EF1-GFP internal standard (six serial dilutions). Three days post-transduction, cells were trypsinized and the titer (TU/ml) was determined by qPCR after extraction of genomic DNA using the Nucleospin tissue gDNA extraction kit (Macherey-Nagel). The titer determined by qPCR and expressed in TU/ml was normalized to the internal standard, the titer of which was previously determined by FACS.

MS2 and PP7-chimeric retrovirus-like particle (LentiFlash®) production, purification, and quantitation by p24 ELISA assay

The non-integrative LentiFlash® particles (Flash Therapeutics) that exploit the bacteriophage MS2 or PP7-Coat and its cognate RNA aptamer were previously described by Prel et al. [20]. Like for the integrative lentiviral particles, three plasmids were used to produce recombinant LentiFlash® particles in HEK293T cells: (i) the pLV-GagPol plasmid encoding the viral gag and pol genes modified to harbor the MS2 and/or PP7-Coat within the gag gene and referred to as pLF-GagPol ZF_PCP and pLF-GagPol MA_MCP.ZF_PCP. pLF-GagPol ZF_PCP was generated using the p8.74 ΔZF_MS2Coat construct, described by Prel et al. [20], by replacing the MS2 coat protein sequence with the capsid assembly-deficient PP7 coat protein PP7ΔFG sequence described by Chao et al. [50]. The human codon-optimized PP7ΔFG coding sequence was synthesized by Geneart (Thermo Fisher Scientific) and cloned, using the In-Fusion® cloning kit (Takara Bio), into p8.74 ΔZF_MS2Coat previously digested with *Hpa*I. pLF-GagPol MA_MCP.ZF_PCP was generated by inserting the MS2 coat protein coding sequence into the pLF-GagPol ZF_PCP plasmid between the codons corresponding to the 127th and 128th amino acid of the MA protein using the In-Fusion® cloning kit (Takara Bio) after PCR amplification of the two fragments; (ii) the pVSVG plasmid encoding the VSV-G glycoprotein; and (iii) the plasmid encoding the RNA cargo, flanked by the bacteriophage aptamers to enable RNA mobilization into lentiviral particles through the interaction with the corresponding coat protein cloned in the Gag sequence. For the ZsGreen reporter, the ZsGreen mRNA was flanked by PP7 aptamers on the RNA transfer plasmid as shown in supplementary Fig. S11, and the pLF-GagPol ZF_PCP was used for transfection of the produced cells. For the CRISPR/Cas9 system, PP7 aptamers were inserted into the tetraloop and stem-loop 2 of the sgRNA scaffold, the Cas9 nuclease mRNA sequence was flanked by MS2 aptamers on the RNA transfer plasmid, as detailed in supplementary Fig. S11, and the pLF-GagPol MA_MCP.ZF_PCP packaging plasmid was used for transfection. All newly generated constructs were verified by restriction enzyme digestion and sequencing. The primer sequences and additional details are available upon request. Production, concentration, and purification of LentiFlash® particles were done as described for the integrative viral particles.

The functionality of LentiFlash® particles carrying multiple RNA molecules encapsidated using a bacteriophage chimeric system, regardless of the position of the bacteriophage coat protein in the gag gene, was demonstrated and patented in 2015 [51]. We evaluated various designs to determine the best localization of the MS2 coat protein in the gag gene. We found that the maximum amount of RNAs is packaged into LentiFlash® particles when the MCP is inserted in the matrix gene. We did not observe any significant decrease of the p24 titers of LentiFlash® batches containing the MCP inserted into MA compared with constructs in which the MCP was inserted in the NC. The p24 titers of these batches remained high, and these particles effectively led to high and rapid level of expression of the gene of interest. Following the first LentiFlash® patent, the functionality of LentiFlash® particles to transfer the CRISPR/Cas9 system was then demonstrated and patented in 2016 [52]. We performed many additional experiments with this MCP-MA/PCP-NC optimized helper plasmid to confirm the best editing efficiency of these particles in different cell types and/or by targeting various genes.

For quantification, the p24 core antigen was detected directly in the viral supernatant with a HIV-1 p24 ELISA kit (Perkin Elmer), as specified by the supplier. The viral titer (expressed in physical particles per ml) was calculated from the p24 amount, knowing that 1 pg of p24 corresponds to 10^4 physical particles.

hiPSC transduction

The day before transduction, hiPSC were plated as single cells (25000 cells/cm^2) in 24- or 48-well plates coated with Geltrex matrix in E8 medium supplemented with 10 μM of Y-27632. Two hours before transduction, the medium was changed with fresh E8 supplemented with 10 μM Y-27632. Transduction was performed using integrative lentiviral particles or LentiFlash® particles in E8 medium supplemented with 10 μM Y-27632 and 8 μg/ml polybrene (Sigma Aldrich) for 16 to 18 h before changing the medium.

Electroporation

For electroporation, 4×10^5 PCD_02:30 iPSC were transfected with 52 pmol Cas9 protein and 60 pmol premixed Alt-R CRISPR-Cas9 tracrRNA and Alt-R CRISPR-Cas9 crRNA (IDT DNA Technologies) in Nucleofector Solution SF (Lonza) in a final volume of 25 μl. Cells were transfected with the Amaxa 4D-Nucleofector (Lonza) device using program CA-137 and then resuspended in

with E8 medium supplemented with 10 μM Y-27632 for 24 h.

Sanger sequencing and ICE analysis

Targeted loci were amplified using the appropriate primers (listed in Supplementary Table S2) and the One-Taq® DNA Polymerase (NEB) following the manufacturer's instruction. After amplification confirmation by electrophoresis of an aliquot on 2% agarose gels, PCR products were purified using the QIAquick PCR Purification Kit (QIAGEN), as recommended by the manufacturer. Purified PCR products were analyzed by Sanger sequencing (Eurofins Genomics). Chromatograms were analyzed with the freely available FinchTV version 1.4.0 (Geospiza) and ICE (Synthego) tools [53].

On-target next-generation amplicon sequencing

Genomic DNA was used as input for PCR (primers described in Table S2) using OneTaq polymerase (New England Biolabs). PCR product was purified using the QIAquick Gel Extraction Kit (Qiagen) according to the manufacturer's instructions and subjected to paired-end read sequencing on an Illumina flow cell MiniSeq Mid-Output at Montpellier GenomiX. Genomic PhiX DNA was spiked-in to increase base diversity. Fastq files were analyzed using the CRISPResso2 software with default settings [54].

Clonal line derivation and validation

Clonal hiPSC lines were obtained by plating transduced cells at low density in 6-well plates coated with Geltrex matrix (from 500 to 10000 cells/well) in E8 medium supplemented with 10 μM Y-27632. The medium was changed every day and Y-27632 was added for the first 2 days. After 6–10 days, clones were manually picked and transferred to a well of a 96-well plate coated with Geltrex matrix in E8 medium. Clones were amplified in E8 medium for 5 to 8 days and passaged as small clumps in two wells of 96-well plates (duplicate). One plate was kept in culture and the second was used for screening.

Screening was performed by extracting DNA with the DNA Extract All Reagents Kit (Thermo Fisher Scientific) or the QIAamp DNA Blood Mini Kit (QIAGEN) followed by HRMA using the LightCycler® 480 SYBR Green kit (Roche) and a standard qPCR program (95 °C for 10 min, followed by 40 cycles of 95 °C for 10 s, 60 °C for 15 s, and 72 °C for 15 s, with a final melting curve including a step of 95 °C for 5 s followed by an increase from 65 to 97 °C with a temperature ramping set to 0.11 °C/s) on a LightCycler 480 (Roche). The identified mutant clones were confirmed by Sanger sequencing as described above.

Newly established clonal lines were validated by (1) Sanger sequencing analysis of off-target sites containing up to three mismatches (primers are listed in Supplementary Table S2), (2) immunofluorescence analysis of OCT3/4, NANOG, SOX2, and SSEA4 expression (pluripotency markers) (antibodies are listed in Supplementary Table S3), and (3) genomic integrity analysis by ddPCR of the copy number variations of the 24 more frequent recurrent genetic abnormalities that cover more than 90% of all recurrent genetic abnormalities found in hPSC (provided as a service by Stem Genomics) [55].

Copy number variation analysis by droplet digital PCR (ddPCR)

Copy number variation was evaluated in a duplex reaction in which the target gene (*GFP* or *CCDC40*-YGT) is amplified using a FAM-labeled probe (IDT DNA Technologies) and the reference gene *RPP30* with a HEX-labeled probe (IDT DNA Technologies), set at two copies. Reaction mixes contained 150 ng of purified genomic DNA, 1x ddPCR Supermix (Bio-Rad), 900 nM of each primer (two primers per assay), and 250 nM of each probe (sequences detail can be found in Supplementary Table S2). Reaction mixes were loaded into DG8 cartridges with 70 μl of droplet oil (Bio-Rad) per sample and the droplets generated using the QX200 Droplet Generator (Bio-Rad), according to the manufacturer's instructions. Emulsions were transferred to a 96-well plate, and samples were amplified in a thermocycler (95 °C for 10 min, followed by 45 cycles of 95 °C for 30 s and 60 °C for 60 s, with a final elongation step of 98 °C for 10 min with temperature ramping set at 2 °C/s). The plate was then loaded on the QX200 Droplet Reader (Bio-Rad), and copy number was determined with the QuantaSoft software.

Gene expression analysis by real-time quantitative PCR

For qPCR experiments, total RNA was extracted from cells using the RNeasy® Mini kit (QIAGEN) following the manufacturer's instructions. Reverse transcription to complementary DNA (cDNA) was performed using the SuperScript™ First-Strand Synthesis System for RT-PCR (Invitrogen) following the manufacturer's instructions. qPCR was performed using LightCycler® 480 SYBR Green I Master (Roche) in 384 plates, in 10 μl reactions, including 1x SYBR Green I Master, 0.5 μM of each primer, and the cDNA. All reactions were performed in triplicate. A negative control (RNAse/DNAse-free water) was included in each run. The qPCR assays were performed on a LightCycler 480 (Roche) using the following program: 95 °C for 10 min, followed by 40 cycles of 95 °C for 10 s, 60 °C for 15 s, and 72 °C for 15 s, with a final melting curve including a step of 95 °C for 5 s followed by an increase from 65 to 97 °C with a temperature ramping set to 0.11 °C/s.

Raw data (Ct values) were analyzed using the comparative Ct method. Gene expression data were calculated as relative to the expression of the *GAPDH* housekeeping gene. The comparative threshold cycle method (ΔΔCT) was used to quantify relative gene expression, and the obtained quantification was transformed to $2^{-\Delta\Delta CT}$ values.

Immunofluorescence

Cells were fixed in 4% paraformaldehyde at room temperature (RT) for 15 min and then permeabilized with PBS containing 0.5% Triton X-100 (Thermo Fisher Scientific) for 15 min. Cells were blocked with 10% donkey serum in PBS containing 1% BSA and 0.1% Triton X-100 at RT for 60 min. Primary and secondary antibodies were diluted (see Supplementary Table S3 for details) in 1% BSA/0.1% Triton X-100/PBS. Samples were incubated with primary antibodies at 4 °C overnight and with secondary antibodies at RT in the dark for 60 min. Nuclei were stained with DAPI (1:2500) for 2 min and then samples were mounted in ProLong Gold (Thermo Fisher Scientific) and stored in the dark at RT. A Zeiss microscope (LMS700) and the ZEN 3.1 (blue edition) software were used for image acquisition and analysis.

Flow cytometry analysis

For CXCR4 staining, cells were harvested by dissociation to a single cell suspension with Versene. Cells were first incubated with Zombie violet (1:1000, Biolegend) at RT in the dark for 15 min to differentiate between live and dead cells. Cell pellets were then incubated with a PE-conjugated anti-CXCR4 antibody (mouse PE, 1:200, BD Biosciences) or its isotype control at 4 °C for 30 min (see supplemental Table S3 for details). For GFP or ZsGreen analysis, cells were harvested by dissociation to single cell suspension using Versene and directly used for flow cytometry analysis.

All cells were analyzed using a Gallios flow cytometer (Beckman Coulter) and the Kaluza Analysis software (Beckman Coulter).

Lactate dehydrogenase cytotoxicity assay and cell counting

LDH cytotoxicity analysis was performed using the Cytotoxicity Detection Kit (LDH) (Roche) following the manufacturer's instructions. Briefly, supernatants of transduced and control cells were harvested every day for 3 days. A cell lysate control was made using a well of not transduced cells lysed in 1% Triton X-100 solution. Fresh E8 medium constituted the blank control. Supernatants, blank, and lysis controls were centrifuged at 5000 rpm for 3 min to remove cells and cell debris. Then, supernatants (100 µl/each) were distributed in duplicate in a 96-well plate. One hundred microliters of reaction mixture containing the catalyst and the dye solution was added to each well, and the plate was incubated in the dark at RT for 15 min. Absorbance was measured at 492 nm using a Varioskan Flash reader (Thermo Fischer Scientific).

Cells were counted manually using a Malassez counting chamber after dissociation to single cells using Versene.

Differentiation to definitive endoderm

hiPSC were differentiated to definitive endoderm as per Ahmed et al. [45]. Briefly, 16 to 18 h before differentiation induction, cells were plated as single cells at 80000 cells/cm^2 in 24- or 6-well plates in E8 medium supplemented with 10 µM Y-27632. Differentiation was induced by replacing the E8 medium with RPMI 1640 (GIBCO) supplemented with B27 without vitamin A (GIBCO), 100 ng/ml activin A (Peprotech), 3 mM CHIR-99021 (Tocris), and 10 µM Y-27632. After 24 h, the medium was changed to RPMI 1640 supplemented with B27 without vitamin A, 100 ng/ml activin A, and 250 nM LDN-193189 (Miltenyi biotec). Cells were then incubated for another 24 h to obtain definitive endoderm.

Differentiation to neural progenitors and transduction

hiPSC were differentiated to neural progenitors using the STEMdiff™ SMADi Neural Induction kit (STEMCELL), following the manufacturer's instructions. Briefly, differentiation was induced by plating hiPSC as single cells at 200,000 cells/cm^2 in 6-well plates coated with Geltrex matrix in STEMdiff™ Neural Induction medium supplemented with SMADi and 10 µM Y-27632. After 24 h, the medium was changed to fresh STEMdiff™ Neural Induction medium supplemented with SMADi. Then, the medium was changed daily for 4 to 5 days before cell passaging. For this, cells were dissociated to single cell using Versene followed by plating 150,000 cells/cm^2 in 6-well plates coated with Geltrex matrix in STEMdiff™ Neural Induction medium supplemented with SMADi and 10 µM Y-27632.

The day prior to transduction, neural progenitors were dissociated to single cell using Versene and 125,000 cells/cm^2 were plated in 48-well plates coated with Geltrex matrix in STEMdiff™ Neural Induction medium supplemented with SMADi and 10 µM Y-27632. Two hours before transduction, the medium was changed to fresh STEMdiff™ Neural Induction medium supplemented with SMADi and 10 µM Y-27632. Transduction was performed using LentiFlash® particles in STEMdiff™ Neural Induction medium supplemented with SMADi, 10 µM Y-27632, and 8 µg/ml polybrene for 16 to 18 h before changing the medium.

Statistical analysis

Data are presented as the mean ± SEM. Differences were evaluated using the two-way ANOVA, Dunnett test. Statistical analyses were performed with GraphPad Prism. A value of $P \leq 0.05$ was considered to be significant.

Abbreviations

Cas9: CRISPR-associated protein 9; cDNA: Complementary DNA; CCDC40: Coiled-coil domain containing 40; COPD: Chronic obstructive pulmonary disease; CRISPR: Clustered regularly interspaced short palindromic repeats; CXCR4: C-X-C chemokine receptor type 4; ddPCR: Droplet digital PCR; DSB: Double-strand breaks; hiPSC: Human induced pluripotent stem cells; hPSC: Human pluripotent stem cells; HRMA: High-resolution melting analysis; ICE: Interference of CRISPR edits; IDRV: Integration-deficient retroviral vector; ILV: Integrative lentiviral vector; LDH: Lactate dehydrogenase; LF-ZsGreen: LentiFlash® particles containing the fluorescent reporter ZsGreen mRNA; LVLP: Lentivirus-like particles; MCIDAS: Multiciliate differentiation and DNA synthesis associated cell cycle protein; MFI: Mean fluorescent intensity; MMEJ: Micro-homology end-joining; NHEJ: Non-homologous end-joining; NT: Not transduced; OT: Off-target; PCD: Primary ciliary dyskinesia; PFV: Prototype foamy virus; qPCR: Quantitative PCR; sgRNA: Single guide RNA; SIN: Self-inactivating; RRE: Rev-responsive element; RT: Room temperature; TRAC: T cell receptor alpha constant; TU: Transduction unit; VSV-G: Vesicular stomatitis virus envelope glycoprotein; WPRE: Woodchuck hepatitis virus post-transcriptional regulatory element; WT: Wild type allele

Supplementary Information

The online version contains supplementary material available at https://doi.org/10.1186/s12915-021-01214-x.

Additional file 1: Figs. S1-S11. Supplementary Figure S1. Transduction of the HY03 hiPSC line with LF-ZsGreen particles allows transient ZsGreen expression and does not affect pluripotency. **Supplementary Figure S2.** LF-ZsGreen particles allow the highly efficient delivery of RNA in different hiPSC lines. **Supplementary Figure S3.** Characterization of the HY03-GFP non-clonal reporter hiPSC line. **Supplementary Figure S4.** NGS analysis of DNAH5 indel size distribution. **Supplementary Figure S5.** LentiFlash® particle-based transduction of the CRISPR/Cas9 system to target the GFP fluorescent reporter sequence in a HCT116-GFP cell line that contains one GFP copy per cell. **Supplementary Figure S6.** Characterization of hiPSC clones in which *DNAH5* or *MCIDAS* was knocked out by CRISPR/Cas9 gene editing using the LentiFlash® system. **Supplementary Figure S7.** LentiFlash® particle-based transduction of the CRISPR/Cas9 components to target specific genes results in high indel formation in different hiPSC lines. **Supplementary Figure S8.** Interallelic gene conversion following iPSC electroporation and following LentiFlash® transduction of neural progenitors obtained from the PCD_02:30 hiPSC line results. **Supplementary Figure S9.** Characterization of hiPSC clonal lines harboring *DNAH5* heterozygous mutations. **Supplementary Figure S10.** Specifically targeting the wild-type allele in hiPSC clones harboring a *DNAH5* heterozygous mutation results in interallelic gene conversion. **Supplementary Figure S11.** Schematic representation of the expression cassettes carried by the plasmids used to produce the integrative lentiviral vector (ILV) that expresses the GFP reporter and of the expression cassettes carried by the plasmids used to produce non-integrative lentiviral particles (LentiFlash®) that express the ZsGreen reporter or the CRISPR/Cas9 systems. **Supplementary Tables S1-3. Supplementary Table S1.** sgRNA sequences. **Supplementary Table S2.** PCR primers. **Supplementary Table S3.** antibodies

Acknowledgements

We wish to thank Montpellier Rio Imaging for access to their flow cytometry facilities (http://www.mri.cnrs.fr/en/). We thank Elena Hauser and Marie Bouaud for technical help and Véronique Pantesco for helping in the amplicon deep sequencing experiment.

Authors' contributions

J.M., C.N.V., A.N., C.B., M.F., E.A., N.M, and F.S. performed the experiments. H.P. and A.L. performed the NGS. J.M. designed the experiments. C.D., N.M., A.I., R.G., S.A. and J.D.V. helped with the experiment design. C.D., N.M., A.I., R.G., F.S., L.L., and P.B. contributed to the development of the LentiFlash vectors used in the experiments. M.F., R.G., P.B., A.B., and S.A. revised the manuscript. J.M., C.D., N.M., A.I., and J.D.V. wrote the manuscript. All authors read and approved the final manuscript.

Funding

This work was supported by grant FDM20170638083 and by the "Investissement d'Avenir" program managed by the Agence Nationale pour la Recherche (contract ANR-10-INBS-09) (MGX).

Availability of data and materials

The datasets analyzed in the current study are available from the corresponding author.

Declarations

Ethics approval and consent to participate

Not applicable.

Consent for publication

All authors read and approved the final manuscript.

Competing interests

S.A. and J.D.V. filed a patent entitled "Non-invasive methods for assessing genetic integrity of pluripotent stem cells", priority number: EP20150306389, and are co-founder and scientific advisor of Stem Genomics S.A.S. that acquired the exploitation rights of this patent. C.D., N.M., A.I., R.G., F.S., L.L., and P.B. work for Flash Therapeutics. J.M., C.N.V., C.B., M.F., E.A., and A.B. declare that they have no competing interests.

Author details

[1]IRMB, Univ Montpellier, INSERM, CHU Montpellier, Hôpital St Eloi, 80 avenue Augustin Fliche, 34295 Montpellier, France. [2]Flash Therapeutics, Toulouse, France. [3]Univ. Montpellier, CNRS, INSERM, Montpellier, France. [4]MGX-Montpellier GenomiX, Univ. Montpellier, CNRS, INSERM, Montpellier, France. [5]PhyMedExp, Univ Montpellier, INSERM, CHU Montpellier, Montpellier, France. [6]Department of Cell and Tissue Engineering, Univ Montpellier, CHU Montpellier, Montpellier, France.

Received: 6 April 2021 Accepted: 2 December 2021
Published online: 07 January 2022

References

1. Rowe RG, Daley GQ. Induced pluripotent stem cells in disease modelling and drug discovery. Nat Rev Genet. 2019;20:377.
2. Shi Y, Inoue H, Wu JC, Yamanaka S. Induced pluripotent stem cell technology: a decade of progress. Nat Rev Drug Discov. 2017;16(2):115–30. https://doi.org/10.1038/nrd.2016.245.
3. Hockemeyer D, Jaenisch R. Induced pluripotent stem cells meet genome editing. Cell Stem Cell. 2016;18(5):573–86. https://doi.org/10.1016/j.stem.2016.04.013.
4. Mianné J, Bourguignon C, Nguyen Van C, Nguyen van C, Fieldès M, Nasri A, et al. Pipeline for the generation and characterization of transgenic human pluripotent stem cells using the CRISPR/Cas9 technology. Cells. 2020;9(5). https://doi.org/10.3390/cells9051312.
5. Haapaniemi E, Botla S, Persson J, Schmierer B, Taipale J. CRISPR-Cas9 genome editing induces a p53-mediated DNA damage response. Nat Med. 2018;24(7):927–30. https://doi.org/10.1038/s41591-018-0049-z.
6. Ihry RJ, Worringer KA, Salick MR, Frias E, Ho D, Theriault K, et al. p53 inhibits CRISPR-Cas9 engineering in human pluripotent stem cells. Nat Med. 2018;24(7):939–46. https://doi.org/10.1038/s41591-018-0050-6.
7. Li XL, Li GH, Fu J, Fu YW, Zhang L, Chen W, et al. Highly efficient genome editing via CRISPR-Cas9 in human pluripotent stem cells is achieved by transient BCL-XL overexpression. Nucleic Acids Res. 2018;46(19):10195–215. https://doi.org/10.1093/nar/gky804.
8. Yu X, Liang X, Xie H, Kumar S, Ravinder N, Potter J, et al. Improved delivery of Cas9 protein/gRNA complexes using lipofectamine

CRISPRMAX. Biotechnol Lett. 2016;38(6):919–29. https://doi.org/10.1007/s10529-016-2064-9.
9. Roberts B, Hendershott MC, Arakaki J, Gerbin KA, Malik H, Nelson A, et al. Fluorescent gene tagging of transcriptionally silent genes in hiPSCs. Stem Cell Reports. 2019;12(5):1145–58. https://doi.org/10.1016/j.stemcr.2019.03.001.
10. Mitzelfelt KA, McDermott-Roe C, Grzybowski MN, Marquez M, Kuo CT, Riedel M, et al. Efficient precision genome editing in iPSCs via genetic co-targeting with selection. Stem Cell Reports. 2017;8(3):491–9. https://doi.org/10.1016/j.stemcr.2017.01.021.
11. Martin RM, Ikeda K, Cromer MK, et al. Highly efficient and marker-free genome editing of human pluripotent stem cells by CRISPR-Cas9 RNP and AAV6 donor-mediated homologous recombination. Cell Stem Cell. 2019;24:821–828.e5.
12. Kim S, Kim D, Cho S-W, Kim J, Kim J-S. Highly efficient RNA-guided genome editing in human cells via delivery of purified Cas9 ribonucleoproteins. Genome Res. 2014;24(6):1012–9. https://doi.org/10.1101/gr.171322.113.
13. Geng BC, Choi KH, Wang SZ, Chen P, Pan XD, Dong NG, et al. A simple, quick, and efficient CRISPR/Cas9 genome editing method for human induced pluripotent stem cells. Acta Pharmacol Sin. 2020;41(11):1427–32. https://doi.org/10.1038/s41401-020-0452-0.
14. Xu X, Gao D, Wang P, Chen J, Ruan J, Xu J, et al. Efficient homology-directed gene editing by CRISPR/Cas9 in human stem and primary cells using tube electroporation. Sci Rep. 2018;8(1):11649. https://doi.org/10.1038/s41598-018-30227-w.
15. Lu B, Javidi-Parsijani P, Makani V, Mehraein-Ghomi F, Sarhan WM, Sun D, et al. Delivering SaCas9 mRNA by lentivirus-like bionanoparticles for transient expression and efficient genome editing. Nucleic Acids Res. 2019;47(8):e44. https://doi.org/10.1093/nar/gkz093.
16. Ortinski PI, O'Donovan B, Dong X, Kantor B. Integrase-deficient lentiviral vector as an all-in-one platform for highly efficient CRISPR/Cas9-mediated gene editing. Mol Ther Methods Clin Dev. 2017;5:153–64. https://doi.org/10.1016/j.omtm.2017.04.002.
17. Mock U, Riecken K, Berdien B, Qasim W, Chan E, Cathomen T, et al. Novel lentiviral vectors with mutated reverse transcriptase for mRNA delivery of TALE nucleases. Sci Rep. 2014;4(1):6409. https://doi.org/10.1038/srep06409.
18. Lindel F, Dodt CR, Weidner N, Noll M, Bergemann F, Behrendt R, et al. TraFo-CRISPR: enhanced genome engineering by transient foamy virus vector-mediated delivery of CRISPR/Cas9 components. Mol Ther Nucleic Acids. 2019;18:708–26. https://doi.org/10.1016/j.omtn.2019.10.006.
19. Knopp Y, Geis FK, Heckl D, Horn S, Neumann T, Kuehle J, et al. Transient retrovirus-based CRISPR/Cas9 all-in-one particles for efficient, targeted gene knockout. Mol Ther Nucleic Acids. 2018;13:256–74. https://doi.org/10.1016/j.omtn.2018.09.006.
20. Prel A, Caval V, Gayon R, Ravassard P, Duthoit C, Payen E, et al. Highly efficient in vitro and in vivo delivery of functional RNAs using new versatile MS2-chimeric retrovirus-like particles. Mol Ther Methods Clin Dev. 2015;2:15039. https://doi.org/10.1038/mtm.2015.39.
21. Ling S, Yang S, Hu X, Yin D, Dai Y, Qian X, et al. Lentiviral delivery of co-packaged Cas9 mRNA and a Vegfa-targeting guide RNA prevents wet age-related macular degeneration in mice. Nat Biomed Eng. 2021;5(2):144–56. https://doi.org/10.1038/s41551-020-00656-y.
22. Yin D, Ling S, Wang D, Dai Y, Jiang H, Zhou X, et al. Targeting herpes simplex virus with CRISPR-Cas9 cures herpetic stromal keratitis in mice. Nat Biotechnol. 2021;39(5):567–77. https://doi.org/10.1038/s41587-020-00781-8.
23. Fieldes M, Ahmed E, Bourguignon C, Mianné J, Martin M, Arnould C, et al. Generation of the induced pluripotent stem cell line UHOMi002-A from peripheral blood mononuclear cells of a healthy male donor. Stem Cell Res. 2020;49:102037. https://doi.org/10.1016/j.scr.2020.102037.
24. Ahmed E, Sansac C, Fieldes M, Bergougnoux A, Bourguignon C, Mianné J, et al. Generation of the induced pluripotent stem cell line UHOMi001-A from a patient with mutations in CCDC40 gene causing primary ciliary dyskinesia (PCD). Stem Cell Res. 2018;33:15–9. https://doi.org/10.1016/j.scr.2018.09.019.
25. Campenhout CV, Cabochette P, Veillard AC, Laczik M, Zelisko-Schmidt A, Sabatel C, et al. Guidelines for optimized gene knockout using CRISPR/Cas9. Biotechniques. 2019;66(6):295–302. https://doi.org/10.2144/btn-2018-0187.
26. Lu Z, Yao X, Lyu P, Yadav M, Yoo K, Atala A, et al. Lentiviral capsid-mediated Streptococcus pyogenes Cas9 ribonucleoprotein delivery for efficient and safe multiplex genome editing. CRISPR J. 2021. https://doi.org/10.1089/crispr.2020.0106.
27. Lyu P, Lu Z, Cho SI, Yadav M, Yoo KW, Atala A, et al. Adenine base editor ribonucleoproteins delivered by lentivirus-like particles show high on-target base editing and undetectable RNA off-target activities. CRISPR J. 2021;4(1):69–81. https://doi.org/10.1089/crispr.2020.0095.
28. Jonkman MF, Scheffer H, Stulp R, Pas HH, Nijenhuis M, Heeres K, et al. Revertant mosaicism in epidermolysis bullosa caused by mitotic gene conversion. Cell. 1997;88(4):543–51. https://doi.org/10.1016/S0092-8674(00)81894-2.
29. Javidi-Parsijani P, Lyu P, Makani V, Sarhan WM, Yoo KW, el-Korashi L, et al. CRISPR/Cas9 increases mitotic gene conversion in human cells. Gene Ther. 2020;27(6):281–96. https://doi.org/10.1038/s41434-020-0126-z.
30. Susani L, Castelli A, Lizier M, Lucchini F, Vezzoni P, Paulis M. Correction of a recessive genetic defect by CRISPR-Cas9-mediated endogenous repair. CRISPR J. 2018;1(3):230–8. https://doi.org/10.1089/crispr.2018.0004.
31. Wu Y, Liang D, Wang Y, Bai M, Tang W, Bao S, et al. Correction of a genetic disease in mouse via use of CRISPR-Cas9. Cell Stem Cell. 2013;13(6):659–62. https://doi.org/10.1016/j.stem.2013.10.016.
32. Adikusuma F, Piltz S, Corbett MA, Turvey M, McColl SR, Helbig KJ, et al. Large deletions induced by Cas9 cleavage. Nature. 2018;560(7717):E8–9. https://doi.org/10.1038/s41586-018-0380-z.
33. Egli D, Zuccaro MV, Kosicki M, Church GM, Bradley A, Jasin M. Inter-homologue repair in fertilized human eggs. Nature. 2018;560(7717):E5–7. https://doi.org/10.1038/s41586-018-0379-5.
34. Burgio G. Gene conversion following CRISPR/Cas9 DNA cleavage: an overlooked effect. Gene Ther. 2020;27(6):245–6. https://doi.org/10.1038/s41434-020-0154-8.
35. Zuccaro MV, Xu J, Mitchell C, Marin D, Zimmerman R, Rana B, et al. Allele-specific chromosome removal after Cas9 cleavage in human embryos. Cell. 2020;183(6):1650–1664.e15. https://doi.org/10.1016/j.cell.2020.10.025.
36. Yoshimi K, Kaneko T, Voigt B, Mashimo T. Allele-specific genome editing and correction of disease-associated phenotypes in rats using the CRISPR-Cas platform. Nat Commun. 2014;5(1):4240. https://doi.org/10.1038/ncomms5240.
37. Ma H, Marti-Gutierrez N. Park SW et al. Nature: Correction of a pathogenic gene mutation in human embryos; 2017.
38. Liang D, Gutierrez NM, Chen T et al. Frequent gene conversion in human embryos induced by double strand breaks. bioRxiv. 2020
39. Ma H, Marti-Gutierrez N, Park SW, et al. Ma et al. reply. Nature. 2018;560(7717):E10–23. https://doi.org/10.1038/s41586-018-0381-y.
40. Canny MD, Moatti N, Wan LCK, et al. Inhibition of 53BP1 favors homology-dependent DNA repair and increases CRISPR-Cas9 genome-editing efficiency. Nat Biotechnol. 2017.
41. Wilde JJ, Aida T, Del Rosario RCH, et al. Efficient embryonic homozygous gene conversion via RAD51-enhanced interhomolog repair. Cell. 2021;184:3267-3280.e18.
42. Blanpain C, Mohrin M, Sotiropoulou PA, Passegué E. DNA-damage response in tissue-specific and cancer stem cells. Cell Stem Cell. 2011;8(1):16–29. https://doi.org/10.1016/j.stem.2010.12.012.
43. Fu X, Cui K, Yi Q, Yu L, Xu Y. DNA repair mechanisms in embryonic stem cells. Cell Mol Life Sci. 2017;74(3):487–93. https://doi.org/10.1007/s00018-016-2358-z.
44. Rocha CRR, Lerner LK, Okamoto OK, Marchetto MC, Menck CFM. The role of DNA repair in the pluripotency and differentiation of human stem cells. Mutation research. 2012
45. Ahmed E, Fieldes M, Bourguignon C et al. Differentiation of human induced pluripotent stem cells into functional airway epithelium. bioRxiv. 2020. Available from: https://doi.org/10.1101/2020.11.29.400358
46. Haeussler M, Schönig K, Eckert H, Eschstruth A, Mianné J, Renaud JB, et al. Evaluation of off-target and on-target scoring algorithms and integration into the guide RNA selection tool CRISPOR. Genome Biol. 2016;17(1):148. https://doi.org/10.1186/s13059-016-1012-2.
47. Osborn MJ, Webber BR, Knipping F, et al. Evaluation of TCR gene editing achieved by TALENs, CRISPR/Cas9 and megaTAL nucleases. Mol Ther. 2015.
48. Schumann K, Lin S, Boyer E, Simeonov DR, Subramaniam M, Gate RE, et al. Generation of knock-in primary human T cells using Cas9 ribonucleoproteins. Proc Natl Acad Sci U S A. 2015;112(33):10437–42. https://doi.org/10.1073/pnas.1512503112.
49. Mali P, Aach J, Stranges PB, Esvelt KM, Moosburner M, Kosuri S, et al. CAS9 transcriptional activators for target specificity screening and paired nickases for cooperative genome engineering. Nat Biotechnol. 2013;31(9):833–8. https://doi.org/10.1038/nbt.2675.

50. Chao JA, Patskovsky Y, Almo SC, Singer RH. Structural basis for the coevolution of a viral RNA-protein complex. Nat Struct Mol Biol. 2008;15(1):103–5. https://doi.org/10.1038/nsmb1327.
51. Bouillé P, Pages JC, Gayon R. Retroviral particle comprising at least two encapsidated nonviral RNAs. US PATENT. 2017 US20180135025A1.
52. Bouillé P, Gayon R, Lamouroux L, Iche A. Particle for the encapsidation of a genome engineering system. US PATENT. 2016 US10870865B2.
53. Hsiau T, Conant D, Rossi N et al. Inference of CRISPR Edits from Sanger Trace Data. bioRxiv. 2018
54. Clement K, Rees H, Canver MC, Gehrke JM, Farouni R, Hsu JY, et al. CRISPResso2 provides accurate and rapid genome editing sequence analysis.[letter]. Nat Biotechnol. 2019;37(3):224–6. https://doi.org/10.1038/s41587-019-0032-3.
55. Assou S, Girault N, Plinet M, Bouckenheimer J, Sansac C, Combe M, et al. Recurrent genetic abnormalities in human pluripotent stem cells: definition and routine detection in culture supernatant by targeted droplet digital PCR. Stem Cell Reports. 2020;14(1):1–8. https://doi.org/10.1016/j.stemcr.2019.12.004.

Publisher's Note

Springer Nature remains neutral with regard to jurisdictional claims in published maps and institutional affiliations.

Ready to submit your research? Choose BMC and benefit from:

- fast, convenient online submission
- thorough peer review by experienced researchers in your field
- rapid publication on acceptance
- support for research data, including large and complex data types
- gold Open Access which fosters wider collaboration and increased citations
- maximum visibility for your research: over 100M website views per year

At BMC, research is always in progress.

Learn more biomedcentral.com/submissions

BMC

REVIEW
COPD

Targeted therapy in eosinophilic chronic obstructive pulmonary disease

Mathieu Fieldes[1], Chloé Bourguignon[1], Said Assou[1], Amel Nasri[1], Aurélie Fort[2,3], Isabelle Vachier[2], John De Vos[1,4], Engi Ahmed[2] and Arnaud Bourdin[2,3]

Affiliations: [1]IRMB, INSERM, Montpellier University Hospital, Montpellier, France. [2]Dept of Respiratory Diseases, Montpellier University Hospital, INSERM, Montpellier, France. [3]PhyMedExp, University of Montpellier, INSERM U1046, Montpellier, France. [4]Dept of Cell and Tissue Engineering, Montpellier University Hospital, Montpellier, France.

Correspondence: Engi Ahmed, Hopital Arnaud de Villeneuve, 371 Av Doyen Gaston Giraud, 34295 Montpellier Cx 5, France. E-mail: e-ahmed@chu-montpellier.fr.

ABSTRACT Chronic obstructive pulmonary disease (COPD) is a common and preventable airway disease causing significant worldwide mortality and morbidity. Lifetime exposure to tobacco smoking and environmental particles are the two major risk factors. Over recent decades, COPD has become a growing public health problem with an increase in incidence. COPD is defined by airflow limitation due to airway inflammation and small airway remodelling coupled to parenchymal lung destruction. Most patients exhibit neutrophil-predominant airway inflammation combined with an increase in macrophages and $CD8^+$ T-cells. Asthma is a heterogeneous chronic inflammatory airway disease. The most studied subtype is type 2 (T2) high eosinophilic asthma, for which there are an increasing number of biologic agents developed. However, both asthma and COPD are complex and share common pathophysiological mechanisms. They are known as overlapping syndromes as approximately 40% of patients with COPD present an eosinophilic airway inflammation. Several studies suggest a putative role of eosinophilia in lung function decline and COPD exacerbation. Recently, pharmacological agents targeting eosinophilic traits in uncontrolled eosinophilic asthma, especially monoclonal antibodies directed against interleukins (IL-5, IL-4, IL-13) or their receptors, have shown promising results. This review examines data on the rationale for such biological agents and assesses efficacy in T2-endotype COPD patients.

@ERSpublications
Patients with severe COPD and eosinophilic inflammation experience uncontrolled symptoms despite optimal pharmaceutical treatment. The development of new biomarkers is needed for better phenotyping of patients to propose innovative targeted therapy. https://bit.ly/2KzWuNO

Cite this article as: Fieldes M, Bourguignon C, Assou S, *et al.* Targeted therapy in eosinophilic chronic obstructive pulmonary disease. *ERJ Open Res* 2021; 7: 00437-2020 [https://doi.org/10.1183/23120541.00437-2020].

Received: 26 June 2020 | Accepted: 14 Dec 2020

Copyright ©ERS 2021. This article is open access and distributed under the terms of the Creative Commons Attribution NonCommercial Licence 4.0.

Introduction

Chronic obstructive pulmonary disease (COPD) is a growing cause of morbidity and mortality worldwide [1]. The Global Burden of Disease Study 2015 estimated approximately 174 million prevalent cases in the world. Over the last two decades, specialists in the field have noticed a significant increase in patient numbers mainly due to global population ageing and environmental factors [2]. Several studies report a high prevalence rate ranging from 2.1% to 26.1% of the adult population depending on age, sex, smoking habits, world region and study inclusion criteria used [2–8]. A higher prevalence is reported among men, but recent data indicate a progressive sex-ratio equilibration due to a rise in tobacco smoking in high-income countries and an increase in environmental exposures in low/middle-income countries [4, 9–13]. As underlined by the ELISABET (*Enquête Littoral Souffle Air Biologie Environnement*) study, considerable heterogeneity in the prevalence of COPD is due to an impressive 76.4% under-diagnosis rate [14].

In 2015, over 3 million people died from COPD in the world [2]. World Health Organization (WHO) projections are quiet alarming and highlight a possibility of 6 million deaths at the 2050 horizon [15]. Healthcare systems and society face a complex economic problem given that COPD is ranked eighth place in terms of disability-adjusted life years (DALYs), accounting for 2.6% of global DALYs [2]. In Europe, the total cost of respiratory diseases, including healthcare and productivity loss, represents more than EUR 380 billion per year, with EUR 48.4 billion being directly imputable to COPD [16]. Costs are clearly associated with exacerbation frequency, hospital admissions and disease severity [17–21]. Indeed, higher severity of COPD is significantly associated with a higher risk of death [22]. There is no curative treatment currently available and disease management is highly focussed on the symptomatic side and limitation of acute exacerbations. New studies based on the triple association of inhaled glucocorticoid (ICS), long-acting β_2-agonist (LABA) and long-acting muscarinic antagonist (LAMA) showed a significant 25% reduction in risk of moderate or severe exacerbations compared with 15% for dual therapy (ICS–LABA and LAMA–LABA) [23]. Emerging evidence highlights the complexity of the disease, with the existence of specific COPD patient endotypes and "treatable traits", such as predominant eosinophilic inflammation [24]. A targeted strategy adapted to the different treatable traits/endotypes appears more appropriate. Hence, anti-eosinophilic drugs developed for asthma bring new hope for patients with COPD. This review aims to discuss results from recently published data reporting evidence of efficacy in some patients with COPD.

Pathophysiology and molecular mechanisms

General pathophysiology

COPD is a preventable disease clinically defined by persistent respiratory symptoms and airflow limitation during forced expiration mainly due to airway and/or alveolar abnormalities [12, 25]. Airflow limitation is due to an increased airway resistance combined with mucociliary clearance failure and progressive accumulation of mucus exudate in distal airway lumens [26].

A local chronic inflammatory response is combined with an abnormal and excessive airway remodelling subsequent to damage repair, leading in turn to an alteration of the epithelial barrier and a thickening of the conducting walls of distal airways (<2 mm of diameter) [27, 28]. In addition to lumen narrowing, a substantial decrease in distal airway numbers has been clearly correlated with the COPD severity grade [29]. Lifetime exposure to tobacco smoking and environmental particles (domestic biomass combustion and air pollution) appear to be the two major COPD risk factors in high-income and developing countries respectively [30, 31].

Atsou *et al.* [3] demonstrate a significant trend between COPD and the amount of tobacco smoking; people consuming over 30 pack–years have a median (interquartile range); 3.73 (2.62–5.29) higher risk of developing COPD [4, 5]. Recently, emerging evidence suggests that accelerated forced expiratory volume in 1 s (FEV_1) decline is just one of the possible disease trajectories. Paediatric roots are involved in more than half of COPD cases, where abnormal development and lung growth during childhood leads to an incomplete pulmonary function at the age of 20 [32–34]. New genome-wide association studies (GWAS) highlight the genetic background in COPD emergence [35–38] with α_1-antitrypsin deficiency as one of the most well-described genetic disorders [39]. Historically the COPD inflammatory profile is mainly characterised by an increase in macrophages, neutrophils and $CD8^+$ T-cells in peripheral airways and lung parenchyma due to non-T-helper cell type 2 mechanisms, thus steroid non-responsive [40–43]. The percentage of neutrophils in the sputum appears to be higher in COPD patients, with more severe airflow obstruction and development of neutrophilic bronchitis during exacerbations [44]. A therapeutic strategy targeting this neutrophilic trait (anti-interleukin (IL)-8 and anti-CXCR2) leads to minimal reduction in inflammation with limited reduced blood neutrophil counts or clinical benefit [45]. Sun *et al.* [46] reported a significant variation in Th1/Th2 cytokines between acute exacerbation and remission of COPD. They demonstrated that the imbalance of cytokines secreted by Th1 and Th2 cells was disrupted in COPD

patients. Indeed, acute COPD exacerbation was associated with a decrease in Th1 cells and a dominance by Th2 cells, with a normalisation of Th1 cell numbers during the remission step [46].

COPD and the eosinophilic airway inflammation trait

Eosinophils are terminally differentiated cells derived from $CD34^+$ eosinophil-basophil progenitors in bone marrow. Progenitors undergo maturation under IL-5, IL-3, granulocyte-macrophage colony-stimulating factor (GM-CSF), IL-33 and thymic stromal lymphopoietin (TSLP) stimulation [47–50]. Eosinophils play pivotal roles in tissue homeostasis and the inflammatory processes harbouring pro-inflammatory genes that appear to be overexpressed in diseases such as asthma [51]. Bafadhel *et al.* [40] reported from a 1-year study a total of 182 exacerbations from 86 COPD cases, of which over one-quarter were associated with sputum eosinophilia. Variations in eosinophil counts according to treatment, exacerbation phase, and sampling time make it difficult to establish clear guidelines on the thresholds for defining eosinophilic inflammation in COPD. Indeed, there is no consensus definition for eosinophilic COPD [41, 49, 52, 53]. Currently, the cellular and molecular pathways leading to eosinophilic airway inflammation are well understood in asthma. Eosinophilic inflammation might not be identical in asthma and COPD. Two different pathogenic pathways of the adaptive or innate immune response are involved: i) Allergic eosinophilic inflammation driven by $CD4^+$ Th2 lymphocytes and cytokines such as IL-4, IL-5 and IL-13. This phenotype is generally well controlled by ICS; ii) non-allergic eosinophilic inflammation probably imputable to IL-5 production by type 2 innate lymphoid cells (ILC2) [54, 55]. Eosinophilic inflammation is thought to be a main feature of asthma on a type 2-mediated airway inflammation background. COPD is known to be a highly heterogeneous disease with many different clinical features. Some patients present phenotypes differing to those from the general pathophysiology, for instance eosinophilic airway inflammation (eosinophilic endotype) [56–58]. Hence, some COPD and asthma patients share similar symptoms. This has been identified as the asthma–COPD overlap (ACO) [49, 59–61]. However, ACO has provided limited clinical and biological benefits regarding the management of chronic airway diseases given its relatively inaccurate diagnostic criteria (particularly the lack of clear-cut thresholds for quantitative parameters) and the heterogeneity of both inflammatory and structural change patterns [60].

It is noteworthy that a range of 20–40% COPD patients present an exacerbated eosinophilic profile in blood and/or sputum, not only during acute exacerbations but also in stable periods [40, 47, 62–65]. It has been demonstrated that blood eosinophil counts in COPD patients are associated with a higher frequency and severity of exacerbations [65–69]. Data from two multicentre and longitudinal cohorts (the ECLIPSE (Evaluation of COPD Longitudinally to Identify Predictive Surrogate End-points) and COPDGene studies) reported respective 22% and 32% ($p=0.006$) increases in risk of exacerbation for COPD patients with a blood eosinophil count threshold of $\geqslant 300$ cells·μL^{-1} [52]. A high number of eosinophils is also associated with a better response to ICS and could be a promising response biomarker [66, 67, 70–72]. Emerging transcriptomic evidence highlights only a small overlap between genes linked to blood eosinophilic inflammation in asthma and COPD [73]. However, the existence of an overlap is still debated. Considering for example the GLuCOLD (Groningen and Leiden Universities study of Corticosteroids in Obstructive Lung Disease) cohort; here the presence of a type 2 signature in the sputum related to a predicted eosinophilic pattern and steroid sensitivity outcome was not tracked by asthma history [74]. At a glance, it seems that type 2 traits and the subsequent eosinophilic patterns carry a significant genetic predisposition [75], whereas the clinical taxonomy plays a limited role and the overall story is far from being elucidated.

Over the last decade, emergence of specific anti-eosinophil molecules, such as monoclonal antibodies (mAb) directed against IL-5, has led to major improvements in asthma control, improving lung function with diminution of exacerbations [76–79]. All these findings suggest that the eosinophilic inflammation pattern is a potential treatable trait in COPD patients. New evidence on this type 2 COPD endotype is rationale for the testing of drugs used for asthma treatment which selectively block eosinophilic and type 2 inflammation (figure 1).

Anti-IL-5 therapies

IL-5 is one of the major cytokines secreted by $CD4^+$ Th2 lymphocytes, eosinophils, ILC2 cells, mastocytes, eosinophils, and basophils, in turn inducing the activation of multiple signalling pathways and the release of cytokines and chemokines [50]. These molecules have a pivotal role in eosinophil recruitment, activation, differentiation, proliferation and survival [80, 81], and, in addition, eosinophil degranulation also has a major effect on airway inflammation [82]. Accordingly, IL-5 has become an interesting drug target in elevated eosinophil numbers among asthma patients. Targeted treatment, such as antibodies directed against the IL-5 cytokine (mepolizumab and reslizumab) or the IL-5 receptor (benralizumab), block eosinophil maturation. Note that the mechanism of action of benralizumab is different from that of mepolizumab and reslizumab, both binding exclusively to IL-5 and leading to a reduction in eosinophils.

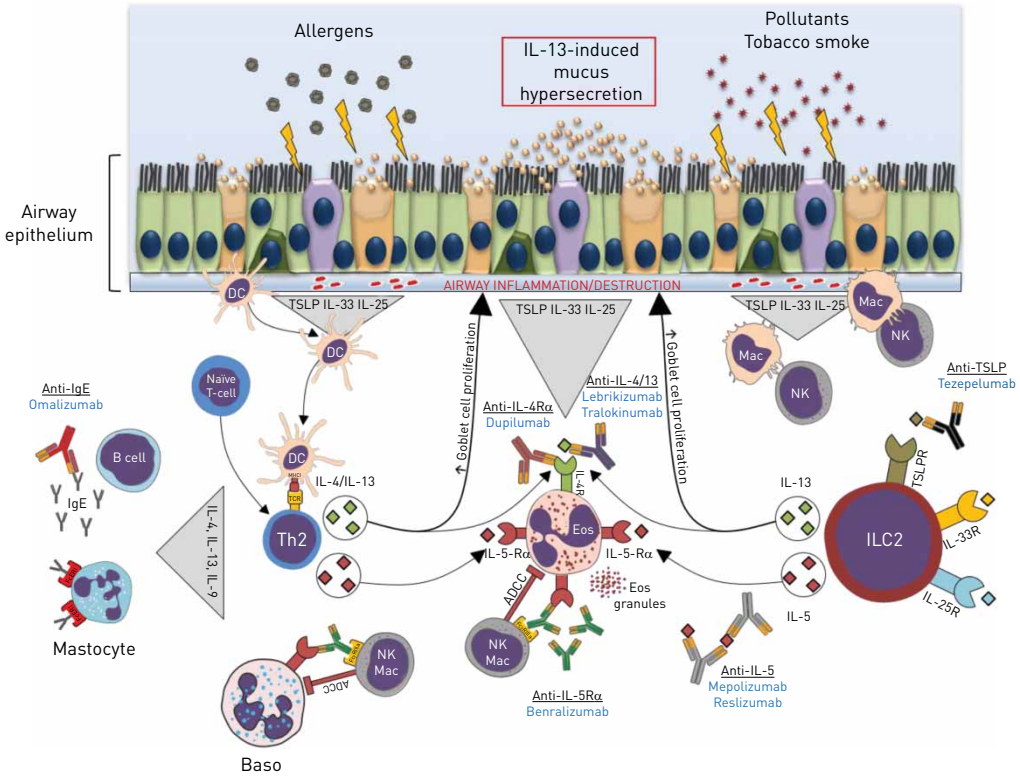

FIGURE 1 Simplified representation of the eosinophilic inflammation pattern in asthma and COPD. Allergens, cigarette tobacco, and other pollutants attack airway epithelial cells and contribute to a local injury. Release of epithelial-derived innate cytokines, interleukin (IL)-25, IL-33, and thymic stromal lymphopoietin (TSLP) in response to environmental factors play key roles in: i) the maturation of T-helper 2 (Th2) cells through dendritic cell activation; ii) the activation of innate immune cells including type 2 innate lymphoid cells. Release of Th2 cytokines (IL-4, IL-5 and IL-13) promotes the activation of resident macrophages and recruitment of innate cells such as basophils and eosinophils. Finally, activation of these several pathways participates in airway remodelling, mucus overexpression, and eosinophilic inflammation maintenance. Therapeutic strategy to control eosinophilic inflammation in asthma and COPD (monoclonal antibodies) are as follows. Benralizumab acts in an antibody-dependent cell-mediated cytotoxicity (ADCC) way resulting in eosinophilic depletion. Mepolizumab and reslizumab target the soluble IL-5 form to limit recruitment and activation of eosinophils. Omalizumab limits mastocyte activation through immunoglobulin (Ig)E depletion. Dupilumab inhibits eosinophil activation *via* IL-4Rα, contrary to lebrikizumab and tralokinumab which target soluble IL-13 cytokine. Tezepelumab blocks type 2 innate lymphoid cells (ILC2) activation by preventing TSLP binding. Baso: basophil; DC: dendritic cell; Eos: eosinophil; IL-5Rα: IL-5 receptor α; IL-25R: IL-25 receptor; IL-33R: IL-33 receptor; Mac: macrophage; MHCII: major histocompatibility complex class II; NK: natural killer cell; TCR: T-cell receptor. Illustrations adapted from Smart Servier under a Creative Commons Attribution 3.0 Unported (CC BY 3.0) license.

Thus, a strategy based on blood eosinophil depletion could play a role in the management of COPD.

Mepolizumab

Mepolizumab was approved in 2015 by the Food and Drug Administration (FDA) as an add-on therapy for the treatment of severe eosinophilic asthma [83, 84]. It is a fully-humanised mAb (immunoglobulin (Ig)G1κ) directed against IL-5, preventing its binding to the α-chain of the IL-5 receptor alpha subunit (IL-5Rα) present on the surface of eosinophils [85]. Pharmacokinetics is proportional to the dose and time independent. The half-life of mepolizumab is about 20 days, with a maximal concentration at 0.5 to 4.8 h after the beginning of perfusion [86]. The drug prevents the formation of the IL-5-receptor complex and blocks the activation of signalling pathways, leading to a limited eosinophil production, incomplete maturation and a decreased half-life [87].

Ortega *et al.* [88] reported from the DREAM (Mepolizumab for severe eosinophilic asthma) and MENSA (Mepolizumab as Adjunctive Therapy in Patients with Severe Asthma) studies a significant 47% reduction in mean exacerbation rate (rate ratio=0.53, p<0.0001) in severe eosinophilic asthma. The authors also found a significant association between mepolizumab efficacy and high baseline blood eosinophil counts (⩾150 cells·μL^{-1}) [88]. A meta-analysis of eight different studies enrolling 1707 participants with

severe asthma and high eosinophil levels concluded an improvement in quality of life and a reduction in asthma attacks without significant benefits on lung function [89].

Dasgupta *et al.* [90] performed a single-centre, double-blind, randomised, placebo-controlled trial for 6 months including 18 patients of 40–80 years old with moderate-to-severe COPD. The authors assessed the effect of monthly injections of mepolizumab 750 mg or placebo in cigarette smoke-related COPD patients with persistent sputum eosinophilia. The primary objective was to determine if mepolizumab induced a significant reduction in sputum eosinophil count. Secondary outcomes were the assessment of the effects on blood eosinophil count, lung function, exacerbation rate, airway remodelling, symptoms and quality of life. Baseline sputum eosinophil counts represented 11% and 7.4% for the mepolizumab-treated arm (n=8) and the placebo group (n=10) respectively. Baseline blood eosinophil counts were 0.7±0.5 cells·mm^{-3} for the mepolizumab-treated and 0.33±0.29 cells·mm^{-3} for the placebo groups. After 6 months, a significant reduction in sputum (0.50 *versus* 2.20%, p<0.05) and blood eosinophil counts (0.03 *versus* 0.26; p<0.05) were reported in the mepolizumab-treated group. However, the additional secondary outcomes showed no significant changes; there was no improvement in lung function or exacerbation rates [90].

Two large cohort studies have also been carried out to assess anti-IL-5 efficacy on patients with moderate-to-severe exacerbations despite an adequate triple inhaled therapy composed of a combination of LABA, LAMA and ICS. These two phase III studies were the METREX (Mepolizumab *versus* Placebo as Add-on Treatment for Frequently Exacerbating COPD Patients) study and the METREO (Mepolizumab *versus* Placebo as Add-on Treatment for Frequently Exacerbating COPD Patients Characterised by Eosinophil Level) study. Both the METREX and METREO trials assessed the efficacy and safety of mepolizumab compared to placebo in patients with COPD and eosinophilic phenotype [91]. The primary outcome for both studies was the annual rate of moderate-to-severe exacerbations. The METREX study included patients with either an eosinophilic phenotype (⩾150 eosinophils·mm^{-3} at screening or ⩾300 in the previous year) or a non-eosinophilic phenotype, contrary to the METREO study in which patient selection was based on blood eosinophil count. Treated patient groups consisted of mepolizumab 100 mg (METREX and METREO) or 300 mg (METREO) compared with placebo in addition to ICS/LABA/LAMA tritherapy every 4 weeks for 52 weeks. Subcutaneous injection of mepolizumab 100 mg once a month for 52 weeks was associated to a lower annual rate of moderate or severe exacerbations only in COPD patients with eosinophilic phenotype (high stratum group) in the METREX study [92, 93]. In this study, exacerbation rates of 1.40 *versus* 1.71 per year were observed in the mepolizumab-treated group compared to the placebo group respectively (rate ratio=0.82, p=0.04). No significant improvements in the overall cohort or impact on emergency department visits were noted. On the contrary, the METREO study did not give any insight into the efficacy on exacerbation rate, at either the 100 mg (rate ratio= 0.80, p=0.07) or 300 mg (rate ratio=0.86, p=0.14) doses [94]. However, both studies reported a well-tolerated mepolizumab treatment with similar incidence of adverse events compared to placebo groups. A dose–response relationship between the increase in eosinophil number and treatment efficacy has already been suggested [56]. Such hopeful results need to be discussed given that further increases in eosinophil count can lead to loss of asthma control after cessation of mepolizumab treatment [95–97]. Overall, the results of these studies are disappointing and contradictory. Stronger evidence of eosinophilic inflammation is now required for the enrolment of patients in the new phase III study MATINEE (Mepolizumab as Add-on Treatment In Participants With COPD Characterized by Frequent Exacerbations and Eosinophil Level; www.clinicaltrials.gov/ct2/show/NCT04133909). This means that the proportion of eligible patients will be smaller than expected. Interestingly, a GWAS performed on patients with COPD and blood hyper-eosinophilia did not demonstrate any robust associations between genetic variants and mepolizumab efficacy (biomarker efficacy) [98].

Reslizumab

Reslizumab is a humanised mAb (IgG4κ) directed against IL-5 and prevents IL-5 binding at the eosinophil surface similarly to mepolizumab [99]. Plasma concentrations are dose-proportional with a maximal peak concentration obtained at 6.9 h after dosing and a reported half-life ranging between 24.5 to 30.1 days [100]. A study with patients aged 18–75 years old with uncontrolled eosinophilic asthma were randomly assigned and received monthly injections of reslizumab at 3 mg·kg^{-1} (n=53) or placebo (n=53) for 12 weeks. Castro *et al.* [101] reported the absence of a significant reduction in exacerbations (p=0.0833), but a significant improvement of 0.24 L in FEV_1 parameter in the reslizumab group (p=0.0023). A significant diminution in eosinophils in the induced sputum (p= 0.0068) and in blood counts (p<0.0001) was also observed [101]. To our knowledge, reslizumab has not yet been evaluated in COPD [41].

Benralizumab

Benralizumab is a humanised mAb directed against IL-5Rα with an 18-day terminal half-life [102]. Excision of the fucose sugar residue in the CH2 region of the antibody (afucosylated antibody) results in a

five- to 50-fold higher affinity for the Fcγ receptor (human FcγRIIIa) expressed on natural killer (NK) cells and macrophages. This modification leads to a 1000-fold increase in antibody-dependent cell-mediated cytotoxicity (ADCC) functions [103] and activation of this ADCC mechanism induces rapid eosinophil depletion [104–106].

Patients under benralizumab treatment with severe and uncontrolled eosinophilic asthma have shown a significant reduction in annualised exacerbation rate, an improvement in pre-bronchodilator FEV_1, and a decrease in oral corticosteroid use [107–109]. A phase II, double-blind, randomised, controlled study was performed on an uncontrolled asthma cohort split into two groups: eosinophilic (n=324) and non-eosinophilic (n=285) phenotypes. At week 52, the authors demonstrated a reduction in asthma exacerbations in the patients treated with benralizumab doses at 20 mg (p=0.019) and 100 mg (p=0.010). In particular, these patients had baseline blood eosinophil counts of at least 300 cells·μL^{-1} [110]. On the contrary, a phase II, double-blind, randomised, placebo-controlled study assessed the effect of benralizumab in COPD in 101 adults aged 40–85 years old with a moderate-to-severe disease and a sputum eosinophil count of ⩾3%. The primary outcome was annual rate of moderate-to-severe exacerbations of COPD at week 56. Patients received a placebo or a benralizumab 100 mg injection, three doses every 4 weeks, followed by five doses every 8 weeks after 48 weeks. The placebo group reported a 0.92 (95% CI 0.67–1.25) and the benralizumab group a 0·95 (95% CI 0.68–1.29) annual rate of acute exacerbations, meaning in all that Brightling *et al.* [111] demonstrated a non-significant reduction of 3% (95% CI −58–33; p=0·94) in exacerbations. On the other hand, benralizumab treatment was associated with a rapid diminution in blood and sputum eosinophils in patients with COPD and incidence of adverse events was similar to the placebo group. A significant improvement in post-bronchodilator FEV_1 in the benralizumab arm was noted as similar to the placebo arm (p=0·014) [111]. Despite this FEV_1 increase, no difference was observed in health status [45]. GALATHEA (Benralizumab Efficacy in Moderate-to-Very Severe Chronic Obstructive Pulmonary Disease with Exacerbation History; n=1044) and TERRANOVA (Efficacy and Safety of Benralizumab in Moderate-to-Very Severe Chronic Obstructive Pulmonary Disease with Exacerbation History; n=1392) were two phase III, double-blind, randomised, placebo-controlled trials. The primary endpoint was to assess the effect of benralizumab on COPD exacerbation rate. Patients of 40–85 years old were assigned in a 2:1 ratio into an eosinophilic (⩾220 cells·mm^{-3}) or non-eosinophilic (<220 cells·mm^{-3}) group. The first three doses were injected every 4 weeks then every 8 weeks, with final assessment at week 56. In both studies patients randomly received placebo or benralizumab at 30 or 100 mg. In the TERRANOVA study, an additional group of patients received benralizumab 10 mg. Results of the GALATHEA study showed no significant improvement in annual rate ratios for exacerbations at any treatment dose: benralizumab 30 mg (0.96; p=0.65) and benralizumab 100 mg (0.83; p=0.05). The same trend was detected in the TERRANOVA study, with corresponding rate ratios of 0.85 (p=0.06), 1.04 (p=0.66) and 0.93 (p=0.40) in the 10 mg, 30 mg and 100 mg benralizumab groups, respectively. No dose effect on benralizumab efficacy was detected and similar adverse events were observed. Interestingly, in both studies a moderate depletion of blood eosinophils was reported [112]. Criner *et al.* [113] identified, from the TERRANOVA and GALATHEA trails, a subtype of patients characterised by i) a baseline blood eosinophil count ⩾220 cells·μL^{-1}; ii) three or more exacerbations in the previous year; and iii) tritherapy as best responder treatment in combination with benralizumab therapy. These patients were associated with a significant reduction in exacerbation rate ratio of 0.70 (95% CI 0.56–0.88) under benralizumab 100 mg treatment every 8 weeks compared with placebo. No improvement was reported for patients treated with benralizumab 30 mg [113].

Altogether, these results are more disappointing than those observed with mepolizumab treatment, even more so given there was no relationship found with the level of eosinophilia. A new phase III study (www.clinicaltrials.gov/ct2/show/NCT01914757) will be relevant for the follow-up of the subset of patients who seemingly responded [113]. However, it is highly likely that if outcomes are yet again not achieved, benralizumab treatment will be ruled out for the treatment of COPD and the overall concept of eosinophilic COPD will be challenged.

To conclude, the European Medicines Agency declares that benralizumab is effective in patients with eosinophilic COPD, whereas the FDA claims there is not robust evidence supporting this.

Anti-IL-13/anti-IL-4 therapy

IL-4 and IL-13 Th2 cytokines are responsible for many functions and are involved in asthma and COPD development [114–118]. IL-13 binding to the IL-13 receptor alpha 1 (IL-13Rα1) induces recruitment of IL-4 receptor alpha 1 (IL-4Rα1), in turn forming a heterodimeric receptor complex responsible for the activation of signalling pathways [114, 119]. IL-4 and IL-13 share similar biological effects, mainly as they bind the same receptor composed of IL-4Rα1 and IL-13Rα1, both expressed in airway epithelium [115, 120–122]. Indeed, IL-4 activates not only through signalling pathways *via* the IL-4Rα and IL-13Rα chains, but also *via*

common gamma chain. Likewise, IL-13 has also been found to use IL-4Rα and IL-13Rα chains [123, 124]. IL-13 is produced by T cells, mast cells, basophils and dendritic cells. It is involved in regulation of inflammatory and immune responses as well as mucous hypersecretion [125, 126]. Eosinophils have shown secretion of IL-13 under GM-CSF and/or IL-5 stimulation [127] and ILC2 cells are also able to secrete IL-5 and IL-13 under stimulation of IL-33 and IL-25 [128]. ILC2s have been found increased in patients with stable COPD or during acute exacerbation [46].

Dupilumab

Dupilumab is a human mAb targeting IL-4Rα leading to inhibition of IL-13 and IL-4 signalling [129]. A randomised, placebo-controlled, phase IIb clinical trial showed a significant increase in FEV_1 parameter and a reduction in the rate of severe exacerbations in patients with uncontrolled asthma under dupilumab treatment. Improvements were consistent in two different treatment groups; dupilumab 200 or 300 mg every 2 weeks regardless of baseline eosinophil count [130]. These encouraging data must be transposed to COPD patients. The BOREAS (A Pivotal Study to Assess the Efficacy, Safety and Tolerability of Dupilumab in Patients With Moderate-to-severe COPD With Type 2 Inflammation) study is underway (NCT03930732) and will give some insights for patients with COPD.

Lebrikizumab

Lebrikizumab is a humanised mAb that binds to soluble IL-13 and blocks activation of IL-4Rα and IL-13Rα1 heterodimers. Two studies related to lebrikizumab are LUTE and VERSE; double-blind, randomised, placebo-controlled studies enrolling 463 patients of 18–75 years old. Hanania *et al.* [131] found an improvement in asthma exacerbation rate and lung function in patients with moderate-to-severe asthma and a high periostin profile [131]. A phase II, double-blind, randomised, placebo-controlled trial for lebrikizumab (NCT02546700) treatment has been recently carried out in patients with frequent COPD exacerbations despite ICS and at least one long-acting bronchodilator inhaler medication. Data are not yet available.

Tralokinumab

Tralokinumab is also a mAb which specifically targets IL-13 [126]. Piper *et al.* [132] noted no significant improvement in asthma symptoms following treatment based on the Asthma Control Questionnaire score (ACQ-6; p=0.375), but a small effect on FEV_1 was shown. Marone *et al.* [118] concluded a putative efficacy of tralokinumab in a highly selected cohort of asthmatics with an overexpression of IL-13. The authors concluded a minor role of IL-13 in severe asthma exacerbations [133]. No study or clinical trial data are available in patients with COPD.

Other targeting strategies: anti-TSLP, anti-IL-33, anti-IL-25 and anti-IgE drugs

Damage to airway epithelial cells induces the release of several cytokines, such as IL-33, IL-25 and TSLP, leading to eosinophilic inflammation through ILC2 and Th2 pathways [129]

Tezepelumab

Human TSLP is involved in activation of dendritic cells [134]. Activated DCs then induce conversion of $CD4^+$ T-cells into Th2 cells able to produce the Th2 cytokines IL-4, IL-5, and IL-13 [135]. Tezepelumab is a human monoclonal antibody directed against TSLP, thus preventing its interaction with the TSLP receptor. Corren *et al.* [136] reported a significant 62%, 71% and 66% ($p<0.001$ for all comparisons with placebo group) diminution of annualised asthma exacerbation rates for tezepelumab treatment at 70 mg every 4 weeks, 210 mg every 4 weeks, or 280 mg every 2 weeks respectively. Pre-bronchodilator FEV_1 was also slightly higher in all tezepelumab-treated groups independently of blood eosinophil counts at the beginning of the study [136]. Currently, COURSE (Tezepelumab COPD Exacerbation Study) is a phase IIa, multicenter, double-blind, randomised trial (NCT04039113) recruiting patients to assess the efficacy of tezepelumab on moderate or severe COPD exacerbation rate ratios.

Anti-IgE therapy

Omalizumab

IgE plays an important role in allergic asthma [137]. Allergen-specific IgE binds to Fc receptors (FcεRI) on the surface of mast cells, basophils and eosinophils. This binding induces allergic reactions through the release of inflammatory molecules [138]. Omalizumab is a recombinant humanised anti-IgE mAb indicated in patients with moderate-to-severe allergic asthma. Omalizumab binds to the Fc region of the IgE antibody, preventing the binding of IgE to high-affinity IgE receptors, and so blocking the signalling pathways responsible for the release of inflammatory mediators. Omalizumab has been shown to limit asthma exacerbation rates and annual rates of hospital admissions [139, 50]. Maltby *et al.* [140] reported an improvement in health-related quality of life in individuals with severe allergic asthma and ACO.

The PROSPERO (Omalizumab in the Prospective Observational Study to Evaluate Predictors of Clinical Effectiveness in Response to Omalizumab) study is a multicentre, single-arm, prospective, 48-week observational study. Study analysis by HANANIA *et al.* [141] showed similar improvements in asthma outcome among patients with and without ACO, but preserved lung function was reported in the ACO group.

Discussion

Eosinophilic airway inflammation is a common trait in patients with asthma and COPD. Some patients with COPD and uncontrolled asthma, despite maximal adequate treatment (ICS, LABA and LAMA), are eligible for treatment with molecules targeting specific components of eosinophilic inflammation in asthma. Mepolizumab has shown encouraging results in the asthma trajectory and has become one of the most studied anti-IL-5 therapies in COPD [142]. Regarding results from the METREX/METREO studies, mepolizumab therapy is thought to reduce the rate of exacerbations in COPD patients with an elevated blood eosinophil level. This trend was only confirmed in the METREX cohort, where patients with hyper-eosinophilia (high stratum) demonstrated a significant reduction in moderate-to-severe exacerbations. No significant trend was found in the METREO cohort regardless of the injection dose (100 or 300 mg). Patients with $\geqslant$300 eosinophils·mm^{-3} benefit more from mepolizumab 100 mg therapy, with a 23% lower mean annual rate of moderate or severe exacerbations (rate ratio=0.77 (95% CI 0.63–0.94)). It is noteworthy that the DREAM/MENSA trial in asthma reported a significant reduction in the mean exacerbation rate of patients under mepolizumab treatment (rate ratio=0.53 (95% CI 0.44–0.62)) [88]. These differences could be explained by higher exacerbation rates in COPD and a weaker impact of IL-5 in the pathophysiology of COPD compared to asthma. Moreover, a decrease in sputum and blood eosinophil counts did not lead to significant improvements in lung function parameters or remodelling patterns, thus questioning the importance of eosinophil involvement in the disease [90]. Regarding the limited proof of efficacy and the cost-effectiveness balance, in 2018, the FDA decided not to approve mepolizumab as an add-on therapy for COPD [56]. No other anti-IL-5 therapies, such as reslizumab use, have been reported in COPD.

Direct targeting of IL-5Rα with benralizumab in the GALATHEA and TERRANOVA trials has reported no significant improvement in annualised COPD exacerbation rate combined with limited diminution of blood eosinophil counts. The authors explain the difference due to different cut-off values for the eosinophil counts, limited patient asthma history characteristics, and variation in previous medications [112]. A subtype of patients in the GALATHEA and TERRANOVA trials with moderate-to-very severe COPD showed elevated peripheral blood eosinophils ($\geqslant$300 cells·μL^{-1}) and experienced more than three exacerbations. This was despite patient triple therapy being associated to a significant reduction in exacerbations. Heterogeneous results along with no reduction in acute COPD exacerbations, contrary to results with mepolizumab treatment, were possibly due to small sample sizes. In addition, no attenuation of symptoms nor impact on quality of life was reported, but surprisingly a significant lung function improvement based on FEV_1 parameter was noted with long-lasting effects [111]. The RESOLUTE (Efficacy and Safety of Benralizumab in Moderate to Very Severe Chronic Obstructive Pulmonary Disease (COPD) With a History of Frequent Exacerbations) trial (NCT04053634) designed to assess the efficacy and safety of benralizumab in highly exacerbated patients with moderate-to-severe COPD will bring new insights on highly selected populations. The limited benefits of anti-IL-5/IL-5R treatment in COPD may relate to different factors: a) patient heterogeneity in clinical trials; currently applied cut-off values for blood eosinophil counts in COPD are less consensual than in asthma, meaning that the population may not be sufficiently enriched; b) mechanisms of airway eosinophilia in COPD might be different from asthma, driven in an IL-5-independent manner. For instance, eotaxin, GM-CSF, IL-13, impaired macrophage efferocytosis [143], CCL5 and alarmins, *etc*, have been shown to be potentially relevant candidates; or c) ambiguous clinical evidence that eosinophilia is differentially linked to COPD exacerbation, steroid sensitivity, or lung function compared to asthma.

It is not clear whether patients with sputum or blood eosinophilia represent a stable COPD phenotype over time. Little is known about the other clinical characteristics of T2 phenotype in COPD patients [144]. Whether eosinophilic airway inflammation arises due to increased bone marrow production and/or increased eosinophil recruitment into the airway is less well-documented than in asthma [145].

In a recent study [73], the authors aimed to identify the transcriptomic signatures in bronchial brushing samples from both patients with asthma and COPD in the U-BIOPRED (Unbiased BIOmarkers in PREDiction of respiratory disease outcomes) and EvA (Epidemiology of Vascular Ageing) cohorts, respectively. Using a blood eosinophil count cut-off of 200 cells·mL^{-1}, no genes were found differentially expressed between the COPD and asthma cohorts. The authors found that only 12 genes were associated with blood eosinophil count in the COPD cohort, *versus* more than 1000 among patients with asthma. These genes were in majority related to type 2-mediated immunity. The only common gene to both eosinophilic asthma and COPD was cystatin-SN (*CST1*). However, in the validation cohorts, *CST1* and

blood eosinophil count were weakly correlated. Cystatin is a cysteine protease inhibitor expressed by the airway and nasal epithelium and implicated in type 2 immunity, such as eosinophilic nasal polyps [146]. Epithelial *CST1* expression is upregulated by the epithelial alarmins TSLP and IL-33, and it also stimulates alarmin release itself. Cystatin can also promote eosinophilic inflammation *via* fibroblast activation and subsequent release of pro-eosinophilic chemokines [146]. This study highlighted very few shared biological mechanisms between eosinophilic COPD and eosinophilic asthma. Unbiased bronchial epithelial gene expression studies have shown that CCL26 is also associated with blood eosinophil counts in COPD patients [74].

Studies based on the IL-4R receptor targeting strategy with dupilumab have shown significant improvement in asthmatic patient lung function combined with a diminution of annualised exacerbation rate [130, 147–149]. These encouraging results have led to the assessment of the use of dupilumab in COPD and a trial is ongoing (NCT03930732). Given the disappointing and disruptive results that have been reported from studies on the anti-IL-13 targeted strategy in uncontrolled and severe asthma, some authors have concluded a minor role of IL-13 in asthma [133]. In COPD, there may be eosinophil-driven mechanisms that may involve non-IL-5T2 cytokines such as IL-13, and therefore anti-IL-5 biologics do not show impressive clinical results. Eosinophil-derived IL-13 was shown to promote alveolar macrophage MMP-12 production and lead to airspace enlargement, indicating IL-13 involvement in the emphysematous progression of COPD [150].

Increased expression of *CST1* and *IL13* genes have been recently shown in eosinophilic COPD airways [151].

These promising sub-studies deduce the hypothesis that a small proportion of patients with COPD may benefit from anti-IL-5 therapy. Indeed, at this point most clinical trial evidence does not support the use of anti-IL-5 treatment in COPD [94, 112]. To our knowledge, no results on patients with COPD have been published for anti-IL-13 and anti-IL-4 treatment. Omalizumab, an anti-IgE treatment, has shown an improvement in health-related quality of life in individuals with severe allergic asthma and ACO. Anti-TSLP strategies are ongoing, with assessment in patients with COPD in a phase IIa, multicentre, double-blind randomised trial (NCT04039113) (COURSE study).

Conclusions

A significant proportion of patients with severe COPD and eosinophilic inflammation experience uncontrolled symptoms despite an optimal pharmaceutical treatment. Recently, targeted strategies directed specifically against cytokines or receptors involved in eosinophilic inflammation have provided significant improvement in asthma. Biological agents used in asthma have limited therapeutic effects on patients with COPD. These disappointing results are thought to be due to the existence of multiple disease origins and a highly complex role of eosinophils. Indeed, several studies have shown the global effects of eosinophilic patterns on exacerbations, but no impacts on the trajectory of the disease, such as lung function decline, were mentioned. A better understanding of such complex cellular mechanisms and a clear consensus on peripheral blood eosinophils are needed to improve patient gradations in routine clinical practice. Not only biomarkers but also elucidation of the role of eosinophilic and type 2 inflammation in COPD is warranted. In conclusion, the development of new biomarkers is mandatory for a better patient selection in order to propose these innovative therapies to the best responder patient profile. This step forward to personalised medical treatments for patients with COPD will match the right targeted treatment to the right patient.

Author contributions: All authors have read and agreed to the published version of the manuscript.

Conflict of interest: M. Fieldes has nothing to disclose. C. Bourguignon has nothing to disclose. S. Assou has nothing to disclose. A. Nasri has nothing to disclose. A. Fort has nothing to disclose. I. Vachier has nothing to disclose. J. De Vos has nothing to disclose. E. Ahmed has nothing to disclose. A. Bourdin reports grants, personal fees, nonfinancial support and other support from AstraZeneca, Boehringer Ingelheim, GlaxoSmithKline and Novartis; personal fees and nonfinancial support from Teva; personal fees, nonfinancial support and other support from Regeneron, Chiesi Farmaceuticals and Actelion; personal fees from Gilead; nonfinancial support and other support from Roche; and other support from Nuvaira, all outside the submitted work.

References

1 IMHE, Institute for Health Metrics and Evaluation (IHME). GBD Compare. Seattle, WA: IHME, University of Washington, 2015. http://www.healthdata.org/data-visualization/gbd-compare Date last accessed: May, 2020; date last updated: May 2020.

2 GBD 2015 Chronic Respiratory Disease Collaborators. Global, regional, and national deaths, prevalence, disability-adjusted life years, and years lived with disability for chronic obstructive pulmonary disease and asthma, 1990–2015: a systematic analysis for the Global Burden of Disease Study 2015. *Lancet Respir Med* 2017; 5: 691–706.

3 Atsou K, Chouaid C, Hejblum G. Variability of the chronic obstructive pulmonary disease key epidemiological data in Europe: systematic review. *BMC Med* 2011; 9: 7.
4 Halbert RJ, Natoli JL, Gano A, *et al.* Global burden of COPD: systematic review and meta-analysis. *Eur Respir J* 2006; 28: 523–532.
5 Buist AS, McBurnie MA, Vollmer WM, *et al.* International variation in the prevalence of COPD (the BOLD Study): a population-based prevalence study. *Lancet* 2007; 370: 741–750.
6 Roche N, Dalmay F, Perez T, *et al.* Impact of chronic airflow obstruction in a working population. *Eur Respir J* 2008; 31: 1227–1233.
7 Menezes AMB, Perez-Padilla R, Jardim JR, *et al.* Chronic obstructive pulmonary disease in five Latin American cities (the PLATINO study): a prevalence study. *Lancet* 2005; 366: 1875–1881.
8 Scholes S, Moody A, Mindell JS. Estimating population prevalence of potential airflow obstruction using different spirometric criteria: a pooled cross-sectional analysis of persons aged 40-95 years in England and Wales. *BMJ Open* 2014; 4: e005685.
9 Beaglehole R, Bonita R, Alleyne G, *et al.* UN High-Level Meeting on Non-Communicable Diseases: addressing four questions. *Lancet* 2011; 378: 449–455.
10 Gershon AS, Warner L, Cascagnette P, *et al.* Lifetime risk of developing chronic obstructive pulmonary disease: a longitudinal population study. *Lancet* 2011; 378: 991–996.
11 Rabe KF, Watz H. Chronic obstructive pulmonary disease. *Lancet* 2017; 389: 1931–1940.
12 Adeloye D, Chua S, Lee C, *et al.* Global and regional estimates of COPD prevalence: Systematic review and meta-analysis. *J Glob Health* 2015; 5: 020415.
13 Ng M, Freeman MK, Fleming TD, *et al.* Smoking prevalence and cigarette consumption in 187 countries, 1980–2012. *JAMA* 2014; 311: 183–192.
14 Quach A, Giovannelli J, Chérot-Kornobis N, *et al.* Prevalence and underdiagnosis of airway obstruction among middle-aged adults in northern France: The ELISABET study 2011–2013. *Respir Med* 2015; 109: 1553–1561.
15 WHO. Projections of mortality and causes of death, 2016 to 2060. www.who.int/healthinfo/global_burden_disease/projections/en/ Date last accessed: April 5, 2020; date last updated: April 2020.
16 The economic burden of lung disease. *In*: Gibson GJ, Loddenkemper R, Sibille Y, *et al.*, eds. European Lung White Book. Sheffield, European Respiratory Society, 2013. www.erswhitebook.org/chapters/the-economic-burden-of-lung-disease/
17 Rehman AU, Hassali MAA, Muhammad SA, *et al.* The economic burden of chronic obstructive pulmonary disease (COPD) in Europe: results from a systematic review of the literature. *Eur J Health Econ* 2020; 21: 181–194.
18 Molinari N, Briand C, Vachier I, *et al.* Hospitalizations for COPD exacerbations: trends and determinants of death. *COPD* 2015; 12: 621–627.
19 Laurendeau C, Chouaid C, Roche N, *et al.* [Management and costs of chronic pulmonary obstructive disease in France in 2011]. *Rev Mal Respir* 2015; 32: 682–691.
20 Toy EL, Gallagher KF, Stanley EL, *et al.* The economic impact of exacerbations of chronic obstructive pulmonary disease and exacerbation definition: a review. *COPD* 2010; 7: 214–228.
21 Hilleman DE, Dewan N, Malesker M, *et al.* Pharmacoeconomic evaluation of COPD. *Chest* 2000; 118: 1278–1285.
22 Mannino DM, Buist AS, Petty TL, *et al.* Lung function and mortality in the United States: data from the First National Health and Nutrition Examination Survey follow up study. *Thorax* 2003; 58: 388–393.
23 Lipson DA, Barnhart F, Brealey N, *et al.* Once-daily single-inhaler triple versus dual therapy in patients with COPD. *N Engl J Med* 2018; 378: 1671–1680.
24 Agusti A, Bel E, Thomas M, *et al.* Treatable traits: toward precision medicine of chronic airway diseases. *Eur Respir J* 2016; 47: 410–419.
25 Global Initiative for Chronic Obstructive Lung Disease. 2020 GOLD Reports - Global strategy for the diagnosis, management, and prevention of chronic obstructive pulmonary disease. www.goldcopd.org/gold-reports/ Date last accessed: 2020; date last updated: 2021.
26 Hogg JC. Pathophysiology of airflow limitation in chronic obstructive pulmonary disease. *Lancet* 2004; 364: 709–721.
27 Jones JG, Lawler P, Crawley JCW, *et al.* Increased alveolar epithelial permeability in cigarette smokers. *Lancet* 1980; 315: 66–68.
28 Agustí A, Hogg JC. Update on the pathogenesis of COPD. Reply. *N Engl J Med* 2019; 381: 2484.
29 McDonough JE, Yuan R, Suzuki M, *et al.* Small-airway obstruction and emphysema in chronic obstructive pulmonary disease. *N Engl J Med* 2011; 365: 1567–1575.
30 Salvi SS, Barnes PJ. Chronic obstructive pulmonary disease in non-smokers. *Lancet* 2009; 374: 733–743.
31 Lelieveld J, Evans JS, Fnais M, *et al.* The contribution of outdoor air pollution sources to premature mortality on a global scale. *Nature* 2015; 525: 367–371.
32 Lange P, Celli B, Agustí A, *et al.* Lung-function trajectories leading to chronic obstructive pulmonary disease. *N Engl J Med* 2015; 373: 111–122.
33 Martinez FD. Early-life origins of chronic obstructive pulmonary disease. *N Engl J Med* 2016; 375: 871–878.
34 Duffy S, Weir M, Criner GJ. The complex challenge of chronic obstructive pulmonary disease. *Lancet Respir Med* 2015; 3: 917–919.
35 Tobacco and Genetics Consortium. Genome-wide meta-analyses identify multiple loci associated with smoking behavior. *Nat Genet* 2010; 42: 441–447.
36 Sakornsakolpat P, Prokopenko D, Lamontagne M, *et al.* Genetic landscape of chronic obstructive pulmonary disease identifies heterogeneous cell-type and phenotype associations. *Nat Genet* 2019; 51: 494–505.
37 Soler Artigas M, Loth DW, Wain LV, *et al.* Genome-wide association and large-scale follow up identifies 16 new loci influencing lung function. *Nat Genet* 2011; 43: 1082–1090.
38 Hobbs BD, de Jong K, Lamontagne M, *et al.* Genetic loci associated with chronic obstructive pulmonary disease overlap with loci for lung function and pulmonary fibrosis. *Nat Genet* 2017; 49: 426–432.
39 Stoller JK, Aboussouan LS. Alpha1-antitrypsin deficiency. *Lancet* 2005; 365: 2225–2236.

40 Bafadhel M, McKenna S, Terry S, *et al.* Acute exacerbations of chronic obstructive pulmonary disease: identification of biologic clusters and their biomarkers. *Am J Respir Crit Care Med* 2011; 184: 662–671.
41 Narendra DK, Hanania NA. Targeting IL-5 in COPD. *Int J Chron Obstruct Pulmon Dis* 2019; 14: 1045–1051.
42 Barnes PJ. Cellular and molecular mechanisms of asthma and COPD. *Clin Sci (Lond)* 2017; 131: 1541–1558.
43 Capron T, Bourdin A, Perez T, *et al.* COPD beyond proximal bronchial obstruction: phenotyping and related tools at the bedside. *Eur Respir Rev* 2019; 28: 190010.
44 D'silva L, Hassan N, Wang HY, *et al.* Heterogeneity of bronchitis in airway diseases in tertiary care clinical practice. *Can Respir J* 2011; 18: 144–148.
45 Yousuf A, Brightling CE. Biologic drugs: a new target therapy in COPD? *COPD* 2018; 15: 99–107.
46 Sun J, Liu T, Yan Y, *et al.* The role of Th1/Th2 cytokines played in regulation of specific CD4+ Th1 cell conversion and activation during inflammatory reaction of chronic obstructive pulmonary disease. *Scand J Immunol* 2018; 88: e12674.
47 Saha S, Brightling CE. Eosinophilic airway inflammation in COPD. *Int J Chron Obstruct Pulmon Dis* 2006; 1: 39–47.
48 Denburg JA. Bone marrow in atopy and asthma: hematopoietic mechanisms in allergic inflammation. *Immunol Today* 1999; 20: 111–113.
49 Tashkin DP, Wechsler ME. Role of eosinophils in airway inflammation of chronic obstructive pulmonary disease. *Int J Chron Obstruct Pulmon Dis* 2018; 13: 335–349.
50 Nixon J, Newbold P, Mustelin T, *et al.* Monoclonal antibody therapy for the treatment of asthma and chronic obstructive pulmonary disease with eosinophilic inflammation. *Pharmacol Ther* 2017; 169: 57–77.
51 Hogan SP, Rosenberg HF, Moqbel R, *et al.* Eosinophils: biological properties and role in health and disease. *Clin Exp Allergy* 2008; 38: 709–750.
52 Yun JH, Lamb A, Chase R, *et al.* Blood eosinophil count thresholds and exacerbations in patients with chronic obstructive pulmonary disease. *J Allergy Clin Immunol* 2018; 141: 2037–2047.e10.
53 Farne HA, Wilson A, Powell C, *et al.* Anti-IL5 therapies for asthma. *Cochrane Database Syst Rev* 2017; 9: CD010834.
54 Brusselle GG, Maes T, Bracke KR. Eosinophils in the spotlight: Eosinophilic airway inflammation in nonallergic asthma. *Nat Med* 2013; 19: 977–979.
55 Spits H, Artis D, Colonna M, *et al.* Innate lymphoid cells: a proposal for uniform nomenclature. *Nat Rev Immunol* 2013; 13: 145–149.
56 Mkorombindo T, Dransfield MT. Mepolizumab in the treatment of eosinophilic chronic obstructive pulmonary disease. *Int J Chron Obstruct Pulmon Dis* 2019; 14: 1779–1787.
57 Han MK, Agusti A, Calverley PM, *et al.* Chronic obstructive pulmonary disease phenotypes: the future of COPD. *Am J Respir Crit Care Med* 2010; 182: 598–604.
58 Lange P, Halpin DM, O'Donnell DE, *et al.* Diagnosis, assessment, and phenotyping of COPD: beyond FEV_1. *Int J Chron Obstruct Pulmon Dis* 2016; 11: 3–12.
59 Barnes PJ. Asthma–COPD overlap. *Chest* 2016; 149: 7–8.
60 Bourdin A, Suehs CM, Marin G, *et al.* Asthma, COPD, and overlap in a national cohort: ACO on a gradient. *J Allergy Clin Immunol* 2018; 141: 1516–1518.
61 Gibson PG, McDonald VM. Asthma–COPD overlap 2015: now we are six. *Thorax* 2015; 70: 683–691.
62 Saetta M, Di Stefano A, Maestrelli P, *et al.* Airway eosinophilia in chronic bronchitis during exacerbations. *Am J Respir Crit Care Med* 1994; 150: 1646–1652.
63 Leigh R, Pizzichini MMM, Morris MM, *et al.* Stable COPD: predicting benefit from high-dose inhaled corticosteroid treatment. *Eur Respir J* 2006; 27: 964–971.
64 Singh D, Kolsum U, Brightling CE, *et al.* Eosinophilic inflammation in COPD: prevalence and clinical characteristics. *Eur Respir J* 2014; 44: 1697–1700.
65 Siva R, Green RH, Brightling CE, *et al.* Eosinophilic airway inflammation and exacerbations of COPD: a randomised controlled trial. *Eur Respir J* 2007; 29: 906–913.
66 Pascoe S, Locantore N, Dransfield MT, *et al.* Blood eosinophil counts, exacerbations, and response to the addition of inhaled fluticasone furoate to vilanterol in patients with chronic obstructive pulmonary disease: a secondary analysis of data from two parallel randomised controlled trials. *Lancet Respir Med* 2015; 3: 435–442.
67 Agusti A, Fabbri LM, Singh D, *et al.* Inhaled corticosteroids in COPD: friend or foe? *Eur Respir J* 2018; 52: 1801219.
68 Liesker JJW, Bathoorn E, Postma DS, *et al.* Sputum inflammation predicts exacerbations after cessation of inhaled corticosteroids in COPD. *Respir Med* 2011; 105: 1853–1860.
69 Vedel-Krogh S, Nielsen SF, Lange P, *et al.* Blood eosinophils and exacerbations in chronic obstructive pulmonary disease. The Copenhagen General Population Study. *Am J Respir Crit Care Med* 2016; 193: 965–974.
70 Brightling CE, McKenna S, Hargadon B, *et al.* Sputum eosinophilia and the short term response to inhaled mometasone in chronic obstructive pulmonary disease. *Thorax* 2005; 60: 193–198.
71 Brightling CE, Monteiro W, Ward R, *et al.* Sputum eosinophilia and short-term response to prednisolone in chronic obstructive pulmonary disease: a randomised controlled trial. *Lancet* 2000; 356: 1480–1485.
72 Tinè M, Biondini D, Semenzato U, *et al.* Reassessing the role of eosinophils as a biomarker in chronic obstructive pulmonary disease. *J Clin Med* 2019; 8: 962.
73 George L, Taylor AR, Esteve-Codina A, *et al.* Blood eosinophil count and airway epithelial transcriptome relationships in COPD versus asthma. *Allergy* 2020; 75: 370–380.
74 Christenson SA, Steiling K, van den Berge M, *et al.* Asthma–COPD overlap. Clinical relevance of genomic signatures of type 2 inflammation in chronic obstructive pulmonary disease. *Am J Respir Crit Care Med* 2015; 191: 758–766.
75 McLeod O, Silveira A, Valdes-Marquez E, *et al.* Genetic loci on chromosome 5 are associated with circulating levels of interleukin-5 and eosinophil count in a European population with high risk for cardiovascular disease. *Cytokine* 2016; 81: 1–9.
76 Nair P, Pizzichini MM, Kjarsgaard M, *et al.* Mepolizumab for prednisone-dependent asthma with sputum eosinophilia. *N Engl J Med* 2009; 360: 985–993.

77 Haldar P, Brightling CE, Hargadon B, *et al.* Mepolizumab and exacerbations of refractory eosinophilic asthma. *N Engl J Med* 2009; 360: 973–984.
78 Pavord ID, Korn S, Howarth P, *et al.* Mepolizumab for severe eosinophilic asthma (DREAM): a multicentre, double-blind, placebo-controlled trial. *Lancet* 2012; 380: 651–659.
79 Ortega HG, Liu MC, Pavord ID, *et al.* Mepolizumab treatment in patients with severe eosinophilic asthma. *N Engl J Med* 2014; 371: 1198–1207.
80 Wang JM, Rambaldi A, Biondi A, *et al.* Recombinant human interleukin 5 is a selective eosinophil chemoattractant. *Eur J Immunol* 1989; 19: 701–705.
81 Jatakanon A, Lim S, Barnes PJ. Changes in sputum eosinophils predict loss of asthma control. *Am J Respir Crit Care Med* 2000; 161: 64–72.
82 Possa SS, Leick EA, Prado CM, *et al.* Eosinophilic inflammation in allergic asthma. *Front Pharmacol* 2013; 4: 46.
83 Fala L. Nucala (Mepolizumab): First IL-5 Antagonist Monoclonal Antibody FDA Approved for Maintenance Treatment of Patients with Severe Asthma. *Am Health Drug Benefits* 2016; 9: 106–110.
84 FDA, Clinical Review - NUCALA (mepolizumab). www.fda.gov/media/95114/download. Date last accessed: 2020; date last updated: 2015.
85 Hart TK, Cook RM, Zia-Amirhosseini P, *et al.* Preclinical efficacy and safety of mepolizumab (SB-240563), a humanized monoclonal antibody to IL-5, in cynomolgus monkeys. *J Allergy Clin Immunol* 2001; 108: 250–257.
86 Smith DA, Minthorn EA, Beerahee M. Pharmacokinetics and pharmacodynamics of mepolizumab, an anti-interleukin-5 monoclonal antibody. *Clin Pharmacokinet* 2011; 50: 215–227.
87 EMA, Nucala: Summary Of Product Characteristics. www.ema.europa.eu/en/documents/product-information/nucala-epar-product-information_en.pdf. Date last accessed: 2020; date last updated: 2015.
88 Ortega HG, Yancey SW, Mayer B, *et al.* Severe eosinophilic asthma treated with mepolizumab stratified by baseline eosinophil thresholds: a secondary analysis of the DREAM and MENSA studies. *Lancet Respir Med* 2016; 4: 549–556.
89 Powell C, Milan SJ, Dwan K, *et al.* Mepolizumab *versus* placebo for asthma. *Cochrane Database Syst Rev* 2015; 7: CD010834.
90 Dasgupta A, Kjarsgaard M, Capaldi D, *et al.* A pilot randomised clinical trial of mepolizumab in COPD with eosinophilic bronchitis. *Eur Respir J* 2017; 49: 1602486.
91 Pavord ID. Biologics and chronic obstructive pulmonary disease. *J Allergy Clin Immunol* 2018; 141: 1983–1991.
92 Shahlav-Monavvar P, Mobasher-Jannat A. Mepolizumab for eosinophilic COPD. *N Engl J Med* 2018; 378: 681.
93 Xia Y, Li W, Shen H. Mepolizumab for eosinophilic COPD. *N Engl J Med* 2018; 378: 680–681.
94 Pavord ID, Chanez P, Criner GJ, *et al.* Mepolizumab for eosinophilic chronic obstructive pulmonary disease. *N Engl J Med* 2017; 377: 1613–1629.
95 Ortega H, Lemiere C, Llanos JP, *et al.* Outcomes following mepolizumab treatment discontinuation: real-world experience from an open-label trial. *Allergy Asthma Clin Immunol* 2019; 15: 37.
96 Haldar P, Brightling CE, Singapuri A, *et al.* Outcomes after cessation of mepolizumab therapy in severe eosinophilic asthma: a 12-month follow-up analysis. *J Allergy Clin Immunol* 2014; 133: 921–923.
97 Moore WC, Kornmann O, Humbert M, *et al.* Outcomes following continuation or stopping long-term mepolizumab treatment in patients with severe eosinophilic asthma: the Randomized Comet Trial. *Am J Respir Crit Care Med* 2020; 201: A4211.
98 Condreay LD, Gao C, Bradford E, *et al.* Yancey, genetic associations with mepolizumab efficacy in COPD with peripheral blood eosinophilia. *Respir Med* 2019; 155: 26–28.
99 EMA, CINQAERO: Summary Of Product Characteristics. www.ema.europa.eu/en/documents/product-information/cinqaero-epar-product-information_en.pdf Date last accessed: 2020; date last updated: 2016.
100 Kips JC, O'Connor BJ, Langley SJ, *et al.* Effect of SCH55700, a humanized anti-human interleukin-5 antibody, in severe persistent asthma: a pilot study. *Am J Respir Crit Care Med* 2003; 167: 1655–1659.
101 Castro M, Mathur S, Hargreave F, *et al.* Reslizumab for poorly controlled, eosinophilic asthma: a randomized, placebo-controlled study. *Am J Respir Crit Care Med* 2011; 184: 1125–1132.
102 Ghazi A, Trikha A, Calhoun WJ. Benralizumab: a humanized mAb to IL-5Rα with enhanced antibody-dependent cell-mediated cytotoxicity--a novel approach for the treatment of asthma. *Expert Opin Biol Ther* 2012; 12: 113–118.
103 Kolbeck R, Kozhich A, Koike M, *et al.* MEDI-563, a humanized anti-IL-5 receptor alpha mAb with enhanced antibody-dependent cell-mediated cytotoxicity function. *J Allergy Clin Immunol* 2010; 125: 1344–1353.
104 Pham T-H, Damera G, Newbold P, *et al.* Reductions in eosinophil biomarkers by benralizumab in patients with asthma. *Respir Med* 2016; 111: 21–29.
105 Tan LD, Bratt JM, Godor D, *et al.* Benralizumab: a unique IL-5 inhibitor for severe asthma. *J Asthma Allergy* 2016; 9: 71–81.
106 Laviolette M, Gossage DL, Gauvreau G, *et al.* Effects of benralizumab on airway eosinophils in asthmatic patients with sputum eosinophilia. *J Allergy Clin Immunol* 2013; 132: 1086–1096.
107 Bleecker ER, FitzGerald JM, Chanez P, *et al.* Efficacy and safety of benralizumab for patients with severe asthma uncontrolled with high-dosage inhaled corticosteroids and long-acting β2-agonists (SIROCCO): a randomised, multicentre, placebo-controlled phase 3 trial. *Lancet* 2016; 388: 2115–2127.
108 FitzGerald JM, Bleecker ER, Nair P, *et al.* Benralizumab, an anti-interleukin-5 receptor α monoclonal antibody, as add-on treatment for patients with severe, uncontrolled, eosinophilic asthma (CALIMA): a randomised, double-blind, placebo-controlled phase 3 trial. *Lancet* 2016; 388: 2128–2141.
109 Bourdin A, Shaw D, Menzies-Gow A, *et al.* Two-year integrated steroid-sparing analysis and safety of benralizumab for severe asthma. *J Asthma* 2021; 58: 514–522.
110 Castro M, Wenzel SE, Bleecker ER, *et al.* Benralizumab, an anti-interleukin 5 receptor α monoclonal antibody, versus placebo for uncontrolled eosinophilic asthma: a phase 2b randomised dose-ranging study. *Lancet Respir Med* 2014; 2: 879–890.
111 Brightling CE, Bleecker ER, Panettieri RA, *et al.* Benralizumab for chronic obstructive pulmonary disease and sputum eosinophilia: a randomised, double-blind, placebo-controlled, phase 2a study. *Lancet Respir Med* 2014; 2: 891–901.

112 Criner GJ, Celli BR, Brightling CE, *et al.* Benralizumab for the Prevention of COPD Exacerbations. *N Engl J Med* 2019; 381: 1023–1034.
113 Criner GJ, Celli BR, Singh D, *et al.* Predicting response to benralizumab in chronic obstructive pulmonary disease: analyses of GALATHEA and TERRANOVA studies. *Lancet Respir Med* 2020; 8: 158–170.
114 May RD, Fung M. Strategies targeting the IL-4/IL-13 axes in disease. *Cytokine* 2015; 75: 89–116.
115 Brightling CE, Saha S, Hollins F. Interleukin-13: prospects for new treatments. *Clin Exp Allergy* 2010; 40: 42–49.
116 Kaur D, Hollins F, Woodman L, *et al.* Mast cells express IL-13R alpha 1: IL-13 promotes human lung mast cell proliferation and Fc epsilon RI expression. *Allergy* 2006; 61: 1047–1053.
117 Howard TD, Koppelman GH, Xu J, *et al.* Gene–gene interaction in asthma: IL4RA and IL13 in a Dutch population with asthma. *Am J Hum Genet* 2002; 70: 230–236.
118 Marone G, Granata F, Pucino V, *et al.* The intriguing role of interleukin 13 in the pathophysiology of asthma. *Front Pharmacol* 2019; 10: 1387.
119 Panettieri RA, Wang M, Braddock M, *et al.* Tralokinumab for the treatment of severe, uncontrolled asthma: the ATMOSPHERE clinical development program. *Immunotherapy* 2018; 10: 473–490.
120 Wang I-M, Lin H, Goldman SJ, *et al.* STAT-1 is activated by IL-4 and IL-13 in multiple cell types. *Mol Immunol* 2004; 41: 873–884.
121 Yang SJ, Allahverdian S, Saunders ADR, *et al.* IL-13 signaling through IL-13 receptor α2 mediates airway epithelial wound repair. *FASEB J* 2019; 33: 3746–3757.
122 White SR, Martin LD, Stern R, *et al.* Expression of IL-4/IL-13 receptors in differentiating human airway epithelial cells. *Am J Physiol Lung Cell Mol Physiol* 2010; 299: L681–L693.
123 Hilton DJ, Zhang JG, Metcalf D, *et al.* Cloning and characterization of a binding subunit of the interleukin 13 receptor that is also a component of the interleukin 4 receptor. *Proc Natl Acad Sci USA* 1996; 93: 497–501.
124 van der Pouw Kraan TCTM, Küçükaycan M, Bakker AM, *et al.* Chronic obstructive pulmonary disease is associated with the -1055 IL-13 promoter polymorphism. *Genes Immun* 2002; 3: 436–439.
125 Grünig G, Warnock M, Wakil AE, *et al.* Requirement for IL-13 independently of IL-4 in experimental asthma. *Science* 1998; 282: 2261–2263.
126 Blanchard C, Mishra A, Saito-Akei H, *et al.* Inhibition of human interleukin-13-induced respiratory and oesophageal inflammation by anti-human-interleukin-13 antibody (CAT-354). *Clin Exp Allergy* 2005; 35: 1096–1103.
127 Schmid-Grendelmeier P, Altznauer F, Fischer B, *et al.* Eosinophils express functional IL-13 in eosinophilic inflammatory diseases. *J Immunol* 2002; 169: 1021–1027.
128 Jiang M, Liu H, Li Z, *et al.* ILC2 s induce adaptive Th2-type immunity in acute exacerbation of chronic obstructive pulmonary disease. *Mediators Inflamm* 2019; 2019: 3140183.
129 Bel EH, Ten Brinke A. new anti-eosinophil drugs for asthma and COPD: targeting the trait! *Chest* 2017; 152: 1276–1282.
130 Wenzel S, Castro M, Corren J, *et al.* Dupilumab efficacy and safety in adults with uncontrolled persistent asthma despite use of medium-to-high-dose inhaled corticosteroids plus a long-acting β_2 agonist: a randomised double-blind placebo-controlled pivotal phase 2b dose-ranging trial. *Lancet* 2016; 388: 31–44.
131 Hanania NA, Noonan M, Corren J, *et al.* Lebrikizumab in moderate-to-severe asthma: pooled data from two randomised placebo-controlled studies. *Thorax* 2015; 70: 748–756.
132 Piper E, Brightling C, Niven R, *et al.* A phase II placebo-controlled study of tralokinumab in moderate-to-severe asthma. *Eur Respir J* 2013; 41: 330–338.
133 Panettieri RA, Sjöbring U, Péerffy A, *et al.* Tralokinumab for severe, uncontrolled asthma (STRATOS 1 and STRATOS 2): two randomised, double-blind, placebo-controlled, phase 3 clinical trials. *Lancet Respir Med* 2018; 6: 511–525.
134 Marone G, Spadaro G, Braile M, *et al.* Tezepelumab: a novel biological therapy for the treatment of severe uncontrolled asthma. *Expert Opin Investig Drugs* 2019; 28: 931–940.
135 Soumelis V, Reche PA, Kanzler H, *et al.* Human epithelial cells trigger dendritic cell mediated allergic inflammation by producing TSLP. *Nat Immunol* 2002; 3: 673–680.
136 Corren J, Parnes JR, Wang L, *et al.* Tezepelumab in adults with uncontrolled asthma. *N Engl J Med* 2017; 377: 936–946.
137 Djukanović R, Wilson SJ, Kraft M, *et al.* Effects of treatment with anti-immunoglobulin E antibody omalizumab on airway inflammation in allergic asthma. *Am J Respir Crit Care Med* 2004; 170: 583–593.
138 Thomson NC, Chaudhuri R. Omalizumab: clinical use for the management of asthma. *Clin Med Insights Circ Respir Pulm Med* 2012; 6: 27–40.
139 Takaku Y, Soma T, Nishihara F, *et al.* Omalizumab attenuates airway inflammation and interleukin-5 production by mononuclear cells in patients with severe allergic asthma. *Int Arch Allergy Immunol* 2013; 161: Suppl. 2, 107–117.
140 Maltby S, Gibson PG, Powell H, *et al.* Omalizumab treatment response in a population with severe allergic asthma and overlapping COPD. *Chest* 2017; 151: 78–89.
141 Hanania NA, Chipps BE, Griffin NM, *et al.* Omalizumab effectiveness in asthma–COPD overlap: *post hoc* analysis of PROSPERO. *J Allergy Clin Immunol* 2019; 143: 1629–1633.
142 Taillé C, Chanez P, Devouassoux G, *et al.* Mepolizumab in a population with severe eosinophilic asthma and corticosteroid dependence: results from a French early access programme. *Eur Respir J* 2020; 55: 1902345.
143 Eltboli O, Bafadhel M, Hollins F, *et al.* COPD exacerbation severity and frequency is associated with impaired macrophage efferocytosis of eosinophils. *BMC Pulm Med* 2014; 14: 112.
144 Singh D, Bafadhel M, Brightling CE, *et al.* Blood eosinophil counts in clinical trials for chronic obstructive pulmonary disease. *Am J Respir Crit Care Med* 2020; 202: 660–671.
145 Salter BM, Sehmi R. Hematopoietic processes in eosinophilic asthma. *Chest* 2017; 152: 410–416.
146 Kato Y, Takabayashi T, Sakashita M, *et al.* Expression and functional analysis of CST1 in intractable nasal polyps. *Am J Respir Cell Mol Biol* 2018; 59: 448–457.
147 Castro M, Corren J, Pavord ID, *et al.* Dupilumab efficacy and safety in moderate-to-severe uncontrolled asthma. *N Engl J Med* 2018; 378: 2486–2496.

148 Rabe KF, Nair P, Brusselle G, *et al.* Efficacy and safety of dupilumab in glucocorticoid-dependent severe asthma. *N Engl J Med* 2018; 378: 2475–2485.
149 Castro M, Rabe KF, Corren J, *et al.* Dupilumab improves lung function in patients with uncontrolled, moderate-to-severe asthma. *ERJ Open Res* 2020; 6: 00204-2019.
150 Doyle AD, Mukherjee M, LeSuer WE, *et al.* Eosinophil-derived IL-13 promotes emphysema. *Eur Respir J* 2019; 53: 1801291.
151 Higham A, Beech A, Wolosianka S, *et al.* Type 2 Inflammation in Eosinophilic Chronic Obstructive Pulmonary Disease. *Allergy* 2020; in press [https://doi.org/10.1111/all.14661].

Stem Cell Research 56 (2021) 102550

Contents lists available at ScienceDirect

Stem Cell Research

journal homepage: www.elsevier.com/locate/scr

Generation of four severe early-onset chronic obstructive pulmonary disease (COPD) patient-derived induced pluripotent stem cell lines from peripheral blood mononuclear cells

Engi Ahmed [a,b], Mathieu Fieldes [a], Joffrey Mianné [a], Chloé Bourguignon [a], Amel Nasri [a], Isabelle Vachier [b,e], Said Assou [a], Arnaud Bourdin [b,c,*], John De Vos [a,d,*]

[a] IRMB, Univ Montpellier, INSERM, CHU Montpellier, Montpellier 34000, France
[b] Department of Respiratory Diseases, CHU Montpellier, Arnaud de Villeneuve Hospital, INSERM, Montpellier 34000, France
[c] PhyMedExp INSERM 1046, University of Montpellier, Montpellier, France
[d] Department of Cell and Tissue Engineering, Saint-Eloi Hospital, Montpellier 34000, France
[e] MedBioMed, Montpellier, France

A B S T R A C T

Evidence highlights the concept of multiple trajectories leading to COPD. Early-life events (i.e., in utero lung development) may influence the maximally attained lung function and increase the risk to develop COPD. Human pluripotent stem cells (hiPSC) represent a unique opportunity to model lung development. We generated hiPSC lines from four highly characterized COPD patients with early onset and severe phenotype. Peripheral blood mononuclear cells (PBMCs) were reprogrammed using integration-free Sendai Virus. The cell lines had normal karyotype, expressed pluripotency hallmarks, and differentiated into the three primary germ layers. These lines offer a tool to study early-life origins of COPD.

1. Resource utility

Early onset of COPD is a poorly understood trajectory of the disease, actually considered to have developmental lung origins (Martinez, 2016). IPSC lines were generated from four severe COPD patients. These cell lines afford a unique model to investigate mechanisms relevant to pathologic lung development, and susceptibility to environmental exposure.

2. Resource details

In this study, peripheral blood mononuclear cells (PBMCs) were obtained from four early onset severe CODP patients. Cells were reprogrammed into iCOPD2 (UHOMi003-A), iCOPD6 (UHOMi006-A), iCOPD8 (UHOMi004-A), iCOPD9 (UHOMi005-A) lines respectively using non-integrating CytoTune-iPSC 2.0 Sendai Reprogramming kit.

PBMCs were isolated by Ficoll gradient centrifugation using Ficoll-Paque PLUS (GE Healthcare)(Vissers et al., 1988) then washed with PBS plus foetal bovine serum (FBS) 10%. PBMCs were cultured in StemSpan with Erythroid Expansion Medium (SSEM, StemCell Technologies), according to the manufacturer's instructions. Erythroid differentiation leads to erythroid progenitor cells expansion. The four reprogramming factors OCT3/4, SOX2, KLF4, and C-MYC were transiently expressed in the erythroid progenitor cells using the integration-free Sendai virus transduction method. The four cell lines had a normal morphology (Fig. 1, panel A, bright field microscopy; scale bar: 50 μm) and karyotype analysis revealed normal number and structure of chromosomes in all four lines (Fig. 1, panel B). The generated iPSC lines were tested for the absence of exogenous reprogramming vector which was analysed by PCR using Sendai virus vector (SeV) specific primers after about 10 passages, (Fig. 1D). The viral sequence was also absent in the negative non transduced human embryonic stem cells (Fig. 1, panel D,) but present in positive control.

Expression of pluripotency genes was evidenced by q-RT-PCR, using previously published Hy03 healthy iPS cell line (UHOMi002-A) as positive control, respectively for SOX2, NANOG and OCT4 (Fig. 1, panel C) (Fieldes et al., 2020).

Expression of pluripotency markers were assessed by immunocytochemistry staining, using antibodies against human OCT3/4 and NANOG (Fig. 1, E scale bar 50 μm) and using surface marker TRA-1–60 (Fig. 1, panel F). The ability of COPD iPSC cell lines to differentiate into the three germ layers in vitro was confirmed by embryoid body (EB)

* Corresponding authors.
E-mail addresses: a-bourdin@chu-montpellier.fr (A. Bourdin), john.devos@inserm.fr (J. De Vos).

https://doi.org/10.1016/j.scr.2021.102550
Received 6 May 2021; Received in revised form 6 September 2021; Accepted 19 September 2021
Available online 27 September 2021
1873-5061/© 2021 CHU de Montpellier. Published by Elsevier B.V. This is an open access article under the CC BY license (http://creativecommons.org/licenses/by/4.0/).

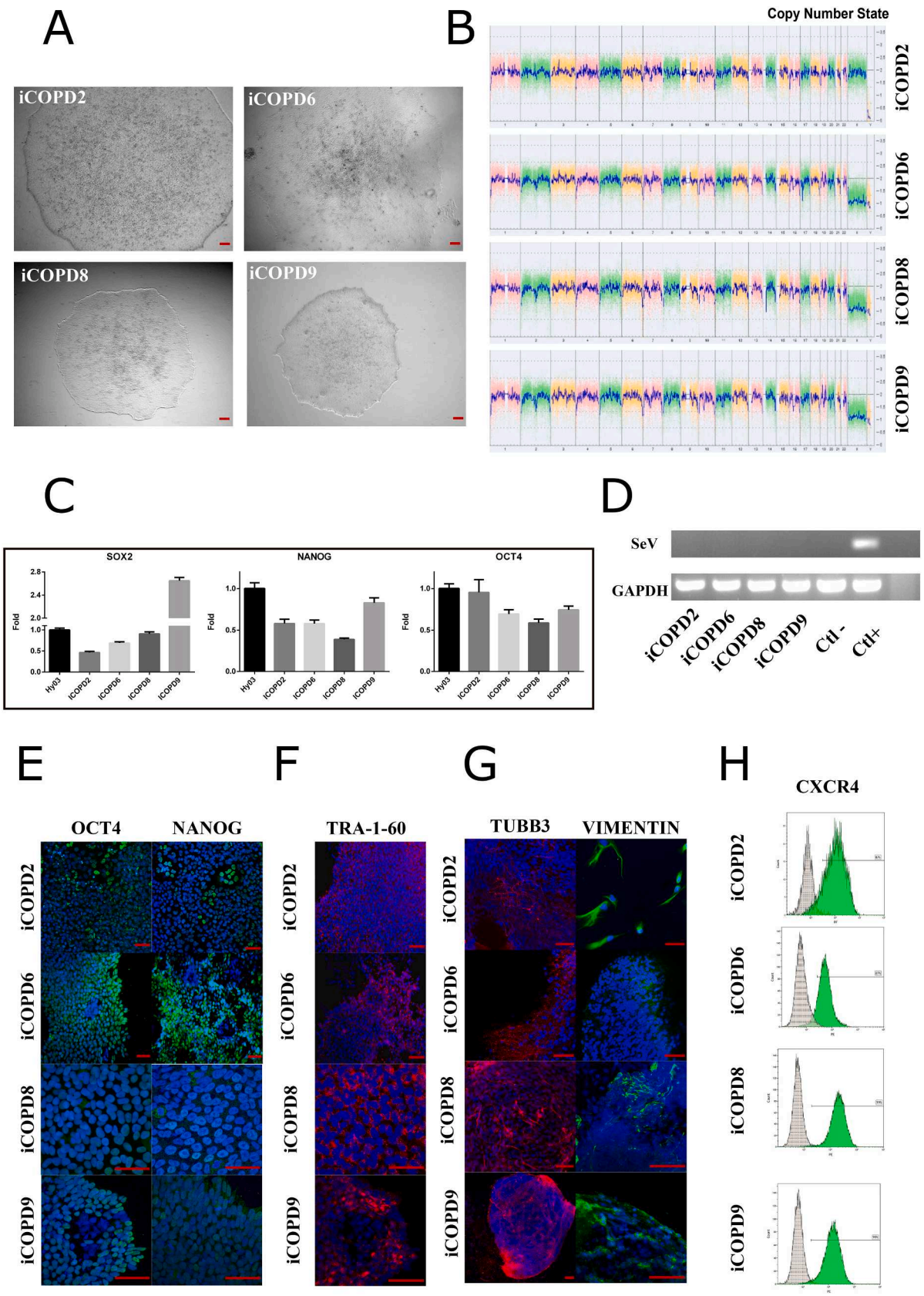

(caption on next page)

Fig. 1. Characterization of the iPS cell lines. A. The four cell lines display a normal morphology (bright field microscopy; scale bar: 50 μm). B. KaryoStat analysis (ThermoFisher) revealed normal number and structure of chromosomes in all four lines. C. Expression of pluripotency genes was evidenced by q-RT-PCR, using previously published Hy03 healthy iPS cell line (UHOMi002-A) as positive control, respectively for SOX2, NANOG and OCT4. D. The iPSC lines were tested for the absence of exogenous reprogramming vector by PCR using Sendai virus vector (SeV) specific primers after about 10 passages. The viral sequence was also absent in the negative non transduced human embryonic stem cells (Ctl-) but present in positive control (Ctl +). E. Expression of pluripotency markers assessed by immunofluorescence, using antibodies against human OCT3/4 and NANOG (scale bar 50 μm). F. Expression of pluripotency markers assessed by immunofluorescence, using antibodies against surface marker TRA-1–6). G. The ability of COPD iPSC cell lines to differentiate into the three germ layers in vitro was confirmed by embryoid body (EB) formation. EB expressed ectodermal (β-III-tubulin) and mesodermal (vimentin) markers as observed by immunofluorescence. H. EB expressed endodermal protein CXCR4 as shown by flow cytometry method.

formation. EB formation was performed by transferring iPSC clumps to low-adhesion dishes (Falcon) in E8 medium. After 24 h, EB were suspended in differentiation medium composed of RPMI-1640 medium (Gibco) supplemented with 10% FBS (Gibco) and 1% Penicillin-streptomycin. The medium was changed every two days for 30 days. After this period, the EB were plated on Geltrex-coated dishes and cultured for about a week. Cells were then fixed in 4% paraformaldehyde for immunofluorescence analysis. They expressed ectodermal (β-III-tubulin), mesodermal (vimentin) (Fig. 1, panel G) and endodermal protein CXCR4 by flow cytometry method (Fig. 1, panel H).

Microsatellite analysis showed matching profiles of short tandem repeats (STR) amplified from genomic DNA UHOMi00 3,4, 5 & 6-A iPS cells and patient-derived PBMCs (matching of 16/16 loci: D8S1179, D21S11, D7S820, CSF1PO, D3S1358, TH01, D13S317, D16S539, D2S1338, AMEL, D5S818, FGA, D19S433, vWA, TPOX and D18S51; available with authors). The four iPS cell lines were also confirmed to be free of mycoplasma. Of note, ratio < 0.9 means that the sample was negative for mycoplasma (Supplemental Table 1).

3. Materials and methods

3.1. Reprogramming of PBMCs to iPSCs

Erythroid progenitor cells (EPC) were transduced by Sendai-virus with the CytoTune®-iPS 2.0 Sendai Reprogramming Kit (Thermo Fisher Scientific), following manufacturer's instruction. The calculated volumes of each of the three CytoTune™ 2.0 Sendai-virus (SeV) were added to the EPC (KOS MOI = 5, hc-Myc MOI = 5, hKlf4 MOI = 3). The colonies with an embryonic stem cells (ES)-like appearance were manually isolated based on morphologic features.

3.2. Cell culture of iPSC cell lines

COPD cell lines were cultured on Geltrex matrix (Thermo Fisher Scientific) in E8 medium (Thermo Fisher Scientific), according to the manufacturer's instruction. The cells were cultivated at 37 °C in normoxic conditions/ 5% CO_2 and passaged manually. They were then adapted by passaging them using EDTA dissociation (Versene Solution, Thermo Fisher Scientific) every week into clumps, using 1:10 split ratio.

3.3. Karyotyping

Karyotyping was performed at mechanic passage 20. Karyotyping was performed using a service provider. The KaryoStat™ assay allows for digital visualization of chromosome aberrations with a resolution similar to g-banding karyotyping. The size of structural aberration that can be detected is > 2 Mb for chromosomal gains and > 1 Mb for chromosomal losses. Genomic DNA purification Cells were prepared according to the Genomic DNA Purification Kit (Catalog #: K0512) and quantified using the Qubit™ dsDNA BR Assay Kit (Catalog #: Q32850). GeneChip® Preparation 250 ng total gDNA was used to prepare the GeneChip® for KaryoStat™ according to the manual and is an array that looks for copy number variants and single nucleotide polymorphisms across the genome.

Table 1
Characterization and validation.

	Test	Result	Data
Morphology	Photography Bright field	*Normal for the four iPS cell lines*	Fig. 1 *panel A*
Phenotype	Qualitative analysis Immunocytochemistry	*Expression of pluripotency markers: OCT4, NANOG, TRA-1–60*	Fig. 1 *panel E & F*
	Quantitative analysis *RT-qPCR analysis*	*Expression of SOX2, NANOG and OCT4*	Fig. 1 *panel C*
Genotype	Karyotype (G-banding) and resolution	*Normal for the 4 cell lines*	Fig. 1 *panel B*
Identity	Microsatellite PCR (mPCR)	*not performed*	*N. A*
	STR analysis	*Specific 16 loci tested, 16/16 matched between iPS cell line and patient derived PBMCs*	*submitted in archive with journal*
Microbiology and virology	Mycoplasma	*Mycoplasma testing by luminescence. Negative*	Supplemental Table 1
Differentiation potential	Embryoid body formation	*Embryoid bodies show the three germ layers formation:* Immunocytochemistry ***ectoderm:*** *βIII-tubulin (TUBB3);* ***mesoderm:*** *vimentin marker.* *Flow cytometry* ***endoderm:*** *C-X-C Motif Chemokine Receptor (CXCR4), respectively UHOMi003-A: 87 %* *UHOMi004-A: 99 %* *UHOMi005-A: 98%* *UHOMi006-A: 87 %*	Fig. 1 *panel G & H*
List of recommended germ layer markers	Expression of these markers has to be demonstrated at mRNA (RT PCR) or protein (IF) levels, at least 2 markers need to be shown per germ layer	Ectoderm: TUBB3/TUJ1, Endoderm: CXCR4 Mesoderm: VIMENTIN	Fig. 1 *panel G & H*
Donor screening (OPTIONAL)	HIV 1 + 2 Hepatitis B, Hepatitis C	*Negative*	*not shown but available with the authors*
Genotype additional info (OPTIONAL)	Blood group genotyping	*N.A.*	N. A
	HLA tissue typing	*N. A*	N. A

3.4. Immunofluorescence labelling

Cells were tested after passage 20 and fixed in 4% PFA for 15 min at room temperature (RT) and washed 3 times in phosphate-buffered saline (PBS, Gibco). The cells were permeabilized with 0.5% Triton X-100 (Sigma Aldrich) for 15 min, blocked with 10% normal donkey serum (Sigma Aldrich) for 1 h at RT. Cells were incubated with the primary antibodies in PBS BSA 1% 0.1% Triton X-100 overnight at 4 °C. (listed in Table 2). Secondary antibodies were used at the dilution of 1:2000 during one hour at RT. Cell nuclei were stained with DAPI (Sigma Aldrich). Images were captured with Zeiss Axioimager Z1 Apotome and Confocal Microscopy Zeiss LMS700.

3.5. Flow cytometry analysis

Cells were tested after passage 20 and harvested using cell dissociation reagent (Versene Solution) and washed twice in PBS. Cells were then incubated 15 min at room temperature with a Live Cell/Dead Cell discriminator staining (Violet Zombie, Biolegend). IPS cells were incubated with a conjugated primary or the control isotype antibody for 30 min at 4° C. After staining, cells were washed twice and analysed by flow cytometry using Beckman Coulter Gallios. Analysis was performed with Kaluza software.

3.6. Testing for Sendai virus clearance

Total RNA was isolated from iPS cells within the first week after transfection with Sendai virus and iPSCs after passage 15. RNA extraction and RT were performed as previously described (qRT-PCR section). PCR was performed using Q5 High-Fidelity DNA Polymerase with the primers listed in Table 2. The PCR mix was composed of cDNA (50 ng), the forward and reverse primers 1.5 µl at 10 µM for each, dNTPs (10 nM), Q5 buffer and Q5 DNA Pol5 (New England BioLabs). DNA was melted for 3 min at 95 °C, then 35 cycles (95 °C) for 15 s, 55 °C for 15 s and 72 °C for 30 s), and final elongation was performed at 72 °C for 2 min using C100 Thermal Cycler (Bio-Rad). Products were analysed on 2.5 % agarose gel, ran at 130 V electric field. Finally, the picture was acquired using ChemiDoc™MP Imaging System (Bio-Rad).

3.7. RT-qPCR analysis

Reverse transcription (RT) was performed on cells around passage 20 using SuperScript™ First-Strand Synthesis System (ref 11904–018, Invitrogen) as recommended by the manufacturer in 20 µl reaction volume that included 1 µg RNA (extracted with RNeasy Mini Kit, ref 74106, Qiagen), Superscript II RT, oligo-dT primer, dNTP mixture, MgCl2, 0.1 M DTT and RNase inhibitor. Quantitative PCR (qPCR) was then performed using the LightCycler® 480 SYBR Green I Master (04707516001, Roche) with 2 µl of the RT reaction product (1:20 dilution) and 0,5µl of each primer diluted at 10 µM (Integrated DNA Technologies IDT) in a total volume of 10 µl. PCR amplifications were carried out using a LightCycler 480 apparatus and the following programme: 1 cycle of 95 °C for 10 s; 40 cycles of 95 °C for 10 s, 60 °C for 15 s; 72 °C for 15 s, 1 cycle 95 °C for 5 s, 65 °C for 1 min, 97 °C forever. Gene expression levels were normalised to the expression of the housekeeping gene GAPDH, using the following formula: 2-ΔΔCt, where ΔΔCt = ΔCt unknown - ΔCt positive control.

3.8. Short tandem repeat analysis (STR)

DNA extraction was performed as described below on cells after passage 10. STR analysis of generated iPSCs and parental PBMCs was performed to detect 16 loci. STR was performed using a service provider (Eurofins). Briefly, DNA isolation was carried out from cell pellet. Genetic characteristics were determined by PCR-single-locus-technology. 16 independent PCR-systems D8S1179, D21S11, D7S820, CSF1PO, D3S1358, TH01, D13S317, D16S539, D2S1338, AMEL, D5S818, FGA, D19S433, vWA, TPOX and D18S51 were investigated. In parallel, positive, and negative controls were carried out yielding correct results.

Table 2
Reagents details.

Antibodies used for immunocytochemistry/flow-cytometry			
	Antibody	Dilution	Company Cat # and RRID
Pluripotency Markers	*Rabbit Polyclonal anti OCT4*	*1:400*	*Santa Cruz Technology Cat# RRID AB_2167703*
	Rabbit polyclonal anti NANOG	*1:250*	*Abcam Cat# ab80892 RRID AB_2150114*
	Mouse monoclonal [TRA-1-60]	*1:100*	*Abcam Anti-TRA-1-60 (R) antibody [TRA-1-60] RRID (ab16288)*
Differentiation Markers	*Mouse anti-CXCR4 (PE)*	*1:200*	*BD BiosciencesRRID 557145*
	Polyclonal goat anti VIMENTIN	*1: 50*	*Santa Cruz Biotechnology Cat# sc-7557, RRID: AB_793998*
	Mouse anti βIII-TUBULIN	*1:1000*	*Covance Research Products Inc. Cat# MMS-435P, RRID: AB_2313773*
Secondary antibodies	*donkey anti mouse Alexa fluor 555*	*1:2000*	*Thermo Fisher Scientific Cat# A-31570, RRID: AB_2536180*
	donkey anti goat Alexa fluor 647	*1:2000*	*Thermo Fisher Scientific Cat# A-21206, RRID: AB_ 2535862*
	Mouse IgG2a, (PE))	*1:200*	*BD Biosciences RRID556653*

Primers		
	Target	Forward/Reverse primer (5′-3′)
Virus clearance (qPCR)	*SeV product size: 181 bp*	*GGATCACTAGGTGATATCGAGC ACCAGACAAGAG TTTAAGAGATATGTATC*
House-Keeping Genes	*GAPDH (PCR) product size: 300 bp*	*CTG GCG TCT TCA CCA CCA TGG CAT CAC GCC ACA GTT TCC CGG*
Pluripotency genes (qRT-PCR)	*OCT4*	*GGG CTC TCC CAT GCA TTC AAA C CAC CTT CCC TCC AAC CAG TTG C*
	SOX2	*GGCCATTAACGGCACACTGCC TTACTCTCCTCTTTTGCACCCCTCC*
	NANOG	*TGA TTT GTG GGC CTG AAG AAA GAG GCA TCT CAG CAG AAG ACA*
House -Keeping Genes	*GAPDH (qRT-PCR)*	*GAC CTG ACC TGC CGT CTA GAA A CCT GCT TCA CCA CCT TCT TGA*

3.9. Mycoplasma testing

Cell culture supernatants were tested around passage 20 using bioluminescence MycoAlert® Detection Kit (Lonza) according to manufacturer's instructions.

Appendix A. Supplementary data

Supplementary data to this article can be found online at https://doi.org/10.1016/j.scr.2021.102550.

References

Fieldes, M., Ahmed, E., Bourguignon, C., Mianné, J., Martin, M., Arnould, C., Vachier, I., Assou, S., De Vos, J., Bourdin, A., 2020. Generation of the induced pluripotent stem cell line UHOMi002-A from peripheral blood mononuclear cells of a healthy male donor. Stem Cell Res. 49, 102037. https://doi.org/10.1016/j.scr.2020.102037.

Martinez, F.D., 2016. Early-Life Origins of Chronic Obstructive Pulmonary Disease. N. Engl. J. Med. 375, 871–878. 10.1056/NEJMra1603287.

Vissers, M.C.M., Jester, S.A., Fantone, J.C., 1988. Rapid purification of human peripheral blood monocytes by centrifugation through Ficoll-Hypaque and Sepracell-MN. J. Immunol. Methods 110 (2), 203–207. https://doi.org/10.1016/0022-1759(88)90104-4.

cells

MDPI

Review

Pipeline for the Generation and Characterization of Transgenic Human Pluripotent Stem Cells Using the CRISPR/Cas9 Technology

Joffrey Mianné [1], Chloé Bourguignon [1], Chloé Nguyen Van [1], Mathieu Fieldès [1], Amel Nasri [1], Said Assou [1,*] and John De Vos [1,2,*]

1 IRMB, Univ Montpellier, INSERM, CHU Montpellier, 34000 Montpellier, France; joffrey.mianne@inserm.fr (J.M.); chloe.bourguignon@inserm.fr (C.B.); nguyenva@etud.insa-toulouse.fr (C.N.V.); m_fieldes@hotmail.com (M.F.); amel.nasri@inserm.fr (A.N.)

2 Department of Cell and Tissue Engineering, Univ Montpellier, CHU Montpellier, 34000 Montpellier, France

* Correspondence: said.assou@inserm.fr (S.A.); john.devos@inserm.fr (J.D.V.)

Received: 22 April 2020; Accepted: 23 May 2020; Published: 25 May 2020



Abstract: Recent advances in genome engineering based on the CRISPR/Cas9 technology have revolutionized our ability to manipulate genomic DNA. Its use in human pluripotent stem cells (hPSCs) has allowed a wide range of mutant cell lines to be obtained at an unprecedented rate. The combination of these two groundbreaking technologies has tremendous potential, from disease modeling to stem cell-based therapies. However, the generation, screening and molecular characterization of these cell lines remain a cumbersome and multi-step endeavor. Here, we propose a pipeline of strategies to efficiently generate, sub-clone, and characterize CRISPR/Cas9-edited hPSC lines in the function of the introduced mutation (indels, point mutations, insertion of large constructs, deletions).

Keywords: hPSC; CRISPR; screening; stem cells; gene editing; gene targeting; disease modeling

1. Introduction

Thanks to their unlimited proliferative potential, their euploid state, and their capacity to differentiate in any cell type, human pluripotent stem cells (hPSCs), either embryonic or induced, have a tremendous potential for disease modeling and for the production of cells for clinical applications [1–3]. Although numerous hPSC lines from patients with various diseases have been established, the generation of hPSC lines for some pathologies or rare genetic mutations is still challenging. Moreover, interindividual genetic heterogeneity can result in biological variations that may render the comparison between lines difficult, especially between hPSCs derived from healthy controls and patients [4,5]. The ability to genetically manipulate hPSCs offers the opportunity to introduce, modify, or correct mutations and to generate genetically matched isogenic control lines, to establish definitive genotype–phenotype links [6,7].

Recent technologies based on site-specific nucleases, including zinc finger nucleases (ZFNs), transcription activator-like effector nucleases (TALENs), and particularly the clustered regularly interspaced short palindromic repeats (CRISPR) system, have enabled the versatile genome engineering of hPSCs [8,9]. Nevertheless, hPSC engineering remains challenging due to the intrinsic properties of such cells, including their relatively poor transfection efficacy and low viability following transfection, difficulty in isolating clonal populations, preferential selection and amplification of aneuploid clones, and spontaneous cell differentiation. To alleviate these problems, several protocols to generate an array of different mutagenesis events have been described [10–14]. While much effort has been focused on improving the methodological procedures to generate transgenic hPSCs, only few studies

assessed the key quality control steps, including screening and in-depth molecular characterization. Yet, appropriate validation is fundamental to establish the relevance of the edited cell lines, but it is made difficult by the high heterogeneity of the allele types that can be generated by CRISPR-based engineering [15,16]. Here, we summarize the main strategies and propose an efficient pipeline to generate, screen, and characterize genetically engineered hPSC lines obtained by knock-out (KO), small or large knock-in (KI), and deletion of genetic elements.

1.1. The CRISPR/Cas9 System

The discovery and adaptation of natural biological systems as site-specific nucleases have revolutionized the field of genetic engineering in the past two decades. The implementation of meganucleases, ZFN, TALEN, and now CRISPR/Cas systems has expanded the opportunities to manipulate the genome of many species, including human cells [17]. Particularly, the CRISPR/Cas system has become the main tool for genome engineering projects due to its simplicity, versatility, efficacy, and low cost [17].

The CRISPR/Cas9 system, derived from *Streptococcus pyogenes* (spCas9), is the first CRISPR system to have been adapted for gene editing [18]. It relies on a universal Cas9 nuclease that can generate a DNA double-strand break (DSB) when combined with a single-guide RNA (sgRNA) to form a ribonucleoprotein (RNP) complex [18]. In this RNP complex, the sgRNA will guide the Cas9 nuclease to a specific locus by Watson–Crick base pairing, thus allowing nuclease activity and cleavage of the target site (Figure 1). The sgRNA can be designed to target any 20-nucleotide-long sequence that must be followed in the targeted genome by a 5′-NGG tri-nucleotide recognition site, called a protospacer adjacent motif (PAM) [18].

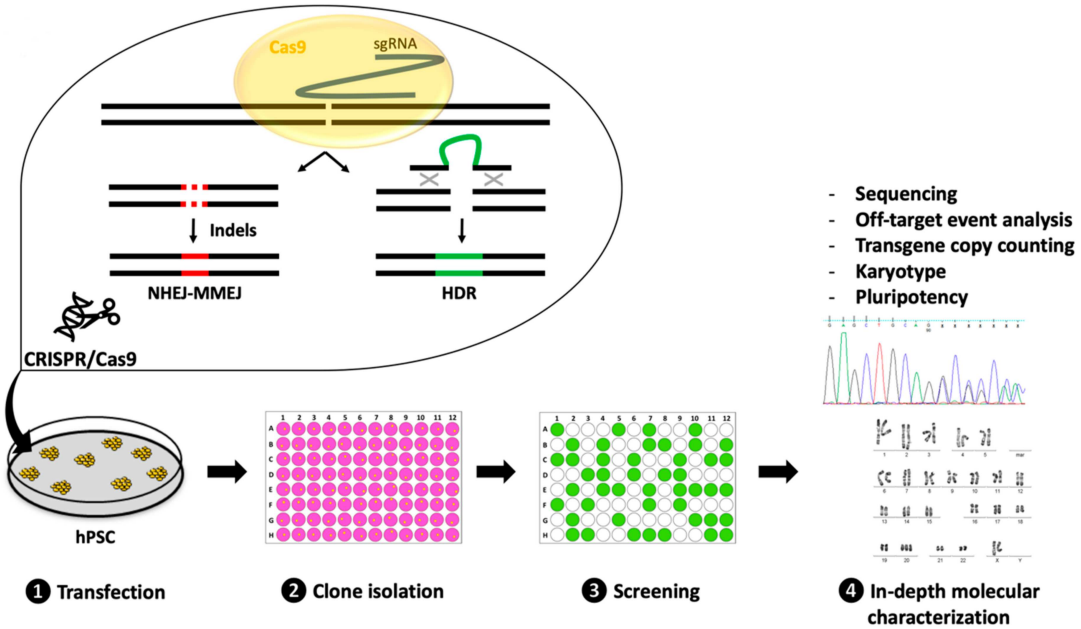

Figure 1. Pipeline to generate CRISPR-edited human pluripotent stem cell (hPSC) lines. Generating transgenic hPSC is a process that includes four mains phases: (**1**) Transfection of CRISPR reagents (single guide RNA, Cas9, and if required, a donor DNA template) in the parental hPSC line to introduce a targeted DNA double strand break (DSB). The DSB will be repaired by the endogenous DNA repair pathways. The non-homologous end-joining (NHEJ) and micro-homology-mediated end-joining (MMEJ) pathways can lead to the introduction of small insertions/deletions (indels), while the HDR pathway introduces exogenous nucleotides; (**2**) Transfected cells are isolated in separate wells to be expanded as clonal populations; (**3**) Following isolation, a high-throughput screening step is performed to select the correctly modified clones; (**4**) The selected clones are finally characterized using a combination of tests.

Although many CRISPR/Cas systems derived from various bacteria or engineered to recognize broader sets of PAMs, to be more efficient or more specific, have now been adapted as site-specific nucleases, this review will only focus and describe the most commonly used spCas9 [19]. However, the strategies and recommendations proposed in this review are applicable to the different CRISPR systems adapted from spCas9 or other DNA-targeting Cas proteins.

1.2. DNA Repair Mechanisms

Introducing a DNA DSB at a targeted locus will lead to activation of the cell endogenous DNA repair mechanisms. Three mechanisms are predominantly activated (Figure 1) [20]. The non-homologous end-joining (NHEJ) and micro-homology-mediated end-joining (MMEJ) pathways are usually considered as error-prone systems. Therefore, by taking advantage of these DNA repair mechanisms, it is possible to introduce small insertion or deletion (indel) events that lead to the disruption of the targeted DNA sequence. On the other hand, the homology-directed repair (HDR) pathway can be exploited to introduce precise nucleotide modifications or exogenous DNA sequences by providing a DNA donor template with homology to the target site. One of the drawbacks of relying on cell endogenous DNA repair mechanisms is our limited ability to preferentially select one of them [20]. This is particularly limiting because HDR events tend to occur at a much lower rate than NHEJ-MMEJ events.

2. Preparing the Experiment

For successful CRISPR-based mutagenesis of hPSCs, it is important to carefully design and plan the experiment. Specifically, before starting laboratory experiments, the following points should be assessed.

2.1. Defining the Project Goal

Clearly defining the project goal is essential for selecting the most time- and cost-efficient approach to obtain the desired cell line. This means specifying the type and purpose of the cell line(s) to be generated. Particularly, it is important to know whether a clonal cell line is required, whether the targeted gene is expressed in and/or is essential for hPSC maintenance, or whether it is expressed only upon hPSC differentiation, and whether the obtained cell lines will be used for basic research, pre-clinical, or clinical purposes. Answering these key questions will ensure the project feasibility, will guide reagent selection, and help to define the quality control (QC) level required to validate the cell line for downstream experiments.

2.2. Defining the Mutagenesis Event to Be Generated

Various type of mutants can be generated using CRISPR technologies. Genes can be KO, single nucleotide polymorphisms (SNPs) can be introduced or corrected, large constructs can be KI to add functional elements (e.g., constitutive protein expression, fluorescent reporters, tags, conditional alleles, inducible systems, etc.), or particular sequences can be deleted. Several mutagenesis events can be obtained in a single experiment. These events can be obtained separately as heterozygous or homozygous variants but can also be found in combination (compound-heterozygosity, e.g., one KO and one KI allele). Determining the mutagenesis event(s) to be generated will specify the experiment design and the screening process to recover the cells with the desired mutation(s).

2.3. Selecting Reagents and Transfection Strategies

The selection of the relevant reagents and transfection strategies are important because this will directly influence the experiment design and the number of QC tests to be performed. The sgRNA/Cas9 reagents can be delivered under various forms, such as plasmids, RNA, or RNP. Plasmids are stable constructs that can be easily engineered to co-express multiple sgRNAs at once, or additional functions

(e.g., fluorescent markers or antibiotic resistance). The addition of fluorescent reporters or antibiotic resistance cassettes can help to assess the transfection efficacy and allow the positive selection of transfected cells. Expression plasmids should carry suitable promoters to avoid transcriptional silencing that can occur in hPSCs [21]. Moreover, when using plasmid expression systems, DNA toxicity, potential unwanted insertion into the genome, and prolonged expression that can increase the chance of introducing undesired CRISPR-induced off-target (OT) mutations should be taken into account [22]. Alternatively, the sgRNA/Cas9 complex can be delivered as RNA or RNP. Although they usually do not allow the co-expression of fluorescence markers or antibiotic selection, they alleviate most of the disadvantages inherent to plasmid transfection due to their low toxicity, absence of genomic integration, and quick transient expression [22]. If required, a DNA donor template can also be added to the system, such as circular or linear double-stranded DNA (dsDNA), and linear single-stranded DNA (ssDNA). dsDNA are easy to synthetize, to manipulate, and can be used to deliver large constructs but come with higher risk of unintended integration into the targeted genome (backbone integration at the targeted locus or random insertion) [16]. Both short (up to 200nt) and long (>200nt) ssDNA are highly efficient templates for homologous recombination, and their single strand nature reduces the odds of unintended integration [14,23–25].

These components can be introduced in cells by electroporation [10], lipofection [26], using biopolymer systems [27], or by viral transduction [28]. The advantages and limitations of each strategy have been discussed elsewhere [29,30]. It is worth noting that electroporation and lipofection are the main transfection approaches for CRISPR/Cas9 gene-editing in hPSCs. Other systems can be interesting but might require optimization for hPSC transfection.

2.4. Characterizing the Targeted Sequence

Although important, the characterization of the hPSC genomic sequence to be modified is often neglected, leading to a waste of time and resources. Indeed, due to the inter-individual genetic heterogeneity, it is not rare to observe small or large nucleotide variations (SNP, insertions, deletions) in one or both alleles compared with the reference genome [31]. Analysis of both alleles by Sanger sequencing before sgRNA selection will ensure that the sgRNA(s) and DNA donor templates are designed in accordance with the actual target sequence.

2.5. Anticipating the Screening Strategy

Another important point in the experiment design is the downstream screening strategy. Screening should be inexpensive and high throughput to allow the processing of as many clones as required (depending on the mutation event complexity and the overall efficacy of the CRISPR/Cas9 system). This is especially true for KI projects that depend on HDR, which is less effective than NHEJ-MMEJ. Strategies to facilitate screening or to reduce the number of clones to be screened should be considered during the experiment design. The selected clones will then require further characterization using more specific but more expensive and time-consuming tests.

2.6. sgRNA Design and Selection

sgRNA selection is a multifactorial evaluation process that can be described as a compromise between specificity and efficacy/probability to obtain the desired modification. For spCas9, sgRNA should recognize a target sequence of 18-20 nucleotides that must be followed by the trinucleotide 5′-NGG PAM sequence at the target site [18]. PAM sequences can differ depending on the chosen CRISPR system [19]. However, irrespective of the CRISPR system to be used, the selection parameters are specific for the modification to be generated. Thus, for protein loss-of-function projects, it is recommended to select sgRNAs that (i) will disrupt a sequence present in all splice variants; (ii) are not too close to the start codon to avoid activation of a downstream alternative start codon; (iii) are not too close to splice-sites, which if deleted, can result in unpredictable new transcripts; and (iv) are as specific as possible, preferentially without OT sites with three or less mismatches. For KI projects, sgRNA selection

is more constrained because the DSB should occur as close as possible to the site of the nucleotide change (typically within 10 nucleotides of either side of the DBS) [14,23,25]. The sgRNA should also be selected to avoid DNA donor cleavage and reprocessing of the allele to be generated following the homologous recombination event. Like for KO projects, the selected sgRNA must be as specific as possible. For deletion projects, the selection of a pair of sgRNAs depends on the nature of the deletion to be generated. If a precise sequence must be deleted (with a defined number of nucleotides to be removed and a precise junction point), then a donor DNA template might be used, and sgRNAs should be selected like described for KI projects [32]. If the deletion does not need to result in a precise junction event, sgRNAs should be selected to introduce a DSB in the region surrounding the sequence to be deleted, and should be as specific as possible.

Many online tools using various algorithms have been developed and are available to help with the experiment design and sgRNA selection depending on their specificity [33]. Moreover, several algorithms can be used to predict sgRNA efficacy and the type of indels that are generated following NHEJ-MMEJ repair of DBS [33,34]. Although these algorithms can be useful to prioritize sgRNA selection, they only give predictions and still have many limitations. Therefore, as sgRNA efficacy can be highly variable, it is important to design two-three sgRNAs and in vitro screen their efficacy by T7 endonuclease 1 (T7E1) assay or by tracking of indels by decomposition (TIDE) analysis with the aim of identifying the most efficient [35,36].

2.7. DNA Donor Template Design

For projects in which exogenous nucleotides will be KI, a DNA donor template must be generated. Its design depends on all of the factors described above, and particularly on the modification to be introduced and the selected sgRNA. The DNA donor template must include the precise sequence to be introduced and also the homology arms to the target. It may also include additional sequences to facilitate the recovery of correctly edited clones. The recommended length for the homology arms is 20-50nt for small ssDNA [14,23], 100-600nt for long ssDNA [24,25], and 300-1000nt for dsDNA (PCR products or plasmids) [13,37]. For ssDNA, phosphorothioate modifications at both donor sequence ends are recommended to improve the ssDNA stability and KI efficacy [23]. The DNA donor template should not include the sgRNA sequence to be used. This can be obtained by selecting sgRNA sequences that will be disrupted by the nucleotides to be introduced, or by adding silent mutations that will prevent tight binding of the sgRNA and facilitate the downstream screening by introducing an enzymatic restriction site.

Of note, strategies based on homology-independent targeted integration have also been described [38]. This might be an interesting alternative; however, their efficacy in hPSC remains to be determined because only limited reports are available [39].

3. Experimental Strategies for the Successful Generation and Characterization of CRISPR-Edited hPSC Lines

Irrespective of the desired modification, the generation of transgenic hPSC lines can be decomposed in four main steps: Transfection, clone isolation, screening, and in-depth molecular validation (Figure 1). Each step can be achieved using various strategies that will be discussed below.

3.1. Transfection

The first step consists in delivering the reagents (sgRNA, Cas9, and DNA donor) into the cells. Its success is influenced by many factors, including the choice of transfection method and the cell line susceptibility. Various tools and protocols have been specifically adapted for the efficient transfection or transduction of hPSCs [26,28,40]. Transfection approaches using electroporation systems or lipofectamine are cheap, have been widely used and optimized, and allow the simultaneous transfer of all reagents (sgRNA, Cas9, and DNA donor) in all possible forms (DNA, RNA, RNP). Other transfection strategies based on polymers or nanoparticles have also been used to deliver CRISPR

reagents. However, these approaches have rarely been tested or optimized for hPSC transfection. Transduction approaches using viral vectors are interesting for their high efficiency, but they usually remain more expensive [28]. Moreover, the inability to package the CRISPR reagents and the donor template into the same particle remains a limitation of transduction strategies [28].

Several points should be taken into account to improve the transfection efficacy. First, hPSCs should be "adapted" to single-cell passaging using the Rho-associated coiled-coil containing kinases (ROCK) inhibitor Y-27632 for four to six passages before starting the experiment [41]. This will ensure optimal cell survival after transfection, and will optimize clone selection. The number of cells to be transfected depends on the transfection system toxicity and the likelihood of obtaining the desired event (depending on its complexity and sgRNA efficacy). Toxicity is also influenced by the quality and quantity of nucleic acids and/or proteins to be transfected. Optimizing these parameters will significantly increase the probability of obtaining the desired event(s). Additionally, it has been reported that hPSC mortality via activation of the tumor protein p53 apoptosis pathway is high after DNA DSB introduction in their genome [42]. It is therefore important to scale up appropriately the number of cells to be transfected. Finally, to promote cell survival after transfection, it is also recommended to culture cells in medium supplemented with the ROCK inhibitor Y-27632 for 24 to 48h [41].

3.2. Clone Isolation

CRISPR-based mutagenesis of a pool of cells will lead to a variety of mutagenesis events. Each cell within the pool will harbor its own combination of wild-type and/or mutant alleles. Although heterogeneous cell populations can be used for some research projects, in most cases, clones that harbor only the desired mutagenesis event must be isolated. This can be obtained by seeding single cells in the wells of 96-well plates. Single cells can be isolated manually by limiting the dilution approach, or by automated cell sorting. Alternatively, a pool of single cells can be plated at low density and later, colonies can be picked and manually transferred in individual wells.

For some projects, clone isolation can be facilitated by adding a positive selection marker (fluorescent reporter, or antibiotic resistance gene) to specifically select the transfected, or correctly engineered cells. Cells that express a fluorescent reporter can be selected by fluorescence-activated cell sorting (FACS), whereas cells that include an antibiotic resistance gene will survive antibiotic selection. These positive markers are usually transiently expressed as part of the transgene and removed at a later stage, or are delivered with the transient Cas9 expression system. If the project aim is to introduce a tagged protein or a gene, the expression of which is controlled by an endogenous promoter, the strategy can be adapted depending on whether this gene is expressed or not in hPSCs. Indeed, if the protein with a fluorescent tag is expressed in hPSCs, correctly targeted cells can be detected and isolated by FACS [13]. Conversely, FACS-based screening is not possible if the tagged protein is not expressed in hPSCs. Innovative approaches have been proposed to overcome this issue. For example, Roberts et al. described a strategy based on a transgene with a constitutively expressed mCherry fluorescence selection cassette that allows selection by FACS of clones that carry the transgene. This was followed by excision of the selection cassette using CRISPR/Cas9 and MMEJ repair [12].

Even when adapted to single-cell passaging, hPSCs remain highly sensitive to cell dissociation and isolation. Consequently, when placed in individual wells, most cells will die within few days. Plating cells at low density will improve survival but will also increase the probability of forming mosaic colonies, derived from two or more genetically different cells. Therefore, irrespective of the used approach, the number of clones to be isolated should be scaled up according to the mortality but also to the likelihood of obtaining the desired event.

Following clone isolation, an intermediate step to expand and duplicate clones is required to maintain cells in culture or to cryopreserve them, while the clone DNA is extracted for screening.

3.3. Clone Screening

Screening can be defined as a single or a combination of high-throughput tests to rapidly and cheaply identify the clones of interest. Two main parameters should be considered when selecting a screening test: (i) The number of clones to be screened, and (ii) the type of modifications introduced (Figures 2 and 3).

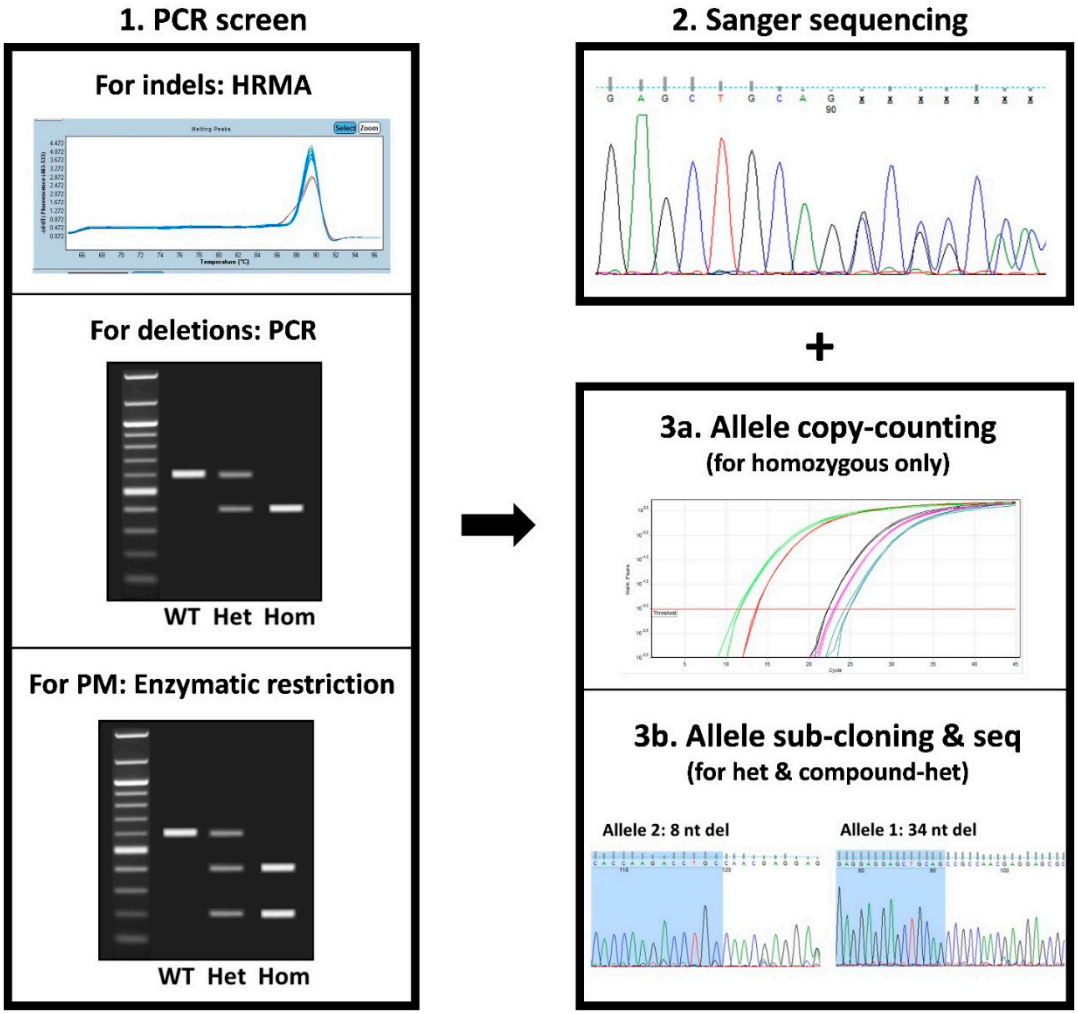

Figure 2. Screening strategies for indels, deletions, and small knock-in (KI). Screening to identify the CRISPR-edited hPSC clones harboring the desired indels, deletions, or small KI can be divided in three steps. The first step is a PCR-based screen to quickly detect clones with the on-target modification(s). For indels, the mutated clones can be identified by PCR followed by high resolution melt analysis (HRMA). To identify clones carrying a deletion, PCR with primers located at each side of the expected deleted sequence can be used. For clones carrying a small KI, if a restriction site has been added to the donor DNA template, enzymatic digestion of the PCR product that includes the targeted sequence will allow the detection of clones with on-target integration of the donor. Positive clones are then checked by Sanger sequencing to determine their exact sequence. This step is important to select clones with the desired modification(s) and to discard clones with unwanted events (i.e., in-frame events for KO projects, imperfect HDR events for a small KI project). Finally, in clones homozygous for the desired mutation, the transgene copy number is evaluated to ensure ploidy, whereas heterozygous and compound heterozygous clones are sub-cloned to determine the exact allelic sequences. PM, point mutation; WT, wild type; Het, heterozygous; Hom, homozygous; seq, sequencing; nt, nucleotides.

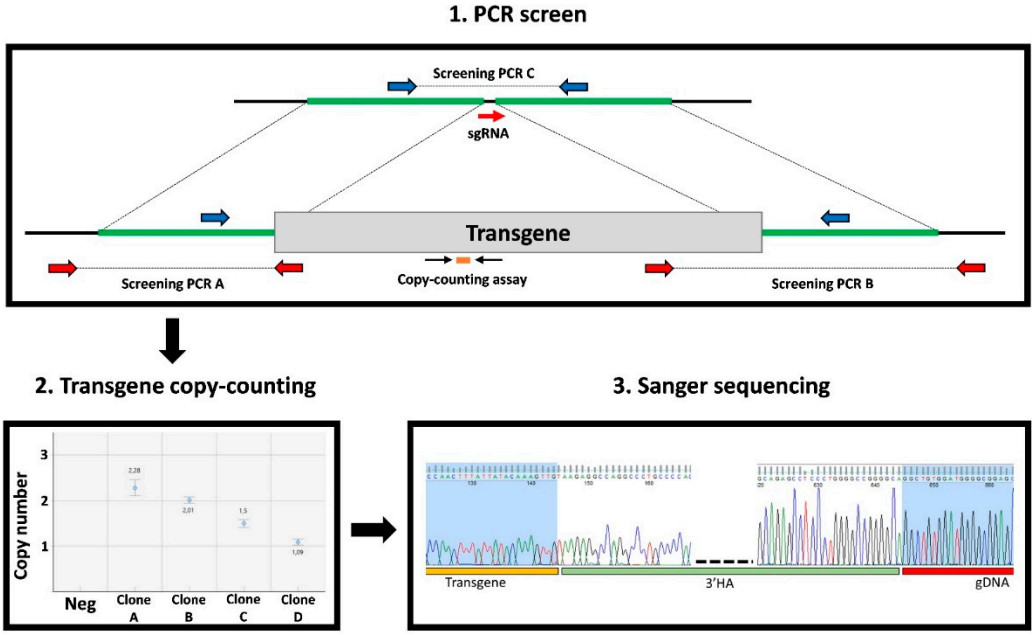

Figure 3. Screening strategies for large KI. Screening CRISPR-edited hPSC clones harboring large KI can be divided in three steps. The first step involves three PCR assays: (i) two PCR assays with primers that bridge between the transgene and the surrounding genomic DNA (screening PCR_A and B) to quickly detect clones with on-target integration of the transgene, and (ii) a third PCR assay using primers that surround the targeted locus (screening PCR_C) to detect alleles without transgene integration. Then, a transgene copy-counting assay by qPCR or ddPCR is performed to determine the transgene copy number. Combining the PCR and copy-counting results will allow classification of the clones in four categories: no transgene integration (PCR_A and B negative, PCR_C positive, copy-counting = 0), heterozygous integration (PCR_A and B positive, PCR_C positive, copy-counting = 1), homozygous integration (PCR_A and B positive, PCR_C negative, copy-counting = 2), other (all the other possibilities, including random insertion of the transgene and mosaic clones). For heterozygous and homozygous clones, the on-target integrated transgene sequence is verified by Sanger sequencing to ensure sequence integrity.

When indels are introduced, different strategies can be employed for clone screening, each of them with its own advantages and limitations (Table 1).

T7E1 or Surveyor nuclease assays are based on the PCR amplification of the targeted sequence, followed by a melting step and random hybridization that can form homo- or hetero-duplexes if one or both alleles within that clone are mutated (the two alleles need to be different for detection). For homozygous clone detection, DNA from the parental cell line must also be amplified and supplemented to the PCR product. Then, these homo- or hetero-duplexes undergo T7E1 or surveyor nuclease enzymatic digestion that will specifically cleave heteroduplexes, thus revealing the mutated clones after electrophoresis [35]. The main limitation of these tests is their low sensitivity to detect some mutations, including single nucleotide variations that are one of the main indel types generated by NHEJ-MMEJ [34,35]. High-resolution melting analysis (HRMA) can also be used for clone screening [43]. This approach consists in following in real time the fluorescence emission of an intercalating dye during the melting of a short PCR product that includes the targeted sequence. Mutated clones will be detected due to the slight modification of their melting curve (Figure 2) [43]. This test is inexpensive and convenient to quickly identify mutants in a large set of clones. Other approaches, such as indel detection by amplicon analysis (IDAA) and droplet digital PCR (ddPCR), can be used for indel identification [44,45]. Both tests are more expensive because they require fluorescent primers or probes. However, IDAA present the advantage of giving information on the allele composition by providing the number of nucleotides added or deleted compared with the wild-type allele (of note,

it only allows the detection of size differences but not nucleotide composition changes) [44]. This is particularly interesting for KO projects to select clones in which both alleles are mutated while avoiding in-frame deletions.

Table 1. Advantages and limitations of the indel screening strategies.

Test (Reference)	Principle	Advantages	Limitations
T7E1 or Surveyor nuclease assay [35]	Enzymatic digestion of PCR heteroduplexes	Quick (few hours) Cheap Medium throughput Basic laboratory equipment	Sensitivity Medium throughput (needs also WT PCR product to detect homozygous clones) No information on the allele composition
HRMA [43]	Melting curve variation	Quick (few hours) Cheap High throughput Sensitive Basic laboratory equipment	Short amplicons required, might miss larger deletion events No information on the allele composition
IDAA [44]	Indel detection by amplicon analysis	Quick (few hours) High throughput Sensitive Information on the allele composition	More expensive Specific laboratory equipment
ddPCR [45]	Indel detection by drop-out of a labeled probe	Quick (few hours) Medium throughput Sensitive	More expensive Specific laboratory equipment No information on the allele composition

Several strategies are available to identify hPSC clones harboring the desired indel(s). WT: wild-type.

For deletion projects, screening usually relies on PCR amplification using primers that surround the region to be deleted to detect the corresponding shorter product after electrophoresis (Figure 2). However, when the deletion size is large, alleles without a deletion event might be difficult to amplify by PCR. Therefore, it is important to combine PCR screening with a copy counting assay by quantitative PCR (qPCR) or ddPCR, to confirm zygosity.

For small KI projects (e.g., introduction or correction of an SNP), the screening strategy depends on the donor design. Introducing a restriction site within the donor facilitates the screening of clones that have integrated the donor on the target. Indeed, positive clones can be identified by PCR amplification of the targeted region followed by enzymatic digestion and electrophoresis (Figure 2). If no restriction site can be introduced in the donor, then primers that will only amplify the expected allele can be designed.

For large KI projects, screening is performed by combining different tests (Figure 3). This includes PCR amplifications using primers that bridge between the transgene and the surrounding genomic DNA (bridge_PCR) to detect clones with on-target transgene integration. An additional PCR to amplify alleles that have not integrated the transgene (NT_PCR) is also performed. Large transgenes are usually delivered as plasmids that may integrate randomly in the genome or in concatemers at the target site [13,16]. To exclude such events, the transgene copy (TC) number must be evaluated by qPCR or ddPCR. Together, the PCR data and TC counting will discriminate clones into four categories: No transgene integration (bridge_PCR negative, NT_PCR positive, TC = 0), heterozygous integration (bridge_PCR positive, NT_PCR positive, TC = 1), homozygous integration (bridge_PCR positive, NT_PCR negative, TC = 2), and others (all the other possibilities, including random transgene insertion and mosaic clones). Alternatively, Southern blot analysis can be performed to identify clones with on-target transgene integration after bridge_PCR.

For all mutation types (KO, deletion, small or large KI), positive clones recovered after these first screening steps will need to be further analyzed by Sanger sequencing to determine the exact allelic sequence composition (Figures 2 and 3). This will allow the selection of only clones with the correct on-target event for downstream in-depth molecular characterization. For homozygous clones, a single sequencing trace will be obtained, directly revealing the sequence of both alleles.

Nevertheless, the ploidy status of homozygous clones should be confirmed by qPCR or ddPCR because large deletion events may sometimes result in hemizygosity (Figure 2) [46]. For heterozygous or compound-heterozygous clones, two overlapping sequences will be obtained and might require sub-cloning to determine the exact sequence of both alleles (Figure 2).

For gene KO projects, only clones in which both alleles contain the frameshift mutation will be kept for further analysis. For clones harboring a deletion, sequencing will give information on the exact sequence that has been deleted, and on the absence of other unwanted modifications (small insertion, inversion) that may be generated at the break points. For KI projects, sequencing is important to confirm the integrity of the newly generated allele, because unperfect repair using donor templates can occur [23–25,47]. Moreover, for heterozygous clones in KI projects, the allele without donor sequence integration should also be characterized because indels may be present [13].

Of note, if only a few clones have to be analyzed, it is possible to directly check them by Sanger sequencing, thus bypassing some of the screening steps.

By the end of the screening process, the clones of interest should have been selected and cryopreserved. Among them, two to five candidates will be selected for in-depth molecular characterization.

3.4. In-Depth Molecular Characterization

At this stage, additional analyses of the selected clones are required to fully characterize and validate them (Table 2). The type and number of tests will depend on the reagents used and the quality level required for the downstream applications. These quality control steps are important to ensure that no unintended event, which may interfere with the genotype–phenotype correlation analysis, has occurred during genome engineering and clonal selection.

Table 2. In-depth molecular characterization tests.

Test	Project Type	Purpose	Methods
DNA integrity	All	Identification of unwanted genomic abnormalities/rearrangements	Screening: qPCR or ddPCR Final characterization: G-banding/microarray/NGS
OT mutation	All	Identification of potential mutagenesis events at off-target sites	HRMA or PCR of the top 5-10 OT sites/HRMA or PCR of OT with up to 3 MMs/whole exome/whole genome
Pluripotency	All	Confirming the pluripotency state of the transgenic iPSC lines	IF/cytometry/embryoid bodies/teratoma
Plasmid integration	All projects in which plasmids are used	Confirming the absence of plasmid backbone integration in the clone's genome	PCR/qPCR/ddPCR
ssDNA donor integration	All projects in which ssDNA are used	Identification of unintended integration of the ssDNA donor oligo(s)	qPCR/ddPCR
p53 function	All	Confirming p53 function	Sequencing

Following screening, clones need to be further characterized to ensure their integrity. NGS: next generation sequencing; MMs: mismatches; IF: immunofluorescence.

Unintended events associated with the mutagenesis process include random genomic integration of the donor DNA or of the used expression systems [13,16,48]. If plasmids have been used to express the CRISPR/Cas9 system or as a donor DNA template, PCR analysis with primers targeting the plasmid backbone should be performed to determine whether they have been integrated. Similarly, the random integration in the genome of the short and long ssDNA used as donor templates should be assessed by copy counting using qPCR or ddPCR [24,25].

Another issue that can arise during CRISPR/Cas9 mutagenesis is the possible generation of OT mutations due to the imperfect specificity of the system [49]. This can occur when the used sgRNAs have a low specificity profile. OT mutations are also more likely to be generated if Cas9 activity is

prolonged [22]. Therefore, the absence of OT mutations should be confirmed, especially if plasmid expression systems have been used because of prolonged exposure to Cas9 activity. Many approaches and protocols have been developed to this aim [50]. While most projects will only require the checking of a few sites that are most likely to be modified by HRMA or Sanger sequencing (top 10 OT sites, or all OT sites with up to three mismatches associated with the used sgRNA), others might need a genome-wide analysis of all possible OT sites [50] or next-generation sequencing approaches (whole-exome or whole-genome sequencing). Another possibility to eliminate potential OT bias is to generate similar mutations using two different sgRNAs (each with its own set of potential OT sites). This will confirm that the obtained phenotype is only due to the on-target event and not to OT mutation(s).

Several options are available to reduce the likelihood of generating OT mutations. They mainly rely on the many Cas protein variants that have been engineered to increase its specificity, or on the use of RNP complexes for quick transient expression of the system [22,50].

Generating transgenic hPSC clones is a stressful process for cells. Single-cell passaging, transfection, and clonal selection can favor the emergence and selection of aneuploid clones. The selection of clones with genomic abnormalities is also facilitated by the fact that several recurrent copy number variants (CNVs) can provide selective growth advantages to cells [51]. Therefore, the DNA integrity of the retained clones should be confirmed using standard cytogenetic procedures, G-banding, microarray, or next-generation sequencing [52]. If many clones have to be analyzed, recurrent CNV can be rapidly detected by qPCR or ddPCR to eliminate these clones before karyotyping [53].

Additional tests can be performed to assess the pluripotency status of the retained clones. The detection of pluripotency markers (e.g., octamer-binding transcription factor 4 [OCT4], NANOG, SRY-Box Transcription Factor 2 [SOX2], stage-specific embryonic antigen-4 [SSEA4]) by immunofluorescence analysis, qPCR, or cytometry analysis can rapidly confirm the pluripotency of the generated clones. As recent research has highlighted the potential preferential selection of p53-deficient hPSCs following CRISPR/Cas9 mutagenesis, it may be useful to check the p53 function or genomic sequence in the selected clones [42].

Finally, for each project, the functionality of the clones that have successfully passed all previous QC tests will have to be assessed. Tests will depend on the nature of the transgenic line that has been generated. It might require hPSC differentiation into the relevant cell type to obtain transgene expression. RNA and protein expression should be monitored in clones harboring indels and deletions. The expression of the modified allele or of the fluorescent reporters should be confirmed after KI.

4. Perspectives

Many protocols to improve the CRISPR mutagenesis rate have been published, but they often overlook the screening and validation steps required to characterize clonal lines. Here, we described a pipeline to efficiently design, generate, and characterize transgenic hPSC lines. Generating CRISPR/Cas9-edited hPSCs is a multi-step process that includes transfection, clone isolation, screening, and in-depth molecular validation. Each step can be performed using different protocols that are chosen in the function of their advantages and limitations. Careful experiment design and planning are crucial to select the most appropriate strategies to reduce the time and costs and to facilitate the generation of the desired hPSC lines.

The available techniques for in-depth characterization are limited by the high sequencing costs, but improving access to more comprehensive approaches, such as whole genome sequencing, should increase the reliability and safety of the edited cell lines in the future.

Furthermore, the development of new genome editing approaches, such as alternative CRISPR systems, base-editing [54], or prime-editing [55], will further facilitate hPSC engineering. It will also broaden the type of changes that can be introduced and expand the genome sequences that can be targeted. These systems should also reduce the risk of introducing unintended modifications. However, more research is needed to fully grasp the on- and off-target effects of these newer techniques in hPSC in order to adapt the screening strategies.

Human PSCs are valuable systems for basic research, disease modeling, pre-clinical, and now also clinical applications [56]. The ability to genetically manipulate these cells using CRISPR technologies to generate tailored transgenic lines that can be differentiated into any cell type is expanding the horizon of their possible applications. This will accelerate basic research by facilitating studies on genotype-phenotype correlations, and consequently increase the number and relevance of hPSC lines for disease modeling. Ultimately, these advances might be translated into autologous gene and cell therapies.

Funding: This work was supported by a grant to C.B. from FRM (FDM20170638083).

Acknowledgments: We thank E. Andermarcher for critical reading of this manuscript.

Conflicts of Interest: S.A. and J.D.V. filed a patent entitled «Non-invasive methods for assessing genetic integrity of pluripotent stem cells», priority number: EP20150306389, and are Co-founder and Scientific Advisor of Stem Genomics S.A.S. that acquired the exploitation rights of this patent. J.M., C.B., C.N.V., M.F. and A.M. declare no conflict of interest.

References

1. Thomson, J.A. Embryonic stem cell lines derived from human blastocysts. *Science* **1998**, *282*, 1145–1147. [CrossRef] [PubMed]
2. Takahashi, K.; Yamanaka, S. Induction of Pluripotent Stem Cells from Mouse Embryonic and Adult Fibroblast Cultures by Defined Factors. *Cell* **2006**, *126*, 663–676. [CrossRef] [PubMed]
3. Shi, Y.; Inoue, H.; Wu, J.C.; Yamanaka, S. Induced pluripotent stem cell technology: A decade of progress. *Nat. Rev. Drug Discov.* **2017**, *16*, 115–130. [CrossRef] [PubMed]
4. Kilpinen, H.; Goncalves, A.; Leha, A.; Afzal, V.; Alasoo, K.; Ashford, S.; Bala, S.; Bensaddek, D.; Casale, F.P.; Culley, O.J.; et al. Common genetic variation drives molecular heterogeneity in human iPSCs. *Nature* **2017**, *546*, 370–375. [CrossRef]
5. Bock, C.; Kiskinis, E.; Verstappen, G.; Gu, H.; Boulting, G.; Smith, Z.D.; Ziller, M.; Croft, G.F.; Amoroso, M.W.; Oakley, D.H.; et al. Reference maps of human es and ips cell variation enable high-throughput characterization of pluripotent cell lines. *Cell* **2011**, *144*, 439–452. [CrossRef]
6. Hockemeyer, D.; Jaenisch, R. Induced pluripotent stem cells meet genome editing. *Cell Stem Cell* **2016**, *18*, 573–586. [CrossRef]
7. Soldner, F.; Laganière, J.; Cheng, A.W.; Hockemeyer, D.; Gao, Q.; Alagappan, R.; Khurana, V.; Golbe, L.I.; Myers, R.H.; Lindquist, S.; et al. Generation of isogenic pluripotent stem cells differing exclusively at two early onset parkinson point mutations. *Cell* **2011**, *146*, 318–331. [CrossRef]
8. Jang, Y.Y.; Ye, Z. Gene correction in patient-specific iPSCs for therapy development and disease modeling. *Hum. Genet.* **2016**, *135*, 1041–1058. [CrossRef]
9. Ben Jehuda, R.; Shemer, Y.; Binah, O. Genome Editing in Induced Pluripotent Stem Cells using CRISPR/Cas9. *Stem Cell Rev. Rep.* **2018**, *14*, 323–336. [CrossRef]
10. Li, X.-L.; Li, G.-H.; Fu, J.; Fu, Y.-W.; Zhang, L.; Chen, W.; Arakaki, C.; Zhang, J.-P.; Wen, W.; Zhao, M.; et al. Highly efficient genome editing via CRISPR–Cas9 in human pluripotent stem cells is achieved by transient BCL-XL overexpression. *Nucleic Acids Res.* **2018**, *46*, 1–21. [CrossRef]
11. Mitzelfelt, K.A.; McDermott-Roe, C.; Grzybowski, M.N.; Marquez, M.; Kuo, C.T.; Riedel, M.; Lai, S.; Choi, M.J.; Kolander, K.D.; Helbling, D.; et al. Efficient Precision Genome Editing in iPSCs via Genetic Co-targeting with Selection. *Stem Cell Rep.* **2017**, *8*, 491–499. [CrossRef] [PubMed]
12. Roberts, B.; Hendershott, M.C.; Arakaki, J.; Gerbin, K.A.; Malik, H.; Nelson, A.; Gehring, J.; Hookway, C.; Ludmann, S.A.; Yang, R.; et al. Fluorescent Gene Tagging of Transcriptionally Silent Genes in hiPSCs. *Stem Cell Rep.* **2019**, *12*, 1145–1158. [CrossRef] [PubMed]
13. Roberts, B.; Haupt, A.; Tucker, A.; Grancharova, T.; Arakaki, J.; Fuqua, M.A.; Nelson, A.; Hookway, C.; Ludmann, S.A.; Mueller, I.A.; et al. Systematic gene tagging using CRISPR/Cas9 in human stem cells to illuminate cell organization. *Mol. Biol. Cell* **2017**, *28*, 2854–2874. [CrossRef] [PubMed]
14. Yang, L.; Guell, M.; Byrne, S.; Yang, J.L.; De Los Angeles, A.; Mali, P.; Aach, J.; Kim-Kiselak, C.; Briggs, A.W.; Rios, X.; et al. Optimization of scarless human stem cell genome editing. *Nucleic Acids Res.* **2013**, *41*, 9049–9061. [CrossRef]

15. Mianné, J.; Codner, G.F.; Caulder, A.; Fell, R.; Hutchison, M.; King, R.; Stewart, M.E.; Wells, S.; Teboul, L. Analysing the outcome of CRISPR-aided genome editing in embryos: Screening, genotyping and quality control. *Methods* **2017**, *121–122*, 68–76. [CrossRef]
16. Canaj, H.; Hussmann, J.A.; Li, H.; Beckman, K.A.; Goodrich, L.; Cho, N.H.; Li, Y.J.; Santos, D.A.; McGeever, A.; Stewart, E.M.; et al. Deep profiling reveals substantial heterogeneity of integration outcomes in CRISPR knock-in experiments. *bioRxiv* **2019**, 841098. [CrossRef]
17. Hsu, P.D.; Lander, E.S.; Zhang, F. Development and applications of CRISPR-Cas9 for genome engineering. *Cell* **2014**, *157*, 1262–1278. [CrossRef]
18. Jinek, M.; Chylinski, K.; Fonfara, I.; Hauer, M.; Doudna, J.A.; Charpentier, E. A programmable dual-RNA-guided DNA endonuclease in adaptive bacterial immunity. *Science* **2012**, *337*, 816–821. [CrossRef]
19. Mitsunobu, H.; Teramoto, J.; Nishida, K.; Kondo, A. Beyond Native Cas9: Manipulating Genomic Information and Function. *Trends Biotechnol.* **2017**, *35*, 983–996. [CrossRef]
20. Yeh, C.D.; Richardson, C.D.; Corn, J.E. Advances in genome editing through control of DNA repair pathways. *Nat. Cell Biol.* **2019**, *21*, 1468–1478. [CrossRef]
21. Zhang, M.; Niibe, K.; Kondo, T.; Kamano, Y.; Saeki, M.; Egusa, H. Gene Delivery and Expression Systems in Induced Pluripotent Stem Cells. In *Interface Oral Health Science 2016*; Sasaki, K., Suzuki, O., Takahashi, N., Eds.; Springer: Singapore, 2017; pp. 121–133. [CrossRef]
22. Kim, S.; Kim, D.; Cho, S.W.; Kim, J.; Kim, J.S. Highly efficient RNA-guided genome editing in human cells via delivery of purified Cas9 ribonucleoproteins. *Genome Res.* **2014**, *24*, 1012–1019. [CrossRef] [PubMed]
23. Renaud, J.B.; Boix, C.; Charpentier, M.; De Cian, A.; Cochennec, J.; Duvernois-Berthet, E.; Perrouault, L.; Tesson, L.; Edouard, J.; Thinard, R.; et al. Improved Genome Editing Efficiency and Flexibility Using Modified Oligonucleotides with TALEN and CRISPR-Cas9 Nucleases. *Cell Rep.* **2016**, *14*, 2263–2272. [CrossRef] [PubMed]
24. Codner, G.F.; Mianné, J.; Caulder, A.; Loeffler, J.; Fell, R.; King, R.; Allan, A.J.; Mackenzie, M.; Pike, F.J.; McCabe, C.V.; et al. Application of long single-stranded DNA donors in genome editing: Generation and validation of mouse mutants. *BMC Biol.* **2018**, *16*, 70. [CrossRef] [PubMed]
25. Li, H.; Beckman, K.A.; Pessino, V.; Huang, B.; Weissman, J.S.; Leonetti, M.D. Design and specificity of long ssDNA donors for CRISPR-based knock-in. *bioRxiv* **2017**, 178905. [CrossRef]
26. Yu, X.; Liang, X.; Xie, H.; Kumar, S.; Ravinder, N.; Potter, J.; de Mollerat du Jeu, X.; Chesnut, J.D. Improved delivery of Cas9 protein/gRNA complexes using lipofectamine CRISPRMAX. *Biotechnol. Lett.* **2016**, *38*, 919–929. [CrossRef]
27. Timin, A.S.; Muslimov, A.R.; Lepik, K.V.; Epifanovskaya, O.S.; Shakirova, A.I.; Mock, U.; Riecken, K.; Okilova, M.V.; Sergeev, V.S.; Afanasyev, B.V.; et al. Efficient gene editing via non-viral delivery of CRISPR–Cas9 system using polymeric and hybrid microcarriers. *Nanomed. Nanotechnol. Biol. Med.* **2018**, *14*, 97–108. [CrossRef]
28. Martin, R.M.; Ikeda, K.; Cromer, M.K.; Uchida, N.; Nishimura, T.; Romano, R.; Tong, A.J.; Lemgart, V.T.; Camarena, J.; Pavel-Dinu, M.; et al. Highly Efficient and Marker-free Genome Editing of Human Pluripotent Stem Cells by CRISPR-Cas9 RNP and AAV6 Donor-Mediated Homologous Recombination. *Cell Stem Cell* **2019**, *24*, 821–828. [CrossRef] [PubMed]
29. Lino, C.A.; Harper, J.C.; Carney, J.P.; Timlin, J.A. Delivering CRISPR: A review of the challenges and approaches. *Drug Deliv.* **2018**, *25*, 1234–1257. [CrossRef] [PubMed]
30. Yin, H.; Kauffman, K.J.; Anderson, D.G. Delivery technologies for genome editing. *Nat. Rev. Drug Discov.* **2017**, *16*, 387–399. [CrossRef] [PubMed]
31. Scott, D.A.; Zhang, F. Implications of human genetic variation in CRISPR-based therapeutic genome editing. *Nat. Med.* **2017**, *23*, 1095–1101. [CrossRef] [PubMed]
32. Wang, X.; Wang, Y.; Huang, H.; Chen, B.; Chen, X.; Hu, J.; Chang, T.; Lin, R.-J.; Yee, J.-K. Precise Gene Modification Mediated by TALEN and Single-Stranded Oligodeoxynucleotides in Human Cells. *PLoS ONE* **2014**, *9*, e93575. [CrossRef] [PubMed]
33. Thomas, M.; Parry-Smith, D.; Iyer, V. Best practice for CRISPR design using current tools and resources. *Methods* **2019**, *164–165*, 3–17. [CrossRef] [PubMed]
34. Allen, F.; Crepaldi, L.; Alsinet, C.; Strong, A.J.; Kleshchevnikov, V.; De Angeli, P.; Páleníková, P.; Khodak, A.; Kiselev, V.; Kosicki, M.; et al. Predicting the mutations generated by repair of Cas9-induced double-strand breaks. *Nat. Biotechnol.* **2019**, *37*, 64–82. [CrossRef] [PubMed]

35. Vouillot, L.; Thélie, A.; Pollet, N. Comparison of T7E1 and surveyor mismatch cleavage assays to detect mutations triggered by engineered nucleases. *G3 Genes Genomes Genet.* **2015**, *5*, 407–415. [CrossRef]
36. Brinkman, E.K.; Chen, T.; Amendola, M.; Van Steensel, B. Easy quantitative assessment of genome editing by sequence trace decomposition. *Nucleic Acids Res.* **2014**, *42*, 1–8. [CrossRef]
37. Zhang, J.P.; Li, X.L.; Li, G.H.; Chen, W.; Arakaki, C.; Botimer, G.D.; Baylink, D.; Zhang, L.; Wen, W.; Fu, Y.W.; et al. Efficient precise knockin with a double cut HDR donor after CRISPR/Cas9-mediated double-stranded DNA cleavage. *Genome Biol.* **2017**, *18*, 1–18. [CrossRef]
38. Suzuki, K.; Tsunekawa, Y.; Hernandez-Benitez, R.; Wu, J.; Zhu, J.; Kim, E.J.; Hatanaka, F.; Yamamoto, M.; Araoka, T.; Li, Z.; et al. In vivo genome editing via CRISPR/Cas9 mediated homology-independent targeted integration. *Nature* **2016**, *540*, 144–149. [CrossRef]
39. Oka, M.; Kobayashi, N.; Matsumura, K.; Nishio, M.; Saeki, K. Exogenous Cytokine-Free Differentiation of Human Pluripotent Stem Cells into Classical Brown Adipocytes. *Cells* **2019**, *8*, 373. [CrossRef]
40. Braam, S.R.; Denning, C.; Van Den Brink, S.; Kats, P.; Hochstenbach, R.; Passier, R.; Mummery, C.L. Improved genetic manipulation of human embryonic stem cells. *Nat. Methods* **2008**, *5*, 389–392. [CrossRef]
41. Watanabe, K.; Ueno, M.; Kamiya, D.; Nishiyama, A.; Matsumura, M.; Wataya, T.; Takahashi, J.B.; Nishikawa, S.; Nishikawa, S.I.; Muguruma, K.; et al. A ROCK inhibitor permits survival of dissociated human embryonic stem cells. *Nat. Biotechnol.* **2007**, *25*, 681–686. [CrossRef]
42. Ihry, R.J.; Worringer, K.A.; Salick, M.R.; Frias, E.; Ho, D.; Theriault, K.; Kommineni, S.; Chen, J.; Sondey, M.; Ye, C.; et al. P53 inhibits CRISPR-Cas9 engineering in human pluripotent stem cells. *Nat. Med.* **2018**, *24*, 939–946. [CrossRef]
43. Thomas, H.R.; Percival, S.M.; Yoder, B.K.; Parant, J.M. High-throughput genome editing and phenotyping facilitated by high resolution melting curve analysis. *PLoS ONE* **2014**, *9*. [CrossRef]
44. Yang, Z.; Steentoft, C.; Hauge, C.; Hansen, L.; Thomsen, A.L.; Niola, F.; Vester-Christensen, M.B.; Frödin, M.; Clausen, H.; Wandall, H.H.; et al. Fast and sensitive detection of indels induced by precise gene targeting. *Nucleic Acids Res.* **2015**, *43*. [CrossRef]
45. Findlay, S.D.; Vincent, K.M.; Berman, J.R.; Postovit, L.M. A digital pcr-based method for efficient and highly specific screening of genome edited cells. *PLoS ONE* **2016**, *11*, 1–17. [CrossRef]
46. Kosicki, M.; Tomberg, K.; Bradley, A. Repair of double-strand breaks induced by CRISPR–Cas9 leads to large deletions and complex rearrangements. *Nat. Biotechnol.* **2018**. [CrossRef]
47. Mccabe, C.V.; Codner, G.F.; Allan, A.J.; Christou, S.; Loeffler, J.; Mackenzie, M.; Malzer, E.; Mianné, J.; Pike, F.J.; Hutchison, M.; et al. Application of long-read sequencing for robust identification of correct alleles in genome edited animals. *bioRxiv* **2019**, 1–27. [CrossRef]
48. Norris, A.L.; Lee, S.S.; Greenlees, K.J.; Tadesse, D.A.; Miller, M.F.; Lombardi, H.A. Template plasmid integration in germline genome-edited cattle. *Nat. Biotechnol.* **2020**, *38*, 163–164. [CrossRef]
49. Haeussler, M. CRISPR off-targets: A question of context. *Cell Biol. Toxicol.* **2020**, *36*, 5–9. [CrossRef]
50. Vakulskas, C.A.; Behlke, M.A. Evaluation and reduction of crispr off-target cleavage events. *Nucleic Acid Ther.* **2019**, *29*, 167–174. [CrossRef]
51. Zhang, J.; Hirst, A.J.; Duan, F.; Qiu, H.; Huang, R.; Ji, Y.; Bai, L.; Zhang, F.; Robinson, D.; Jones, M.; et al. Anti-apoptotic Mutations Desensitize Human Pluripotent Stem Cells to Mitotic Stress and Enable Aneuploid Cell Survival. *Stem Cell Rep.* **2019**, *12*, 557–571. [CrossRef]
52. Assou, S.; Bouckenheimer, J.; De Vos, J. Concise Review: Assessing the Genome Integrity of Human Induced Pluripotent Stem Cells: What Quality Control Metrics? *Stem Cells* **2018**, *36*, 814–821. [CrossRef] [PubMed]
53. Assou, S.; Girault, N.; Plinet, M.; Bouckenheimer, J.; Sansac, C.; Combe, M.; Mianne, J.; Bourguignon, C.; Fieldes, M.; Ahmed, E.; et al. Recurrent Genetic Abnormalities in Human Pluripotent Stem Cells: Definition and Routine Detection in Culture Supernatant by Targeted Droplet Digital PCR. *Stem Cell Rep.* **2020**, *14*, 1–8. [CrossRef]
54. Brookhouser, N.; Tekel, S.J.; Standage-Beier, K.; Nguyen, T.; Schwarz, G.; Wang, X.; Brafman, D.A. BIG-TREE: Base-Edited Isogenic hPSC Line Generation Using a Transient Reporter for Editing Enrichment. *Stem Cell Rep.* **2020**, *14*, 184–191. [CrossRef] [PubMed]

55. Anzalone, A.V.; Randolph, P.B.; Davis, J.R.; Sousa, A.A.; Koblan, L.W.; Levy, J.M.; Chen, P.J.; Wilson, C.; Newby, G.A.; Raguram, A.; et al. Search-and-replace genome editing without double-strand breaks or donor DNA. *Nature* **2019**, *576*, 149–157. [CrossRef]
56. Haake, K.; Ackermann, M.; Lachmann, N. Concise Review: Towards the Clinical Translation of Induced Pluripotent Stem Cell-Derived Blood Cells—Ready for Take-Off. *Stem Cells Transl. Med.* **2019**, *8*, 332–339. [CrossRef]



© 2020 by the authors. Licensee MDPI, Basel, Switzerland. This article is an open access article distributed under the terms and conditions of the Creative Commons Attribution (CC BY) license (http://creativecommons.org/licenses/by/4.0/).